This Thesis is Submitted in Partial Fulfilment of the requirements of

the Award of

Doctor of Philosophy

Title of Thesis:

Spark Breakdown Voltage Sampling During Early Stage Compression

-

A Method for Cycle by Cycle Combustion Control

This Degree is awarded by

OXFORD BROOKES UNIVERSITY

to

Michael James Austin

September 2015

ABSTRACT

This thesis proposes a novel methodology to enable cycle by cycle control of a two-stroke cycle type engine. These engines are well known for offering high specific power density solutions, however, this advantage cannot be fully exploited without new technologies enabling significantly reduced emissions and improved fuel economy. If this could be provided, working with direct fuel injection, new highly efficient, low emission, power units could result.

One of the main reasons why this has not previously been achieved has been the inability to accurately measure and quantify the amount of combustible charge available for metering of the Air/Fuel ratio. This is due to the highly dynamic gas conditions in the engine which cause significant cyclic variations of scavenging and trapping efficiencies. Existing combustion control methods are unable to accurately compensate for these conditions because fuel quantity is determined using the results of previous combustion events which do not reflect the actual gases available for each combustion.

This thesis proposes a different approach, whereby accurate fuel quantities could be determined cyclically from in-cylinder measurements ahead of each combustion event. The intention being, for optimal fuel quantities and ignition initiation timings to be calculated and provided for each cycle. This technology would significantly improve the ability to achieve an optimal combustion of each individual combustion event.

The principle of measurement uses and extends proven existing extensive scientific knowledge of the relationships between the value of Spark Break-Down Voltage (SBDV) to gas density and speciation. The methodology presented, applied pulses of voltage to the spark plug, which is normally used only to initiate ignition, to also function as a non-intrusive in-cylinder sensor.

Experimental results were obtained using three items of equipment purposely designed and manufactured for the present work. These consisted of a) A new high frequency spark breakdown voltage electronic circuit. b) A static volume sparking chamber. c). A motored test engine into which exhaust gas was supplied from an auxiliary engine via an air mixing system. The novel use of an auxiliary engine enabled a wide range of mass fractions to be subjected to cyclic compression events for evaluation independent of test engine conditions.

The new SBDV system was used to evaluate the potential of various spark plugs to function as a measurement and diagnostic sensor. Experimental results were obtained providing SBDV calibration measurements in Air, O_2, CO, CO_2 and N_2 over pressures in an engine cylinder during the early stage of compression. From these measurements mathematical expressions were obtained. Additionally, a novel method to identify these gases was demonstrated. Resulting from this work, a spark plug was modified which successfully improved the stability of the SBDV signal proposed for measurement and diagnosis.

Qualitative tests of a wide range of exhaust gas fractions were also carried out. In the present work, SBDV pulses were generated at a relatively high frequency of around 94 kHz to enable an in-cylinder samples to be obtained within 1ms time periods during the initial stage of closed compression in a motored engine. The tests successfully demonstrated the potential to differentiate between different mass fractions of trapped exhaust gases burnt in a wide range of Air/Fuel ratios, during successive cycles.

Directions for substantial further research work are provided to develop and exploit the novel methodology presented for a wide range of in-cylinder measurements. Opportunities for diagnostics capabilities and combustion control applications which have not previously been achievable are presented.

The novel contributions of the present work are a). The use of the spark plug to determine the density and speciation of the different gases. b). To apply this method cyclically, during the gas exchange period and subsequent early stage of each closed compression. This provides the potential to determine fuel and ignition requirements ‘a priori’ for each cycle to enable cycle by cycle control.

ACKNOWLEDGEMENTS

This work could not have been completed without the help, support and encouragement of a large number of people.

Firstly, I would like to thank my parents and grandparents for their past support and efforts and to see ‘the engineer’ in me. Rest their souls.

My passion for two-stroke engines has been enlightened over the years by many people but special thanks to Mick Scutt, Jack Wilkin, Jan Theil and Dolph van de Woude from whom I learn so much.

Thank you to my friends Tom Miller and Guy Pearson for many years of support and unselfish help, making and advising me on all sorts of items and parts. Thanks also to Tom Snow for his ever-enthusiastic work building the motored test rig in his workshop. My thanks also to Mark Pollard for his friendly help, cups of tea and biscuits in the Oxford Brookes University test cell area.

Thanks also to my work managers Mike Lowe and Aron Pain who enthusiastically supported me through the university process and allowed me the time to complete the thesis.

For around twenty years I have been supported with electronics by my good friend Richard Armitage of GEMS Ltd. Without his continued enthusiastic support, this research would simply not been possible. Thank you.

Thank you also to Bob Graves without whom I would not have started this work. Sadly, but also happily, I know how much the results would have interested him. Rest his soul.

My sincere thanks my university supervisor Dr. Denise Morrey who has been a great support. Similarly, Dr. John Durodola who quietly helped steer me through the PhD process especially when time extensions requests were unavoidable. Special thanks to my supervisor Dr. Stephen Samuel who taught me so much with great patience and who gave his full support through many difficult periods. Finally, to my friend Professor Geoffrey Goddard for his enthusiastic help, support and knowledge, without which I would not have dreamt of starting this work.

My thanks and congratulations also to the hundreds of researchers that contributed the inspiring knowledge that I have tried to investigate and learn from.

My sincere thanks go to Didier De Lille (MSc.) for his help assembling and formatting the thesis, in time for submission.

My sincere thanks go also to Andrea Carretti for his loyal enthusiastic assistance with the research testing and for writing of ‘Matlab’ code.

To all my family, I owe you a massive debt. You all allowed me the selfish time and encouraged me to fulfil a dream to carry out this research and to commit to the effort, writing, reading and thinking. My daughters Lucy, Katie and Nancy all helped so many times in and helpful and practical ways. Also, my grandchildren Eben, Daisy and Grace all of whom I missed time together with, which I look forward to rebalancing from now onwards. Many thanks to you all.

Finally, I save my last and deepest thanks to my wife, Lesley. She has supported my efforts unwavering through thick and thin in this endeavourer and many more before. She is my love, my support and my best friend.

I thank you all, with all my heart.

Mike Austin

TABLE OF CONTENTS

LIST OF FIGURES

LIST OF TABLES

LIST OF SYMBOLS AND ABBREVIATIONS

SYMBOL	NAME	UNIT
Engine, physical geometry, dimensions and physical quantities		
bhp	Brake Horse Power	
bsfc	Brake Specific Fuel Consumption	g/kw-hr
bmep	Brake Mean Effective Pressure	kPa
CE	Charging efficiency	
CR_g	Geometric Compression Ratio	
CR_t	Trapped compression ratio	
C_{thr}	Throttle area ratio	
BDC	Crankshaft position at bottom dead centre	
TDC	Crankshaft position at top dead centre	
BTDC	Crankshaft position relative to top dead centre	
^{0}atdc	Crankshaft angle after top dead centre	degrees of angle
^{0}btdc	Crankshaft angle before top dead centre	degrees of angle
θ	Crankshaft angle	degrees of angle
b^0	Combustion period	degrees of angle
$\overline{P}$	Average peak pressure	bar
P_{at}	Atmospheric Pressure	mbar/ bar
T_{at}	Atmospheric Temperature	K (or ^{0}C) as noted
DR	Delivery ratio	
SR	Scavenging ratio	

TE	Trapping efficiency	
SE	Scavenging Efficiency	
rpm	Speed of crankshaft rotation	rev/min

Engine, performance - related parameters

AFR	Air/Fuel, Air-to-Fuel ratio	
AFR_s	Air-to-Fuel ratio, stoichiometric	
AFR_t	Air-to-Fuel ratio, trapped	
CDI	Capacitor Discharge Ignition	
COV	Coefficient of variation	
HT	High Tension (ignition lead)	
MFB	Mass Fraction Burned	
MTB	Maximum Brake Torque	
RGF	Residual Gas Fraction (of burned exhaust gases)	
λ	Air/ Fuel equivalence ratio	
Ø	Fuel/Air equivalence ratio	
C_{lb}	Burning velocity, laminar	cm/s
η_c	Combustion efficiency	
η_{se}	Combustion efficiency with respect to charge purity	
η_{af}	Combustion efficiency with respect to fueling	

Gases

CO	Carbon Monoxide	
CO_2	Carbon Dioxide	

HC	Hydrocarbon	
N_2	Nitrogen	
NO_X:	Oxides of Nitrogen	
O_2	Oxygen	

Gas, properties

m	mass of gas	kg
m_{ar}	Mass of residual unburned air	kg
m_{as}	Mass of fresh charge	kg
m_{dref}	Reference mass required to fill swept volume	kg
m_{ex}	Mass of exhaust gas charge	kg
m_{tas}	Mass of delivered trapped air	kg
m_{ta}	Mass of trapped air	kg
m_{tr}	Total Mass of trapped charge at exhaust port closure	kg
m_{sref}	Reference scavenge mass required to fill swept volume	kg
P_{tr}	Pressure of trapped gas	mbar/bar
T	Temperature	K (Kevin)
$T\,^oC$	Temperature	C (Celsius)
T_{tr}	Temperature of trapped gas	K
V_{cv}	Volume, clearance (in cylinder head)	cm^3
V_{tr}	Volume or trapped gas	cm^3
V_{sv}	Volume swept by piston stroke	cm^3
V_{ts}	Volume, swept trapped	cm^3

ρ_{at}	Gas density at atmospheric conditions	kg/m^3
$\bar{R}$	Gas constant, universal	J/kgmolK
R_a	Gas constant, air	J/kgK
R_{tr}	Gas constant, trapped gas	J/kgK
ρ	Density	kg/m^3
Π	Purity of trapped charge	

Spark, energy, breakdown and ionization mechanisms

A	Neural ion, gas	
A^+	Positive ion, gas	
Å	Wavelength of light	Ångström
AC	Alternating electrical current	Ampere
c	Speed of light	m/sec
c_{sp}	Capacitance, electric, stray	Farad
DC	Direct Electrical Current	Ampere
E	Electric field: electric force per unit charge	Coulomb
E_{sp}	Energy, maximum available per spark	Joule
e^-	Electron, gas, negatively charged	
h	Planck's constant	
hv	Energy, photon	Joule (micro)
I	Electrical current	ampere
I_o	Electrical current at breakdown	ampere
k	Townsend's spark criteria in a uniform field	

r	Sphere electrode radius	cm
S	Spark gap distance	cm
V	Electrical voltage	Volt
V_i	Ionizing potential of gas	Volt
V_s	Spark breakdown voltage (SBDV)	Volt
$\overline{W}$	Molecular kinetic energy, mean	Joule
$\bar{u}$	Molecular velocity, mean	(m/sec)
δ	Air density correction factor	
α	Townsend's First ionization coefficient	
λ_i	Townsend's Secondary ionization coefficient	
λ	Wavelength of incident radiation	10^{-6} cm

<u>General</u>

CBC:	Cycle by Cycle
CSV	Comma Separated Variable (computer data file)
excel	Computer program
f	Function of:
FFT	Fast Fourier Transform
Matlab	Computer program
S.I.	Spark Ignited
UV	Light, ultra-violet

This page is intentionally left blank

CHAPTER ONE

INTRODUCTION

1.0 INTRODUCTION

Intensive research and development has been carried out for more than a century to increase the fuel efficiency and reduce the emitted emission levels of all types of internal combustion engines. This effort is justified economically, recognising the unsustainable demand for fossil fuel, but is driven primarily, with increasing urgency, due to environmental and public health concerns.

Increasing personal incomes and larger populations are resulting in ever larger global fleets of vehicles of all types. Significant air polluting emission reductions have been made by fitting improved combustion controls to vehicles in the high-cost automotive sector. However, improved combustion control is required for all engines and relative vehicle cost prevents the application of the same level of sophisticated combustion control being applied to small engines used in many applications worldwide.

One challenging aspect to this issue is to reduce the air polluting emissions of small engines used in two and three wheeled vehicles. There are approximately 200 million motorcycles, including mopeds, motor scooters, motorized bicycles, and other powered two and three-wheelers in use worldwide. This number equates to about 33 motorcycles per 1,000 people. Economically, this market place is significant whereby the global motorcycle market in 2010 reached a total industry value of approximately $63.5 billion. Market growth is expected to accelerate to a yearly rate of 6% between 2010 and 2015, to reach almost $85 billion.

The greatest proportion of two and three-wheeled transport occurs in Asia where it is expected for the urban population fraction to increase from 37% to 54% between 2000 and 2030. In 2014, a manufactures association report (MECA, 2014) commented that world-wide motorcycle usage is increasing at a rapid pace, especially in the urbanized areas of Asia where the average annual rate of growth for the region is 15%. Annual growth rates are at or above 5% in most Asian countries.

To demonstrate the effect of emissions from these vehicles. Considering the Asian region, the contribution to air pollution from two and three wheeled vehicles form significant proportions of the total vehicle emissions. The health impact from all vehicle emissions in

that region is extremely significant whereby an estimated 3 – 6 million people die yearly from air pollution related issues (W.H.O., 2000).

The engines used in small two and three wheeled vehicles must be compactly packaged and have low-maintenance costs. They are usually small capacity, single cylinder engines which operated at a high average percentage of their load/speed capability. Two-stroke cycle type engines are ideally suited to these requirements and have been the traditional power plant of choice for these applications. However, typically, these engines have poor emission performance which results from minimal combustion control where fuel is supplied by simple carburation and ignition timing variations are also limited and simple. Subsequently, these two-stroke cycle type engines are estimated to produce up to 70% of the total Hydrocarbon (HC) emissions, 40% of the total Carbon Monoxide (CO) together with a substantial proportion of particulate matter under 10 microns (pm10) (Shah & Harshadeep, 2001). Not all the vehicle air pollution is caused by two-stroke cycle type engines but the proportion of small vehicles powered by these engines in various Asian countries is significant as is shown in table T1-1 (Wijeyakulasuriya & Nalim, 2007).

Table T1-1: Two-Stroke Cycle engine usage in some Asian cities

Country	Bangladesh	India	Nepal	Pasistan	Sri Lanka
Year	1999	1997	1999	1999	1997
% Two-Stroke	51	62	47	45	52

Additionally, considerable global efforts have been made to reduce greenhouse gases especially CO_2 with increasing stringent worldwide targets for emission reductions for all types of vehicles including two-wheeled transport (Hirz, et al., 2004). Atmospheric trace gas measurements made by the Carbon Dioxide Information Analysis Centre (CDIAC), noted that CO_2 levels have increased from pre-1750 levels of 280 ppm to 386 ppm in 2009. In response to this increase, the European Commission aims to reduce CO_2 emissions from light-duty vehicles to 95 g/km by the year 2020 (Smokers, et al., 2006). Such emission concerns led to questions into the future suitability of the two-stroke cycle type engine which resulted in subsequent worldwide limitations on engine capacities. Increasingly

replacement by four-stroke cycle type engines, which require around twice the engine capacity for the same performance, is occurring.

It has been recognised however, that “the challenge is to achieve lower emissions and to adopt more efficient smaller capacity engines with lower heat and frictional losses which could provide down-sized performance comparable with larger engines” (Hardcastle, 2013).

Ultimately, the relatively high-power output capabilities and power / density of the two-stroke cycle type engine cannot be ignored in a world which demands high efficiency solutions. And, it has been recognised “the high-performance potential of two-stroke cycle type engine should receive OEM attention and consideration in future strategic planning if the opportunities for reduced emissions could be achieved” (Schmidt, et al., 2004).

Therefore, the question is how can the unfavourable emission characteristics the two-stroke cycle type engine be improved whilst retaining or enhancing the undoubtedly basic performance advantages over other engine types.

Research incorporating direct fuel injection has shown the opportunity for small two-stroke cycle type engines to re-emerge for many vehicle applications (Wyczalek, 1991) which could match or exceed the potential of small capacity four-stroke cycle type engines (Kirchberger, et al., 2007), (Oswald, et al., 2010). Other significant emission reductions from two-wheeled vehicles equipped with two-stroke cycle type power plants can comply with stringent hydrocarbon and carbon monoxide emission standards by using catalyst technology. “Therefore, in markets where the cost of basic transport and higher specific power output are important, two-stroke cycle type power plants will continue to find widespread use” (MECA, 2014).

Legislation demands further and continuing emission reductions. Future combustion control systems when applied to two-stroke cycle engines will need to compliment the fundamental simplicity of construction which is the basis of its power / density advantages whilst adapting to the associated complexity of the gas exchange process.

Briefly described, the gas exchange process in a two-stroke cycle type engine is complex because the inlet and exhaust phases overlap whereby fresh charge and exhaust gases enter and leave through holes or ports in the sides of the cylinder. These ports are opened and closed by the piston such that each complete combustion cycle is achieved in two piston strokes or 360 Degrees of crankshaft rotation. This process is different in four-stroke cycle type engines where the inlet and exhaust phases are separated by an additional engine stroke

with mechanically actuated valve. Each complete combustion cycle is achieved in four strokes of the piston or 720 Degrees of crankshaft rotation.

The mass flow of fresh charge through the two-stroke cycle type engine varies and increases with engine speed and load thereby causing the fuel and ignition timing requirements vary across the operating range (Tsuchiya & Hirano, 1975). However, the dynamic gas behaviour in the exhaust system forms an additional, almost independently variable effect which continues each cycle until the exhaust port is shut around 90 Degrees BTDC. Until the exhaust port is closed the cylinder may be under-scavenged, or over-scavenged. This causes significant differences to the mass, contents, pressure and temperature of the trapped charge depending on the relative quantities of un-scavenged burned or fresh charge.

Loss of fresh charge by 'short-circuiting' releases unburned gases directly into the exhaust system and into the atmosphere. Quantities of short circuited gases of between 25% - 40% of the swept volume have been measured (Batoni, 1978). Where traditional carburation fuelling methods or in-direct fuel injection is used, fuel is mixed into the fresh charge at the engine inlet. This causes any fresh charge loss to also contains unburned fuel. Computational Fluid Dynamic (CFD) analysis has identified several mechanisms (Rosskamp, et al., 2001), which contributor to the high HC emissions and fuel consumption of the two-stroke cycle type engine. However, the largest individual contributor to these emissions is 'short circuiting' where fresh charge is lost directly into the exhaust system without contributing to combustion. This effect can and has been reduced by a combination of various mechanical devices and port arrangements, but this loss mechanism cannot be eliminated if the fresh charge also delivers fuel. The introduction of both high and low-pressure injection systems have enabled fuel to be added to the fresh charge in the cylinder following closure of the exhaust port. Thus, although fresh air charge can be lost by short circuiting this gas will not contain significant quantities of unburned fuel. However, the loss of fresh air charge does cause the amount of air trapped in the cylinder available for the subsequent combustion to vary.

In addition to cyclic variations of the trapped mass charge available for combustion the quantity of trapped residual gas significantly effects the speed of each combustion. The speed of combustion effects the crankshaft position at which maximum pressure occurs and hence the torque developed. This is compensated by varying the crankshaft position when ignition of the combustible mixture by spark is initiated.

By a combination of these and other effects, which are described in the following chapters, the mass of trapped combustible charge varies cycle by cycle. These effects cause irregular combustion (Tsuchiya, et al., 1983), cylinder pressure variations and varying combustion efficiencies for each event. Thus, due to the cyclic variations of trapped charge both fuel quantity and ignition timing require cycle by cycle correction and optimisation. These effects are worse when the engine is operating at low speed and low load conditions where the mass flow rate through the engine is small in comparison to its maximum capacity (Lu & Lee, 1996).

Current combustion control systems are unable to compensate for the cycle by cycle variations described briefly above. Therefore, the problem remains, of how to provide accurate fuelling which reflects the relatively large cyclic variations of total trapped mass or available combustible charge. Consequently, new combustion control technologies are required which overcome these difficulties for application to two-stroke cycle type engines. Previous introductions of retrofit direct injection kits for small two-stroke cycle type engines (Lorenz, et al., 2005) and developments of low cost solution digital electronics (Ugale, 2014) have shown such technology can be retrospectively introduced in addition to being provided as part of original equipment.

To be globally significant, as noted above, such technologies must provide low cost solutions which are simple to install and maintain but enable combustion control to a level compatible with those applied in higher cost automobile applications.

The present work addresses the characteristics, issues and difficulties described above with the aim of optimising the fuelling and ignition timing for each individual combustion event.

1.1 MOTIVATION FOR THE RESEARCH AND THESIS

The authors' personal interest in engines significantly pre-dated the embarkation into the present work. This practical experience emphasised a close and real connection between spark energy and in-cylinder contents and conditions. The author realised that to investigate this phenomenon further required additional formalised and recorded research which thus provided the motivation for the present work.

The research described in this thesis is primarily focused on the two-stroke cycle type engine. This focus is justified by the author for two reasons. Firstly, the engine type represents a significant technical challenge for combustion control for which a solution is

urgently required. Secondly, for pragmatic research reasons, the simple construction of the two-stroke cycle type engine enables simple and cost effective, use and modification for test engine purposes.

1.2 RESEARCH APPROACH

The initial approach taken was to review the gas exchange process which occurs in a two-stroke cycle type engine. The existing work which has investigated the contributing causes of poor combustion was reviewed together with strategies which could offer optimum control of combustion. This led to the conclusion that in an engine where the amount of combustible gas varied significantly for each individual combustion event, the content of that gas requires individual determination for each cycle. Further, this determination was required to be available in time to calculate the appropriate amount of fuel required for and in advance of each individual combustion event.

The gas exchange processes occur in the engine until the exhaust port is covered by the piston and the gas contents in the cylinder become closed. Therefore, to ensure the accurate determination of the gases within the cylinder, this process is required to take place following this closure event. The operational constraints described above defined the requirements for a new gas sensing system which could operate at high speed within the cylinder of an engine.

The literature review contained in chapter two outlines the existing sensing methodologies which were evaluated for potential use or adaptation to enable the required sensing capabilities. The review of existing technologies uncovered the relationship between the voltage required for an electrical spark to pass between electrodes and the species and density of gas between those electrodes. These relationships were first researched in the Eighteenth century and where subsequently formulated into a Law of physics in the nineteenth century (Paschen, 1889). This relationship between spark break-down voltage and gases is reflected practically in the recognised link between Air/Fuel ratio, combustion pressure and the spark voltage required to enable reliable ignition (Sher, 1986), (Silsbee, 1925). From this, the potential of the spark plug, to act as a gas sensor using these proven relationships was thus realised.

1.3 RESEARCH OBJECTIVES

The overall aim of this research project was to improve the combustion efficiency of the internal combustion engine in a simple and practical manner applicable to all S.I. engines.

The research efforts investigating the use of the spark plug as a gas sensor from which the mass of combustible gas can be determined cyclically. The questions listed below were addressed as part of that effort.

a) Could the spark across the electrodes of a spark plug respond to gas species and gas conditions in a reliable and predictable manner in the same way as found in previous electrical and physics research?
b) Could the spark plug be used as a gas sensor could the voltage required in different pressures and gas species be used for diagnostic information?
c) Could the information be obtained sufficiently quickly and reliably from within the cylinder of an internal combustion engine to enable cycle by cycle combustion control?

These questions led to the development of the following thesis objectives:

- Develop an electronic system for using Spark breakdown Voltage events to determine gas density.
- Manufacture test apparatus to determine Spark Breakdown Voltage values for various gases and pressures.
- Investigate the characteristics and experimental variability of typical spark plugs when subjected to Spark Breakdown Voltage events and suitability as a sensor.
- Derive reliable gas density values from Spark Breakdown Voltage events obtained from cycle by cycle events.
- Investigate the relationship between Spark Breakdown Voltage and the density /speciation of gases present in the combustible charge trapped in the cylinder of an engine.

1.4 LAYOUT OF THE THESIS

Following this introductory Chapter 1.0, Chapter 2.0 begins by reviewing the challenges facing combustion control in all engines and work which has investigated the associated difficulties. The Chapter continues with an overview description of the two-stroke cycle type engine and focuses on the features which are responsible for traditionally high

emissions. The work which has investigated or developed solutions to improve those characteristics or investigated the causes and effects of variations in residual burned fraction, combustion, knock and causes of cyclic variability are covered. This review also includes research which used or developed sensor arrangements or derive mathematical solutions to investigate in-cylinder gas exchange processes and behaviours in two and four-stroke type engines. Finally, the Chapter concludes with a review of spark plug including and work which has investigated it's use as an in-cylinder sensor.

In Chapter 3.0 the theories of Spark Breakdown Voltage (SBDV) and its relationship to gases are investigated. The theoretical background and the mathematical basis for spark breakdown and its relationships with gases is provided from published work.

In Chapter 4.0 the three items of test apparatus which were manufactured for the present work to obtain data in both static and dynamically varying cyclic events are decribed. Design and construction details are included of the sparking chamber and test rig incorporating a motored test engine and the auxiliary engine which supplied burnt exhaust gases. Details are also provided of the new SBDV circuit electronic circuit developed to generate spark breakdown events. The manner the events were gathered and used to process the SBDV and instrumentation signals captured by the PICOSCOPE 4824 are explained.

Chapter 5.0 contains a short-summary of testing carried out for this thesis to guide and assist the reader.

In chapter 6.0 the subject matter covered is the spark plug and calibration evaluations as a SBDV sensor. The testing reported in this chapter was carried out in air. The spark break-down characteristics of three types of spark plug types were investigated using a novel comparison technique which is proposed to offer a method of individualised calibration. Testing was also carried out to evaluate the effect of spark shielding from gas flow. These tests obtained SBDV signals from within the test engine cylinder which was motored. Comparative results are presented showing cycle-by-cycle SBDV vs Pressure and averaged results.

Chapter 7.0 contains details of the testing carried out to determine the spark breakdown voltage relationships to Air and various gases significant to combustion. The testing procedures used are described. The results obtained are explained, aided with graphs and tables. Mathematical expressions for the different gases tested are listed and compared with expressions obtained from previous research. Finally, investigations of SBDV signals obtained from Air, O_2, CO_2 CO and N_2 using Fast Fourier Transforms (FFT) are included.

These results consider all the frequencies which contribute to the characteristic shapes of 10 individual spark break-down events.

In Chapter 8.0 two types of testing are described used to investigate spark break-down Voltage signals obtained from exhaust gases. The results for these tests, consisting of two separate series, were obtained from within the cylinder of the test engine as stored compressed exhaust gases were not available. The first series was ‘quasi-static’, displaced a modified piston very slowly, this attempted to mimic the static testing described in Chapter 7.0. The second series was conducted in a motored test engine. Exhaust gases were supplied by a separate ‘auxiliary’ engine. The testing procedures used are described. Justification for this testing method is explained. Test results are provided with graphs and discussion. Finally, the characteristics of SBDV signals obtained from various exhaust gases investigated using FFT are included and compared.

In Chapter 9.0 the testing carried out to identify the SBDV characteristics obtained from within a dynamically changing environment is presented. Results containing significant information were successfully obtained cycle by cycle. The mathematical expressions previously obtained for exhaust gas mixtures, representing a very wide range of residual mass fraction of burned gases were converted into pressure. These are shown plotted against pressure signals obtained using a proprietary pressure sensor for nine continuous motored cycles.

In Chapter 10.0 potential concepts for cycle by cycle engine control are introduced. The inclusion of this chapter enables the explanation of how the information from the SBDV signal could be incorporated into a new type of combustion control system. Engine control factors which could be influenced by using Spark Breakdown Voltage enabled cycle by cycle control and those which would not be are discussed.

In Chapter 11.0 conclusions are drawn from the work, the limitations to the results are explained and recommendations for further work are given.

The references for the published works included in the thesis are listed within the final work section.

CHAPTER TWO

LITERATURE REVIEW

2.0 INTRODUCTION

This thesis concerns combustion and methods to improve the control of that process for engines which use an electrical spark to initiate that process. In such engines, combustion is a process where the addition of heat from the electrical spark, propagates into a mixture of air and fuel which then oxidises in an exothermic reaction. The heat energy released from that reaction causes an expansion of the trapped gases and drives down the piston, turning the crankshaft to produce motive output torque. The amount of energy released from each combustion event depends heavily on the ratio of Air/Fuel trapped in the cylinder.

The greatest amount of energy occurs when the Air/Fuel ratio is 'Stoichiometric' which is a word taken from Greek words '*Stoicheion'*, meaning 'element' and '*Metron'*, meaning "Measure". Less energy is released from combustion which occurs in mixtures of Air/Fuel ratios containing less fuel, termed 'Lean' and more fuel, termed 'Rich', however, these may be required to optimise various engine operating conditions. Generally, a 'Lean' ratio is used when engine load demands are relatively low, giving an opportunity for fuel consumption reduction. Alternatively, a 'Rich' ratio is used when engine load demands are high, such as during acceleration, which results in increased fuel consumption. Engine development has extended the Air/Fuel ratio limits to optimise overall engine performance and fuel efficiency.

The products of combustion consist of pollutants, the relative proportions of which vary depending upon the Air/Fuel ratio burned. When combustion or burning, is initiated, the flame spreads, radiating outwards spherically, consuming the fuel present in the combustion chamber and cylinder. The speed which the flame spreads and the heat created, is significantly affected by the Air/Fuel ratio and the amount of residual burned gas present (Quader, 1976). The heat created by combustion causes the pressure in the cylinder to increase although no correlation exists between local flame propagation and the in-cylinder pressure history (Spicher & Backer, 1990). The amount of motive torque generated by this process is heavily influenced by the crankshaft position when the greatest cylinder pressure occurs. Therefore, the crankshaft position at which ignition is initiated must consider the rate at which pressure will increase with respect to the contents in the cylinder (Daniels, 1998). In-cylinder pressure has been used for engine control strategies, however the

primary function of the combustion control system is to optimise the amount of fuel in the cylinder to achieve the Air/Fuel ratio required for the operational requirements and the crankshaft position where spark ignition is initiated (Kawamura, et al., 1988). This objective is further complicated due to the dynamic nature of operation where the delivery and trapping of fresh mases of air for each cycle changes for different engine speeds and loads. These conditions change primarily due to variations of mechanical efficiencies and wave dynamics in the inlet and exhaust systems. These produce the pressure differentials which cause gases to flow into and out of the cylinder. The rate of change of engine speed results in considerable overlap and mismatch between the gas flows and engine speed. Naturally, the amount of fresh air trapped in the cylinder for each cycle can vary.

Additionally, the ability of the engine to evacuate the burned gases from the cylinder is also primarily influenced by the gas flow and differential pressure overlaps. Depending on these, the burned gases may be over-extracted or under-extracted. In cycles when the burned gases are not extracted from the cylinder they remain and become a residual part of the next charge (Ohigashi & Hamamoto, 1971). Burned or residual exhaust gases are largely depleted of oxygen and therefore consist of gases which do not contribute to oxidising, hence combustion process. However, the gases and proportions of these gases in these residual exhaust gas vary depending upon the Air/Fuel ratio and residual gases contained in the charge in which they, themselves were burned. There also exist, multiple numbers, of complex and inter-related influences and contributing factors which cause variations of individual combustions and subsequent cycles (Matekunas, 1983), (Ozdor, et al., 1994). These principally involve the early development of the flame kernel and conversion into early flame development as influenced by local conditions around the spark plug electrodes during that process (Keck, et al., 1987), (Herweg, et al., 1988).

Researchers have used many different measurement techniques and mathematical methods applied to all types of engines at various levels of complexity and sophistication to determine in-cylinder gas contents and associated combustion efficiencies (Smith, et al., 1999), (Namazian, et al., 1980), (Cowart, 2002), (Streit & Borman, 1971), (Subramniam, et al., 2010). Work on this issue accelerated due to the development of variable geometry engines and Homogeneous Charge Compression Ignition (HCCI) combustion (Ivansson, 2003), (Karagiorgis, et al., 2006). Obtaining detailed cycle-by-cycle in-cylinder information has currently only been achieved using expensive, specialised equipment (Hunicz, et al., 2004). A method by which cycle-by-cycle corrections can be determined in an operating engine across a realistic operating range has not yet been developed.

In a directly injected engine, fuel is added to the trapped charge following the mechanical isolation of the charge in the cylinder. The amount of fuel added is adjusted by an electronic control system based upon an estimate or measurement of the trapped mass of fresh charge and remains constant over numbers of engine cycles. The potential result of these cyclic variations of the in-cylinder contents trapped at the point of mechanical closure of the cylinder is shown diagrammatically in Figure F2-1 below. Visual comparison of the relative proportions of the contents show the Air/Fuel ratio and combustibility vary each cycle. From this it can be seen, that achieving a pre-defined and consistent Air/Fuel ratio will be impossible unless the amounts of fresh charge and residual exhaust gases are known for each cycle and the fuel quantity added is adjusted to suit.

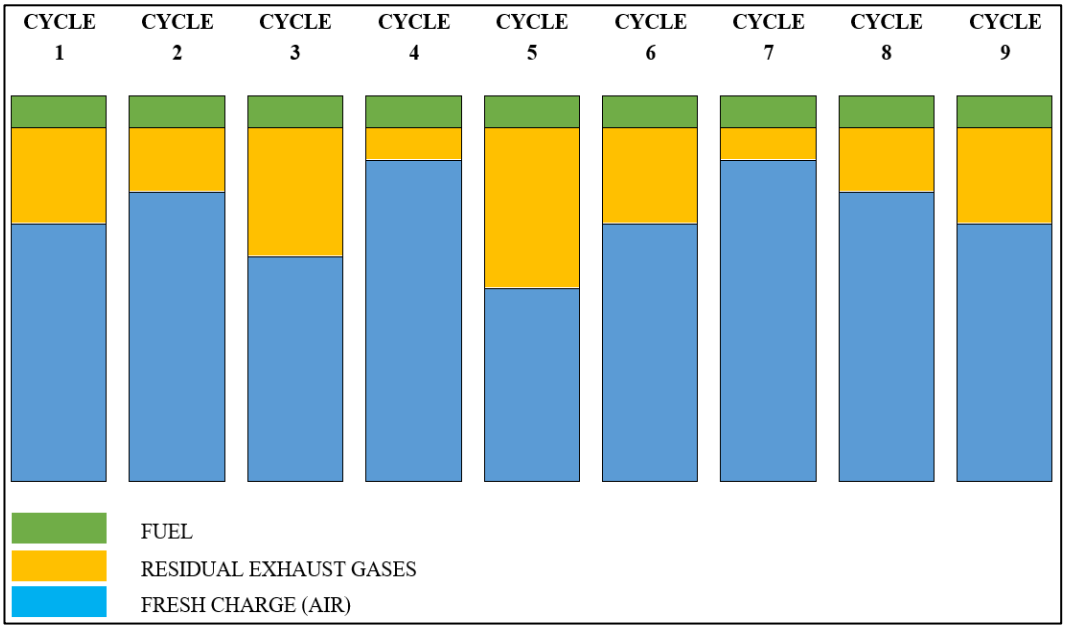

Figure F2-1: Diagrammatic representation of Cyclic Variations to Trapped In-Cylinder contents

The individual in-cylinder contents represented in Figure F2-1, include all those which are then compressed by the ascending piston to be available for the subsequent combustion event.

This chapter consists of a review of existing work which has investigated the causes and effects contributing to variations of trapped in-cylinder gas masses. This review includes different types of instrumentation, sensing systems and mathematical estimating methods which have been used or developed to determine the mass and or speciation of trapped in-cylinder gases for all engine types.

2.1 THE TWO-STROKE CYCLE TYPE ENGINE

For the reasons given in chapter one, this review of existing work especially concerns the loop scavenged two-stroke cycle type engine. Therefore, the review begins with an overview of this type of engine and how its basic design presents the greatest challenge to cycle-by-cycle engine control.

2.1.1 HISTORY OF THE LOOP SCAVENGED CRANKCASE COMPRESSION TWO-STROKE CYCLE ENGINE

The invention of the two-stroke cycle type engine is attributed to Sir Dugal Clerk in 1878. Two-strokes of the piston were used to complete each combustion cycle to avoid a slightly earlier patent using four strokes of the piston, by Nikolus August Otto. The Clerk engine used one of two cylinders to pump fresh charge into the other.

In 1891, Joseph Day invented an improved two-stroke cycle type engine configuration made more compact and efficient by using the pressures created in the crankcase by piston movement (Torrens, 1991). Additional improvements by Fredric Cock, simplified the arrangement further, allowing the fresh charge to be inducted into the crankcase through a port in the cylinder which was opened and closed by the piston skirt. Fresh charge was pumped by the descending piston, when the inlet port was closed, into the combustion space above the piston through transfer ports for compression by the ascending piston. This engine proved ideal for mass production techniques.

The design and simple construction features introduced by Day and Cock were later adapted very successfully, for motor-cycle racing by Alfred Angus Scott. In 1929, the 500cc twin cylinder version engines produced approximately 20bhp at 5000 rpm or 40bhp/litre, (The Scott Owners Club, 2016).

In 1927, a German company, introduced an innovation which directed the fresh charge, pumped from the crankcase, into the cylinder in a new ‘loop’ flow formation. This innovation, attributed to the DWK chief engineer ‘Dr. Schuerle enabled a 125cc engine, to achieve 15bhp or 120bhp/Litre.

The deliberate harnessing of the dynamic pressure waves in the exhaust system was first exploited by a German engineer, Walter Kaaden, who, working for MZ motorcycles in 1952, enabled a 125cc engine to achieve 25bhp or 200bhp/Litre (Oxley, 2009).

The Japanese motor industry committed significant research and effort into two-stroke cycle type engine development for road, off-road and GP racing from the early 1960's through to 2009. In 1968, a Yamaha, four-cylinder 125cc engine developed 44bhp or 350bhp/Litre (Naito & Taguchi, 1966), (Naitoh & Nomura, 1971). Development continued in many motorcycle companies, driven by racing as a sales window. Despite already very high specific power outputs, Powell noted in 1978 that two-stroke engine theory was not well developed at that time (Powell, 1978). Significant research continued which investigated all aspects of the two-stroke cycle engine.

With the growing concern of pollution, much work focused on ways of improving that aspect of the engines behaviour whilst continuing to exploit the types inherent potential (Laimbock, 1991), (Heywood & Sher, 1999). These developments and associated research and measurements are reviewed below. On the race track the search for maximum performance continued such that a Dutch engineer, Jan Theil, working for Aprilia in 2009, is attributed with the development of a 125cc engine for Grand Prix motorcycle use which achieved 54bhp or 430bhp/Litre (Theil, 2014).

Due to racing rule changes and subsequent reduction in engine development, this remains the highest published performance figures for a loop scavenged, crankcase compression, normally aspirated two-stroke cycle type engine.

The following sections in this chapter describe the behaviour of gases in a two-stroke type engine and the research which has investigated those behaviours. Sections have been separated into the different phase of gas movements through the engine to explain the key complexities and difficulties involved in obtaining in-cylinder measurements.

2.1.2 GENERAL

The amount of power that any engine produces is a function of the mass flow of air which passes through the engine and the efficiency of each combustion event. The mass flow rate increases with engine speed and throttle opening until the sizes and opening durations of the inlet and outlet ports limit the process. These factors determine the overall charging efficiency, which is a product of the *delivery ratio* and the *trapping efficiency*. It is the delivery ratio which is the dominant effect (Andersson, 2004) (Komotori & Watanabe, 1969). The *delivery ratio* (DR) of an engine is the mass of air supplied as a function of the mass which would fill the swept volume (Blair, 1996). Very high-performance engines can achieve delivery ratio of 1.5 (Sweeney, et al., 1985).

The following sections introduce the phases through which the mass of air passes through a two-stroke cycle engine and the effects the performance and emissions produced.

2.2 INDUCTION

In a two-stroke cycle type engine the flow of gas from the inlet into the combustion chamber, takes place in two stages. During the first stage, fresh charge passes from the atmosphere (or a representative air box) into the crankcase which is used as a storage volume.

The flow of inlet air entering the engine is adjusted by varying the open-area of a throttle valve. Traditionally, the pressure drop in the middle of a venturi profile corresponding to the throttling point, is used draw fuel from a storage chamber into the stream of fresh air. The traditional use of a device termed ‘a carburettor’ provided a homogeneous Air/Fuel charge into the engine which included lubricating oil added to the fuel. Alternative fuel delivery systems have been developed providing high and low pressure, indirect and indirect fuel injection which are described in section 2.9.

The inlet passage feeds into the crankcase storage volume and is opened and closed by a mechanical valve. Three different valve arrangements have been developed. The simplest form of inlet valve, uses the piston to expose or close the inlet port as it moved up and down. This provides a fixed port timing and duration, controlled by the piston skirt, to allow fresh charge to enter the crankcase volume. The piston port arrangement is simple to implement but provides a symmetrical open and closing angle which is not optimal for all engine speeds and loads. The rotary disc valve is a device which allows fixed asymmetric opening and closing valve timing and enables very short inlet ducts to be used which allows greater charging efficiencies and higher power output potential than is possible with piston port induction (Komotori & Watanabe, 1969), (Naitoh & Nomura, 1971). The third valve type is termed ‘the reed valve’ which opens and closes depending on pressure difference. The performance of the valve depends on the size, number, thickness and material of the reeds which can be optimised by calculation (Blair, et al., 1979), (Fleck, et al., 1987). The advantage of this valve is the opening duration changes dynamically to suit the pressures available and provides a simple and effective device to implement (Jennings, 1973). Additional fuel economy and performance improvements have been achieved using an intermediate storage volume, positioned close to the reed valve (Hata, et al., 1981).

The relative dimensions of any inlet system can be optimised to provide optimum delivery efficiencies. The maximum delivery ratio is achieved by aligning the three quarters length

of the first order standing pressure wave at the inlet valve face. Generally, for any given port area, there is an engine speed which results in the maximum delivery ratio. That engine speed increases with crankcase volume (Nagao & Shimamoto, 1967). Due to the dynamic nature of the pressure waves in the system, ultimate efficiencies cannot be achieved uniformly across the entire engine operating range. Minimalising reverse inlet gas flow (which contains fuel) results in reduced specific fuel consumption (Zhou, et al., 1984)

The inlet flow and resulting delivery ratio relate to gas density and are therefore influenced by ambient pressure and temperature as reported by (Watanabe & Kuroda, 1981), (Sher, 1984), (Harari & Sher, 1993).

2.3 THE TRANSFER OR SCAVENGING PROCESS

The second part of the gas flow process in a two-stroke cycle type engine transfers the charge stored in the crankcase into the cylinder which includes the combustion chamber, above the piston. This transfer of gas charge is driven by differential pressures between the crankcase volume and the cylinder volume through transfer passages which lead to' transfer ports' in the cylinder wall. The differential pressures which increase the scavenging and charging efficiencies result from two effects.

a) Compression of the gases trapped in the crankcases by the downward motion of the piston. The compression pressure achieved is related to the crankcase volume and swept volume which defines the primary compression ratio.

b) The extraction effect of the exhaust system design which produces a significant pressure reduction in the cylinder (Weclas, et al., 1997).

The alternative influences of crankcase compression or exhaust system contribution represent one of the design optimisations to best suit the intended engine application. The effect on the design of various engine components optimised for different applications was demonstrated by (Holzleitner, 1991). In general, engine which are optimised to operate predominantly at low speeds do not have highly effective exhaust systems and the crankcase compression effect dominates the charging process. Alternatively, in engines which are optimised for high speed performance the charging efficiencies are dominated by the exhaust system characteristics (Cartwright, 1994).

The transferred charge flows into the cylinder in a looped shaped pattern which forces the transfer charge against the wall of the cylinder on the opposite side to the exhaust port.

Using the cylinder wall in this way provides a solid partial boundary which helps to maintain the homogeneity of the fresh charge and prevent mixing with the residual burned gases in the cylinder. This flow continues to develop, displacing the residual charge from the combustion chamber and cylinder to scavenge the burned gases out into the exhaust port. However, the stability of the transfer gas streams changes with mass flow rate which varies every cycle causing variable mixing to occur at the boundary between the fresh charge and the residual burned gases during this 'gas exchange process'. Thus, as this is the primary mechanism to scavenge the residual burned gases from the cylinder the amount remaining in the cylinder also varies every cycle.

2.3.1. CALCULATION OF SCAVENGING PERFORMANCE

In a two-stroke cycle type engine calculation of the trapped mass of combustible charge is complex and requires consideration of the effects of mixing between the fresh and burnt charges and the relative gas dynamics of each charge.

At the point when the scavenging process is complete and the transfer ports are just closed, a mass of fresh charge, m_{as}, has passed through the crankcase from the atmosphere. By measuring the ambient pressure p_{at} and temperature, t_{at} the air density is given by, ρ_{at}. From the equation of state, where R_a is the gas constant for air:

$$\rho_{at} = \frac{P_{at}}{R_a t_{at}} \qquad \text{(Eq. 2-1)}$$

The success of the scavenging process is evaluated principally by the following relationships:

The delivery ratio, DR of an engine defines the mass of air supplied during the scavenging period as a function of a reference mass, m_{dref}, which is the mass of gas required to fill the swept volume, V_{sv} under the prevailing atmospheric, conditions. i.e.:

$$m_{dref} = \rho_{at} V_{sv}$$

Therefore:

$$DR = \frac{m_{as}}{m_{dref}} \qquad \text{(Eq. 2-2)}$$

The scavenge ratio, SR defines the mass of air supplied during the scavenging period as a function of reference mass m_{sref}, which is the mass of gas that could fill the entire cylinder volume under prevailing atmospheric conditions. i.e.:

$$m_{sref} = \rho_{at}(V_{sv} + V_{cv})$$

Therefore: $$SR = \frac{m_{as}}{m_{sref}}$$ (Eq. 2-3)

If the scavenging process were 100% successful, the scavenging efficiency SE would equal the scavenging ratio SR. The scavenging efficiency is defined as the mass of delivered air trapped m_{tas}, by comparison with the total residual mass of charge m_{tr} at exhaust port closure. The trapped charge contains only the fresh charge trapped, m_{tas}, and exhaust gas m_{ex}, and any remaining air left unburned from previous cycles, m_{ar},

Where: $$m_{tr} = m_{tas} + m_{ex} + m_{ar}$$

Hence the scavenging efficiency, SE, defines the effectiveness of the scavenging process, hence:

$$SE = \frac{m_{tas}}{m_{tr}} = \frac{m_{tas}}{m_{tas} + m_{ex} + m_{ar}}$$ (Eq. 2-4)

The first methods for analysis of scavenging flows in a two-stroke cycle type engine proposed concepts of 'perfect mixing' and 'perfect displacement' (Hopkinson, 1914). The Hopkinson 'perfect displacement' and 'perfect mixing' scavenging models were idealised versions of actual processes which represented simplified extremes. They did not involve any fluid dynamic calculations but were easy to use to provide a quantifiable evaluation of scavenging performance.

The perfect displacement model shown diagrammatically, in Figure F2-2, assumes a) No mixing between gases. b) No direct loss of exhaust gas into the exhaust port. Hence all the air entering the cylinder is retained and 'perfectly displaces' the exhaust gas.

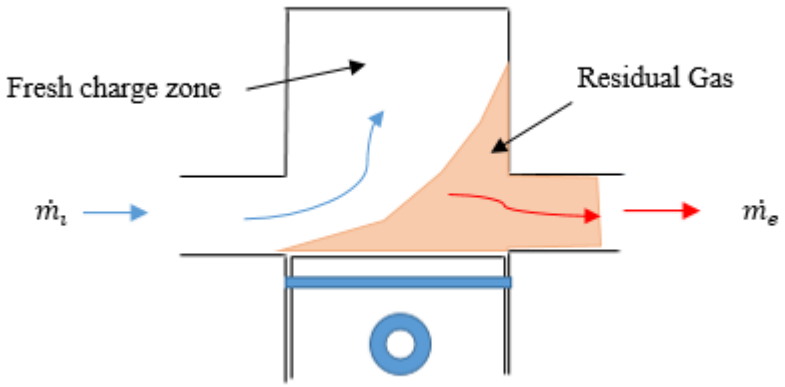

Figure F2-2: Hopkinson's Perfect Displacement Scavenging Model

The perfect mixing model shown diagrammatically, in Figure F2-3, assumes the fresh charge entering the cylinder mixes perfectly and instantly with the residuals. The mixed gas is an ideal gas and the mixed gas is contained by adiabatic cylinder walls. Further, there is a difference between the inlet gas temperature and the mixed charge at the end of the scavenging period. The gas leaving the cylinder is a mixture in the ratio of the two gases caused by the process. However, the results obtained were noted to not enable directly comparison with theoretical work which differentiated between the perfect displacement model and the prefect mixing models proposed by (Hopkinson, 1914).

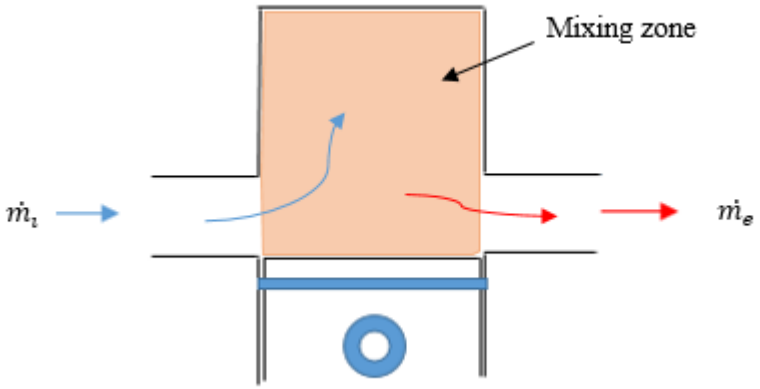

Figure F2-3: Hopkinson's Perfect Mixing Scavenging Model

The perfect displacement model assumes residual gases are *perfectly* displaced by the incoming charge. Hence, no mixing occurs between the fresh and burned charges and there is no direct loss of fresh charge out of the cylinder into the exhaust port. Considering the scavenging process is a function of delivery ratio (DR), the perfect displacement model produces the greatest charging efficiency and is used as a reference model. This mathematical model is shown diagrammatically in Figure F2-3 and consists of one phase and one zone. It assumes. a) No heat is transferred across the boundary walls. b) The volume and Pressure are constant. c) No heat or mass transfer occurs between the fresh charge and burned charges. d) The fresh charge replaces the residual burned charge by a perfect displacement mechanism.

During the scavenging period both the transfer ports and exhaust port are open which results in complex flow processes. Various models were developed, with increasing sophistication and complexity, to calculate the movement of gases in the cylinder and resulting scavenging processes, (Wallace & Nasif, 1954), (Maekawa, 1957), (Benson & Brandham, 1969), (Wallace & Cave, 1971), however, they all incorporated simplifying assumptions.

Changyou and Wallace categorised the models into two classes: 1) Thermodynamic models which omit fluid dynamic behaviour and give only a description of the thermodynamic properties. These are based on artificial flow and zonal assumptions. 2) Fluid Dynamic models which provide all information and do not use flow and zonal assumptions. The researchers then investigated and compared the various 'isobaric' and 'isochoric' models created between 1917 and 1980 to present a generalised thermodynamic model which was reported to give good estimations provided five parameters are well chosen (Chen & Wallace, 1987).

Increasing availability of powerful personal computers enabled fast numerical solutions of differential equations and enabled the development of more complex zonal models which better matched experimental results (Chen & Wallace, 1987), (Blair, 1988). The more sophisticated models considered the scavenging process to be divided into several phases with assumptions applied to each. In these, the cylinder was assumed to consist of various sections or zones, 'Residual Gas Zone', 'Fresh Charge Zone' together with 'one or more mixing zones' with additional consideration of short circuiting. The effect of gas temperature was introduced by (Benson, 1977), (Chen & Wallace, 1987). Blair included unsteady gas dynamic equations based on results obtained from a single cycle test rig (Sweeney, et al., 1985). The non-isothermal behaviour of the scavenging process in a firing engine was accounted for by the inclusion of a parameters $K_{T.}$ The introduction of this related the exhaust gas temperature to the inlet air and cylinder temperature and was found to be a strongly related to engine speed but less to load (Blair, 1993).

Sher modelled exhaust gas purity assuming a time variation of an 'S' shaped flow of fresh air mass fraction of fresh air content in the gas passing through the exhaust port. This related mass fraction to scavenging efficiency with an additional 'Crest' feature related to trapped purity functions (Sher, 1985), (Sher, 1990).

The later models used time step functions and are used for engine simulations. These models were compared with measurements obtained from motored engines calculations (Amsden, et al., 1992) and further validated against three dimensional models (Haworth, et al., 1993). The various models were later summarised and compared by (Merker & Gerstle, 1997).

Despite increasing sophistication these remined simplified scavenging models of the actual processes. The parameters involved in the various assumptions were empirical constants which were determined by fitting the predicted scavenge or charging efficiency to results obtained experimentally from test rigs or engines. Additionally, the geometry of engines is

three dimensional and predictions of flow are not accounted for in these methods which limits the predict accuracy without experimental data nor do the methods predict cyclic variations unless supplied with the parameters from previous cycles from the engine.

2.3.2. TESTING AND MEASUREMENT

Various practical testing methods were developed to determine scavenging flow characteristics and measure the efficiency of the process. Early aeronautical applications for two-stroke cycle type engines resulted in considerable experimentation of transfer passageway shapes. These tests used interchangeable porting to maximise the flow of fresh charge and the effectiveness of the transfer period multiple port arrangements (Rogowski & Bouchard, 1938), (Foster, et al., 1949). Other testing methods have been developed from which the resulting flows have been tested using a variety of test arrangements and instrumentation.

Blair classified these testing methods into a) those based on firing engines and b) those based on test rig models (Sweeney, et al., 1985).

A row or 'comb' of pitot tubes suspended in the cylinder of a motored engine was used by Jante, to obtain three dimensional in-cylinder flow distributions (Jante, 1968). This method enabled practical performance potential comparisons between different good' and 'bad' transfer port arrangements. The most sensitive performance indicator was noted to be the mean flow velocity and the second being the shape and asymmetry of the flow velocity map (Sanborn, et al., 1980). The accuracy of this method was affected by the necessary removal of the cylinder head and blockage caused by the row of pitot tubes.

The availability of 3D printed models later enabled practical testing of accurate physical representations of actual engine parts. Such models were used in conjunction with a single anemometric (pitot) probe which was moved in three dimensional patterns by a computer controlled mechanism (Kinoshita & Motoyama, 1999). This arrangement retained the cylinder head which enabled the full loop pattern to be developed in the cylinder and hence overcoming the limitations of Jante's method. The researchers considered that extensive previous work had not clearly confirmed the relationships and that transfer port design and considered development of transfer ports was based on experience. This was confirmed during later conversations between the author and J. Theil (Theil, 2014). Eleven transfer port shape variable were flow tested. The flow results were compared and correlated with actual engine tests, from which a numerical comparison method was developed. This work

showed the transfer port shape factors which are most influential on engine power output are a) The tangential inclination angles. b) The inner duct radius of the main transfer port.

A different type of practical test used two fluids of different densities, to simulate burned gases and fresh charge. These fluids were displaced by an apparatus with flow transferred within actual engine components of transparent cylinders. The different fluids used by various researchers included Water and Water with dye, Sodium Hyroxide Solution and Water, Cyclohexane and Tetrachloroethylene, Zinc Chloride Solution and Water, Sugar Solution and Water, Kerosene and Water and De-Ionised water and Water which proved to be a very practical combination (Sanborn & Roeder, 1985). A single-cycle pumping system using air and Carbon Dioxide was used by (Sweeney, et al., 1985) to evaluate and compare the scavenging performance of six different scavenging port arrangements. This was reported to produce accurate and consistent results. A different liquid system was later developed to provide a method to enable visual assessment of transfer port flows and resulting in-cylinder separation of fresh and burned charges (Stueck, et al., 2003). Cudina also used a transparent model and various liquids to duplicate the operating conditions and geometry of the scavenging system (Cudina, 2004). from which an equation and was developed to calculate of the efficiency of scavenging processes.

The unsteady, turbulent flows in the transfer ports was noted to be significantly affected by the stirring motion of the crankshaft, in the crankcase, at the entry end of the transfer ports (Rosskamp, et al., 2001).

SCAVENGING MEASUREMENTS IN FIRING ENGINES

Blair's second classification of scavenging testing has been investigated using both motored and fired engines. Noting that scavenging efficiency can be assessed based only on the power produced by the engine whereby, higher power output indicates greater efficiency (Tobis, et al., 1994). Four general methods have been used to measure the scavenging performance of two-stroke cycle engines. These are a) In-cylinder pressure/temperature measurement b) Tracer gas techniques. c) Skip-firing techniques d) Gas sampling techniques using a valve in the cylinder head.

The scavenging performance of a firing two-stroke type engine was measured at engine speeds up to 8000 rpm using pressure and temperature gathered close to exhaust port closing (Hashimoto, et al., 1982). Additionally, the Air/Fuel ratio was measured in the exhaust system. This work showed a very close relationship between BMEP and charging efficiency. The arrangement used a fine wire thermocouple to measure gas temperature

which would not be viable in a normal operating engine. Unfortunately, a more robust thermocouple would not react quickly enough to provide valid measurements. The researchers stated their intention to progress with an optical temperature measurement system. However, such a system would be unrealistic and impractical to add into a normally operating engine.

A number of researchers have used metered quantities of various tracer gases introduced into the inlet and then analysed the exhaust gases to measure scavenging efficiency and provides a measure of short-circuiting. This method has limitations due to gas toxicity and their effect on the stoichiometric chemistry during combustion. The chosen tracer material should be consumed completely by combustion and not react in the exhaust passage. The gases used by different researchers have included, Oxygen for gasoline engines and *n*-Butane for diesel engines were used by (Huber, 1971) who also noted the gas be extracted from a location where it has not yet undergone a chemical change. Monomethyl amine was used by (Scheitzer, et al., 1942) and (Isigami, et al., 1963). Carbon Monoxide was used by others (Bazika & Rodig, 1963), (Wallace & Cave, 1971). However, none of these gases were perfect due to toxicity and interference with combustion chemistry especially in low load / partial combustion conditions.

The oxygen content in the exhaust gas of a two-stroke cycle engine was measured by (Hamamoto, 1971) to calculate scavenging. This technique requires all the oxygen to be consumed by combustion and hence is limited to Air/Fuel ratios of stoichiometric ratio or richer. These researchers also used a high speed electromechanical sampling valve which was opened for selected cycles which were preceded by previous cycles in which peak pressures had been recorded. This work observed calculated values of these gases were within approximate agreement with measured values but the values fluctuated severely in comparison with a four-stroke cycle type. It was noted that trapping efficiency can be determined from measurement of O_2, CO_2, CO or HC. However, evidence was presented from which was concluded that the concentration of O_2 in-cylinder or exhaust gases O_2 varies with the rate of misfiring and with the engine stroke volume.

Sample valves have been used by a number of researchers to extract gases from the cylinder of a two-stroke cycle engine to determined scavenging efficiency. This type of arrangement is simplified relative to a four-stroke cycle engine due to the absence of inlet and exhaust poppet valves. A large mechanically driven poppet valve was used to obtain single samples from each eleventh cycle at engine speeds up to 8000 rpm from four different cylinder by (Blair & Ashe, 1976). These experiments were conducted before high speed

electromechanical valves or modern fast accurate emissions equipment was available. An electromagnetically operated poppet valve in the cylinder head was used to enable large volume samples (from short duration opening periods) by (Asanuma & Yanagihara, 1962). These comprehensive experiments demonstrated that scavenging efficiency correlates well with engine torque characteristics.

In-cylinder sampling via a fast-acting electromechanical valve was used to determine the scavenging efficiency of a firing two-stoke cycle engine using gas composition measurements (Tobis, et al., 1994). This work stated that scavenging efficiency (SE) can be related to gas composition measurement by:

$$SE = \frac{[CO_2]_b - [CO_2]_u}{[CO_2]_b - [CO_2]_{air}} \quad \text{(Eq. 2-5)}$$

Where: Subscripts b, u and air refer to burned, unburned and ambient respectively.

The work also showed that calculated scavenging efficiency matched measured values over a wide range of Air/Fuel ratios between 800 – 3000 rpm using the flowing relationship:

$$SE = \frac{1 - exp\left(-A(R\Lambda)^B\right)}{1 - g(\phi)\, exp(-A(R\Lambda)^B)} \quad \text{(Eq. 2-6)}$$

Where: A and B are model constants, R is a reference mass ratio, Λ is delivery ratio, ϕ is the equivalence ratio and g is a function which could relate to temperature if measured exhaust gas temperature was available.

The mass of fresh charge trapped in the cylinder after exhaust port closure was investigated using a skip firing technique to determine the scavenging characteristics of a two-stroke cycle type engine (Ku & Trimble, 1956). Which work noted in conclusion, that, "It is interesting to note that the mass fraction in the cylinder was, within experimental accuracy, a function of scavenging ratio only, regardless of individual values of engine speed, inlet pressure, or exhaust pressure (within the range of variables investigated)". Ku and Trimble's research used a testing system incorporating a scavenging pump to supply fresh charge to the cylinder measured by orifice plates. The experimental arrangement was similar to that previously developed (Taylor & Rogowski, 1956), in which the researchers proposed to rationalise the mass of fresh charge supplied by the scavenging pump per unit time using the term 'scavenging ratio' R_s which was defined as:

$$R_s = \frac{M_g}{\rho_s V_d N} \quad \text{(Eq. 2-7)}$$

Where: M_g = mass of fresh charge supplied by the scavenging pump per unit time.

Noting: This value could be assumed to be the mass of charge at BDC (+/- 5 Degrees) measured by the SBDV system.

ρ_s = density of fresh charge retained in the engine cylinder after exhaust port closure, per unit of time (this term was used as exhaust pressure rather than inlet pressure have greatest influence on the density of the gas in the cylinder at the time of exhaust port closure).

Noting: This value could be assumed to be the mass of the charge measured by the SBDV system from EPC to EPC +10 Degrees.

V_d = displacement volume (this term was used to define the mean effective pressure)

N = engine speed, revolutions per unit time.

The mass of fresh charge retained in the cylinder after exhaust port closure, per unit time (M_r) to the volume at the point of exhaust port closure

$$M_r = \epsilon \rho_x V_x N \quad \text{(Eq. 2-8)}$$

Where: ϵ = mass fraction of fresh charge in the cylinder after port closure.

ρ_x = average density of the cylinder contents at the instant of port closure

V_x = cylinder volume at the instant of port closure

Then where:

ρ_s = density of fresh charge computed on the basis of inlet temperature and exhaust pressure

V_d = cylinder displacement volume

Scavenging efficiency was then expressed as:

$$SE = \epsilon\left({}^{\rho_x}/_{\rho_s}\right)\left({}^{V_x}/_{V_d}\right) \quad \text{(Eq. 2-9)}$$

Ku and Trimble noted the ratio ${}^{\rho_x}/_{\rho_s}$ represents and provides a measure of the influence of heat transfer between the fresh charge and engine internals, flow resistance through the

engine (including the exhaust system) and the dynamics of flow in the scavenging system. They proposed the following relationship:

$$\rho_x/\rho_s = (\rho_x/\rho_i)(\rho_i/\rho_s) = (\rho_x/\rho_i)(p_i/p_e) \quad \text{(Eq. 2-10)}$$

Where:

ρ_i = density of fresh charge at inlet temperature and inlet pressure

p_i = inlet pressure (absolute)

p_e = exhaust pressure (absolute)

$$SE = \epsilon(\rho_x/\rho_i)(p_i/p_e)\left(V_x/V_d\right) \quad \text{(Eq. 2-11)}$$

An electromagnetically controlled poppet valve was used to sample over 30% of the trapped charge at speeds up to 3000 rpm by (Foudray & Ghandhi, 2003). This work developed a physical model which characterised the scavenging performance of a directly injected engine based solely on the measured trapped gas composition. This approach avoided the need to measure the and compare the gas composition of the post-combustion trapped charge. The measured scavenging efficiency agreed well with the non-isothermal two-zone, perfect mixing limit and showed for the engine tested, scavenging efficiency decreases with increasing Air/Fuel ratio and was nearly independent of engine speed. The work modelled the trapped mass as:

$$m_{tr} = \frac{\rho_{res} V_{epc}}{1 - SE(1-\tilde{\rho})} \quad \text{(Eq. 2-12)}$$

Taking: $$\tilde{\rho} = \rho_{res}/\rho_{del}$$

Where: ρ_{res} is the density of the residual burned gas, ρ_{del} is the density of the fresh charge delivered, V_{epc} is the cylinder volume at EPC, $\tilde{\rho}$ is the density ratio.

The solution determined a scavenging efficiency using the concentration of one gas constituent. Equations were developed to describe the dilution process, the change of in-cylinder concentration due to combustion and provided an estimate of the trapped mass. The advantage of the method was that samples of burned gas were not required. However, as the non-isothermal model requires knowledge of the density ratio '*a priori'* the universal perfect displacement or perfect mixing limit could not be defined.

Measurements showed the actual scavenging performance characteristics to lay between perfect displacement and perfect mixing curves but closer to perfect mixing as indicated in Figure F2-4 (Tobis, et al., 1994).

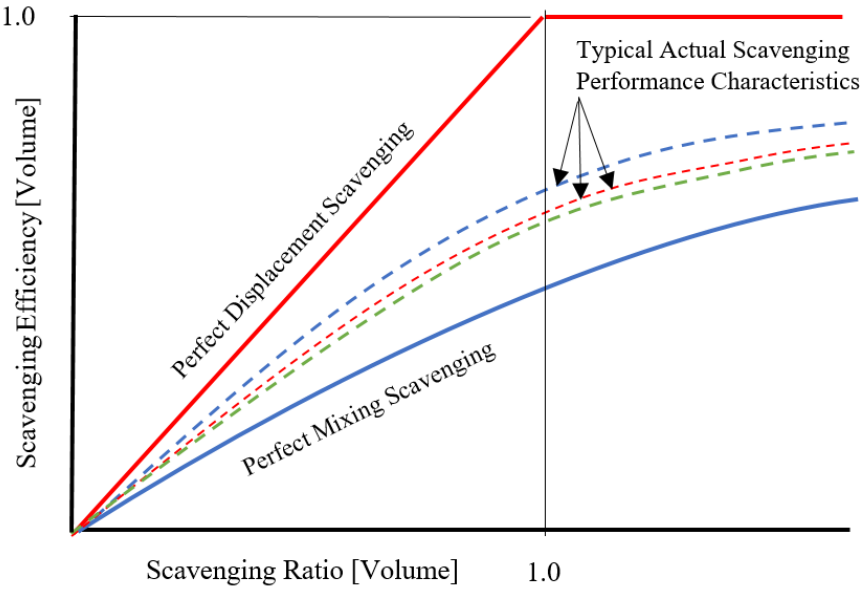

Figure F2-4: Comparison of Hopkinson Perfect Scavenging Models and Actual results

2.4 THE TRAPPING PROCESS

The scavenging period is completed when the transfer ports are closed by the ascending piston. However, although the flow of fresh charge through the transfer ports is prevented the gases in the cylinder continue to change as the exhaust port remains open for approximately thirty degrees more crankshaft movement. The period between the closure of the transfer ports and the closure of the exhaust port is perhaps the most complex period of gas flow and gas exchange until the trapping process is completed.

As the piston ascends in the cylinder from BDC the flow of charge through the transfer ports continues until there is insufficient differential pressure to cause the flow of charge into the cylinder. The pressure in the cylinder is significantly affected by the timing of the returning exhaust pressure wave.

An early exhaust pressure wave return raises the pressure in the cylinder and reduces (or stops), the mass flow rate through the transfer ports. Whereby, insufficiently strong extraction of gases into the exhaust system prevents the removal of burned gases from the cylinder. This reduces the homogeneity of the incoming fresh charge which causes increased gas mixing and reduces the scavenging of residual burned gases out of the

cylinder. Such residual hot burned gases then occupy volume which should have been replaced with fresh charge entering from the transfer ports.

Conversely, a late arrival of the return exhaust wave increases the scavenging flows to the extent fresh charge enters the exhaust port to be lost to atmosphere. This effect is worsened by designs of port flow areas which maximise mass flow rate which widens the transfer ports and results in minimal distances between the transfer and exhaust ports. During the scavenging period, the pressure changes in the cylinder continue to be primarily influenced by the exhaust system. Strong extraction effects generated in the exhaust system, coupled with weakening transfer streams causes loss of fresh charge from the transfer ports closest to the exhaust ports directly into the exhaust system to be lost directly to atmosphere without taking any part in combustion (Nuti & Martorano, 1985). This behaviour is termed 'short circuiting'. Notably, in engines where the fuel is added by carburetion, or by indirect fuel injection before the fresh air mass enters the cylinder the shorted circuiting includes unburned hydrocarbons. The optimum solution requires the exhaust system to provide a low pressure at the cylinder wall to assist a strong flow of fresh charge into the engine to enable excellent scavenging of residual exhaust gases out of the cylinder. High performance levels are then assisted by the deliberate over-scavenging of fresh charge into the first part of the exhaust port. The cooling provided by the surrounding walls of the exhaust port in this section should be maximised. The exhaust system should then be constructed to produce a positive pulse of pressure. This pressure pulse should occur after the transfer ports have been closed to avoid back-flow and trapped charge loss. Conceptually, the returning high pressure exhaust pulse should then push back the over-scavenged fresh charge which was held in the section of exhaust port close to the cylinder. This high-pressure pulse should continue until the exhaust port is closed by the top edge of the ascending piston. The resulting effect being to charge the cylinder with a greater mass of fresh charge than would be contained in its swept volume at atmospheric pressure. As the dimensions of the exhaust system are fixed these pressure wave dynamics cannot be achieved across the entire engine operating range. Additionally, these dynamic effects are not constant and vary with pressure wave overlapping, juxtaposition and super-positioning effects. Further, the regular and optimal timing of the pressure pulses, cannot be maintained in synchronisation with rapidly the changing engine speeds and or load requirements in which such engines are expected to operate. However, the speed range over which a close compromise can be achieved is broadened by progressive delaying of the onset of combustion. This is enabled using a characteristically retarding ignition timing curve.

The present work is not concerned directly with the optimisation of the exhaust pressure pulse or the design of the exhaust system to achieve this which is explained in detail in many related studies including those by (Cartwright, 1994), (Blair, 1996) and (Winterbourne & Pearson, 1999).

Various mechanical methods have been proposed or introduced to minimise losses of fresh charge including short circuiting losses. Hill proposed an additional transfer port passageway to obtain a stratified charge (Hill & Blair, 1983). A different method was presented which separated the mixtures generated by a carburettor into lean and rich zones which were diverted by finely controlled scavenging flows (Onishi, et al., 1984).

A different arrangement involving a two-section exhaust port was presented which enabled exhaust gas from the lower section of the exhaust port to be diverted back via a one-way valve to the engine inlet. The horizontal split which divides the exhaust port was positioned level with the transfer ports. It was proposed gas flowing in this lower exhaust port duct contains large proportions of short-circuited or over-scavenged fresh charge (Saxena, et al., 1989).

A further different approach used a Helmholz resonator which was positioned in the front section the exhaust pipe. This device showed selective sizing of the chamber could reduce the magnitude of returning pressure waves in the exhaust system. The frequency of the device can be matched to those which occurred at inconvenient frequencies/engine speeds (Bella & Chiatti, 1989) to reduce the pressure of the returning wave which is detrimental to engine performance.

Various exhaust flow throttling devices have been developed which minimise short-circuiting and improve engine performance. Systems which use a valve close to the exhaust port wall where reported by (Hata & Lio, 1981), (Nomura, et al., 1983), (Shimizu, 1991), (Fujikawa & Ohtsu, 1991). An alternative exhaust valve arrangement was presented which is operated by pressure in the exhaust port (Bendix, 1993). A butterfly valve located in the exhaust port away from the cylinder wall recognised that the construction of the two-stroke cycle engine could not prevent short-circuiting (Tsuchiya, et al., 1980). This work showed significant reductions in cyclic combustion variations at low throttle openings and engine speeds which could be achieved by throttling the exhaust port area.

2.4.1. CALCULATION OF TRAPPING EFFICIENCY

The preceding section is intended to convey the fact that the effects of the exhaust system which is an essential contributor to the characteristic high performance of the two-stroke

cycle type engine is the primary cause of significant cyclic variations of in-cylinder conditions and gas contents. Hence, the relative proportions of burned to fresh trapped charge at the point of exhaust port closure represent the charge purity available for subsequent combustion. The following definitions were provided by (Blair, 1996).

The purity of the entire trapped charge, $\prod$, is defined as the ratio of air trapped in the cylinder before combustion, m_{ta} to the total mass of cylinder charge, where:

$$m_{ta} = m_{tas} + m_{tr}$$

$$\Pi = \frac{m_{ta}}{m_{tr}} \qquad \text{(Eq. 2-13)}$$

Trapping efficiency, TE is defined as the capture ratio of the mass of delivered air that has been trapped, m_{tas} to that supplied, m_{as}

where: $$TE = \frac{m_{tas}}{m_{as}} \qquad \text{(Eq. 2-14)}$$

$$TE = \frac{m_{tr}\, SE}{m_{sref} SR}$$

The charging efficiency CE expresses the ratio of the cylinder filling with air compared to the 100% filling with air at the start of compression. The overall design objective is to fill the cylinder with the maximum amount of air in order to burn a maximum amount of fuel with that air. Hence charging efficiency CE is:

$$CE = \frac{m_{tas}}{m_{sref}} \qquad \text{(Eq.2-15)}$$

Therefore: $$CE = TE\ x\ SR = \frac{m_{tas}}{m_{as}}\ x\ \frac{m_{as}}{m_{sref}}$$

The scavenging process fills the cylinder with a mass of air, $m_{ta,}$ with a total trapped charge mass, m_{tr} . Where for a given engine the trapping volume, V_{tr} is constant.

$$V_{tr} = V_{ts} + V_{cv}$$

In a two-stroke cycle type engine, at the point of exhaust port closure the gases in the cylinder are trapped the total mass is very dependent on the trapping pressure as shown by the equation of state:

$$m_{tr} = \frac{P_{tr} V_{tr}}{R_{tr} T_{tr}} \qquad \text{(Eq. 2-16)}$$

A simulated calculation of trapping efficiency to within 11% with reduced computational effort has been shown possible (Carlucci, et al., 2015). This calculation was made using measurements of the molar concentrations of CO_2 and O_2 at the inlet and exhaust tailpipe. These are compared to an 'Oswald Diagram' for the fuel used. The method requires two gas sensors and the Carlucci stated "the method provides a quick average not cycle by cycle trapping efficiency".

2.4.2. TESTING AND MEASUREMENT

The trapping efficiency depends heavily on the amount of air which is lost out of the cylinder by short circuiting which are not included in samples of in-cylinder gases. Therefore, calculation of trapping efficiency requires to know the total exhaust gas composition which consists of the gases exhausted as a result of combustion plus the short-circuited air. The molar fraction of short circuited fresh air (Y_{short}) in the exhaust gases measured in the tailpipe (tp), can be obtained by a modified version of equation (Eq. 2-17) for scavenging efficiency (Tobis, et al., 1994):

$$Y_{short} = \frac{[CO_2]_b - [CO_2]_{tp}}{[CO_2]_b - [CO_2]_{air}} \quad \text{(Eq.2-17)}$$

And trapping efficiency can be determined from:

$$TE = \frac{(\dot{m}_{del} + \dot{m}_{fuel}) * Y_{short} * M_{air}}{\dot{m}_{del}[Y_{short} * M_{air} + (1 - Y_{short}) M_b]} \quad \text{(Eq. 2-18)}$$

Where: $\dot{m}_{del}$ is mass flow rate of delivered air, $\dot{m}_{fuel}$ is mass flow rate of delivered fuel and M_{air} is the Molecular weight of air.

The estimation of trapped air mass has been the subject of considerable research effort. Most practical solutions have used pressure sensors to achieve this (Hart, et al., 1998), (Sellnau, et al., 2000).

Mathematical estimation method to determine the enclosed mass was presented by (Caicedo, et al., 2012). This method uses a 'High gain strategy to allow the design of an observer that handles the uncertain part of the estimation of enclosed mass. The focus of this work being highly variable VVT four stroke cycle type engines. In these the estimation of enclosed mass is complicated by amounts of burned exhaust gases and unsteady flow through valves which do not close at the same point every cycle. This method uses a virtual engine, measurements of in-cylinder pressure and observed temperature during the early compression stroke. In this regard, the method is similar in difficulty and intent to the two-

stroke cycle type engine and approach proposed in this work. The model was later improved (Caicedo, et al., 2012), which used a physical model instead of a virtual model. The work concluded that the method of enclosed mass estimation can be achieved in 0.1ms with a simulation time step of 50 μs and before ignition timing point for most engines up to 4500 rpm. Further combustion modelling would not be necessary. These results showed very close correlation with measured values.

Measurements of bi-directional exhaust gas flows were obtained using a spark plug modified to contain four electrodes made from 0.5mm diameter platinum wire (Ohigashi, et al., 1969). The gas velocities were noted to be proportional to the time taken for a spark to pass between two electrodes in an ionized region and variations in the 'ion-drift' duration.

Similar work using a similar butterfly valve arrangement (although not shown in detail) reported a HC emission reduction of 28% could be achieved over a wide range of engine speeds together with a bsfc reduction of 15% while engine power, especially at low speeds could be increased by about 20% (Sher et al, 1990). Further, it was noted the optimum port area reduction is closely related to hydrocarbon emissions across the entire range of engine operating conditions dependent on engine speed by mainly on engine load.

2.5 RESIDUAL TRAPPED EXHAUST GAS

Previously, the mechanisms which cause burned gases to be un-scavenged and trapped, in cyclically varying quantities within the cylinder of a two-stroke cycle engine was described. This behaviour has been improved by the study of port and in-cylinder gas flows and exchange processes working together with the various mechanical devices developed as described. However, the retention of burned gases in cyclically varying quantities remains a fundamental aspect of the loop-scavenged two-stroke type engine design.

Exhaust gases created during combustion may be present in subsequent trapped charges (Blair, 1996). The proportion of exhaust gases and fresh charge trapped in the cylinder varies cyclically either due to not being evacuated from the cylinder or returned back from the exhaust system as previously described. Trapped gases can be assumed to consist of two major components, namely air and burned exhaust gases (Mendra, 2004). This is significant for combustion as the oxygen present in exhaust gases can be considered negligible in comparison to that present in the fresh air charge, (Heywood, 1988), (Sher, 1986). The proportion of the trapped charge occupied by exhaust gas has a major influence on combustion flame speed and reduces the amount of oxygen available for the subsequent

combustion event (Bizard & Keck, 1974). As such it is important to know the composition of the trapped gases available for combustion (Ohigashi & Hamamoto, 1971).

Research to determine or estimate the relative amounts of fresh charge to residual burned gases which ratio is termed 'residual gas fraction' (RGF) has been carried out for two-stroke cycles engines to investigate its effect on combustion. Similar work has also been carried out for Homogeneous Charge Compression Ignition (HCCI) and four stroke cycle engines. In these engine types, high peak combustion temperatures cause high levels of NOx emissions. The peak combustion temperature and resulting NO_X emissions are reduced by increasing the RGF by recirculation or by deliberate trapping using variable geometry inlet and exhaust valve timing. Control systems for these require accurately determined RGF values.

In-cylinder gas sampling during compression requires fast emission measurement systems which have superseded slower in-cylinder emissions analysers and mechanical sample valves to extract gas samples.

Residual Gas Fraction can be estimated using in-cylinder pressure and the associated thermodynamic relationships of gas exchange (Miadek & Onder, 2000). Continuous, direct RGF measurements can be obtained from the comparison of HC or CO_2 levels contained in the exhaust gases with those in the fresh charge. However, to obtain reasonably accurate estimates very detailed analysis is required which should include consideration of specific heat capacities of gas fraction and temperature (Galindo, et al., 2010).

2.6 THE COMPRESSION PROCESS

The trapping process is completed when the exhaust port is closed by the ascending piston and the compression process starts when gas is prevented from entering or leaving the cylinder by exhaust port closure. If relatively minor amounts of gas which can leak past the piston ring(s) are ignored, the gases trapped in the cylinder are contained in a 'closed' thermodynamic system.

During closed cycle compression, the change of in-cylinder gas pressure due to piston movement is considered a 'Polytropic' process whereby the relationship between pressure and volume remain constant.

Additionally, as the compression event occurs very quickly it is considered that no heat flows into the gas from the cylinder walls, piston or cylinder head which classifies the compression phase as an adiabatic process.

Hence the behaviour of the trapped gases during the compression phase is represented by:

$$\mathrm{PV}^{\gamma} = \mathrm{CONSTANT}$$

This equation allows the cylinder pressure to be calculated at any crankshaft angle during compression based on the value of the pressure, P_0 and the volume V_0 at EPC.

The volume of the cylinder is a function of crankshaft angle, and crank train geometries. The factor γ represents the ratio of specific heat of the trapped gases at constant pressure to constant volume and is generally taken to equal 1.3 during compression (Heywood & Sher, 1999).

Hence: $$\mathrm{P_1V_1} = \mathrm{P_2V_2} = \mathrm{CONSTANT}$$

The instantaneous combustion volume is the sum of the combustion chamber volume and the volume displaced by the piston which is dependent on crankshaft angle calculated by:

$$V_{sv} = V_{cc} + \frac{\pi {d_c}^2 S}{8} * \left[\sqrt{\left(1 + \frac{1}{\lambda}\right)^2 - e^2 - \cos(\alpha) - \sqrt{\frac{1}{\lambda^2}}} - (\sin(\alpha) - e)^2 \right] \quad \text{(Eq. 2-19)}$$

and: $V_{cc} = \frac{V_d}{CR-1}$

Where:

CR is the geometric compression ratio. λ is the crank and connecting rod ratio. S is the stroke and α is the crankshaft angle (Degrees)

The gases in the cylinder of an engine combustion before combustion starts and significant reactions occur, can be regarded as an ideal gas (Heywood & Sher, 1999). This is not completely true as some chemical reactions have been noted to occur during scavenging (Hamamoto, 1971). However, this is a reasonable assumption which simplifies the assumptions and calculations of the behaviour during compression before combustion is initiated. therefore. Considering the ideal gas equation:

$$m = \frac{PV}{RT} \quad \text{(Eq. 2-20)}$$

Hence: $$PV = nRT \; and \; N = {}^{m}/_{MW} \quad \text{(Eq. 2-20)}$$

Where: P = Pressure, V = Volume, n = Number of moles, T = temperature, m = mass, MW=Molecular Weight and R is the Ideal Gas Constant.

An estimation of air mass contained in the compression stroke of a four-stroke cycle engine was proposed by (Hart, et al., 1998) which consisted of three parts. Proportional pressure, the influence of residual gas m_{RG} and the influence of vaporised fuel . m_{fuel}:

$$m_{air} = \frac{p_2 * V_2}{R * T_{AF}} * \left[\frac{V_2}{V_2}\right]^{n-1} - \frac{T_{RG}}{T_{AF}} * m_{RG} - . m_{fuel} \qquad \text{(Eq. 2-21)}$$

The temperature of fresh charge increases due to differing amounts of residual burned gas can be assumed to be consistently close to the engine coolant temperature rather than the intake manifold temperature commonly used by other researchers (Lancaster, 1976). A calculation for the temperature rise during compression was presented by (Abraham & Prakash, 1992) which uses mass and energy conservation equations:

$$\frac{dT}{dt} = -T * \left[\frac{\gamma - 1}{V} * \frac{dT}{dt} * \frac{q'' * A_w * (\gamma - 1)}{P * V}\right] \qquad \text{(Eq. 2-21)}$$

Where: V is the instantaneous cylinder volume, q'' is the heat flux, A_w is the area for heat transfer, γ is the Air/Fuel mixture and P is the instantaneous pressure.

The pressure changes during closed cycle compression vary for every cycle although such variations are not significant in comparison to the in-cylinder pressures achieved due to combustion. These variations, shown diagrammatically in Figure F2-2, reflect the relative contents, pressure, temperature and compressibility of the trapped gases and the influence of the gas exchange process of the engine and the heat of the surroundings.

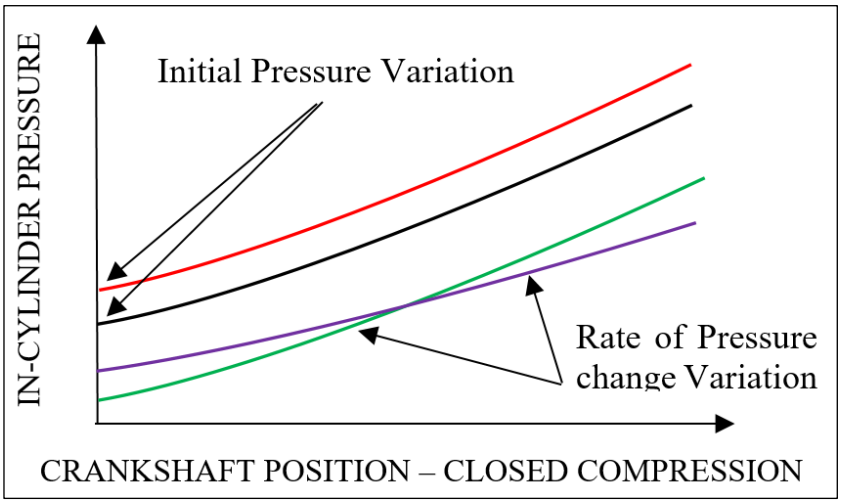

Figure F2-5: In-Cylinder Pressure Variations following Cylinder closure

2.7 ENGINE CONTROL METHODS

The gas flow processes into, through and out of an engine all occur in an unsteady manner. The definition of unsteady flow is where the pressure, temperature and gas particle velocity in a duct vary with respect to time (Blair, 1996).

Intensive research has sought to improve combustion efficiency to reduce fuel consumption and reduce polluting exhaust emissions. Combustion control systems are primarily concerned with the determination of the amount of fuel to be injected and the timing of ignition initiation. Improving the accuracy of these factors requires increased accuracy of the mass of charge available for combustion and the amount of fuel required to be added. The actual Air/Fuel ratio burned significantly affects the speed of combustion. The speed of combustion represents the time the flame takes to oxidise and is dominated by the turbulence in the engine. To extract maximum benefit from the fuel burned it is common for combustion control systems to seek to burn approximately 50% of the fuel at a crankshaft angle of approximately 15 Degrees ATDC (Heywood, 1988), (Sellnau, et al., 2000). This also aligns the point of maximum flame acceleration with TDC. Determining the turbulence characteristics resulting from a given engine design have been the focus of considerable research. However, this influence is largely fixed for a given engine design and it has therefore been the accuracy of the Air/Fuel ratio which concerns combustion control strategies. These factors and control settings thus have a sound basis from which they can be accurately determined. However, the factor which currently remains impossible to determine accurately with sufficient speed and accuracy to enable these values to be determined to vary cycle by cycle is the mass of trapped combustible charge.

The simplest automotive engine combustion control systems use two or three dimensional ‘maps’ representing interdependencies which are stored in the Electronic Control Unit (ECU) memory. These ‘maps’ are produced by series of long and expensive engine calibration tests. The ‘maps’ separately relate engine speed and throttle opening to fuel required and engine speed and throttle opening to ignition timing required. This is also the most reliable method as it uses the minimum of sensors. For this reason, the method is also used on complex systems as ‘get you home’ fall back if multiple sensor faults occur and for this duty is likely to remain so whatever control system improvements are introduced.

To improve the accuracy of fuel and ignition control, current combustion control systems incorporate sophisticated algorithms which consider the averaged results of around 100 combustion cycles to determine a fuel or ignition value change. Depending upon cost and complexity, current control systems use information gathered from various and alternative

sensors. Theses may include combinations of the following: a) Throttle position, b) Engine speed, c) Rate of change of engine speed, d) Manifold absolute pressure (depression), e) Cylinder pressure from intrusive or non-intrusive pressure, f) Ion sensing, g) Measured mass flow rate of fresh air through intake system, h) Oxygen (measured using UEGO sensor) in the exhaust system, i) Cooling water temperature and others.

Such control systems were developed primarily for four stroke engine applications. In these, the cycle by cycle variations of incoming charge and amount of residual charge are small. The only variation to trapped charge gases in these engines comes gases from previous cycles and, or the quantities of exhaust gases deliberately introduced into the cylinder to reduce the combustion temperature and reduce NO_X production. The amount of these gases values is known to the system which controls the amount introduced. Hence the control systems currently in use did not need to react to individual cyclic variations and development has been slow to react to this requirement. Clearly, if combustion control is based on monitored past results or data stored from testing the results can only, at best, predict the amount of fuel and ignition timing required for forthcoming events. As microprocessor speed increases, mathematical estimates of residual burnt and trapped masses are being developed for four-stroke and derivative engines (Leroy, et al., 2008), (Subramniam, et al., 2010), (Koehler & Bargende, 2004). Such estimates were previously only possible for simulation tools and development will no doubt continue. However, they will remain estimates and will require a range of sensors from which calculations will be based.

2.8 FUEL INJECTION

The combustion process in a two-stroke cycle engine in which fuel is supplied by direct injection, presents two primary challenges:

A) The extremely short, time duration available for combustion preparation.
B) How much fuel is required.

Irrespective of how injection is achieved, the cylinder filling and relative proportions of and distribution of fresh charge and residual burned gases are principle concerns (Mitianiec, 2003). The interaction between combustion and gas dynamics are likely to be determined by Computational Fluid Dynamic (CFD) pre-calculations to ensure satisfactory fuel spray and gas dynamics will occur for combustion to occur over the entire engine operational range (Schmidt, et al., 2004), (Arnone, et al., 2001). Simulations will consider and optimise the spray patterns and injection durations and flow rates (Pontoppidan, et al.,

2004), and the manner in which these interact with the cylinder and surroundings (Casarella, et al., 1997), (Han, et al., 1997). Such simulation effort will also be followed by extensive engine testing to determine arrangements for optimum acceleration and emission performance (Winkler, et al., 2008). Recommended practices have been created to allow common and regulated methods to determine gasoline fuel injector spray measurements and characterizations (Hung, et al., 2008).

In a direct injection engine where fuel is added following exhaust port closure, loss of fresh charge occurs due to short circuiting. In consequence of the loss of fresh air the Air/Fuel ratio during combustion cannot be determined by mass measurements of the fuel and air supplied to the engine or by overall exhaust gas analysis. Thus, the Air/Fuel ratio of the trapped charge and the fraction of residual burned gases should be determined (Tobis, et al., 1994).

The traditional issue for the two-stroke cycle type engine is that it is predominantly used for low cost, low-maintenance applications for which the carburettor was an ideal fuelling device. In an engine in which fuel is added by a carburation device or by indirect fuel injection, the fresh charge which enters the cylinder via the transfer ports will contain fuel (and oil). The disadvantage of this arrangement, as previously noted, is that any fresh charge lost directly into the exhaust system, and hence atmosphere contains unburned Hydrocarbons (HC). Carburettors use a variety of proportioning devices such as the shape of the air slide cut out, fixed fuel jets and needles to adjust the fuel in reaction to air pressure changes generated in a venture shaped working area. Although these systems were made increasing sophisticated they cannot sufficiently control the Air/Fuel ratio across the entire engine operating range and create rich and lean regions. In recognition for improvement, carburettors were developed by which the fuel delivery was controlled electronically not by Bernoulli's effect. A device which used an electronically controlled solenoid to adjust the air compensation system was presented by Osakabe. The opening of the solenoid was controlled in accordance with a throttle position sensor and a pre-programmed 3D map with settings suitable for steady state fuel requirements. Additional fuel for acceleration was controlled via a duty cycle correction (Osakabe, 1991). This work did not address one fundamental issue with carburettors used in two-stroke cycle engine applications. This results from using short inlet lengths for packaging and to harness the greatest pressure from the first or second harmonic wave, air entering the inlet system can shuttle backwards and forwards across the working section (Khou & Yang, 1984). Thus, even with accurate fuel control, a shuttle or flow oscillation event will induce three fuel additions to the same parcel of inlet air and result in a very rich mixture. A more sophisticated device was

reported later by which fuel adjustments were made in response to engine speed variations determined directly from the ignition pick-up, (Berlusconi & Colombo, 2001). This work recognised the significant cycle-by-cycle combustion variations which progressively increase either side of stoichiometric combustion and are manifested by torque oscillations and engine speed variations. This device was applied in research to a small four-stroke cycle type engine and successfully reduced the CO by 75% and HC emissions by 50%. However, NOx emissions rose by almost 300% which rendered the nett emission effect as negligible. No results were given for two-stroke cycle type engine testing which would have reduced NOx emissions due to the inherently lower combustion temperatures in comparison with four-stroke cycle type engines.

The application of a programmed-indirect fuel injection applied to 250cc twin cylinder and 500cc, four cylinder, two-stroke cycle type engine for motorcycle racing was presented by Honda Racing Corporation (HRC). The first application was to the 250cc engine (Kusano & Kurosaka, 1991). The fuel control system responded to throttle position, Manifold Absolute Pressure (MAP), water temperature and combustion pressure. Air demand up to around 50% throttle opening was noted to respond according to MAP but then diminished to levels at which differences were negligible and impractical to apply compensation. The combustion pressure was monitored to detect 'misfire' or detonation using an under-spark plug piezoelectric ring (Soda & Sato, 1999). Fuel was added in accordance with a pre-determined strategy to limit the number of detonation events. The density of the gases in the crankcase was adjusted based on water temperature and residence duration. Improved throttle response was reported together with a 120 g/kw-hr reduction in Brake Specific Fuel Consumption (bsfc) across the entire engine operating region. Air/Fuel ratio was shown to be held closely between 11.75 – 12.25:1 in steady state conditions and the significant variations measured using carburation were avoided. Average bsfc at full load was reduced by 5% and 20% at $1/8^{th}$ throttle opening. Overall fuel consumption under steady and actual circuit conditions was reduced by approximately 5 -10%. The system was modified for application to the 500cc engine (Honda Racing Corporation, 1993). The butterfly throttle valve was replaced by a slide valve, additionally, the MAP and combustion signals were modified to improve accuracy. Further improvements to Air/Fuel ratio control and fuel consumption were reported. Neither of these systems were applied to road vehicles presumably because they did not significantly effect HC emissions.

Direct fuel injection adds fuel into the trapped gases following the closure of the exhaust port or relatively late in the compression phase. The objective being to avoid the direct loss of unburned fuel which is manifested by HC emissions. The location and orientation of the

injector can be arranged to ensure the Air/Fuel ratio in the combustion chamber around the spark plug is optimised (Aas, 2010). Early systems were presented using high pressure fuel pressure. This work presented exhaust emission maps for HC, CO, between 1000 – 5000 rpm which compared carburation and direct injection showing low emission levels could be achieved. (Yamagishi, et al., 1972). Other high-pressure systems were presented by (Yui & Ohnishi, 1969), (Pichard, 1977). Low pressure fuel pressure systems were reported by (Jaulmes, 1977), (Vieilledent, 1978). Direct and indirect injection low pressure injection was investigated by (Gozy, 1974). Douglas and Blair used a fuel pressure of 280 kPa which delivered fuel into the cylinder at alternative locations during the transfer port opening period which concluded that "fuel injection can only be applied if power reductions are acceptable", (Douglas & Blair, 1982). Nuti proposed a direct injection system for two-stroke SI engines in road vehicle use (Nuti, 1986). A fuel pressure of 2 MPa was used by Sato and Nakayama in conjunction with an evaluation of three different injector locations. The work also reported optimum dynamic injection timing and time elapse from beginning and duration of injection in relationship to MBT ignition timing from 1000 to 5000 rpm. The work concluded MBT injection timing corresponds to the time required to vaporise the fuel in the cylinder. The work also showed exhaust HC concentration could match four-stroke engine values and that engine power could be doubled whilst improving fuel consumption by 30% (Sato & Nakayama, 1987). A hybrid direct injection system termed 'FAST' was presented which used a carburettor to pre-mix a rich mixture which was delivered into the cylinder head which had been scavenged and charged with only air (Nuti, et al., 1997). The dominant design philosophy being low cost and no electrical system dependence. The comparative exhaust emissions on EEC R47 Driving Cycle, presented in this work, for this system are shown in Table T2-1.

Table T2-1: Comparative Exhaust Emissions (Nuti, et al., 1997)

IMAGE REMOVED TO AVOID ANY POTENTIAL COPYRIGHT ISSUES

A direct fuel injection system for outboard motors using an injection pressure of 5MPa (700psi) was presented which used a belt driven fuel pump. Air -Fuel ratio control was achieved using an exhaust Lambda sensor (Sogawa & Kato, 2001). The life of such sensors is limited by lubricating oil especially those containing silicon. Such devices have been developed which have very fast reaction times especially if fitted close to the cylinder. Boat

engines have a very different speed/load requirement to engines for road use and this obviously allows their successful adaption in this application.

Low pressure direct injection systems have been developed to provide low emissions solutions for both two-stroke and four-stroke cycle type small vehicle engines (Archer & Bell, 2001). The choice of which type of engine used (two or four stroke cycle) depends upon a number of considerations for specialist vehicles (Anderson, et al., 2003) although package optimisation can achieve significant performance gains and emission reductions (Hull, et al., 2003), (Davenport, et al., 2003).

The research and development work reviewed above show that direct injection using both low and high-pressure fuel delivery systems can be successfully applied to two-stroke cycle type engines for a variety of different applications. The work has demonstrated significant emission reductions over those attributable to carburetted engines with which traditional emissions and fuel consumption values are associated. These systems have incorporated various methods to determine the amount of fuel required to achieve pre-defined Air/Fuel ratios.

2.9 COMBUSTION

The design of any engine must focus on the combustion process as this defines the performance, emissions and efficiency of the engine. The function of all other processes and mechanisms are to prepare the optimum conditions for combustion to occur. In an S.I. engine, the combustion process starts when a small but intense source of heat is added to initiate the oxidisation process whereby the potential thermal energy in the fuel is released.

Ignition is initiated at different crankshaft positions depending on engine speed and load and effects exhaust emissions and engine performance (Hallgren & Heywood, 2003) (Zareei & Kakaee, 2013). However, the timing of ignition initiation represents the time required to release the heat energy in the trapped combustible mixture so that the resulting gas pressure exerts maximum benefit to produce crankshaft torque (Quader, 1976). This position can to be determined using a predicted rate of burning and hence flame speed (Hires, et al., 1978). This requires a) knowledge of what factors influence the burn rate. b) at what crankshaft position the maximum pressure must occur.

When the initiating heat source is provided by an electrical spark there is a short-period of time taken for the energy in the electrical spark to form a kernel between the electrodes of the spark plug which has sufficient heat energy to be self-sustaining. Typically, the initial

self-sustaining flame kernel is approximately 1mm diameter (Halldin, 1992). The time taken for this to occur is generally taken to represent 3 to 5% of the total combustion period. The formation of this kernel is critical to the complete combustion process such that delays in formation progress through the entire process and are not recovered (Alger, et al., 2006). There are several influences on the mechanism involved (Herweg, et al., 1988), in this process including the spark energy provided (Silsbee & Randolp, 1925), (Sher, 1986), (Song, et al., 2000). Any delays in which, are carried through to affect the complete overall combustion (Stone, et al., 1996), (Mantel, 1992). Reliable kernel formation thus depends on favourable local conditions which are predominantly influenced by the following functions:

a) The Air/Fuel ratio around the spark plug which should be slightly richer than stoichiometric.
b) The amount of Residual burned gas present.
c) The temperature of the gases and surroundings.
d) The ignition energy, hence the heat input into the spark.
e) The gas flows over and around the flame kernel.
f) The Spark Plug Electrode design and Orientation

Increasing ignition energy has been noted to extend the Air/Fuel ratio limits (Rivin, et al., 1999) and commercial ignition systems seek to optimise calorimetric values in which the general trend is for the total energy delivered to the gas increases with glow duration and ignition probability increases with ignition energy (Franke & Reinmann, 2000), (Rohwein, 1997). Ignition systems are being continually updated principally to reduce costs (Ugale, 2014), or to extend ignitability limits in 'Lean' mixtures (Schemmann, 2003). Recent advances in ignition technology have reported using high frequency spark repetitions but have focused on the effects of improved ignition (Yamada, et al., 1999) (Tanoue, et al., 2010). Proprietary multi-spark ignition systems deliver sparks at 1ms intervals, or 10KHz (Zublin, 1997). Four-Stroke type engine using 'Coil On-Plug' (COP) 'Kettering' or inductive systems have tested using 14 and 34kHz variations of multi-sparking (Czekala, et al., 1998). Capacitor Discharge Ignition systems, conventionally used for Two-Stroke Cycle type engines have characteristically short spark durations of approximately 75μs while multi-spark CDI and transistorised systems have been tested which provide patterns of sparking rates between 1 and 40kHz (Grupp & Martin, 2002).

Silsbee provided a calculation for the heat energy per spark (Silsbee, 1920):

$$joules\ per\ spark = \frac{watts\ x\ 60}{sparks\ per\ rev.x\ r.p.m.} \quad \text{(Eq. 2-22)}$$

The spark plug electrode configuration, material and orientation also effect mixture ignitability and energy required (Arcoumanis & Bae, 1992), (Daniels & Scilzo, 1996).

The combustion process progresses into a phase which is dominated by gas turbulence (Lancaster, 1976), (Gorczakowski & Jarossinski, 2000), (Bjerkborn, 2011). At this point the flame kernel is growing and will not be extinguished by the surrounding conditions. The speed in which the flame spreads is influenced by the following:

A) The Air/Fuel ratio in the charge.
B) The amount of Residual Burned gas present.
C) The temperature of the gases and surroundings.
D) The large scale and small scale turbulence.
E) The in-cylinder pressure

As the flame spreads throughout the mixture in the cylinder, heat is released. The amount of heat released is proportional to the mass fraction of the fuel available. Faster flame speeds therefore correspond to a faster rise of cylinder pressure (Brunt & Emtage, 1998). The increase in cylinder pressure is proportional to the mass fraction of fuel burned (Rassweiler & Withrow, 1980 (originally published 1938)), (Gatowski, et al., 1984). The maximum pressure and the maximum rate of change of pressure occurs when 50% of the mass fraction of fuel is burned (Sellnau, et al., 2000). Pressure exerted onto the piston before TDC is negative work which is minimised if the start of combustion, and hence increase of cylinder pressure, can be delayed towards TDC. This effect is significant (Stone, 2012). Therefore, to optimise the flame speed and extract heat from combustion, engine designs, of all types, seek to maximise the turbulence of gases in the cylinder head (Mantel, 1992), (Herweg, et al., 1988), (Halldin, 1992). These turbulent flows promote turbulent combustion in which the flame speed is increased to reduce the time taken heat to be obtained from the combustible charge (Peters, 1997).

To exert the maximum average force on the crankshaft the maximum pressure and hence 50% of the mass fraction of fuel available should be burned at a crankshaft angle termed Maximum Brake Torque (MBT). This position is a function of the crankshaft geometry and is generally around 15 Degrees ATDC (Sher, 1986). The crankshaft angle at which maximum pressure is developed varies cyclically (Litak, et al., 2008). The gas turbulence assists the spread of the flame (Lancaster, et al., 1976), (Spicher & Backer, 1990) and is considered to increase in proportion to the engine speed (Heywood, 1988). Direct

measurements of the burning velocities in this phase have been made (Witze & Mendes-Lopez, 1986), (Russ, et al., 1997), (Witze, 1989).

The combustion flame moves forward in a thin spherical corridor, away from the source of ignition, consuming the oxygen in the gases at the advancing interface (Gillespie, et al., 2000) (De-Swart, et al., 2006). Keck noted that unless the equivalence ratio is very close to the ignition limit the fuel type and the residual burned gas fraction have a larger effect on the laminar burning speed than the equivalent ratio (Keck, 1982).The speed at which the flame progresses is dependent on the relative amount of fuel and oxygen at the interface and the length of the burning corridor (Knaus, et al., 1999) and rises with pressure (Spicher & Velji, 1984), (Litak, et al., 2008). The influence of the ratio of fuel and oxygen available is significant, showing a significant peak (Heywood & Sher, 1999) which can be seen in Figure F2-6. To predict the rate of burning the relative ratio of fuel to oxygen available must be known and burning time compensated. Additionally, increased gas velocity has been shown to require a fuel enrichment to achieve the rate of burning. This effect was found to be more pronounced in 'Lean' Air/Fuel ratios (Bolt, 1967) .

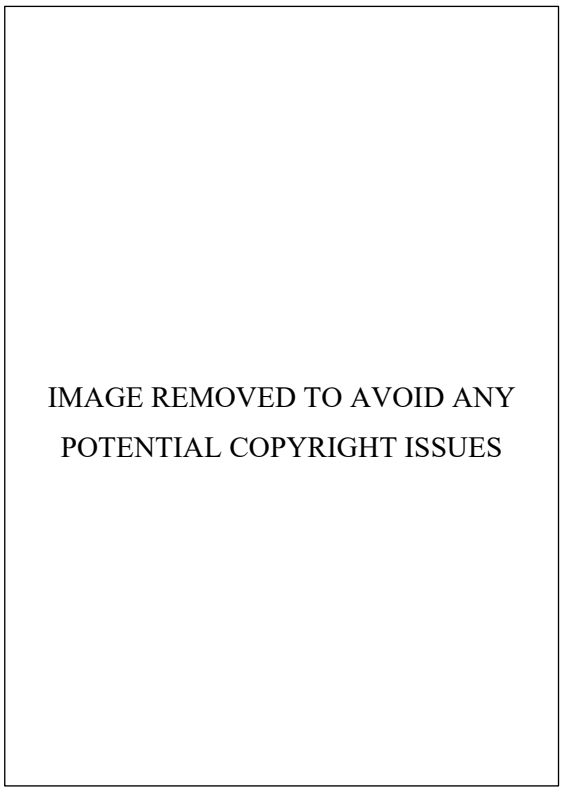

Figure F2-6: Laminar Burning Velocity of Gasoline as a function of Fuel/Air equivalence ratio at 1atm and 300 K (Heywood & Sher, 1999)

The homogeneous distribution with the cylinder to enable a predictable combustion progression is controlled by the distribution of fuel into the cylinder and characteristic of mixing (Shelkin, 1947), (Alger, et al., 2000) . These are in turn influenced by the fuel injector characteristics and the density and turbulence of the gas into which the fuel is dispersed (Ghandi, et al., 1994), (Ghandi & Bracco, 1995), (Wagner, et al., 1998), (Honda et al, 2004). The burn rate is generally considered to be proportional to the rate of gas turbulence which is in turn generally regarded to be proportional to engine speed (Heywood & Sher, 1999). The turbulent combustion process has been modelled using specific turbulence structures. The primary factors controlling these structures being, turbulence intensity, and integral length scale coherent with assumed isotropic relationships (Tabaczynski & Ferguson, 1977). Turbulence has the effect of lengthening the burning corridor which is bent and distorted in two planes by large and small gas flow vortexes (Hill & Kapil, 1989). However, the flame corridor length is also increased if the path of the flame is obliged to move around pockets of gas which resist flame migration. Residual burned gases in the combustible charge act as such barriers and force the advancing flame to move around them to proceed and spread. This action forms wrinkles, dendrites or fingers which considerably lengthen the flame corridor and increase the overall burning rate (Heywood, 1994), (Taylor, 1991), (Akkerman, 2007). However, such residual gases are largely inert compared to fresh charge. Therefore, there is an optimum amount of residual gas which will assist combustion before it becomes detrimental to the overall process. The residual gases cause a faster but cooler combustion. Notably, faster combustion is known to produce reduced levels of NOx which is also lessened by cooler combustion temperatures. In four-stroke cycle type engines, it is common to deliberately introduce burned exhaust gases into the combustible charge to achieve this effect. In two-stoke cycle type engines the residual burned exhaust gases are poorly scavenging due to the inherent design of the engine type, such these exist without deliberate intrusive introduction (Blair, 1996), (Heywood & Sher, 1999). However, cycle by cycle variations are known to increase with large proportions of residual exhaust gases present in the combustible charge especially in coincident ‘lean’ mixture conditions.

Overall, if the mass fraction of residual exhaust gases were known and the Air/Fuel ratio was controlled at pre-determined values the flame speed could be calculated with improved accuracy. Using that information, the appropriate ignition initiation timing lead could be determined which could be arranged to align maximum flame acceleration with TDC, (Prucka, 2008). This would enable a stable, defined target which aligns the maximum cylinder pressure at MBT timing and thus extracts the maximum torque on the crankshaft without variation. This could be validated without specialist test cell instrumentation using

non-intrusive Pressure sensors (Soda & Sato, 1999), (Sellnau, et al., 2000) or UEGO sensing of O_2 (Cowart, 2002).

COMBUSTION

In an SI engine, the effect of combustion starts after the initiation of ignition by electrical spark (Rassweiler & Withrow, 1980 (originally published 1938)). This behaviour forms the basis of combustion analysis by investigating cylinder pressure variations (Annand, 1985), (Annand, 1995), (Pinca-Bretotean & Stoica, 2012).

When a homogeneous gas mixture burns in a combustion chamber, the pressure and temperature of the gases rise as the flame propagates. Therefore, the temperature history of the unburned gases provides knowledge of burning velocities in various gas mixtures and the influence of ignition on the processes involved.

Various methods have been used to obtain temperature histories of unburned gases. The relationship between the velocity of sound in a gas and its proportionality with gas temperature and mixture composition was successfully applied to measure the end-gas temperature in an engine with a specially modified cylinder head over a short distance (Livengood, et al., 1958). The basic procedure for this method uses two transducers, placed a known distance apart, across a volume containing the gases of interest.

A sound signal is sent across the gas medium and the received signal is recorded to obtain the time of flight from which the average speed of sound 'c' is inferred (Eq. 2-23).

$$c = \sqrt{\gamma RT} \qquad \text{(Eq. 2-23)}$$

Dadd, measured gas temperatures, as a minimum, in the range of 300 K – 1000 K in a Stirling engine (Dadd, 1983). The method has also been used to measure the exhaust gas temperatures of a diesel engine over a complete engine cycle (Higashino, et al., 1966). In-cylinder and exhaust gas temperatures were obtained over a whole engine cycle, in a single cylinder Ricardo MKIII test engine running at 1000 rpm (Bauer, et al., 1997), over measurement distances of up to 100mm.

The temperature of the unburned mixture in the end gas region ahead of the flame in an engine operating between 600 - 1200 rpm heavily adapted to enable optical measurement using a fibre optical, laser interferometer system. This method recognises the change of gas density by changes to the optical path length of a test beam which corresponds to changes to the refractive index. Simultaneous pressure measurement and comparison with changes

of the interference signal enabled the temperature history of the unburned gas to be determined.

Knock, which was known to automotive engineers as early as 1882 (Clark, 1926), is characterised as a sudden, very violet completion of the burning in the engine cylinder after a part of the burning has taken place at a normal rate. This effect limits the rate of flame propagation and thermal efficiency which can be achieved. However, although often discussed as one, autoignition and knock are not the same. Photographs taken at rates between 2250-5000 frames/s (Withrow & Rassweiler, 1936), were considered to have recorded autoignition. However, 40,000 frames/s were required to capture images of knock, which takes place in an extremely short time of $5x10^{-4}$ sec or less (Miller, 1941).

Various theories were proposed and for the cause of this phenomena, the two most favoured (Downs & Wheeler, 1951), being: a) Knock is a detonation event caused by the development of shock waves developed during the propagation of the regular spark-ignited flame front and is initiated by a reaction of the end gas when travelling through the yet un-burned unburned end gas mixture. b) Knock is a homogeneous phenomenon, similar to the slow reaction found in cool flames when a section of the end gas homogenously reacts when influenced by high temperatures and pressures. Early investigations of ionization in the spark gap conclude that autoignition (termed 'pressure ignition' by the researcher) occurs in the end zone (Weinhart, 1939). The 'ringing frequencies' associated with Knock were found to differ in firing and motored engines which indicated high and low temperature knock could occur with different underlying processes. This was included as part of the theoretical and experimental investigations of the knocking process work to create a thermal combustion model (Maly & Ziegler, 1982), where (Eq. 2-24), the ratio between these frequencies is a function of relative gas densities and temperatures:

$$\frac{c_f}{c_1} = \frac{\left(\gamma_{f*p}/\rho_f\right)^{1/2}}{\left(\gamma_{i*p}/\rho_i\right)^{1/2}} = \left(\rho_i/\rho_f\right)^{1/2} = \left(T_f/T_i\right)^{1/2} \qquad \text{(Eq. 2-24)}$$

Where:

c_f = Velocity of Sound at T_f , c_1 = Velocity of Sound at T_i, T_f = Flame Temperature, T_i = Ignition Temperature, p = Cylinder Pressure, ρ_f = Mass density at T_f and ρ_i = Mass density at T_i.

Ohita, later considered there was no faultless fundamental explanation for engine knock (Ohita, 1989). He accepted that engine knock is due to a local rapid combustion caused by

autoignition ahead of the flame front. However, he believed this could not be explained over the range of engine conditions in which knock occurs by 'traditional' High and Low temperature approaches and sources other than autoignition due to turbulent flame acceleration (Maly & Ziegler, 1982). Studies showed that knocking at engine speeds above 3000 rpm could be explained by three mechanisms: a) Short Compression Duration which noted the duration taken to compress the mixture has a profound influence on the ignition delay even when the same temperature and pressure end conditions are established. b) Chemical Inhibitory Effect which postulated 'stressed' end-gas slowdown flame propagation. c) Shear-Layer Entrained Knocking where mixing cools the gases which process results in rapid high-temperature, aerodynamic flame and pressure vibrations.

Engines have been modified for testing with quartz windows to allow visualization of flame growth (Pischinger & Heywood, 1988). Flame development have also been obtained using combinations of Ion sensing, optical fibres, and accessible engines allowing high speed capture of flames using Schlieren Cinematography (Backer, 1990). Early flame development has also been measured unobtrusively using spark plugs modified to contain multiple optical fibres (Geiser, et al., 1998). Turbulent flame frequency has been correlated to heat release using wavelet analysis of LDV measurements (Soderbeg & Lindoff, 1998). End flame propagation before and during knocking has been investigated using high speed CCD cameras (Stiebels & Sakak, 1996), Laser Doppler Velocimetry and hot wire Anemometry have been used to measure internal engine flows (Witze, 1980), (Fansler & French, 1988). These systems have response times which are sufficiently fast to capture cycle by cycle events but have not or cannot (for practical reasons) been used in production applications. Additionally, research has focused on measuring the results or effects of combustion and it is common for combustion measurements to be represented, for combustion control purposes by an average of a minimum of 100 engine cycles.

Heat transfer to the walls of the combustion chamber is increased by engine knock. Above knock intensities above 0.2 MPa influence heat flux. Above 0.5 MPa, the peak heat flux can rise to 2.5 times that for a non-knocking cycle (Grandin & Denbratt, 2002). A study carried out in an L-shaped combustion chamber with temperature probes along the flame pathway found the heat transfer coefficient increased in both the near knock and outside knock regions for knock intensities above 0.6 MPa, (Harigaya, et al., 1989). Increased heat flux in combination with very high pressures can cause serious engine damage (Essig, 1981), (Betz & Ellermann, 1981), (Fritton & Nates, 1996), (Maly, et al., 1990). The temperature history of the end gas prior to knock was measured using Dual Band Rotational

Coherent Anti-Stokes Raman Spectroscopy CARS, (Grandin & Denbratt, 2002) and (Bradley, et al., 1994) to study the effects of knock intensities from 0 to 1 MPa.

The third stage of combustion is generally regarded to be the completion phase when turbulence combustion has interacted with the surrounding chamber walls (Rivas, et al., 2011). During this period, bulk of heat available in the trapped charge has been extracted and in Four-Stroke Cycle engines is not considered to be less significant than the turbulent phase to the overall combustion efficiency. However, in a two-stroke type engine which utilises the pressure waves in the exhaust system the effects of this phase are important. It is the thermal energy of combustion in this phase which is utilised to increase the mas flow rate of charge through the engine and is therefore responsible for the high inherent power output of these engines.

GASES PRODUCED BY COMBUSTION

A large number of gases are produced by combustion in any engine. These consist of a very great number of different compounds and molecules. However, although individual molecules have different toxicity levels two predominant gases are produced in significant quantities by combustion.

The first of these gases being, Carbon Monoxide (CO) which is formed as a by-product of incomplete combustion processes where the amount of oxygen available is insufficient. The second gas being, Carbon Dioxide (CO_2) which is formed as a by-product of combustion processes.

The relative amounts of gases present in the exhaust gases indicates the Air/Fuel ratio provided for combustion as shown diagrammatically in Figure F2-7. From this diagram, it is apparent that at Air/Fuel ratios between 14 and 15:1, close to stoichiometric, Carbon Monoxide (CO) emission levels are low but Carbon Dioxide (CO_2) levels reach peak. The reduced emissions levels of these gases resulting from achieving combustion using lean Air/Fuel ratios between 17 and 18:1 is apparent especially if unburned Hydrocarbons (HC) can be reduced. Overall, Figure F2-7 shows the following points:

a) Air/Fuel ratio closely controls the gases and relative masses, present in any fraction of trapped residual burned gas.

b) The amount of CO and CO_2 in a sample of trapped gas, the mass fractions of burned gas and fresh charge and hence the mass of oxygen available present, can be reliably determined using stoichiometric combustion chemistry.

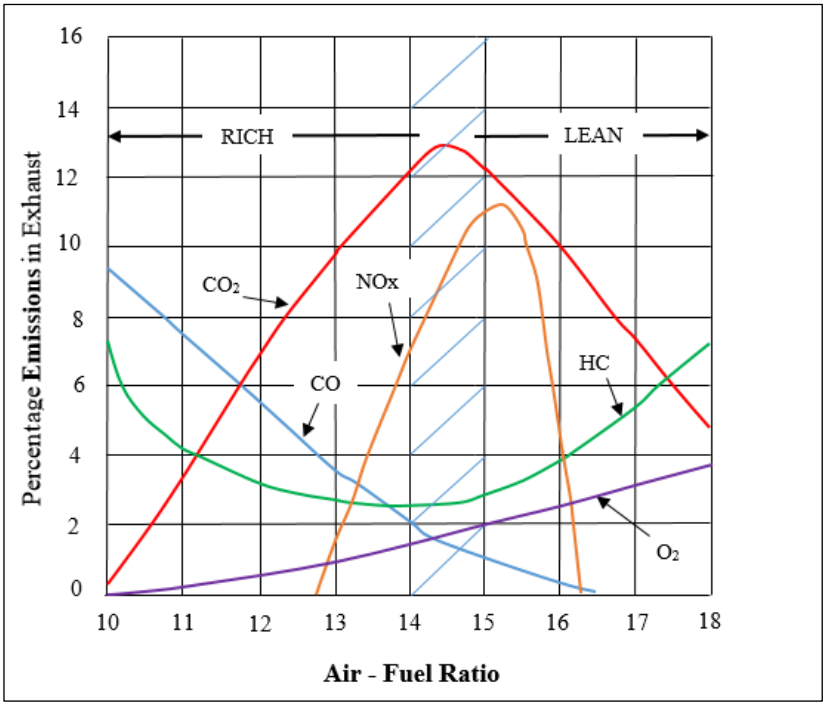

Figure F2-7: Emission gases resulting from Combustion Air/Fuel variations

The proportion of the trapped charge occupied by exhaust gas has a major influence on combustion flame speed and reduces the amount of oxygen available for the subsequent combustion event. Combustion variability increases as the Air/Fuel ratio becomes leaner above stoichiometric (Quader, 1976), (Stone, 2012), which presents additional challenges to combustion control systems. This is significant for combustion as the oxygen present in exhaust gases can be considered negligible in comparison to that present in the fresh Air charge (Heywood, 1988).

TESTING AND MEASUREMENT

A number of different sensing systems have been developed identify different gases, or indicators of their presence, in the exhaust pipe or inside the engine cylinder. In addition to a very large array of research using intrusive and non-intrusive pressure sensors. Combustion has been monitored or measured from gas samples extracted from the exhaust pipe using Infrared absorption (Tomita & Kwahara, 2004) and by Fast Flame Ionization Detector (FID) systems, (Collings, 1988) or from the combustion chamber via electronically controlled sample valves have been routed to FID gas mass spectrometers (Yucel, et al., 2013), (Ladammatos, 1992), (Crawford & Wallace, 1996). Still more complex arrangements have linked in-cylinder pressure measurements to Horiba Universal Exhaust Gas Oxygen (UEGO) sensing of O_2 and FID to measure HC (Karagiorgis, et al., 2006). Gas temperature measurements during combustion have been obtained using

ultrasonic sound waves, (Yamaga & Shibata, 1969) and by Emission-Absorption Spectroscopy (Aust, et al., 1999). Single shot temperature and pressure measurements have been obtained using Laser Induced thermal grating spectroscopy (Stevens & Ewart, 2003). Engine Knock has been investigated by recording the cylinder pressure, flame travel and gas temperature using Coherent Anti-Stokes Raman Spectroscopy (CARS), (Bradley, et al., 1994), (Choi, et al., 2000). The equivalency ratio of flames has been obtained using variations of 'Chemiluminescence' intensity using 'Cassegrain' optical sensors in burner flames (Hardalupas, et al., 2004) and inside high speed Four-Stroke engines (Ikeda, et al., 2008) (Kubota, 2010) . In-Situ measurements of Hydrocarbon (HC) fuel concentrations near the spark plug have been obtained by 3.392um Infrared Laser Absorption (Nishiyama, et al., 2003). Intra-cycle variations of crankshaft acceleration have been used to estimate engine torque and cylinder pressure (Ball, et al., 2000), (Davaine, 1993).

2.10 CYCLE BY CYCLE COMBUSTION VARIATIONS

Two-stroke cycle engines suffer from irregular combustion especially and predominantly under light load conditions showed that even slightly retarded burning precedes cycles in which combustion pressure is greatest (Lu & Lee, 1996). This retarded burning was proposed to allow high temperature gases to remain in the cylinder promoting combustion in the subsequent cycle (Tsuchiya, et al., 1983).

Cycle-by Cycle combustion variations have been investigated by many researchers (Young, 1981) and are readily observed as variations in cylinder pressure development. These occur in all engines and for a variety of reasons, the principle causes are shown diagrammatically in Figure F2-8 which is an adaption taken from the results of an experimental study (Ozdor, et al., 1996), which is relevant for all SI engine types.

Patterson recognised that if these variations were eliminated the operational characteristic of engines would be improved and fuel economy increases between 10 – 20% could be realised without higher octane fuels (Patterson, 1966). Young proposed cyclic-by cycle combustion variations are attributable to two major causes. The first being chemical factors including Air/Fuel ratio and residual exhaust gas concentrations (Young, 1981). The second being physical which include, spark plug location and number, ignition energy, combustion chamber shape, compression ratio, air flow motion, Air/Fuel homogeneity and turbulence intensity.

Research observed flame growth using Schlieren photography and simultaneous pressure records using a square piston transparent engine (Gatowski & Heywood, 1985),

(Namazian, et al., 1980). This work also suggested the major causes of cycle-by-cycle variations result from variations in flame growth rate and the location of the flame kernel at very early formation stage. This condition is worse in 'Lean' mixture conditions which results in heat variations (Yamamoto & Misumi, 1987). The homogeneity of the Air/Fuel mixture was found to effect cycle-by-cycle combustion variations such that if homogeneity is improved grater excess air can be present before cyclic variations will occur. The amount of excess air which could be used before cycle-by-cycle combustion variations started to increase above a stoichiometric level in a four-stroke cycle engine was found to be 1.20 (Ceviz, et al., 2011). The flame kernel formation speed was also found to be delayed by reduced mixture homogeneity (Pundir, et al., 1981). The principle cause of cyclic variation, was validated by comparison of experimental and observed behaviour in small two-stroke cycle engines (Abraham & Prakash, 1992). Non-Linear combustion processes and cycle-by-cycle variations concluded these resulted from deficiencies in originating at the point-source of ignition leading to slow development of the early flame (Hu, 1996). A study using a Pulsed Jet igniter patented (Oppenheim, et al., 1990) and previously reported (Oppenheim, 1988) which provides a uniformly rich mixture at the point of ignition spark confirmed COV increased with residual gas fraction as varied by skip-firing, but was improved by the mixture control during kernel formation (Robinet & Higelin, 1998). Martin suggested two super-imposed combustion variation modes are responsible (Martin, et al., 1988). The first being random cyclic variations in ignition, mixture composition and turbulent flow fields local to the spark plug (Johansson, 1996) and the second being the variations of residual gas composition resulting from prior cycle burning. Cycle-by-cycle combustion variations in the burning rate during the fast-burning turbulent stage of combustion has been concluded to result from variations of the spherical burning area produced by variations in the position of the wall contact flame centre (Keck, et al., 1987). The trends for cycle-by-cycle combustion variations due to Laminar flame speed, turbulence intensity and velocity were determined by CFD in a four-stroke cycle engine to provide a mathematical relationship with Indicated Mean Effective Pressure (imep) (Galloni, 2010).

Mathematical models using three dimensional studies of flame kernel formation and kernel development have been produced (Pischinger & Heywood, 1990), (Mantel, 1992). The effect of heat losses from the spark plug electrodes was shown to be a major factor in flame kernel development (Pischinger & Heywood, 1990). Simulations of cyclic variation showed that in load conditions cycles can switch between burn and no burn combustion which could be improved by increasing the flame speed (Lu & Wang, 1995).

CALCULATION OF CYCLE-BY CYCLE VARIATION

The change of pressure in an engine after ignition, is directly related to combustion and variations between cycles are caused by variations which take place during that process. Cyclic variations can be quantified by a Coefficient of Variance (COV) in terms of either 'mean' or 'maximum' cylinder pressure.

Coefficients of variation in indicated mean effective pressure (imep) is the standard deviation in imep, divided by the mean imep (Heywood, 1988), usually expressed in percent as:

$$COV_{imep} = \frac{\sigma_{imep}}{imep} \, x \, 100 \qquad \text{(Eq. 2.25)}$$

The indicated mean effective pressure provides a measure of the work produced for an engine cycle and is expressed as:

$$imep = \frac{W_c}{V_d} \qquad \text{(Eq. 2.26)}$$

Where: V_d is engine displacement volume and W_c is the work done per cycle, defined as:

$$W_c = \int PdV \qquad \text{(Eq. 2.27)}$$

Coefficients of variation in maximum in-cylinder pressure (Pmax) is the standard deviation in maximum in-cylinder pressure, divided by the mean maximum in-cylinder pressure, usually expressed in percent as:

$$COV_{Pmax} = \frac{\sigma_{imPmax}}{imPmax} \, x \, 100 \qquad \text{(Eq. 2.28)}$$

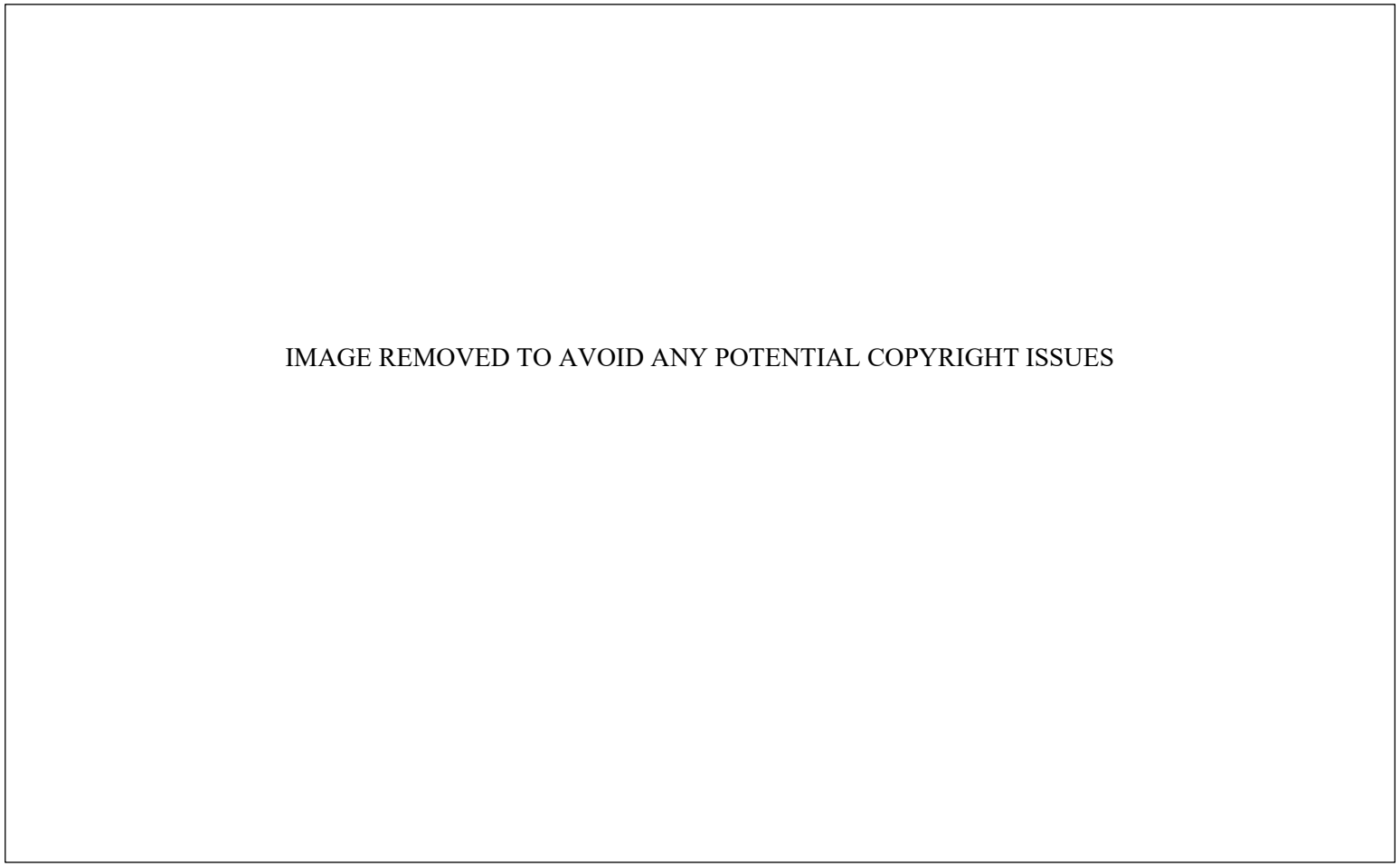

Figure F2-8: Diagram showing causes of Cyclic Combustion Variability

2.11 IN-CYLINDER SENSING

ION CURRENT SENSING

The use of ionization probes for measuring Air/Fuel mixtures in engines was first described in 1931 (Schnauffer, 1934). In the simplest form, a probe consists of two electrodes, where one is connected to a positive voltage of between 150 to 400V DC and the other is connected to ground. An electric field is generated between the electrodes through application of the voltage. The process of combustion causes gas molecules to break apart then reform and recombine into completely different molecules and these processes cause free ions to be released. The presence of free ions causes a reduction of electrical conductivity in the gases using a probe in the combustion chamber. Typically, however, the ion current in the SI engine is measured using the spark plug which is negatively biased.

The ion current signal in an SI. engine consists of two major phases consisting of three current peaks. Not all the factors influencing the ion-current in Spark ignited combustion are not fully understood.

The first ionization peak, termed 'the Ignition Phase' commences with ignition and progresses to approximately 10 Deg. btdc. The ion current signal in this phase falls rapidly after spark breakdown has occurred.

The second ionization peak, termed 'the Flame Front Phase' is caused by chemical ionization in the flame that surrounds the electrodes immediately after the discharge of the electric spark. This follows at the completion of the ignition phase and progresses until approximately 5 Deg. atdc. This peak is caused by the high levels of ions associated with the chemical reactions in the flame front phase which produce one or more characteristic current sub-peaks and its magnitude is related to the local equivalence ratio close to the electrode gap. This peak which is the highest, is considered most suitable for the feedback control of an engine.

The third ionization peak, termed 'the Post-Flame Phase'. The cause of this peak was theorised by (Yoshiyama, et al., 2000) to result from flame front ionization. This was concluded from a bomb experiment which showed the peak occurred when the flame front contacts the wall of the combustion chamber. The major factor influencing this peak being the thermal ionization of NO around the spark plug. However, (Franke, et al., 2003) theorised that thermal ionization of NO was the major influence at high flame temperatures exhibiting high sensitivity, but alkali metals (potassium), become the major influence at

lower temperatures where insufficient NO is formed. These processes are not fully understood although detailed investigations of combustion temperature from ionization current signals have been investigated (Andersson, 2004). The ions generated by the flame have different recombination rates with some occurring quickly to more stable molecules while others exhibit longer residual durations. Following the greatest flame activity, the ion current signal follows the temperature of burned gases and hence the cylinder pressure. The highest part of this peak is located close to the point of greatest cylinder pressure which decays and flattens only when more stable ions remain (Saitzkoff, et al., 1997). Under light loads, the third ion current peak tends to disappear as NO+ concentration decreases. Further significant contributions to the electron density might originate from secondary effects at the cathode (Ahmedi, et al., 2003).

Other types of ion sensors have been developed to monitor the movement of the flame in and across the cylinder head. A printed circuit embedded into a head gasket noted the flame movement was biased towards the exhaust valves in a four-stroke cycle engine (Russ, et al., 1997). Curry, used 49 ion current sensors to carry out a three-dimensional, study of flame propagation (Curry, 1963). Combustion analyses techniques involving twenty-five, ion current sensors set into and around the cylinder head were developed and used in a spark ignition engine at 16000 rpm (Kato, et al., 2007). A 300 Volt negatively biased 300 Volt ion current was applied to the probes with isolated single core wires with ground to the engine casing. This arrangement was coupled with a miniature camera gathering pictures of flame movement at 40 frames/s and fast response thermocouples. An array of twelve twin wire, ion current sensors including four closely fitted around the spark plug, was used to investigate tumble and swirl in a Formula One type engine running up to 17,000 rpm. An arrangement using the ion current measured at the spark plug and at three other probe positions radially dispersed were used for combustion analysis in a 69cc two-stroke engine (Beck, et al., 2008). These were used in conjunction with eight optical fibres fitted radially within the spark plug body plus an additional optical fibre viewing transversely across the cylinder head at engine speeds up to 9,000rpm. The work provided new insights into cycle by cycle combustion behaviour. These arrangements provided excellent results but required careful machining and preparation of the cylinder heads to apply. Witze fitted eight ion current sensors radially spaced in a cylinder head gasket and obtained cycle resolved flame arrivals at the cylinder bore (Witze, et al., 1990). Meyer linked cycle resolved cylinder head gasket, eight location ion current detection with an optical in spark plug pressure sensor but considered the equipment needed further development especially, to distinguish between flame non-arrival and low strength signals (Meyer, et al., 1993).

Later, new cylinder head gasket materials and manufacturing techniques enabled embedded four position ionization current detection within production engines (Clarke, et al., 2002). A cylinder head gasket incorporating eight separate segments was developed to measure the flame front arrive time and associated flame speed (Nicholson & Witze, 1993). Ion current measurement showed the variation of signal strength depending on exposed sensor area. Other work concluded ion current variations are large when cycle by cycle variations of flame propagation is large (Yoshiyama, et al., 2003). Investigation of ionization in the spark gap was used to conclude that autoignition (termed 'pressure ignition' by the researcher) occurs in the end zone (Weinhart, 1939).

Ionisation in a HCCI Two-stroke engine was investigated by (James, et al., 2010). Combustion and combustion control in such engines is complex but this work showed the Ion current could be used to predict the peak pressure position with an average error over three operating conditions of 5.24% indicating combustion timing and could be used for timing feedback. A relationship between combustion duration and the peak value of the rate of ionisation showed an inverse relationship with timing location of peak pressure. Using Ion sensing to determine pressure avoids the installation of a pressure sensor used by other researchers (Olsson., et al., 2001).

Mass fraction burned curves from ion sensing signals recorded at the spark plug and found the results compared very well with those created from recorded cylinder pressure (Daniels, 1998). Ion current signals have been interpreted to replace cylinder pressure measurements to determine combustion variations (Byttner & Rognvaldsson, 2001) and heat release (Eriksson, 1998).

Engine misfiring and knock can be identified from ion current signals (Daniels, et al., 2003). This capability was used by (Forster, et al., 1999) and a closed loop control system presented. Some aspects of signal behaviour were reported including the improvements to the signal if spark plugs with a large central electrode and gap distance up to 1.1mm are used. Ion current signals reaction to fuel additives was investigated which showed signal increases of up to five times if Methylcyclopentadienyl Manganese Tricarbonyl (MMT) or Methyl-tert-butyl-ether (MTBE), which are used in unleaded gasoline to increase octane rating, was present. This behaviour increased with combustion temperature.

Ion current sensing was also adapted to determine late combustion resulting from EGR within the exhaust system for possible application for feedback control (Brehob, 1989) and gas density fluctuations to detect transient misfire (Chae & al, 1999)

An AC Ion current sensing system was developed which offers increased reliability at lower cost (Wilstermann, et al., 2000). The use of an AC Ion current sense signal was obtained from within the combustion chamber Diesel engines using an adapted probe which replaced the pre-heater element (Glavmo, et al., 1999). This work concluded that ion current contains different information depending upon the direction of the current. Nilsson investigated AC ion current signals on the basis that if it were possible to measure the ion current flowing in both directions more information could be obtained but more work electronic development was required (Nilsson, 2008).

Ion current sensing technology provides a practical cost-effective method by which air/fuel ratio, pressure, heat release and knocking have been identified and feedback control systems created (Malaczynski, et al., 2013). If the spark plug is used to collect the associated signal, additional cylinder head adaptions and additional parts are avoided. However, the definition of the ion current signal is heavily dependent on the design and location of the sensor and in particular the area of the electrode. Additionally, the process of free ion creation and reformation is somewhat chaotic and cyclically variable, such that signal results of 100 combustion cycle used and cycle by cycle interpretation is limited. However, a major advantage of ion sensing is the ability to operate and provide equivalent pressure values in high temperatures (Zdenek & Anthenien, 2004) .

2.12 THE SPARK PLUG

The first spark plug design is attributed to Edmond Berger, however, the first patent for this device was awarded to Sir Oliver Lodge (1903). Alternative designs were first produced around the same time by Albert Champion and Robert Bosch. The basic design concepts have remained whereby the high voltage which is used to produce an ignition spark, is delivered to a central electrode which is insulated from the threaded outer body which provides the electrical (conventionally negative polarity) earth. The key areas of development for this apparently simple device have been: a) The electrode geometry and gap. b) The electrode materials. c) The insulation material d) The gas sealing.

The spark plug is a mass-produced item, not an accurately machined piece of laboratory equipment with carefully controlled electrode surfaces. Many types and shapes of electrodes have been developed (Adbel-Rehim, 2013) using specially optimised materials (Hori, et al., 2003) to reduce electrode erosion (Javan, et al., 2012) and increase resistance to fuel containments (Shoobert, 1962). Further, the rapidly varying environment inside an engine which contributes to cyclic variations of combustion efficiency especially in lean

mixture conditions cannot easily be directly compared with controlled laboratory conditions, (Daniels & Scilzo, 1996), (Ozdor, et al., 1996), (Heywood & Sher, 1999), (Ozdor, et al., 1994). The design of the spark plug has evolved to provide efficient ignition initiation allowing sparks to pass between its electrodes in a consistent manner at voltages up to around 35kV (Silsbee, 1925), (Lee, et al., 2000), (Lee, et al., 2005), (Manivannan, et al., 1995). The voltage required to form a reliable ignition spark at different pressures and temperatures was investigated for early aero-piston engines and reported by (Loeb & Silsbee, 1920).

Electrode design and plug orientation are both noted to be causes of cyclic combustion variability (Ozdor, et al., 1996). Spark plug development has moved to incorporate small diameter centre 'power' electrodes with similar local protuberant additions to the 'earth' electrodes (Daniels & Scilzo, 1996), (Hori, et al., 2003). These additions are manufactured from specialised Iridium and Platinum alloys which can withstand the additional heat from reduced mass and erosion due to reduced electrode surface area. These materials also have lower ionisation potential characteristics which encourages breakdown to occur in more defined channels. Formation of the flame kernel is assisted due to the reduced heat transfer to the electrodes. The overall effect of these developments has however, been focused on improving ignition reliability and reducing the Coefficient of Variance (COV) between combustion events. Evaluation of different earth electrode arrangements have shown variations of the voltage required to achieve combustion with the low COV and emissions levels (Lee, et al., 1990). Simulation and visualisation of ignition has been carried out to evaluate electrode designs (Yorita, et al., 2007). The variation of mass burning rates due to the number of earth electrodes showed multiple electrodes slowed down the early flame development. The amount of heat loss from the spark plug leads towards higher cyclic variability (Adbel-Rehim, 2013).

Spark plugs represent 'non-intrusive' sensors and are therefore attractive to modified or adapt gain in-cylinder access. Subsequently, they have been adapted to fit small pressure sensors (Bertola, et al., 2015), incorporate valves to sample gases around the electrodes or fit multiple bundles of fibre optics to provide optical observation of kernel growth and subsequent flame propagation (Beck, et al., 2008).

ELECTRODE SHAPES.

A huge variety of electrode shapes and configurations have been presented since its invention. It has been proven by researchers that electrode design exerts a significant

influence on mixture ignitability, (Pischinger & Heywood, 1990), (Pischinger & Heywood, 1988). Perhaps the widest range of spark plug designs was assessed during the period when piston engine designs for automotive and airplanes were developing rapidly during the 1920 - 1940's. Silsbee reported tests of 107 different configurations (Silsbee, 1920). In all designs, the primary objectives are to maximise the spark energy which is passed into the surrounding gases to improve mixture ignitability and ensure a preferred spark path between the electrodes. The most common configuration provided by a 'J' shaped earth electrode. Different configurations provide more protrusion into the gas, away from the earthed body. Other designs include the surface discharge arrangement where the earthed body closes to surround the central electrode. These are used commonly in aircraft engines, two-stroke engines and high performance four stroke engines (Craver, et al., 1970). They provide a more shielded environment for the spark in engines with high turbulence but run cool so need greater sparking voltages. Other commonly available earth electrode designs include a straight cantilever which the author has termed the 'R' type. This arrangement provides good access for gases to the spark kernel and improved mixture ignitability (Daniels & Scilzo, 1996), but provides greater shielding from gas turbulence that the 'J' type. Other recent designs include a double spark arrangement in which a metallic ring is inserted into the ceramic nose. No earth electrode is used and the path to earth for the spark from the centre electrode passes first to the inserted ring in the nose and then in a second pass to the earthed body (Astanei, et al., 2011). This design results in a longer than conventional spark gap distance which requires increased sparking voltage. The impact of multiple earth (or ground) electrodes reported considerable differences in mass fraction burned and concluded a complete picture was far from clear (Adbel-Rehim, 2013). Designs using a 'shroud' in which a 'corona wind' is created showed great potential for reducing emissions but have not been developed commercially (Sher et al, 1992). Pischinger, investigated the effects of electrode configuration, material and gap distance thoroughly in work that included detailed sparking voltage assessments (Pischinger, 1989). Different measures have been used to identify the effects of different spark plug electrode designs. Although COV is commonly used as a measure of mixture ignitability (Daniels & Scilzo, 1996) proposed that the duration required to achieve 2% of mass fraction burned burn was a more accurate measure although 10% has been used although others.

The lean limit Air/Fuel ratio comparison is also used (Nishio, et al., 1994). Hood used a time based, misfires count in lean limit conditions (Hood, 1990).

The shape and size of the spark plug electrodes represents varying 'uniformity' which influences the field concentration as spark voltage increases (Pedersen, 1967), (Hutton,

1947). It is easier to initiate a spark in a gap with a strongly non-uniform distribution of the electric field between the electrodes, because this requires a lower voltage (Bazelyan, 1988). This influences the voltage at which electrons are released from the electrode surface to move across the gap towards the earth electrode. This in turn influences the spark breakdown event which leads to the formation of the spark which subsequently causes ignition of the combustible gas mixture.

ELECTRODE MATERIALS.

Spark plug electrode material has a fundamental influence on the formation of the spark breakdown process which results in the creation of the ignition spark. Each time a spark forms, material is removed from the electrode surface (Walker, et al., 2005). Therefore, for the service life to be increased, harder materials, which could better resist erosion, were required (Rager, et al., 2006). This was especially so when higher ignition voltages are used to improve the reliability of mixture ignitability in lean Air/Fuel ratio mixtures (Osamura, 2000). Additionally, to improve this performance and reduce emissions spark plug electrodes have are required to be smaller and run at hotter temperatures. New electrode designs incorporating very small electrodes with new materials have been developed to meet these requirements (Hanashi, et al., 2001), (Hori, et al., 2003), (Nishioka, et al., 2008) and to achieve high ignition reliability (Shimanokami, et al., 2004). The surface condition of the electrodes changes as repeated sparking events known as ‘conditioning’ also affects the ionization process (Lucas, 2001) and this effect would need to be considered if the spark plug were to be used as a sensor. The space taken in the combustion chamber, particularly in for stroke cycle engines has driven research to reduce the physical size of the spark plug (Ishiguro, et al., 2005). This affects the performance as smaller items are unable to transfer as much heat away from the hot electrodes to the threaded body and into the engine. The tendency for the spark to track across directly to the plug body is increased due to the shorter distance (Craver, et al., 1970). Although not commonly reported, the formulation and influence of insulation material had been investigated from pioneering work on aero piston engines (Silsbee & Honaman, 1920).

2.13 SPARK BREAKDOWN VOLTAGE OF SPARK PLUGS

The relationship between the sparking voltage and cylinder contents has been studied extensively and understandably, to improve the reliability of combustion (Silsbee, 1925), (Burgett, et al., 1972), (Teets & Sell, 1988), (Mc Allister, et al., 1989). Ignition systems are designed to ensure a spark occurs in all operating conditions and hence, concern of the

voltage supplied to the spark plug becomes focused on obtaining a reliable ignition event. However, in addition to providing the means to apply an ignition spark, the spark plug is also known to be an indicator of engine condition and combustion. The condition of the spark plug electrodes and ceramic are traditionally recognised to be key indicators of engine condition and operational settings. Prior to the introduction of Capacitor Discharge Ignition (CDI) systems which release stored electrical energy faster than inductive types, two-stroke cycle engines suffered badly with misfires and irregular combustion (Mogi, et al., 1992). This occurred because the voltage supplied to the spark plug was often insufficient to overcome the electrical isolation provided by the gas between the spark plug electrodes. This was made worse because oil, mixed into the fuel to provide lubrication (which is not deliberately added into the fuel for four-stroke cycle engines), significantly further increased the resistance to sparking. This resistance was greatest when the engine was under full load with greatest cylinder pressure. Reducing the electrode gap distance being a regular remedial fix. Traditional 'tuners' of two-stroke cycle racing engines would learn to 'read' the discolouration of the spark plug to help judge if the engine settings were correct (Jennings, 1973). These simple observations show a direct relationship between spark voltage and the gases in the cylinder.

The relationship between sparking voltage and different gases has been extensively researched by physicists and electrical engineers but these findings have been largely ignored by researchers who have focused primarily on designing ignition systems to produce sufficient voltage to avoid misfiring. Although researchers have used analysis of the spark plug voltage to analyse combustion (Shimasaki, et al., 1993).

The geometry and arrangement of the spark plug is known to affect the breakdown voltage (Craver, et al., 1970), (Brereton & Rani, 1998), (Adbel-Rehim, 2013).

Silsbee noted the variables which effect the voltage required by a spark plug included: 1). Spark gap length and electrode shape. 2). The gas density which depends upon the pressure and temperature (plus others). He concluded, "the effects of items 1 and 2 have been the subject of a very great amount of research so that relatively little remains to be done on them" (Silsbee, 1925). From tests conducted by Silsbee, on 25 different spark plugs he found a +/- 20% variation of sparking voltage in air compared with Paschen's law and noted the results were similar with those obtained from atmospheric pressure to 98 lb/in^2 by (Patterson & Campbell, 1918). Silsbee also presented a simple linear relationship which he stated, fitted the observed data "fairly well" and was convenient to use (Silsbee, 1925).

He noted that the density of gas increases the spark voltage approximately linearly according to the equation (Eq. 2-29).

$$E_\delta = E_1 (1 + K(\delta - 1)) \qquad \text{(Eq. 2-29)}$$

Where: δ = density of air relative to normal temperature and pressure, E_1 = sparking voltage at relative density =1, E_s = sparking voltage at relative density = δ, K = a constant which varies from 0.5 to 0.7 for different shapes of electrodes, the larger value corresponding to blunter electrodes.

Research noted the sensitivity to the orientation of the earth electrode effects from tests in firing engines (Pischinger & Heywood, 1990), (Burgett, et al., 1972) and the orientation of the electrodes relative to gas flows in the cylinder (Heywood & Sher, 1999). The effect was attributed to changes in the flow field in the vicinity of spark plug electrodes, electrical spark energy loss to the electrodes and the heat transfer between the flame kernel and the electrodes. Some researchers believed the effects of the earth electrode orientation have often been neglected in engine tests (Lee, et al., 1990). Others considered this as one of the contributing reasons for cyclic combustion variability, (Ozdor, et al., 1996). Other research had focused on ignition spark breakdown voltage and shown this was affected by in-cylinder mass air flow rates in order to formulate their calculations (Adbel-Rehim, 2013) for spark plugs with different electrode numbers and arrangements.

The variation of contact area between the electrodes and the flame due to kernel elongation is influenced by the changes in the flow field (Pischinger & Heywood, 1990). The mean flow velocity and turbulence intensity influence from the electrodes was noted by (Halldin, 1992). The variation of the voltage required to achieve ignition in propane and air mixtures using different electrode materials and gaps in stream velocities between 15 - 75 m/s were comprehensively reported in a series of works between 1948 - 1955 (Swett, 1948), (Swett, 1949), (Swett, 1951), (Swett & Donlon, 1953), (Swett, 1954), (Swett, 1955). More recently, (Ballal & Liefebvre, 1975), investigated the effect of gas flow over spark plug electrodes on the minimum spark energy required to initiate ignition.

The apparatus shown schematically, in Figure F2-9 was used to apply a direct jet of air across spark plug electrodes (Kim & Anderson, 1995). The accuracy of the bulk flow predicted by this technique was considered moderate overall showing weak correlation at low velocities but good correlations at higher flow velocities up to 15m/s.

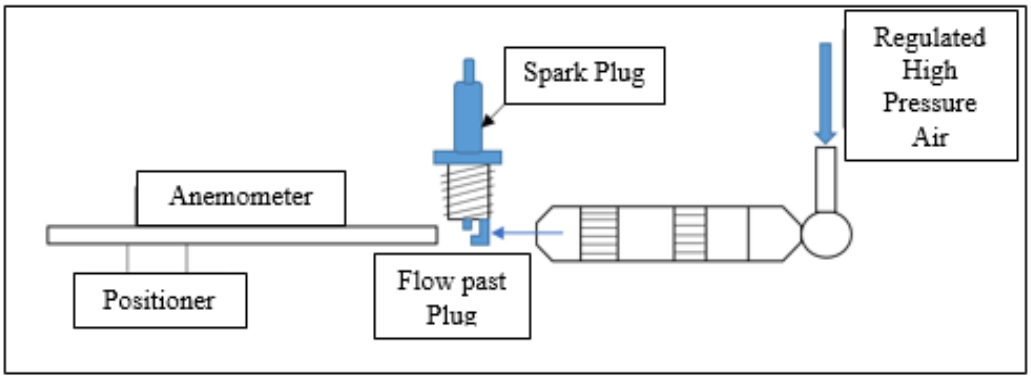

Figure F2-9: Schematic of Air Flow Test apparatus (Kim & Anderson, 1995)

This work calculated the variation of time in the spark event due to a rectangular, 'U' shaped deflection of the spark during the glow discharge phase although the method could be used in a motored engine.

The deflection of the spark path used was noted to be a simplification of the more irregular and fluctuation spark shown by (Maly, et al., 1983). The results of the work noted above used single event breakdown spark events using Direct Current. In-cylinder pictures showing sparks being deflected by flowing gases in a running engine are shown by (Aleiferis, et al., 2000). These pictures confirm the spark length varies as the spark twists and contorts when exposed to different gas flows with the plug electrode in different orientations.

A method to use the change of spark breakdown voltage to calculate the gas flow rate past the spark plug electrodes and to provide a value for local gas turbulence was presented by (Pashley & Stone, 2000).

Han reported the interpretation of spark breakdown voltage required for ignition to derive the Air/Fuel Ratio of the charge. This work reported a mathematical expression relating the spark breakdown voltage used for ignition with burned exhaust gas in the cylinder (Han, 1997). Analysis of the spark plug voltage has also used to monitor combustion (Shimasaki, et al., 1993).

The relationship between secondary ignition voltage and cylinder pressure was also investigated with respect to ignition in gas fuelled engines (Mitianiec, 2012). A mathematical expression relating secondary voltage with electrode gap and compression ratio was presented. Plotted curves were provided which show how these varied with electrode gaps between 0.3 to 0.9 mm obtained from measurements in a calorific chamber similar to that used in the present work. More recently (Grasso, et al., 2013), used spark

breakdown current to measure in-cylinder pressure at an applied frequency of 60kHz. They included an expression for spark breakdown voltage for pressure which includes a temperature term from which they derived gas temperature.

A series of four papers were published which described the use of Spark Breakdown Voltage applied across the spark plug repeatedly during the non-ignition sparking period. The proposed a possible method of in-cylinder pressure measurement included a plot of a whole cycle of Spark Breakdown Voltage simultaneously recorded against cylinder pressure (Martychenko, et al., 1999). The work concluded that it was much too early to discuss the accuracy of the method. However, it also includes a comment which the present work is based upon: “The method based on breakdown voltage gives the possibility to estimate in-cylinder pressure not only during combustion but in any cycle”. The second work concerned the proposed use of Spark Breakdown Voltage to detect misfire and its intensity (Park, et al., 1999). This work also included recorded plots showing whole cycle comparisons between Spark Breakdown Voltage and Cylinder Pressure. It concluded this new method could detect engine misfires regardless of engine speed or load. The third paper presents a method and formula by which gas temperature may be interpreted from Paschen’s relationship for Breakdown Voltage against pressure corrected for gas density (Park, et al., 2000). Plots of calculated temperature against crankshaft angles over the combustion period were presented. The calculations were favourably compared with results for a two-zone combustion model. The fourth work proposes a method by which fluctuations of in-cylinder gas density are used to detect misfire which applied multiple sub-ignition level voltages across the spark plug to investigate combustion. The work showed that in-cylinder gas pressure and density values could be obtained throughout entire engine cycles using the relationship between the voltage required to overcome the dielectric properties of gas.

2.14 CHAPTER SUMMARY

This chapter has attempted to describe the difficulties which researchers have faced to investigate the processes occurring inside SI engines of both two and four-stroke cycle types. Many different testing arrangements and instrument devices and measurement techniques were reviewed. These had been used to measured or calculate, the gas flow into and through engines, the pressure, speed and timing of combustion and determined resulting engine efficiencies. The review of this extensive work showed how the increased understanding of these issues and improved mechanical engine designs led to significant efficiency improvements and emission reductions. However, the objectives of the present

work require the combustible mass to be determined during the compression stroke ‘a priori’ of ignition and combustion. The extensive review of published work revealed only one sensing method (Martychenko, et al., 1999), (Chae & al, 1999), (Park, et al., 1999), (Park, et al., 2000), which demonstrated the potential to determine the in-cylinder gases in a practical and cost-effective manner in an operating engine during the compression period. The direct applicability of using spark breakdown voltage to determine in-cylinder conditions was further verified and emphasised by reference to early work carried out on aero engines (Silsbee, 1925)

Accordingly, the subsequent research and development for the present work focused on the use of spark breakdown voltage using the spark plug as the sensor. The following chapter could be viewed as an extension of this literature review which is specifically concerned with the history, development of ‘spark breakdown’ theory and its background relative to spark plugs in engines.

CHAPTER THREE

SPARK BREAKDOWN VOLTAGE THEORY

3.0 INTRODUCTION

At normal pressures and temperatures all gases are excellent electrical isolators which mechanism prevents electrical charge passing to ground. However, when subjected to an electrical field of sufficient strength, gases 'break-down' and suddenly become very good electrical conductors (Wadhwa, 2007). The resistive ability of a gas to 'break-down' is termed 'dielectric strength' (Volt per gap distance). 'Breakdown' results when the gases between the electrodes are 'ionised' to provide a highly electrically conductive path down which an electrical spark can pass. This chapter explains the theoretical basis for this phenomenon and the factors which influence the behaviour.

The relationship between gases and electrical voltage was a fundamental part of early electrical science experiments by Coulomb reported in 1785. However, the earliest measurements to determine the potential voltage differences required to produce an electrical spark through gas were made using air at atmospheric pressure, by Lord Kelvin (Thomson, 1860). In atmospheric conditions 'dry air' is considered to have a dielectric strength of approximately 30kV/cm of spark gap distance (Kuffel, et al., 2000). Such is the consistency of the dielectric strength of Air, the gap distance between spherical electrodes has been used for over a century, using simple equipment (Figure F3-1) as the standard method to determine the value of High Voltages (Chubb & Fortesque, 1913), (Clark & Ryan, 1914), (Peek, 1914), (Karmakar, 2012).

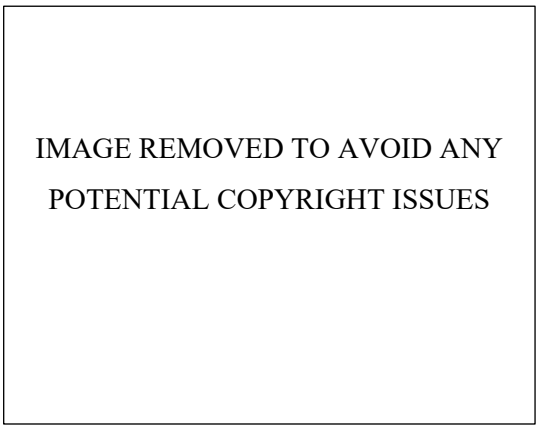

Figure F3-1: Spark Breakdown Measuring equipment (Clark and Ryan, 1914)

The standard sphere gap apparatus requirements for vertical and horizontal testing is specified in BS: 358, 1929, 1939 and 1960 as shown in (Figure F3-2). This standard also references the Guide on High Voltage Testing Techniques contained in BS: 923, 1940, 1972, 1980 and 1990.

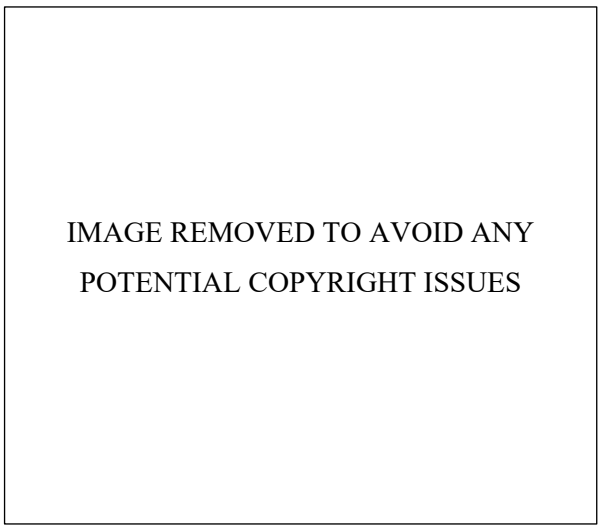

Figure F3-2: Standard Arrangement of Vertical Gap Testing - BS. 358

The 'Standard Measurement' tests are conducted slowly in a carefully controlled manner requiring an experimental procedure (Valavala & Kanchanapalli, 2013) listed as follows:

Step 1. Adjust the gap distance between spheres to the value required to be tested.

Step 2. Slowly raise the applied voltage until a faint hissing audible sound is heard. (This is the beginning of corona and the Corona Inception Voltage).

Step 3. Slowly increase the voltage until a faint visible glow appears the power electrode. (This represents the Visible Corona Inception Level).

Step 4. Slowly decrease the applied voltage until the audible hissing sound disappears. (The Voltage at this point is called the Corona Extinction Voltage).

Step 5. Slowly increase the voltage again until breakdown occurs at which point a spark will pass between the sphere electrodes.
(This Voltage is called The Breakdown Voltage).

Notably, these 'standard' steps obtain 'spark Breakdown Voltage' in a slow and controlled manner which is very different from the application proposed in the present work.

The standard High-Voltage test method shows that 'Breakdown Voltage' is proportional to gap distance and electrode radius where Breakdown Voltage' reduces as the gap distance and sphere radius is reduced.

The spherical electrodes shape is used to prevent localised concentrations of electrical field strength. Such electrode shapes are termed 'uniform' electrodes. Those which have sharper shapes which promote localised concentrations of electrical field strength are termed 'non-uniform' electrodes. Thus, electrical field strength changes with electrode profile and increases as the profile becomes sharper in 'non-uniform electrodes'.

These effects are witnessed in everyday life where, in electrical storms lightning seeks out sharply pointed objects on earth. Early work to understand and protect from lighting strikes led to an improved appreciation of how the profile and material of sharp objects react to electrical charges (Linss, 1887), (Elster and Geitel, 1900).

Most of us are familiar with the consequences if electrical isolation distances between electrical contacts in household electrical items. Investigations have enabled physicists and electrical engineers to design high voltage overhead power lines and similar equipment to prevent electrical discharge to local objects (Sigmond, et al., 2004), (Kuffel, et al., 2000) and to specify safe working clearances for high voltage equipment (Mc Allister, et al., 1989). In low-voltage electronic circuits very small separation distances between components are required.

Thus, everyday observations demonstrate that different gap distances provide electrical isolation which are representative of the voltage involved and the nature of the electrodes.

Other early research investigated the formation of the spark itself (Walter, 1899) or sparking in Air (Pen-Tung-Sah. A., 1927).

The conduction of electricity through gases other than Air, and at pressures other than ambient, was the focus of considerable scientific effort and associated work through the late nineteenth century by Baille, Liebig, Paschen, Peace, Orgler, Strutt, Earhart, Carr and Russell, Hobbs and Kinsley, (Thomson, 1908). The electrical breakdown characteristics of gases was formulated into a law (Paschen, 1889). Paschen proposed the breakdown voltage was a product of the electrode gap distance (d) and gas pressure (p) (actually density):

$$V = f(pd)$$

The work to understand the behaviour of electricity through gases continued through the twentieth century (Meek & Craggs, 1953), (Cobine, 1958), continuing to date to include investigations as to the potential influence on electronic packages of specific extra-terrestrial atmospheres (NASA, n.d.) (Stumbo, 2013).

The 'Breakdown Voltage' required to ignite combustible gases has been studied extensively with the primary aim to achieve reliable ignition and engine performance. It has been shown that spark Breakdown voltage required to ignite explosive mixtures varies as a simple additive property of the composition of the mixture (Silsbee, 1925).

3.1 GAS IONIZATION

The conversion of the dielectric property of the gas was found to result from ionization of the gas molecules which process allows a spark to pass through channels of ionized gas formed in the gap between the electrodes. This property is reversible and self-healing when the voltage is reduced below the 'breakdown voltage' limit.

Ionization is the process by which an electron is liberated from a gas molecule with the simultaneous production of a positive ion (Naidu & Kamaraju, 1996).

The electrical conductivity of all gases is reduced by the presence of ions. Ions occur naturally in the atmosphere (about $1/cm^3$). Ionization present in the atmosphere results from cosmic radiation, radioactive substances (present in the earth and atmosphere), electrical or magnetic fields, combustion, "or by any agent which introduces ions into the field" (Thomson, 1908).

In the absence of electrical or magnetic fields gases are only weakly ionised, however due to the random motion of the gas, molecular collisions occur. These collisions are considered to obey the Laws of classic kinetic gas theory (Kuffel, et al., 2000) which assume the following:

a) Gas consists of spherical molecules of same mass.
b) The molecules move randomly with a distribution in speeds which do not change
c) The molecules undergo simple mechanical elastic collisions with other molecules and walls but otherwise exert no forces on each other.
d) The number of Molecules is very large
e) The molecules obey Newton's laws of physics

Under these conditions the mean kinetic energy per molecule relates to its effective velocity to temperature such that:

$$\overline{W} = \frac{1}{2} m u^2_{eff} = \frac{3}{2} k \qquad \text{(Eq. 3-1)}$$

Table T3-1: Mean molecular velocities @20°C & 760 Hg
(Kuffel. Zaengl. and Kuffel, 2000)

TABLE REMOVED TO AVOID ANY POTENTIAL COPYRIGHT ISSUES

3.2 GAS IONIZATION PROCESSES

Two theories are considered to describe the manner which ionization occurs a) the Townsend theory, b) the 'Streamer' or 'Avalanche' theory, (Kuffel, et al., 2000), (Naidu & Kamaraju, 1996). Between 1897 and 1901, J.S. Townsend proposed the first fundamental processes which cause ionization of gases (Thomson, 1908).

These consist of:

a) PRIMARY processes being which occur when an electron accelerates in an imposed electric field, collides with a neutral molecule to create another electron and a positive ion.
b) SECONDARY processes being which change the primary ionization process contributing to further ionization of the gas by positive ions or photons. Or by the release of an electron from the cathode electrode due to the impact of a positive ion, photon, or excited atom.

More recently a variation on these was proposed in a new theory by which multiplications could occur in streamers and avalanches (Ficker, 2009).

3.3 PRIMARY IONIZATION BY COLLISION

As the strength of the electric field increases charged particles gather on the surface of the cathode, which in this case is the positively charge central electrode (or cathode) of a spark plug. The charged particles gather preferentially, at the sharp shape at the edges of the electrode. Initial detachment if electrons from the surface of the Cathode in an open environment is assisted by irradiation from Ultra-Violet (UV) light (Weidemann & Ebert, 1888). In the cylinder of an engine, for this application, during the scavenging and early

stage of compression, this will not be available. The same situation occurs when an ignition spark is initiated. This absence may cause variations of time lag to breakdown (Meek & Craggs, 1953). In an operating engine, it is considered the presence of free ions in residual combustion gases, hot electrodes will reduce this effect and increase the speed at which electrons are released for the initial breakdown. The free electrons are attracted towards the 'earthed' in this case 'negatively' charged electrode, or anode, which is earthed through the outer body of the spark plug into the engine. As electrons move through the gas, they are obliged to move across in a zig-zag path resulting from collisions with the molecules of the gases between the electrodes. If the energy (ε) gained during the transit between collisions exceeds the ionization potential of the gas (V_i), which is defines as 'the energy required to dislodge an electron from the outer atomic shell', then ionization will occur. This process is represented numerically by equation Eq.3-2.

$$e^- + A \quad \varepsilon > V_i \quad + A^+ + e^- \qquad \text{(Eq.3-2)}$$

Where: A is the atom, A^+ is the positive ion and e^- is the electron. The collision simultaneously produces an additional, new 'free' electron and a positively charged ion to be produced in a process termed 'ionization by collision'. Ionization by electron collision is the most significant contribution to the overall ionization processes. The two electrons continue to move through the gas under the acting force provided by the electric field *'E'* resulting from the 'potential voltage difference between the electrodes. The additional electrons produced from each collision then, contribute to further collisions as the process repeats and expands. This process increases in the electron current, since the number of electrons reaching the Anode per unit time is greater than the number liberated from the Cathode. The elastic collisions cause electrons to be detached, or liberated from the gas molecules, is represented graphically for an individual collision event by Figure F3-3 and for multiple collision events in Figure F3-7.

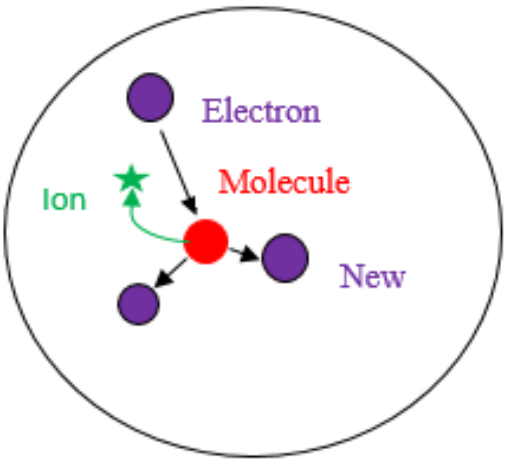

Figure F3-3: Ionization by Collision

3.4 IONIZATION BY RADIATION OR PHOTO-IONIZATION

Ionization also occurs if radiation energy absorbed by a gas atom exceeds the ionization energy (Kuffel, et al., 2000), (Meek & Craggs, 1953).

This ionization process is represented by: $A + hv \longrightarrow A^{+} + e$

Where: 'A' is a neutral atom of molecule of gas and 'hv' is the photon energy. If the photon energy is less than the ionization energy, it may be absorbed whereby raising the atom to a higher energy level known as 'photoexcitation'. Radiation can be absorbed by atoms or molecules if the atom is excited to a higher energy state or by dissociation of a diatomic molecule. An excited atom emits radiation which the electron returns to a lower or ground state which is a reversible process.

Ionization occurs when: $\lambda \leq c * \frac{h}{V_i}$

Where: 'h' is Planck's Constant, 'c' is the velocity of light, 'λ' is the wavelength of the incident radiation and V_i is the atomic ionization energy.

Substitution of 'h' and 'c' yields:

$$\lambda \leq \left[\frac{1.27}{V_i}\right] x\ 10^{-6}\ \text{cm} \qquad \text{(Eq. 3-3)}$$

Where: V_i is electron volts (e^V).

As ionization energy increases the wavelength which causes radiation, reduces. Radiation of wavelength 1250A° is capable of photo-ionization of almost all gases. This is thought to be a factor in the manner by which the voltage required to cause high-frequency is significantly less than values quoted in textbooks (Cobine, 1958), (Meek & Craggs, 1953), (Thomson, 1908).

3.5 TOWNSEND'S FIRST IONISATION COEFFICIENT

A mechanism of how the ionised path 'breaks-down' was first proposed by Townsend (Townsend, 1915). He investigated this by applying a varying electrical current using a pair of parallel plates, as shown in Figure F3-4 and measuring the current change as function of voltage.

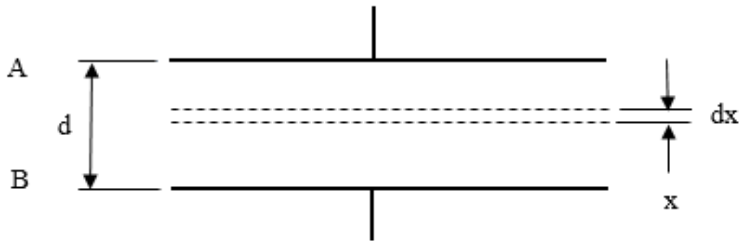

Figure F3-4 Townsend's first Ionization Coefficient Experiment

When no electric field was initiated the arrangement is in equilibrium. However, when a strong electric field is initiated variation of current occurs as a function of voltage. Townsend found that initially the current increased proportionally with voltage. However, as the applied voltage was increased the current remained almost constant at a value of i_0 due to saturation. If the cathode was irradiated by ultra-violet light the value of i_0 increased to show the emitted photo current. When the voltage was further increased the current increased above i_0 at an exponential rate, given by equation Eq.3-5, as shown in Figure F3-5.

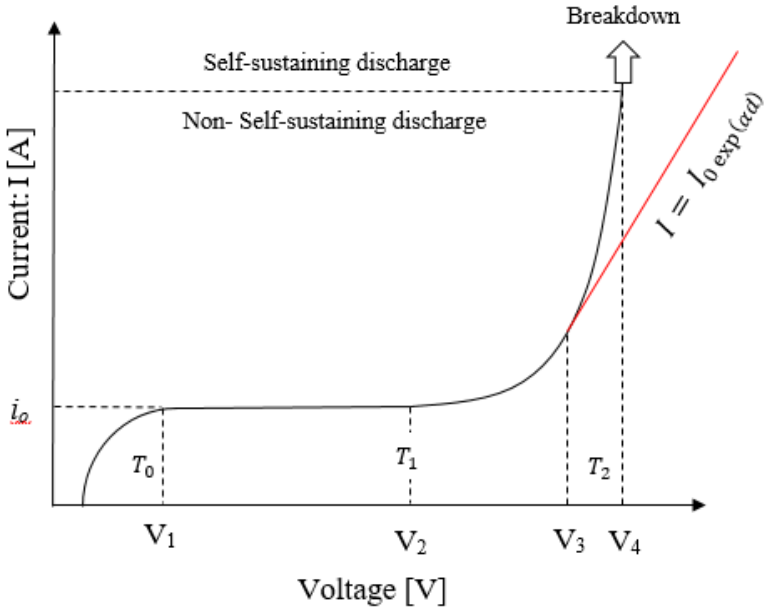

Figure F3-5: Current-Voltage relationship in Pre-Spark Ignition

Townsend proposed the behaviour of the current was due to ionization of the gas between the plates by electron collision. Townsend proposed that as the electric field increased beyond the point identified as V_2, electrons leaving the cathode are accelerated to create increasing numbers of collisions with gas molecules between the plates. This would increase until the electrons created by collisions, themselves caused collisions which caused more electrons to be produced. To explain this behaviour, Townsend introduced the quantity 'α' which is known as 'Townsend's first ionization coefficient. This is defined as: 'The number of electrons produced by an electron per unit length of path in the direction of the field'.

If a number of electrons '*n*' at a distance '*x*' from the cathode in the applied field direction, the increase in electrons '*dn*' the number of additional electrons that will be produced from an additional change in distance 'dx' will be represented by:

$$dn = \alpha n dx$$

Or $$\frac{dn}{n} = \alpha\, dx$$

Or $$\ln n = \alpha x + A$$

At x = 0, where n = n_0. $$\ln n_0 = A$$

Or $\ln n = \alpha x + \ln n_0$

Or $\ln \frac{n}{n_0} = \alpha x$

At x = d, where $n = n_0$

Therefore, in terms of current: $I = I_o e^{\alpha d}$ (Eq. 3-4)

3.6 SECONDARY IONIZATION PROCESSES – CATHODE EFFECTS

Secondary Ionizations are defined as "are those which sustain a discharge following establishment by primary processes or Collision or Photo-Ionization.

The ions produced from each collision, shown for an individual collision event in Figure F3-3, and in multiple collisions in Figure F3-7, drift back towards the cathode, in the opposite direction to the electron flow. As the positive ion approaches the Cathode it can cause emission of electrons as it losses its kinetic energy by impact. If the total energy consisting of the kinetic energy of impact plus the ionization energy exceeds two times the 'work function' of the Cathode material, one electron will be ejected and a second electron will neutralise the ion. The probability of this occurring is termed 'Townsend's Secondary Ionisation coefficient' (λ_i) which is defined as "the net yield of electrons per positive ion collision" (Kuffel, et al., 2000). This (λ_i) increases with ion velocity which is dependent on the nature of the gas and the material of the electrode. For an electron to be released for the Cathode material the energy is required to be greater than the surface potential barrier. Contributions of energy can include photon impact from UV light of the frequency is sufficient.

Electron emission by positive ion is the principle secondary process in the Townsend spark discharge mechanism. Atom excitement or interactions with metastable molecules on the cathode surface can also release electrons from the Cathode surface.

3.7 TOWNSEND SECOND IONIZATION COEFFICIENT

Townsend observed the current in his parallel plates gap experiment increased more rapidly with increased voltage compared with the expression provided by the First Ionization Coefficient (Eq. 3.5). To compensate for this difference Townsend suggested that a second mechanism must be affecting the current. He suggested the additional current must result from the presence of positive ions and photons.

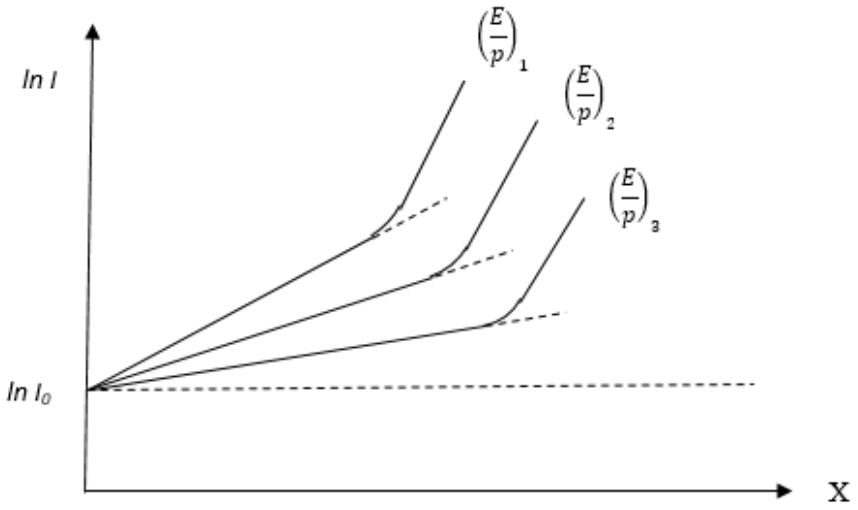

Figure F3-6: Variation of Gap Current / Electrode Spacing in Uniform Field 'E'

Using Eq. 3-4 where: $I = I_o e^{\alpha d}$

Taking log of both sides yields: $\ln I = \ln I_0 + \alpha d$ (Eq. 3-5)

Equation Eq.3-5 provides a linear equation with slope α which intercepts $\ln I_0$. This relationship is shown in Figure F3-6.

Positive ions can liberate electrons from the surface of the Cathode by mechanisms previously described. Where this results in self-sustained discharge, n_0 represents the number of electrons released from the Cathode by Ultra-Violet radiation. And n_+ the number of electrons released form the Cathode due to positive ion surface impingement. And n the number of electrons reaching the Anode. Where, γ represents Townsend's Second Ionization Coefficient defined as "the number of electrons released from the Cathode per positive ion incident.

Then: $n = (n_0 + n_+)e^{\alpha d}$ (Eq. 3-6)

The number of electrons released from Cathode is $(n_0 + n_+)$ and those reaching Anode, n.

Therefore, the total number of electrons released from the gas is given by: $n - (n_0 + n_+)$

From each electron released from the gas, one positive ion will be produced assuming each positive ion releases γ effective electrons from the Cathode.

Then: $n_+ = \gamma[n - (n_0 + n_+)]$

Or $n_+ = \gamma n - \gamma n_0 - \gamma n_+$

Or $(1 + \gamma)n_+ = \gamma(n - n_0)$

Or $n_+ = \frac{\gamma(n-n_0)}{1+\gamma}$

Substituting in Eq.3-6 $n = \left[n_0 + \frac{\gamma(n-n_0)}{1+\gamma}\right] e^{\alpha d}$

$$n = \frac{(1+\gamma)n_0 + \gamma_n - \gamma n_0}{1+\gamma} e^{\alpha d}$$

$$n = \frac{n_0+\gamma_n}{1+\gamma} e^{\alpha d}(n + \gamma n)$$

$$(n + \gamma n) = n_0 e^{\alpha d} + \gamma n e^{\alpha d}$$

$$(n + \gamma n) - \gamma n e^{\alpha d} = n_0 e^{\alpha d}$$

$$n[(1 + \gamma) - \gamma n e^{\alpha d}] = n_0 e^{\alpha d}$$

Therefore: $n = \frac{n_0 e^{\alpha d}}{[(1+\gamma) - \gamma n\, e^{\alpha d}]}$

Or: $n = \frac{n_0 e^{\alpha d}}{1-\gamma(e^{\alpha d}-1)}$

Which in terms of Current: $I = \frac{I_0 e^{\alpha d}}{1-\gamma(e^{\alpha d}-1)}$ (Eq. 3-7)

The current becomes infinite if: $1 - \gamma(e^{\alpha d} - 1) = 0$ (Eq. 3-8)

Or $\gamma(e^{\alpha d} - 1) = 1$ (Eq. 3-9)

Since $e^{\alpha d} \gg 1$ (Normally) $\gamma e^{\alpha d} \approx 1$

From the above equations. Three conditions are possible (note a) and c) are for reference

a) $\gamma e^{\alpha d} = 1$ (Eq. 3-10)

This represents a condition when the number of ion pairs produced in the gas is sufficiently large to cause repetitions of the avalanche process.

Therefore: $\gamma e^{\alpha d} = 1$ defines the threshold sparking condition.

b) $\gamma e^{\alpha d} > 1$ (Eq. 3-11)

This represents a condition when ionization produced by avalanche is cumulative. Spark discharge grows more rapidly as $\gamma e^{\alpha d}$ rises above 1.

c) $\gamma e^{\alpha d} < 1$ (Eq. 3-12)

This represents a condition when current is not self-sustaining and I_0 stops when the source is removed.

In practice, the effects of positive ions, photons or metastable processes may contribute such that γ represents the sum of all cathode or secondary ionization effects. Additionally, γ is dependent on the work function of the cathode material. If the work function is low for the same conditions, more emissions will result. As the value of γ is relatively small at low values of E/p there will be more positive ions and photons possessing sufficient energy to cause ionization when impacting on the surface of the cathode. The influence of γ is only applicable to the Townsend breakdown mechanism whereby Eq.3-9 rationalises calculated and measured breakdown voltages and the formation predicted matches observed spark formations in formulations where *'Pd'* exceeds 1000 Torr. The Townsend mechanism is considered to be relevant at gas pressures between 0.01 to 300 Torr. Hence this mechanism is considered, from observation, to be relevant at low pressures corresponding to *pd* (gas pressure x gap distance values of 1000 Torr or less).

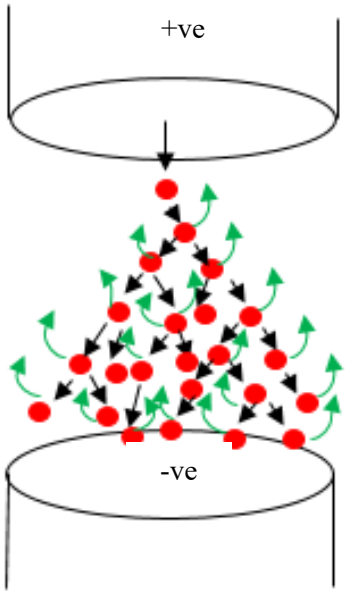

Figure F3-7: Representation of Townsend's Breakdown

3.8 THE STREAMER BREAKDOWN MECHANISM

The Townsend breakdown mechanism display some inconsistencies with observed sparking behaviour (Wadhwa, 2007), (Meek & Craggs, 1953). The Townsend process, proposes only ionization causes current growth. However, breakdown voltage was found to depend upon the gas pressure and electrode gap distance. Additionally, actual sparking occurs much faster than predicted by Townsend. In contradiction, the Townsend mechanism predicts a very diffused for of discharge which does not match the formation of sparking observed which is filamentary and irregular. Subsequently, three scientists Loeb, Raether and Meek independently proposed an alternative breakdown mechanism termed "the streamer theory". This is also known as the 'Kanal' mechanism due to a German spelling for the shape of the spark formation and pathway predicted (Wadhwa, 2007).

The streamer theory predicts the development of a spark discharge which results from a single avalanche. This develops the avalanche into a plasma streamer.

A criterion was proposed (Meek & Craggs, 1953), to estimate the electric field that converts the avalanche into a streamer where the electric field E_r produced by the space charge at radius r is given by equation Eq. 3-13:

$$E_r = 5.27\ x\ 10^{-7}\ \frac{\alpha e^{\alpha x}}{\sqrt{(x/p)}}\ \text{(V/cm)} \qquad \text{(Eq. 3-13)}$$

Where: α is Townsend's first ionization coefficient, p is gas pressure (Torr), and x is distance into which the streamer extends into the gap before converting into a plasma.

Meek proposed the minimum breakdown voltage occurs when:

The electric field $E_r = E$ and $x = d$ in Eq.3-9.

Whereby

Eq. 3-9 simplifies to: $$\alpha d + \ln\left[\frac{\alpha}{p}\right] = 14.5 + \ln\left[\frac{E}{p}\right] + 0.5\ \ln\left[\frac{d}{p}\right]\text{V/cm} \qquad \text{(Eq. 3-14)}$$

3.9 THE MEAN FREE PATH

The 'Zig-Zag' path describing the random collision path of a charged particle or electron at it moves between the positive and negative electrodes is termed 'the free path' (λ). This

is defined as: 'The distance molecules or particles travel between collisions'. The average distance between collisions is termed 'the mean free path'. This has been determined by slightly different approaches. Considering Serway's approach (Serway & Jewett Jnr, 2014).

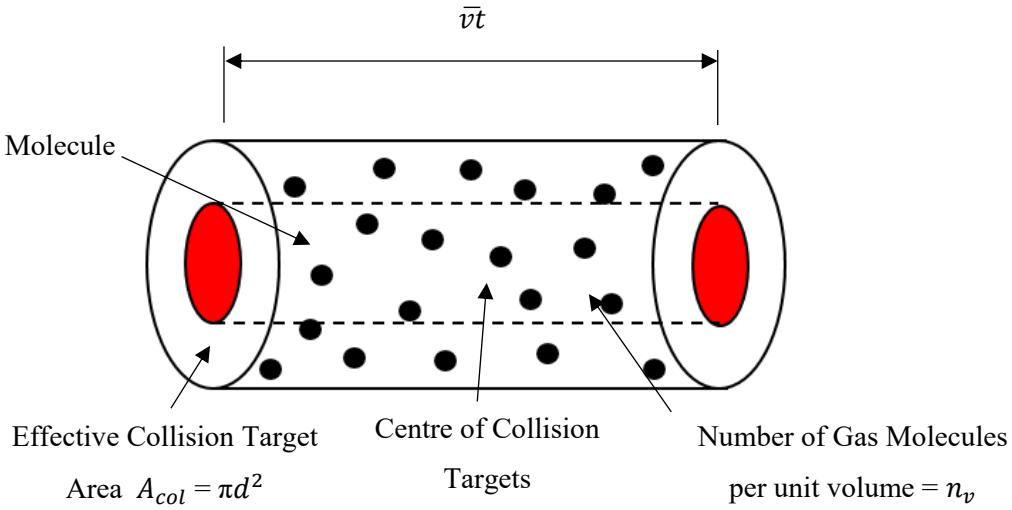

Figure F3-8: Mean Free Path Collision Volume

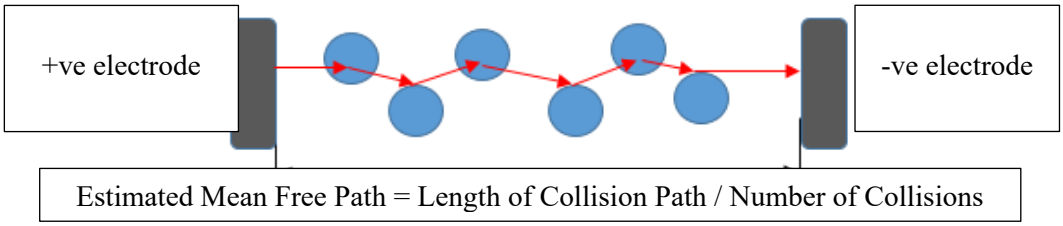

Figure F3-9: Graphical representation of the Estimated Mean Free Path

The estimated mean free path is expressed mathematically by equation Eq. 3-15

$$\text{The Estimated Mean Free Path} = \frac{\bar{v}t}{\pi d^2 \bar{v}t * n_v} \longrightarrow = \frac{1}{\pi d^2 n_v} \qquad \text{(Eq. 3-15)}$$

The effect of dynamic collisions and the relationships with 'the ideal gas law' were included by (Kuffel, et al., 2000) to calculate the Mean Free Path.

Where: The Mean Free Path: $\bar{\lambda} = \frac{RT}{\sqrt{2\pi d^2 N_A P}}$ (Eq. 3-16)

The Mean Free Path and the effect of the collisions are fundamental to the value of the Spark Break Down Voltage for any gap length, gas pressure or species. This process is described in greater detail in section 3.11.

3.10 THE SPARKING VOLTAGE

The voltage at which a spark will form in a uniform field gap, as a function of gap distance and pressure can be obtained using the Townsend criteria as given previously by equation Eq. 3-10. Which stated: $\gamma e^{\alpha d} = 1$

This expression requires using appropriate values of Townsends first and second ionization coefficients $\bar{\alpha}/p$ and γ, corresponding to values of E/p.

Hence: $\bar{\alpha}/p = f\left(E/p\right)$ (Eq.3-17)

Or: $\frac{\bar{\alpha}}{p} = \frac{k}{V}\frac{E}{p}$

Inserting: $e^{f(E/p)pd} = \frac{1}{\gamma} + 1$

Or: $f\left(E/p\right)pd = \ln\left(\frac{1}{\gamma} + 1\right) = k$

For a uniform field: $E = \frac{V_b}{d}$

Therefore: $f\left(\frac{V_b}{pd}\right)pd = k$

Or: $f\left(\frac{V_b}{pd}\right) = \frac{k}{pd}$

Or: $V_b = f\,(pd)$ (Eq.3-18)

The relationship shown by (Eq 3.18), established experimentally, is known as Paschen's Law (Paschen, 1889) which shows the Breakdown Voltage for a uniform field gap is a unique function of the product of gas pressure and a gap distance for any particular gas and electrode material. The relationship does not show that Breakdown Voltage is directly proportional to the product '*pd*' however, testing has shown a linear relationship over some ranges. The typical shape of the plotted relationship between V_b and '*pd*' is shown in Figure F3-11. For any gas, the minimum (critical) value of V_b occurs at a unique value of $pd_{min.}$

From testing of any gas and electrode gap arrangement the values of the ionization coefficient and the field strength provided by (Eq. 3-17) can be plotted to obtain a curve with a generic shape shown in Figure F3-10. The limiting value of $\left({}^{E}/_{p}\right)$ corresponds to the start of ionization as indicated.

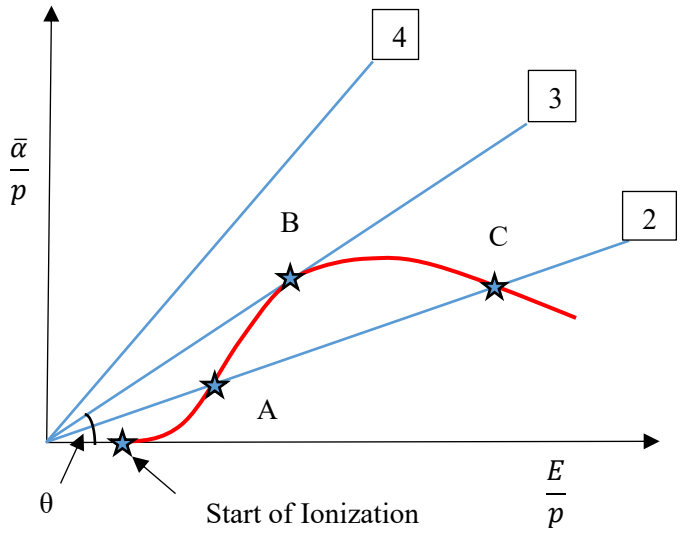

Figure F3-10: The relationship between Townsend's and Paschen's criterion

Noting the Townsend criteria may be expressed as: $\frac{\bar{\alpha}}{p} = \frac{k}{V}\frac{E}{p}$ and considering Figure: F3-10. The slope of a straight lines '2', '3' and '4' for a constant value of K depending on the value of applied voltage is given by:

$$\tan\theta = \frac{{}^{\theta}/_{p}}{{}^{E}/_{p}} \qquad \text{(Eq. 3-19)}$$

At low voltage 'V' values, there are no intersections between the curve of $\frac{\bar{\alpha}}{p} = f\left({}^{E}/_{p}\right)$ and line '4'. This indicates that at small voltages below 'Paschen's minimum' no breakdown events will occur. This relationship is valid irrespective of the values (or product of) pressure *'P'* or gap distance *'d'*.

At larger voltage 'V' values, for a given constant pressure (and gas) there must exist two Breakdown Voltages. One occurring at small values of *'P'* and *'d'* shown at intersection 'A' and the other at intersection point 'C' corresponding to the product of a larger gap and greater pressure *'Pd'*.

The tangent point at ‘B’ corresponds to the lowest ‘Breakdown Voltage’ or ‘Minimum Sparking Voltage’. The corresponding positions for points ‘A’, ‘B’ and ‘C’ on what is regarded as a typical ‘Paschen Curve’ are shown in Figure F3-11.

3.11 THE SPARK BREAKDOWN PROCESS

As previously described, the Ionization of the gases in the electrode gap is possible when the amount of energy caused by collision, electromagnetic radiation or secondary processes exceeds the ionization energy. The amount of ionization depends on the electric field strength E, and the ionizing in proportion to the mean free path $\bar{\lambda}$, (Kuffel, et al., 2000).

The collisions cause the electron’s kinetic energy to transform into potential energy by ionizing the struck molecule. This process continues as other collisions occur along the path between the electrodes. Ionization caused by this process is termed ‘ionization by collision’ and is the largest contributor to the overall process. The zig - zag path which the electrons are forced to take due to collisions with gas molecules varies in overall length in proportion to the gas pressure and hence number, or density of the gas molecules present. The individual steps between these collisions is termed ‘the free path’. The average length of the path between individual collisions is termed ‘the Mean Free Path’, shown in Figure F3-9, is a primary factor used in calculations of the overall process described.

This pathway progressively builds an ionized corridor of high electrical conductivity between the electrodes through otherwise very low conductivity gases. When the corridor is completed the two electrodes are effectively, electrically joined. At that point, electric current flows from the positively charged cathode through the ionized path to discharge its energy to earth through the negatively charged anode. The point at which the discharged electric current reaches the earthed anode completes what is termed as the spark breakdown. The voltage which is required to achieve the completion of the ionized corridor between the electrodes is termed ‘the Spark Break-Down Voltage’, from now referred to as SBDV. This voltage changes dependent on the gas or gases present in relation to the size, or mass of the gas molecules and the ease which an electron can be detached from the outer ring and the gas compressibility. If the ionized corridor is not completed, the cathode and anode electrodes are not effectively electrically ‘linked’ and the spark breakdown will not occur. However, each individual spark breakdown and hence the voltage required SBDV is an individual representation of the difficulty or effort required to create the ionized corridor.

If the number of molecules present is very small, as would occur in low pressures, towards vacuum, very little, if any, ionization would occur. Similarly, when the gap between the electrodes is reduced, the number of collisions and subsequent ionization is reduced. The number of collisions which will occur is proportional to the number of electrons moving between the electrodes and their energies caused primarily by collisions. These are increased if the voltage is increased. Similarly, fewer collisions occur if the gap between the electrodes, number of molecules is reduced and subsequent ionization is reduced. Proportionally more and more voltage is required to create a less and less likely collision with the reducing number of molecules present. This is represented graphically in Figure F3-11 at point 'A' which corresponds to the same conditions discussed previously for Figure F3-10. As the gas pressure increases, the number, or density, of gas molecules in the path of the electrons moving across the gap increases, the number of collisions and resulting ionization increases. There reaches an optimum condition, where the zig-zag path of the electrons moving across the electrode gap causes the maximum ionization. At this point the product of the acceleration of the electrons and number of collisions in which an additional ion and free electrode is produced, is maximised. At this point the total ionisation in the gap is maximised which causes the maximisation of ionization in the gap which provides the path for the breakdown and subsequent spark to occur. The voltage required and hence the number of free electrons moving between the electrodes, reaches an optimum condition in proportion to the number, or density of gas molecules per gap distance. The process is affected by temperature because associated variations of electron mobility alter the effective mean free path length. This influence is greater as the gas pressure is reduced towards vacuum (Koliatene, et al., 2011). The optimum condition where the smallest voltage is required to cause breakdown for any given product of pressure gap length is termed the 'Minimum Sparking Voltage' or is graphically represented at point 'B' in Figure F3-11.

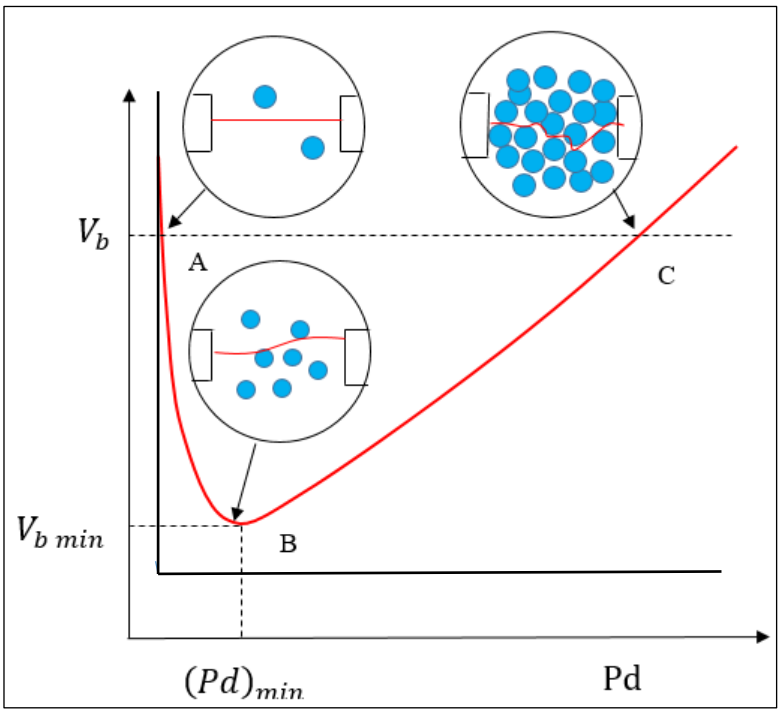

Figure F3-11: Effect of Mean Free Path variation in a typical 'Paschen' Curve

As the gas pressure is further increased, above the optimum, (if the relatively minor effects of secondary ionization γ, resulting from Cathode considerations, are neglected for values of $Pd > (Pd)_{min}$) the electrons crossing the gap collide more frequently with increased numbers (or densities) of gas molecules than at $(Pd)_{min}$ as the number or density of molecules in the gap increased proportionally. As a result, the distance between the gas molecules and the distances in the zig-zag path, which free electrons moving across the gap, becomes progressively less and less. The acceleration and hence kinetic energy which the free electrons can obtain, between collisions are proportional to their mass and velocity squared. The mass of the free electrons is small but (as they are produced from similar atoms) is overall constant for any gas. However, the achievable acceleration becomes progressively less as pressure increases. Therefore, as pressure or gap increases, in order to ionize the entire gap, progressively more voltage and hence free ions are required. The voltage needed to cause the number of collisions required to ionize the entire gap is proportional to, the molecules in any given gas, at a given pressure, or density and gap distance. Eventually, if the pressure or gap is increased, the voltage available and hence the number of free electrons moving across the electrode gap cannot cause sufficient collisions for sufficient ionization to be present in the whole gap. Hence no spark will form, the condition is represented in Figure F3-11 at 'C'.

A mathematical expression for the curve defining the 'Minimum Spark Breakdown Voltage', relating $V_b min$ and $Pd_b min$, is provided by equation (Eq, 3-10) which defines the sparking threshold: $e^{\alpha d} = 1$

As $E = {}^{V}/_{d}$

Then: $\frac{\alpha}{p} = Ae^{\left(\frac{Bp}{E}\right)}$ (Eq. 3-20)

Townsend provides: $\gamma e^{\alpha d} = 1$

Where: α– First Ionization coefficient and γ- Second Ionization coefficient

$$\alpha d = ln\left[1 + \frac{1}{v}\right] \quad \text{(Eq. 3-21)}$$

From (Wadhwa, 2007) $d = \frac{e^{{Bpd}/{Vb}}}{pA} . ln\left[1 + \frac{1}{v}\right]$

Assuming v to be constant, let $ln\left[1 + \frac{1}{v}\right] = k$ (Eq. 3-22)

Then: $d = k * \frac{e^{{Bpd}/{Vb}}}{pA}$

Paschen's relationship provides: $V_b = f(pd)$

Therefore: $d = k . \frac{e^{{Bpd}/{Vb}}}{pA}$

Multiplying both sides of by Pa and Divide by k.

We obtain: $\frac{dpA}{k} = k . \frac{e^{{Bpd}/{Vb}}}{pA} . \frac{pA}{k}$

Cancelling leaves: $\frac{dpA}{k} = e^{{Bpd}/{Vb}}$

Taking ln of both sides: $ln\left(\frac{dpA}{k}\right) = \frac{Bpd}{V_b}$

Transposing provides: $V_b = \frac{Bpd}{ln\left(\frac{dpA}{k}\right)}$ (Eq. 3-23)

Differentiating V_b w.r. to pd and equating the derivative to zero: Noting $\frac{d}{dx}n^x = nx^{n-1}$

Then: $\frac{d\,V_b}{d(pd)} = \frac{d}{d(pd)}\left[\frac{Bpd}{ln\left(\frac{dpA}{k}\right)}\right]$

Where: U = Bpd and V = $ln\left(\frac{Apd}{k}\right)$ and U^1 = B and $V^1 = \frac{k}{Apd}.\frac{A}{k}$

Then: $\frac{d}{dx}\left(\frac{u}{v}\right) = \frac{u^1v - v^1u}{V^2}$

Thus: $\frac{d\,V_b}{d(pd)} = \frac{\text{B}.ln\left(\frac{dpA}{k}\right) - \frac{k}{dpA}.\frac{A}{k}.Bpd}{\left(ln\left(\frac{dpA}{k}\right)\right)^2} = 0$

Leaving: $\frac{d\,V_b}{d(pd)} = \frac{B.ln\left(\frac{dpA}{k}\right)}{\left(ln\left(\frac{dpA}{k}\right)\right)^2} - \frac{\text{B}}{\left(ln\left(\frac{dpA}{k}\right)\right)^2}$

For minimum sparking value: $\frac{d\,V_b}{d(pd)} = 0$

Thus: $\frac{\text{B}.ln\left(\frac{dpA}{k}\right)}{\left(ln\left(\frac{dpA}{k}\right)\right)^2} - \frac{\text{B}}{\left(ln\left(\frac{dpA}{k}\right)\right)^2} = 0$

Or: $\text{B}.\,ln\left(\frac{dpA}{k}\right) * - \frac{\text{k}}{dpA} * \frac{A}{k} * Bpd = 0$

Cancelling leaves: $ln\left(\frac{dpA}{k}\right) = 1$

So that: $\frac{dpA}{k} = \text{e}$

and hence $dp = \text{e}\,\frac{k}{A}$

Therefore: $(pd)_{min} = \frac{e}{A}\,.\,\text{k}$

At: $V_{b\,min} = \frac{Be\left(\frac{k}{A}\right)}{1}$ Where: $\frac{B}{A} * ek$ Then: $V_{b\,min} = \frac{Bek}{A}$

Note: Exponential = 2.718 and k = $\ln\left[1 + \frac{1}{v}\right]$

Thus: $V_{b\,min} = 2.718.\frac{B}{A}.\ln\left[1 + \frac{1}{v}\right]$ (Eq. 3-24)

Values for the constants A and B and v are obtained by testing which enables, *(pd) min* and V_b can be obtained.

Typical values for Air (Naidu & Kamaraju, 1996) are: A = 12, B = 365, v = 0.02

A quadratic expression between $^{\alpha}/_{p}$ and $^{E}/_{p}$ was suggested, were ionization occurs in a uniform field (as in Townsend's experiments).

Where $\left(^{E}/_{P}\right)_{C}$ is the minimum value of E at which effective ionization starts, P is pressure and c is a constant (Schumann, 1923).

$$s\frac{\alpha}{p} = c\left(\frac{E}{p} - \left(\frac{E}{P}\right)_{C}\right)^{2} \qquad \text{(Eq. 3-25)}$$

In a uniform field where, $\alpha d = k$ and $k = \left(1 + {}^{1}/_{v}\right)$

Townsend's spark criteria being: $\frac{k}{dp} = c\left(\frac{E}{p} - \left(\frac{E}{P}\right)_{C}\right)^{2}$

Or: $\frac{k}{c} \cdot \frac{1}{dP} = \left(\frac{E}{p} - \left(\frac{E}{P}\right)_{C}\right)^{2}$

Or: $\left(\frac{k}{c} \cdot \frac{1}{dP}\right)^{\frac{1}{2}} = \frac{E}{p} - \left(\frac{E}{P}\right)_{C}$

Or: $\frac{E}{p} = \left(\frac{k/c}{dP}\right)^{\frac{1}{2}} + \left(\frac{E}{P}\right)_{C}$ (Eq.3-26)

Where: $E = \frac{V_b}{d}$

Then: $\frac{V_b}{d} = \left(\frac{k/c}{dP}\right)^{\frac{1}{2}} + \left(\frac{E}{P}\right)_{C}$

Hence: $V_b = \left[\left(\frac{k/c}{dP}\right)^{\frac{1}{2}} + \left(\frac{E}{P}\right)_{C}\right] \text{pd}$

And: $V_b = (k/C)^{\frac{1}{2}} \cdot \frac{1}{pd^{\frac{1}{2}}} \cdot \text{pd} + \left(\frac{E}{P}\right)_{C} \cdot \text{Pd}$

Or: $V_b = (k/C)^{\frac{1}{2}} \cdot (pd)^{\frac{1}{2}} + \left(\frac{E}{P}\right)_{C} \cdot \text{Pd}$

Where: Constant 'B' = $\left(\frac{k}{C}\right)^{\frac{1}{2}}$ and Constant 'A' = $\left(\frac{E}{P}\right)_{C}$

Min. Spark Breakdown Voltage: $V_b = (k/C)^{\frac{1}{2}} . (pd)^{\frac{1}{2}} + \left(\frac{E}{P}\right)_C . \text{Pd}$

$$V_b = B\sqrt{pd} + \text{A}(pd)$$

Or: $$V_b = \text{A}(pd) + B\sqrt{pd} \quad \text{(kV)} \qquad \text{(Eq. 3-27)}$$

Values for constants 'A' and 'B' for Air $(\text{p} = 1 \text{ bar @ temperature} = 20 \text{ deg. C})$. Have been suggested by (Wadhwa, 2007). Reference values for 'A' and 'B' constants for the formulation, Eq. 3-27 were given by (Sohst, 1962) and Schroder (Schoder, 1961).

Where for Constant 'B': $K/C = 45.16 \ {(kV)^2}/{cm} \quad 'B' = \sqrt{\frac{K}{C}} = 6.72$

And for Constant 'A': $E_c = 24.36$ kV/cm = 'A'

Thus Providing: $$V_b = 24.36(pd) + 6.72\sqrt{pd} \text{ (kV)} \qquad \text{(Eq. 3-28)}$$

The work which provides the relationship between spark breakdown voltage, pressure and gap length was carried out in the late 1800, early 1900's. This work was primarily interested in the behaviour of high voltages for the 'new' electricity generation and distribution industry. Therefore, the focus was the behaviour in air in atmospheric conditions (at 20º C and in a pressure of 760 mmHg), produced by voltages applied at 50Hz for gaps up to 12cm.

To maximise the accuracy of the influence of the gas and gap length the experiments used large spherical electrodes of various radii and large gaps. The use of large radius electrodes sought to avoid the influence of locally intensified fields which would reduce the breakdown voltage. Such fields are termed 'uniform fields'. The spherical shape was later improved and optimised and tests typically used specially shaped electrodes of 3 different diameters, 8.5, 18 and 45cm (Rogowski & Rengier, 1926).

Tests, with an estimated accuracy of +/- 0.8% which resulted in a uniform distribution of electrical charge on the electrode surfaces. Where V= Breakdown voltage, d = Electrode gap (cm). The results were expressed by the following relationship presented by Ritz (Ritz, 1932).

$$V_b = 24.55d + 6.66\sqrt{d} \text{ [kV]} \qquad \text{(Eq. 3-29)}$$

Later, (Holzer, 1932) used a single Rogowski profile electrode of 60 cm diameter in similar conditions in Air. The results were expressed by the following relationship:

$$V_b = 23.85d + 7.85\sqrt{d} \text{ [kV]} \quad \text{(Eq. 3-30)}$$

Later again, (Bruce, 1947) increased the accuracy of the breakdown voltage calculation down to approximately 0.15% using Rogowski profile electrodes of 5.7, 11.2 and 19.8 cm diameter in similar conditions in Air. The results were expressed by the following relationship:

$$V_b = 24.22d + 6.08\sqrt{d} \text{ [Kv]} \quad \text{(Eq. 3-31)}$$

The Breakdown Voltages obtained by the three researchers are summarised in Table T3-2. Note the spark gap distances are large in relation to a typical spark plug gap < 1mm.

Table T3-2: Comparison AC Breakdown Voltages in uniform fields in Air @ 20°C & 760mm Hg of Breakdown Voltage (kV) Testing

Gap	Researcher / Breakdown Voltage (kV)		
(cm)	Ritz	Bruce	Holzer
1	31.35	30.30	31.66
2	58.70	57.04	61.20
3	85.80	83.19	86.94
4	112.00	109.00	113.04
5	138.50	134.70	137.80
6	163.80	160.20	163.44
7	189.00	185.60	187.74
8	215.00	211.00	212.88
9	240.00	236.30	237.78
10	265.00	261.40	263.00

More recent of sphere gap voltage measurements (Sankar, 2011), (Karmakar, 2012), have provided the more elaborate mathematical expression given below in Eq. 3-32. The results of the testing by Karmakar are shown in Figure F3-12, which show an accurate correlation between Spark breakdown voltage and air pressure.

$$\text{Vs (Air)} = \left(\frac{27.2\delta r\left(1+0.\frac{54}{\sqrt{\delta r}}\right)\frac{S}{r}}{0}\right) * 2S\left(\frac{S}{r} + 1 + \sqrt{\left(\frac{S}{r}+1\right)^2 + 8}\right) \quad \text{(Eq. 3-32)}$$

Where: Vs (Air) = Spark Breakdown Voltage in Air. r = the sphere electrode radius (cm), S = The gap distance between spheres (where the electric field between the gap is $^{V}/_{d}$ in which d is gap between electrodes (cm), δ is the Air density factor = $293b$ / $760(273+t)$, b = air pressure (mmHg) and t = air temperature (°C).

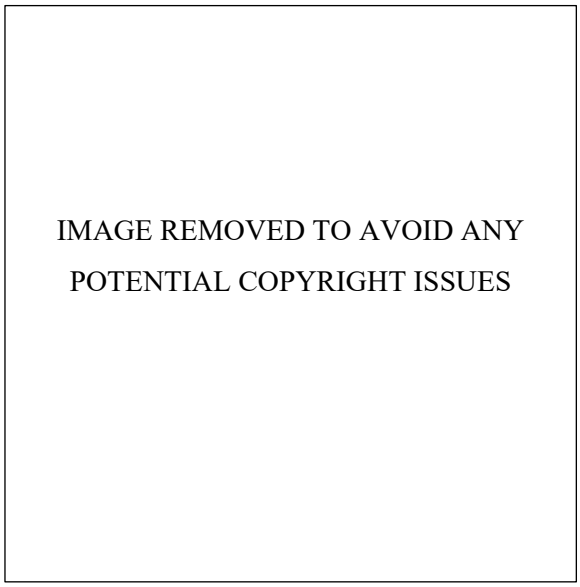

Figure F3-12: Experimental vs Calculated SBDV for Sphere Gap in Air (Karmakar, 2012)

3.12 SBDV CORRECTION FOR AMBIENT CONDITIONS

The effect of gas density variations relating temperature, pressure as represented by changes to ambient conditions required compensation from 'standard' values. This was provided by equation Eq. 3-33. (Wadhwa, 2007).

$$\delta = \frac{3.92\ b}{273+t} \qquad \text{(Eq.3-33)}$$

Where: b is atmospheric pressure in cm of Hg and t (the temperature) deg. C

The influence of density for ρ = 0.8 – 1.0. where 1.0 corresponds to Air @ 20°C & 760mm Hg was studied by Ritz and Holzer which provided the following modification of their equations for density:

Ritz: $$V = 25.55d + 6.66\sqrt{(\rho d)}\ \text{[kV]} \qquad \text{(Eq. 3-34)}$$

Holzer: $$V = 23.85d + 7.85\sqrt{(\rho d)}\ \text{[kV]} \qquad \text{(Eq. 3-35)}$$

The electrodes used were spheres manufactured from either Brass or Copper machined to different radii, typically between 1 to 5.5 cm, although diameters up to 200cm were used. It should be noted the objective of the testing carried out by these researchers was to use the sphere gap method to measure the value of electrical discharge [kV] rather than to identify gases. The spherical electrode arrangements used by these researchers are termed 'uniform' as they do not lead to concentrations of ionic formation behaviour which occur with sharp edged electrodes termed 'non-uniform'. This explains the reason why large radii, spherical shaped electrodes and large gap distances were used for 'classic' or 'standard' tests which emphasised the voltage measurement and diminish the influence of the electrodes.

The published expressions provided by three researchers relating spark break-down voltage and the pressure of Air, is provided below. These are repeated from chapter three for the reader's convenience. The expressions include values for 'A' and 'B' constants which relate to empirically derived characteristics of the electrodes used.

$$V(Air)_s = Apd + B\sqrt{pd} \qquad \text{(Eq. 3-36)}$$

The constants derived by the researchers can be noted as being slightly different. It will be seen from comparison with SBDV results, the differences in theses constants used may have been the alterative use of Peak or Mean spark break-down voltage values.

(Ritz, 1932) $$V_s(Air) = 24.55pd + 6.66\sqrt{pd}\ \text{(kV)} \qquad \text{(Eq. 3-37)}$$

(Holzer, 1932) $$V_s(Air) = 23.85pd + 7.85\sqrt{pd}\ \text{(kV)} \qquad \text{(Eq. 3-38)}$$

(Bruce, 1947) $$V_s(Air) = 24.22pd + 6.08\sqrt{pd}\ \text{(kV)} \qquad \text{(Eq. 3-39)}$$

The expressions relating spark break-down voltage to air pressure were modified by the respective researchers to relate spark break-down voltage to Air density. The reported accuracy given by Ritz = 0.8% and Bruce = 0.15%.

(Ritz, 1932) $$V_s(Air) = \left[24.55 + 0.41\left(\frac{e}{10} - 1\right)\right]\rho d + 6.66\sqrt{\rho d}\ \text{(kV)} \qquad \text{(Eq. 3-40)}$$

(Holzer, 1932) $$V_s(Air) = 23.85\rho d + 7.85\sqrt{\rho d}\ \text{(kV)} \qquad \text{(Eq. 3-41)}$$

(Bruce, 1947) $$V_s(Air) = 24.22\left[\frac{293pd}{750T}\right] + 6.08\sqrt{\left[\frac{293pd}{750T}\right]}\ \text{(kV)} \qquad \text{(Eq. 3-42)}$$

Later a different expression was provided by Cobine (Cobine, 1958), provided an expression for air which relates to pressure for a sphere (uniform) gap distance of 0.1cm.

Where: $V_s(Air) = 30\mathrm{d} + 1.35$ (kV) (Eq. 3-43)

Correction factors for relative air density were provided for standard sphere gap testing such as those shown in Table T3-3 below. The tabulated correction values were multiplied by the spark break-down voltage to account for the effects of air density.

IMAGE REMOVED TO AVOID ANY POTENTIAL COPYRIGHT ISSUES

Table T3-3: Relative Air Density variation using Standard Spheres (Karmakar, 2012)

3.13 THE INFULENCE OF HUMIDITY

Thomson found, later clarified by Warburg (Warburg, 1896), the potential difference in extremely dry still air was up to three to four times than if less dried gas is used (Thomson, 1908). The effects of humidity in air on breakdown subjected to high AC voltages were investigated by (Winkelnkemper & Baucke, 1969). Similarly, the effects of humidity in air on breakdown subjected to high DC high were investigated by (Peschke, 1969) which work showed humidity does affect the breakdown voltage, but the measured variation depends on the electrode configuration. Feser, observed that if breakdown occurs without 'pre-breakdown' the effect of humidity on breakdown is slight (0.25% / gr/m). However, impulse-like pre-breakdown glow corona precedes the breakdown at the positive electrode

and is greatly influenced by humidity and has been found to have a linear relationship with pressure (Guindehi. S, 1970), (Feser, 1972).

Impulse-less glow corona being described as a form of discharge which can be observed in AC and DC voltages particularly at sharp edges and on thin wires confirmed breakdown voltage in a nonhomogeneous field (as is the case with all spark plugs) is influenced by the absolute humidity. However, the observation was conditionally obtained from impulse-less glow corona. Feser, predicted the reduction of breakdown voltage as humidity increases could lie in the absorption of photons the breakdown characteristics or rod gaps are influenced by humidity, the effect depending on the form, polarity and over-breakdown voltage this is consistent to correlate breakdown voltage data the measure values are corrected to a standard humidity of 11 grams of water per cubic meter of air, corresponding to a relative humidity of 64% at 20°C

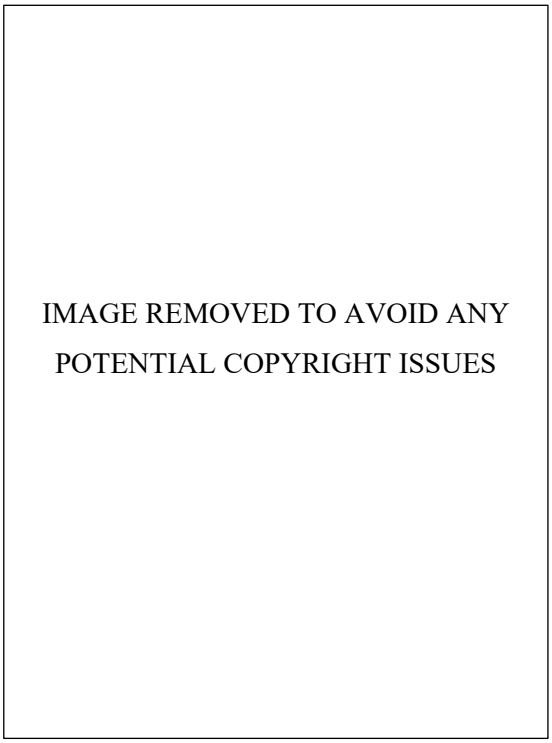

Figure F3-9: Correction factor Spark Breakdown Voltage vs Absolute Humidity (Rod-gaps: +/-1/50, +/- 1/5 and 50Hz)

3.14 THE INFULENCE OF ELECTRODE SHAPES

As the focus of standard High-Voltage testing is the accurate measurement of the voltage, accurately machined spherical electrodes are used which minimise the influence on all except the voltage itself. Use of parallel plates as electrodes, creates a problem whereby the electrical stresses at the edges of the plate are significantly greater than those required to be the working section. This localised increased electrical stress causes high localised fields which encourage ionization and subsequent break-down, to occur preferentially at the edges. Thus, the edges of the plate are non-uniform. For accurate voltage measurement, the highest electrical stress should be present in the homogenous field, where the plates are parallel and the gap length is constant. A scientist named Rogowski conceived a profile shape which has curved edges such that the field strength at the curved edges never exceeds the value of:

$$H_0 = \frac{2g}{\pi} (\omega + 1 + e^{\omega})$$

Where: V = The applied voltage and 2g = the distance between the parallel plates.

The 'Rogowski' profile shape has been used in spark gap testing as it is more convenient to manufacture and is more space efficient than spherical electrodes. Ostiguy noted the Rogowski profile can be defined as "the profile which makes the vertical component of the flux density in the pole, constant along the pole surface", (Ostiguy, 1993).

The uniform shapes used for spark gap voltage measurements are typically not those found in practical engineering installations. Therefore, the influence and effect of 'non-uniform' electrodes on the value of spark breakdown voltage has the subject of considerable research. Testing has determined spark breakdown voltage values for a great variety of rod to rod profiles and rod to plate profiles with different radii, gaps and sharpness. This has informed electrical engineers concerned with the safe distance required between high voltage equipment made with objects with squared or sharp edges (Karmakar, 2012), (Mc Allister, et al., 1989), (Bregnsbo, 1979). These concerns include testing to understanding of how atmospheric lightning is preferential attracted to sharp objects (Sigmond, et al., 2004).

Early observations of electrical current in a spark gap noted that even with uniform electrodes the electrical field is not uniform, but larger at one or both electrodes (Thomson, 1860). Other early work (Faraday, 1844), found that when electrodes of differing sizes are used, the spark potential varies if the smaller electrode is positive or negative. Overall, it is easier to initiate a spark in a gap with a strongly non-uniform distribution of electric field between the electrodes, because this requires a lower voltage (Aleksandrov & Bazelyan,

1999). This behaviour has significant influences on the spark breakdown voltage characteristics of spark plugs design and the development of their electrode developments.

3.15 THE INFLUENCE OF FREQUENCY

The value of a sparking voltage was noted by Faraday to reduce significantly if a spark had passed across the gap within a few minutes and a considerably lesser voltage is required to keep up the sparks once started (Faraday, 1844). This was investigated and by later research which found the value of spark breakdown voltage has been found to be reduced if applied at a frequency of 60kHz, (Clark & Ryan, 1914), (Reukema, 1928), (Brown, 1951), (Biswas & Mitra, 1979). The effect of application of voltage within 'radio frequencies' was specifically investigated (Oler, 1954).

3.16 SPARK BREAKDOWN VOLTAGE IN GASES OTHER THAN AIR

Different gases (from Air) are known to have different dielectric strengths and these values change with pressure, (Hayashi, 1914), (Cobine, 1958). It is known that the value of the SBDV varies proportionally to the gas density and is also dependent on the gas species (Meek & Craggs, 1953), (Townsend, 1915).

SBDV relationships with different gases both pure (Cobine, 1958), (Hayashi, 1914) and combustible mixtures, (Patterson & Campbell, 1919), have been determined by physicists working in laboratories. These relationships vary predominantly with the gap distance between the electrodes but also with electrode geometry, material, surface condition and temperature (Naidu & Kamaraju, 1996).

Despite the difference of detailed interest, the fundamental processes are shared irrespective of gap distance. For example, Pedersen (Pedersen, 1989), noted, greater concentrations of electronegative gases (of which Oxygen is one), places greater limits on electrode non-uniformity. This translates to potential inaccuracies or signal reliability as oxygen levels increase.

The mathematical expression for the relationship between spark breakdown voltage and pressure for various gas were developed and found to form the second order polynomial format following that for air. However, various researchers offer slightly different variables (Meek & Craggs, 1953) and 'Paschen' curves for each gas is different (Cobine, 1958), (Stumbo, 2013). The relative values for the dielectric properties of some common gases in terms relative to Air as shown in tables T3-4, 5 & 6.

Table T3-4: The dielectric properties of gases (Cobine, 1958)

IMAGE REMOVED TO AVOID ANY POTENTIAL COPYRIGHT ISSUES

Table T3-5: Relative Spark Breakdown Strength of Gases (Cobine, 1958)

IMAGE REMOVED TO AVOID ANY POTENTIAL COPYRIGHT ISSUES

Table T3-6: SBDV (kV) vs Gap (sphere) distance (Cobine, 1958)

IMAGE REMOVED TO AVOID ANY POTENTIAL COPYRIGHT ISSUES

3.17 CHAPTER SUMMARY

This chapter provides a basic introduction to the theories concerning how the dielectric properties of gases overcome by the application of electrical energy. The present work is not concerned on exactly how the breakdown occurs, whether by Townsend, Streamer or other mechanisms. The theories of how ionisation and breakdown occurs are however, directly transferable to the gases and conditions in an engine. The relative dielectric properties of gases other than air were noted.

The chapter provides a background to the 'classic' testing procedures used to derive relationships between 'spark break-down voltage' (V_s) and the product of pressure and gap distance *'Pd*'. It was noted these results were obtained using the standard sphere gap method using brass or copper spheres or special uniform electrode shapes which deliberately negated the effect of electrode shapes. The mathematical basis for the derived relationships was provided together with coefficient values from published information. Text book commentary, (Meek & Craggs, 1953), (Naidu & Kamaraju, 1996), (Thomson, 1908), (Wadhwa, 2007), consistently notes these parameters should be determined by testing due to the significant influence of the electrodes used.

This chapter shows that proven relationships between spark breakdown voltage and pressure in various gases had been demonstrated but these were dependant on electrode

variables. Notably, the electrode shapes of spark plugs are ‘non-uniform’ and formed from materials which are known to have significantly influence on the ionization process.

This provided the justification for testing to determine the mathematical relationships between spark breakdown voltages and the gases in the cylinder of an engine using spark plugs.

CHAPTER FOUR

THE TEST APPARATUS

4.0 INTRODUCTION

This chapter presents and describes the three items of test apparatus purposely designed and manufactured for the present work, to investigate high frequency spark breakdown voltage applied to spark plugs. The apparatus described enabled calibration tests of air and other gases at different pressures in static conditions and separate tests of air and exhaust gas mixtures in dynamically conditions. The items manufactured and used for testing consisted of the items listed below:

1) A prototype electronic SBDV system. (Figure F4-2)
2) A constant volume chamber in which spark breakdown events were obtained in various gases in controlled steps of static pressure. (Figure F4-12)
3) A dynamic sparking chamber in which spark breakdown events were obtained in air and exhaust gas mixtures. A motored test engine was used as the test chamber with a separate auxiliary engine used to supply exhaust gases. (Figure F4-19)

4.1 THE NEW SPARK BREAKDOWN VOLTAGE CIRCUIT

A new electronic circuit was developed which generated the spark breakdown events for these tests. Instrumentation was added to enable the monitoring and capture of relevant information for post-test analysis which is described in later chapters of this work. The electronic circuit used for the testing was based on an arrangement presented by (Martychenko, et al., 1999) which was described in Chapter two. The new circuit was developed to use the same principles applied in a different manner and purpose, as specified by the author, in a collaborative effort, with a specialised automotive electronics company 'GEMS Ltd'. The new spark breakdown voltage circuit was designed and developed to meet two primary objectives.

A) To provide voltage peaks at a frequency which would enable the gases in the cylinder to be sampled during a small period of crankshaft movement during the early stage of closed cycle compression.

B) To provide a spark voltage which would achieve reliable 'Breakdown' events for the range of gas pressures which would occur during the required crankshaft period and gas conditions likely to occur.

4.1.1 THE SPARKING FREQUENCY

As previously described, for cycle by cycle combustion control to occur, the amount of combustible gases trapped in the cylinder of an engine must be determined during the early stage of each closed cycle compression. In a two-stroke cycle type engine this period is limited due to the completion of a combustion cycle during each rotation of the crankshaft. Following the closure of the exhaust port, typically at approximately 95 º BTDC the period of closed cycle of compression is short. In a directly injected engine, this period must include the determination of the fuel quantity to be injected and subsequently supplied.

In a closed cylinder during the early stage of compression, the mixture of gases may be considered constant, however the pressure will increase as the piston ascends. The compression of the trapped gases will cause the gas temperature to change and would be expected to increase. The temperature of the gases at the start of each compression period can be expected to vary depending upon the relative masses of fresh and residual burned gases present. Additionally, a generally slower temperature variation will occur due to heat transfer from and to the piston and surrounding cylinder.

Based on these limitations, the period of crankshaft movement over which spark breakdown sampling of the trapped gases could be obtained was assumed, for the present work, to be 10 Degrees. It was assumed that during the 10 Degree period of crankshaft movement, a minimum of 10 samples would be required to describe those gases and conditions. The maximum engine speed at which such sampling would be required was assumed to be 15,000 rpm.

Thus, the frequency / sample rate required was:

$$15{,}000\ rpm = \frac{15000}{60} = 250\ rps$$

$$or\ 250 * 360 = 90{,}000\ \ spark\ breakdown\ events/s$$

This arrangement provided the minimum frequency = 90 kHz which is believed to operate ≈ 90 times faster than the circuit presented by (Martychenko, et al., 1999).

4.1.2 THE SPARKING VOLTAGE

The second design objective for the new SBDV circuit was to achieve a voltage which would be sufficient to create a spark between the electrodes of a spark plug at a suitable maximum cylinder pressure.

The spark breakdown electronic circuit used in previous work, described in chapter two, proved able to break-down the in-cylinder gases through entire engine cycles up to a quoted, in-cylinder pressure of 6.5 MPa (65 bar or 942.745 psi). This met the requirements of those workers which was to use SBDV to replace a combustion pressure sensor working in associated high pressures. However, unlike previous work the present work is differentiated because it is required to only collect pressure data for the first 10 Degrees of closed cycle compression hence a considerably lower maximum pressure would be sufficient for this range. Further, the test apparatus, described later in this chapter, would provide gases at or close to ambient pressure.

It was known the SBDV reduced as gas temperature increased (Meek & Craggs, 1953). Hence it was realistically expected that whatever crankshaft rotation angle breakdown was achieved at ambient temperature, the crankshaft rotation angle over which Spark Breakdown Voltage signals could be obtained, would increase in a hotter operating engine as gas density decreases. Therefore, the second design objective was to achieve dielectric breakdown in air at approximately 2 bar at ambient temperature. These objectives were met using the electronic circuit shown in Figure F4-2.

The breakdown voltage required to initiate ignition had also been shown to relate to burned Air/Fuel ratio and burned gases concentration (Han, 1997). Han used the ignition spark with the engine operating at 2,500 rpm which represents a spark frequency of 2500/60 = 41.66 spark break-down events/sec or 0.041 kHz.

Continuous sparking in a cylinder full of a combustible mixture of gases is likely to cause ignition which must be avoided. In order to initiate combustion by an electrical spark, there has to be sufficient energy in the electrical spark to overcome the loss of heat to the surroundings leaving enough to initiate the chemical process termed combustion (Craver, et al., 1970), (Daniels & Scilzo, 1996), (De-Soete, 1983), (Lee & Boehler, 2005). This minimum sparking energy varies with gas pressure, temperature and Air/Fuel ratio proposed a minimum ignition energy of 0.3mJ (Silsbee, 1925).

The maximum energy E_{sp} available per spark was calculated by (Martychenko, et al., 1999), using equation Eq.4-1. This calculation used a value of 5pF for the stray capacitance C_{sp} in the spark plug and connecting High Tension (HT) ignition leads and plug cap. A value of 7kV was assumed as a characteristic breakdown voltage V_s value in typical conditions in the cylinder.

Where: $$E_{sp} = \frac{C_{sp} * {V_s}^2}{2} = \frac{5*10^{-12} * (7* 10^3)}{2} \approx 0.12 * 10^{-3} \text{ J} \quad \text{(Eq. 4-1)}$$

It was noted this value was well below 0.3 mJ especially when taking into account the full value for stray capacitance would not be available. The work also considered the sparking events, occurring at 1kHz to be individual events with no addition of residual heat contributing to the heat from subsequent sparks.

It was considered unlikely to be the case if the same spark energy was delivered at 94kHz. However, the energy delivered per spark used in the new SBDV electronic circuit was limited by the components used.

If the proposed SBDV system is used in combination with direct injection, as described in Chapter three, the cylinder will not be full of a combustible mixture. Additionally, the proposed system will be turned off after 10 degrees of compression following the closure of the exhaust port. At this point the contributing effects of increased pressure and temperature are not significant additions.

4.1.3 CRITICAL SPARKING FREQUENCY

The new SBDV circuit output generated is AC but with the breakdown heavily negatively biased to DC. This differed from the standard spark breakdown voltage testing carried out using DC generation. In the presence of an AC field, relatively few of the energised particles formed in the breakdown attach to the electrodes and remain active in the electrode gap.

Where high frequency events are generated, this improves the efficiency of successive breakdowns by limiting the secondary generation of electrons generated by ion impacts with the electrode. This is an important difference to the breakdown process using DC discharges where (Brown, 1951) noted the ionization processes “are hence limited primarily to diffusion” and observed that in an AC field, other phenomena occur apart for diffusion, such as recombination and attachment. Therefore, the AC voltage form was expected to require less voltage to cause breakdown events than if a DC form was used.

Other researchers observed the voltage required to ignite a fresh plasma is significantly higher than the succeeding, re-breakdown, voltages operating in the continuous mode (Nam, et al., 2011). The effect of Breakdown frequency has been investigated with much concentration of values in Mc/s (Pim, 1948), (Brown, 1951), (Chu, 1992). Work which investigated a lower range of frequencies between 20 kHz to 425 kHz in gap distances up to 25mm, observed there was not much change in the Breakdown Voltage versus frequency (from individual events), until the frequency approaches 20 kHz. there is a gradual decrease in the range between 20 - 60 kHz above which there is little change up to 425 kHz (Reukema, 1928).

The gap distance and Breakdown frequency are related to each other such that both are optimised at 'critical values'. This relationship was not investigated in the present work and these values or the effect of the interaction between them is unknown. However, the following formula relating 'the critical gap' at a given frequency is provided by (Chu, 1992) which was noted to match that provided earlier by (Pim, 1948).

$$g_{ce} = \frac{2KE}{7wp}\left[6 - \sqrt{15 - \frac{21p^2B_0}{AE^2}}\right] \quad \text{(Eq. 4-2)}$$

Where:

k = a proportional factor between velocity and E/p

$v = k\,E/p$ (k = 3.9x 10^5 (cm/sec), (mm Hg) and (V/cm)

E = Peak Electric Field (V/cm)

$w = 2\pi f$

p = Gas pressure (mm Hg) (p = 760mm Hg @ Atmospheric pressure)

B = Loss Coefficient representing electron loss due to recombination, radial outward spread of electrons, B = 0.0116 in DC conditions. B = 0.0133 @ atmospheric pressure and E = 34 Kv/ cm^3. B is proportional to gas pressure. B assumed to be 0.01333

A = An empirical value = 1.58 x 10^{-5} (mm Hg) / $(V/cm)^2$

SBDV CIRCUIT DETAILS

The SBDV circuit developed for the present work, consists of three sections. These are shown together in Figure F4-2.

The new SBDV circuit functions in the following manner. In the first input regulator section, from a 9 pin D-Type connector and a 12 Volt source, current passes through a Linear Voltage Regulator via Diode D1. Both sides of the regulator are protected by earthed high and low value capacitors which help to filter out undesired electromagnetic pulses.

The 5 Volt output from the regulator then feeds into the second section of the circuit which forms an oscillator in which the high frequency is produced by a relaxation oscillator system using NAND U1A, which is maintained in 'ON' state, by resistor R3. Capacitor C6 then charges up, when its voltage exceeds the 'ON' voltage of NAND U1A its output pin3 turns low. This starts to discharge C6 when the voltage drops below the 'OFF' voltage the output of NAND U1A goes back to high restarting the cycle.

The charging and discharging rates are controlled separately by the two arms; R2 D4 for charging, R1 D2 for discharging. The circuit 'self oscillates' at a frequency equal to the inverse of the sum of the charge and discharge mark space ratio times which in this case is set to 90kHz. The two rates adjusted to a 30%/60% ratio by varying the values of resistors R1 and R2. The oscillating signal is converted into a square waveform by the Schmitt trigger as shown in Figure F4-1.

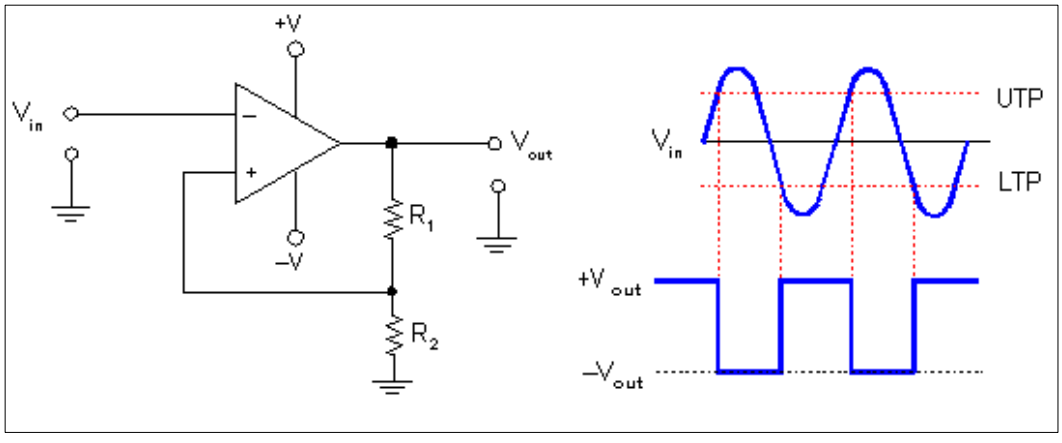

Figure F4-1: The function of a Schmitt trigger

The signal then passes through three additional Schmitt triggers. These are configured to speed up testing with an external signal applied to the OVERRIDE pin if the function 'DISABLElow' is activated. The signal is presented to pin 2 input of a High-Power Driver, decoupled by dual value capacitors C3 C8. The signal that exits the High-Power Driver at pin 4, is typically 12 Volts and passes on to the third 'power' section of the circuit through a resistor R7 to the switch function of a transistor.

The third section of the circuit is separately powered with 12 Volts through a 3amp fuse F1 to pin 1 of the 250:1 turns ratio Transformer T1 which exits at pin 2 and is earthed by the transistor switch (driven at 90kHz). The transformer produces an AC voltage output but with a negative DC voltage bias. When the transistor is turned on by the driver signal, a low positive voltage occurs across the transformer. When the transistor is turned off, a high negative voltage, termed as a fly-back voltage, is created by the collapse of the field in the primary winding of the transformer between pins 1 and 2.

The transformer was found during bench testing to produce the most energy when in resonance with the whole circuit including the plug leads, cap and plug. A high tension (HT) cable is routed from the negatively charged step up side of the coil (Pin 3) to the spark plug which is earthed through the body of the engine. Measurement of the output voltage signal was obtained via a screened branch of the HT cable that is routed to a BNC connector with a resistive divider consisting of two resistors R8 (50MOhm) and R9 (10kOhm). This arrangement provided a voltage signal at a 5001:1 ratio to enable safe connection directly to the PICOSCOPE 4824 oscilloscope.

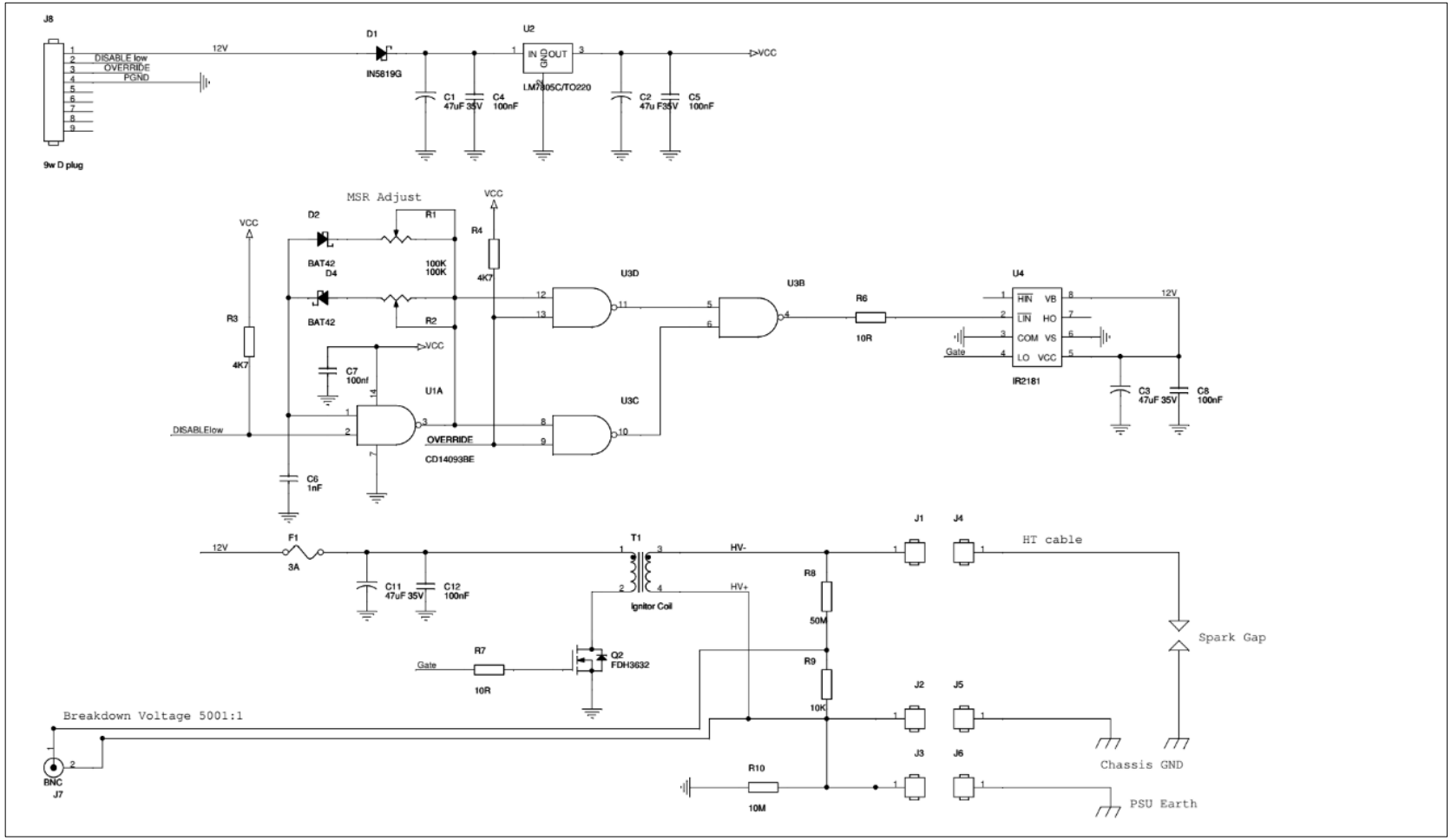

Figure F4-2: The new SBDV circuit developed, manufactured and used for Thesis testing

4.2 RECORDING OF THE SPARK BREAKDOWN EVENTS

The spark breakdown voltage events produced by the new SBDV generation circuit were captured as individual events via the measurement branch of the new electronic circuit, using a PICOSCOPE 4824 high speed oscilloscope shown in Figure F4-3. As previously described the overall SBDV signal was formed by separate SBDV events which were generated at approximately 94kHz.

The Nyquist limit imposes to record the signal using a frequency at least double of the characteristic one (in this case ~ 190 kHz); however, to implement the accuracy the maximum recording frequency was used instead. Since the PICOSCOPE 4824 unit is capable of simultaneously recording 8 channels each at a maximum sampling frequency of 10MHz or 10k samples per millisecond. This allowed the SBDV signal for each event to be defined by:

$$\frac{10{,}000{,}000}{94{,}000} \approx 106 \text{ datapoints per spark events}$$

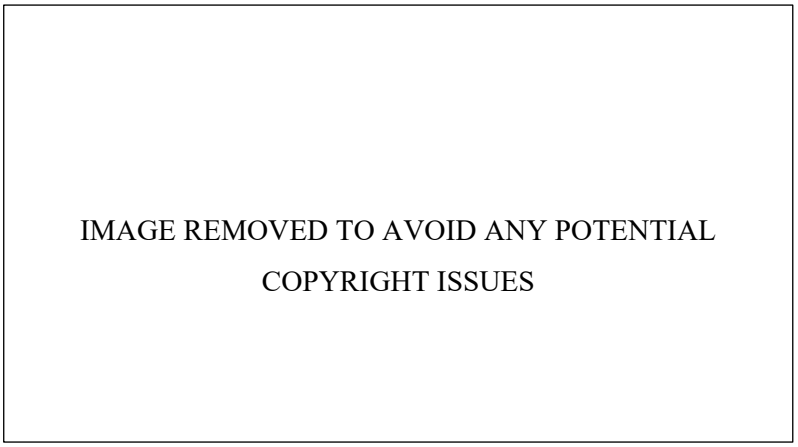

Figure F4-3: The Picoscope 4824 - 8 Channel Oscilloscope unit

The work carried out to investigate the breakdown voltage signal and associated behavior when used in spark plugs is reported in Chapter 6. The 0 - 5V output signal from the SBDV circuit was fed via the RS232 port connection into one channel of the PICOSCOPE 4824. Initially, the performance of the output from the SBDV circuit and the detail that would be produced was unknown. Therefore, a second comparative signal from the new SBDV circuit was gathered by a standard Picoscope automotive application accessory. This item

(Picoscope Part No. PP178) shown in Figure F4-4, was clipped over the HT close to the SBDV circuit box and connected directly to the PicoScope 4824 unit to provide an additional direct HT voltage measurement.

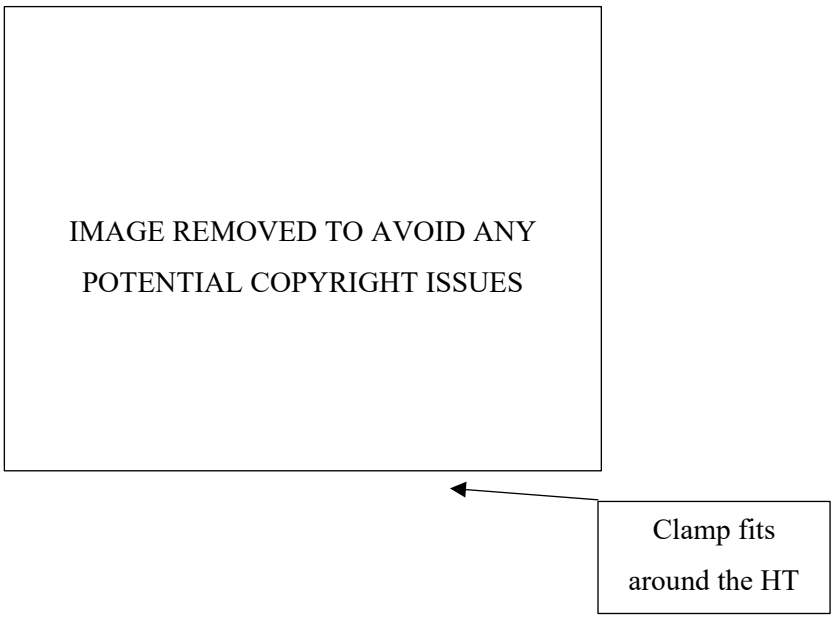

Figure F4-4: Direct inductive HT measurement - Picoscope Part No. PP178

The SBDV events, using two different systems, were recorded synchronously on two separate channels which allowed direct visual and functional comparison. The channel recording the signal from the SBDV circuit was assigned the colour GREY on the PICOSCOPE screen. The second channel from the inductive clamp around the HT lead, was assigned the colour PURPLE on the PICOSCOPE screen. Testing showed a close correlation between the two signals. Therefore, the output signal taken directly from the SBDV electronic circuit was focused on and used for analysis of the breakdown voltage events for the testing reported in the present work.

4.3 BENCH TESTING OF THE NEW SBDV CIRCUIT

The break-down process is known to be influenced by the abundance of residual ions in the gap during previous breakdown events (Kuffel, et al., 2000). It was not known if and by how much, the high frequency of breakdown events produced by the new SBDV system would affect the voltage required. Previous work reported the voltage required for a single breakdown event in air, is reduced by 13% at frequencies of 60,000 cycle/sec and above, (Reukema, 1928). However, the existing data was obtained using a Poulsen arc generator

between accurately machined and polished brass spheres 6.25cm diameter which generated a uniform field. An additional 3.5% reduction of breakdown voltage occurred if the sphere gap was flooded with UV (ultra-violet) light.

The first test produced a single breakdown event in air, across a 0.6mm gap using an Automotive Capacitor Discharge Ignition (CDI) system used to initiate ignition in a four-stroke cycle engine. The event was recorded on a PicoScope 2205 and is shown in Figure F4-5 below. The resulting breakdown can be seen to occur at almost 8 kV.

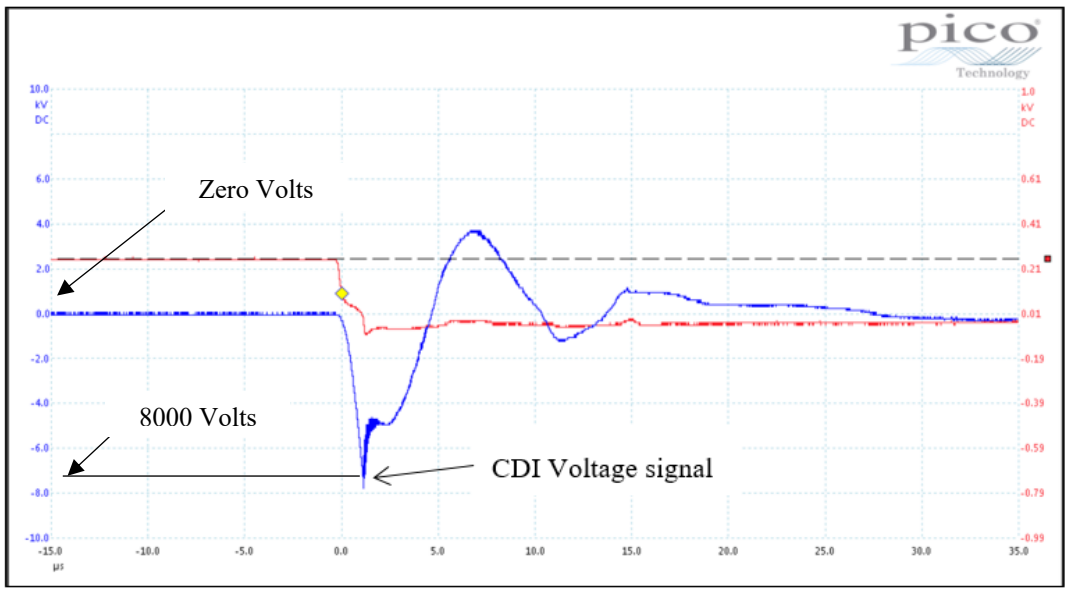

Figure F4-5: A single CDI spark in Air at standard conditions

The second test was carried out with the Resistors R1 and R2 adjusted to achieve an equivalent to a 50%/50% mark turns ratio as shown in F4-10. This resulted in an over voltage supply, in which a breakdown plasma 'overpowers' the spark gap. However, as shown in Figure F4-6, the progression to 'start-up' of the breakdowns occurred in just 3 attempts.

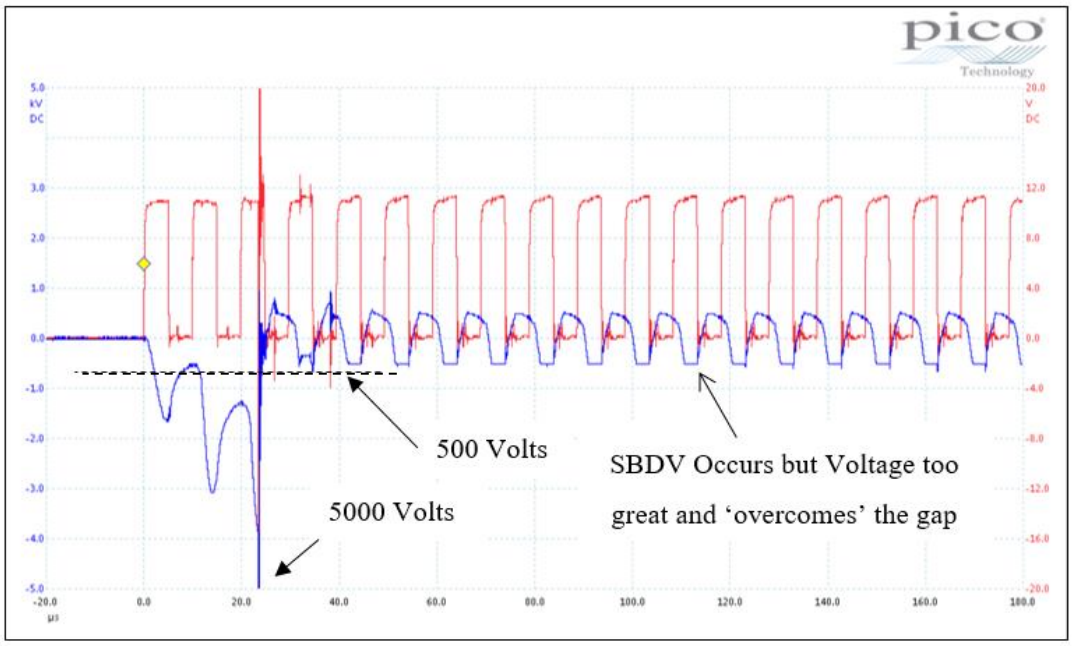

Figure F4-6: Breakdown is overcome when voltage is too great

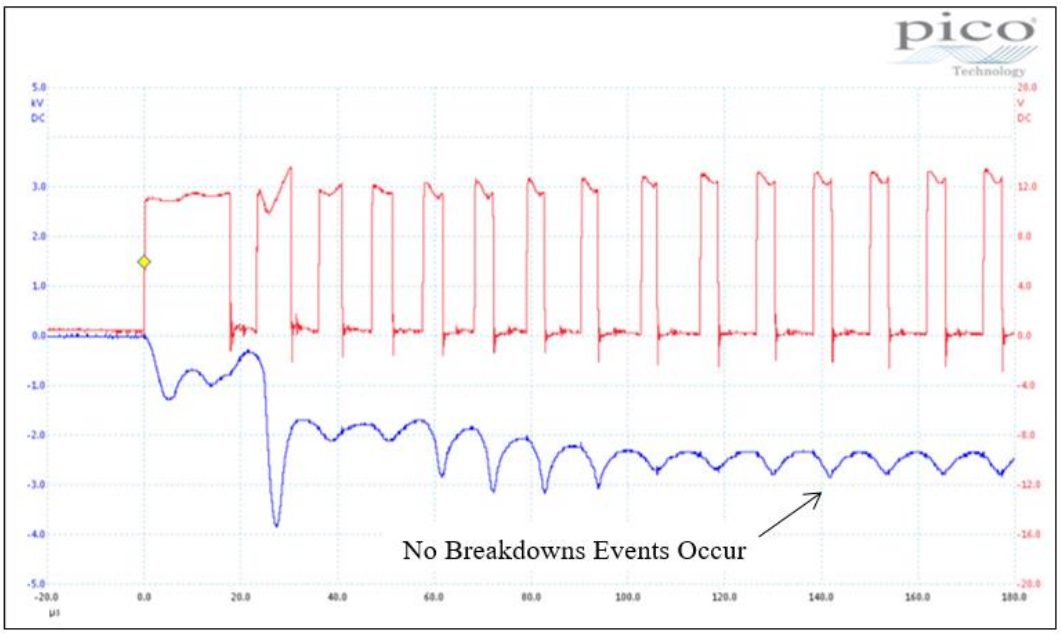

Figure F4-7: No Breakdown events occur with insufficient input voltage

The values of R1 and R2 resistors were then adjusted to the equivalent of a 30%-30% mark turns ratio, until well defined individual spark break-down events were generated. However, as can be seen in Figure F4-8, the events did not stabilise until at least 78 attempts. This was a compromised adjustment arrangement used in the circuit which had just enough power to produce the test results required. The initial test showed the breakdown voltage in air in standard conditions eventually stabilised at around 1000 Volts. The 'stabilised voltage' was noted to be considerably less than the first successful breakdown event of around 3600 Volts. The circuit appears to oscillate after the initial breakdown until reliable breakdown at the lower voltage occurs. This behaviour was thought to show the effect of increased ionization in the gap between the electrodes and potentially the heating of the ionized gas. This increased ionization would then reduce the voltage required to achieve breakdown. It was also considered the surface condition of the electrodes may also change to produce a more irregular surface with high local non-uniformities. It was not known from this initial bench test, at what pressure the SBDV circuit would produce breakdown events that would be stable. The behaviour of interest being the 'stabilised' breakdown events and how these would change in controlled conditions. This was the subject of the testing reported in the present work.

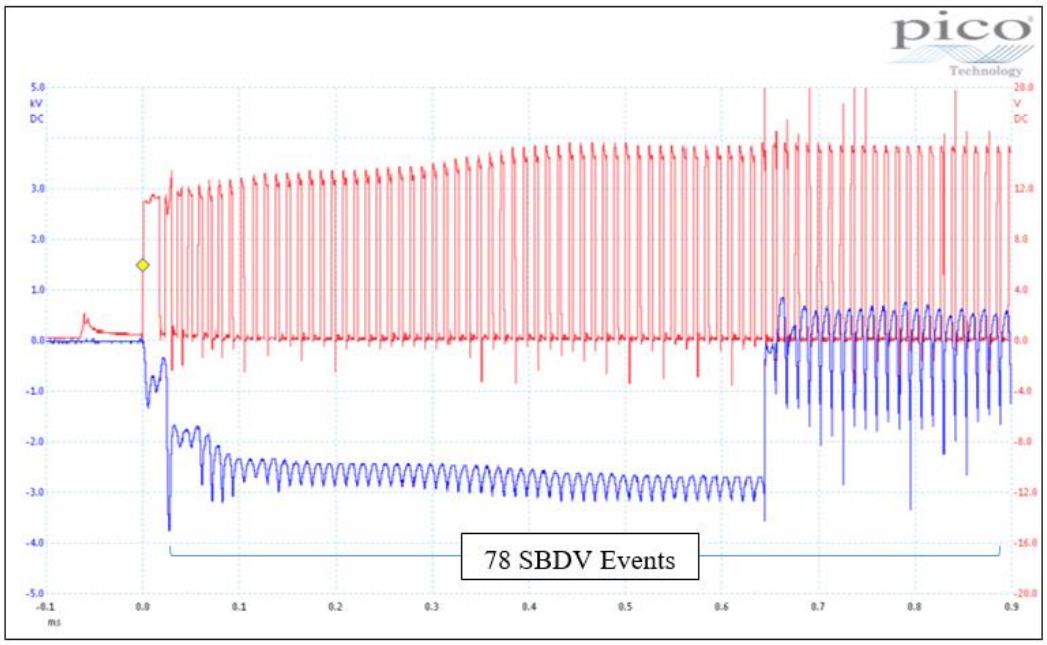

Figure F4-8: SBDV signal initiation as used for Thesis tests

4.4 THE SBDV SIGNAL USED FOR TESTING

A typical view of a 50 milli-second window of the generated SBDV signal, with a resolution x 1, is shown below in Figure F4-9. The apparently solid trace actually consists of many separate SBDV events. The raw signal generated is negative, therefore the trace is inverted. The reader is therefore required to understand a greater numerical value is represented on the screen by a lower value.

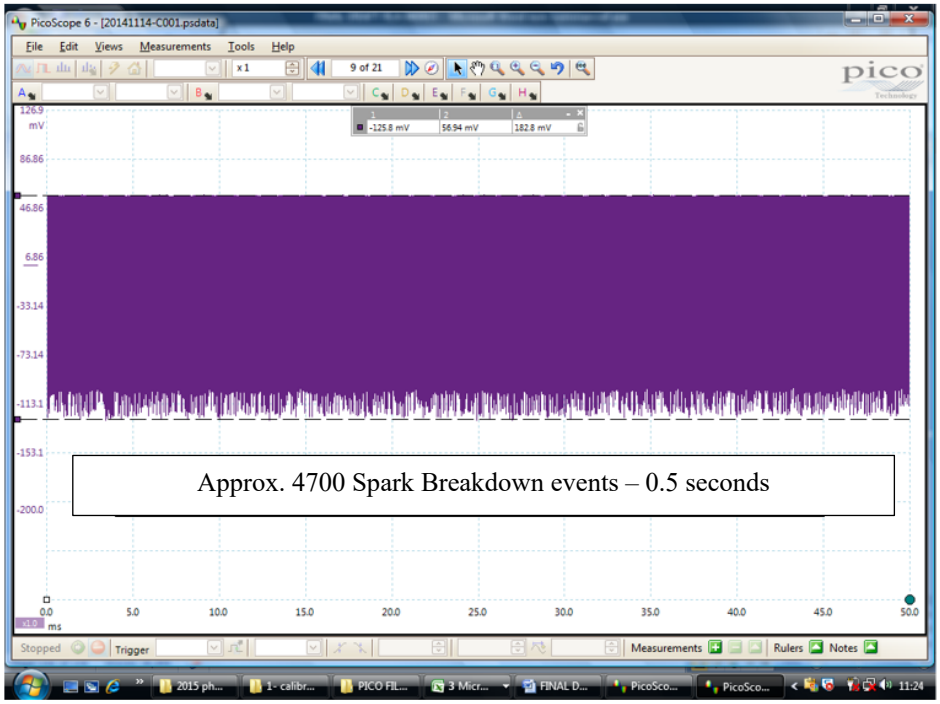

Figure F4-9: Example of a single screen of SBDV events

A 'raw' signal of SBDV recorded in PICOSCOPE is shown with a resolution x 1000, below in Figure F4-10. Five individual locations are identified showing the peak voltages associated with spark breakdown events. The voltage is negative as the new SBDV circuit is negatively earthed. The vertical axis shows the recorded signal voltage before conversion to actual Breakdown voltage.

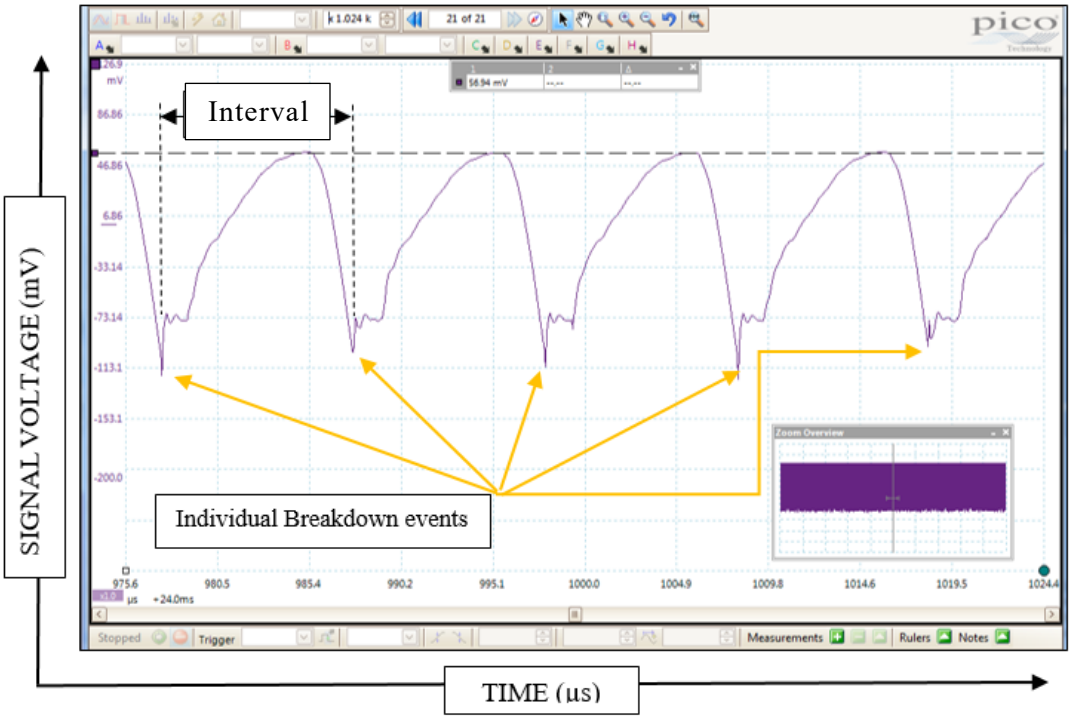

Figure F4-10: Five Spark Breakdown events (Interval approximately 0.00001s)

Each SBDV event is a record of the voltage required to 'breakdown' or overcome the resistance of ions generated at the central electrode to reach the earth electrode. Each breakdown event is a separate event which reflects the molecular activity and conditions between the electrode gap. The activity which enables this to occur is described in Chapter 3. Three such consecutive spark breakdown events are shown in Figure F4-11 which were obtained from test 310-28-03-2015-26, in air at atmospheric pressure, using spark plug 10 which features an 'R' type earth electrode arrangement. From visual inspection, it can be seen the 'Breakdown' event itself starts at the top of the 'ramp' after a period of 'build-up'. Following each 'breakdown' there is a very short 'arc' phase. The period of the 'arc' phase is short and the energy passed into the gas is therefore small. There is no significant 'glow' phase. Investigation of the SBDV signal shows a variation in the absolute value of the 'breakdown' voltage. Within that variance in this value shows the chaotic distribution of gas molecules in the gap at any instance. Small variations and sensitivity can be noted. The signals produced by the new SBDV circuit are unlike those presented by (Maly & Vogel, 1979), showing typical ignition events.

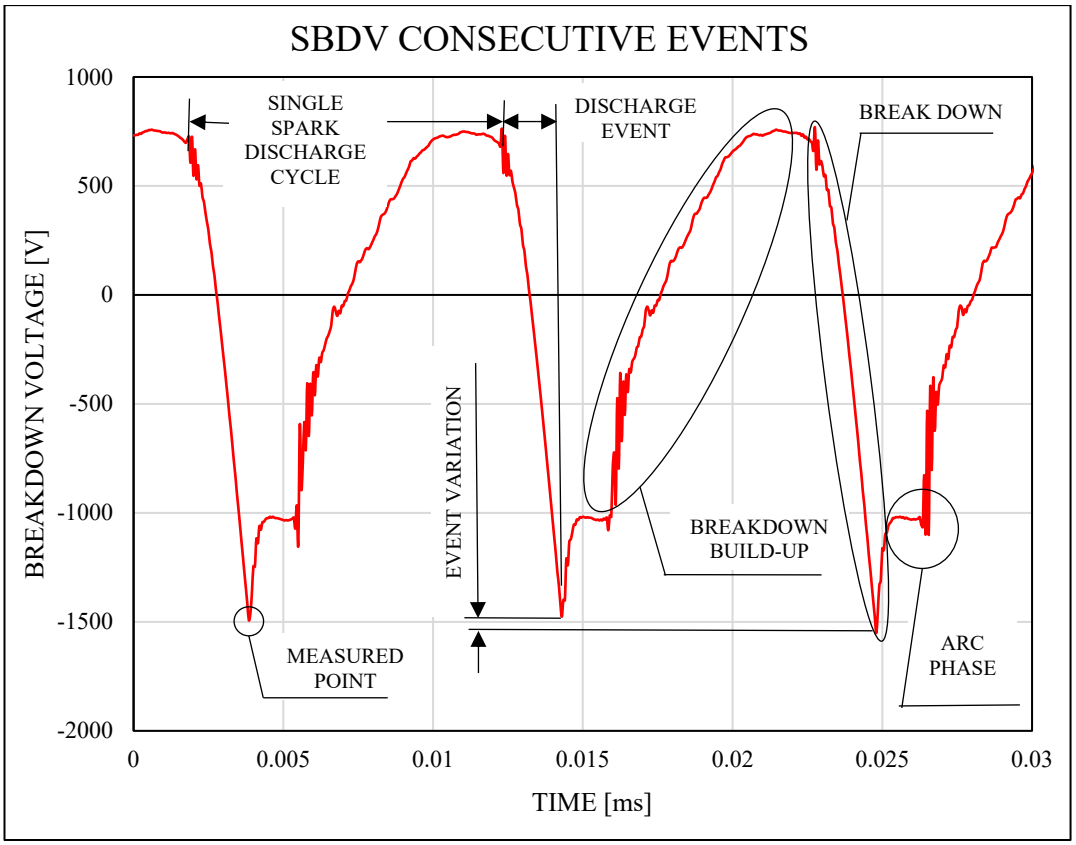

Figure F4-11: Plot showing two individual Spark Breakdown events

4.5 SBDV SIGNAL FILTERING

The sampling rate used to record the SBDV events guaranteed sufficiently high accuracy. This value is higher than the frequency of surrounding electrical, electronic and mechanical background noise from various sources including other electrical devices, computers, and even radio waves. However, the research required investigation of each spark breakdown event and due to the high signal variability and speed of the SBDV signal the internal filtering within the PICOSCOPE 4824 was not used during data acquisition. Therefore, no filtering was applied to the spark breakdown voltage signals from the new circuit or the inductive clamp.

Additional filtering was however, applied to all the non-spark breakdown voltage signals including the OPTRAND pressure sensor. For these, the built-in Low Pass Filter of 1 kHz provided as a standard setting within the PICOSCOPE software was used. The signal filtering and processing applied to the spark breakdown voltage and in-cylinder pressure signals are described below.

Different signal processing routines were required for the in-cylinder pressure and spark breakdown voltage signals. To enable these to be completed efficiently with automatic outputs into excel, 'Matlab' programs were developed and used.

4.6 THE PRESSURE SIGNAL

The 'OPTRAND' PSI 'S' pressure sensor is a dynamic device which therefore only provides a signal when the pressure was changing. The sensor was thus used for DYNAMIC (motored) and not STATIC tests. The value of pressure was relative and therefore required 'pegging' against a reference value representing ambient pressure. In each 'motored' test the output of the pressure sensor at BDC assumed to be ambient and the associated pressure in the test cell was used. Each sensor is factory calibrated and has a conversion factor, which relates the millivolt output from the sensor into pressure (psi). The conversion factor for the 0-70 bar, and 0-7 bar pressure range was 4.24 mV/psi and 38.49 mV/psi respectively.

4.7 PICOSCOPE FILE STORAGE AND CONVERSION

The simultaneously recorded signals of all channels are displayed on computer screen and stored as complete files consisting of 'waveform' sections. The complete file or individually selected sections were then converted as from individually selected 'waveforms' into several different formats including Matlab, CSV and excel. The complete files of all signal outputs for each 'static' test was recorded and stored by PICOSCOPE. To achieve a reasonable file processing duration, the on-screen records for each individual complete test file were then visually examined. For each test, a single 'waveform' was manually selected which showed consistent or relatively stable Spark Breakdown Voltage signals. From this file, a 10millisecond period was selected, then converted and stored as a separate CSV file to represent each individual test.

As previously described, two types of test were carried out for the present work. The first, static tests were used to obtain calibration curves for spark breakdown voltages in different gases at different pressures. The second series were 'dynamic' tests which sought to prove representative data of the gases and conditions in a 'motored' engine. These tests were fundamentally different in intent and detail and therefore, the data recorded and stored for signal processing was different. Hence, the signal storage rate was selected and set on-screen at two different speeds depending on the test carried out. For tests carried out in static conditions approximately 10 consecutive on-screen periods were recorded and

displayed by PICOSCOPE software. Each screen display showed approximately 1,000,000 samples for each 0.5 second duration. During each dynamic test, approximately 32 consecutive on-screen periods were recorded and displayed by PICOSCOPE software. Each screen display showed approximately 2,000,000 samples for each 0.2 second total duration. Thus, each screen displayed around 8 consecutive engine cycles at 2500 rpm.

4.8 SBDV PEAK SELECTION

The voltage values, output from the new SBDV circuit were captured and recorded against time by PICOSCOPE. This 'raw data' contained separate signature shapes representing the breakdown events occurring at approximately 94,000 times per second. The 'shape' of these events consists of and includes many individual frequencies, some at very high frequencies. However, the values of each voltage 'peak' is known to represent the gas density and conditions at that point in time. They required to be graphically plotted for the many tests carried out. However, before 'post processing' could be achieved it was necessary to extract the 'peak' voltage values from the raw data. This extraction was termed 'peak selection' and was achieved efficiently using a 'Matlab' program. The key feature of the mathematical procedure developed was to divide complete strings of data containing many breakdown events into sections. The whole string was broken down into discrete windows, each one containing one SBDV event, and the lowest value within each window was identified. The length of the string was initial imposed as it was thought the frequency of breakdown events was fixed by the parameters of the new SBDV circuit. However, during initial testing it was noted the SBDV frequency changes as one of the responses to different gases and applied conditions. In response to this behavior, the 'Matlab, program was modified to optimize and adapt according to the actual value of the SBDV frequency for each sample and test. To obtain adaptive response of the program to the signal the option of using temporal variation (or values derivate) was considered. However, the time derivative of the signal cannot be reliably distinguished from that of other secondary peaks typically present in the SBDV trace. Comparing the high level of complexity of the latter with the 4% maximum error produced by the discrete division method, it was opted for the last one.

4.9 MECHANICAL TESTING APPARATUS

The SBDV circuit presented previously, was used in combination with two separate items of mechanical apparatus which consisted of the following:

1) A constant volume chamber in which spark breakdown events were obtained in various gases in controlled steps of static pressure (Figure F4-12)
2) A dynamic sparking chamber in which spark breakdown events were obtained in air and exhaust gas mixtures. A motored test engine was used as the test chamber with a separate auxiliary engine used to supply exhaust gases (Figure F4-19).

These items of apparatus are presented and described separately below. The instrumentation incorporated and features included are shown on diagrams with associated photographs of key features. Details of the operating sequences used for testing are included.

4.10 THE STATIC TEST CHAMBER APPARATUS

The static chamber was used to provide a controlled environment to test the performance of the new SBDV circuit and evaluate the characteristics of different spark plugs. The test apparatus shown schematically in Figure F4-12, consisted of the static test chamber, a gas supply, manual pressure control and vacuum purging system. Manual adjustment provided controlled pressure steps of 0.1bar from atmospheric pressure up to approximately 3 bar.

Initial tests were carried out using air, which was supplied from the compressed air utility distribution system. Additional tests were carried out using gases significant to combustion which were supplied from pressurised gas bottles. The pressurised gases were separately connected to the apparatus supply system for individual tests with intermediate vacuum purging.

The cylinder head from the test engine was used so to duplicate the local environment around the spark plug. Internal pressure for each ‘static’ test was obtained from a large diameter pressure gauge. The ‘OPTRAND’ pressure sensor which was fitted to the cylinder head could not be used for this purpose as it responses only to dynamic pressure changes.

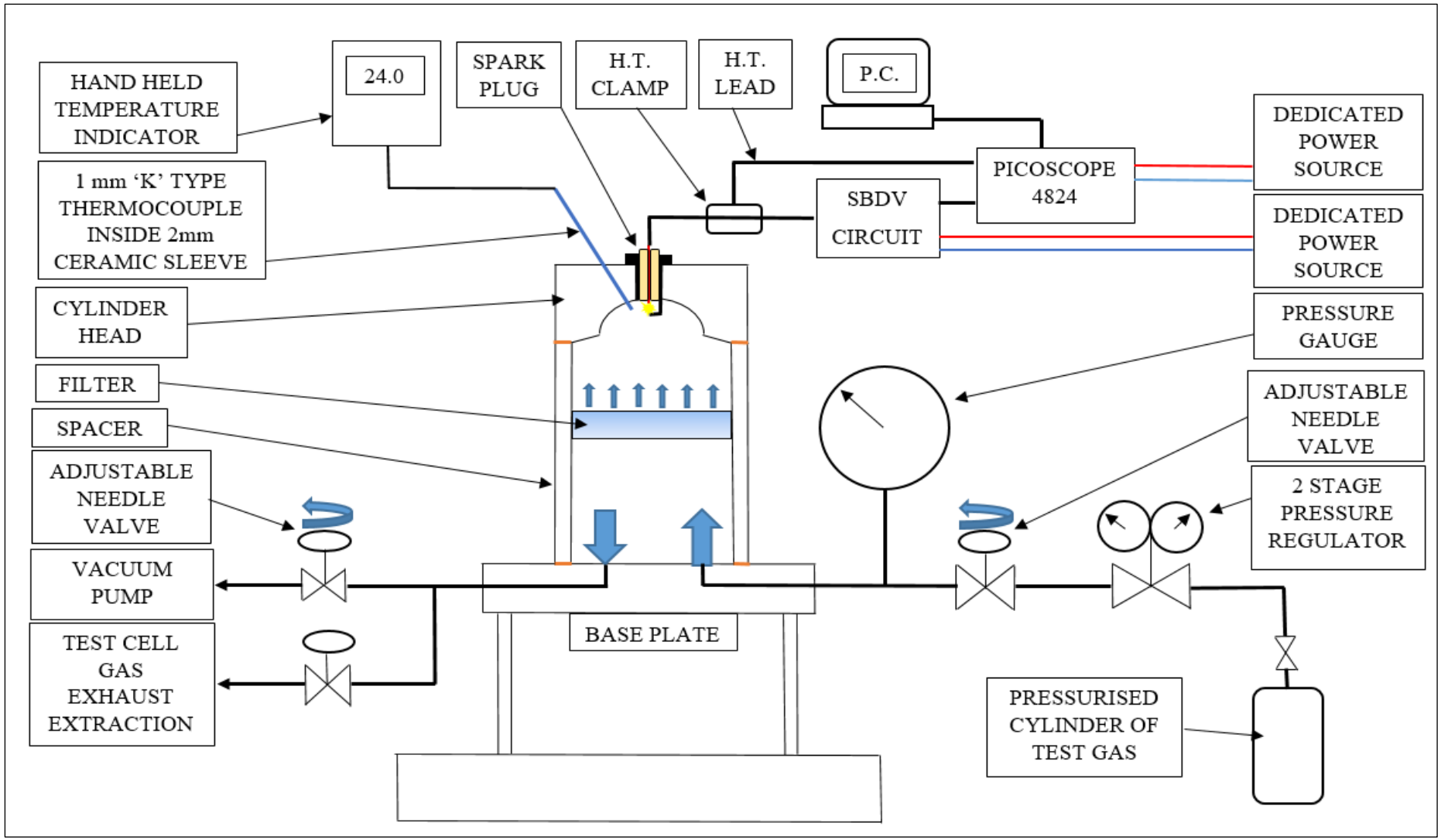

Figure F4-12: Schematic Diagram of the 'Constant Volume Sparking Chamber' apparatus

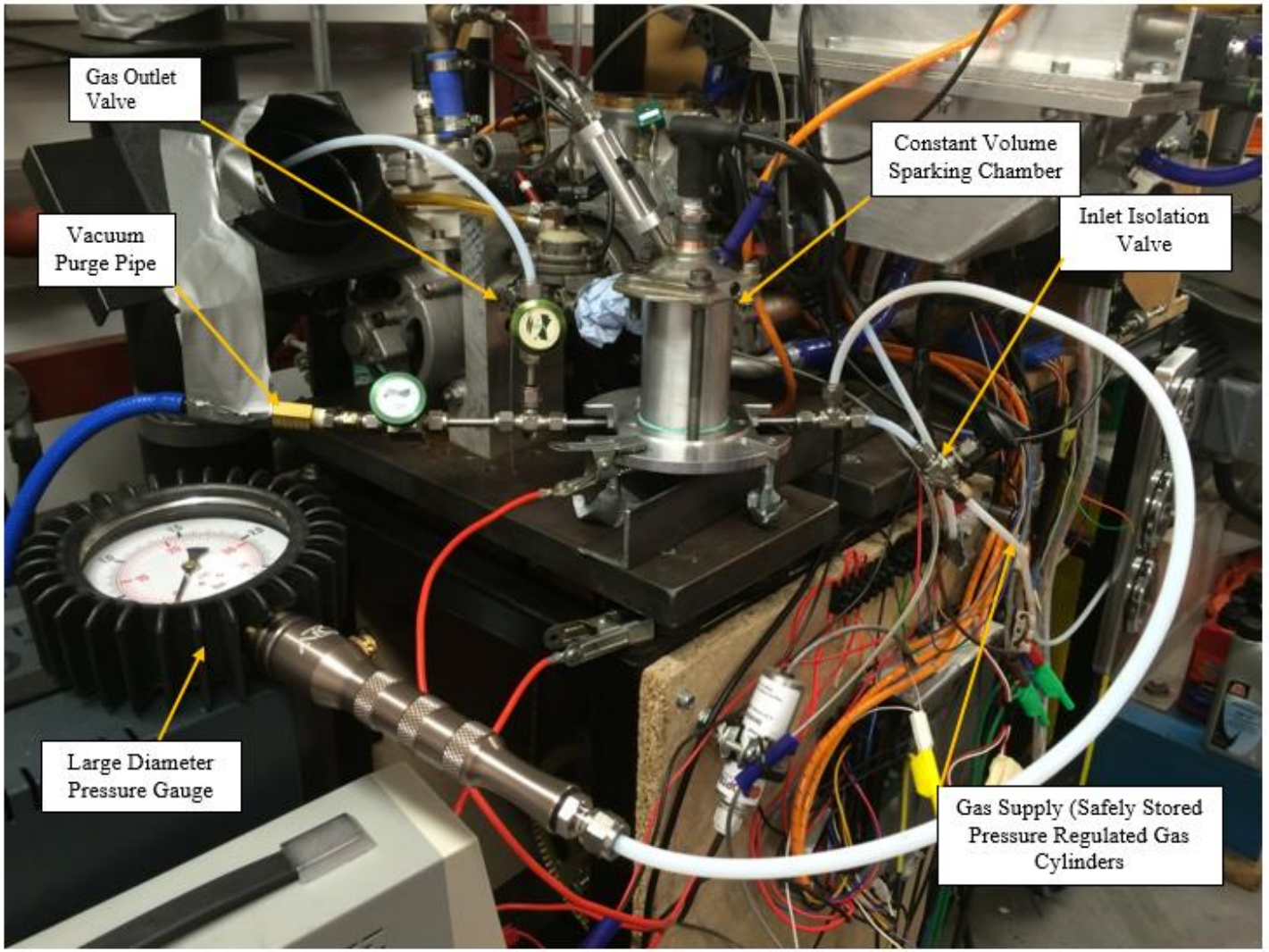

Figure F4-13: The Constant Volume Sparking Chamber (Standing on the Motored test rig)

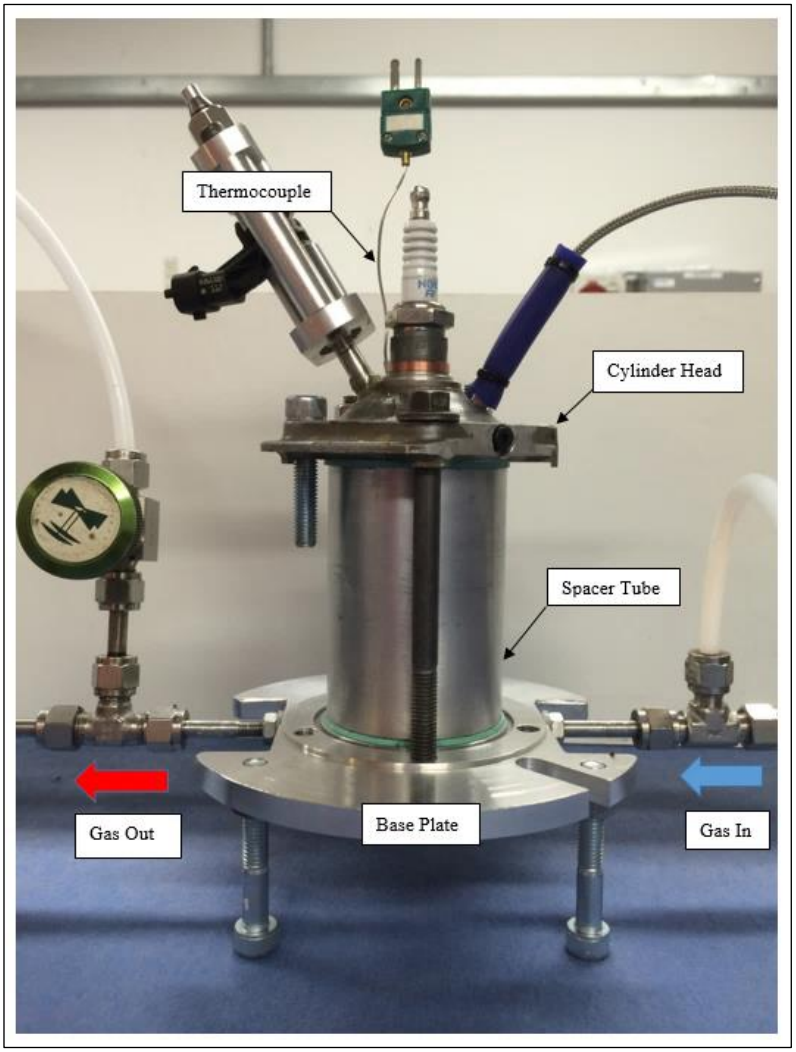

Figure F4-14: The Constant Volume Sparking Chamber

4.10.1 BASE PLATE

The base plate of the chamber was machined from 12 mm thick T6061 T6 aluminium alloy. To keep the chamber approximately 50mm clear of the support surface three cap head bolts provided simple and stable adjustable supports. Gas inlet and outlet passageways of 3mm diameter, were cross-drilled through the plate leading from opposite sides of the base plate to the chamber area. Where these entered the chamber the drillings were angled at approximately 45 Degrees to the vertical. The inlet and outlet passageways in the chamber were drilled such that they faced opposite directions. The intention being to spin the gas and avoid short circuiting when the gas was evacuated from the chamber. External connections from each side of the base plate were made for both M6 stainless steel compression couplings to link into the gas delivery and extract system as shown in Figure F4-14.

4.10.2 CYLINDER HEAD

The top of the chamber was provided by the cylinder head from the 'Rotax Senior Max' test engine. This was a pragmatic solution which avoided the manufacture of an additional part and duplicated the shape, environment, instrumentation and spark plug arrangement used in the test engine. However, additionally, it is known that heat conduction from the spark into the area local to the spark plug is a factor influencing the spark formation and also the formation of the flame kernel. Even though this mechanism would not occur in the tests, as combustion would not occur, it was considered important to gather data from a local environment which duplicated that in an operating engine.

The cylinder head component was modified to incorporate features described below predominantly for dynamic testing. The simple construction of the two-stroke cycle engine component, which does not include inlet and exhaust valves, made these modifications straightforward. An internal view of the modified cylinder head is shown in Figure F4-15.

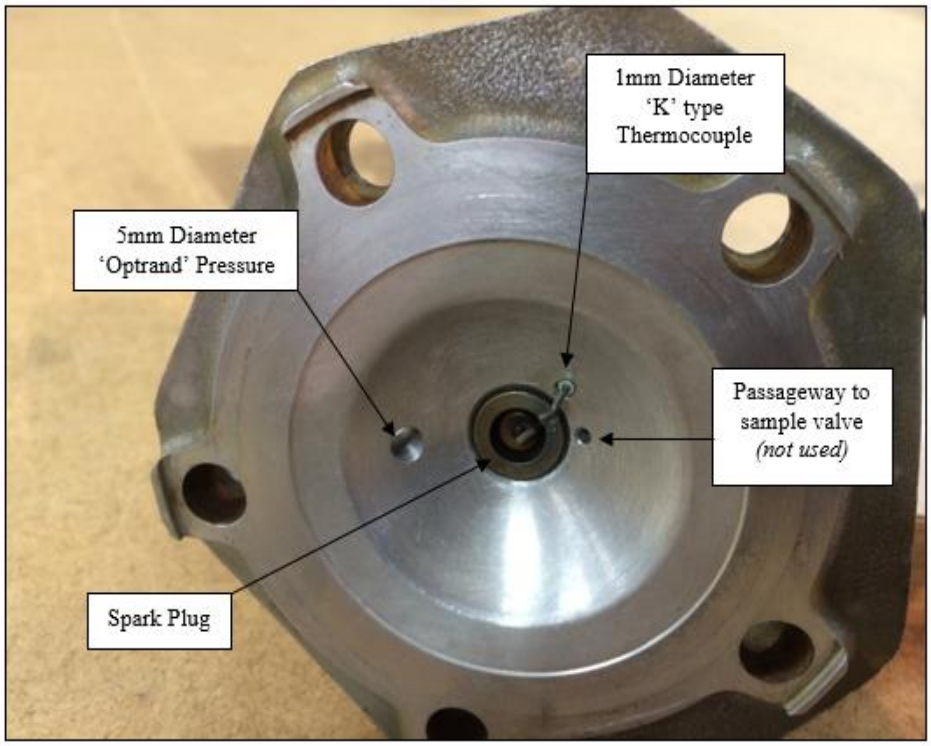

Figure F4-15: Modifications to the Test Engine Cylinder Head

4.10.3 THERMOCOUPLE IN THE HEAD

The modifications to the cylinder head included a 1mm diameter 'K' Type thermocouple. Despite the small dimensions, the response time is not fast enough for dynamic testing, but

it can be reliably used for static tests. As the temperature measurement was not considered dynamic a hand held twin channel digital indicator was used to provide the temperature reading. The thermocouple was fitted into a 2.0mm outside diameter silicon carbide sleeve. The tip of the thermocouple was placed at a distance of 3mm from the cylinder head wall. The incorporation of the sleeve provided thermal isolation from the cylinder head metal into the thermocouple sheath which ensures the temperature at the tip is measured not that of the metal surroundings. The sleeved thermocouple arrangement was fitted into the cylinder head using high temperature Loctite 535.

4.10.3 THE SPACER TUBE

A plain spacer tube was manufactured from Aluminium alloy to provide clearance between the base plate and cylinder head. No general rules for the volume of gases to be tested could be found. However, because the primary objective of the static tests was to record spark breakdown events in constant gas conditions it was thought a volume of gas greater than the swept volume used in dynamic testing should be used. Subsequently, a 90 mm long spacer tube shown in Figure F4-16, was trapped between the cylinder head and base plate to increase the total chamber volume to approximately 225cc. The joints between the spacer and base plate and cylinder head joints were sealed using 1.5mm thick gaskets cut from cardboard.

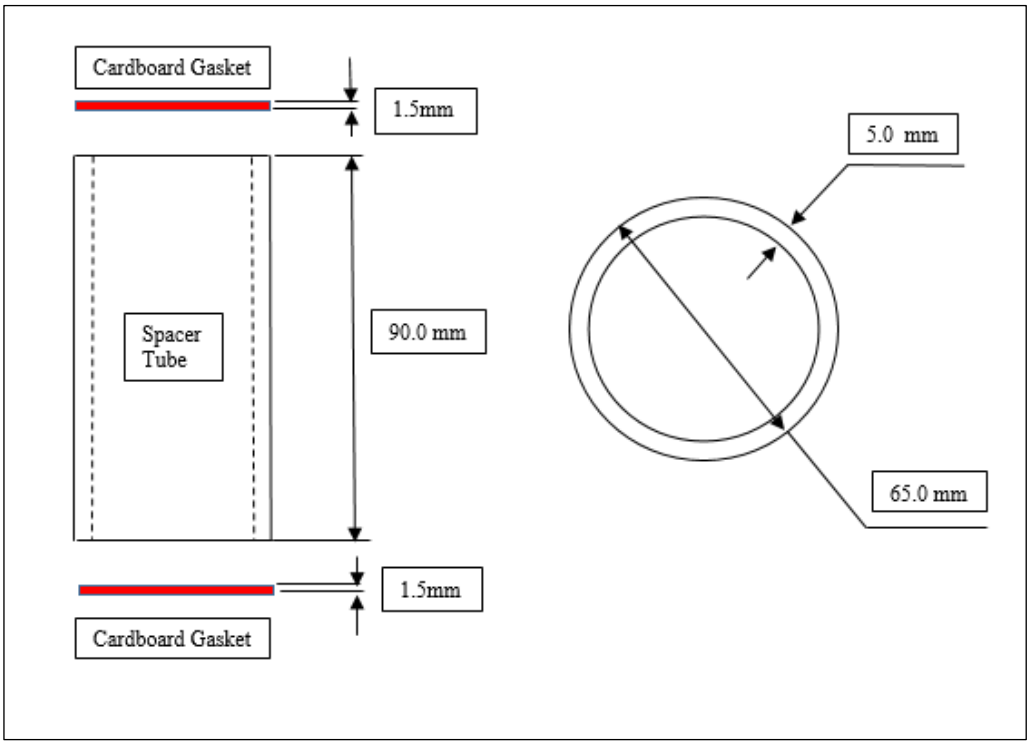

Figure F4-16: The Static Chamber Spacer Tube

4.10.4 THE FILTER SCREEN – USED TO LIMIT GAS TURBULENCE

Initial testing of the Constant Volume Sparking Chamber used the cylinder head bolted directly to the base plate. However, the spark breakdown voltage signal behaved very erratically. Additionally, it was noted the signal was very sensitive to small variations of inlet gas flow. It was known that the spark path could be deflected by gas flows (Pashley & Stone, 2000), (Swett & Donlon, 1953). To reduce the gas turbulence in the cylinder head, the volume of the sparking chamber was increased by adding the spacer tube detailed in section 4.11.3. This decreased increased the distance between the gas inlet point and reduced the variations in the Spark breakdown voltage signals. The variations in the spark breakdown voltage signals were further reduced by to addition of a 20mm thick circular section of plastic foam filter which was cut to fit snuggly, approximately half way down the spacer tube. This filter was prevented from being pushed upwards by inlet gas towards the spark plug by a 1.5mm thick steel washer with a 25mm central hole, fitted above the filter with a small interference fit into the spacer tube. With this filter fitted the stability of the spark breakdown voltage signals was significantly improved. In air, the pressure at which stable spark breakdown voltage signals could be obtained increased from 0.8 bar to 2.5 bar. No further filter arrangement designs were evaluated. The filter material was noted to become degraded following tests using oxygen and was accordingly replaced.

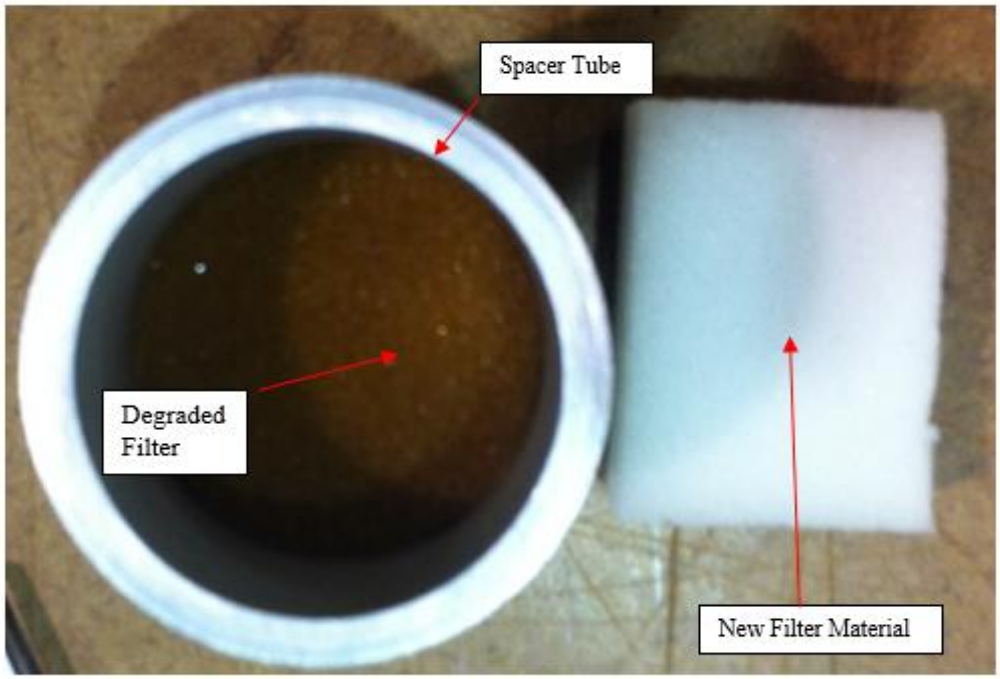

Figure F4-17: Chamber Spacer and Filter Material

4.10.5 GAS SUPPLY AND EVACUATION SYSTEM

The function of the Static Test Cell required various gases to be delivered into the chamber and maintained in a steady range of pressures. A simple, manually controlled gas delivery system was created. A diagram of the gas delivery system is provided in Figure F4-12.

Gas was delivered into and to the various components via 6mm nylon pipes connected by compression couplings. Proprietary pressurized cylinders were used to provide Air, CO, CO2, O2, N_2 gases. These gases were stored safely to avoid accidental damage but within the test cell. Air was obtained directly from the plant air distribution system in the test cell. This was dried by the in-house plant air drier system. No additional drying was installed for the SBDV tests. The relative humidity of the gas was not recorded. This could have contributed to inaccuracy of SBDV values gathered and to variability between various tests using air. It is known that the water vapour content of the gas effects the value of spark breakdown voltage significantly as water vapour is an electro-negative gas which effects the ionization process. Research has shown SBDV varies in a linear relationship over a wide range of humidity in air. (Feser, 1972), (Peschke, 1969), (Guindehi. S, 1970). The present work did not deliberately vary the humidity for the testing carried out. The effect of the humidity variations that occurred naturally is shown in Chapter Seven. The control of the gas pressure in the Static Test Cell was enabled by manual adjustment. Where gas was stored in gas cylinders, the two stage regulators at the cylinder outlet were adjusted to approximately 3.0 bar. Gas flow rate control was enabled by vertical ball flow-meters. These were adjusted to provide a gas flow rate of approximately 0.5 litres/min. The dry plant air pressure was set and adjusted locally at 4.0 bar. No flow control system was used.

In cylinder pressure adjustment and monitoring was enabled by fine adjustment of small needle isolation valves. Pressure values were obtained using an accurate 100mm diameter pressure gauge with a 0-2.5 bar range.

To ensure the gases contained in the Static Test Cell for individual tests not contaminated by other gases a gas evacuation system incorporating a vacuum pump was added. This was operated between tests to evacuate the Static Test Cell of the gas contained in the whole distribution system from the associated storage source.

4.11 THE DYNAMIC TEST APPARATUS

The thesis objectives stated in Chapter one, required the investigation of SBDV signals from in-cylinder gases trapped during the early stage of cycle by cycle compression events.

In a firing, operating engine, the gases trapped in the cylinder following exhaust port closure consist of fresh charge together with mixtures of residual burned and unburned gases which were not scavenged from previous cycles. The relative percentages of these gases can vary significantly cyclically to represent the influence of the gas exchange process which takes place prior to the start of each closed cycle compression. These variations produce random cyclic differences to the starting pressure and the rate of change of pressure as described practically and mathematically in chapter two and shown graphically in Figure F4-18.

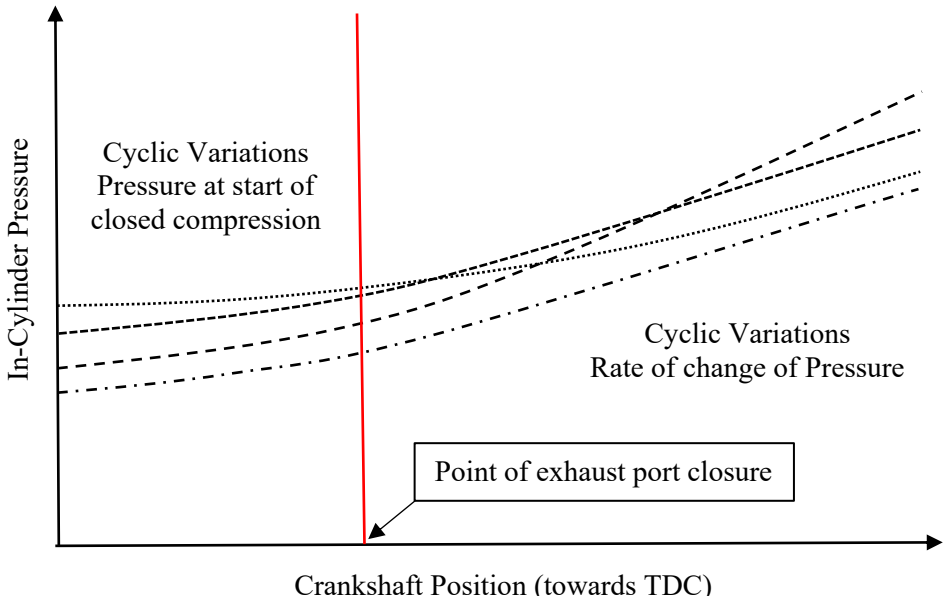

Figure F4-18: Variations of closed cycle In-cylinder pressure before ignition

The gas pressure at the start of closed compression is predominantly driven by the arrival timing and pressure of the return exhaust pulse. The rate of pressure change during closed compression, prior to ignition represents the trapped gas species, gas conditions, gas compressibility and heat transfer characteristics.

The pressure changes during closed compression in an operating engine have been noted to be small and vary cyclically. However, these events have been largely ignored by researchers focused on the monitoring of actual subsequent combustion events. The rate of change of cylinder pressure during closed compression starts to diverge strongly following

ignition, when the heat of combustion starts to occur. The work of (Rassweiler & Withrow, 1980 (originally published 1938)) presented a process which deducted the motored pressure history from the fired pressure history to obtain the contribution of pressure resulting from combustion. Later work confirmed this approach which isolates the contributions of pressure changes in the cylinder due to non-combustion and combustion by improving the definition of pressure change to fuel quantity burned (Sellnau, et al., 2000). This confirmed the following two points relative to considering the in-cylinder activity during the early stage of compression before ignition is initiated:

a) This activity does not form part of 'conventional' combustion analysis.
b) The isolation of this activity would not interfere with the procedures or results of 'conventional' combustion analysis.

It was realised monitoring in-cylinder pressure and gas variations is complex. Further, monitoring of the results of actual combustion events were not required for the present work. Therefore, the use of a firing engine was not necessary for generating cyclic pressure changes in the cylinder. Accordingly, the test engine from which SBDV signals were obtained, was motored. The use of a motored, rather than fired, test engine provided consistent cyclic pressure histories which resulted predominantly from volume changes due to piston movement only. The use of a motored engine rather than a fired engine also avoided unnecessary mechanical and thermal complexities which would have occurred from combustion.

In addition to monitoring in-cylinder pressure variations during the early stage of closed compression it was essential to monitor the effect of different combinations of fresh charge and exhaust gases during this period. The test apparatus was therefore required to deliver a wide range of such mixtures for monitoring in the motored test engine. This was achieved by using a firing auxiliary engine from which exhaust gases were bled off and mixed with fresh charge for supply to the motored test engine. The fuel supply of the auxiliary engine being adjusted to provide exhaust gases representative of a wide range of operating Air-Fuel ratio settings.

The use of a motored test engine limited the cyclic in-cylinder pressure variations and avoided the heat of combustion. This simplified the selection of a suitable in-cylinder pressure sensor and avoided concerns for wide range temperature compensations. The avoidance of combustion also allowed a conventional thermocouple to be inserted into the combustion chamber space and by limiting the temperature variation to that resulting from

compression only allowed comparable temperature readings to be obtained from this simple equipment.

Accordingly. the second item of mechanical test apparatus was designed and purpose manufactured to obtain SBDV signals from simulated gas variations which would occur in an operating engine.

The design requirements of the dynamic test apparatus are summarised as follows:

a) To provide a two-stroke cycle type test engine.
b) To provide a mechanism to motor the test engine at a consistent speed.
c) To provide an auxiliary engine to produce exhaust gas.
d) To provide a method to combine different mixtures of fresh air and exhaust gases.
e) To include the SBDV system, pressure sensing and instrumentation to obtain and record simultaneous signals relative to crankshaft position.
f) To mount onto an independent, moveable and transportable unit.

The above design requirements were met and combined to provide the dynamic test apparatus shown schematically below in Figure F4-19 and then described in detail.

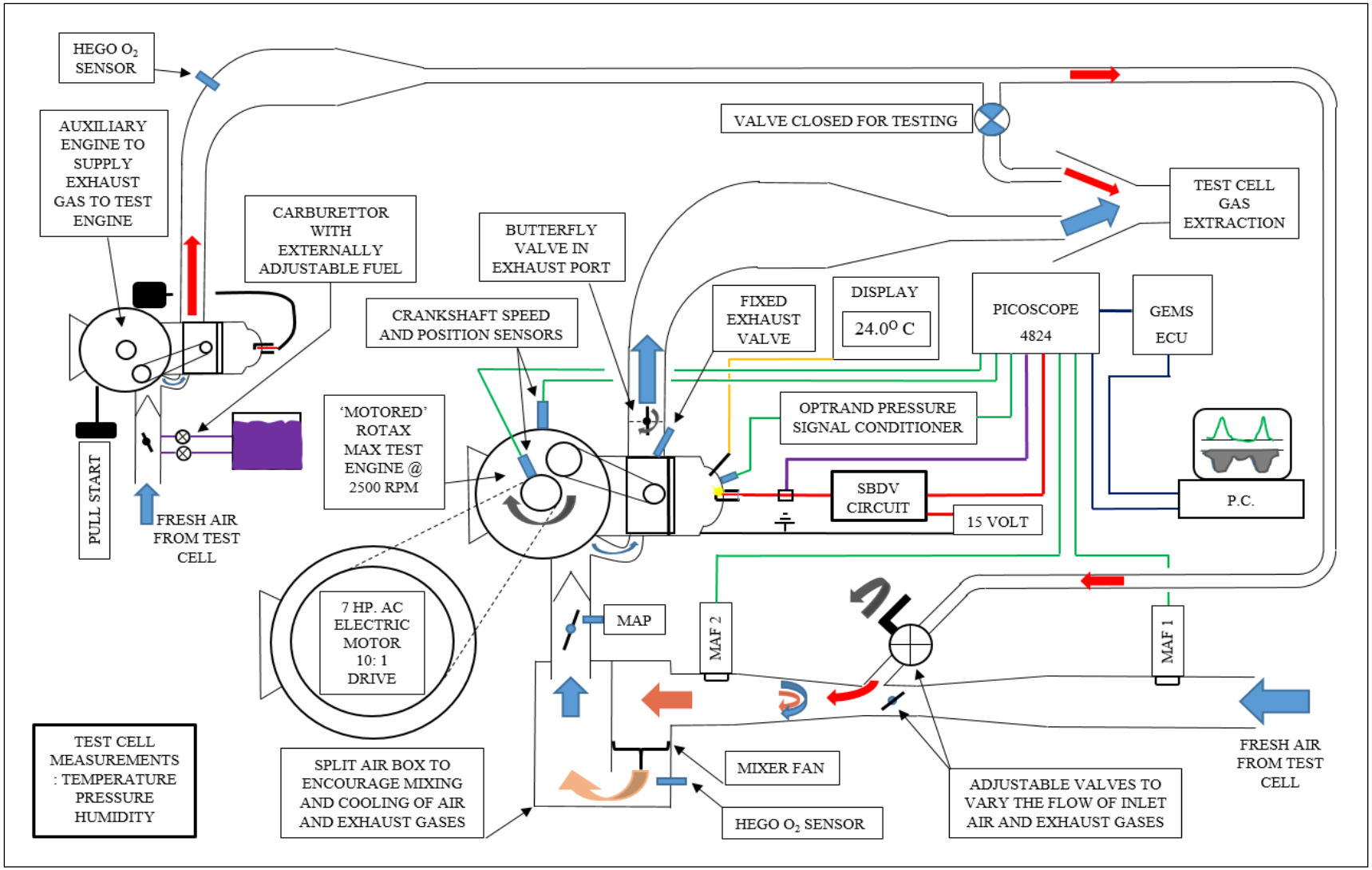

Figure F4-19: Diagram showing the Test Engine Inlet System with Exhaust Gas mixing

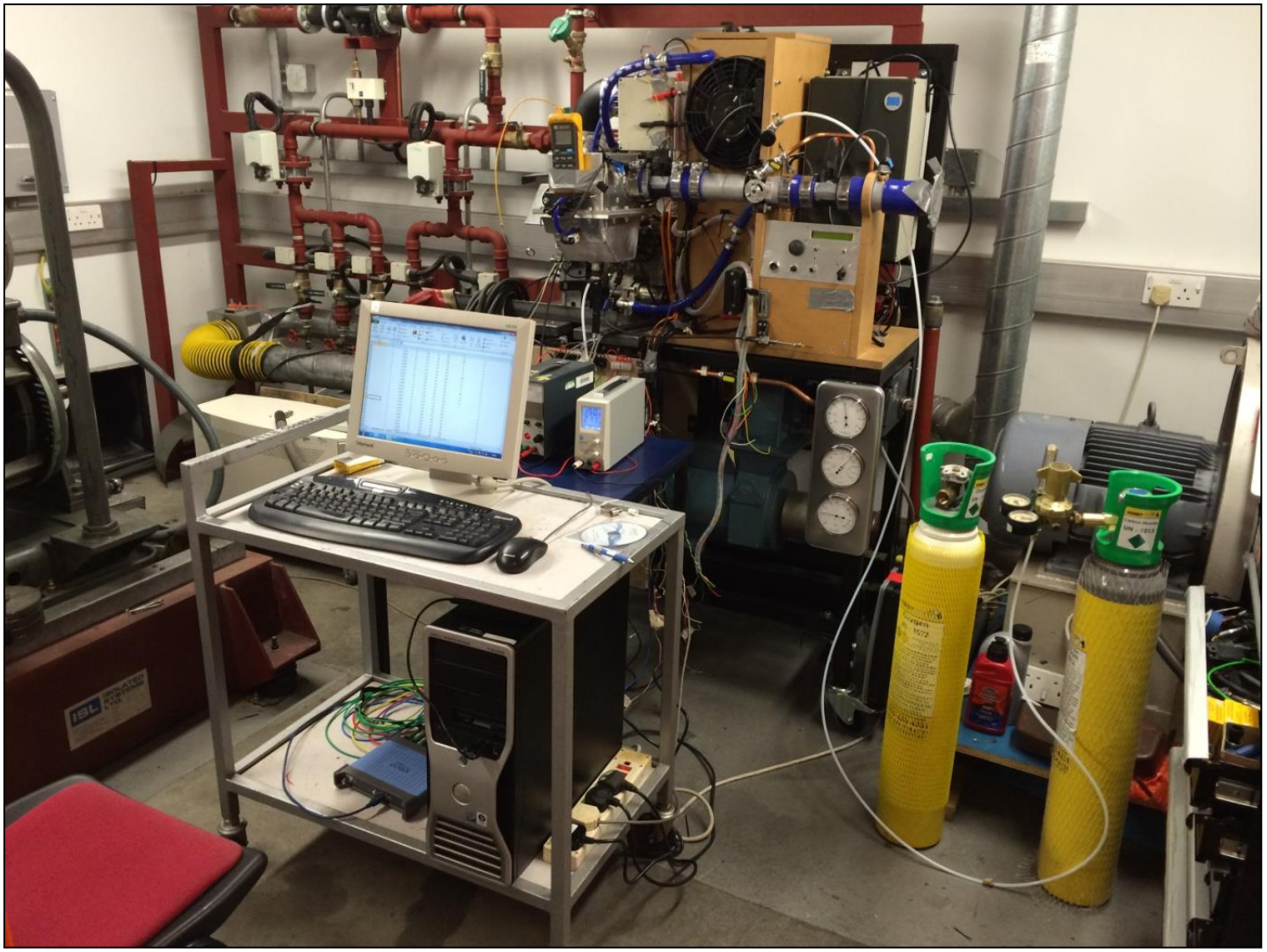

Figure F4-20: The ‘Motored’ Testing apparatus

4.11.1 GENERAL CONSTRUCTION DETAILS

The ‘Motored’ test apparatus was constructed in two main frames made from 40mm x 40mm x 2.5mm Hollow Steel Section. The main base frame carried the AC electric motor which was mounted on two longitudinal 152mm x 76mm Rolled Steel Channel members. These beams were bolted to the bottom members of the base frame to reduce the overall centre of gravity height.

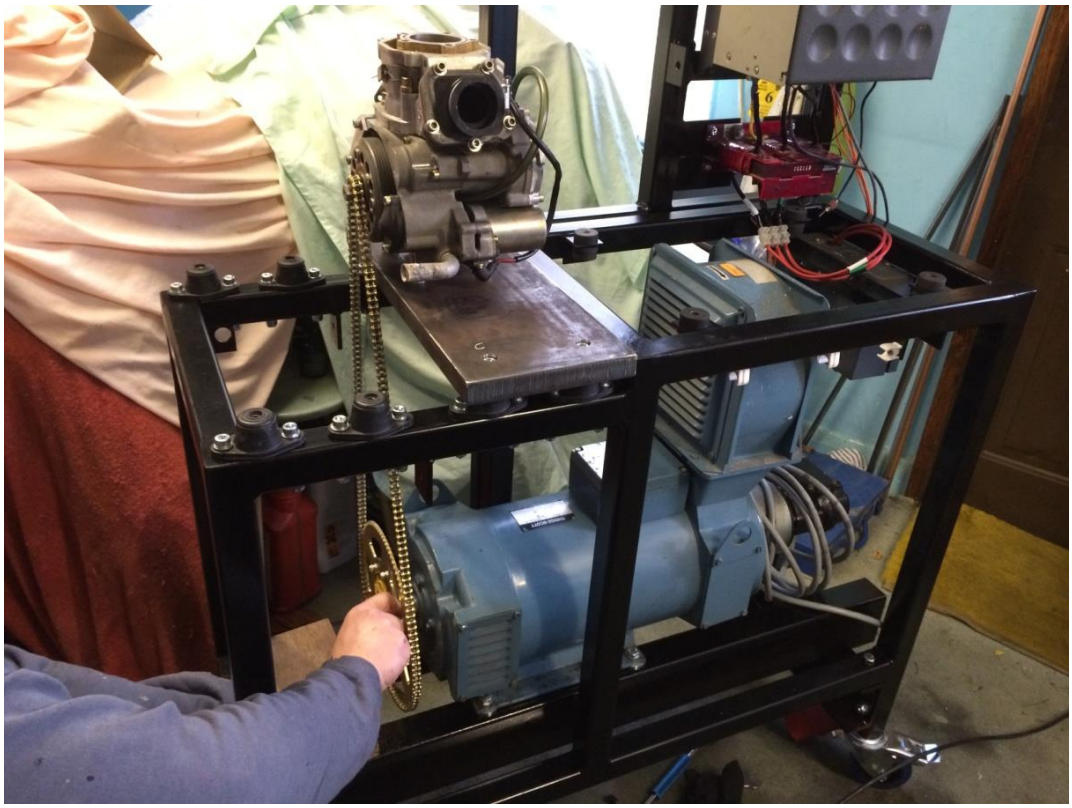

Figure F4-21: AC Motor and Test Engine sprocket drive arrangement

The crankshaft of the test engine was rotated, or ‘Motored’ by a variable speed, 7hp three phase 330 Volt, AC electric motor via a chain drive using a 10:1 sprocket ratio as shown in Figure F4-21. The test and auxiliary engines were bolted onto separate 25mm thick carbon steel base plates to provide simple, flat and independently vibration isolated engine mountings as shown in Figure F4-22. The base plates were separated by a 50mm gap through which drive chain of the test engine could pass unobstructed between engine sprocket(s) and the electric drive motor and absorber shaft below.

To the right-hand side of the top a 20mm thick Multi-Directional Fibre board MDF worktop provided a flat base form mounting of ancillary equipment. This to MDF section was also independently mounted on rubber isolation mounts.

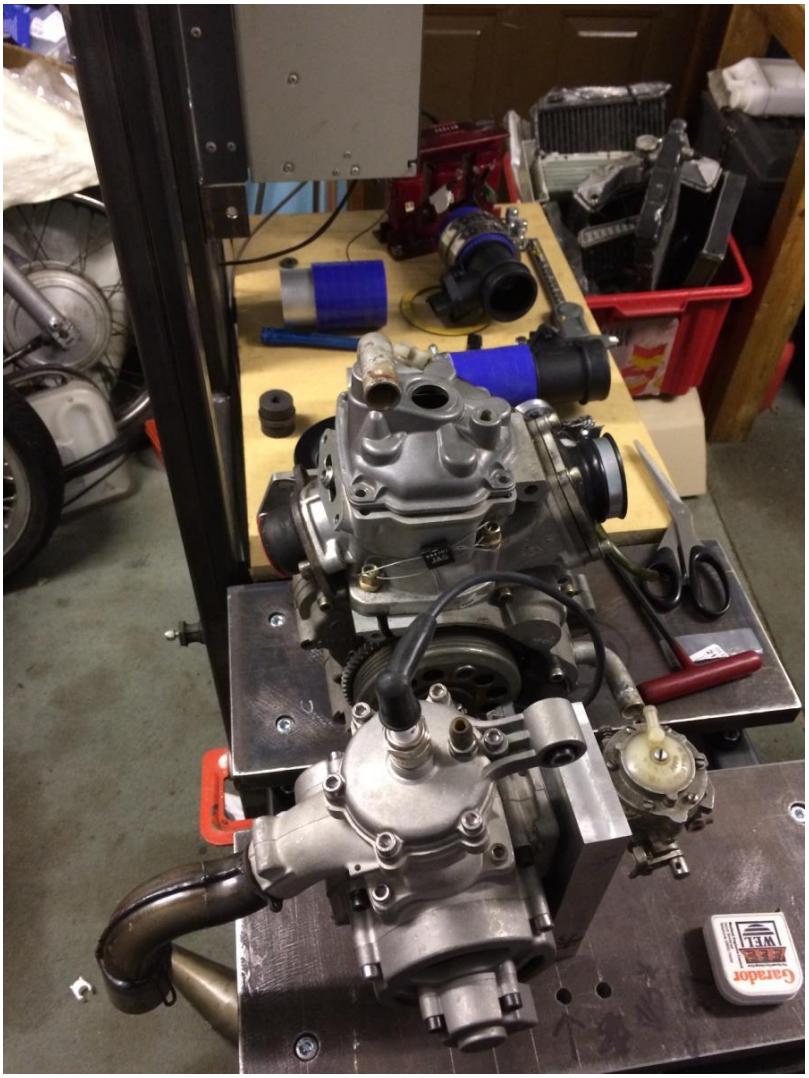

Figure F4-22: Engines on separate mountings – Far: Test engine. Near: Auxiliary engine

The second frame formed a vertical backing to the base frame. This frame was again fixed on separate rubber mounts to provide vibration isolation from the base frame. The Inverter for the AC motor was fixed back to the vertical frame and mounted at the opposite end to the test engine mounting plates to minimise any transmitted vibration from the auxiliary engines to the inverter electronics.

The second vertical frame also provided fixing points for an MDF box into which is mounted two separate air/water radiators independent for the test and auxiliary engines. These were mounted one behind the other to save space. A 200mm diameter electric fan

was mounted at the front of the MFD box to provide air to both radiators. A large 12volt, lead acid battery was installed underneath the radiators to provide an on-board independent power supply for short term cooling fan operation.

4.12 THE TEST ENGINE

The test engine used for ‘Motored’ tests was a ’Rotax Senior Max’. This two-stroke cycle type engine shown in Figure F4-23, is used for kart racing (MSA, 2011). It was chosen because it’s design and construction represents reliable current technology, it is easy to mount and replacement parts are available at reasonable cost. The engine is also compact and features a blade type exhaust valve and reed valve inlet control into the crankcase. Details of the standard engine are provided in Table T4-1.

Figure F4-23: Test engine: Rotax Senior Max 125cc

Table T4-1: Specification of Test Engine

Main Specification Details of Test Engine	
Manufacturer / Model	Rotax / Senior Max
Intended use	Karting
Capacity (Nominal)	125cc
Inlet Type	Reed Valve
Scavenging Type	Crankcase Scavenged Loop
Cylinder Bore (Nominial)	54.00 mm
Stroke	54.5mm
Connecting Rod Length	100mm
Geometric Compression Ratio	12.55:1
Clearance Volume (as tested)	11cc
Transfer Ports (5) - Total Duration	115 Degrees
Exhaust Port Closing (valve open)	82 Degrees BTDC
Exhaust Port Closing (valve closed)	97 Degrees BTDC

4.12.1 MODIFICATIONS TO THE TEST ENGINE

The standard ‘Rotax Senior Max’ engine was modified for the testing carried out for the present work. As the engine was to be ‘motored’ the ignition system was not required nor the carburettor, so these were removed. As the heat of combustion would not have to be removed, the engine cooling system was not connected. This allowed the outer water jacket of the cylinder head to be dispensed with for testing. This allowed the inner cylinder head ‘skull’ to be exposed and gave freedom of access for instrumentation which additions are shown in Figure F4-15.

4.12.2 PRESSURE SENSOR

The modifications to the cylinder head also included the fitting of an ‘OPTRAND’ Model: Psi-S pressure sensor. The sensor head of this unit, shown in Figure F4-24 below was mounted into the cylinder head using an M5 X 0.5 thread which was very compact.

Figure F4-24: The ‘Optrand’ PSI S Sensor

The manufactures specification for the unit used for testing is given in Table T4-2. The actual values of each unit vary slightly from the quoted data. The ‘Optrand’ package used is quoted to be equivalent to ‘Kistler’ Model 6051B. To maximise the accuracy of the pressure sensor unit, the manufacturers were requested to modify the sensor to optimise the response at the low end of the pressure range while still retaining its maximum pressure capability. This ‘optimisation’ made the sensor more suitable as a single item for the range of motored and static tests conducted while retaining the capability to be used in the cylinder head of a fired engine.

Table T4-2: Specification – Optrand pressure sensor used for testing

Technical Specification of In-Cylinder Pressure Sensor	
Manufacturer / Country of Manufacture	Optrand / USA
Model	PSI 'S'
Pressure Range	0 -70 Bar (Custom optimised)
Allowable Over-Pressure	2 x 1.5 x Rated Pressure: 210 Bar
Temperature Range (Continuous use)	-40 to + 300°C
Temperature Range (Intermittent use)	Combustion
Temperature Range (Cable)	-40 to + 200°C
Temperature Range (Signal Conditioner)	-40 to + 65°C
Frequency Response	0.01Hz to 30 kHz
Linearity / Hysteresis: Non-Combustion	+/- 0.25 to +/- 0.5% Full Scale Output
Linearity / Hysteresis: Combustion	+/- 1 to +/- 2% Full Scale Output
Temperature Coefficient of Sensitivity	+ 0.03 % per °C
Signal to Noise Ratio	2000:1 @ 15 kHz
Sensor Output	0.5 to 5.0 Volt
Sensor Diagnostic Output	0.5 to 3.6 Volt
Guaranteed Service Lifetime	1 Billion Cycles or 5 Years

The ‘OPTRAND’ sensor does not incorporate piezoelectric elements but operates by sensing the variations of ‘time of flight’ to an LED signal. The ‘time of flight’ variations are caused by varying deflections of a stainless steel disc element at the sensor head shown in Figure F4-25 and converted to pressure variations.

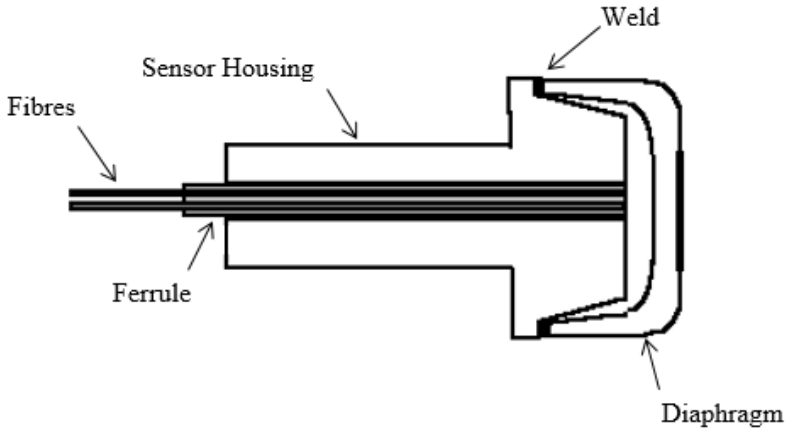

Figure F4- 25: The ‘Optrand’ Sensor head

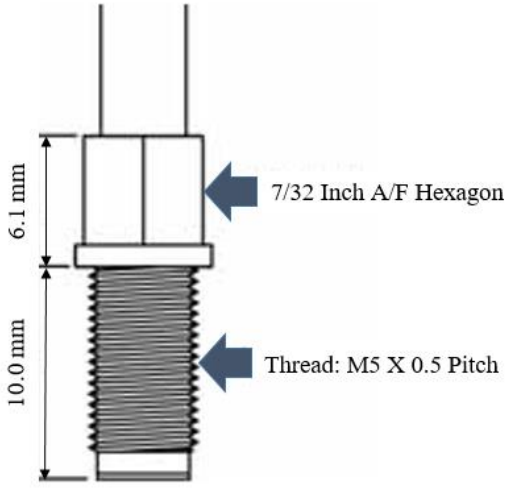

Figure F4- 26: The mounting dimensions of the ‘Optrand’ Sensor head

The ‘Optrand’ sensor was supplied with a conditioning unit which has a conversion value from millivolts to pressure. Each individual unit has a different conversion factor to account for a reference pressure. The item used for the present work had a conversion value of 4.24 mV /1.0 psi. The Resonant frequency of the sensor diaphragm was 120kHz which is almost

6 times the individual unit's frequency response of 1.0 – 25 kHz. Under constant temperature conditions such as when used in the Constant Volume Sparking Chamber. The individual unit has a stated non-linearity of +/- 0.55% of its rated range = 0.385 Bar. While in combustion conditions this stated non-linearity rises to +/- 1 to 3 of its rated range equals 2.1 Bar. F4-24 shows the sensor head mounting dimensions. The maximum pressure achieved in the cylinder head during static testing when used in the Constant Volume Sparking Chamber was approximately 3 Bar. The maximum pressure achieved in the cylinder head during motored testing was approximately 35 Bar. The maximum allowable pressure for the unit is 210 Bar. The operating pressure range of the sensor is 0 -70 Bar, with a maximum operating temperature of +350° C. The item is suitable for use in a combustion environment.

Significant heat build-up which would result from motored engine compression was prevented by limiting the duration of individual tests to a maximum of 15 seconds. A minimum time of 5 minutes was allowed between tests to allow for heat dissipation. The gas temperature inside the engine close to the spark plug was monitored.

Piston friction was limited by the Teflon coating on the piston skirt applied on the skirt of the standard piston. A small amount of oil was applied to the piston skirt prior to tests. Crankshaft bearing friction was prevented by adding a small amount of lubricating oil into the lubrication passageways prior to tests.

Two proximity sensors were used to monitor crankshaft position. One sensor was triggered by a hole in the periphery of the crankshaft to provide a 'one time per crankshaft revolution' absolute position. This feature is provided for the triggering of the standard ignition system but was adapted to fit the sensor used for testing. A second proximity sensor was located to the outside of the engine such that it was triggered by the profile of the 72 tooth gear provided in the standard engine for starting. The same type and specification of proximity sensor was used in both locations to avoid confusions which might arise from signal differences

The starter gear drive is fixed to the crankshaft and is free to rotate separately from the outer flywheel and chain drive sprocket. The centrifugal clutch mechanism is designed to function in a manner whereby the engine drives and is not driven. Therefore, to allow the test engine to be driven by the AC electric motor the functioning clutch could not be retained. Consequently, the starter gear was fixed to the flywheel / drive sprocket by three spacers. The spacers were machined with two outer diameters. The smaller diameter was

sized to be a light push fit into flywheel lightening holes in the flywheel drum which can be seen in Figure F4-27. The inner larger diameter then trapping the spacer inside the flywheel drum.

The test engine was motored via a chain drive by the AC electric motor at 2,500rpm for all tests.

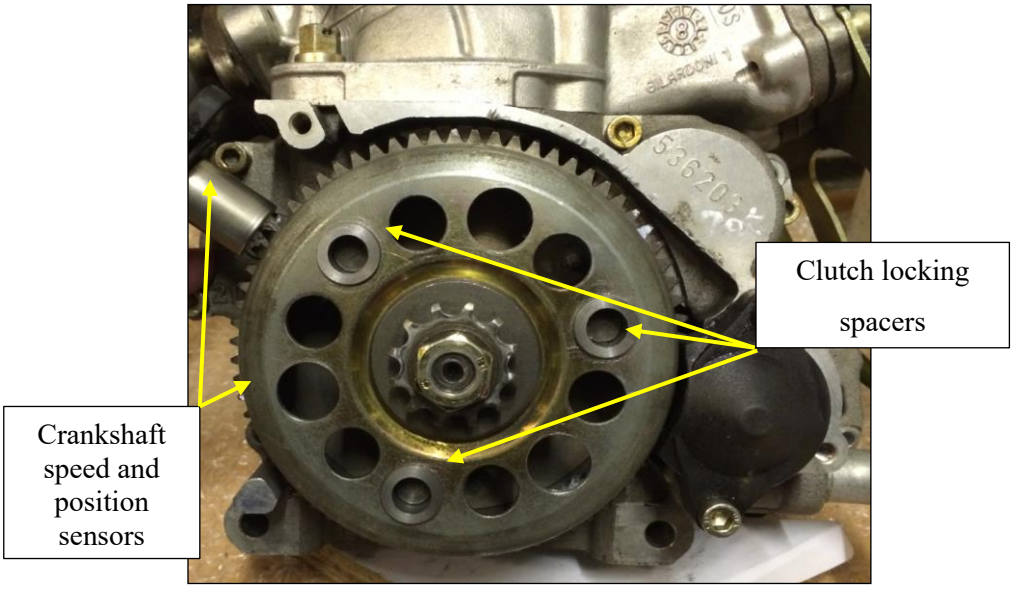

Figure F4-27: Drive locking arrangement to allow the Test Engine to be 'Motored'

The 'Dellorto' carburettor fitted as standard to the 'Rotax Senior Max' test engine, was replaced by a 'Lectron' item of 34mm bore. The replacement item was stripped of the fuel bowl and fuel control floats and internals. This item was fitted in an inverted position and was used only as an intake gas throttle. The throttle slide was fitted with a short throttle cable and held fully open for all tests by a threaded, adjustable/ lockable end fitting. A rubber tube was pushed over the central jet tube which normally supplies fuel into the venturi section and connected to a 0-3 Bar Manifold Absolute Pressure (MAP) sensor. The inverted arrangement was intended to prevent any 'drop-out' from gases passing across the slide building up in the MAP sensor. The inlet end was connected via a rubber pipe to the aluminium air box which was manufactured as part of the inlet gas delivery and mixer system described in section 4.16

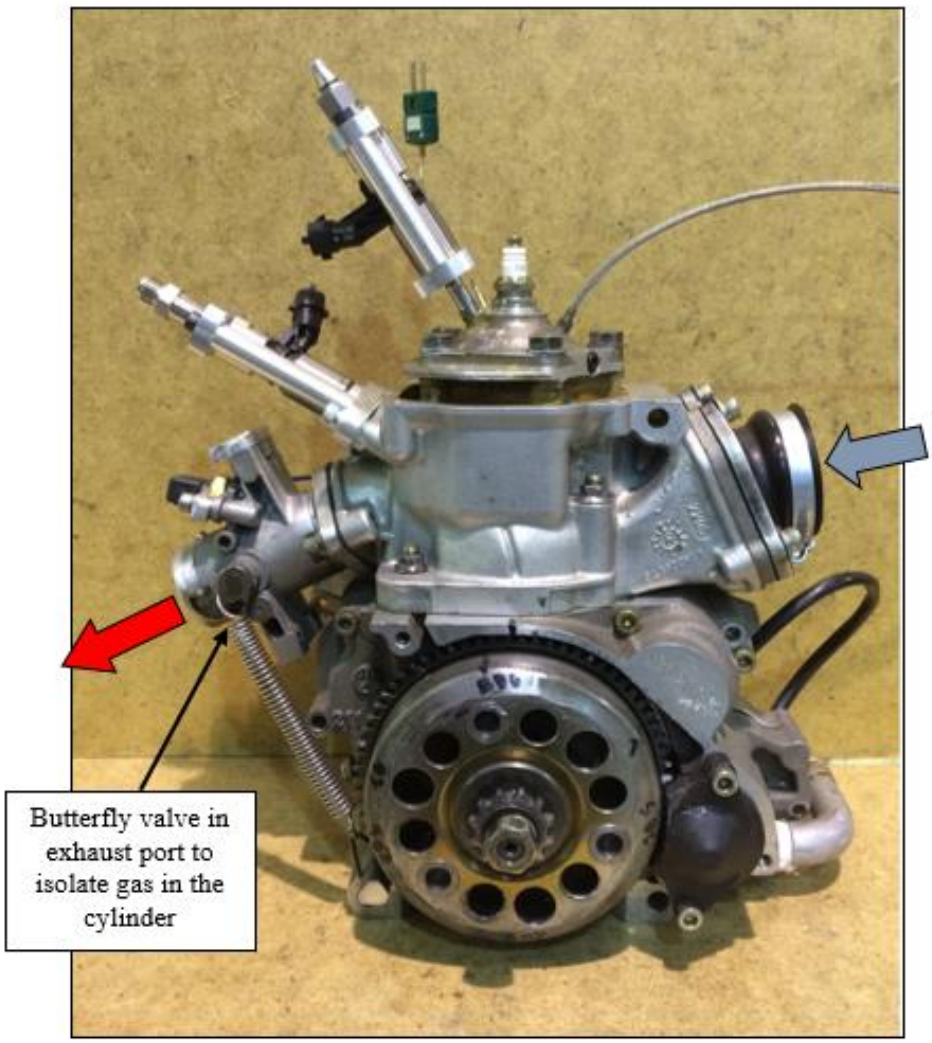

Figure F4-28: The Modified Rotax ‘Max’ Test Engine

The primary intention of dynamic tests was for air or mixtures of air and exhaust gases to pass through the test engine moved by the pumping action of the motored piston. It was intended for this to show the change of SBDV signal resulting from compression and the gas exchange period when the gas was moving through the open exhaust and transfer ports. However, to demonstrate the signal was showing this behaviour it was necessary to prevent the gas which entered the engine from exiting. It was thus intended for the SBDV signals to show the differences of compression and gas flow in open and closed engines. This function was provided using a butterfly valve throttle body which could be manually opened or closed. This item was modified and bolted to the exhaust port outlet flange. This item is shown in Figure F4-28. The same type of butterfly throttle body (modified differently) was fitted to the gas inlet/ mixing system to control and mix the flows of fresh

air and exhaust gases. The exhaust pipe fitted to the test engine consisted of a carbon steel 38mm outside diameter rubber mounted and routed to the test cell exhaust gas evacuation system.

4.13 THE AUXILARY ENGINE

An auxiliary engine was used to deliver burned exhaust gas to the test engine. The unit used, shown in Figure F4-29 being a 40cc ‘Origami B1 Blata Replica’, two-stroke cycle type engine normally fitted to ‘mini-moto’ fun moto-bikes.

This engine was chosen as the auxiliary engine as it was small, reliable and self contained with an integral ignition unit and pull cord starter. The specification of the engine is listed in Table T4-3.

Figure F4-29: The Auxiliary Engine - As supplied

Table T4-3: Specification- Auxiliary engine

Main Specification Details of Auxiliary Engine	
Manufacturer / Model	Origami (Blata Replica) / B1
Intended use	MiniMoto
Capacity (Nominal)	40cc
Inlet Type	Reed Valve
Scavenging Type	Crankcase Scavenged Loop
Cylinder Bore (Nominal)	37.00 mm
Stroke	36.00 mm
Connecting Rod Length	70mm
Geometric Compression Ratio	16.5:1
Clearance Volume (as tested)	2.5cc
Transfer Ports (x5) - Total Duration	120 Degrees
Exhaust Port (x2) Closing Angle	90 Degrees BTDC

4.13.1 MODIFICATIONS TO THE AUXILARY ENGINE

No internal modifications were made to the auxiliary engine as its function was to provide the exhaust gases which were fed into the test engine via the inlet gas delivery and mixing system. The auxiliary engine did not need to be run under load and therefore no drive system was required. An aluminium mounting arrangment was manufactured to

fix the auxiliary engine rigidly to its indendent 25mm thich carbon steel mounting plate as shown in Figure F4-30.

The ‘as supplied’ auxiliary engine featured a conventional fixed jet carburettor which was replaced as it did not provide easy and quickly adjustable fuel control. This facility was required because a fundamental requirement of the dynamic testing apparatus was to be able to change the Air-Fuel ratio of the exhaust gases supplied for mixing with fresh charge to the Rotax Max test engine for evaluation by the SBDV system.

The standard carburettor was changed to a ‘Tillotson’ HL series carburettor which is commonly used in Karting. This item is shown installed on the Auxiliary engine in Figures F4-30 and as a separate item in F4-31.

Note: The thickness of the mounting block ofr the Auxiliary engine shown in Figure F4-30 maintained the same overall inlet length as that with the standard fixed jetting carburettor which was replaced to ensure comparable engine tuning variables.

Figure F4-30: The Auxiliary Engine mounted with adjustable fuel control

4.13.2 THE ADJUSTABLE CARBURETTOR

The ‘Tillotson’ HL carburettor features two externally adjustable fuel jets for high speed and low speed running. This provided an easily changed wide range of fuel flow adjustment. This fuel adjustment was used to provide variations of burned air/ fuel ratio for the tests detailed in chapter nine to identify SBDV signals for different burned exhaust gases in the test engine cylinder.

Figure F4-31: The Tillotson HL Series Carburettor with externally adjustable fuel control

4.13.3 THE AUXILIARY ENGINE EXHAUST SYSTEM

The exhaust system supplied with the Auxiliary engine was retained but modified enable exhaust gases to be routed to the test cell exhaust outlet system or diverted to the Rotax Max test engine inlet mixing system. The diversion arrangement incorporated a by-pass system which could be isolated and diverted using manual valves as shown schematically in Figure F4-19 and below in Figure F4-32. The diversion system piping was manufactured from copper to encourage the heat transfer to atmosphere and reduce the temperature of the exhaust gases delivered to the test engine gas inlet system. The piping was routed to be integral with the overall dynamic test apparatus design.

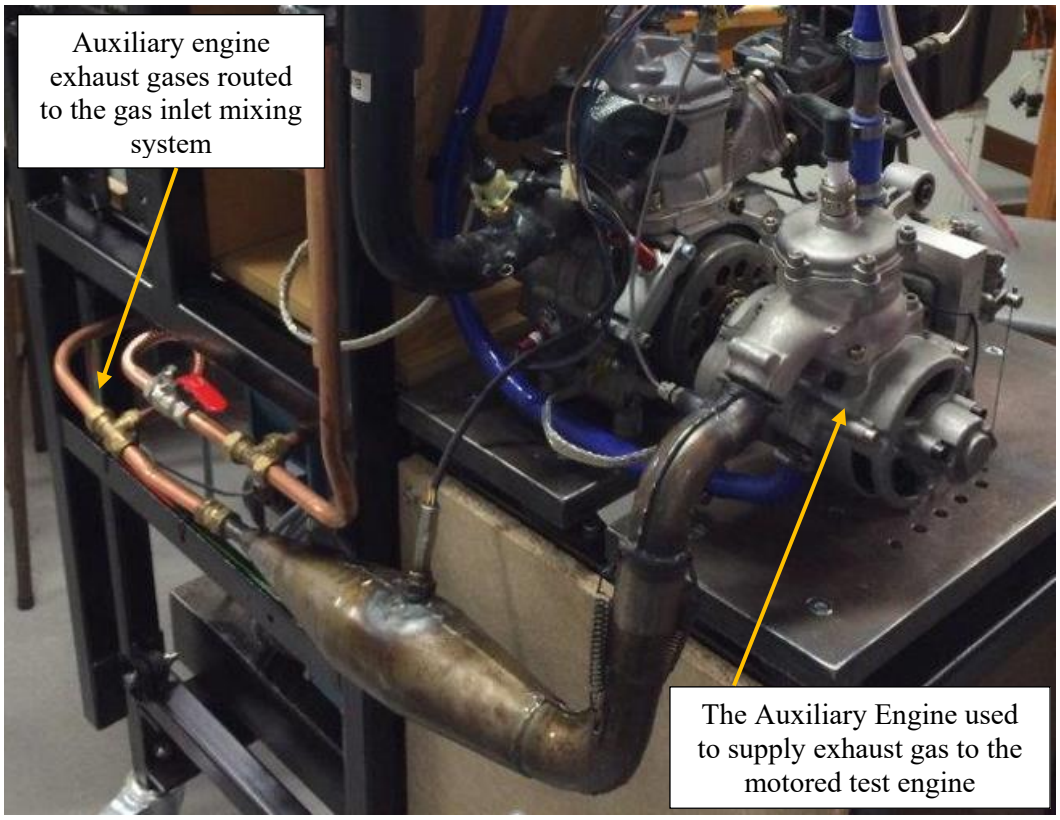

Figure F4-32: The Auxiliary Engine Exhaust Gas Piping arrangement

4.14 THE INLET GAS DELIVERY AND MIXING SYSTEM

The exhaust gases from the Auxiliary engine were delivered via the diversion piping for mixing with fresh charge to the inlet mixing system of the Rotax Max test engine. A simple system was devised and manufactured and assembled from three main separate parts. The design of this system enabled simple manufacturing, cleaning, maintenance and provided options to modify if required. For ease of assembly and maintenance the main items were joined together and connected using rubber sleeves.

The overall arrangement is shown schematically in Figure F4-19 and as an assembly in Figure F4-33. The main three items consisted of the following:

a) An Inlet Pipe.

b) A Mixing Valve.

c) An Air Plenum.

The three main parts of the gas inlet and mixing system listed above, were manufactured from aluminium alloy. This material was chosen, to act together with the copper piping of the exhaust gas diversion system, for its good thermal conductivity characteristics.

The temperature of the inlet gas streams at the point of mixing was expected to increase in proportion to the quantities of exhaust gases added, hence it was considered necessary to encourage heat transfer from the inlet mixed gases to the surroundings before entering the test engine. The objective of the system design and materials used was to limit the temperature variations of all the combinations of exhaust gases and fresh charge delivered into the test engine. For consistency, the gases would enter the engine at the ambient temperature of the test cell so that the SBDV signals obtained would reflect only variations of pressure and temperature changes resulting from motored compression of the gas species in the various gas mixtures tested.

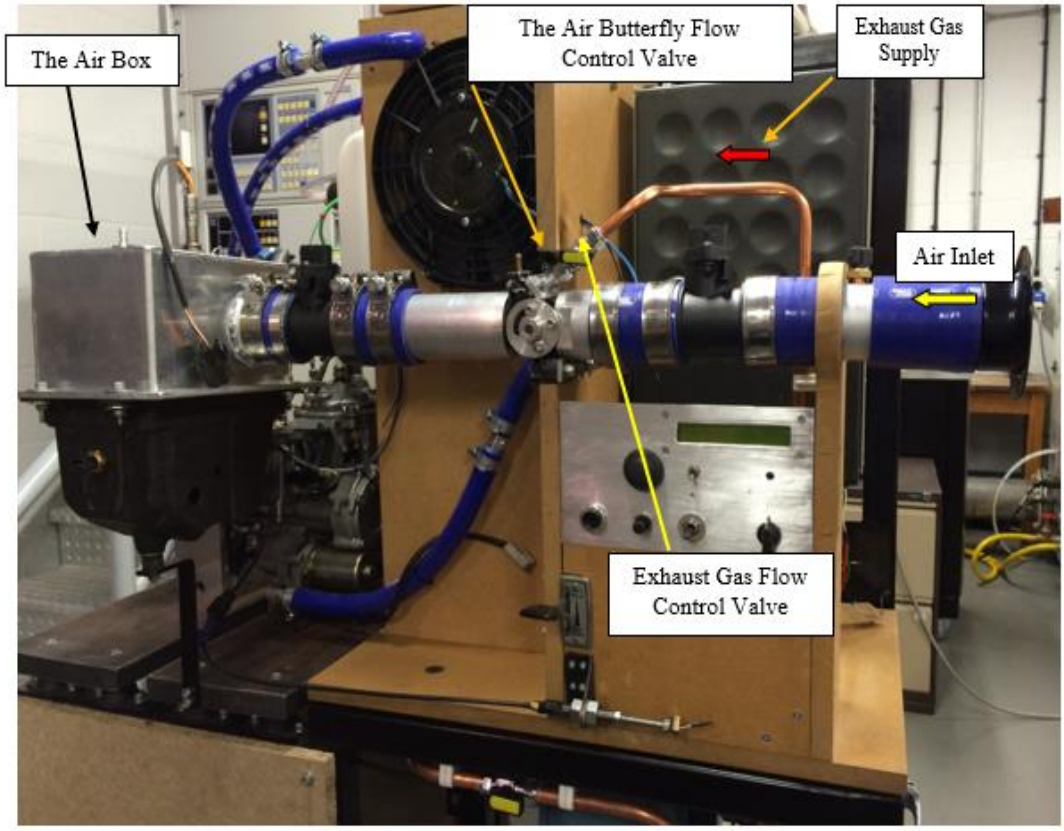

Figure F4-33 The Inlet Gas Delivery and Mixing System

4.14.1 THE INLET PIPE

The inlet pipe was taper bored machined in two parts from aluminium alloy in the form of a venturi shape. This shape increases the speed of the gas and reduces its pressure in the reduced bore central section. The inlet and outlet bore was 50mm and the reduced central bore was 34mm. A cross section of the venturi section of the inlet pipe assembly is shown in Figure F4-34. Upstream and downstream parallel bored sections of aluminium alloy pipe were used to maximise the length of the inlet pipe assembly within the mounted apparatus. Two 50mm bore automotive hot film type mass air flow sensors of the same type were included in the gas inlet system, one upstream and one downstream of the venturi section.

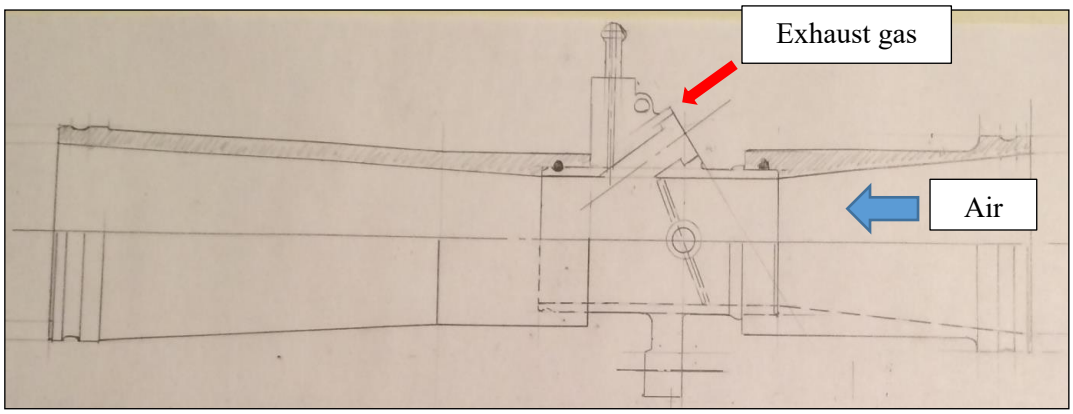

Figure F4-34: Cross section drawing through the Mixing Pipe

4.14.2 THE INLET SYSTEM GAS MIXING VALVE

The centre section of the inlet gas venturi was formed by 34mm bore fuel injection butterfly valve throttle body. The butterfly throttle mechanism provided the means to adjust the fresh air entering the test engine. This item was modified to enable the upstream and downstream connections to the ventruri sections to be sealed gas tight using 3mm section ‘O’ rings.

The protruding boss provided in the throttle body casting for a fuel injector was modified to enable the connection of the exhaust gas diversion piping from the Auxiliary engine. The piping was connected to the throttle body via a closely mounted ½” ball valve using standard compression fittings, as shown in Figure F4-35.

Manual adjustment of the ball valve thus controlled the amount of exhaust gas from the Auxiliary engine entering the test engine inlet gas mixing system. The use of the fuel injector location for incoming exhaust gas ensured the gas fed into the turbulent, low pressure zone immediately downstream of the butterfly valve which encouraged mixing of the two gas streams.

An external plate was fixed to the throttle body by which the butterfly valve could be locked into pre-marked positions. The throttle body was supported from the frame of the dynamic test apparatus using rubber vibration isolation mountings.

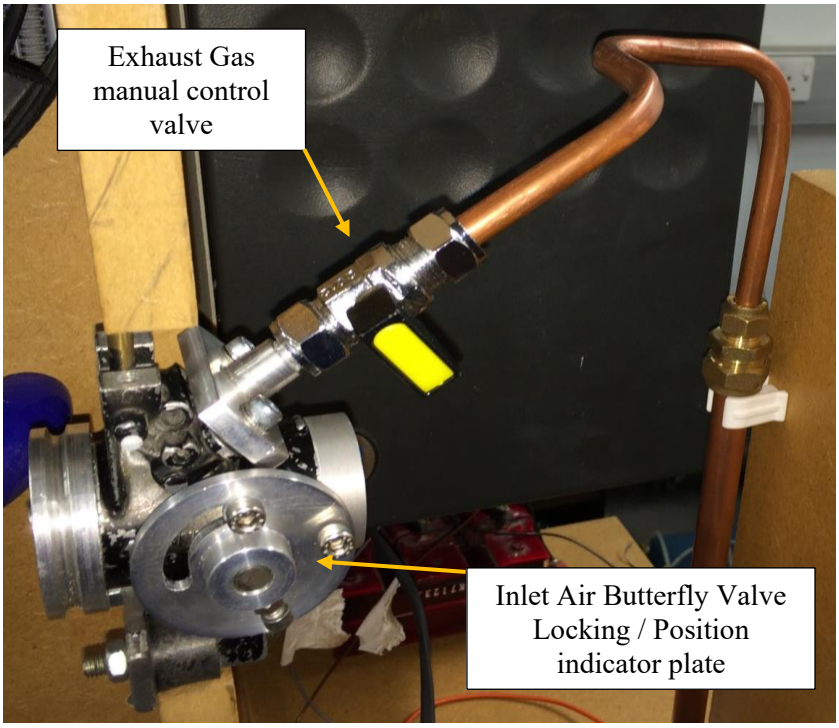

Figure F4-35: The Inlet System Gas Throttle Butterfly and Exhaust Flow Control Valves

4.14.3 THE INLET SYSTEM AIR BOX

The standard Rotax Senior Max engine is supplied for racing with a two-piece plastic Plenum Air Box. In this standard item, which is required by kart racing regulations features a foam filter, trapped between the upper and lower plastic halves with plastic supports. Unfortunately, the inlet connection to this standard item did not enable a satisfactory arrangement for the inlet gas mixing system of the dynamic test apparatus. The Plenum Air Box concept and overall volumes were retained for the test apparatus, but the items were both modified.

Initially, the lower plastic section of the air box was retained together with the standard rubber connector as this was a practical way to adapt the air box to the inlet slide valve. However, initially, the top section of the standard plastic air box was replaced with an item manufactured from Aluminium alloy which incorporated a side entry feed from the inlet

gas mixing pipe. This provided a satisfactory arrangement for the routing of the gas mixing inlet system.

To encourage gas mixing, the top and bottom sections of the Air Plenum Box were separated with a 3mm thick flat aluminium alloy plate. The gases between the two sections were obliged to transfer from the top to bottom sections through two 20mm inside diameter diverter tubes in the opposite end to the inlet pipe connection as shown in Figure F4-37. To further assist gas mixing and to ensure the delivery of a homogenous mixture of air and exhaust gases into the test engine a 12 Volt, 75mm fan (normally used for electronic cooling), was located into the top section of the air box between the inlet gas connection and the 20mm diverter tubes as shown in Figure F4-36.

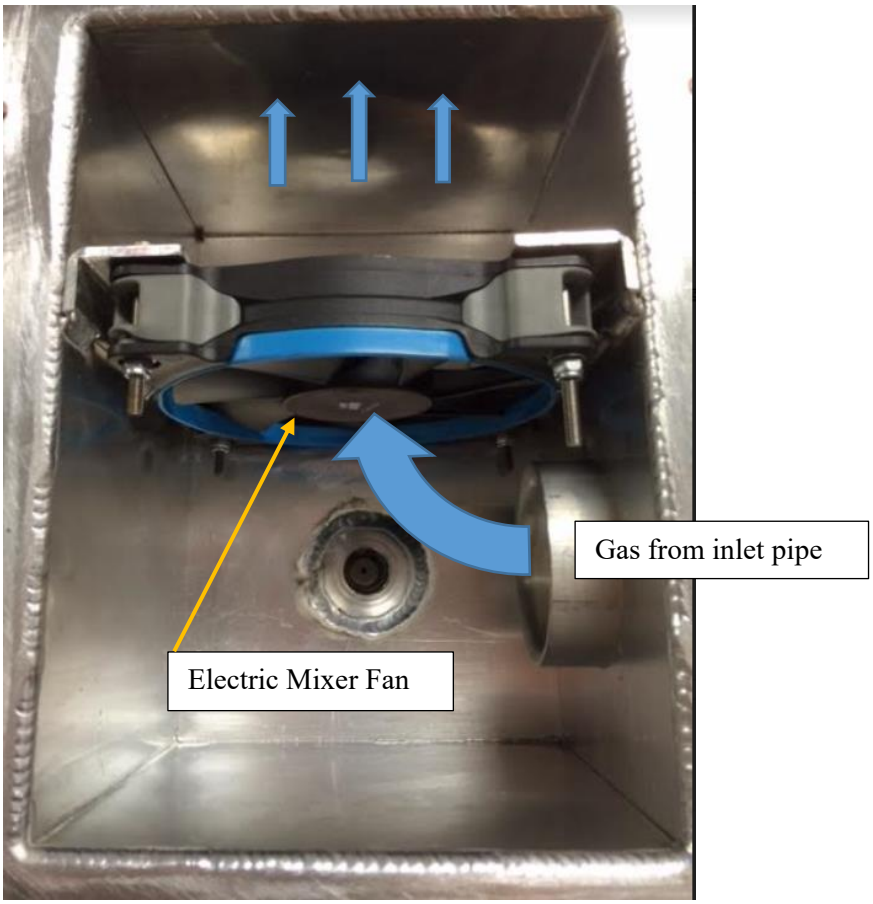

Figure F4-36: The (inverted) Top section of the Air Box

Later, the plastic bottom section of the air box was replaced by a fabricated aluminium alloy item as shown in Figure F4-37. This arrangement forced the inlet gas to a long turbulent flow path which prevented short circuiting, maximised the gas mixing and heat transfer and was used for all the tests reported in the present work.

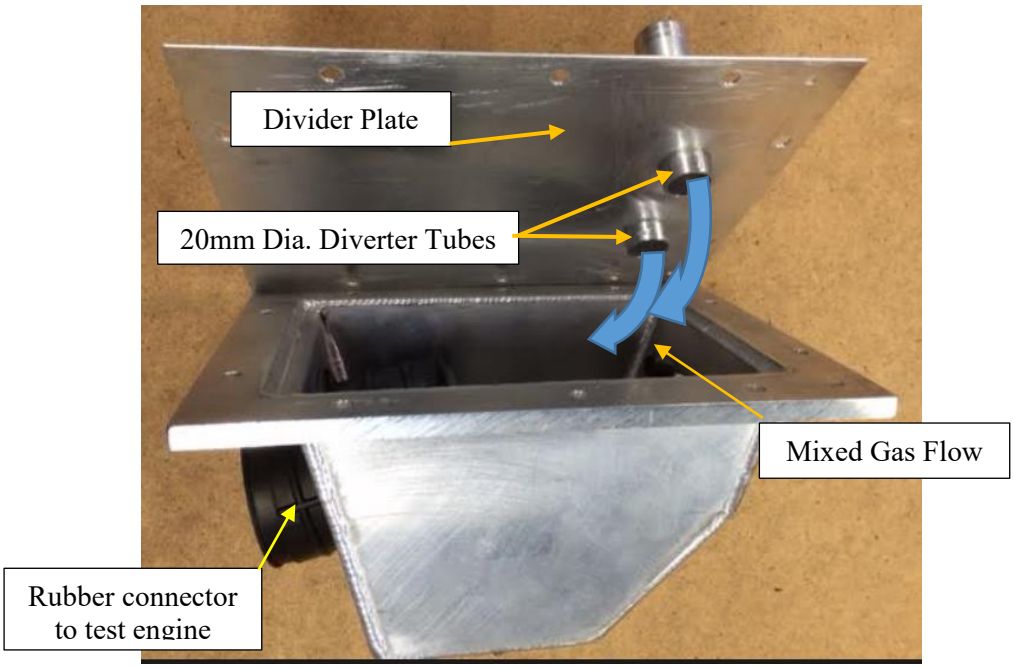

Figure F4-37: The Bottom section of the Air Box with Divider Plate and Flow Tubes.

4.15 CHAPTER SUMMARY

The test apparatus described in this chapter is not complex and does not use expensive equipment. The use of such apparatus matches the basis of the present work which was to determine information in a simple practical way which would be transferable for use in everyday vehicles.

The use of an auxiliary engine to supply exhaust gases to a separate motored test engine appears to be novel as this has not been described in any reference papers investigated. Using exhaust gases produced in an engine under separate control from the motored test engine enabled a wide range of tests to be carried out for the present work.

The test equipment later proved to function acceptably and proved essential to provide the results presented in the following chapters of this work.

CHAPTER FIVE

SCHEDULE OF EXPERIMENTS

5.0 INTRODUCTION

This chapter summarises four stages of testing carried out to determine the capabilities and characteristics of the new SBDV system. The various tests carried out for the present work are listed and described with Chapter references, to assist the reader.

5.1 STAGE 1: SBDV CALIBRATIONS OF SPARK PLUGS IN AIR.

These tests were required to evaluate the spark breakdown voltage signals generated by the new electronic circuit using the spark plug as a sensor.

A first series of tests was carried out to evaluate the sparking characteristics of a range of commercially available types of spark plugs in Air. These tests showed that Spark Distribution Curves can be produced which indicate the characteristics of individual spark plugs at different pressures. These curves are thought to represent a new spark plug calibration method which would be essential for items used as a gas sensor in the new SBDV system.

A second series of tests was carried out to assess the effect of air flow over spark plug electrode specifically to understand how the SBDV signal responded to different amounts of shielding from the incoming gas flow.

Tests were carried out using Air as the dielectric gas, within the test engine both with the engine static with the piston fixed at BDC and also with the test engine motored at 2500 rpm.

These tests confirmed previous work which showed sparking behaviour can be significantly influenced by gas flows around the spark plug. To reduce these effects, a spark plug was modified to improve the stability and response of the SBDV signal in unstable gas flow conditions.

5.2 STAGE 2: SBDV CALIBRATIONS FOR VARIOUS GASES

It is known that spark breakdown voltage varies for different gases and that behaviour changes at different gas pressures / densities. The following chapters investigate those relationships using a number of spark plugs incorporating three different electrode arrangements.

The test results are presented in graphical form with tabulated mathematical expressions provided for each gas for different spark plug types. Further analysis is presented which shows the potential to identify different gases within 1ms.

5.3 STAGE 3: QUASI-STATIC AND DYNAMIC SBDV TESTING OF EXHAUST GASES

A first series of tests were carried out using the test engine, manually turned (hand cranked) at low speed. Exhaust gases were supplied by an auxiliary engine. to obtain SBDV signals and values for various exhaust gas mixtures. The results from these tests are presented graphically with associated mathematical expressions.

A second series of tests were carried out using the test engine motored at 2500 RPM. Exhaust gases were supplied by an auxiliary engine. A number of tests were conducted to represent a very wide range of residual trapped gases. From these tests values for the area under the curve of Power Spectral Density curves which were obtained using Fast Fourier Transform were obtained. These are presented graphically to show a linear relationship which could be used to obtain values of trapped combustible mass within 1ms.

5.4 STAGE 4: DYNAMIC SBDV SIGNALS OF TRAPPED TXHAUST GASES

Tests were carried out to obtained SBDV signals cyclically with air passing freely through the engine. The SBDV signals show cyclic variations of gases during the gas transfer period which are significantly more pronounce than simultaneously recorded values of changing pressure. The validity and interpretation of these signals is confirmed by a second series of cyclically SBDV signals obtained from ‘blocked-in’ tests, where the air was trapped in the cylinder by a butterfly valve in the exhaust port. This arrangement trapped the exhaust gases in the cylinder so that they could not change during the test period. In these tests, the cyclic variations of mass flow during the ‘scavenging’ periods are absent.

Further investigations of SBDV obtained from continuous motored engine cycles with are gas flow through the engine are also reported. Plots of nine consecutive motored cycles in which cylinder pressure changes are compared with SBDV signals converted into pressure using the mathematical relationships for different gases presented in Chapters Seven and Eight. The differences between the SBDV signals representing a wide range of exhaust gas mass fractions are apparent. The chapter also shows reduced sections of each of the nine motored cycles localised around the crankshaft positions proposed by the present work to be used for cycle by cycle control.

CHAPTER SIX

SPARK PLUG CALIBRATION

6.0 INTRODUCTION

This chapter reports the testing carried out to evaluate the functional behaviour and characteristics of various spark plugs to act as SBDV gas sensors.

From previous investigations reported in chapter two and three, it was known that spark breakdown voltage is a function of gas condition, spark length and electrode arrangement which includes geometry, material and condition. These factors are all considerably different in spark plugs than used in classical SBDV tests which used spherical electrodes and spark lengths of several inches. Spark plug design and development has focused on creating a mass-produced item to provide a reliable source of ignition. These ignition sparks occur at significantly lower frequencies and voltages than delivered by the new SBDV electronic circuit. Therefore, the behaviour and characteristics of spark plugs with different electrode configurations, materials and gap lengths required investigation. The spark plugs used were selected as being representative of spark plugs with electrode configurations commonly used for two-stroke cycle type engine applications. These are described in section 6.1.

All the tests reported in this chapter were carried out using ‘air’ as the dielectric test gas. This was a deliberate choice which was relevant and pragmatic for the following reasons:

a) Differences noted were primarily due only to differences in electrodes.
b) Air is a very important gas for an engine, as it forms a large part of the fresh charge and is the carrier of the oxygen required for combustion.
c) Air is the easiest gas to supply and use.
d) Air has been most extensively used gas for ‘classic’ SBDV testing.

Testing prior to that reported in this chapter had been carried out on the bench, in the open atmosphere. However, these tests would be carried out with spark plugs mounted in the cylinder head of the test engine. It was unknown how various spark plugs would function in these alternative conditions and if individual spark plugs could be effectively ‘calibrated’ for use as SBDV gas sensors.

The influence of gas species and conditions is investigated in subsequent chapters.

Therefore, the objectives of this chapter were:

a) Investigate the effect of different spark plug electrode geometries.
b) Investigate if spark plugs function in a reliably consistent manner when subjected to the SBDV generated by the new electronic circuit.
c) Investigate if standard spark plugs can be calibrated individually as SBDV sensors.
d) Investigate how would the SBDV signal be affected by the in-cylinder environment.

6.1 THE SPARK PLUGS USED FOR TESTING

Three basic types or variations of spark plugs were evaluated by testing which were chosen because they are commonly used in two-stroke cycle type engines. These incorporate different electrode configurations, electrode materials and surface condition (resulting from used and new condition). It is known from Paschen's Law the electrode gap distance is the most significant parameter in the relationship between breakdown voltage and gas pressure/density. To evaluate this effect, the electrode gap distance of some spark plugs of the same type were adjusted up to +/- 0.2mm. The details of all the spark plugs used for testing, are provided in Table T6-1.

Table T6-1: Details of Spark Plugs used in Tests

PLUG	PLUG	GAP	MATERIAL	CONDITION	REAL PEAK SBDV	VARIATION	FREQUENCY
Ref. No.	TYPE - HEAT	GAP(mm)	centre/earth		[V]	%	(KHz)
1	R7282A-10.5	0.55	IRIDUIUM/PLATIUM	new	1027.75	27.76	96.15
2	R6120-10.5	0.5	PLATIUM/PLATIUM	new	910.63	36.33	96.40
3	R6120-10.5	0.5	PLATIUM/PLATIUM	new	1025.81	42.87	96.15
4	R6120-10.5	0.55	PLATIUM/PLATIUM	used	999.50	30.47	97.56
5	R7282A-10.5	0.55	IRIDUIUM/PLATIUM	new	1199.00	59.55	96.15
6	R6120-10.5	0.35	PLATIUM/PLATIUM	used	806.50	30.81	96.62
7	R6120-10.6	0.35	PLATIUM/PLATIUM	used	869.50	35.02	97.56
8	R6120-10.5	0.35	PLATIUM/PLATIUM	new	890.00	27.13	97.56
20	IW29 - 9.0	0.6	IRID/PLAT	new	1001.25	33.03	95.24
21	IW29 - 9.0	0.5	IRID/PLAT	new	906.25	24.28	95.24
22	IW29 - 9.0	0.6	IRID/PLAT	new	1069.50	24.60	95.24
23	IW29 - 9.0	0.7	IRID/PLAT	new	1054.82	23.72	95.78

The first spark plug type evaluated by calibration testing, shown in Figure F6-1, is recommended for use with the test engine when used in kart racing. The 'earth' electrode configuration of this plug is a conventional 'J' shaped hook. The tip centre electrode protrudes past the threaded body by 2 mm. This arrangement locates the spark away from the wall of the combustion chamber to limit heat loss of the ignition spark. The 'power' centre electrode for these plugs is tipped with a short section of 0.4mm diameter Iridium

Alloy. The receiving section of the ‘J’ shaped electrode is platinum. Four new plugs of this type, were obtained and a sample from these new plugs was retained as a reference. The other three plugs were re-gapped 0.1mm either side of the recommended 0.6mm value.

Figure F6-1: DENSO IW31 Spark Plug ‘J’ type Earth Electrode

The second and third type of spark plugs evaluated by calibration testing are used in Grand Prix motorcycle racing engines with high heat demands. The ‘earth’ electrode configuration for both of these spark plug types is provided by a 1.0 mm square section made from Platinum alloy. The Platinum alloy earth electrode used for both spark plugs is formed by a straight cantilever from the threaded body over the centre electrode not the ‘J’ shape used for the spark plug type shown in Figure F6-1.

Figure F6-2: NGK R6120 Spark Plug ‘R’ type Platinum Electrodes

The key difference between these types shown in Figures F6-2 and F6-3 being the detail and material used for the central ‘power’ electrode. The first being of 1mm diameter made from Platinum material (Figure F6-2) and the second being 0.4mm diameter made from Iridium alloy (Figure F6-3).

Figure F6-3: NGK R7282A Spark Plug ’R’ type Platinum / Iridium Alloy Electrodes

The smaller diameter central electrode increases the Non-Uniformity of the electrode. This feature increases the localisation of the electric field and reduces the Spark Breakdown Voltage required to pass between a gap of equal distance in an equivalent dielectric gas. This characteristic satisfies a key focus of the design of spark plugs which is to minimise the voltage required to pass between the electrodes. This accepts the actual voltage may vary as this is not conventionally measured by ignition systems. Spark plugs which have small, sharp sided electrode configurations therefore exert considerable influence on the characteristics of the spark breakdown and ionisation mechanisms (Alger, et al., 2006). The replacement of Platinum alloy with Iridium alloy is only possible because it has been developed to better resist erosion for sparking in a reduced cross-sectional area (Nishioka, et al., 2008).

It can be expected that as spark plug electrodes are mass produced they can vary significantly from item to item even for the same design, Therefore, standard values for uniform or non-uniform spark breakdown voltage for any gap cannot be relied upon and each item must be calibrated individually. The dominant influence of electrodes also diminishes the influence of the gas through which the spark breakdown occurs and was expected to represent a challenge to calibrate spark breakdown voltage against different gases.

6.2 THE FIRST SERIES OF SPARK PLUG TESTS

Two separate series of tests were carried out to investigate the characteristic behaviours of various spark plugs. Both series were carried out using the cylinder of the Rotax Senior Max test engine as the test chamber and the spark plugs previously described in section 6.1.

The objectives of both series of tests was listed previously in section 6.0. The primary difference between the test series being the first series used the test engine as a stationary engine as a static volume chamber. These tests focused on investigating the effect on SBDV resulting from the following variations:

a) Spark Plug type.
b) Electrode configuration.
c) Electrode materials.
d) Electrode condition (New or Used plug).
e) Earth electrode orientation relative to inflowing gas.
f) Spark Gap length.
g) Input Voltage supply to SBDV circuit.
h) Air flow (Varied air inlet system valve position).

6.3 APPARATUS FOR THE FIRST SERIES OF SPARK PLUG TESTS

The apparatus arrangement used for the first series of spark plug tests in shown in Figure F6-4. To avoid potential changes to the engine volume during and between individual tests, the test engine crankshaft, was locked into position at BDC. This also ensured the transfer and exhaust ports were fully open and the risk of turbulence resulting from diverted flow past the piston was avoided. The exhaust pipe was connected to the test cell exhaust gas extraction system. Bench testing of the new SBDV system had shown the temperature of the spark plug body is raised by repeated sparking. This is due to the sparking energy being transferred into the spark plug electrodes which then transfers through the porcelain insulation into the plug body. As the SBDV varies on demand in response to the gas species and gas conditions, the heat input and resulting electrode / plug body temperature will vary. These effects were not investigated in the present work. However, when carrying out tests of any kind it is critical to avoid creating changes apart from those being investigated. It was known that SBDV changes with gas density and this varies with gas temperature. Therefore, to avoid increasing the temperature and thus density of the air in the test chamber increasing a small air flow through the engine was created. It was considered important for this flow to be consistent. This flow was created using the suction of the test cell gas

extraction system which has a large volume and functions at constant extract fan speed. Air was thus drawn through the engine via the intake system including the 'air box' and intake butterfly air valve. The majority of tests were carried out with the intake air butterfly valve adjusted to and locked in different positions ranging from fully open (1.0). However, an initial evaluation of varying the pressure in the test chamber was made by restricting the air flow into the test chamber while the suction produced only by the test cell exhaust gas evacuation system remained constant. The air pressure in the cylinder was not recorded in these tests as the objective was only to note if changes occurred. The test cell ambient pressure, temperature and humidity were recorded to enable inlet air density corrections.

The test engine was fitted with the modified cylinder head as shown in Figure F4-15, which had been modified to include a 1mm diameter 'K' type thermocouple. The spark voltage generation circuit was connected to a dedicated power supply unit to avoid electrical interferences from other electrical devices. The electronic signals from the various apparatus sensors including those from the SBDV circuit were connected to a 'Pico-scope' 4824, high speed, 8 channel oscilloscope. This equipment was also powered by a separate dedicated power supply and provided with a separate earth connection to avoid electrical interference. This was connected to a PC to display the data signals from all sensors simultaneously gathered by the PICO 4824 unit.

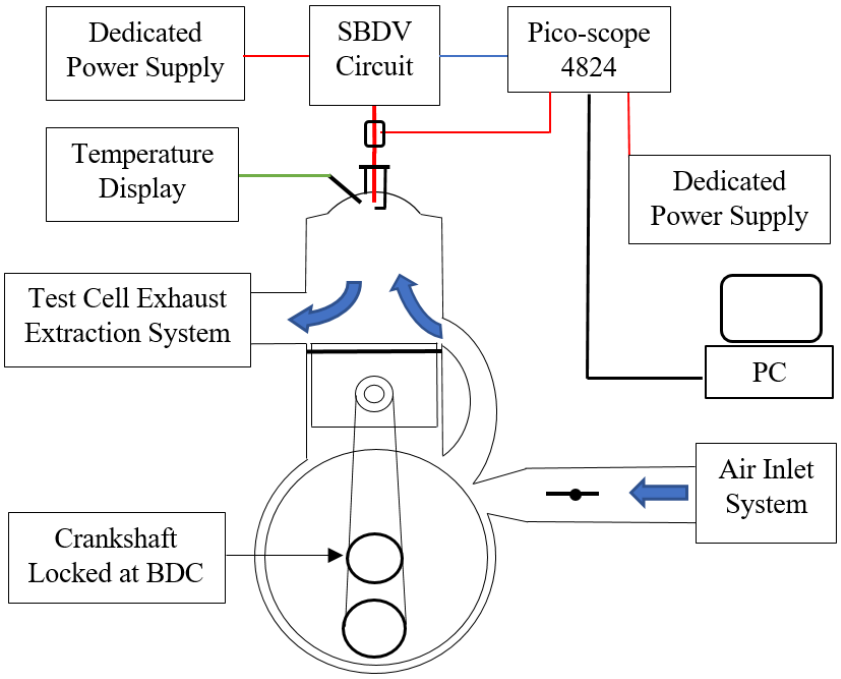

Figure F6-4: Apparatus arrangement scheme for the First series of Spark Plug Tests

6.4 PROCEDURE FOR FIRST SERIES OF SPARK PLUG TESTS

For each individual calibration test the process of obtaining and extracting data followed the procedure is summarised below.

a) The test cell extraction system was started and after 30 seconds (to establish a steady air flow through the engine), the SBDV system was started and run for approximately 10 seconds.
b) The record of spark breakdown voltage events was recorded at a sample rate of 10MHz using a 'Pico-scope' file and saved following each test.
c) Each test file was manually reviewed to check the required signal was recorded.
d) From each 'Pico-scope' test file a reduced sample of one 50 millisecond trace was selected, converted (by 'Pico-scope' software) and stored into separate 'Excel' files.
e) These were compared on the base of data analysis computed on selected 10 millisecond samples (corresponding to about 20000 spark break-down events).

6.5 RESULTS OF THE FIRST SERIES OF SPARK PLUG TESTS

The results of the first test series, comprising 60 individual tests are summarised in Table T6-2.

Table T6-2: Summary of Spark Plug Calibration tests (sheet 1 of 2)

SPARK PLUG CALIBRATION TESTS IN AIR (Sheet 1 of 2)																	
TEST	WAVE	GAS	INTAKE	SPARK	TYPE	PLUG	ELECTRODE			SBDV CIRCUIT		MEASURED SBDV PARAMETERS			AMBIENT CONDITIONS IN TEST CELL		
Ref. No.	FORM	TYPE	VALVE	PLUG	OF	HEAT	GAP	PLUG	ORIENTATION	POWER SUPPLY		REAL PEAK SBDV	VARIATION	FREQUENCY	TEMP	PRESSURE	HUMIDITY
14/11/2014	CAPTURED		POSITION	Ref. No.	PLUG	RANGE	[mm]	CONDITION	[Degrees]	[Volt]	[Amp]	[V]	[%]	[kHz]	[Deg. C]	[Millibar]	[%]
C001	9	AIR	1.00	4	R6120	10.5	0.55	USED	0° [IN-LINE]	14.50	1.97	999.50	30.47	97.561	13.00	995.00	15.00
C002	7	AIR	1.00	5	R7282A	10.5	0.55	NEW	0° [IN-LINE]	14.50	1.98	1199.00	59.55	96.154	13.00	995.00	15.00
C003	13	AIR	1.00	20	IW29	9.0	0.60	NEW	0° [IN-LINE]	14.50	2.07	972.50	32.75	95.238	12.50	995.00	14.50
C004	1	AIR	1.00	21	IW29	9.0	0.50	NEW	0° [IN-LINE]	14.50	2.06	870.50	18.09	95.238	12.80	996.00	15.00
C005	17	AIR	1.00	22	IW29	9.0	0.60	NEW	0° [IN-LINE]	14.50	2.06	1134.00	18.21	95.238	13.00	996.50	14.30
C006	17	AIR	1.00	23	IW29	9.0	0.70	NEW	0° [IN-LINE]	14.50	2.03	979.00	17.88	95.694	13.00	997.50	14.20
C007	13	AIR	1.00	1	R7282A	10.5	0.55	NEW	0° [IN-LINE]	14.50	1.97	1030.00	26.17	96.154	13.00	997.20	13.80
C008	10	AIR	1.00	1	R7282A	10.5	0.55	NEW	0° [IN-LINE]	14.50	2.01	1025.50	29.35	96.154	11.80	992.50	34.70
C009	9	AIR	1.00	6	R6120	10.5	0.35	USED	0° [IN-LINE]	14.50	1.92	896.50	30.81	96.618	12.00	992.70	33.50
C010	27	AIR	1.00	7	R6120	10.5	0.35	USED	0° [IN-LINE]	14.50	2.02	869.50	35.02	97.561	12.00	992.50	32.80
C011	18	AIR	1.00	8	R6120	10.5	0.50	NEW	0° [IN-LINE]	14.50	2.03	890.00	27.13	97.561	12.40	993.00	32.00
C012	25	AIR	1.00	2	R6120	10.5	0.50	NEW	0° [IN-LINE]	14.50	1.99	909.50	38.87	97.561	12.60	992.70	29.00
C013	32	AIR	1.00	2	R6120	10.5	0.50	NEW	45°	14.50	1.99	909.50	38.87	97.561	12.70	992.70	27.80
C014	22	AIR	1.00	2	R6120	10.5	0.50	NEW	345°	14.50	2.00	907.50	34.33	95.238	12.60	993.00	26.30
C015	12	AIR	1.00	2	R6120	10.5	0.50	NEW	285°	14.50	2.00	916.00	33.24	95.238	12.50	992.50	24.50
C016	17	AIR	1.00	3	R6120	10.5	0.50	NEW	0° [IN-LINE]	14.50	2.00	966.00	28.27	96.154	12.50	992.80	22.20
C017	18	AIR	1.00	3	R6120	10.5	0.50	NEW	180°	14.50	1.97	993.00	31.72	96.154	12.50	993.00	20.50
C018	14	AIR	1.00	3	R6120	10.5	0.50	NEW	270°	14.50	1.98	993.00	42.30	96.154	12.50	993.30	20.00
C019	23	AIR	1.00	3	R6120	10.5	0.50	NEW	0° [IN-LINE]	14.50	1.98	1011.50	36.33	96.154	12.50	993.00	20.00
C020	20	AIR	1.00	3	IW29	10.5	0.50	NEW	0° [IN-LINE]	15.00	2.08	960.50	41.54	96.154	12.30	994.00	20.50
C021	18	AIR	1.00	20	IW29	9.0	0.60	NEW	0° [IN-LINE]	15.00	2.14	1030.00	33.30	95.238	12.50	993.80	21.00
C022	29	AIR	1.00	21	IW29	9.0	0.50	NEW	0° [IN-LINE]	15.00	2.12	942.00	30.46	95.238	12.30	994.00	21.00
C023	7	AIR	1.00	22	IW29	9.0	0.60	NEW	0° [IN-LINE]	15.00	2.12	1005.00	31.00	95.238	12.50	994.00	21.00
C024	2	AIR	1.00	23	IW29	9.0	0.70	NEW	0° [IN-LINE]	15.00	2.11	1050.50	61.30	96.154	12.40	994.20	20.80
C025	23	AIR	1.00	3	R6120	10.5	0.50	NEW	0° [IN-LINE]	15.00	2.15	960.50	51.38	96.154	12.20	1014.50	15.80
C026	27	AIR	1.00	3	R6120	10.5	0.50	NEW	0° [IN-LINE]	15.00	2.15	960.50	51.38	96.154	12.20	1014.50	15.80
C027	31	AIR	1.00	3	R6120	10.5	0.50	NEW	0° [IN-LINE]	15.00	2.15	1038.50	40.40	96.154	12.20	1014.50	15.80
C028	29	AIR	1.00	3	R6120	10.5	0.50	NEW	0° [IN-LINE]	15.00	2.09	1035.50	50.00	96.154	12.20	1014.50	15.80
C029	8	AIR	1.00	3	R6120	10.5	0.50	NEW	0° [IN-LINE]	15.00	2.06	1038.50	40.40	96.154	12.20	1014.50	15.80
C030	9	AIR	1.00	3	R6120	10.5	0.50	NEW	0° [IN-LINE]	15.00	2.06	1075.50	44.60	96.154	12.60	1014.20	14.00

Table T6-2: Summary of Spark Plug Calibration tests (sheet 2 of 2)

SPARK PLUG CALIBRATION TESTS IN AIR (Sheet 2 of 2)																	
TEST	WAVE	GAS	INTAKE	SPARK	TYPE	PLUG	ELECTRODE			SBDV CIRCUIT		MEASURED SBDV PARAMETERS			AMBIENT CONDITIONS IN TEST CELL		
Ref. No.	FORM	TYPE	VALVE	PLUG	OF	HEAT	GAP	PLUG	ORIENTATION	POWER SUPPLY		REAL PEAK SBDV	VARIATION	FREQUENCY	TEMP	PRESSURE	HUMIDITY
14/11/2014	CAPTURED		POSITION	Ref. No.	PLUG	RANGE	[mm]	CONDITION	[Degrees]	[Volt]	[Amp]	[V]	[%]	[kHz]	[Deg. C]	[Millibar]	[%]
C031	15	AIR	1.00	3	R6120	10.5	0.50	NEW	0° [IN-LINE]	15.00	2.07	1043.00	36.60	96.154	12.80	1014.30	13.20
C032	15	AIR	0.75	3	R6120	10.5	0.50	NEW	0° [IN-LINE]	15.00	2.07	1037.50	54.70	96.154	12.80	1014.30	13.20
C033	10	AIR	0.50	3	R6120	10.5	0.50	NEW	0° [IN-LINE]	15.00	2.07	1056.00	44.70	96.154	12.80	1014.30	13.20
C034	11	AIR	0.25	3	R6120	10.5	0.50	NEW	0° [IN-LINE]	15.00	2.07	1043.00	51.00	96.154	12.80	1014.30	13.20
C035	14	AIR	0.00	3	R6120	10.5	0.50	NEW	0° [IN-LINE]	15.00	2.04	1043.00	48.00	96.154	12.80	1014.30	13.20
C036	28	AIR	1.00	3	R6120	10.5	0.50	NEW	0° [IN-LINE]	15.00	2.04	1057.00	39.10	96.154	12.80	1014.00	11.80
C037	31	AIR	0.75	3	R6120	10.5	0.50	NEW	0° [IN-LINE]	15.00	2.04	1049.50	39.70	96.154	12.80	1014.00	11.80
C038	29	AIR	0.50	3	R6120	10.5	0.50	NEW	0° [IN-LINE]	15.00	2.04	1030.00	42.80	96.154	12.80	1014.00	11.80
C039	21	AIR	0.25	3	R6120	10.5	0.50	NEW	0° [IN-LINE]	15.00	2.04	1038.50	39.10	96.154	12.80	1014.00	11.80
C040	27	AIR	0.00	3	R6120	10.5	0.50	NEW	0° [IN-LINE]	15.00	2.11	1049.50	41.40	96.154	12.80	1014.00	11.80
C041	28	AIR	1.00	23	IW29	9.0	0.70	NEW	0° [IN-LINE]	15.00	2.11	1112.50	26.10	95.694	12.60	1013.70	12.00
C042	28	AIR	0.75	23	IW29	9.0	0.70	NEW	0° [IN-LINE]	15.00	2.11	1070.00	26.50	95.694	12.60	1013.70	12.00
C043	26	AIR	0.50	23	IW29	9.0	0.70	NEW	0° [IN-LINE]	15.00	2.11	1044.00	16.10	95.694	12.60	1013.70	12.00
C044	28	AIR	0.25	23	IW29	9.0	0.70	NEW	0° [IN-LINE]	15.00	2.11	1025.50	17.10	95.694	12.60	1013.70	12.00
C045	29	AIR	0.00	23	IW29	9.0	0.70	NEW	0° [IN-LINE]	15.00	2.11	1010.50	14.50	95.694	12.60	1013.70	12.00
C046	28	AIR	1.00	23	IW29	9.0	0.70	NEW	0° [IN-LINE]	15.00	2.11	1087.50	24.80	95.694	12.60	1013.70	12.00
C047	26	AIR	0.75	23	IW29	9.0	0.70	NEW	0° [IN-LINE]	15.00	2.11	1082.00	22.70	95.694	12.60	1013.70	12.00
C048	31	AIR	0.50	23	IW29	9.0	0.70	NEW	0° [IN-LINE]	15.00	2.11	1094.00	23.70	95.694	12.60	1013.70	12.00
C049	30	AIR	0.25	23	IW29	9.0	0.70	NEW	0° [IN-LINE]	15.00	2.11	1095.00	22.40	95.694	12.60	1013.70	12.00
C050	29	AIR	0.00	23	IW29	9.0	0.70	NEW	0° [IN-LINE]	15.00	2.11	1005.00	20.70	95.694	12.60	1013.70	12.00
C051	28	AIR	1.00	23	IW29	9.0	0.70	NEW	0° [IN-LINE]	15.00	2.11	1057.00	24.50	95.694	12.50	1013.50	14.20
C052	25	AIR	0.75	23	IW29	9.0	0.70	NEW	0° [IN-LINE]	15.00	2.11	1068.00	21.30	95.694	12.50	1013.50	14.20
C053	25	AIR	0.50	23	IW29	9.0	0.70	NEW	0° [IN-LINE]	15.00	2.11	1083.00	27.10	95.694	12.50	1013.50	14.20
C054	22	AIR	0.25	23	IW29	9.0	0.70	NEW	0° [IN-LINE]	15.00	2.11	1043.00	17.80	95.694	12.50	1013.50	14.20
C055	26	AIR	0.00	23	IW29	9.0	0.70	NEW	0° [IN-LINE]	15.00	2.11	1025.50	18.80	95.696	12.50	1013.50	14.20
C056	25	AIR	1.00	3	R6120	10.5	0.50	NEW	0° [IN-LINE]	15.00	2.03	1025.50	42.70	96.154	12.70	1013.30	14.30
C057	18	AIR	0.75	3	R6120	10.5	0.50	NEW	0° [IN-LINE]	15.00	2.03	1019.00	42.90	96.154	12.70	1013.30	14.30
C058	25	AIR	0.50	3	R6120	10.5	0.50	NEW	0° [IN-LINE]	15.00	2.03	1049.50	43.40	96.154	12.70	1013.30	14.30
C059	18	AIR	0.25	3	R6120	10.5	0.50	NEW	0° [IN-LINE]	15.00	2.03	1049.50	47.70	96.154	12.70	1013.30	14.30
C060	25	AIR	0.00	3	R6120	10.5	0.50	NEW	0° [IN-LINE]	15.00	2.03	1049.50	42.40	96.154	12.70	1013.30	14.30

It was observed from Table T6-2 that SBDV values are not the same for all spark plug types or electrode gaps. This confirmed SBDV measurements using spark plugs were sensitive to key variables which is the major attribute required. However, it was not known how SBDV variations respond to the key variables and therefore further investigation was required. These investigations using data recorded from the tests summarised in Table T6-2 are presented below.

6.6 SPARK DISTRIBUTION CURVES

For each test sample, a graph was created to plot the distribution of spark breakdown voltage vs the repetition of the number of spark events at each voltage. These graphs were termed 'Spark Distribution Curves'. These curves show the distribution and absolute values of breakdown voltages and were found to differ for each individual spark plug and response to variables. The curves thus represent 'signature' curves which could be used as calibrations. The author has not found any previous examples of such behaviour. These curves represent a random running sample so do not include any start-up or shut-down effects. Examples of two individual spark distribution curves are presented below. These curves are considered to show a great deal of information relating to the spark breakdown processes which primarily include, electrode gap length, configuration and material, gas species and pressure. However, how the information shown in such 'distribution curves' relates to these key variables requires to be understood and a straightforward means to differentiate these between samples.

The first investigation was required to determine if the individual spark break-down events recorded during a sample period occurred at the same voltage or if the voltage required varied. The spark distribution curves thus represent the distribution of the number of spark breakdown events over the range of voltages which occurred. The outline shape shown is a trace through the number of repetitions at each voltage. It was expected that not all the break-down events would occur at the same voltage. It was considered such variations would result from 'mass produced' electrode surface irregularities and effects of electrode non-uniformity. The results were surprising and showed that individual spark plugs have a characteristic SBDV 'signature'.

The 'Peak' value indicates the breakdown voltage value at which the greatest number, or 'repetitions' of events occurred. The 'Mean' value of breakdown voltage was calculated as the arithmetic mean of all events during the sample period. The 'Peak' and 'Mean' values

have been indicated in Figures F6.6 and F6-7. The comparative difference between the 'Peak' and 'Mean' values was calculated as a percentage variation.

Where:- $$Percentage\ variation = \frac{Peak\ Voltage - Mean\ Voltage}{Range\ of\ voltages\ of\ sample} \quad \text{(Eq. 6-1)}$$

The differences between the Peak voltages in the two examples shown may be due to the electrode condition, as one is new and the other pre-used. As conditioning occurs the surface irregularities are reduced by erosion and material deposition by the sparking mechanism. This effect would reduce non-uniformity of the electrode surfaces and subsequently reduce the differences of local ionization. This in turn directly effects the voltage at which spark break-down occurs. This may explain the reduced variation of 'Peak', 'Mean' and 'percentage variation'. Alternatively, the differences may result from the different electrode materials of each plug. However, the differences, in this case are not due to different spark gap lengths as both were set at 0.55mm.

The first example, Figure F6-6, is taken from test C001 waveform 9 which was representative of the stable signal of the recorded period. The data was obtained from a 'R' (6120) type plug (No. 4). This spark plug was pre-used condition with an electrode gap of 0.55mm.

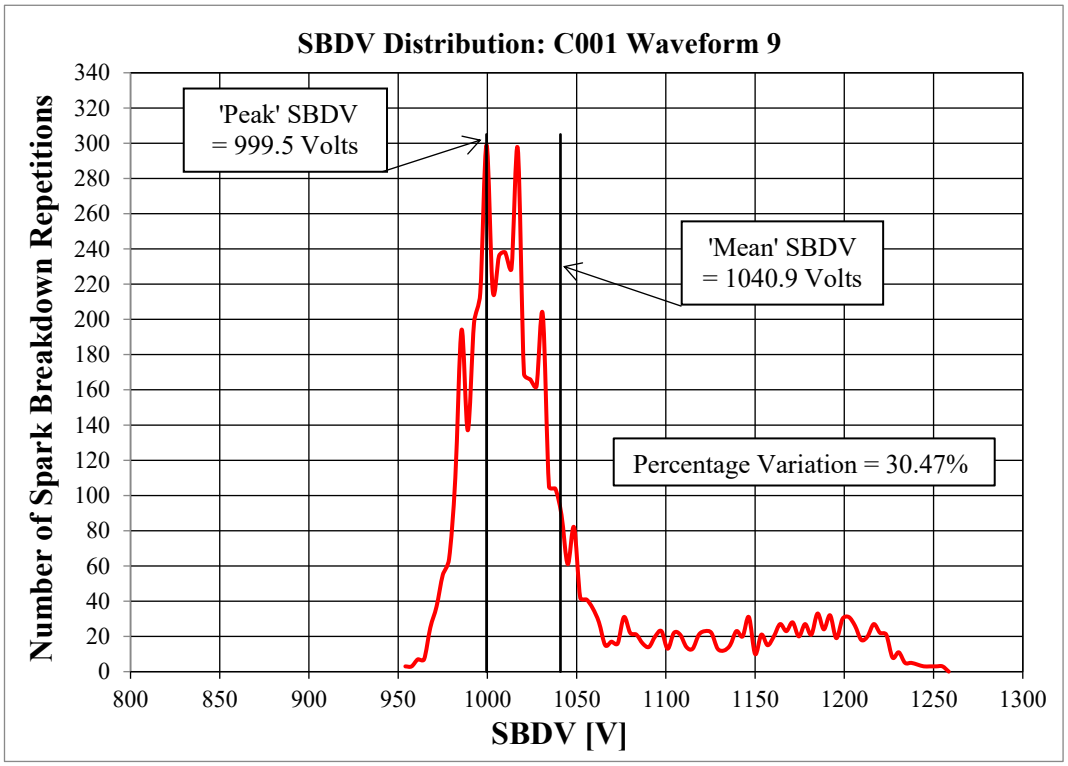

Figure F6-6: Distribution of Spark Breakdown Voltage file: C001 Waveform 9

The second example, Figure F6-7, is taken from test C002 waveform 7 which was representative of the stable signal of the recorded period. The data was obtained from a 'R' (7282A) type plug (No. 5). This spark plug was new condition with an electrode gap of 0.55mm.

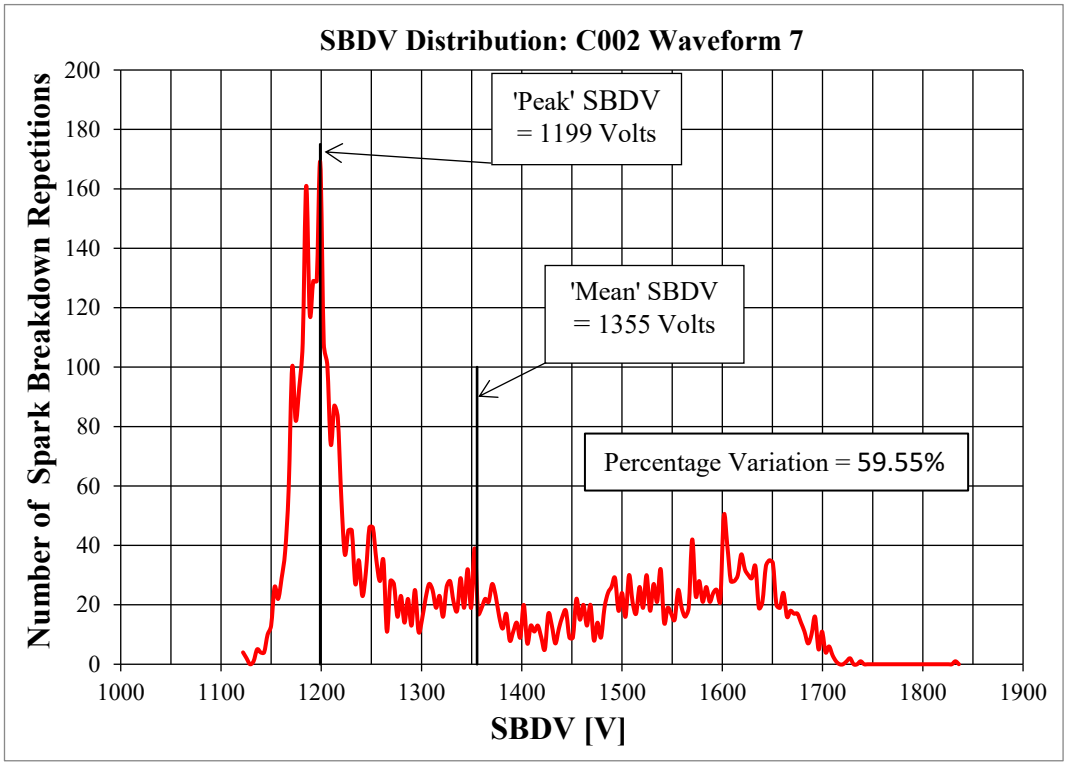

Figure F6-7: Distribution of Spark Breakdown Voltage file C002 Waveform 7

Further investigations of the shape differences between the spark distribution curves by statistical analysis was not included in the present work.

6.7 THE EFFECT ON SBDV OF SPARK PLUG TYPE

A comparison of the spark distribution curves obtained in air, from three different spark plugs, summarised in Table T6-3, and are shown overlaid, in Figure F6-8.

Table T6-3: Files used to create Figure F6-8

Files used to create Figure F6-8			
Spark Plug Ref. No.	Plug 2	Plug 3	Plug 8
File Ref. No.	C012	C016	C011

With reference to the test summary Table T6-2 (Page 1). Plug Numbers 2, 3 and 8 are all new ‘R 6120’ type spark plugs and therefore have the same type electrode configurations. All three spark plugs also have the same heat range (10.5) and therefore similar insulator ceramic shapes and volumes around the central electrode. The input voltages supplied to the SBDV circuit were the same for all three tests with only a 2% variation of current. The dielectric gas used in all three tests was ‘Air’ at very similar ambient temperature and pressure but with a 10% variation of humidity levels Plug 2: 29.00%, Plug 3: 22.2% and Plug 8: 32.00%. Further, the orientation of the earth electrode for these three tests was the same such that the earth electrode was in-line at 0^{o} orientation. The spark distribution curves for these tests are shown in Figure F6-8. The graphs show the number of spark breakdown repetitions which occurred at each breakdown voltage. The recorded spark breakdown events occurred over a range of voltages with varying numbers of repetitions for each. The distribution of the spark breakdown repetitions for all three spark plugs was noted to have a similar overall profile at voltages below and above a defined peak. Notably, the distribution curves appear to be displaced by the SBDV at which the ‘Peak’ number of breakdown repetitions occurred. The similarity of overall spark voltage distribution contours for the three spark plugs caused the spark breakdown voltage at which the average or ‘Mean’ number of repetitions to be displaced by a similar amount as the ‘Peak’, approximately 11%. Spark plug No. 8 displays the smallest variation of voltage to achieve spark breakdown and the greatest number or ‘Peak’ of spark breakdown repetitions occurred at 869.5 Volts. While spark plug No. 3 showed a similar repetition profile but required a higher spark breakdown voltage of 966 Volts. In these three tests, the ‘Peak’ number of spark breakdown events was noted to decrease as the voltage increased.

The results shown in Figure F6-8 were taken to show that spark plugs require individual ‘calibration’ irrespective of their specification and similarity.

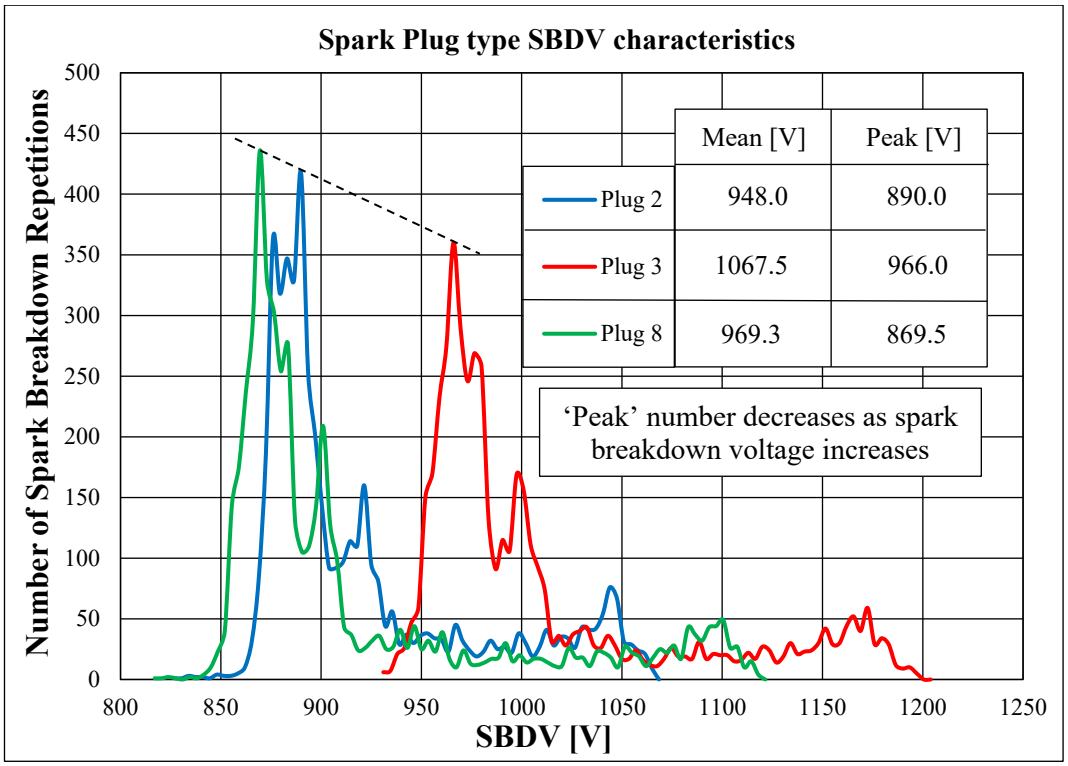

Figure F6-8: Effect of Spark Plug type on Spark Breakdown Voltage Distribution

6.8 THE EFFECT ON SBDV OF THROTTLE OPENING

A comparison of the spark distribution curves obtained in air, from five air inlet positions are summarised in Table T6-4, and are shown overlaid, in Figure F6-9.

Table T6-4: Files used to create Figure F6-9

Files used to create Figure F6-9					
Throttle Position	100%	75%	50%	25%	0%
File Ref. No.	C041	C042	C043	C044	C045

The relationship between the voltage required to 'breakdown' the dielectric gas at different pressures was described in Chapter 4. In an operating engine, the throttle position is a major influence on the cylinder pressure and this would be an important behaviour for the SBDV sensor to respond to. The potential for the SBDV system to differentiate the effect of changing cylinder pressures was achieved in the test engine by changing the position of the inlet butterfly throttle valve against the extraction effect from the exhaust duct. This is more thoroughly investigated and reported in chapter 7. However, an initial assessment showing the effect on the spark breakdown voltage for five throttle valve positions from fully open to fully closed is shown in Figure F6-9. The overlaid spark distribution curves were

obtained using the same spark plug. This shows the 'Peak' breakdown voltage reduces as the air inlet valve position closes and the cylinder pressure reduces. The 'Mean' breakdown voltage does not respond so progressively at low throttle openings. This indicates that using the voltage at which the peak number of samples is obtained rather than the voltage at which the mean or average number of samples is obtained would provide the more consistent relationship with throttle position. This assumption is reasonable for this spark plug but cannot be assumed to be a generalised for all spark plugs or types.

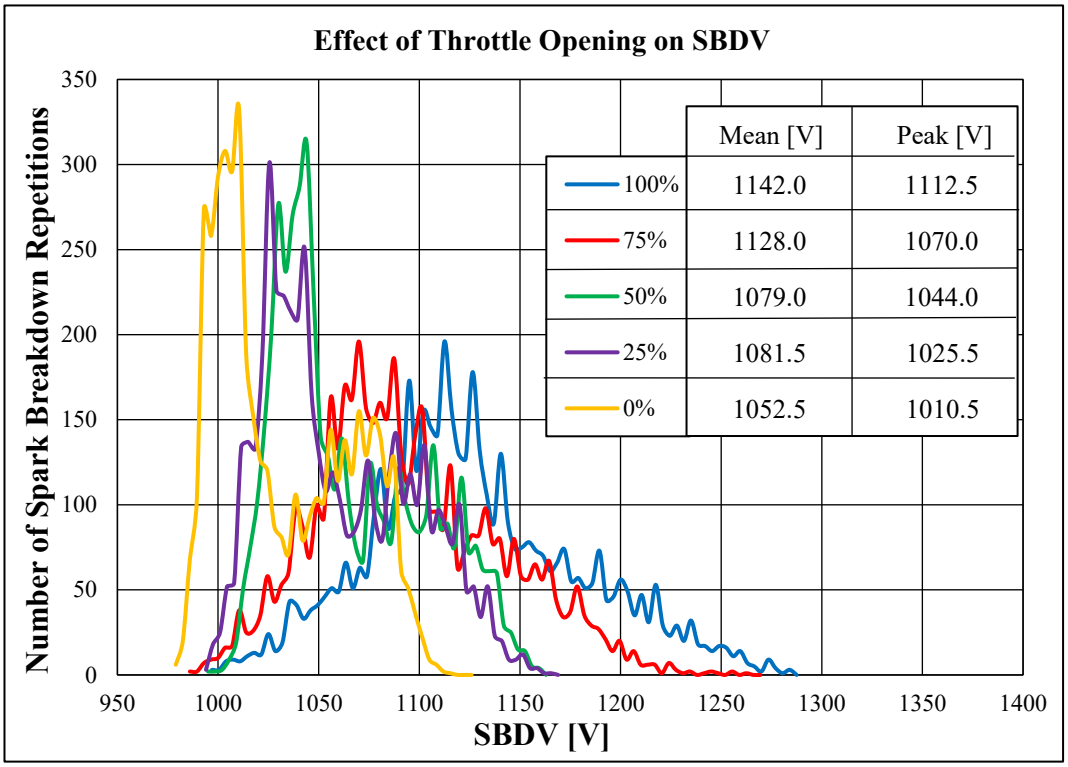

Figure F6-9: Effect of Throttle Opening on Spark Breakdown Voltage Distribution

6.9 THE EFFECT ON SBDV OF INPUT VOLTAGE

A comparison of the spark distribution curves obtained in air, of an input of 14.5 Volts or 15.0 Volts are summarised in Table T6-5, and are shown overlaid, in Figure F6-10.

Table T6-5: Files used to create Figure F6-10

Files used to create Figure F6-10				
Input Voltage	14.5 [V]		15.0 [V]	
Spark Gap (mm)	0.5	0.7	0.5	0.7
File Ref. No.	C004	C006	C022	C024

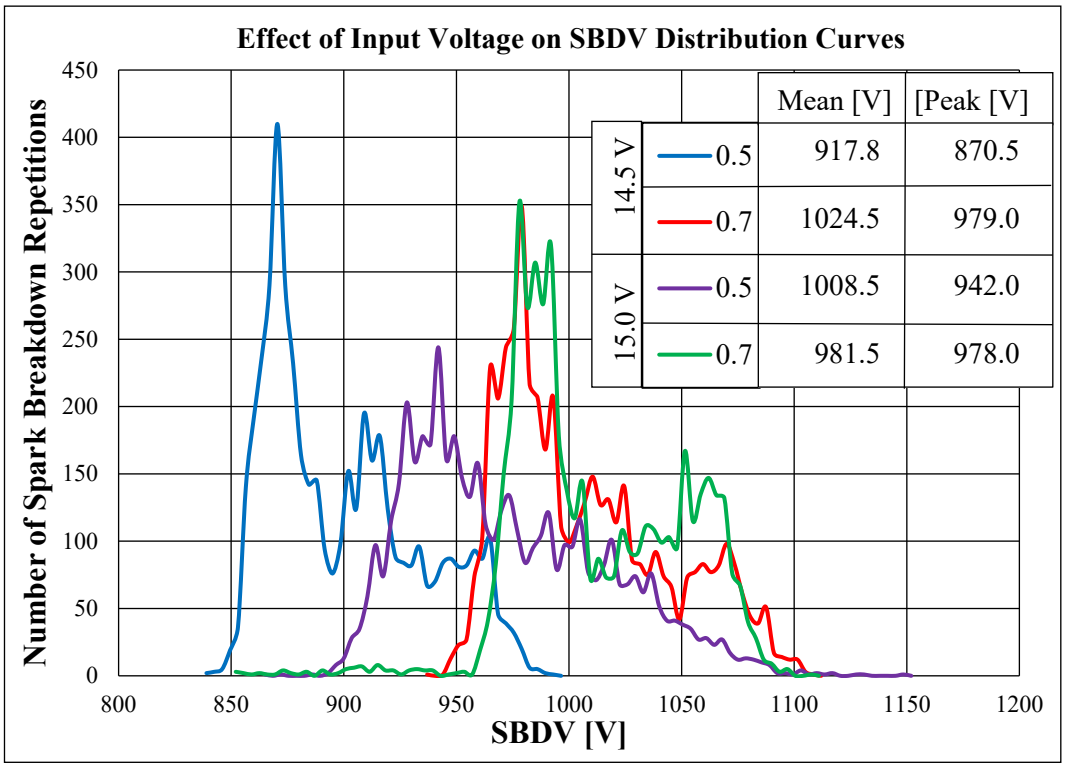

Figure F6-10: Effect of Input Voltage on Spark Breakdown Voltage Distribution

This series of tests were carried out to assess the effect on the sparking behaviour shown by the 'Peak' and 'Mean' spark distribution if the circuit input voltage was changed.

Note: The input voltage to the SDBV circuit was accurately controlled for all tests by using a dedicated power supply. The input voltages used for the tests reported in this section were set at 14.5 Volts and 15.0 Volts.

The effect of changing the input voltage by 0.5 Volts for two spark plugs with two different plug gaps is shown in Figure F6-10. Spark plug No. 21 (0.5mm Spark Gap) and No. 23 (0.7mm Spark Gap), see Table T6-5, were used at both voltages. These spark plugs are both type IW29 and hence have 'J' shaped electrodes. Both spark plugs were in new condition and orientated in the same position at 0° for all tests.

The spark distribution curves for both spark plugs change in response to both input voltage and electrode gap. The effect is more pronounced for the plug with a 0.5mm spark gap distance where the distribution curve spreads and the breakdown voltage increases as the input voltage is increased. Intuitively, this would be due to a greater number of locations or higher electrons density on the electrode surface of the earth electrode where the breakdown could focus. This would reduce the probability of breakdowns occurring in a uniform manner. However, this behaviour is not repeated when the spark plug electrode

gap distance is increased to 0.7mm where the ‘Peak’ voltage differs by only approximately 1%. However, it is further evidence that the breakdown behaviour of each spark plug cannot be assumed to be consistent.

b) To assess the accuracy to which the input voltage requires to be controlled.
c) Increasing the SBDV circuit input voltage causes the components to run hotter and potentially less reliably.

6.10 ELECTRODE CONDITION

The effect of electrode condition was assessed by testing a pre-used NGK ‘R’ type plug the electrodes and ceramic of which were ‘coked-up’ as would commonly be seen in a spark plug from a heavily used engine. Unfortunately, no data existed as to the age or the mileage this item had covered. This racing type plug had electrode materials at the centre: Iridium and tapered earth electrode of Platinum. Tests results showed that this plug can provide a SBDV signal with the least variation when compared to any conventional plug tested. This characteristic was interesting evidence as to the positive effect of ‘electrode conditioning’ on SBDV stability (Lucas, 2001). This plug was designated for future reference as (R10). A photograph of the electrode face of this plug is shown in Figure F6-11.

Figure F6-11: Condition of ‘as tested’ R10 Spark Plug electrodes

6.11 THE EFFECT OF SPARK PLUG ORIENTATION

A comparison of the spark distribution curves obtained in air, of the earth electrode positioned in four positions are summarised in Table T6-6, and shown overlaid, in Figure F6-12. The rotational positions are shown schematically in Figure No. F6-13.

Table T6-6: Files used to create Figure F6-12

Files used to create Figure F6-12				
Earth Electrode Orientaion	0°	45°	345°	285°
File Ref. No.	C012	C013	C014	C015

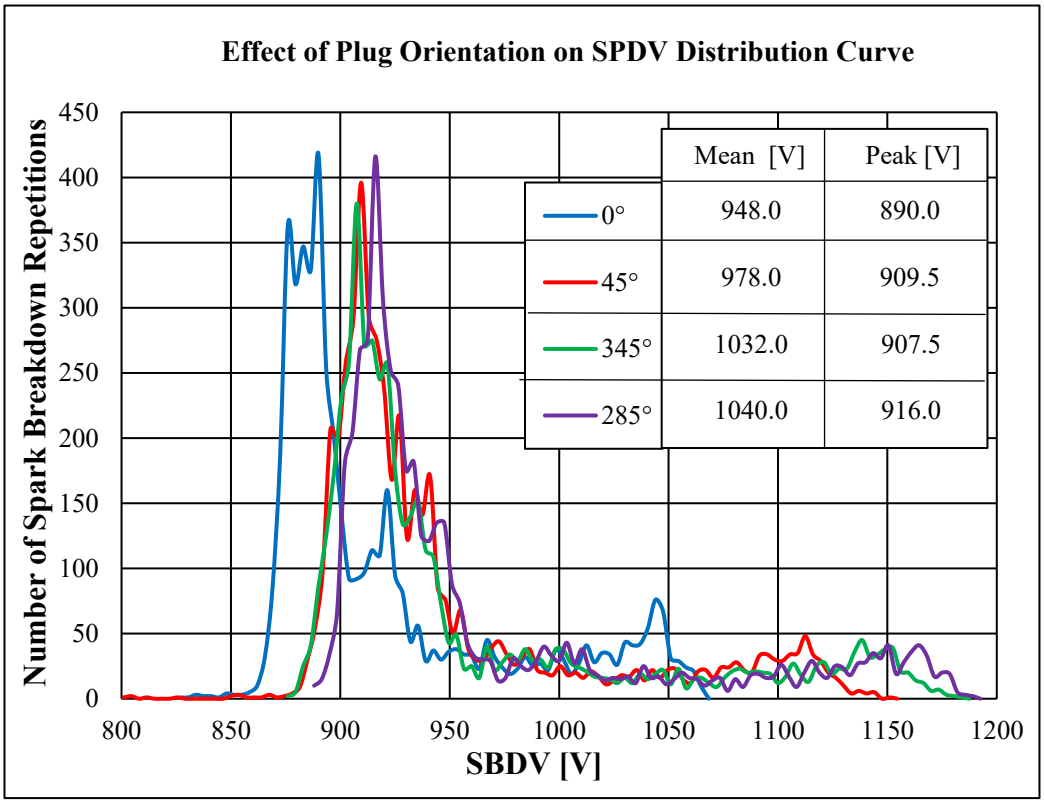

Figure F6-12: Spark Distribution Curves – Four earth electrode orientations.

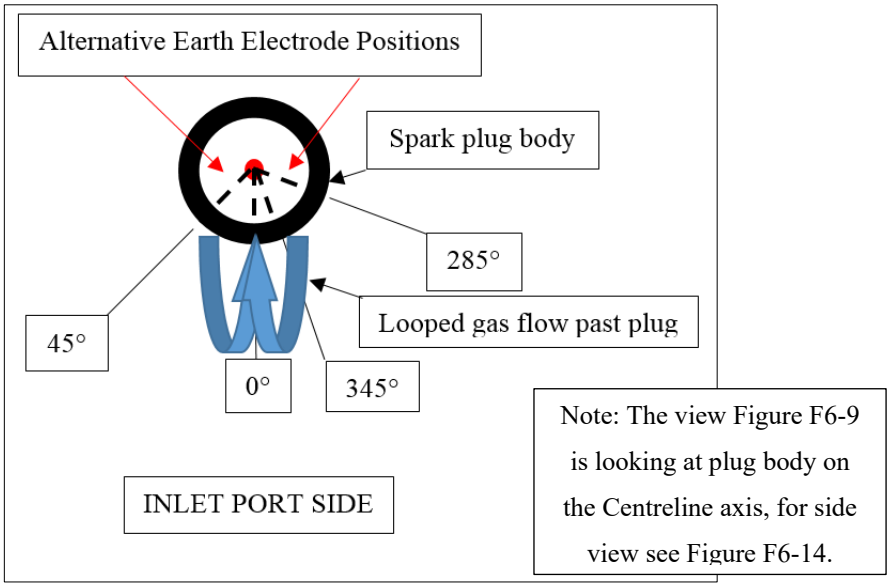

Figure F6-13: Spark Plug earth electrode rotational orientations

The apparatus arrangement used for the first series of tests created a small flow of air through the engine. Four of the initial tests were carried out with Spark plug No. 2 mounted in the different rotational orientations as shown in Figure F6-13 to enable an initial assessment of the influence of the spark plug earth electrode orientation.

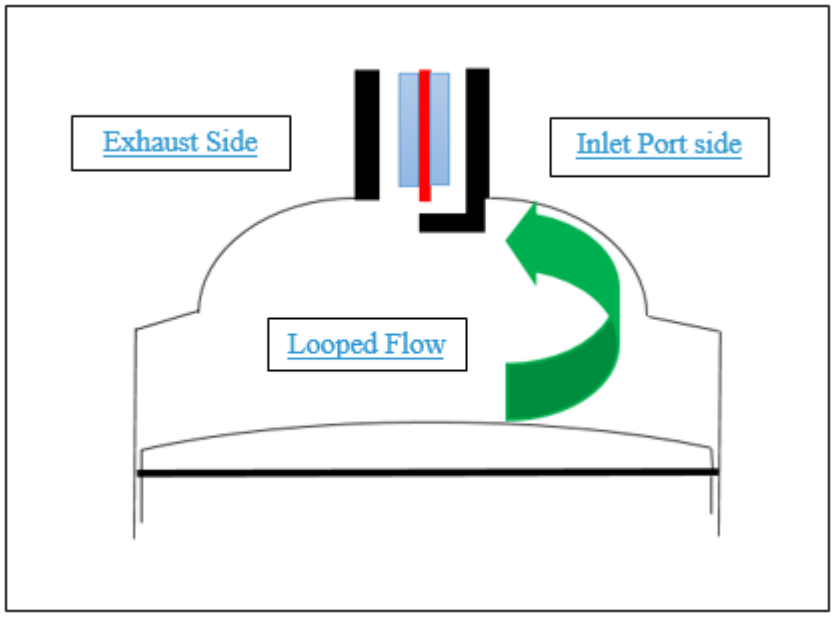

Figure F6-14: Air Flow direction relative to Spark Plug earth electrode

With the spark plug mounted at 0° the earth electrode provided shielding from the air flow in the cylinder conforming to the 'loop scavenged' pattern as shown in Figure F6-14.

The three alternative rotational positions were achieved by varying the thickness of the washer under the spark plug so that when the spark plug was tightened down, it was aligned at three different angles (45°, 285°, 345°). When rotated into these positions, the shielding effect provided by the earth electrode positioned at 0 Degrees was reduced.

The four spark distribution curves in Figure F6-11, shows the significant sensitivity of spark breakdown voltage to earth electrode position. These curves show both the 'Peak' and 'Mean' breakdown voltage change in response to decreased shielding from the air flow. It was noted the characteristic shape of the curves for all the unshielded electrode positions were similar to each other, but differed from that of the shielded position. The greatest shielding results in the lowest spark breakdown voltage which increases in the other three cases as the shielding decreases. Air flow across the spark plug electrodes causes the ionized spark path to become elongated as shown in Figure F6-15.

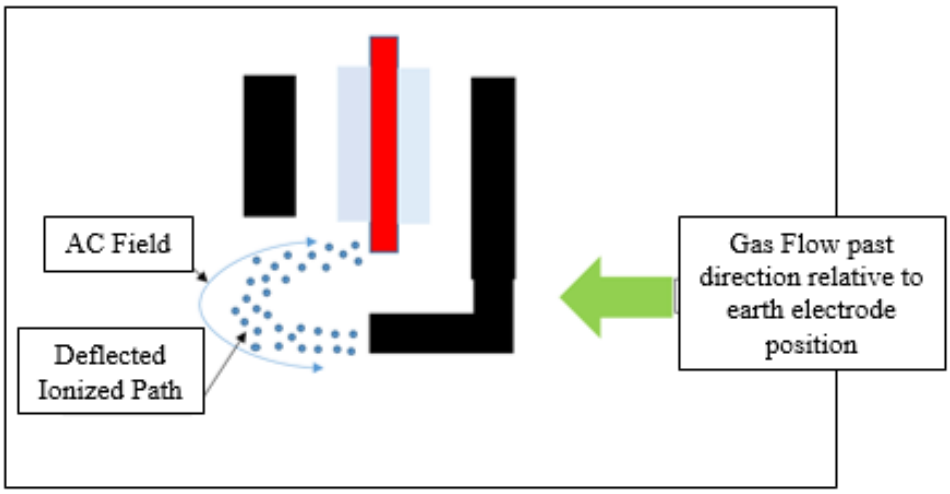

Figure F6-15: View showing effect of an Ionized path deflection by gas-flow.

In an ignition event, an elongation of the ionized spark path length causes a delay to the ignition event and increases the amount of spark heat lost to the surroundings. If this is sufficiently great, the spark will have insufficient heat to sustain the initial flame kernel growth and a misfire will occur. However, this effect is more critical if the spark breakdown voltage is being used as a sensor the increased ionization path length will be interpreted as an increase in gas pressure / density. The four tests carried out had demonstrated how sensitive the SBDV signal would be to such effects. An additional indication was that in some recordings the SBDV signal became 'rippled' shaped as if a repetitive cycle had occurred. This was not a universal feature, but this was taken as further indication of flow effects.

6.12 THE BLOW TEST

The second series of tests examined the effects of in-cylinder air flow on SBDV in greater detail. However, it was realised the application of SBDV events at 94 kHz as indicated by Figure F6-15, represents an almost continuous ionized stream which would be easier to influence than a single ignition spark event. The greater ionized material retention resulting from the continuous high frequency AC events generated by the SBDV system were considered likely to increase the potential for deflection and elongation of the ionized path to occur. Therefore, before the second series of tests were carried out a very simple test was made to assess how sensitive the sparking created by the SBDV system would be and how easily this path could be diverted.

To evaluate the potential for ionized path diversion, a very simple test was carried out, termed 'the blow test'. This consisted of blowing a simple puff of air from the author's mouth, (estimated at 0.5m/sec), blown towards the spark plug from a distance of approximately 150mm. This showed how the SBDV spark stream could be diverted. This admittedly, very simple, non-scientific, evaluation was carried out on both the plug types 'with 'J' shaped and 'R' type electrodes. The results and conclusions cannot be classified as other than indicative.

6.12.1 THE BLOW TEST ON SPARK PLUG WITH 'J' SHAPED ELECTODES

When the 'blow test' was applied to a 'J' shaped electrode, the SBDV spark was easily pushed to move away from the overhanging earth electrode onto the threaded body of the plug. This behaviour can be seen clearly in a photograph of the test, see Figure F6-16. The total detachment of the spark from the earth electrode produces an almost instantaneous switch to the spark plug body. Once attached to the body the spark ran around the circumference of the body attempting to 'find' the path of least resistance. Additionally, once detached the SBDV spark stream and resisted relocation back onto the overhanging earth electrode. This phenomenon was observed by (Griffin, et al., 1998) and termed 'rimfire' noting its detrimental effects on combustion.

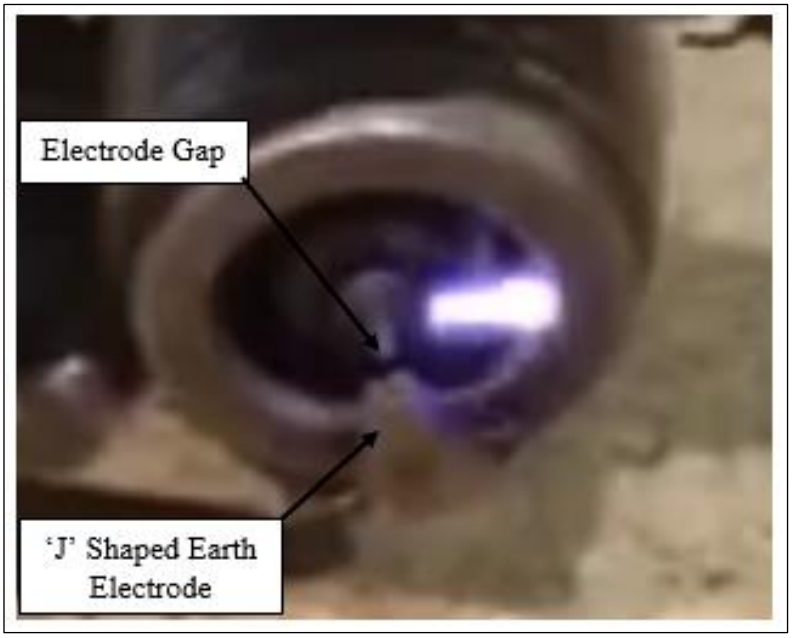

Figure F6-16: 'J' Shaped Electrode Blow Test. Spark direct to plug body

The reason why the SBDV spark stream detaches from the earth electrode can be recognised by considering Figure F6-17. As the air flow elongates the SBDV spark stream the grounding point moves further along the earth electrode. This mechanism continues until the distance from the central electrode to the 90 Degree corner of the 'J' shaped electrode is greater than the distance to the spark plug body. At this point the SBDV spark stream jumps to the spark plug body. The spark plug body represents an earth of less resistance which decreases the potential difference and encourages the jump to occur.

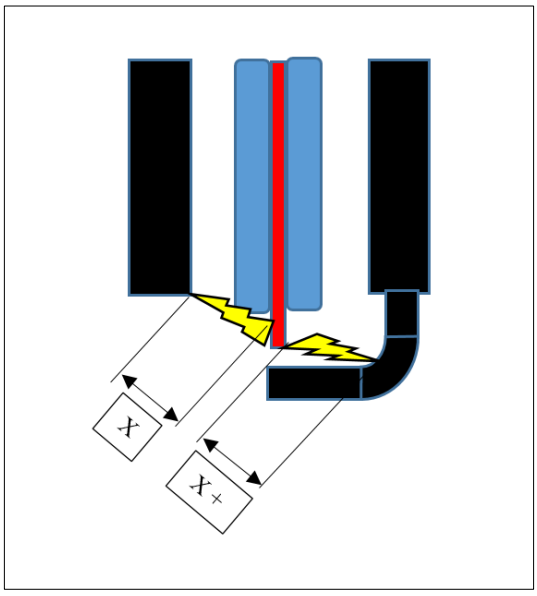

Figure F6-17: 'J' Shaped Electrode. Deflected Sparking Distance

6.12.1 THE BLOW TEST ON SPARK PLUG WITH ‘J’ SHAPED ELECTODES

When the ‘blow test’ was applied to a ‘R’ shaped electrode plug, the SBDV spark stream was observed to be very resistant to diverting off the earth electrode onto the spark plug body. This difference is considered to occur due to the straight cantilever shape of the earth electrode where the distance along the cantilevered earth electrode increases progressively, always offering a shorter path than that to the spark plug body. During the blow test the spark moved along the cantilevered earth electrode and back towards the shortest distance in the central position when the air velocity was reduced. This behaviour can be observed in Figure F6-18 and the mechanism visualised in Figure F6-19. This behaviour could be used to provide a measurement technique for the turbulent gas flow past the plug in an enhanced manner than previously achieved (Pashley & Stone, 2000).

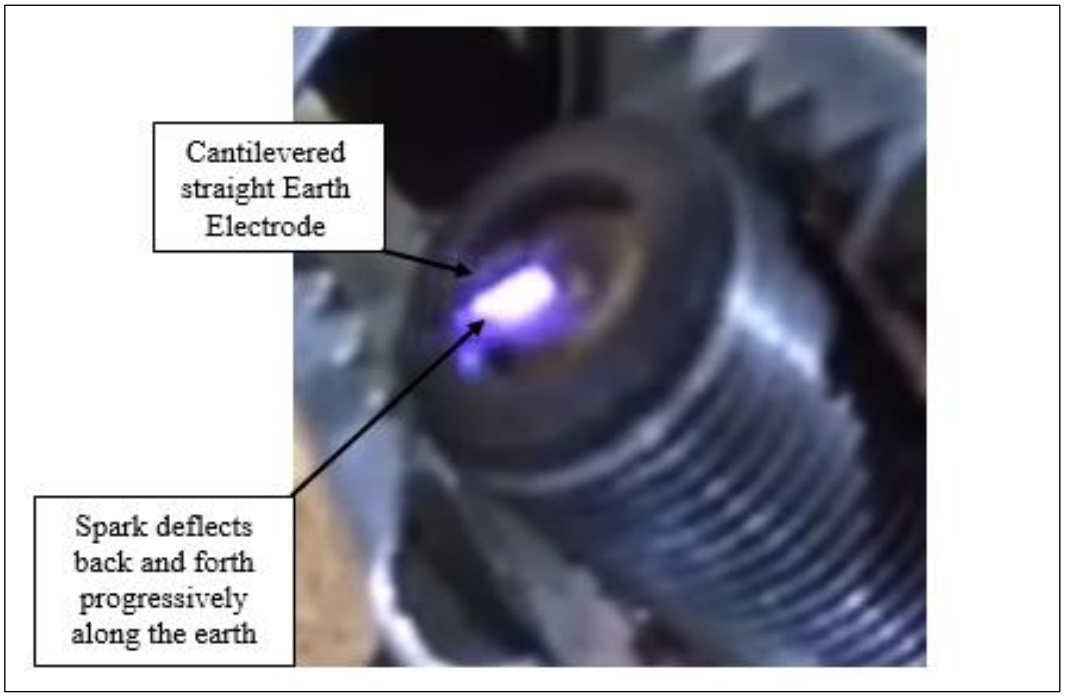

Figure F6-18 ‘R’ Shaped Electrode Blow Test. Spark follows earth electrode

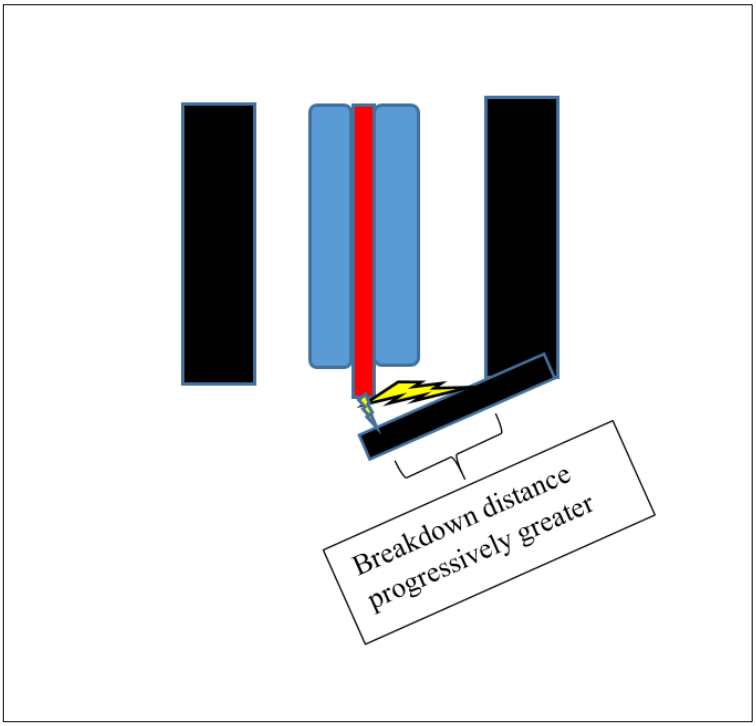

Figure F6-19 ‘R’ Shaped electrode. Progressive sparking distance

6.13 THE SHROUDED PLUG

Spark plug developments have been focused on improving ignition reliability and reducing COV. Previous research has shown that electrode design and plug orientation are both noted to be causes of cyclic combustion variability (Ozdor, et al., 1996). Evaluation of different earth electrode arrangements has shown variations of the voltage required to achieve combustion with the low COV and emissions levels (Lee, et al., 1990). The variation of mass burning rates due to the number of earth electrodes showed multiple electrodes slowed down the early flame development. The amount of heat loss from the spark plug leads towards higher cyclic variability (Adbel-Rehim, 2013).

Spark plug development has moved to incorporate small diameter centre ‘power’ electrodes with similar local protuberant additions to the ‘earth’ electrodes (Daniels & Scilzo, 1996), (Hori, et al., 2003). These additions are manufactured from specialised Iridium and Platinum alloys which can withstand the additional heat from reduced mass and erosion due to reduced electrode surface area. These materials also have lower ionisation potential

characteristics which encourages breakdown to occur in more defined channels. Formation of the flame kernel is assisted due to the reduced heat transfer to the electrodes.

Tests described previously indicated the sensitivity which would occur in a firing engine due to different electrode shapes, positions and shielding. It was considered this would add significantly to the variability of the SBDV signal and cause interpretation complexities in a firing engine. This behaviour was expected to require the development of a spark plug electrode arrangement which would combine excellent ignition and SBDV sensing. However, the work of this thesis concerns only the sensitivity and stability of the SBDV signal.

Consequently, a spark plug design was conceived which would provide a more consistent SBDV behaviour and signal particularly when exposed to flowing gases. Manufacture of a completely new spark plug was not an option. Additionally, any adaptation or modification for the present work had to be simple to implement.

6.13.1 SHROUDED PLUG DESIGN CONCEPT

The work previously reported in this chapter had shown that a critical design feature for a spark plug which is to be used as a SBDV sensor is the maintenance of constant spark gap. This is because for a gas of the same density and temperature the voltage required to breakdown the dielectric properties of that gas being proportional to the electrode gap or as shown, more correctly, the ionized path length. Therefore, for a spark plug to function consistently as a SBDV gas sensor it is critical the same ionized spark length occurs irrespective of gas flow strength or direction.

The spark plug design conceived for a SBDV sensor design is shown schematically in Figure F6-20 and modifications are described in section 6.13.2. The primary feature of the design is an earth electrode which surrounds the central electrode with a constant gap distance. This also provides a greater shroud effect to the spark than an exposed electrode arrangement.

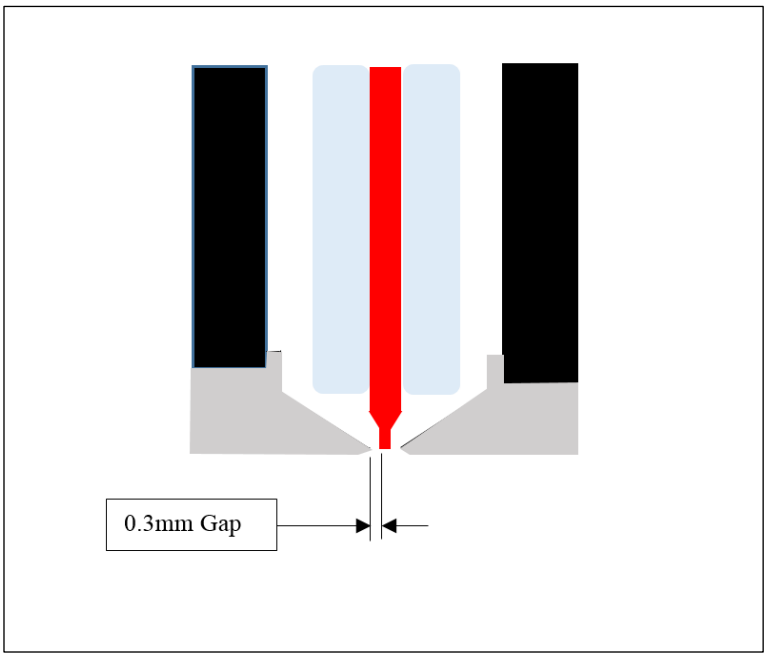

Figure F6-20: Modification scheme to produce ‘The Shrouded Plug’

As the spark voltage provided by the new SBDV circuit used for this research, was limited, the electrode gap length was reduced from the 0.55mm - 0.6mm used for a spark plug for ignition, to 0.3mm. This distance would enable SBDV signals to be obtained in higher gas pressures.

The electrode to electrode configuration was intended to provide the maximum encouragement for the spark breakdown to be maintained between the 0.3mm gap distance. The profile of the surrounding earth electrode was tapered to a sharp point in both directions. This shape presents a strongly non-uniform arrangement which reduces the breakdown voltage required and encourages the spark to strike on the shortest distance. Additionally, because the gap surrounds and shrouds the central electrode any spark deviation caused by gas flow could only result in spark being deflected a minimal distance inwards or outwards axially. From observations of ‘R’ and ‘J’ plug sparking behaviour it was considered any sparks displaced by air flow would be encouraged by the electrode profile to return to back, towards the central sharp point.

The arrangement looks similar to a ‘surface discharge’ type plug which is commonly used in aero engines, rotary type engines and also in Formula 1 engines. Notably, these engine applications develop very high levels of gas turbulence to promote combustion efficiency. However, the spark in the shrouded is kept away from the central electrode insulating

ceramic to deliberately avoid tracking and encourage the spark to only move to the surrounding earth electrode. It is recognised this arrangement may not be suitable for engines where the electrode is deliberately extended into the combustion chamber in order to be positioned in specific zones of favourable combustible charge. It is also recognised the shrouded plug earth electrode will act as a heat sink which may affect the spark energy required for reliable ignition. Further the reduced gap distance of 0.3mm used for the present work smaller than the 0.55 - 0.6mm gap recommended for ignition sparking and may require changing when also used for ignition initiation. Such evaluations were not within the scope of the present work which was focused on the requirements for SBDV performance.

6.13.2 SHROUDED PLUG MANUFACTURE

The surrounding earth electrode for the shrouded plug is formed by a 2.5mm thick washer machined from carbon steel (EN8 specification). The washer was stepped to provide a simple means of light push fit, self-alignment between the spark plug body and central electrode. Two such items are shown in Figure F6-21.

The inner profile of the washer was set at 120° profile which could be machined simply by drilling. The outer surface was finished flat but with a 0.5mm deep 120° chamfer simply to avoid a sharp edge.

Figure F6-21: Two machined earth electrode extension washers.

The body of the shrouded plug was manufactured from a modified, pre-used, NGK: TYPE BR10EV spark plug. The plug had completed 200 miles in a racing two-stroke engine which ensured the electrode surfaces were ‘conditioned’ (Lucas, 2001).

The existing ‘J’ shaped earth electrode was removed. The modified plug body and earth electrode washer are shown in Figure F6-22.

Figure F6-22: The modified donor Spark Plug body and electrode extension washer.

The earth electrode extension washer was then silver soldered into the end of the donor spark plug body. The two items are shown before joining in Figure F6-23. This method was acceptable as the heat required was insufficient to damage the ceramic insulator within the plug and was sufficient to operate inside the motored (non-operating) test engine.

Figure F6-23: The Shrouded Plug components ready for joining.

The components shown in Figure F6-23 were modified after joining to flatten the outer ‘dome’ shape. It was considered this obscured the spark from the gases present at the

surface. The final shrouded plug electrode arrangement used for testing is shown in Figure F6-24.

Figure F6-24: The finished Shrouded Plug used for Testing

6.13.3 SHROUDED PLUG BLOW TEST

The simple ‘blow test was repeated, applied to the shrouded plug. A photograph taken during this test is shown in Figure F6-25. Despite significant attempts the SBDV spark stream could not be dislodged. The spark was observed to revolve around but maintain the same gap distance.

Figure F6-25: A photograph showing the Shrouded Plug Spark Path

6.13.2 SHROUDED PLUG BENEFITS AND LIMITATIONS

The design of the shrouded plug looks similar, to the surface discharge plug design. That plug design is commonly used in Formula One and aircraft piston engines and other applications where consistent sparking behaviour is critical. In such spark plugs the earth electrode is a circular inward extension of the spark plug body. This arrangement provides a circular earth electrode which surrounds the central electrode. Such spark plugs are available with various spark gap lengths. However, the design conceived was intended to extend the surrounding earth electrode to provide a greater shroud effect to the spark and to improve the accuracy of the sparking distance. Additionally, in a surface discharge plug the spark tracks across the end of the insulating ceramic which increases the predictability of the spark path distance. The intention for the shrouded plug design was to keep the spark away from the central electrode insulating ceramic and encourage the spark to only move to the surrounding earth electrode at the minimum distance.

The 0.3mm gap used in the shrouded plug is smaller than the 0.55-0.6mm gap recommended for ignition sparking. It is recognised this arrangement may not be suitable for engines where the electrode is deliberately extended into the combustion chamber and be positioned in specific zones of favourable combustible charge. It is also recognised the shrouded plug earth electrode will act as a heat sink which may affect the spark energy required for reliable ignition. Further the reduced gap distance of 0.3mm used for the present work may require to be changed and the design further optimised when also used for ignition initiation. Such evaluations were not within the scope of the present work which was focused on the requirements for SBDV performance.

6.14 THE SECOND SERIES OF SPARK PLUG TESTS

The second series of spark plug tests were carried out to extend the investigation of earth electrode shielding and evaluate the influence on SBDV of a moving piston and air flow past the spark plug. These tests were carried out in a motored engine to evaluate behaviour of spark plugs when working as SBDV sensors in a dynamically changing environment.

The first series of spark plug testing included an initial assessment of the effect of electrode orientation on the SBDV signal. This showed significant sensitivity to small gas flows over the plug. As a result, of that testing the shrouded plug was manufactured. This item was added to the spark plugs used in the first test series described in section 6.1 and listed in Table T6-1 for evaluation in second series of spark plug tests.

The second series of tests was carried out recognizing the potential effects of turbulence and the SBDV signal variations due to these conditions. As a simple measure to increase the shielding of both the 'J' and 'R' plugs the plugs were tested in the standard position with the threaded body flush with the combustion chamber wall and retracted back into the threaded hole. The retracted position was controlled by additional copper washers under the plugs. Two retracted positions were evaluated +2.5mm and +5.0mm (Figures F6-26 to 28). Additionally, the position of the earth electrode relative to the incoming fresh charge was noted. The incoming direction of the fresh charge is controlled by the loop scavenging transfer port flows. This flow regime which is a fundamental aspect of two-stroke cycle engine design, brings the fresh charge up along the cylinder wall on the opposite side to the exhaust port. In all tests, the fresh charge (dielectric gas) was air.

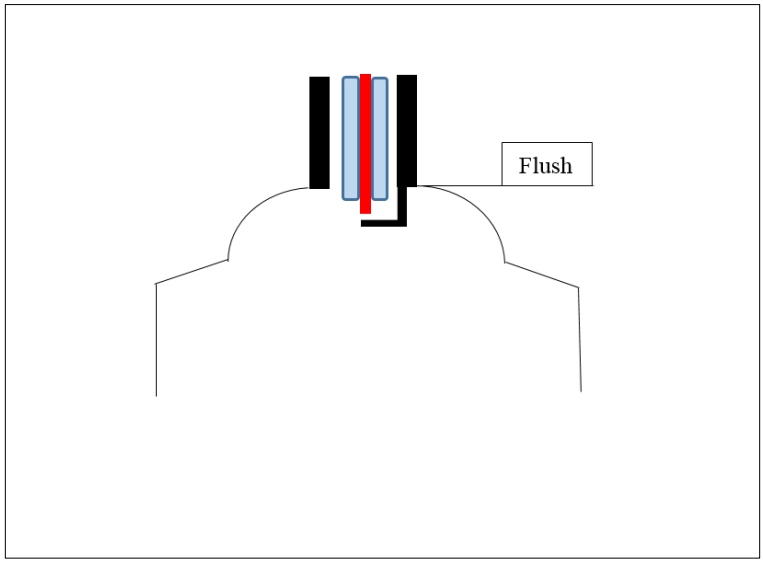

Figure F6-26: Schematic of Spark Plug flush mounted for Motored Testing

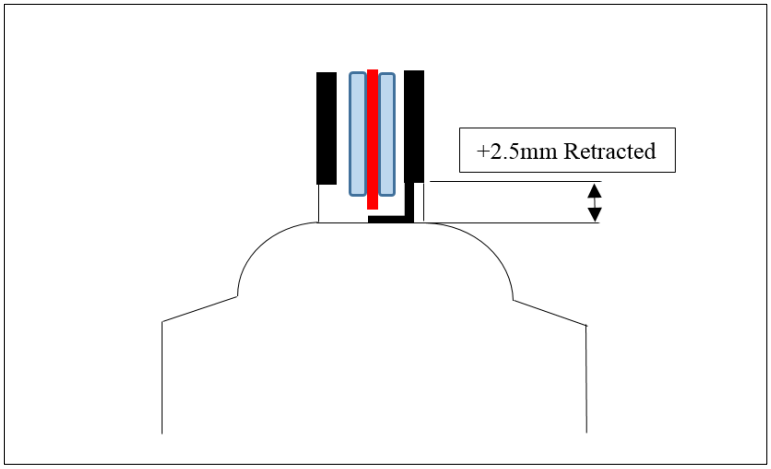

Figure F6-27: Schematic of Spark Plug retracted +2.5mm for Motored Testing

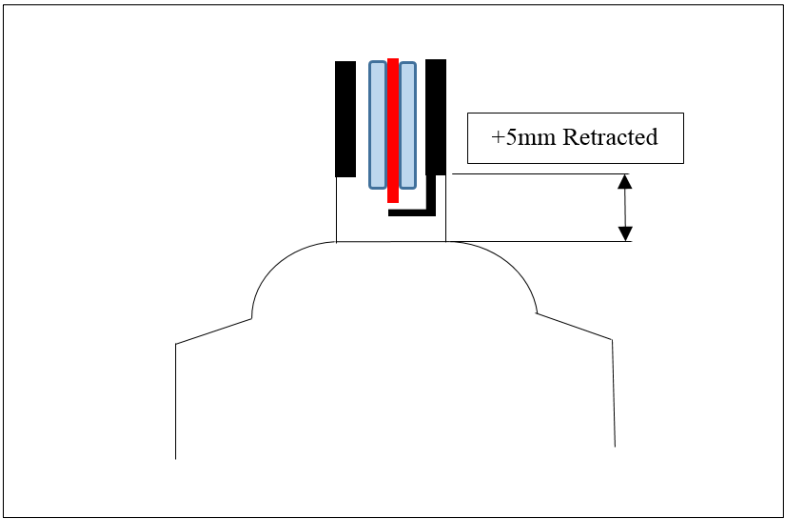

Figure F6-28: Schematic of Spark Plug retracted +5mm for Motored Testing

6.15 APPARATUS FOR SECOND SERIES OF SPARK PLUG TESTS

The second series of tests were carried out using the Rotax Max test engine. However, unlike for the first series of spark plug tests this was motored by an AC electric motor, set to a constant speed of 2500 rpm which was used for all testing. The apparatus used for the second series of spark plug tests is shown schematically in Figure F6-25.

Air was supplied to the motored test engine through the intake system including the 'air box' and intake butterfly air valve. In these tests, only air from the test cell, was supplied to the test engine.

Tests were carried out with the intake air butterfly valve adjusted to and locked in different positions ranging from fully open (1.0) to fully closed (0). The exhaust pipe was connected to the test cell exhaust gas extraction system which has a large volume and functions at constant extract fan speed.

The test engine was fitted with the modified cylinder head as shown in Figure F4-15, which had been modified to include a 1mm diameter 'K' type thermocouple connected to an RS 206-3750 converter, and recorded manually.

The air pressure in the cylinder was obtained from a 0-70 bar 'Optrand' pressure sensor connected to the 'Pico-scope' 4824 unit set at 20 ms per division for the duration of 0.2 second. The procedure followed to process the data followed that described in Chapter 4.

The electronic signals from the various apparatus sensors including those from the SBDV circuit were connected to a 'Pico-scope' 4824, high speed, 8 channel oscilloscope which was powered by a separate dedicated power supply to a PC. The spark voltage generation circuit was connected to a dedicated power supply unit to avoid electrical interferences from other electrical devices. The test cell ambient pressure, temperature and humidity were recorded to enable inlet air density corrections.

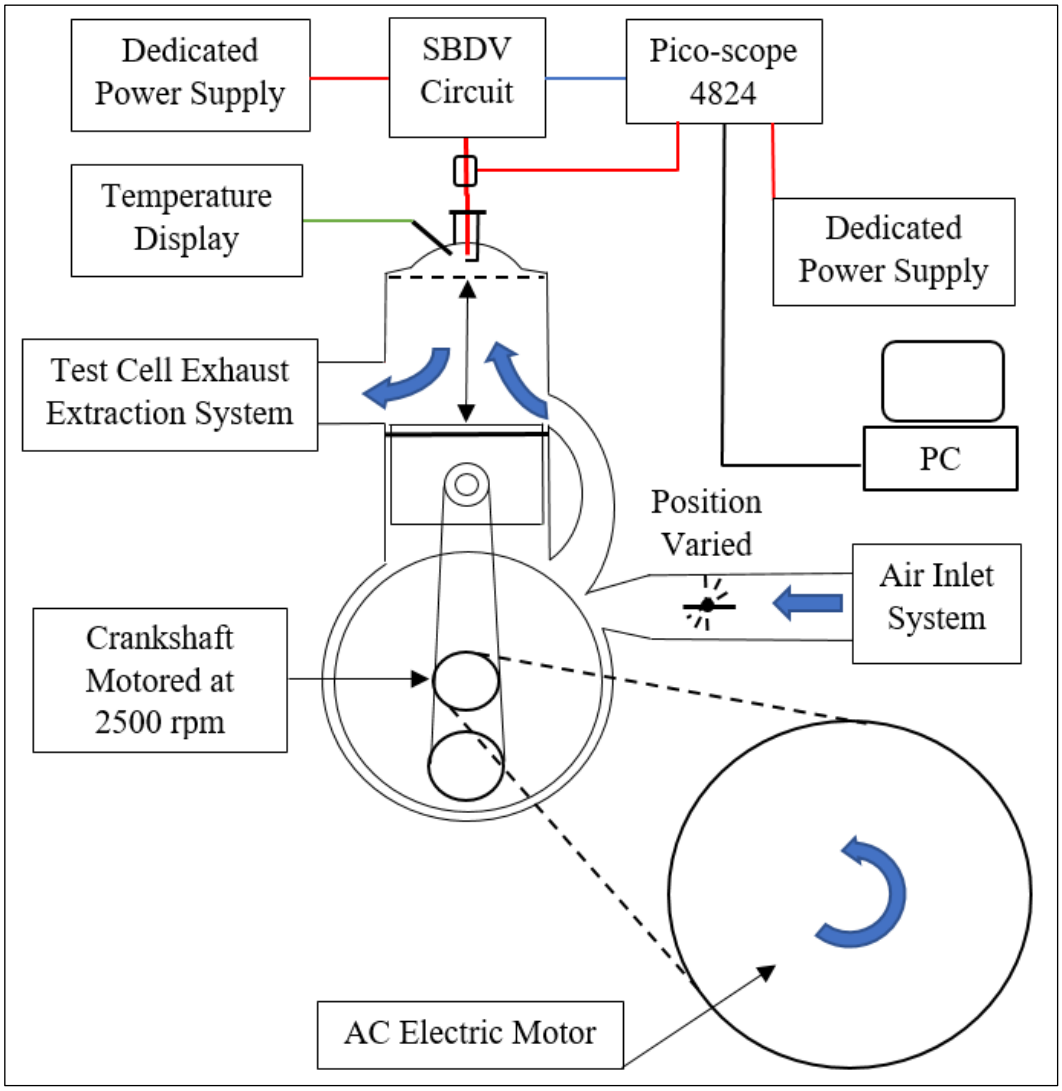

Figure F6-29: Apparatus arrangement for the Second series of Spark Plug Tests

6.16 RESULTS OF THE SECOND SERIES OF SPARK PLUG TESTS

The results of the second series, comprising of 14 individual tests, listed in Table T6-7.

Table T6-7: Summary of 2nd Series of Spark Plug Tests - Effect of Earth Electrode Shielding

SUMMARY OF TESTS TO EVALUATE THE EFFECT OF EARTH ELECTRODE SHIELDING OF IN-CYLINDER GAS FLOW

Notes:

1. THE TESTS SUMMARISED BELOW WERE CARRIED OUT TO EVALUATE THE EFFECT OF SHIELDING THE IONISED SPARK PATH FROM THE INCOMING GAS FLOW INTO THE CYLINDER.
2. THE INCOMING GAS FLOWS TOWARDS THE SPARK PLUG FROM 0O ORIENTATION. THE EARTH ELECTRODE AT 0^0 THEREFORE OFFERS GREATEST OBSTRUCTION TO THE FLOW FROM DISTUBING THE IONISED SPARK
3. POTENTIAL SHIELDING WAS ALSO PROVIDED BY RECESSING THE SPARK PLUG FROM ITS NORMAL 'FLUSH' POSITION UP BY EITHER 2.5mm OR 5.00mm.

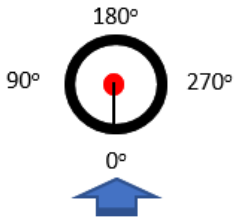

VIEW LOOKING AT PLUG

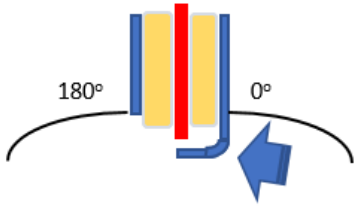

GAS FLOW DIRECTION

TEST Ref. No. 02/06/2015	SPARK PLUG Ref. No.	TYPE OF PLUG	SPARK PLUG CONDITION	PLUG HEAT RANGE	SPARK GAP [mm]	GAS IN CYLINDER	AIR VALVE POSITION	GAS TEMP IN-HEAD	EARTH ELECTRODE ORIENTATION [Degrees]	RECESS DEPTH [mm]	AMBIENT CONDITIONS IN TEST CELL		
											TEMP [Deg. C]	PRESSURE [Millibar]	HUMIDITY [%]
14	2	R6120	NEW	10.5	0.50	AIR	1.00	24.50	0	UP 2.5	20.40	1025.00	34.30
15	2	R6120	NEW	10.5	0.55	AIR	1.00	24.90	355	FLUSH	20.40	1025.00	34.30
16	5	R6120	NEW	10.5	0.55	AIR	1.00	22.60	350	FLUSH	20.40	1025.00	34.30
17	5	R6120	NEW	10.5	0.50	AIR	1.00	23.00	340	UP 2.5	20.40	1025.00	34.30
18	3	R6120	NEW	10.5	0.50	AIR	1.00	27.00	340	FLUSH	20.40	1025.00	34.30
19	3	R6120	NEW	10.5	0.50	AIR	1.00	26.50	340	UP 2.5	20.40	1025.00	34.30
20	1	R7282A	NEW	10.5	0.55	AIR	1.00	22.90	355	FLUSH	20.40	1025.00	34.30
21	1	R7282A	NEW	10.5	0.55	AIR	1.00	25.00	60	UP 2.5	20.40	1025.00	34.30
22	2	R6120	NEW	10.5	0.50	AIR	1.00	24.20	60	UP 5.0	20.40	1025.00	34.30
23	3	R6120	NEW	10.5	0.50	AIR	1.00	25.40	5	UP 5.0	20.40	1025.00	34.30
24	5	R6120	NEW	10.5	0.50	AIR	1.00	25.30	355	UP 5.0	20.40	1025.00	34.30
25	8	R6120	NEW	10.5	0.50	AIR	1.00	25.80	350	UP 5.0	20.40	1025.00	34.30
26	20	IW29	NEW	9.0	0.60	AIR	1.00	32.10	180	UP 2.5	20.40	1025.00	34.30
27	20	IW29	NEW	9.0	0.60	AIR	1.00	35.90	170	UP 5.0	20.40	1025.00	34.30

Figure F6-30 shows a screen shot taken from one ‘Picoscope’ Waveform sample of nine separate motored cycles. The green trace represents the cylinder pressure variations for each cycle which were recorded simultaneously from a 5mm diameter 0-70 bar ‘Optrand’ pressure sensor. The upper blue trace shows the mass flow rate measured in the intake system monitored for reference only. The light red castellated trace shows the once per revolution trigger from the test engine crankshaft. The lower dark red trace represents the 70 per revolution crankshaft positions taken from the starter gear behind the clutch of the test engine.

The purple coloured trace shows the SBDV variations measured by an inductive clamp around the HT ignition lead to the spark plug. As the SBDV signal is negative the profile of the lower trace is the one to be considered. A Standard 4824 type ‘Picoscope’ with associated software, described in Chapter Four was used to provide a comparative signal to confirm the accuracy of that taken directly from the SBDV measurement branch of the SBDV box referred to below.

The grey coloured trace is the SBDV output signal from the GEMS circuit. As the SBDV signal is negative the profile of the lower trace is the one to be considered. This can be seen to vary roughly in proportion to pressure.

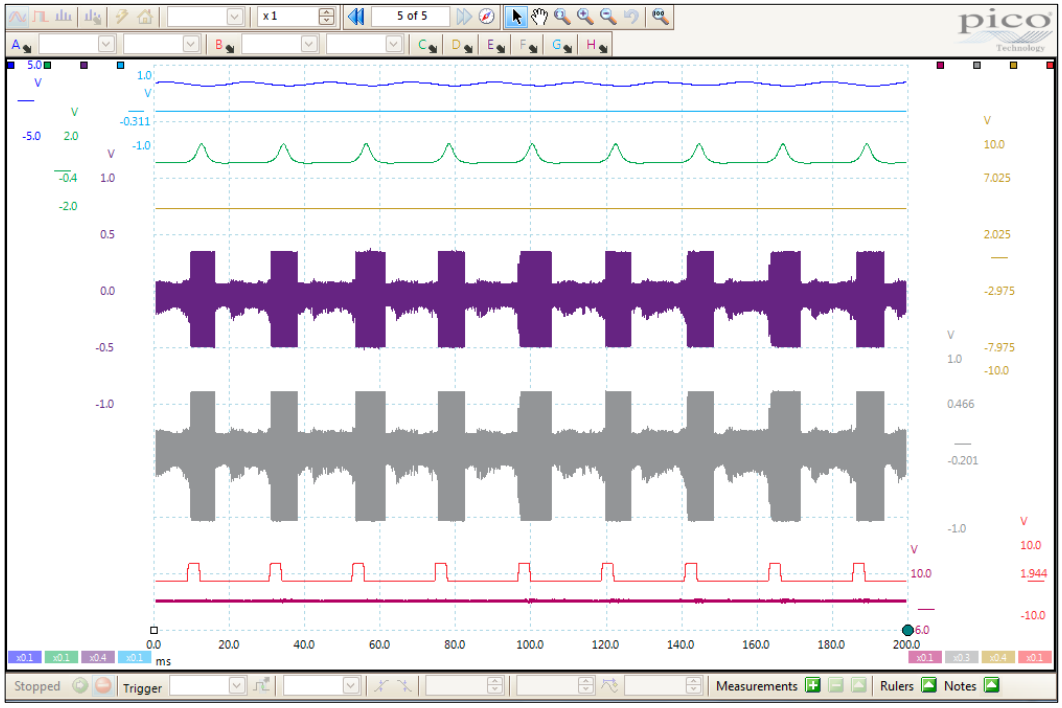

Figure F6-30: Sample ‘Picoscope’ recording of file 006-02-06-2015 Waveform 5

There are two important signal profiles to note from the SBDV traces. Firstly, the central bulges that occur every cycle at roughly BDC represent the change in gas density which results from the incoming fresh charge. This is barely discernible in the pressure signal. Secondly, the flat profile to the SBDV signal which occurs as the cylinder pressure increases shows the SBDV signal to be 'off'. This is simply because the SBDV spark is not able to pass between or jump across, the electrodes as the cylinder pressure increases. This is a self-limiting effect dependent upon the voltage potential of the SBDV system, the spark plug gap, electrode material and condition and the gas type.

The signal period of focus to this thesis is the first 10 degrees of closed cycle compression. Therefore, the SBDV peak trace for this period was focused on in the present work.

The 'once per revolution' crankshaft trigger pulse position was used for the first series of tests. The raw SBDV signal from the Pico-scope 4824 was processed by a 'Matlab' program to extract all of the 'peak' values and produce a trace of those values. The start of the trace was taken to be 0.5 milliseconds before and finish 1.0 millisecond after the trigger leading edge. The crankshaft period was thus obtained relative to the time.

The SDBV signal was converted to pressure using the mathematical expression representing the relationship derived for each plug by calibration testing air as summarised Tables T7-1 to 4 in Chapter Seven.

Comparative SBDV [V] signals were converted to pressure (with subscript 'p') SBDVp vs pressure recorded simultaneously by the OPTRAND sensor for eight continuous motored cycles. Such recordings were made for J20 and R10 plugs mounted in flush and retracted positions previously described. (Note in all three figures, 'STD' or standard, corresponds to threaded body flush with combustion chamber).

The multi-cycle plots show the signal variation for each test. Following the multi-cycle overlay comparisons, a summary graph is provided which shows the average signal for each position. This shows the effect of the retraction and associated effect of shielding from direct gas flow. Only one test was recorded using the shrouded 'S' plug which was with the plug mounted flush as the objective was to compare its characteristics only in this position.

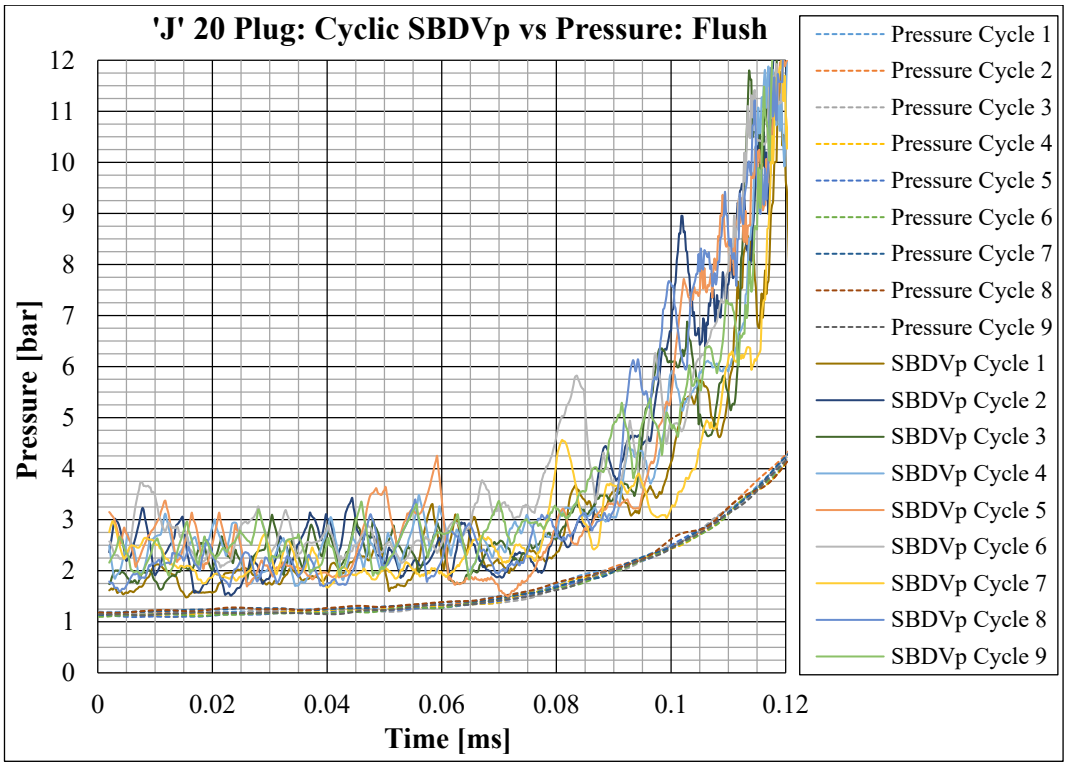

Figure F6-31: 'J' 20 Plug: Nine Motored Cycles SBDVp vs Pressure – Mounted Flush

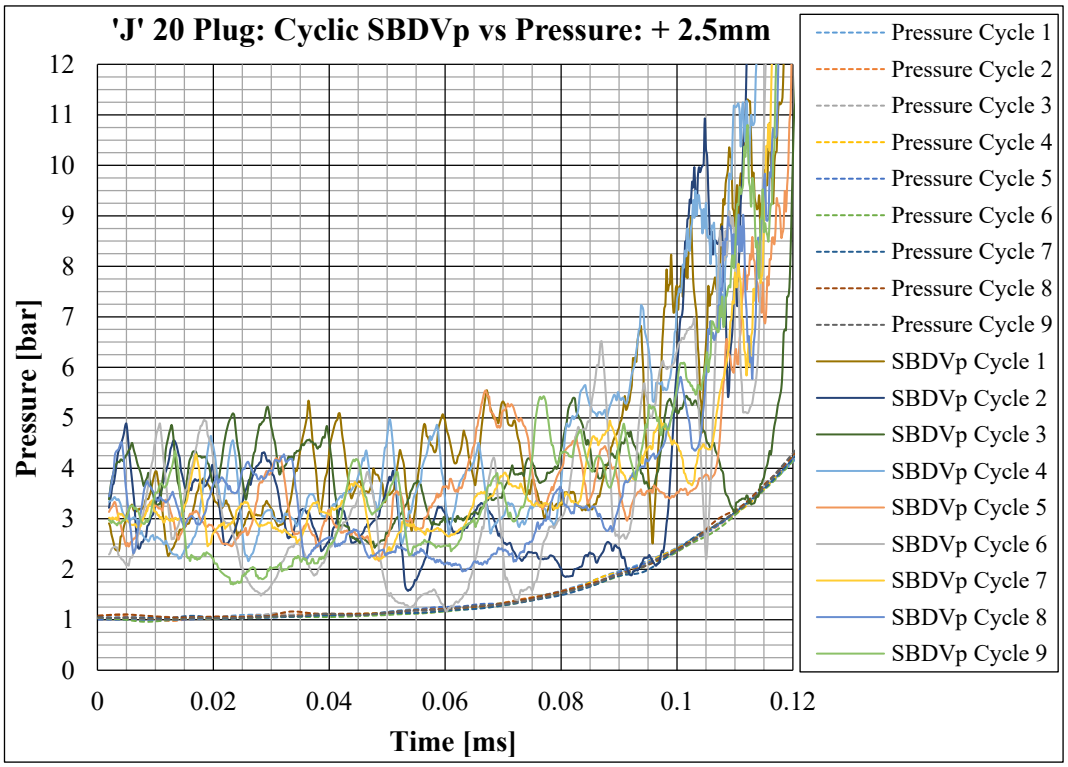

Figure F6-32: 'J' 20 Plug: Nine Motored Cycles SBDVp vs Pressure -Mounted +2.5mm

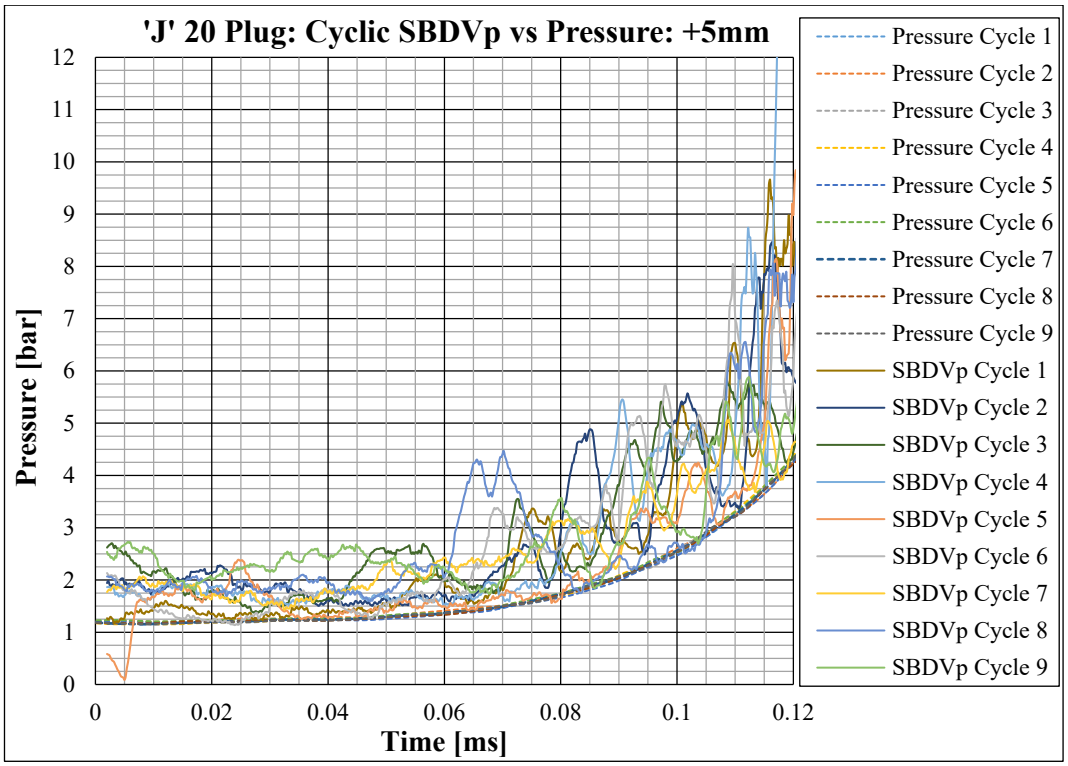

Figure F6-33: 'J' 20 Plug: Nine Motored Cycles SBDVp vs Pressure – Mounted +5mm

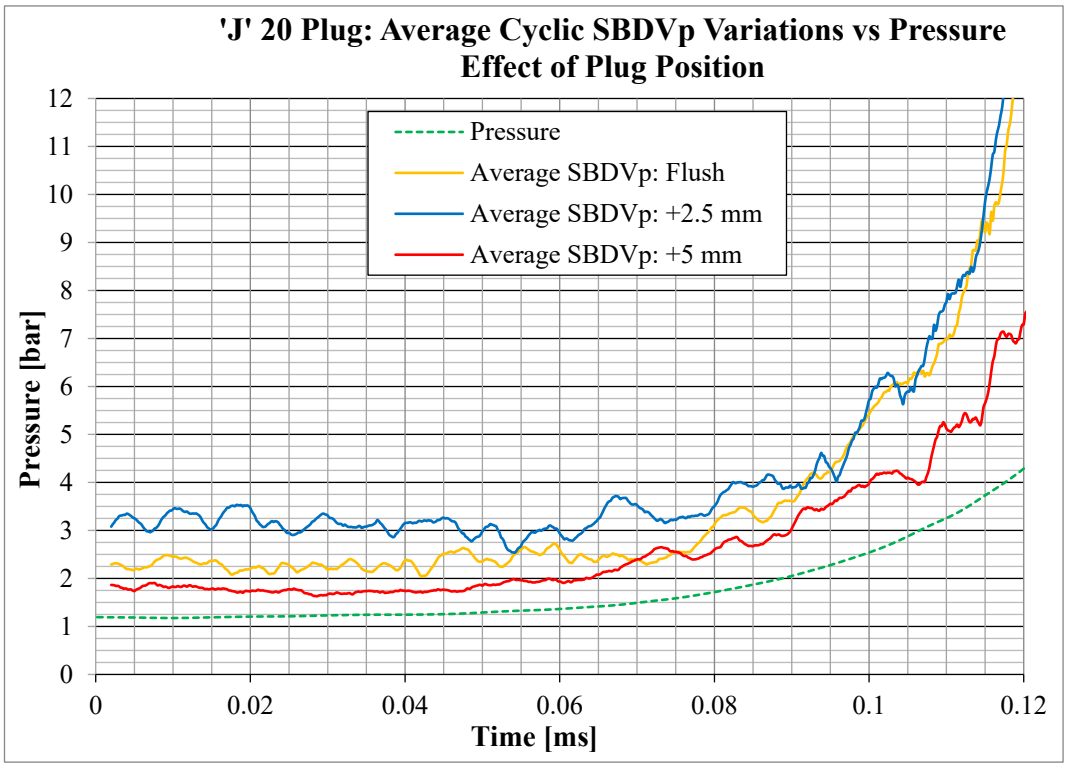

Figure F6-34: 'J' Plug: Nine Cycle Average SBDVp Variation vs Motored Pressure (Effect of Mounting Position)

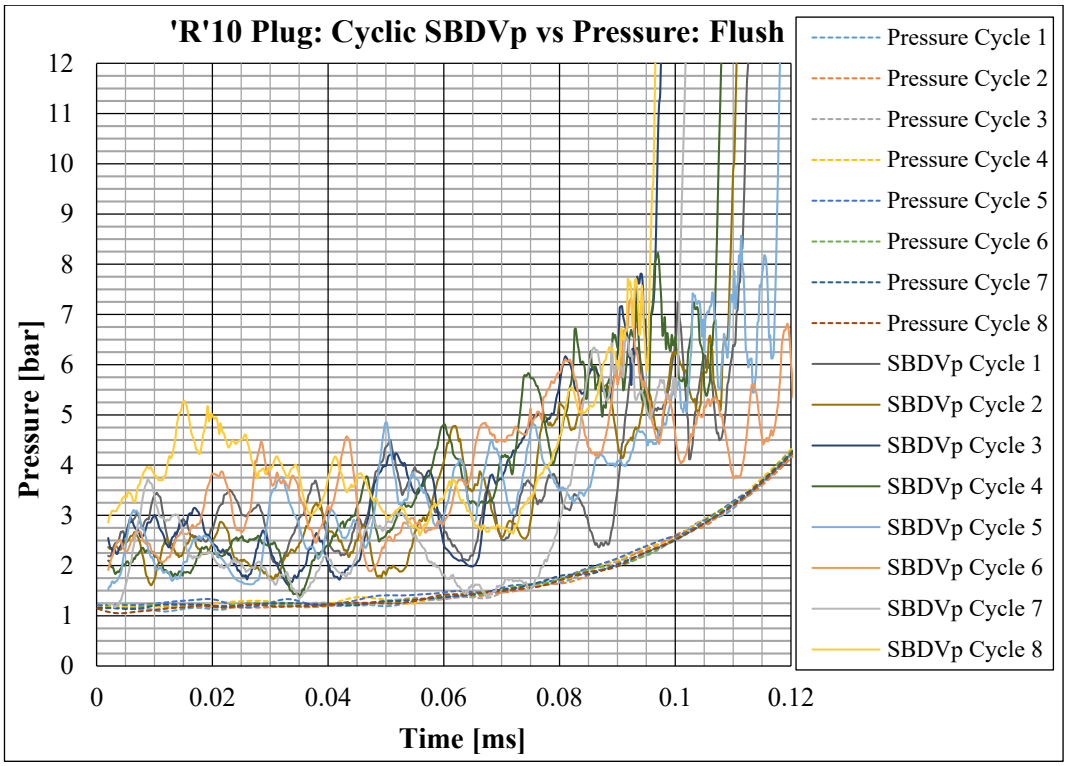

Figure F6-35: 'R'10 Plug: Nine Motored Cycles SBDVp vs Pressure – Mounted Flush

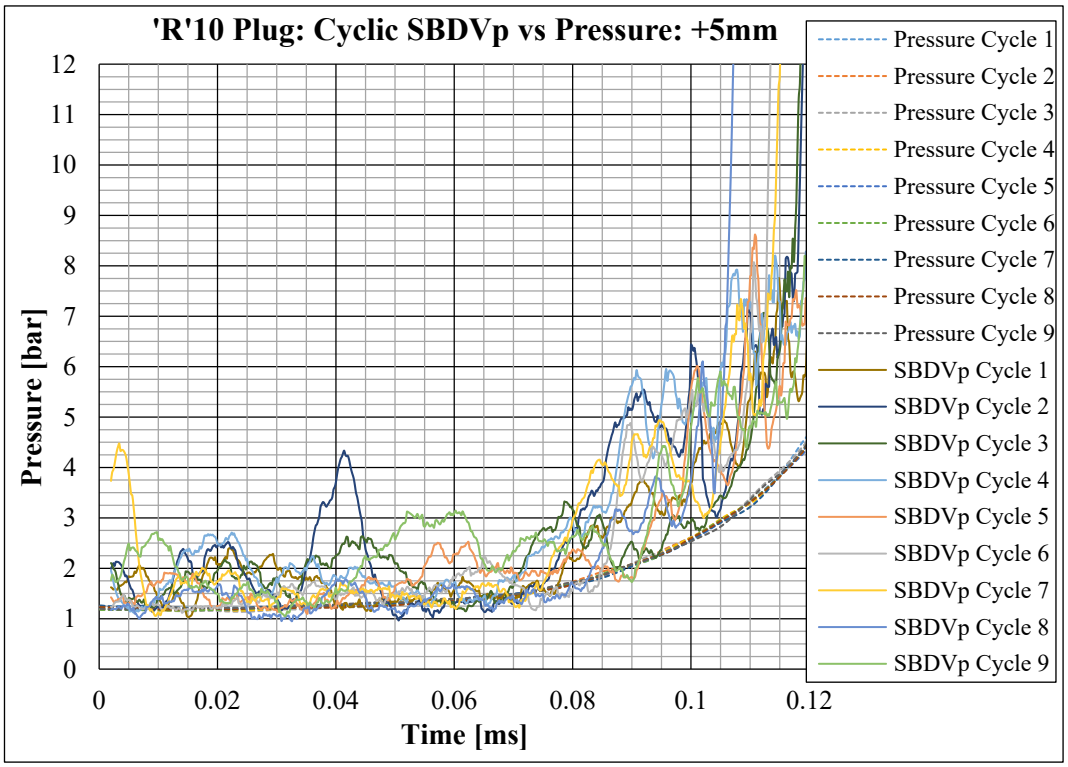

Figure F6-36: 'R'10 Plug: Nine Motored Cycles SBDVp vs Pressure – Mounted +5mm

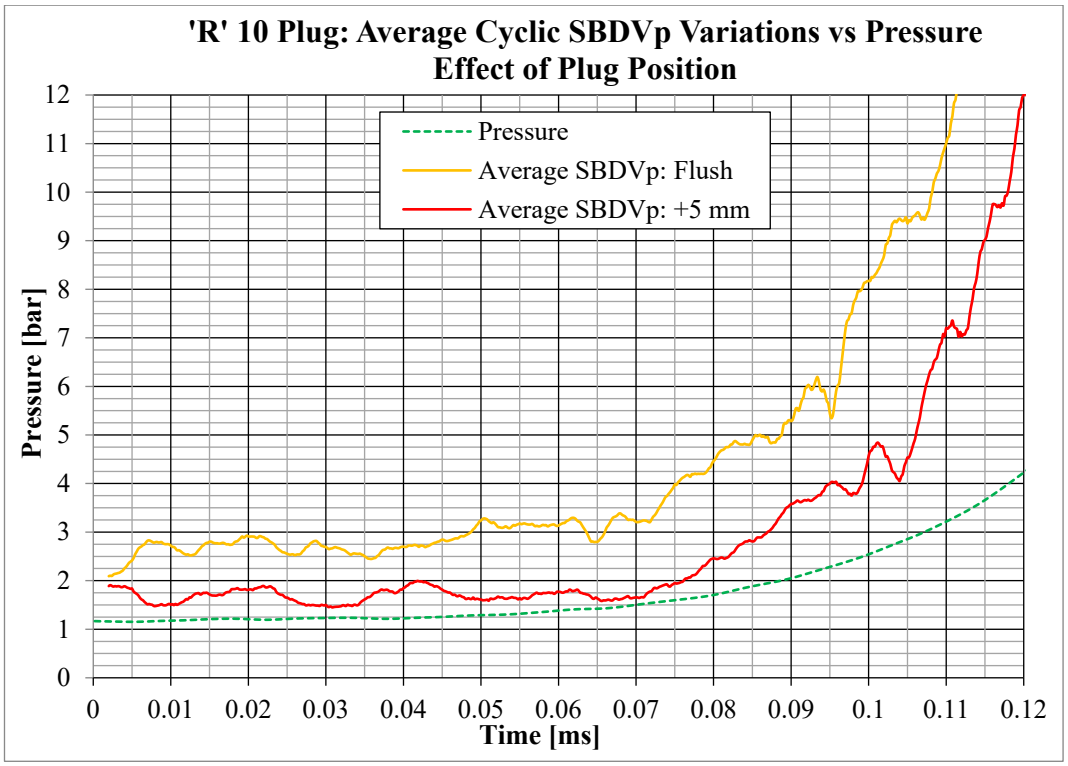

Figure F6-37: 'R'10 Plug: Nine Cycle Average SBDVp Variation vs Motored Pressure (Effect of Mounting Position)

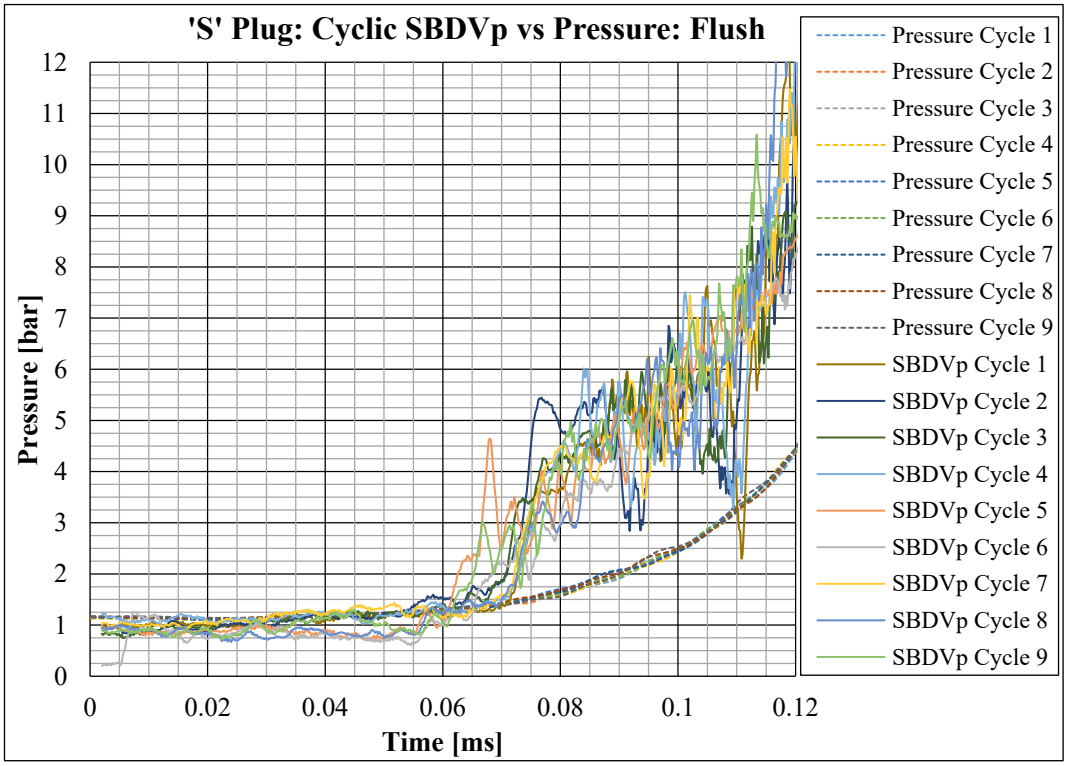

Figure F6-38: 'S' Plug: Nine Motored Cycles SBDVp vs Pressure – Mounted Flush

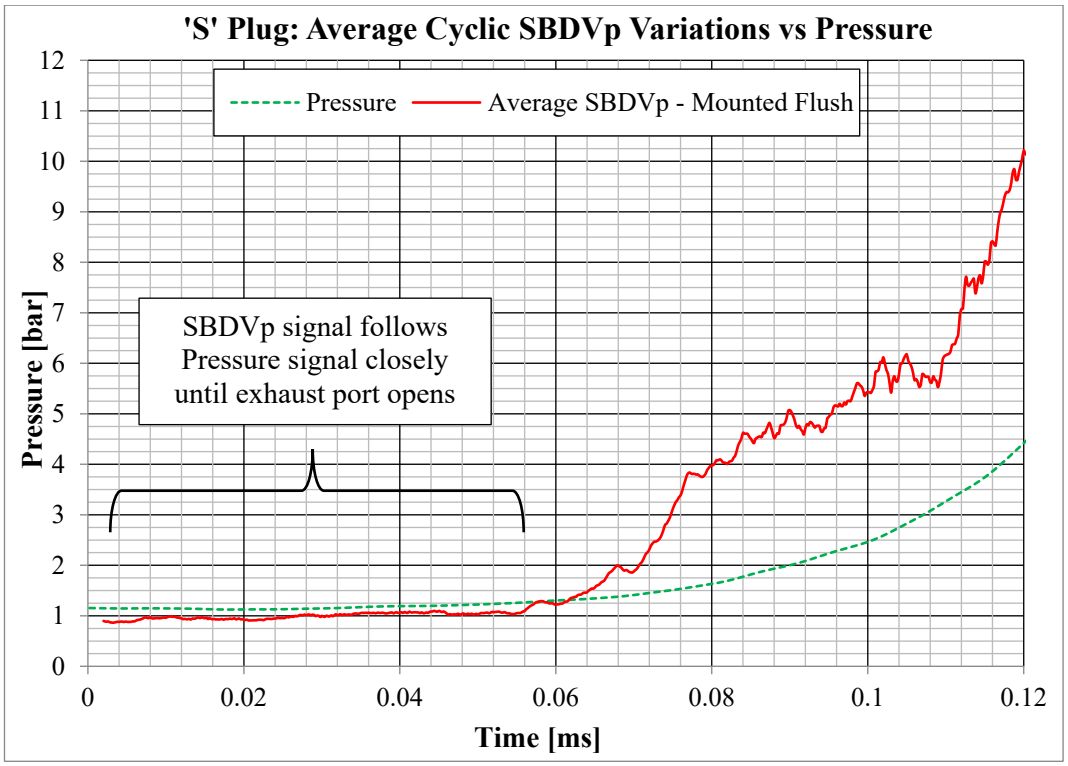

Figure F6-39: 'S' Plug: Nine Cycle Average SBDVp Variation vs Motored Pressure

6.17 CHAPTER SUMMARY

Tests described in this chapter were carried out to determine if the SBDV signal would be affected by the gas flows and turbulence in the combustion chamber. Comparisons of SBDV signals from a spark plugs fitted in different orientations and recess distances were investigated. The 'J' type and 'R' type plugs were both affected by the retracted depth position and hence the stand-off length of the electrodes relative to the combustion chamber wall. It is considered the differences show the effect of local turbulences caused in the spark plug hole resulting from the air flow over the hole.

The results confirm the SBDV signals are sensitive to electrode shape and the amount of shielding provided by the earth electrode. The stability of the SBDV signal is better for the 'R' type than the 'J' type plug. The shrouded plug gave the most consistent SBDV signal which additionally responded clearly to the rapid change of pressure in the cylinder following the closure of the exhaust port.

It should be remembered these signals were obtained within a dynamically changing environment during a 10 ms sample period.

The test method used enabled by the SBDV system was very simple and the results obtained for cycle by cycle events are consistent. From the graphs and summary charts above it can be seen there is a considerable variation of behaviour across the spark plugs tested. The surface condition varies with use and has shown the spark breakdown value changes and becomes more stable as the electrode surface is 'conditioned' (Lucas, 2001). This effect was noted during SBDV testing. In general, the new spark plugs showed unstable SBDV behaviour when initially used. Usually, the SBDV signal from every spark plug tested became more stable after a short running duration. The difference between 'PEAK' spark breakdown voltage value as opposed to the mathematical 'MEAN' is apparent. The spark distribution curves show considerable variations occur between individual spark plugs. The simple 'Blow Tests' show that deflection of the spark can occur, which effect lengthens the channel over which ionization has to be created in order for sparking to occur as described in Chapter Three. Depending upon the form of the earth electrode, a progressive increase of sparking length, (where the spark is deflected and migrates along the earth electrode) can jump 'rimfire', across to the threaded body.

This behaviour must occur because the threaded body is a direct earth and therefore offers less electrical resistance. The 'jump' directly across to the threaded body occurs almost instantaneously producing a pronounced 'step' in the Spark Breakdown Voltage signal. Once the spark has 'jumped' directly to the threaded body of the spark plug it does not easily return onto the earth electrode. This effect thus does not show a progressive change of Spark Breakdown Voltage signal relative to pressure but instead, a pronounced step which cannot easily be analysed. This behaviour was not fully investigated for the present work, which was more focused on general characteristics. However, the more regulated sparking which occurred using the R type plug earth electrode design was apparent in improved signal stability. This stability and sensitivity was further improved using the shrouded plug design. This confirms spark distribution curves should be generated for all spark plugs which are intended to be used in the SBDV system.

The data was collected using air from the test cell at ambient conditions varied by only 1.8 degrees C during the complete series of 60 tests. The individual tests were completed within 15 minutes. The results also show the SBDV system is very sensitive to differences which must be attributable to the spark plug electrodes. Although the variation of humidity in the air is known to influence spark breakdown voltage (Feser, 1972), this was not fully evaluated for the present work.

CHAPTER SEVEN

SBDV OF AIR AND OTHER GASES SIGNIFICANT TO COMBUSTION

7.0 INTRODUCTION

This Chapter reports on testing carried out to determine the SBDV characteristics in the gases which are present in the cylinder of an engine and which are individually significant to combustion. The gases tested were, Air, Oxygen (O_2), Carbon Dioxide (CO_2), Carbon Monoxide (CO) and Nitrogen (N_2). These were investigated as individual gases and not mixtures, other than those present in Air, in the present work.

For the proposed combustion control strategy to function it is essential for the new SBDV system to differentiate the presence of other gases which will be present within the engine.

Air is the most important gas for an engine. Air is a mixture of gases, the majority of the mixture consists of 79% Nitrogen (N_2), and almost 21% Oxygen (O_2). Air is therefore the carrier of Oxygen which is critical for combustion to occur as it is the oxidising agent. However, the other gases tested, Carbon Dioxide (CO_2), Carbon Monoxide (CO) and Nitrogen (N_2) are also independently significant to combustion. Carbon Dioxide (CO_2) is a natural constituent of Air represented by approximately 0.4% of the atmosphere but is a product of combustion. The peak value CO_2 is produced when stoichiometric Air/Fuel ratios are burned. Carbon Monoxide (CO), is not a natural constituent of Air but is a product of combustion and is poisonous. The amount produced increases in proportion to the amount of fuel added to air. Therefore, the relative amounts of CO_2 and CO present is a key indicator of combustion quality. Nitrogen form the largest part of Air and the atmosphere. Nitrogen reacts with oxygen during combustion to produce Nitrous Oxides (NOX) which are considered harmful. The production rate of these is proportional to and increases with combustion temperature. Hence the amount produced peaks when slightly lean stoichiometric Air/Fuel ratios are burned.

The pressure range over which tests were carried out was limited between ambient to the maximum which spark break-down could occur as a function of the dielectric strength of each individual gas and the maximum voltage generated by the new SBDV system. The tests presented below, follow on from the investigations into the basic characteristics of spark break-down behaviour in spark plugs reported previously in chapter six.

The overall objective of this chapter was to determine if SBDV, applied across various spark plugs, could differentiate between the individual gases over the pressure range tested. This objective was separated into the following list of tasks:

a) Investigate SBDV characteristics for each gas from ambient to the maximum attainable pressure using the new SBDV circuit.
b) Obtain SBDV values for each gas from ambient to the maximum attainable pressure/density using the new SBDV circuit.
c) Obtain mathematical expressions for each gas from ambient to the maximum attainable density using the new SBDV circuit.
d) Compare the mathematical expressions obtained with previously published information.
e) Investigate features of SBDV signals which could be used to differentiate between the various gas species tested.

This chapter begins by describing the apparatus used for the testing carried out for this chapter. The content progresses by investigating Spark Distribution Curves for the various gases. Then, SBDV behaviour in Air is investigated which is then followed by similar investigations of the other gases list above. This is followed by comparison of results with published work. The chapter is concluded with an investigation into other potential methods to determine gas species.

7.1 APPARATUS AND PROCEDURES USED FOR TESTING

To determine the SBDV in various gases and pressures, the Constant Volume Sparking Chamber shown schematically in Figure F4-14 was used.

Spark plugs representing the three types as discussed in Chapter six were used for the tests reported in this chapter (‘J’ type, ‘R’ type and SP type).

The supply and pressure of the gases supplied into the test chamber were manually adjusted to that indicated by a 100mm diameter pressure gauge. This procedure was initiated at atmospheric pressure and was increased in 0.1 bar steps. The individual tests were carried out one after the other without the deliberate stabilisation period used with standard sphere gap testing. When the pressure value was stable at each pressure step, the SBDV signal was captured by the Pico-scope which was manually initiated.

Approximately 30 samples of 50 milliseconds giving a total of around 1.5 seconds of duration, were captured and stored for post processing. The selection of each sample stored for post processing was a judgment based on an even and regular pattern SBDV appearance.

This process was then repeated for increased pressure steps until the voltage supplied was not able to breakdown the dielectric properties of the gas being tested. The maximum pressure that could be tested was therefore limited by the maximum voltage generated by the new SBDV circuit and the dielectric properties of the gas tested.

Contamination between different gas tests was prevented by purging. For each gas tested the test chamber was subjected to a minimum of six successive gas purges with vacuum pressure applied between purges. Following the final vacuum evacuation, the Sparking Chamber cylinder was re-filled at a rate of 0.5 l / min. with the gas to be tested.

The gas temperature during the tests was monitored using a 1mm diameter 'K' type thermocouple. The tip of this item was located close to the spark plug electrodes shown in Figure F4-15. This position was used for all testing and was therefore not adjusted to be a consistent distance from the electrodes if the shape or orientation of those differed.

Static testing to investigate the sparking characteristics of various spark plugs, reported previously in Chapter six, had noted the effect of gas turbulence on the spark breakdown voltage signals. Those tests had been carried out in air using the test engine locked at BDC.

Initial tests carried out in Constant chamber consisting of the cylinder head bolted directly to the base plate. The SBDV signals of these tests using air, showed significant signal variations and instabilities which prevented testing above approximately 1.0 bar. It was considered these SBDV signal variations were probably due to gas turbulence resulting from the very small purge gas flow through the cylinder. This purging was considered essential to ensure the gas trapped in the cylinder was not contaminated and the gas temperature was as constant as possible for all test steps. To reduce the gas turbulence in the cylinder, the volume of the test chamber volume was increased. This was achieved by adding an aluminium tube extension spacer tube as shown in Figure F4-16. Additionally, a foam rubber filter was added approximately half way up the extension spacer tube as shown in Figure F4-16. This filter was retained in place by a large tight-fitting washer. The extension spacer and foam filter are described in section 4.10. The combination of increased chamber volume and flow calming filter more than doubled the maximum gas pressure for which stable SBDV values could be obtained in air.

Despite these modifications some variance and what appeared to be ultrahigh speed wave resonances in the SBDV signals were observed. These occurred differently at different gas pressures and were eventually thought to be due to unavoidable unsteady flow through the purge gas needle valves. These variations in the SBDV signal were very small and thought to be insignificant to signals variations which would occur in a firing engine. These variations were not investigated further in the present work.

The source for compressed air was the universities service air system. The air used was not additionally filtered or dried. For species of gas other than air, the gas feed arrangement was connected to a compressed gas cylinder containing the specific gas required to be tested. The outlet stage of the pressure regulator fitted to the pressurized cylinders was set at 3.5 bar which minimized the gas pressure difference required to be manually varied and provided a safety limit to the maximum pressure that could occur in the test chamber.

7. 2 SBDV DISTRIBUTIONS FOR TEST GASES AND PRESSURES

The first evaluation of the SBDV signals recorded for each gas was obtained from observing the behaviour of all spark break-down events recorded for each test gas at each pressure step. The objective being to determine if the spark break-down voltage was consistent and if that changed dependant on spark plug type.

Plots were made showing the magnitude of spark break-down voltage against the number of break-down events occurred at each voltage to provide a comparative distribution. The graphic representations of these results were termed ‘Spark Break-Down Voltage’ (SBDV) distributions. The voltage values used were extracted from tests carried out using the static pressure chamber for Air, O_2, CO_2, CO and N_2 at each 0.1 bar pressure step tested. The samples for each plot were taken from a duration of approximately 10 ms which represent approximately 1000 individual spark break-down events. This method followed the procedure used to determine the spark break-down characteristics of different spark plugs in Air, presented in chapter six.

It was found that spark break-down voltage and characteristic SBDV distributions vary differently for each gas, pressure step and spark plug type. The results of these tests are presented below in Figures F7-1 to 14 below, which show the differences between the SBDV distributions. To present these differences clearly, the distributions included are limited to between four to six different pressures, as noted by a key in each gas.

The upper pressure and spark break-down voltage values were limited as previously noted, by the relative dielectric strength of each gas and the voltage limit of the generation circuit used for the present work. It was shown that spark gap distance, electrode material and surface condition also influence the spark break-down voltage of spark plugs.

The spark distribution behaviour in each gas at each pressure tested for each spark plug type is noted and summarised in section 7.3.

7.2.1 SBDV distribution in Air

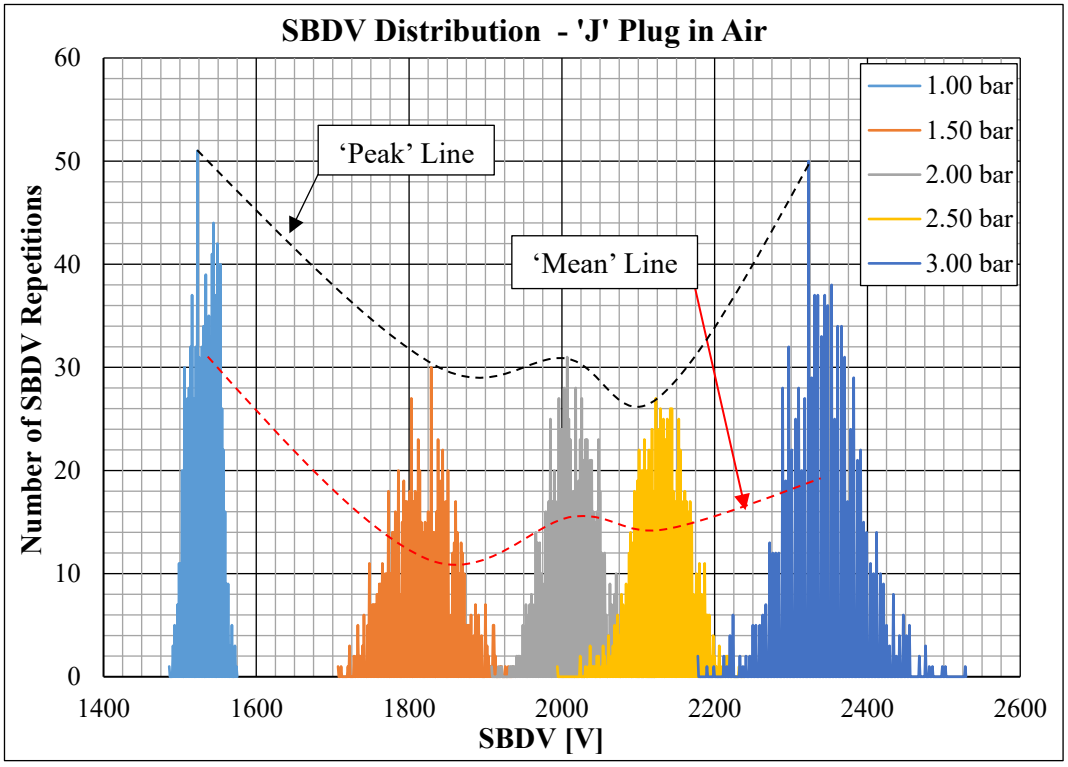

Figure F7-1: SBDV Distribution Curves – 'J' Plug in Air (Ambient to 3.00 bar)

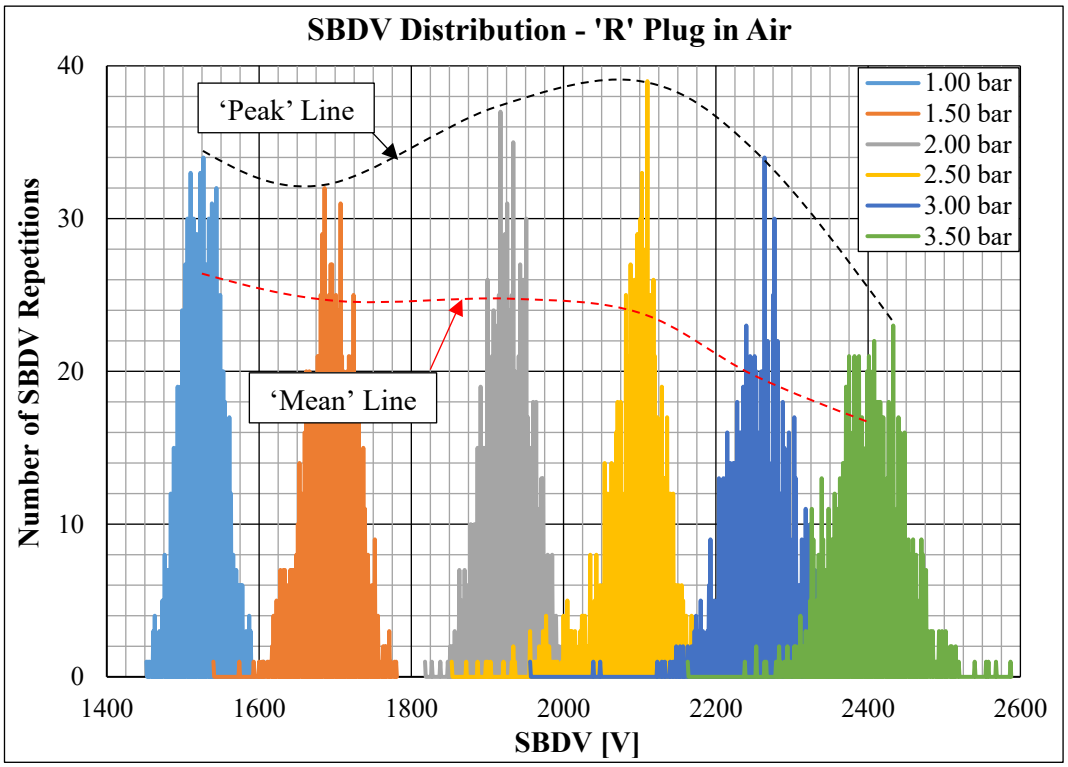

Figure F7-2: SBDV Distribution Curves – 'R' Plug in Air (Ambient to 3.50 bar)

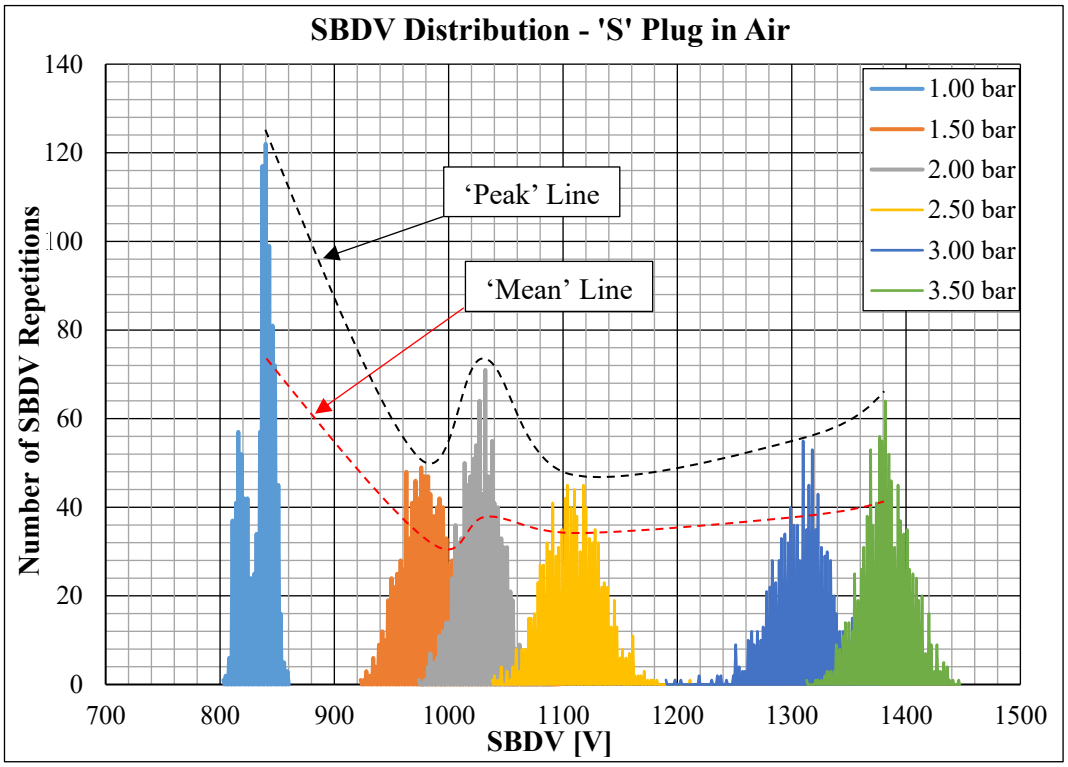

Figure F7-3: SBDV Distribution Curves – 'S' Plug in Air (Ambient to 3.50 bar)

Observations: SBDV (Air)

In Air, for the three spark plug types shown, the voltage at which the 'Peak' number of spark break-down repetitions occurs increases almost proportionally with increasing pressure. The 'shape' of the spark break-down repetition distribution is most consistent with the 'R' plug. The general trend for the characteristic shape of the spark break-down distribution is to widen with increasing pressure. The narrowest distribution shape consistently occurs at ambient pressure.

The spark break-down voltage for each pressure is confirmed graphically to increase with spark gap distance where the values are 'J' plug = 0.6mm, 'R' Plug = 0.55mm and 'S' Plug = 0.3mm. The difference between the voltage required is noted to be significant. Additionally, the maximum pressure in which spark break-down occurred was limited for the 'J' plug relative to that obtainable using the 'R' and 'S' plugs.

SBDV distribution in Carbon Dioxide (CO_2)

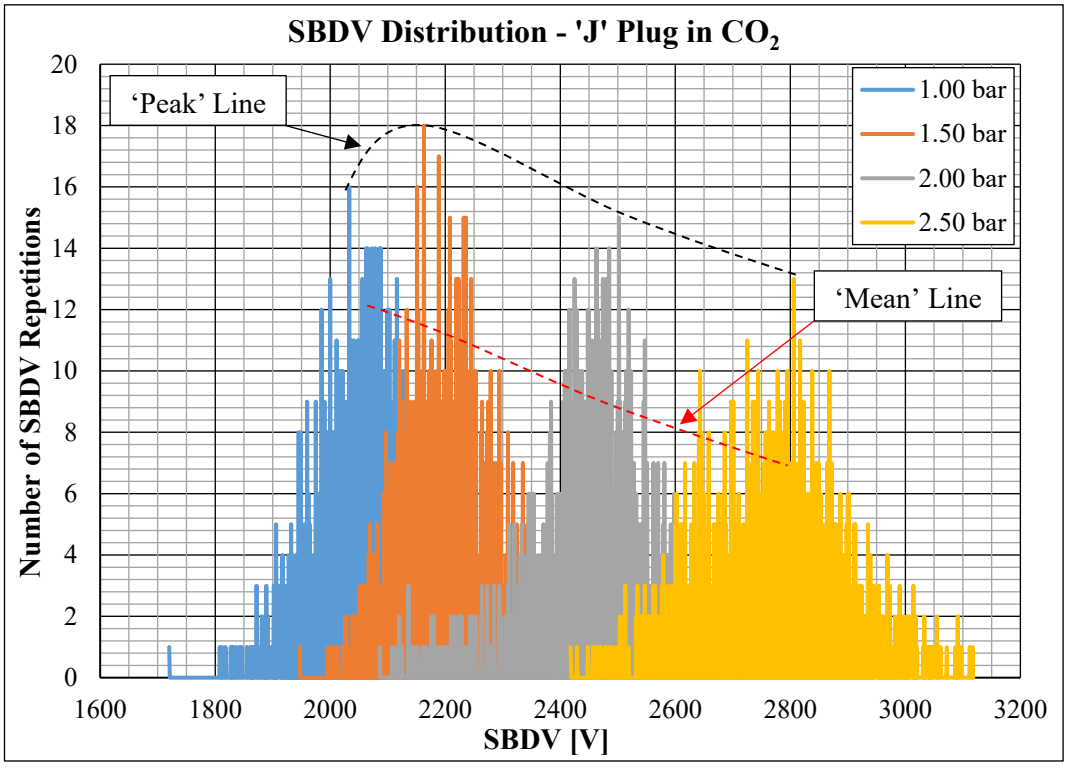

Figure F7-4: SBDV Distribution Curves – 'J' Plug in CO_2 (Ambient to 2.50 bar)

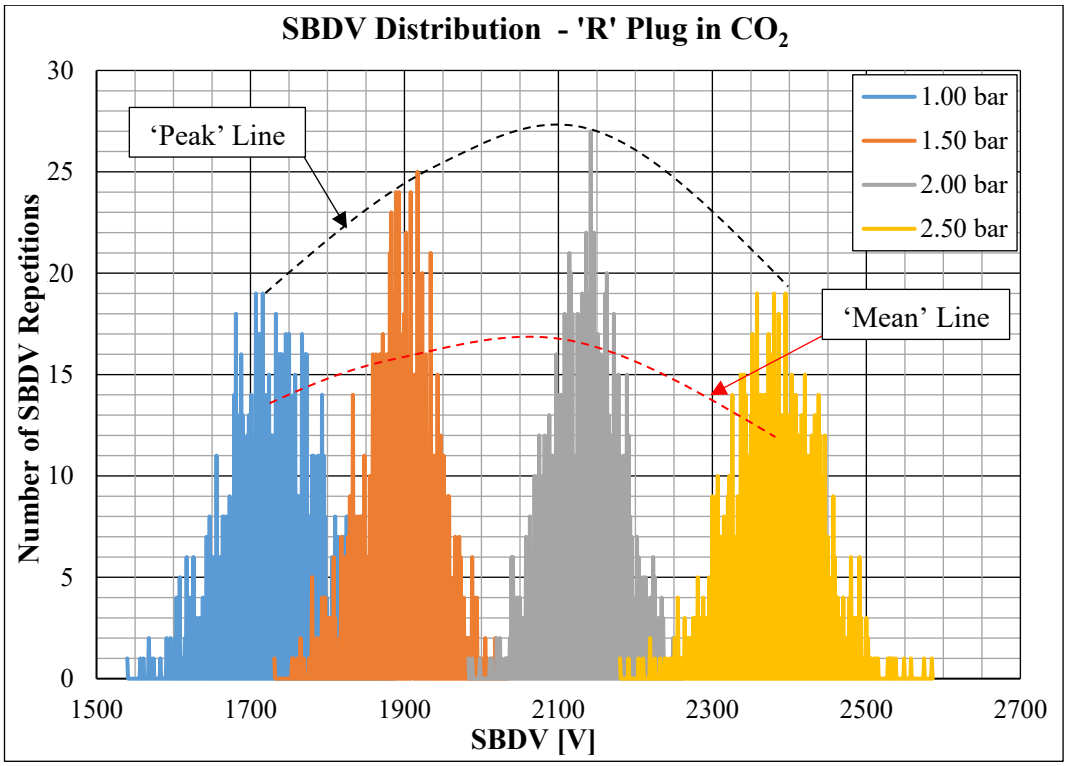

Figure F7-5: SBDV Distribution Curves – 'R' Plug in CO_2 (Ambient to 2.50 bar)

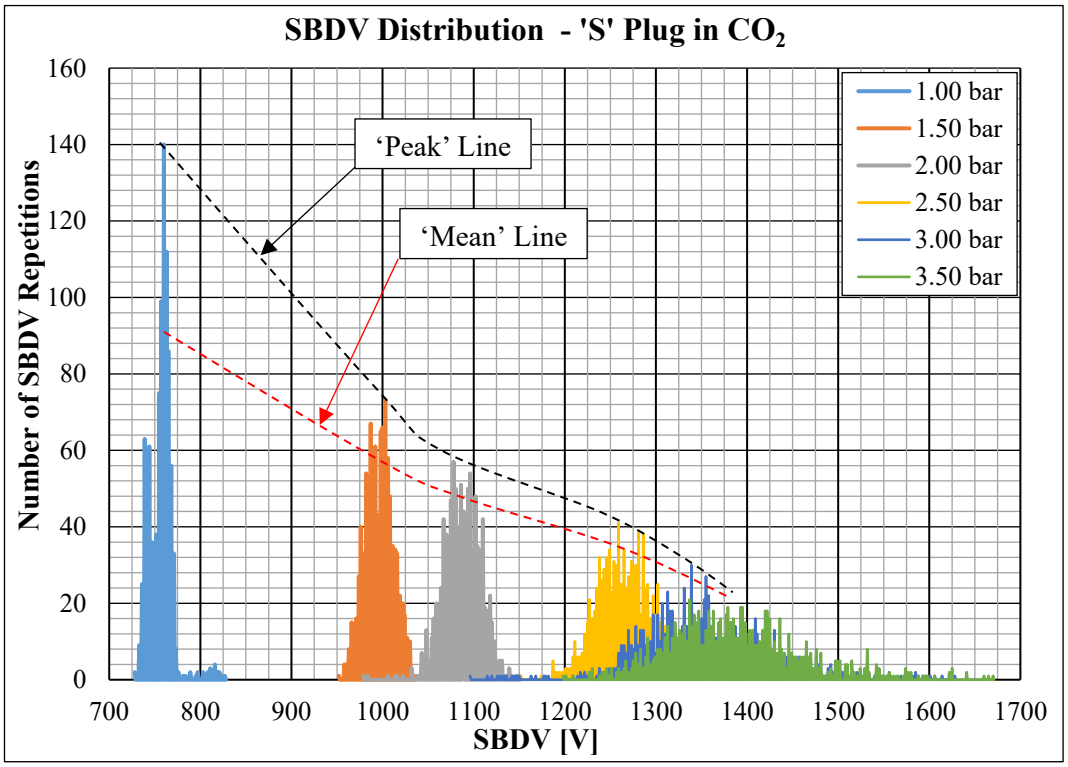

Figure F7-6: SBDV Distribution Curves – 'S' Plug in CO_2 (Ambient to 3.50 bar)

Observations: SBDV in Carbon Dioxide

In Carbon Monoxide (CO_2), the characteristic shape of spark break-down voltage repetition was noted to be general visually consistent using both the 'J' and 'R' type spark plugs. This behaviour for the 'S' plug was noted to be erratic and significantly less consistent over the pressures tested. However, this behaviour changes significantly at pressures above which spark break-down events could not be generated using the 'J' or 'R' type spark plugs which both have larger spark gap distances.

Visual comparison of the voltage at which the 'Peak' and 'mean' number of spark break-down repetitions occurs is significantly different for each spark plug. These voltages (judged visually) are shown by the black arrows (Peak) and red arrows (Mean). The visual trend for reducing voltage as pressure increases appears to be more consistent and greater over the pressure range tested in CO_2 using the 'S' plug.

SBDV Distribution in Carbon Monoxide

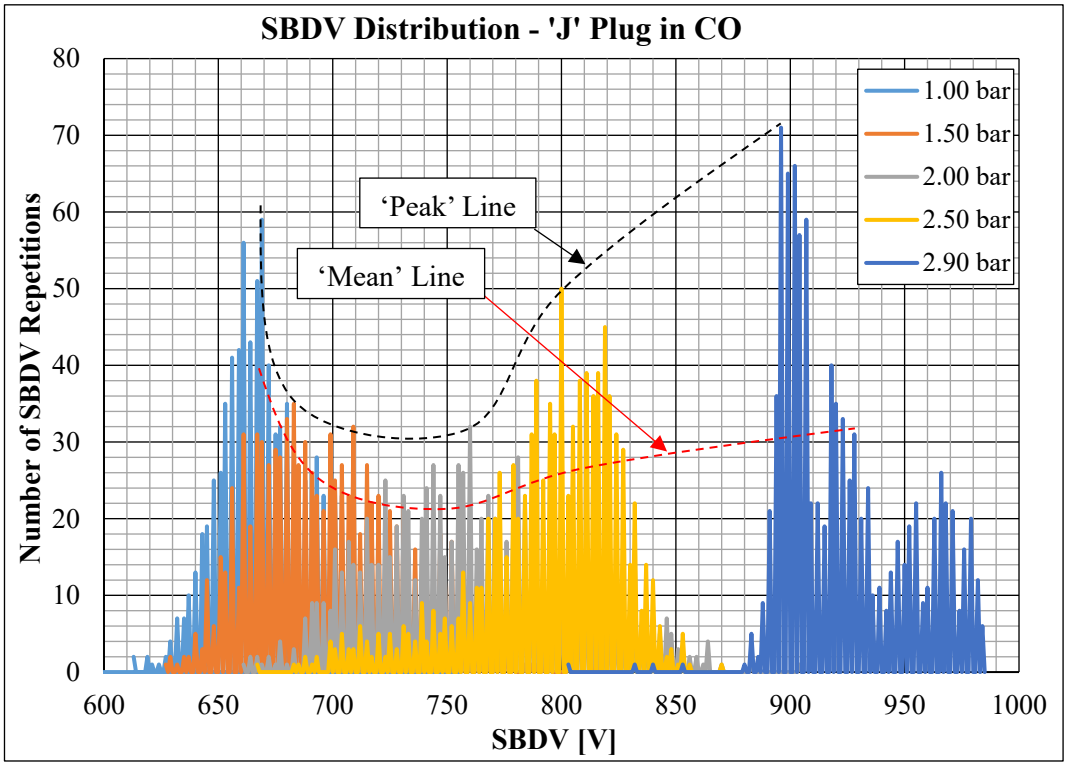

Figure F7-7: SBDV Distribution Curves – 'J' Plug in CO (Ambient to 2.90 bar)

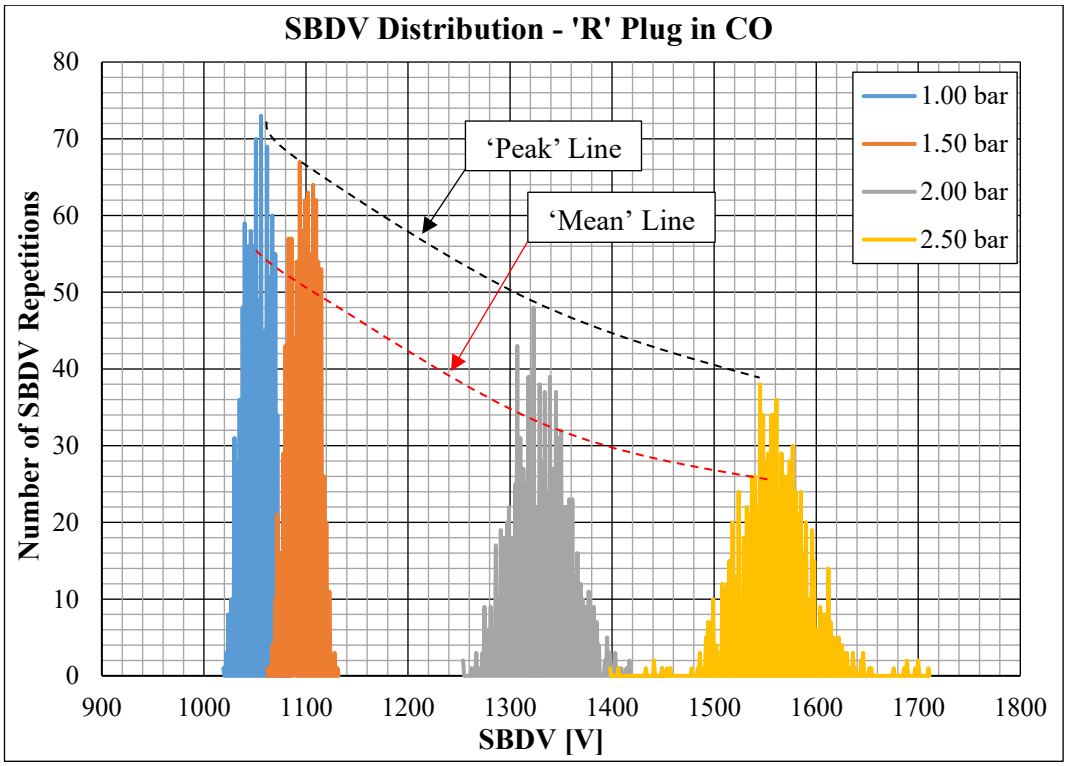

Figure F7-8: SBDV Distribution Curves – 'R' Plug in CO (Ambient to 2.50 bar)

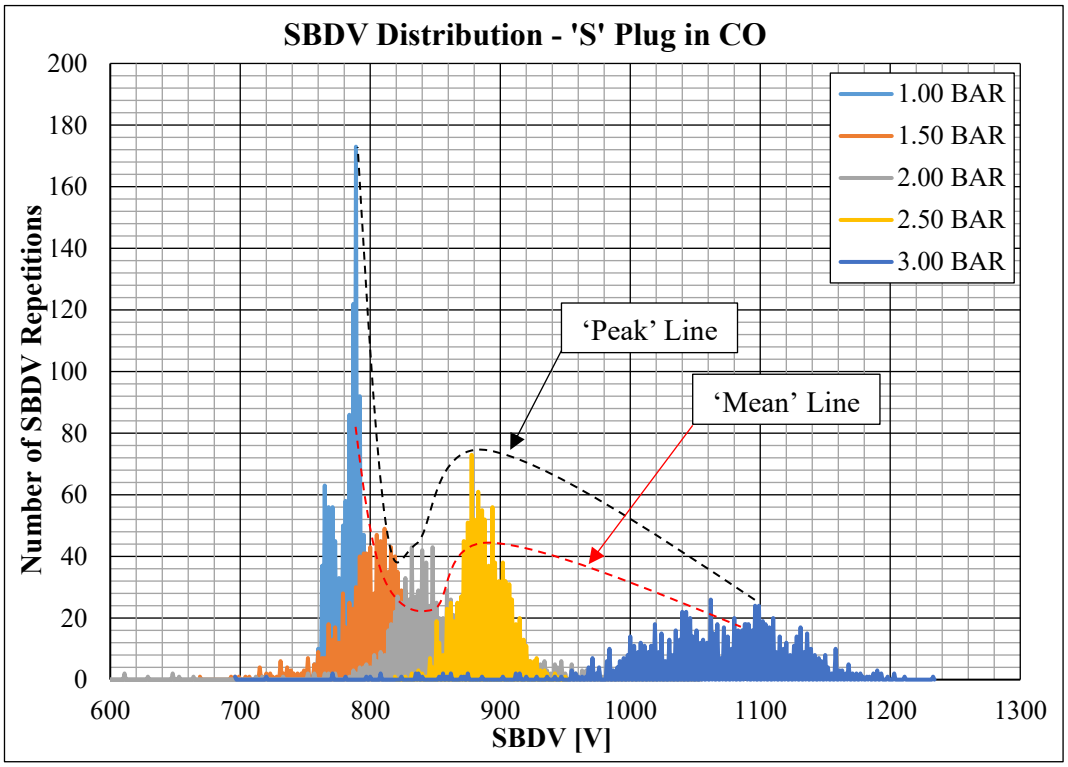

Figure F7-9: SBDV Distribution Curves – 'S' Plug in CO (Ambient to 3.0 bar)

Observations: SBDV in Carbon Monoxide

In Carbon Monoxide (CO), the characteristic shape of spark break-down voltage repetition was noted to be general visually consistent using the 'R' type spark plugs. This behaviour for both the 'J' and 'S' plugs was noted to be erratic and significantly less consistent over the pressures tested. However, this behaviour changes significantly at pressures above which spark break-down events could not be generated using the 'J' or 'R' type spark plugs which both have larger spark gap distances.

Visual comparison of the voltage at which the 'Peak' and 'mean' number of spark break-down repetitions occurs is significantly different for each spark plug. These voltages (judged visually) are shown by the black arrows (Peak) and red arrows (Mean). In both the 'J' plug and 'S' plug the 'Peak and 'Mean' spark break-down voltage dipped relatively at pressures 0ne bar above atmospheric.

SBDV distribution in Oxygen (O_2)

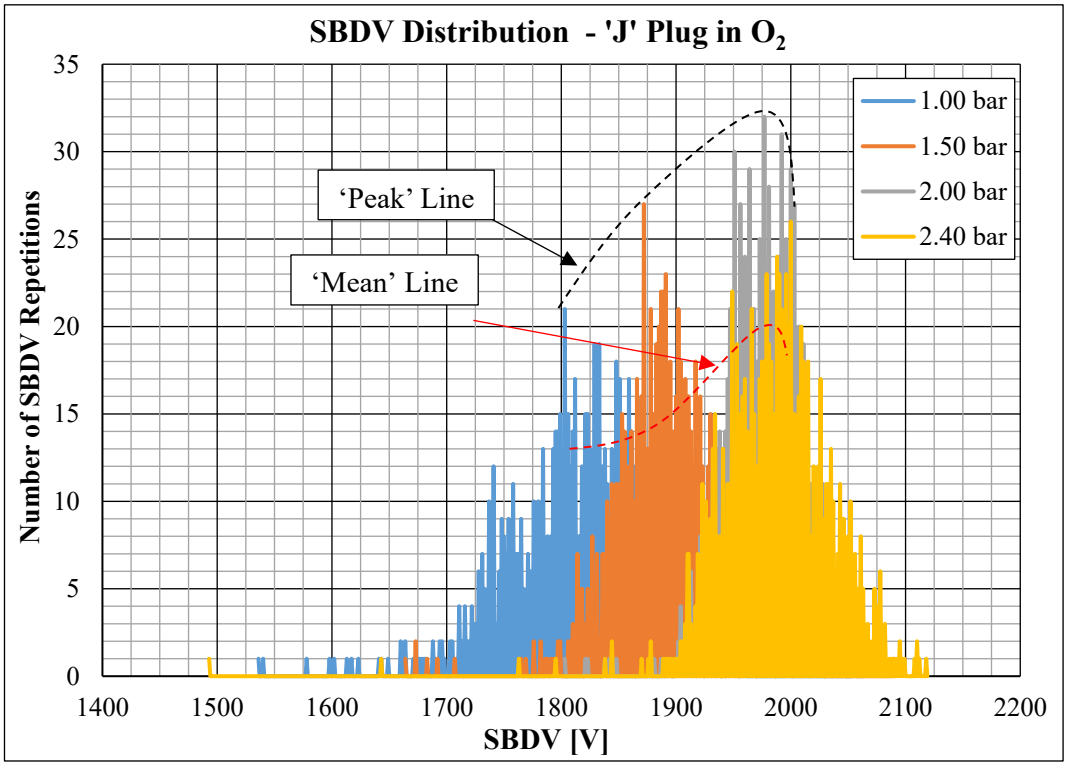

Figure F7-10: SBDV Distribution Curves – 'J' Plug in O_2 (Ambient to 2.40 bar)

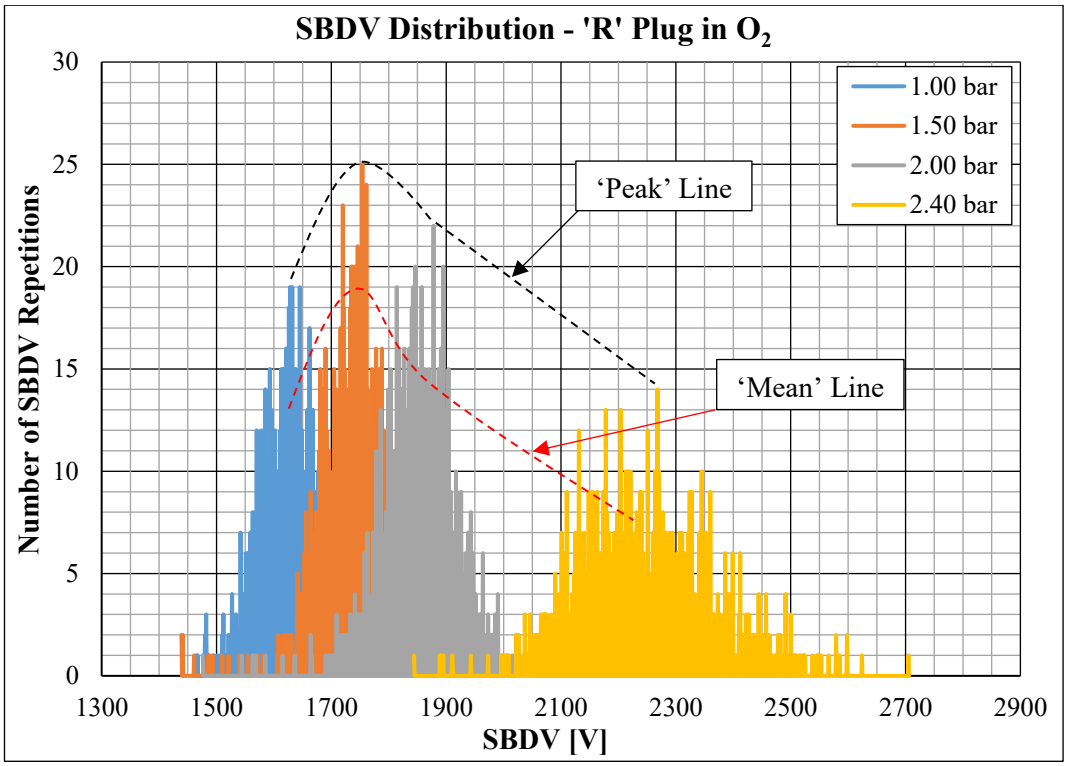

Figure F7-11: SBDV Distribution Curves – 'R' Plug in O_2 (Ambient to 2.40 bar)

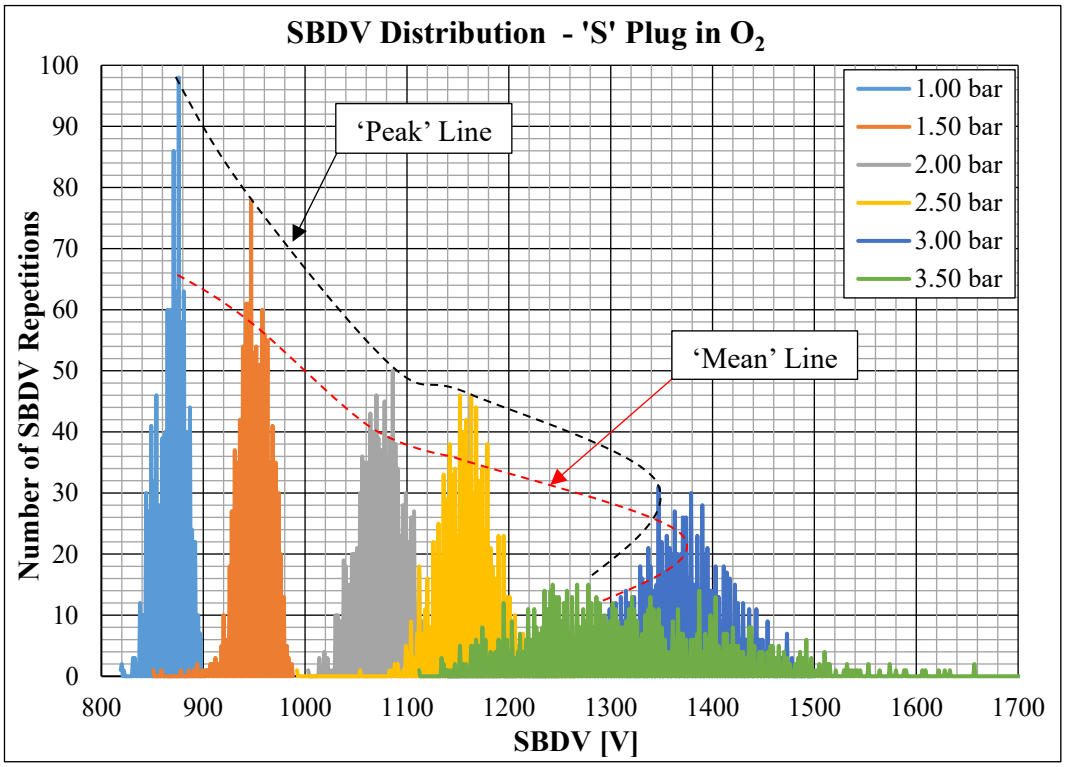

Figure F7-12: SBDV Distribution Curves – 'S' Plug in O_2 (Ambient to 3.5 bar)

Observations: SBDV in Oxygen

In Oxygen (O_2), the characteristic shape of spark break-down voltage repetition was noted to vary significantly for each plug type. The distribution shape is wide at atmospheric pressure but becomes narrower with increasing pressure using the 'J' plug. This characteristic is reversed using the 'R' plug. The trend is more consistent using the 'S' plug until pressures over which spark break-down would not occur using the 'J' and 'R' plugs, at which pressure the distribution becomes very widely spread.

Visual comparison of the voltage at which the 'Peak' and 'Mean' number of spark break-down repetitions occurs is significantly different for each spark plug. These voltages (judged visually) are shown by the black arrows (Peak) and red arrows (Mean). The pressures in which spark break-downs occur was noted to be greater using the 'S' plug than the other two types. However, at the higher pressure both the 'Peak' and 'Mean' voltage reduce.

SBDV distribution in Nitrogen (N_2)

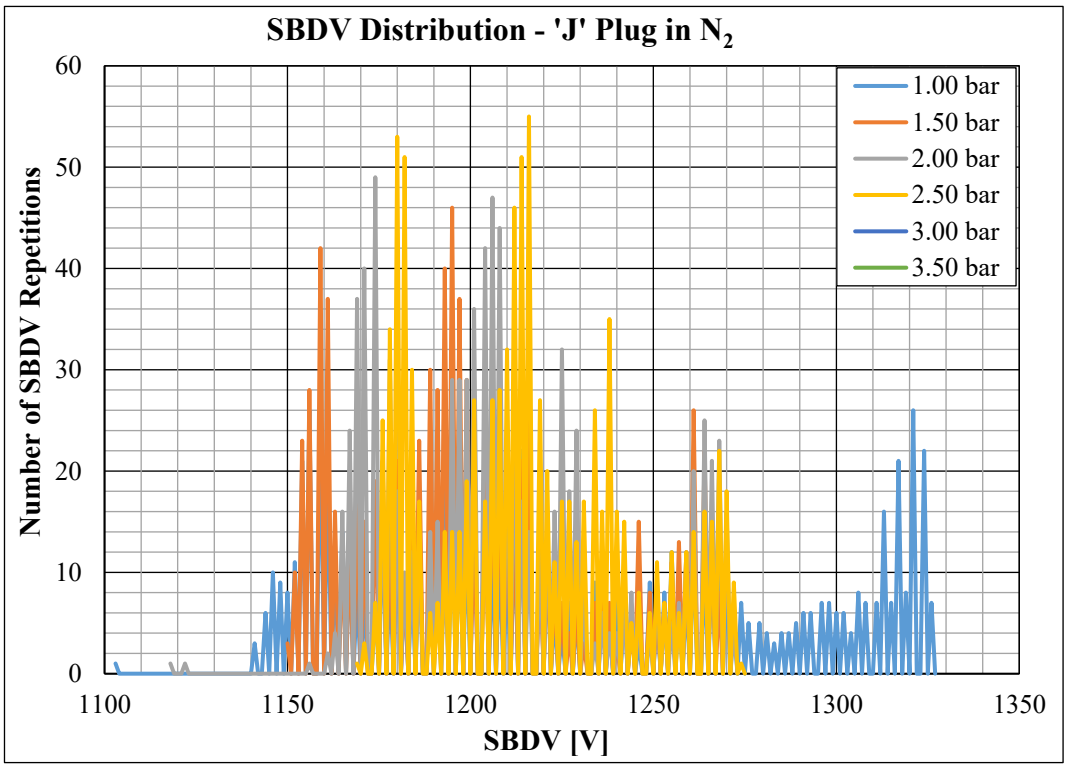

Figure F7-13: SBDV Distribution Curves – 'J' Plug in N_2 (Ambient to 3.50 bar)

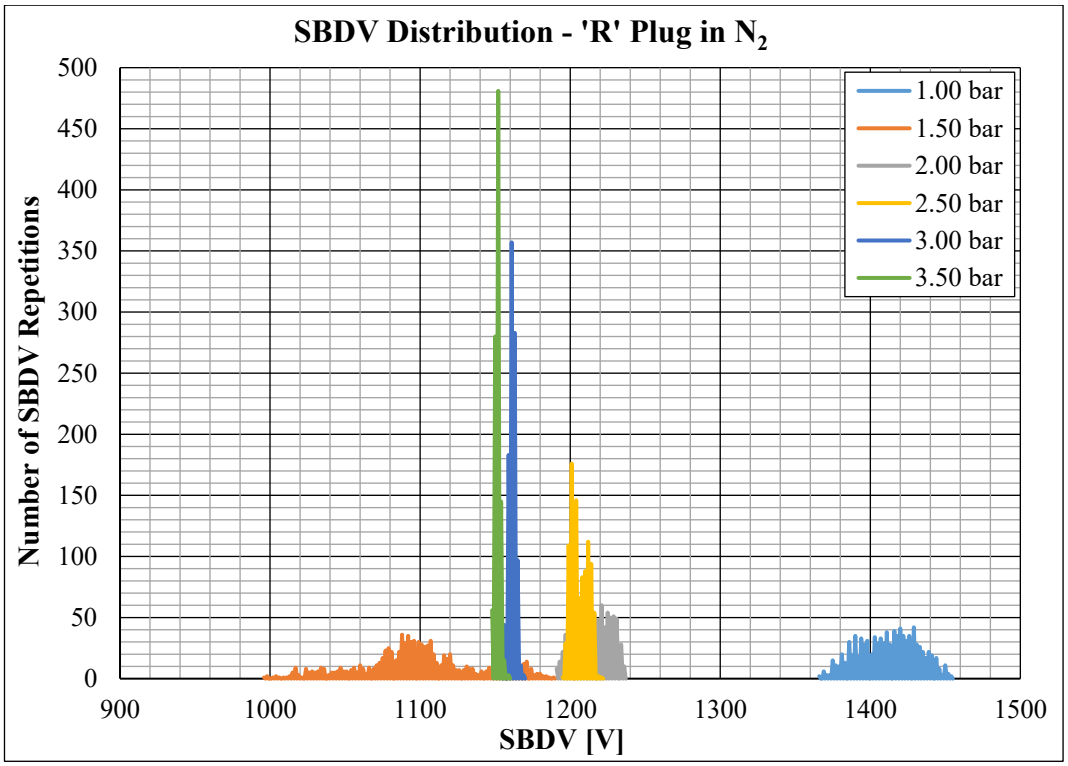

Figure F7-14: SBDV Distribution Curves – 'R' Plug in N_2 (Ambient to 3.50 bar)

Observations: SBDV in Nitrogen

Spark break-down distributions were obtained from testing in Nitrogen for only the 'J' and 'R' type spark plugs. The characteristic shapes of the distributions were found to be completely contradictory. Using the 'J' plug, the distribution shape is very wide and indistinct. This is repeated for all pressures. In contrast, the spark break-down distributions at all pressures using the 'R' plug are very narrow and closely defined at some pressures and wide at other pressures. Additionally, the 'Peak' and 'Mean' voltages do not increase with pressure. The behaviour of both plugs is so confusing the visual assessment of the voltages where the Peak number of spark break-down repetitions occur or where the Mean number of such repetitions occur is impractical.

7.3 SBDV DISTRIBUTION SUMMARY

The SBDV behaviour relative to increasing pressure was found to be generally consistent whereby the spark break-down voltage increased with pressure. This is expected from previous published information and was most consistent in Air. However, the behaviour was not directly proportional or consistent in other gases. Additionally, the spark break-down distribution varied considerably for different plugs. This varied behaviour was found to be most defined in Nitrogen where the distribution using the 'J' plug was very broad but very defined and narrow using the 'R' plug and inconsistent over all pressures.

Visual comparison of the overall shapes of the spark break-down distributions shows the voltage at which the 'Peak' number of break-down repetitions varies from the voltage at which the 'Mean' number of repetitions occurs. The voltage at which the 'Peak' and 'Mean' number of spark break-down repetitions occurs varies at different pressures in each gas and with each spark plug type. This behaviour is clearly demonstrated in the present work because the large numbers of spark break-down events represent a very large sample size. Such sample numbers are unlikely to have been recorded during sphere gap testing and it is considered possible the mathematical expressions published by previous researchers represent the difference between 'Peak' and 'Mean' spark break-down voltages.

7.4 SBDV CALIBRATION OF AIR AND OTHER GASES

For the proposed combustion control strategy to function it is essential for the new SBDV system to differentiate the presence of gases which will be present within the engine. This requires the value of SBDV for those gases to be converted into equivalent pressure. The same process used to produce these relationships for Air was followed for the other gases.

As previously listed, the other gases consisted of Oxygen (O_2), Carbon Dioxide (CO_2), Carbon Monoxide (CO) and Nitrogen (N_2). All these gases are independently significant to combustion. Oxygen is critical for combustion to occur as it is the oxidising agent. Carbon Dioxide (CO_2) is a natural constituent of Air and represents approximately 0.4% of the atmosphere. However, CO_2 is produced as a product of combustion, the peak value occurring when stoichiometric Air/Fuel ratios are burned. As such, the relative amount of CO_2 present is a key indicator of combustion quality. Carbon Monoxide (CO), is not a natural constituent of Air but is a product of combustion and is poisonous. The amount produced increases in proportion to the amount of fuel added to air. Therefore, as with CO_2, the relative amount of CO present is a key indicator of combustion quality. Nitrogen form

the largest part of Air and the atmosphere. Nitrogen reacts with oxygen during combustion to produce Nitrous Oxides (NOx) which are considered harmful. The production rate of these is proportional to and increases with combustion temperature. Hence the amount produced peaks when slightly lean stoichiometric Air/Fuel ratios are burned.

This section reports the results of testing to determine the spark break-down voltage required to overcome the dielectric strength of gases at various pressures. The test procedure described in section 7.1 was used to obtain spark break-down voltages at pressures between atmospheric and approximately 2.5 bar above atmospheric using the static pressure test chamber described in chapter four.

The results for each gas tested are graphically presented to show the relative relationship between Spark Break-Down Voltage (SBDV) vs Pressure and Spark Break-Down Voltage vs Density. These results are compared for the spark break-down voltage at which the Peak and Mean number of breakdown repetitions occurred. Both comparisons are included because each have been previously described to be most appropriate for different gases and pressures using different spark plugs. The results are reported for each gas tested in the following order, Air, Oxygen, Carbon Dioxide, Carbon Monoxide and Nitrogen. The observations from the results of each gas are included.

From the plots of SBDV vs Pressure and SBDV vs Density, mathematical expressions were obtained for Linear, Polynomial and Exponential relationships. These are presented in Tables T7-4, 5, 6 and 7. Regression analysis is included for each mathematical relationship to show the relative level of accuracy. It can be noted the Power Law relationship provides a slightly more accurate value than the Linear equation. However, due to ease of use and because the relative inaccuracy was comparatively small the ‘Linear’ relationships were used in later calculations to convert spark break-down voltage (SBDV) values to equivalent pressure (SBDVp) and density (SBDVd).

The section concludes by comparing the polynomial expression for air pressure obtained from the tests for both Peak and Mean SBDV with published information in section 7.6.

7.4.1 CONVERSION SBDV IN AIR

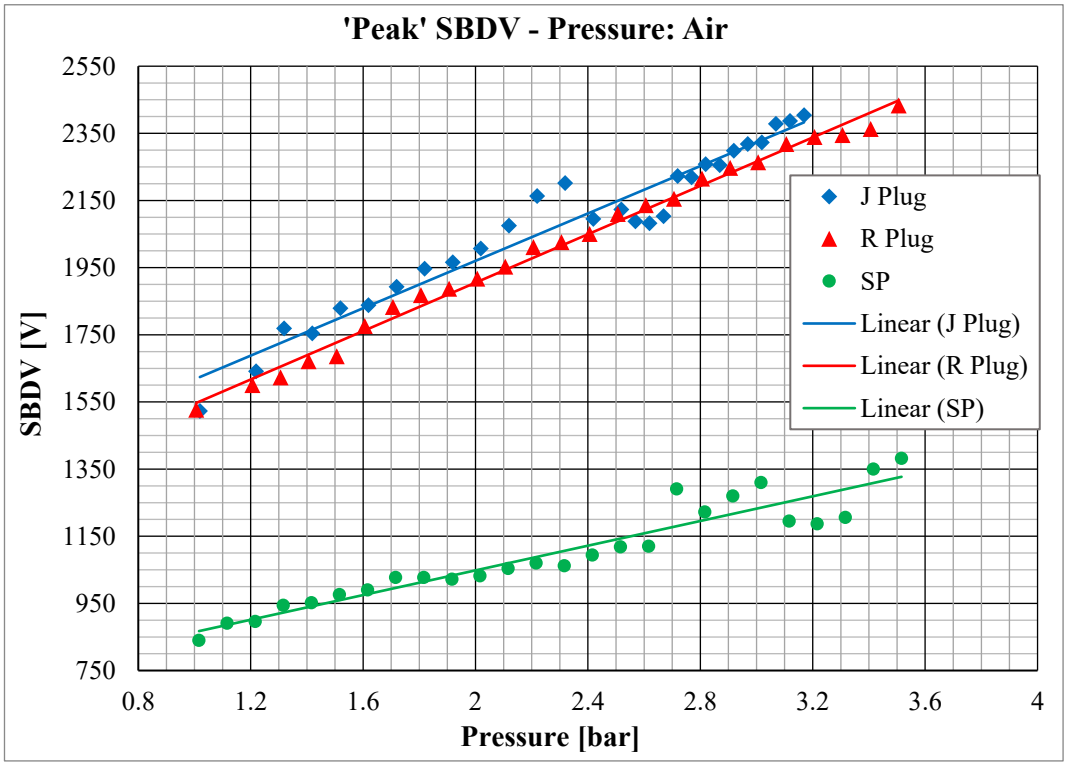

Figure F7-15: SBDV 'Peak' values vs Pressure in Air ('J','R' &'S' Spark Plugs)

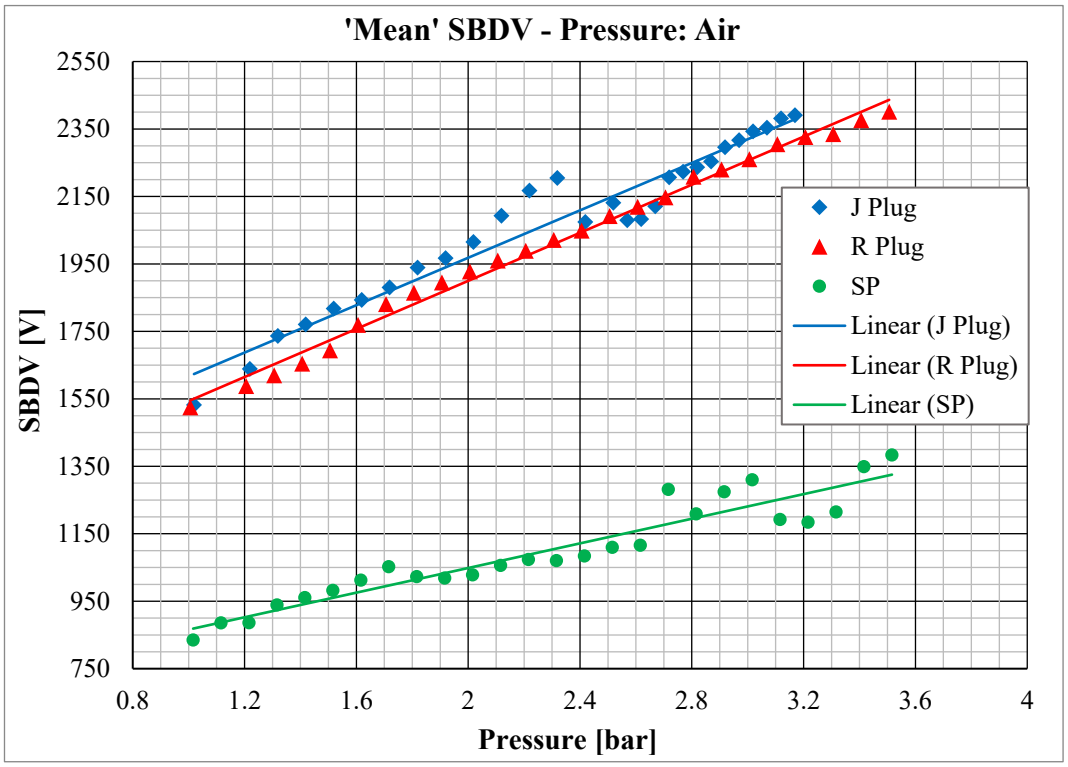

Figure F7-16: SBDV 'Mean' values vs Pressure in Air ('J','R' &'S' Spark Plugs)

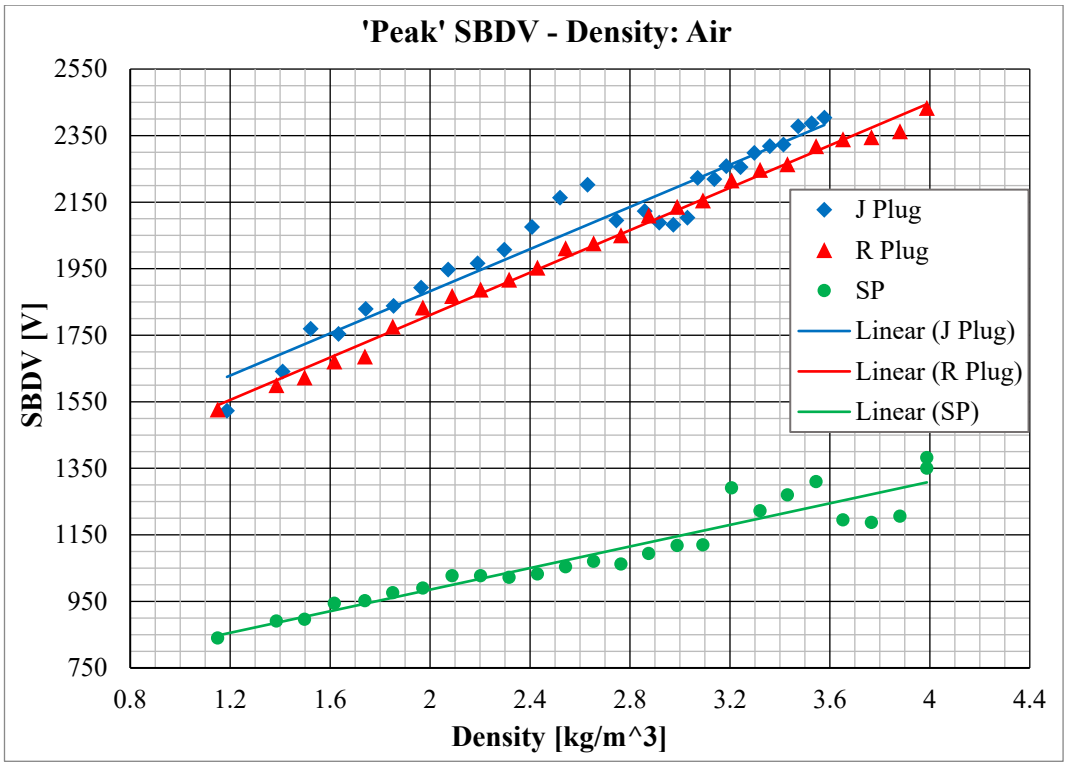

Figure F7-17: SBDV 'Peak' values vs Density in Air ('J', 'R' &'S' Spark Plugs)

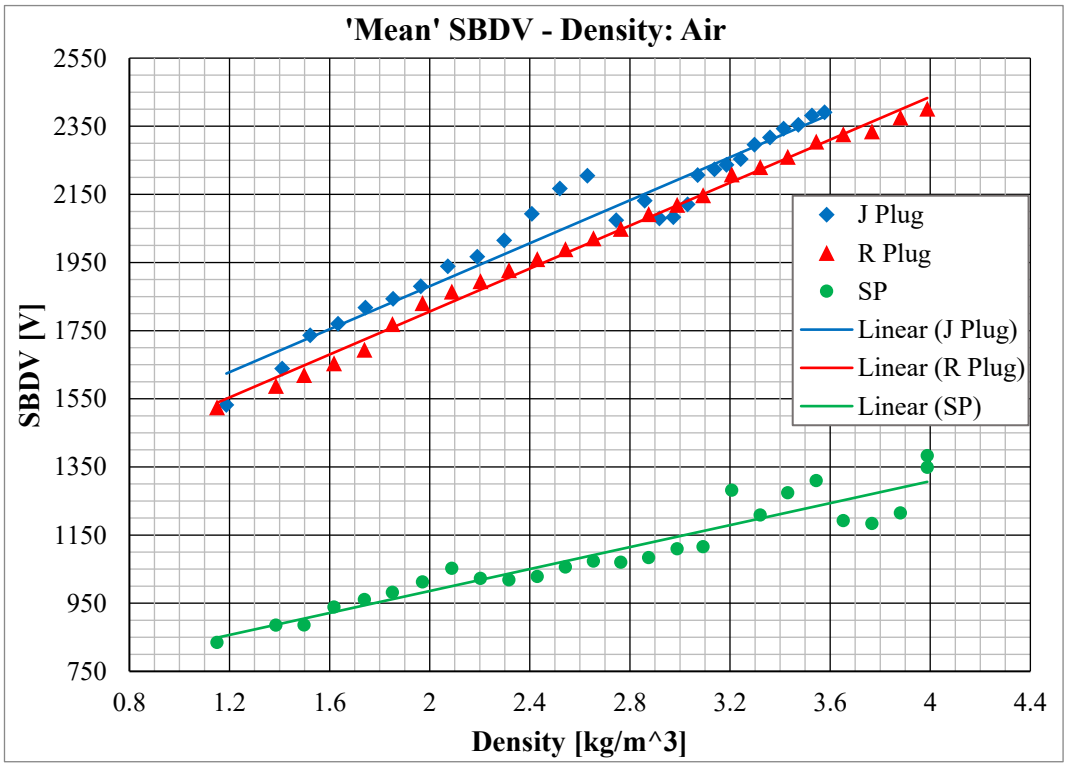

Figure F7-18: SBDV 'Mean' values vs Density in Air ('J','R' &'S' Spark Plugs)

7.4.2 OBSERVATIONS OF SBDV RESULTS FOR AIR

The SBDV values obtained in Air using all three type of spark plugs was consistent with pressure. The best ‘fit’ (with least variance) to increasing pressure was obtained using the ‘R’ plug. The maximum pressure in which spark break-down signals were obtained reached 3.5 bar using both the ‘R’ and ‘S’ plug which was 0.5 bar greater than those obtained using the ‘J’ plug.

The difference of spark-break-down voltage between the ‘J’ and ‘R’ plugs is small but consistent. The voltage difference between the ‘J’ and ‘R’ plugs and ‘S’ plug is disproportionate to the reduced spark gap difference but consistent across the pressure range.

7.4.3 SBDV IN OXYGEN

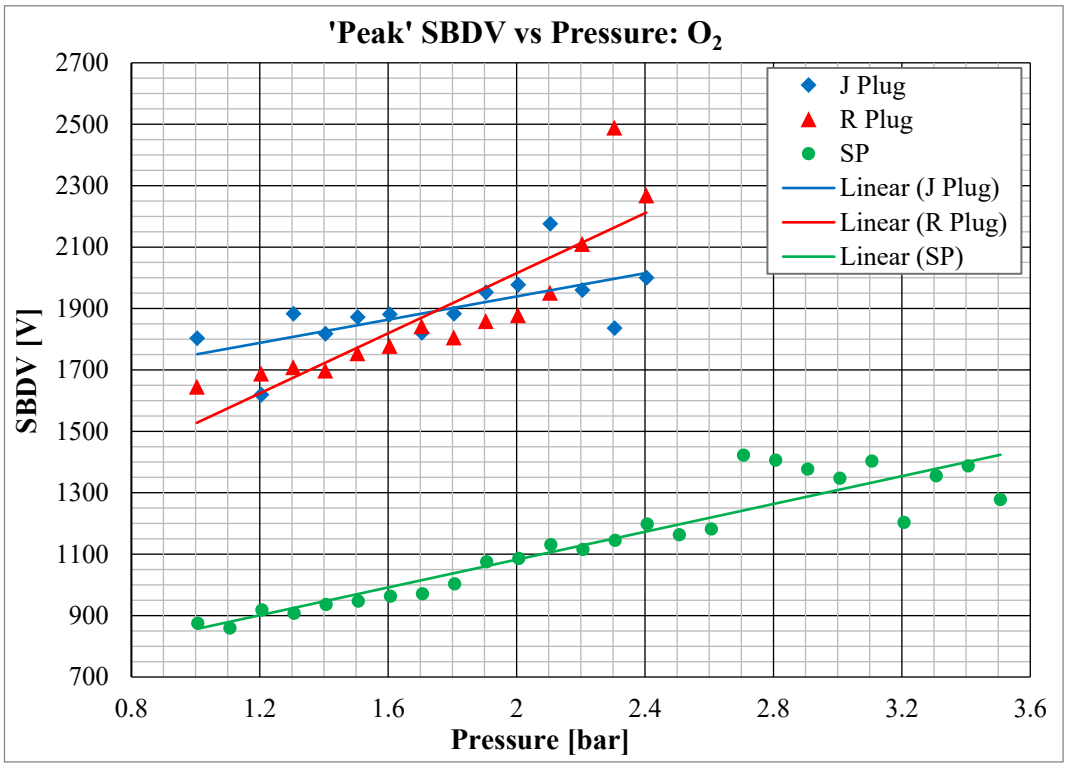

Figure F7-19: 'Peak' SBDV vs Pressure in O_2

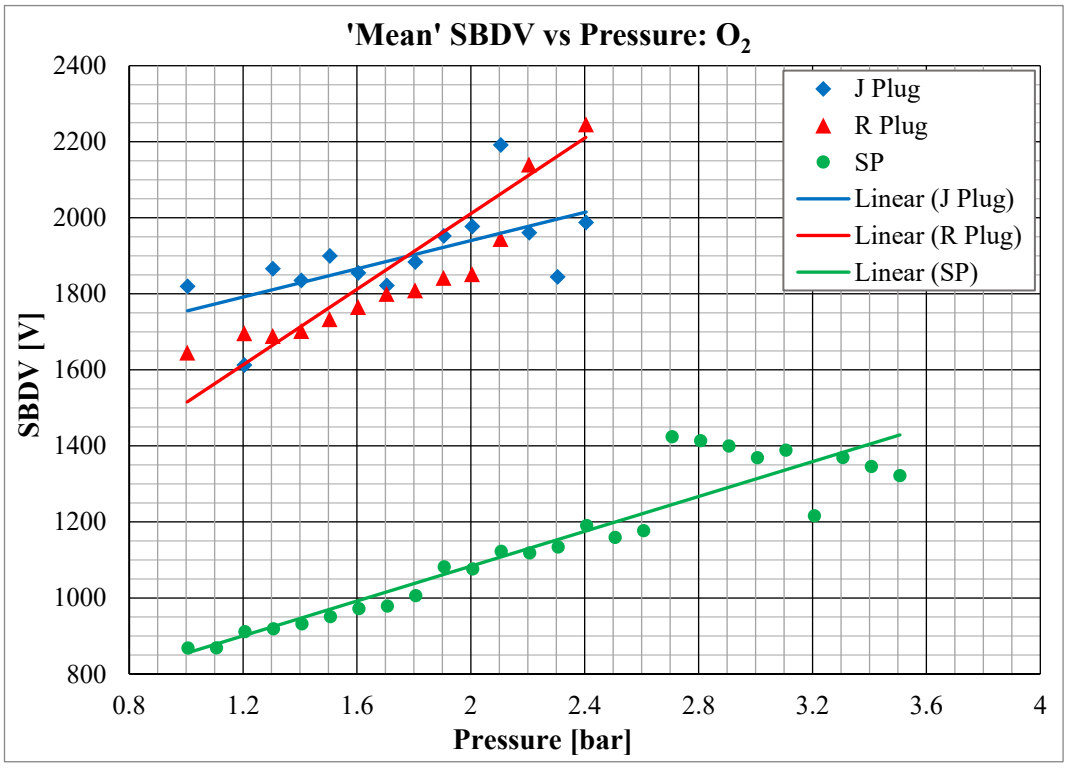

Figure F7-20: 'Mean' SBDV vs Pressure in O_2

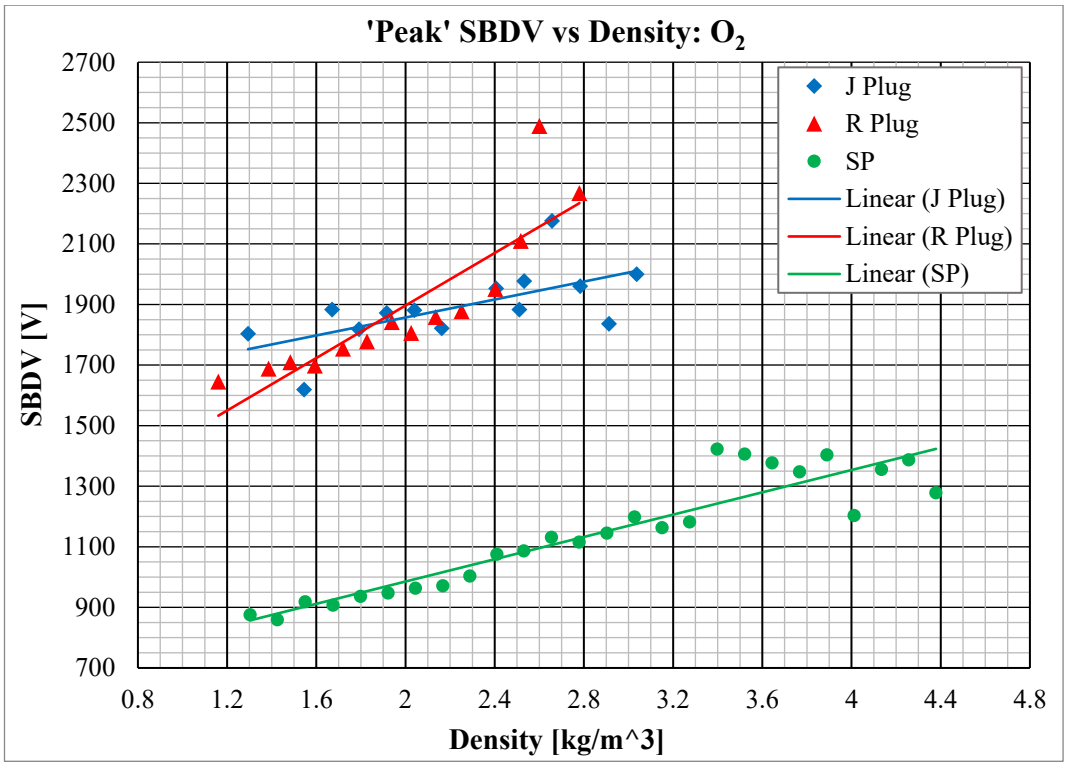

Figure F7-21: 'Peak' SBDV vs Density in O_2

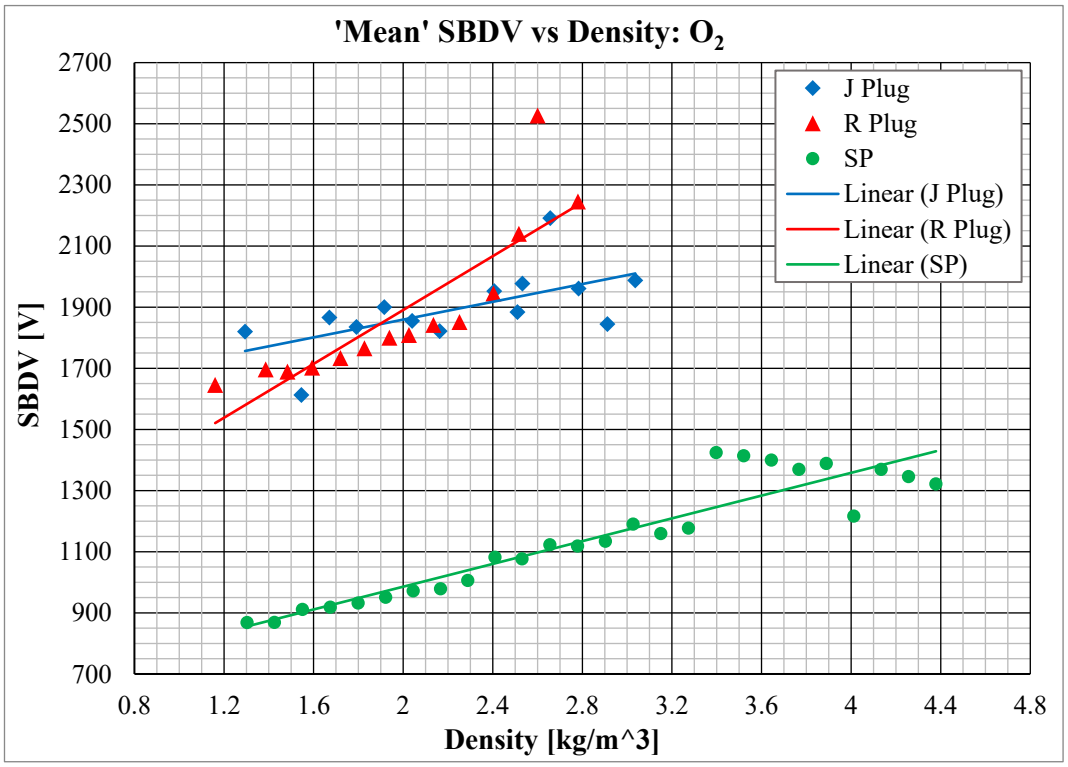

Figure F7-22: 'Mean' SBDV vs Density in O_2

7.4.4 OBSERVATIONS OF SBDV RESULTS FOR OXYGEN

The SBDV values obtained in Oxygen are less consistent than those obtained in Air. The maximum pressure in which spark break-down events could be generated using the ‘J’ and ‘R’ plugs was approximately one bar less than those obtained in Air. The trendline for the ‘J’ and ‘R’ plugs were significantly different but consistent. The trendline for the ‘S’ plug to both pressure and density was consistent but showed increased variance in the upper pressure range. The effect of the smaller spark gap distance of the ‘S’ plug is apparent in the spark break-down voltage values required at all pressures.

7.4.5 SBDV IN CARBON DIOXIDE

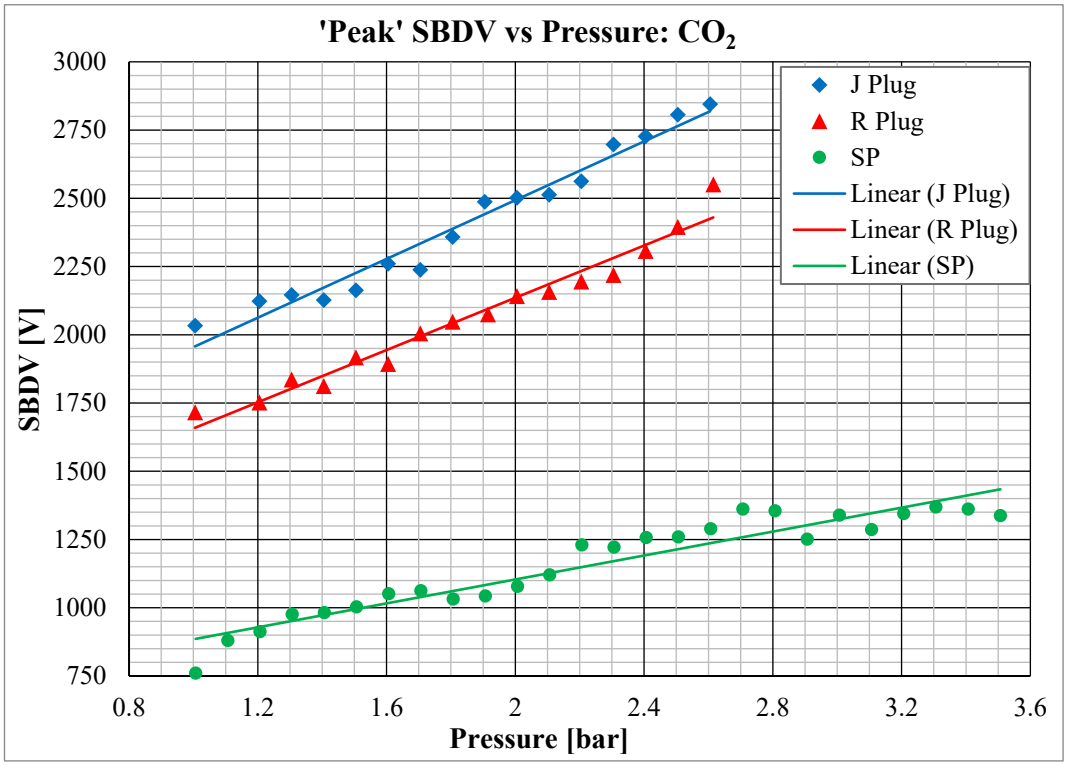

Figure F7-23: 'Peak' SBDV vs Pressure in CO_2

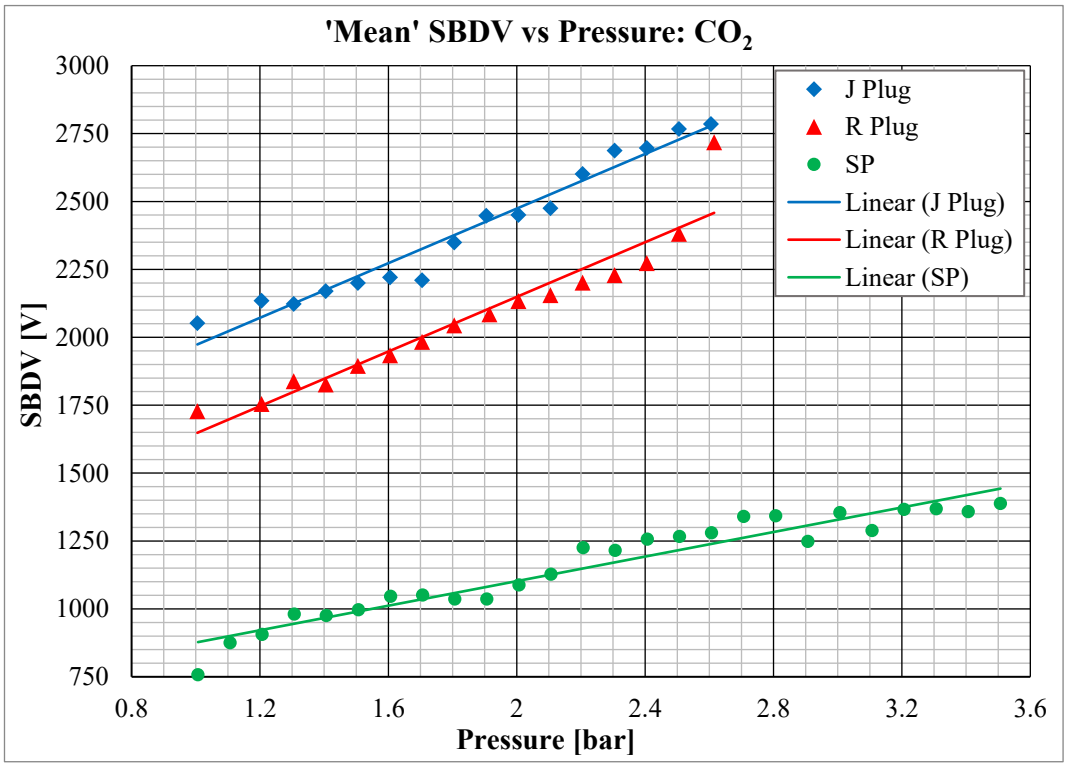

Figure F7-24: 'Mean' SBDV vs Pressure in CO_2

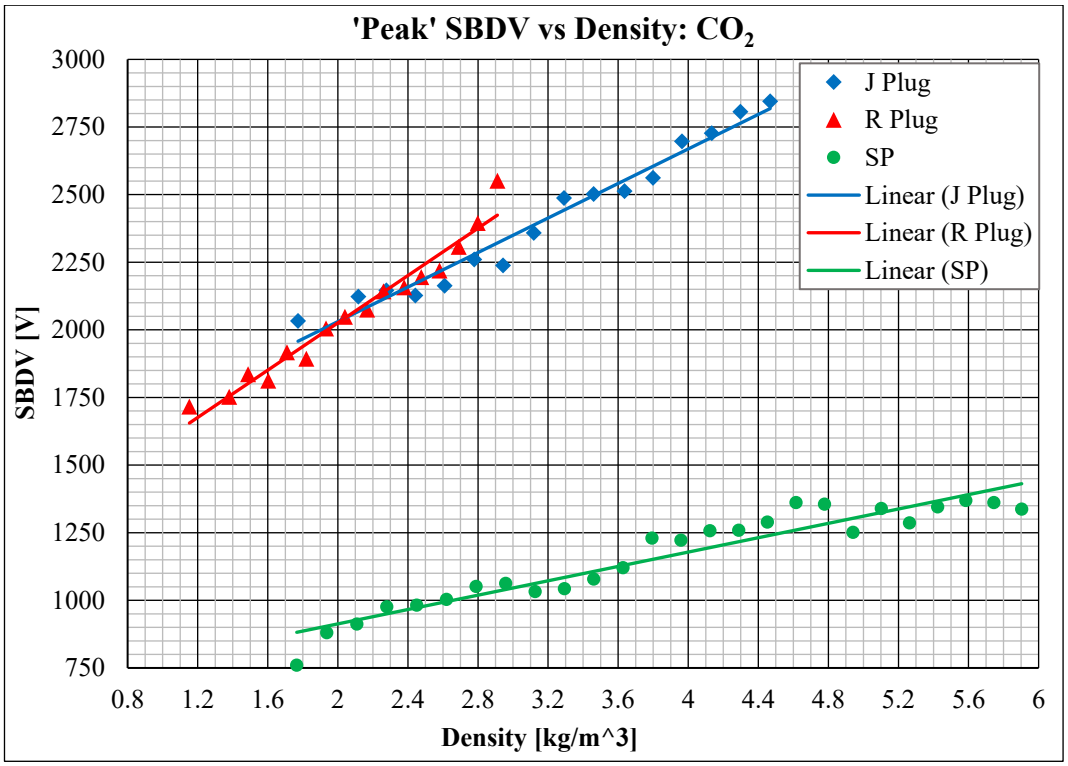

Figure F7-25: 'Peak' SBDV vs Density in CO_2

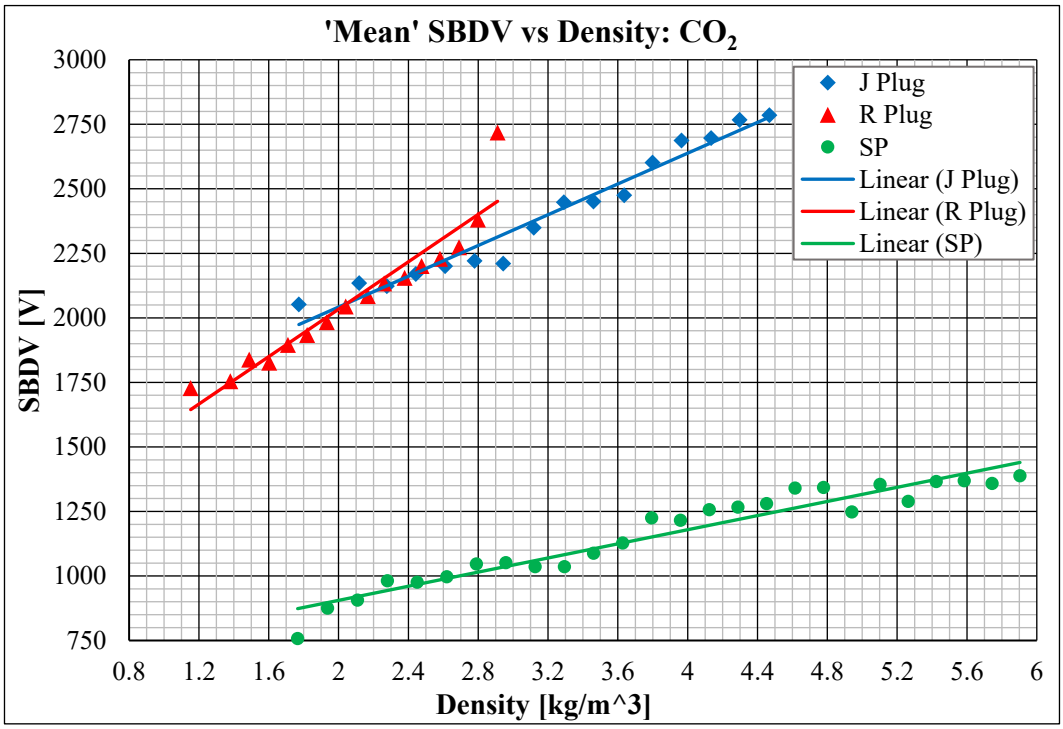

Figure F7-26: 'Mean' SBDV vs Density in CO_2

7.4.6 OBSERVATIONS OF SBDV RESULTS FOR CARBON DIOXIDE

The SBDV values obtained from testing using Carbon Dioxide are consistent. The difference between the use of ‘Peak or ‘Mean’ values is negligible. The difference in the voltage required by the ‘S’ plug in comparison with the ‘J’ and ‘R’ types is significant. The voltages required for the three types of spark plug is distinct. The trendline for pressure and density is significantly different using the ‘J’ and ‘R’ types but similar using the ‘S’ type.

7.4.7 SBDV IN CARBON MONOXIDE

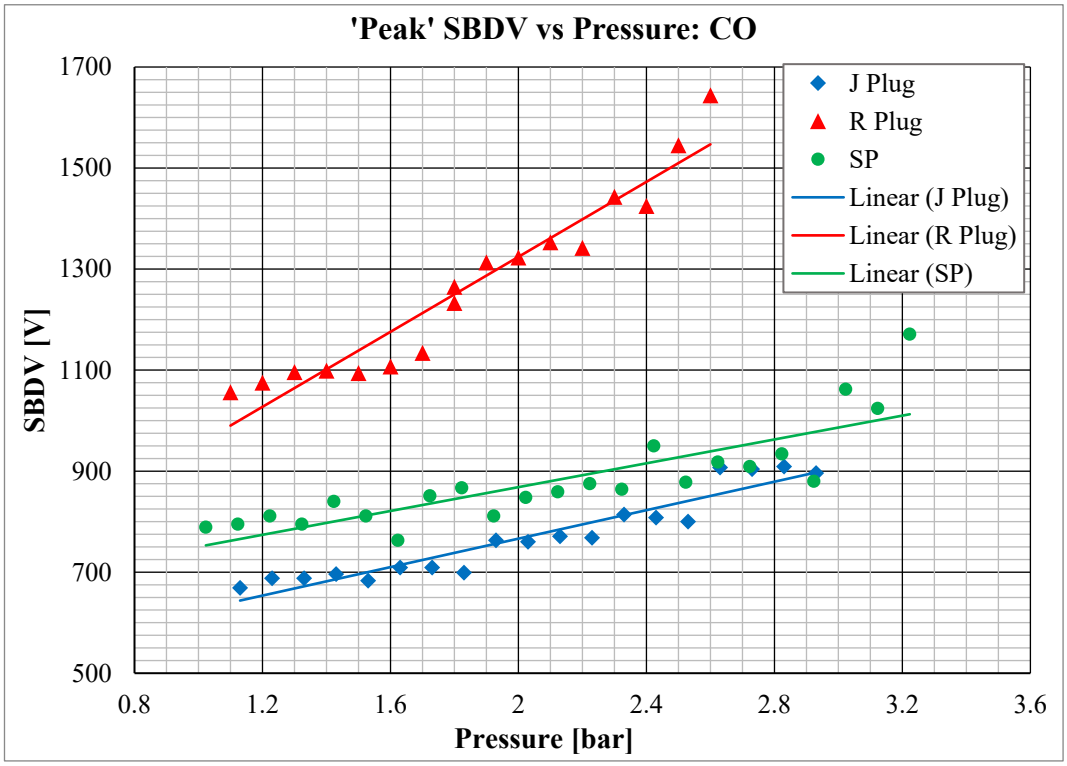

Figure F7-27: 'Peak' SBDV vs Pressure in CO

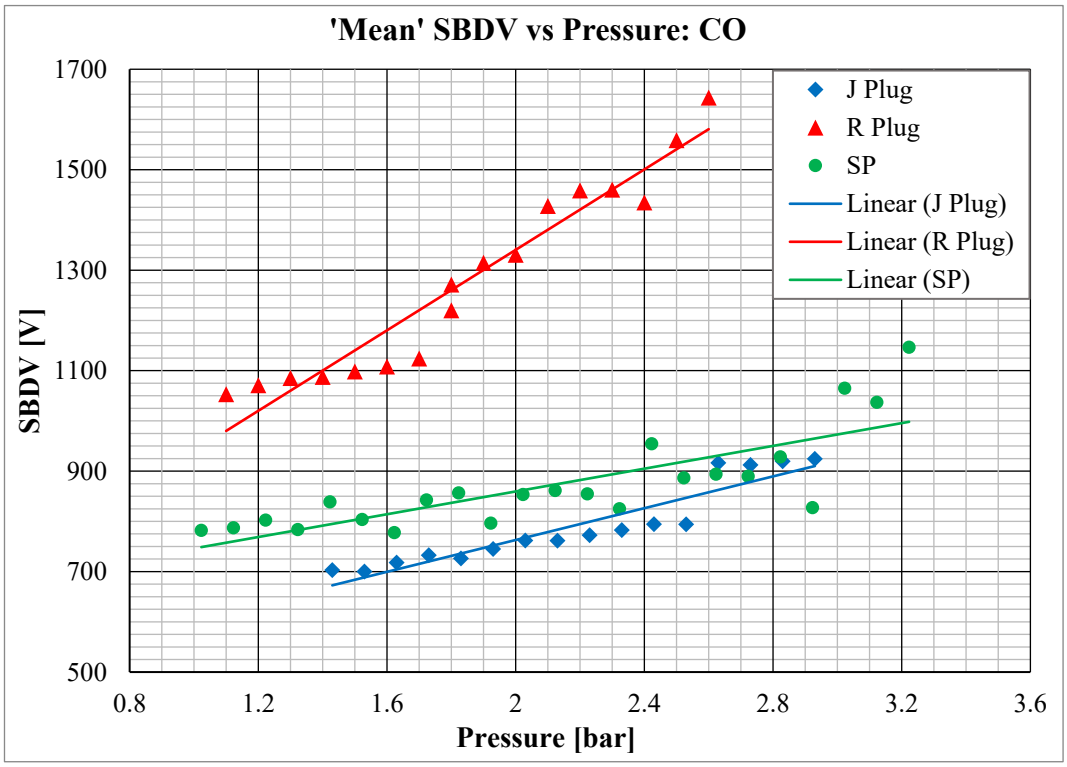

Figure F7-28: 'Mean' SBDV vs Pressure in CO

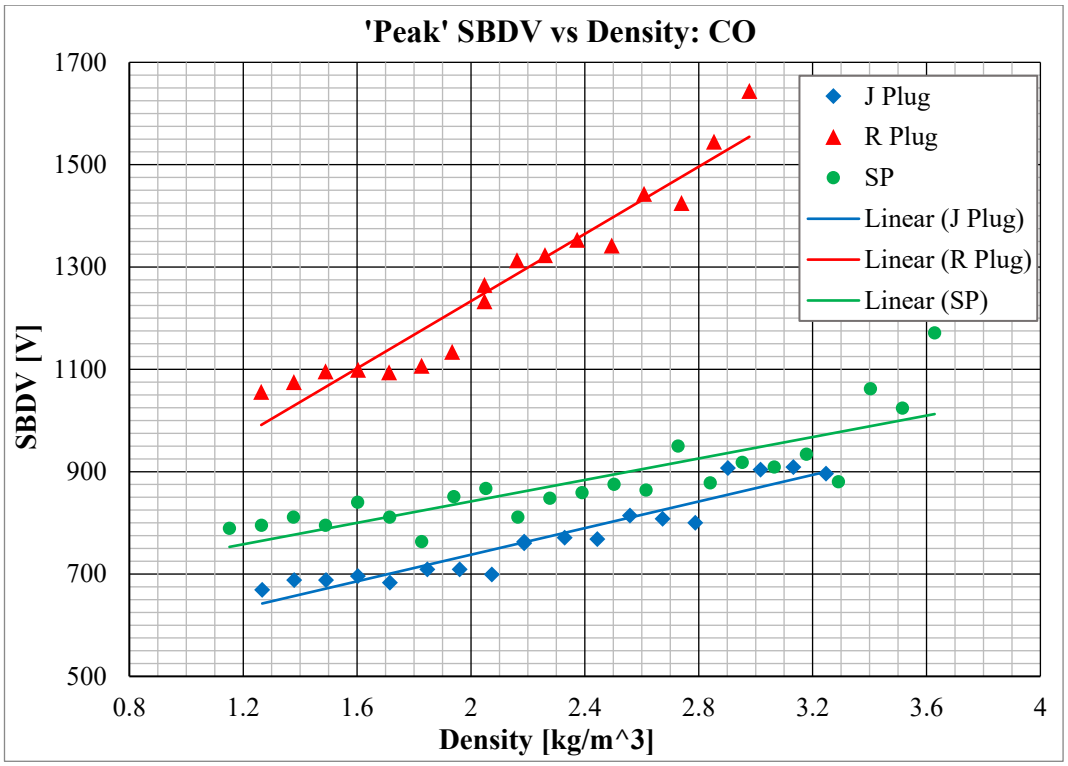

Figure F7-29: 'Peak' SBDV vs Density in CO

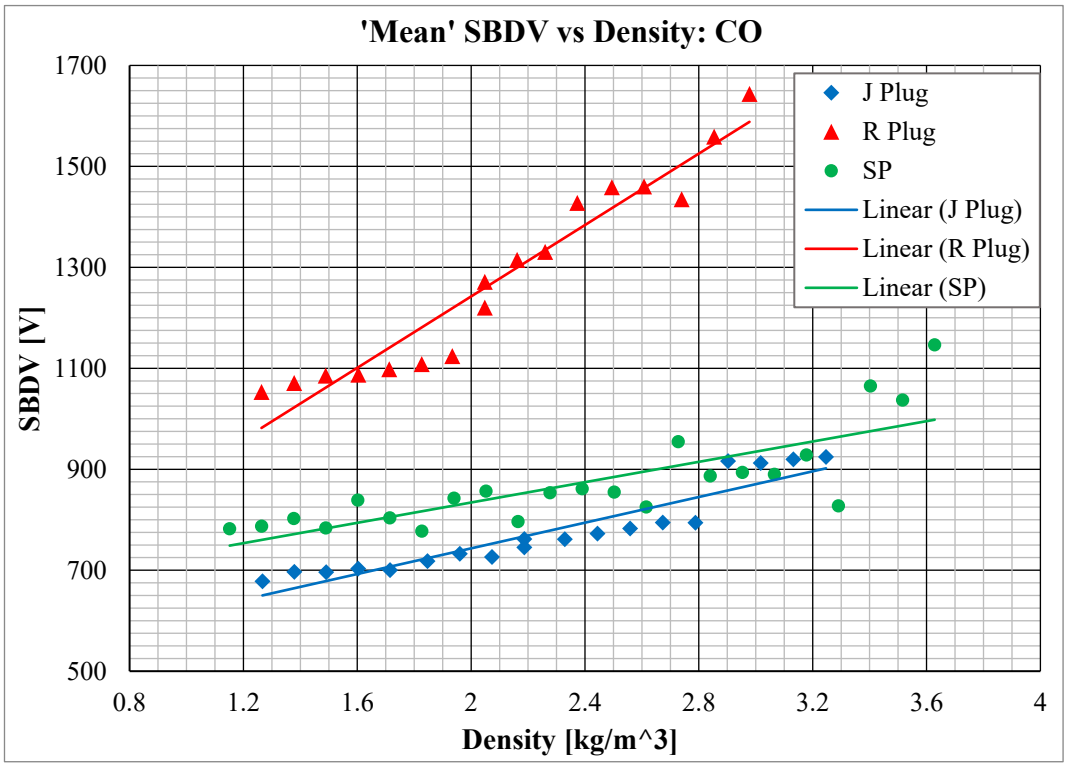

Figure F7-30: 'Mean' SBDV vs Density in CO

7.4.8 OBSERVATIONS OF SBDV RESULTS FOR CARBON MONOXIDE

The spark break-down voltages obtained using the ‘J’ plug in CO are less than the ‘S’ plug despite the significantly smaller spark gap distance. However, the trendline slopes and relative voltage differences are consistent.

7.4.9 SBDV IN NITROGEN

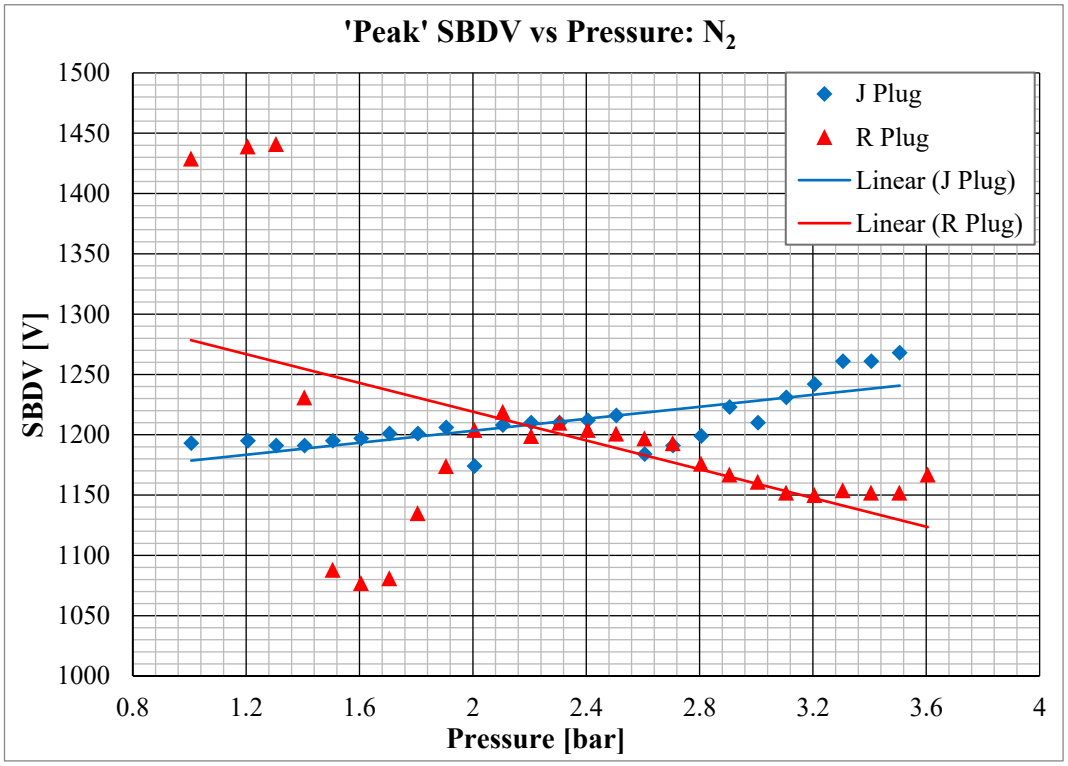

Figure F7-31: 'Peak' SBDV vs Pressure in N_2

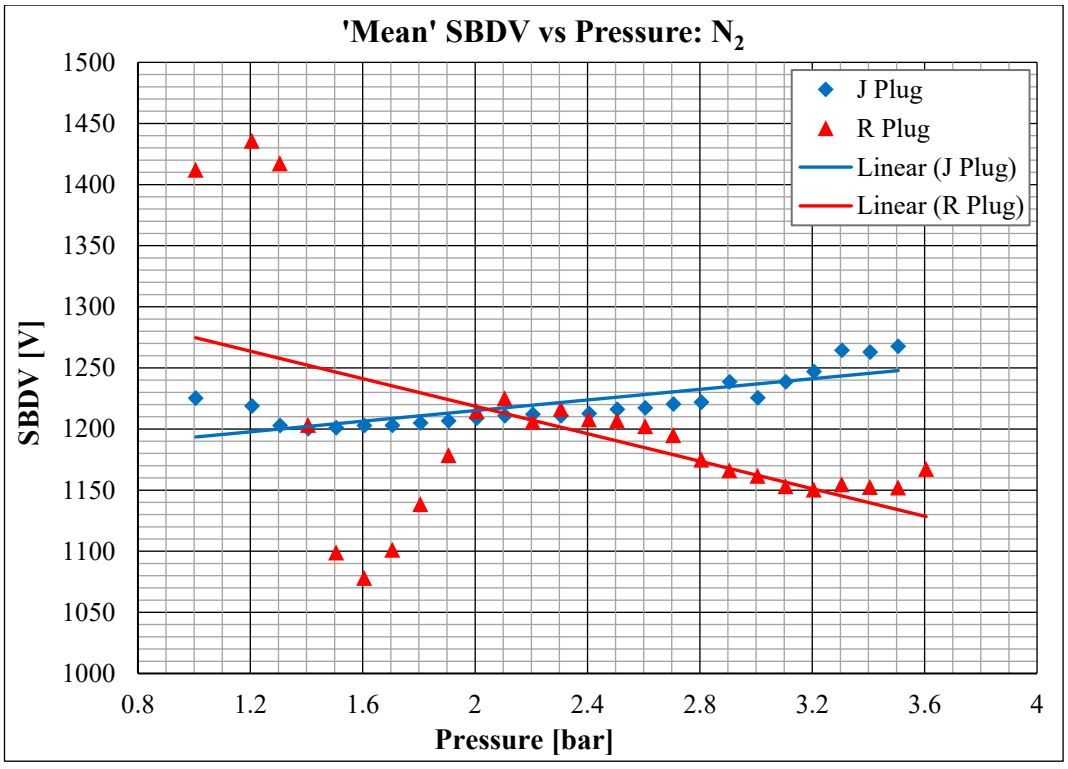

Figure F7-32: 'Mean' SBDV vs Pressure in N_2

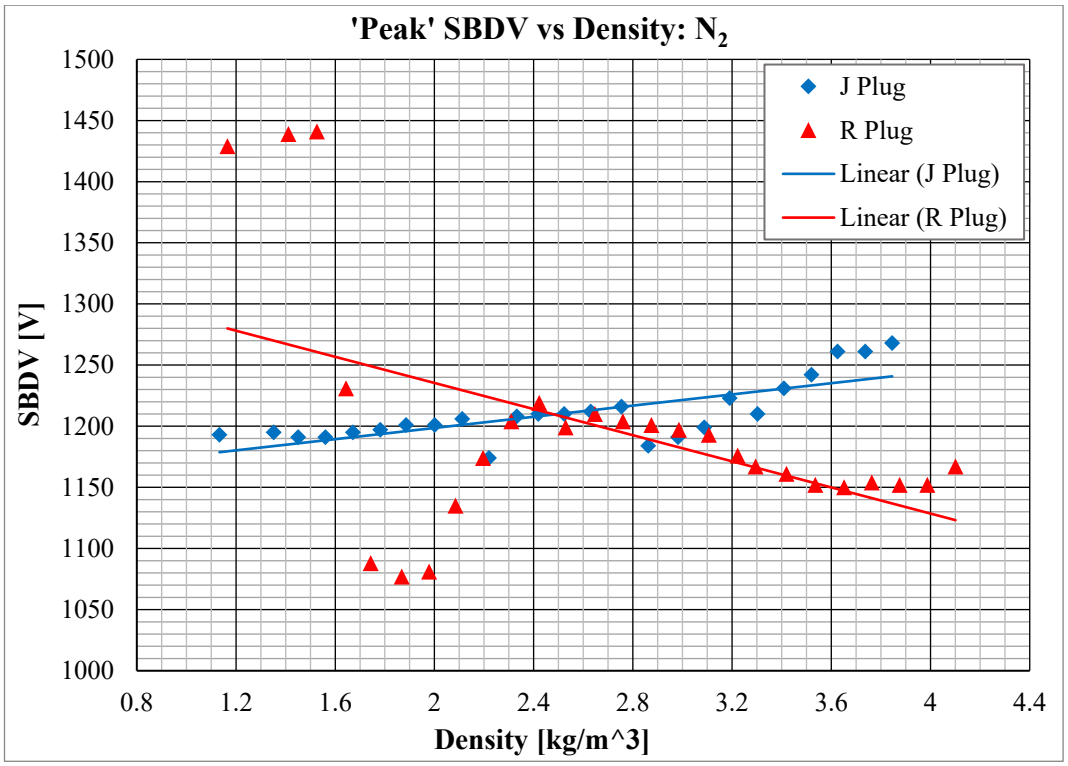

Figure F7-33: 'Peak' SBDV vs Density in N_2

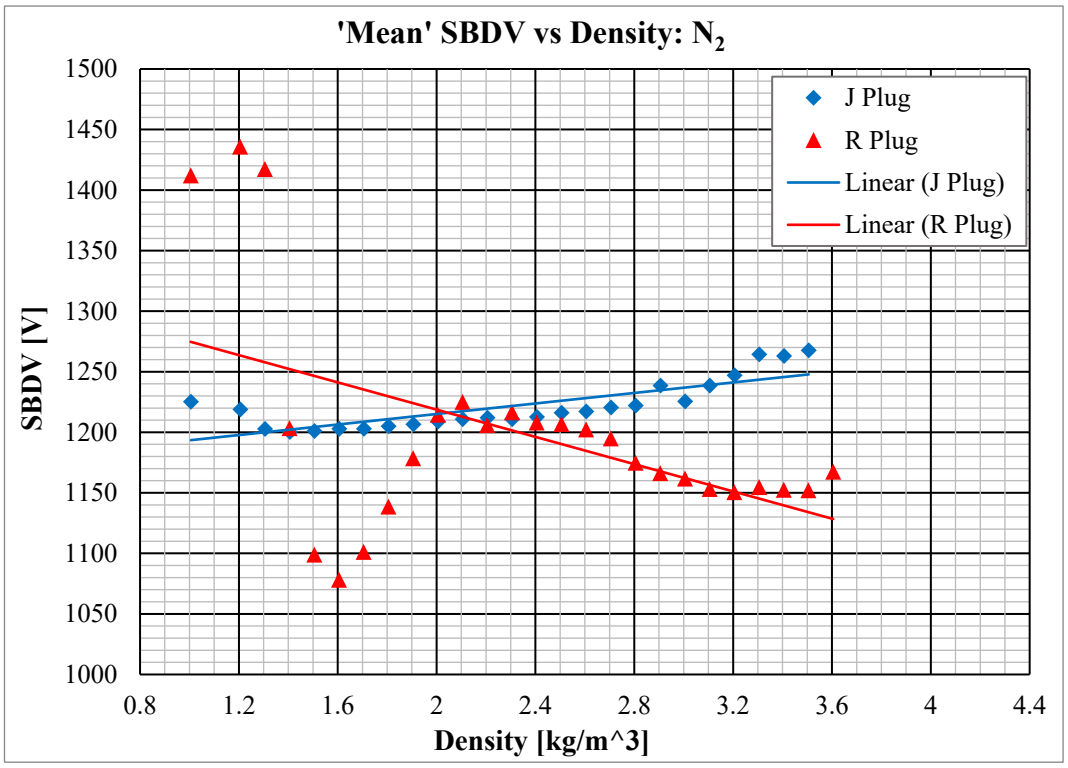

Figure F7-34: 'Mean' SBDV vs Density in N_2

7.4.10 OBSERVATIONS OF SBDV RESULTS FOR NITROGEN

The spark break-down voltages obtained by testing in Nitrogen showed opposing characteristics between the ‘J’ and ‘R’ plugs. The pressure range over which spark break-down could be generated was large and consistent between the two plug types. Nitrogen behaves in a unreactive and benign manner and spark break-down, hence gas ionization would appear to be less effected by pressure increase than any of the other gases tested.

7.4.11 COMPARISON OF 'PEAK' &' MEAN SBDV - VARIOUS GASES

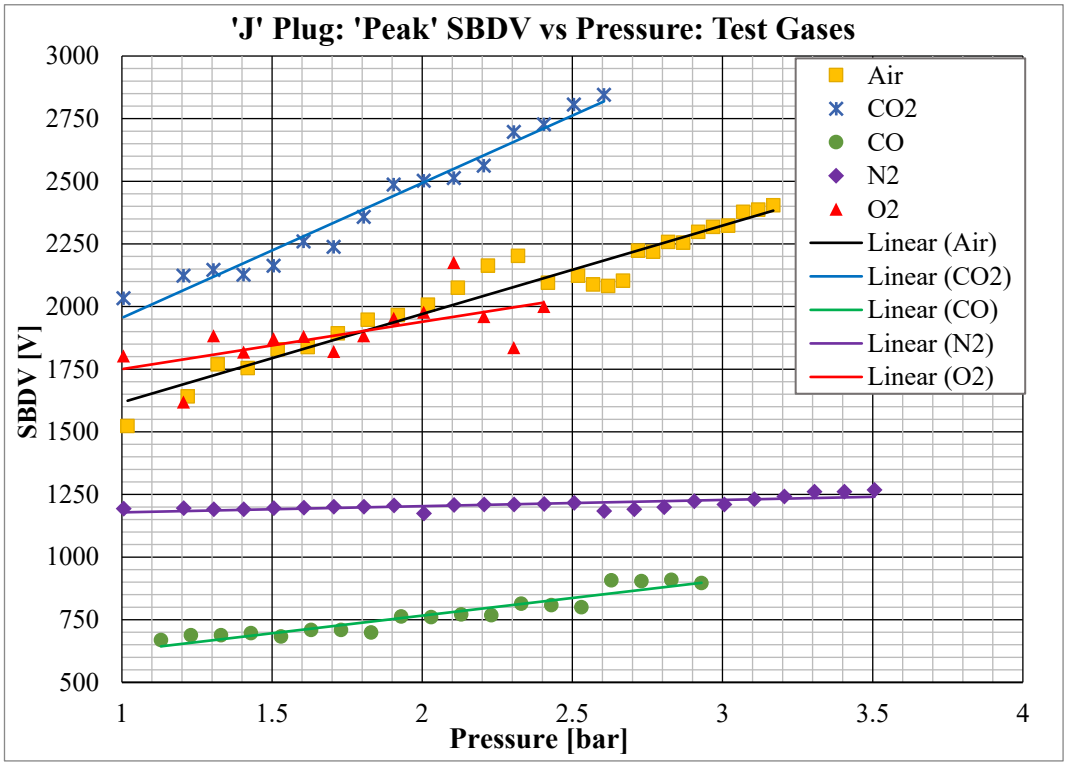

Figure F7-35: 'Peak' SBDV vs Pressure of Test gases using the 'J' Plug

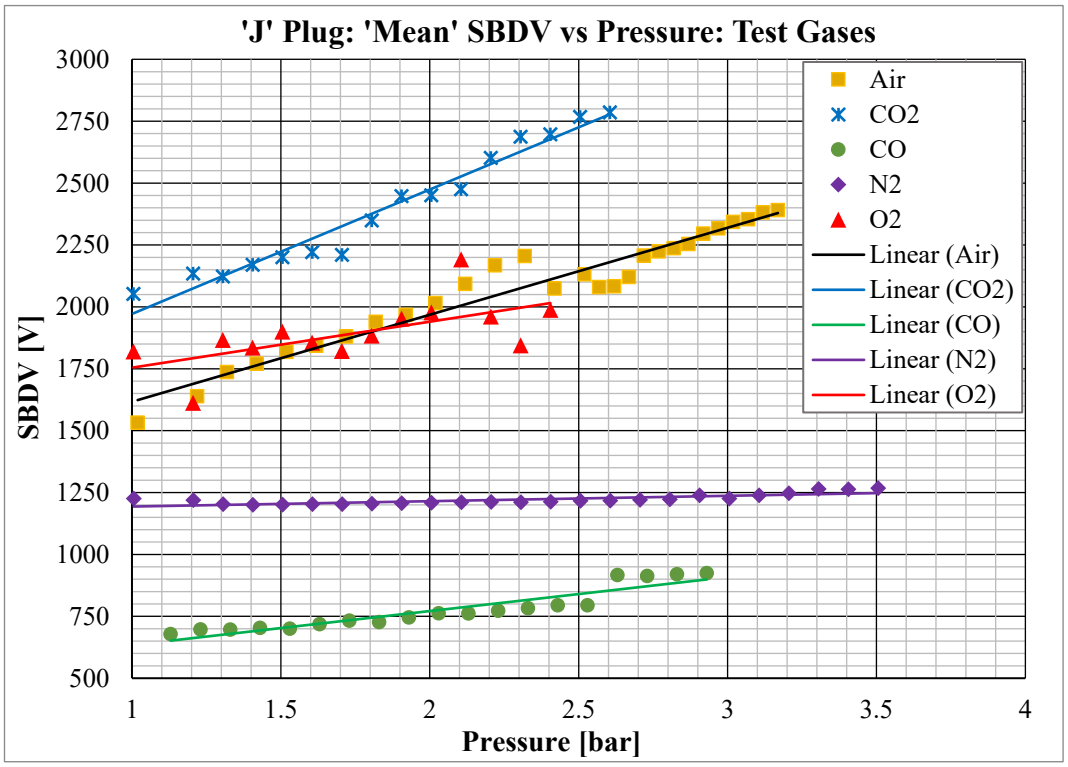

Figure F7-36: 'Mean' SBDV vs Pressure of Test gases using the 'J' Plug

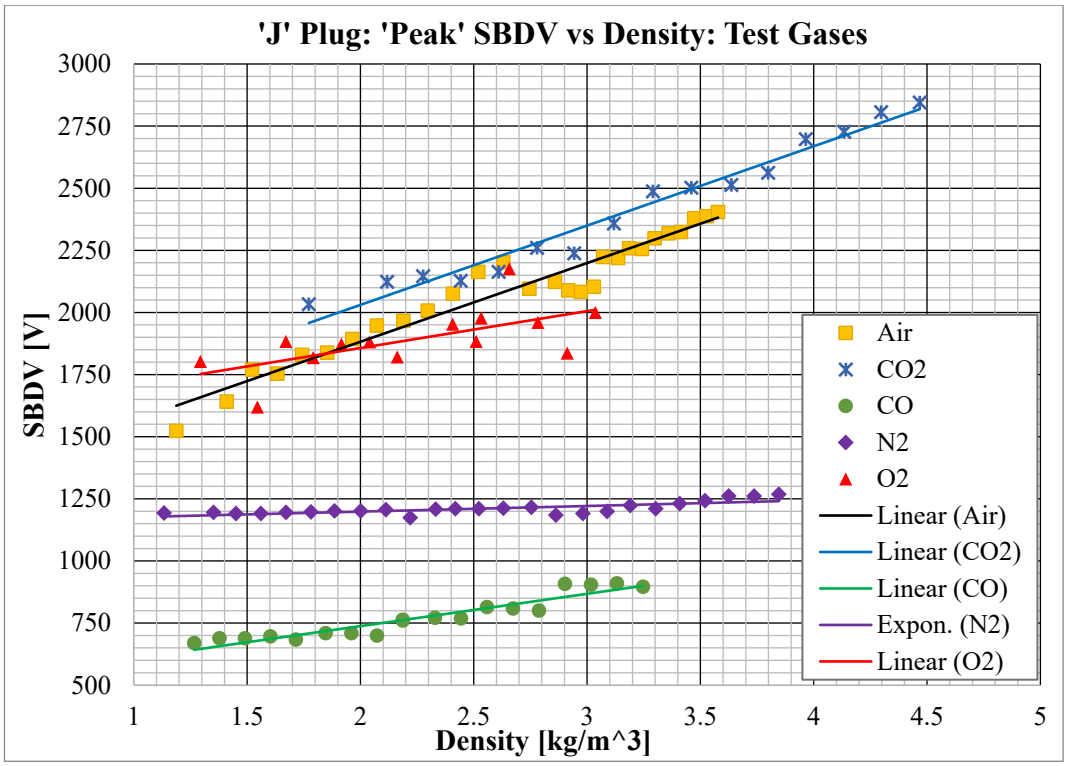

Figure F7-37: 'Peak' SBDV vs Density of Test gases using the 'J' Plug

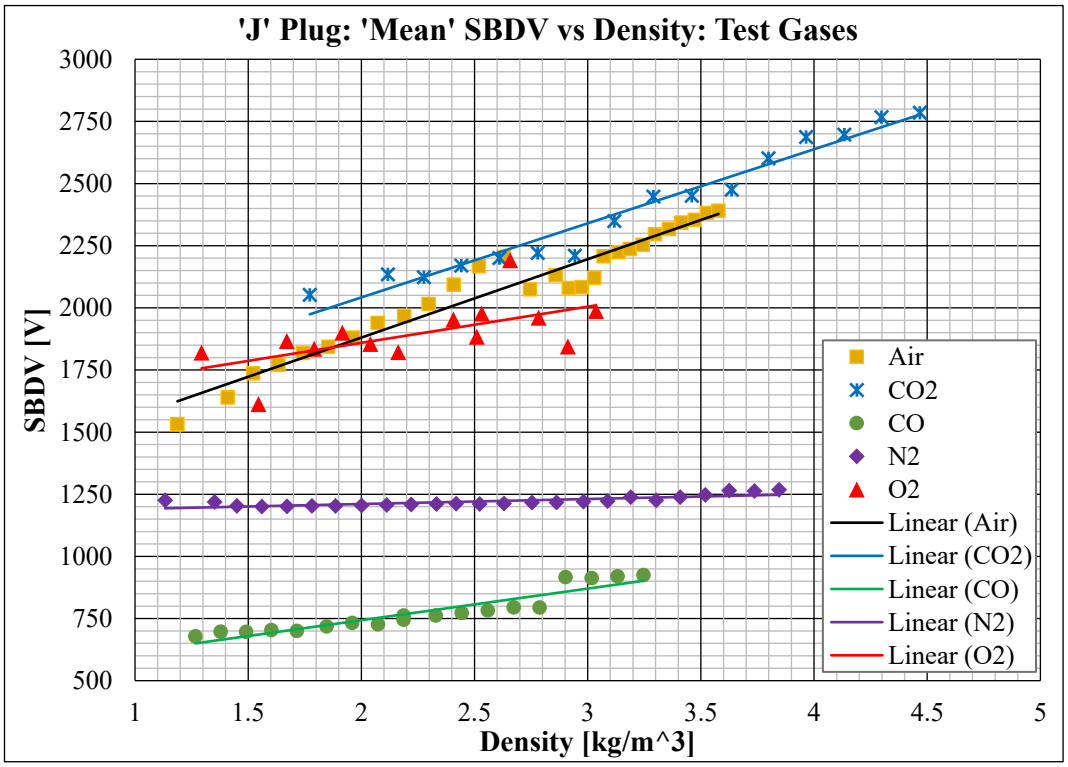

Figure F7-38: 'Mean' SBDV vs Density of Test gases using the 'J' Plug

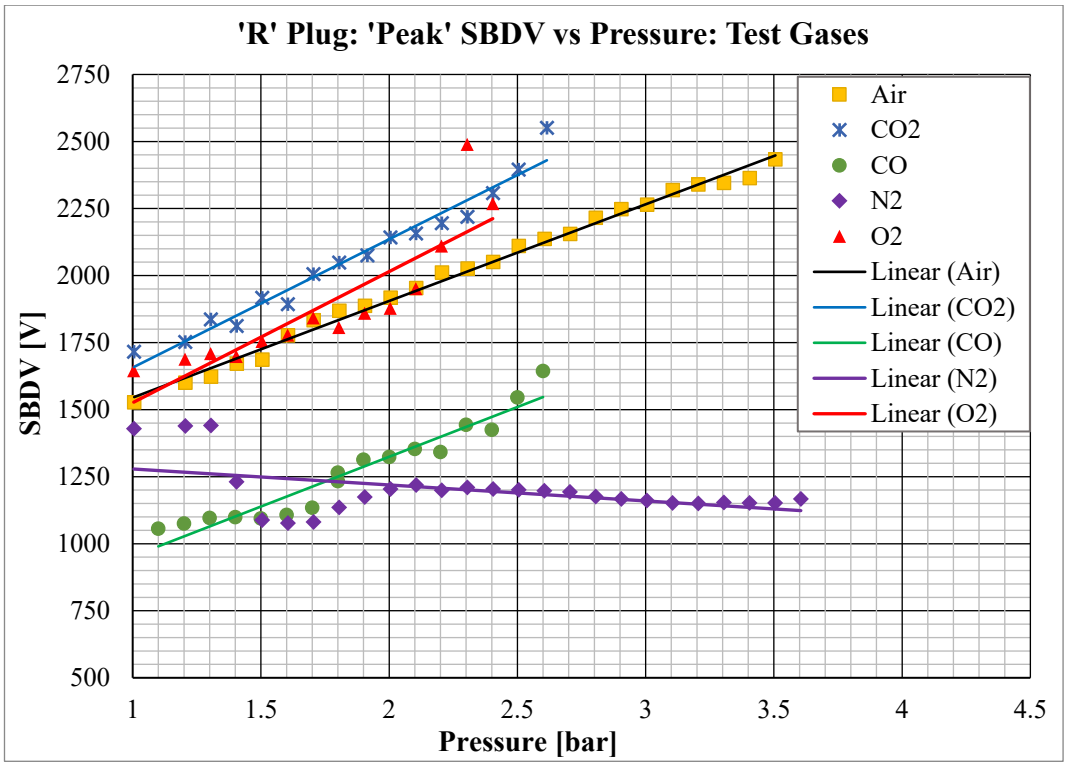

Figure F7-39: 'Peak' SBDV vs Pressure of Test gases using the 'R' Plug

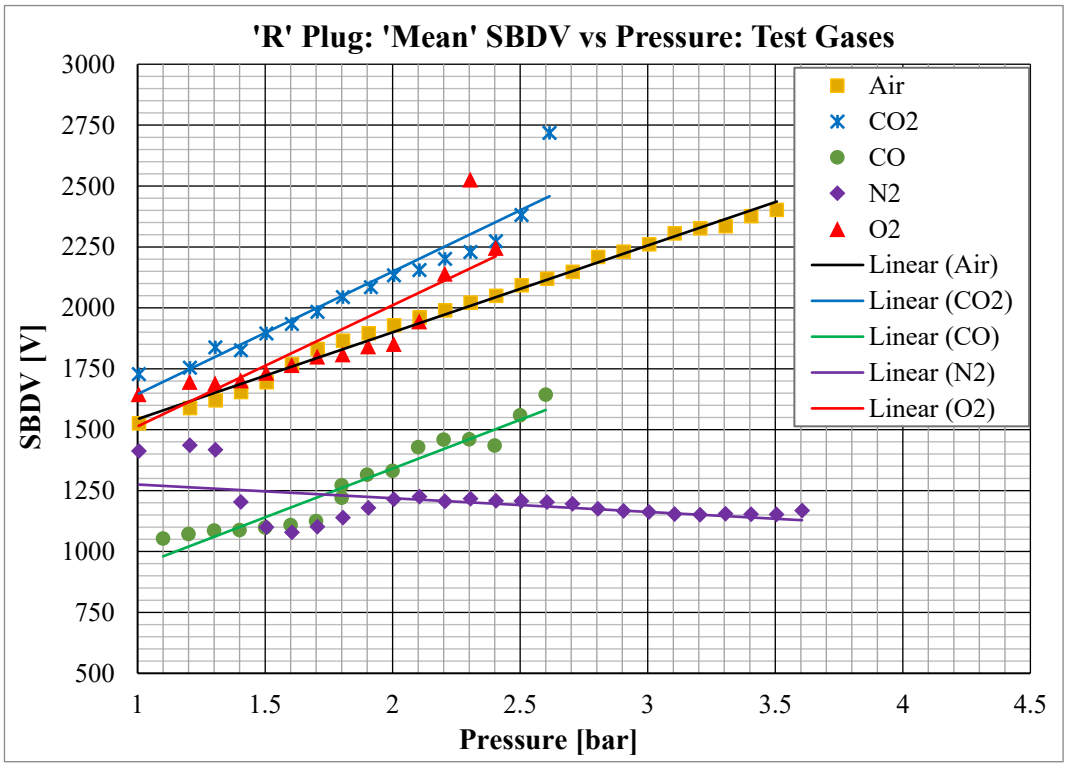

F7-40: 'Mean' SBDV vs Pressure of Test gases using the 'R' Plug

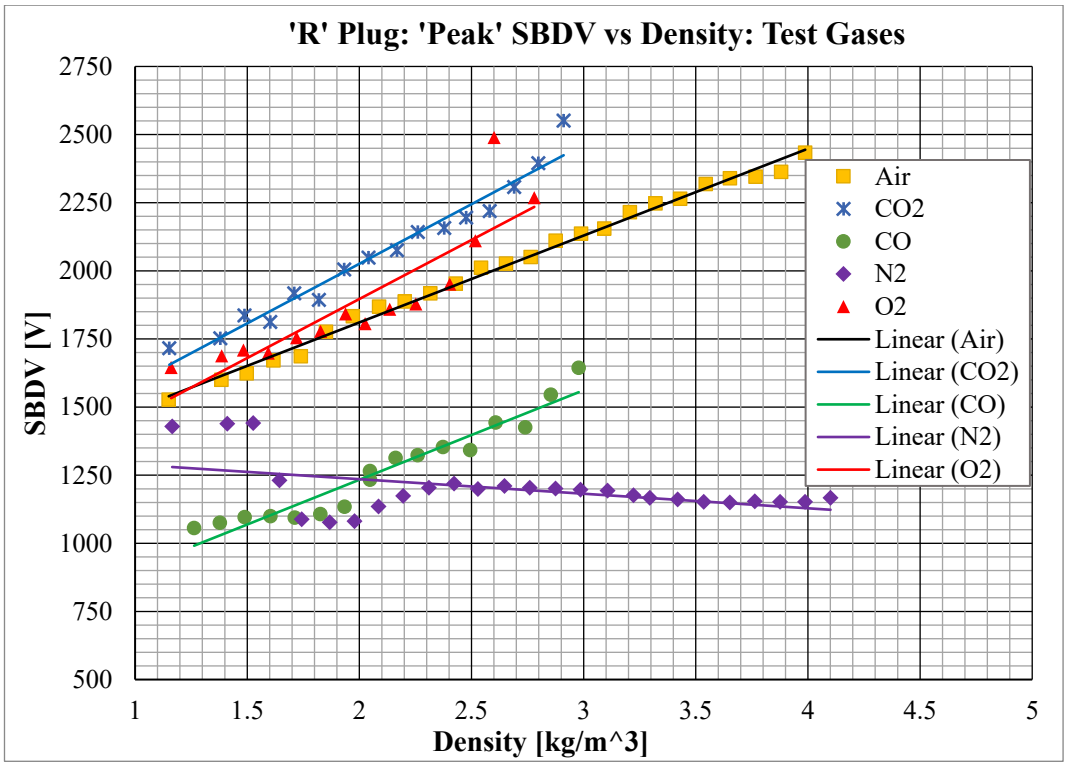

Figure F7-41: 'Peak' SBDV vs Density of Test gases using the 'R' Plug

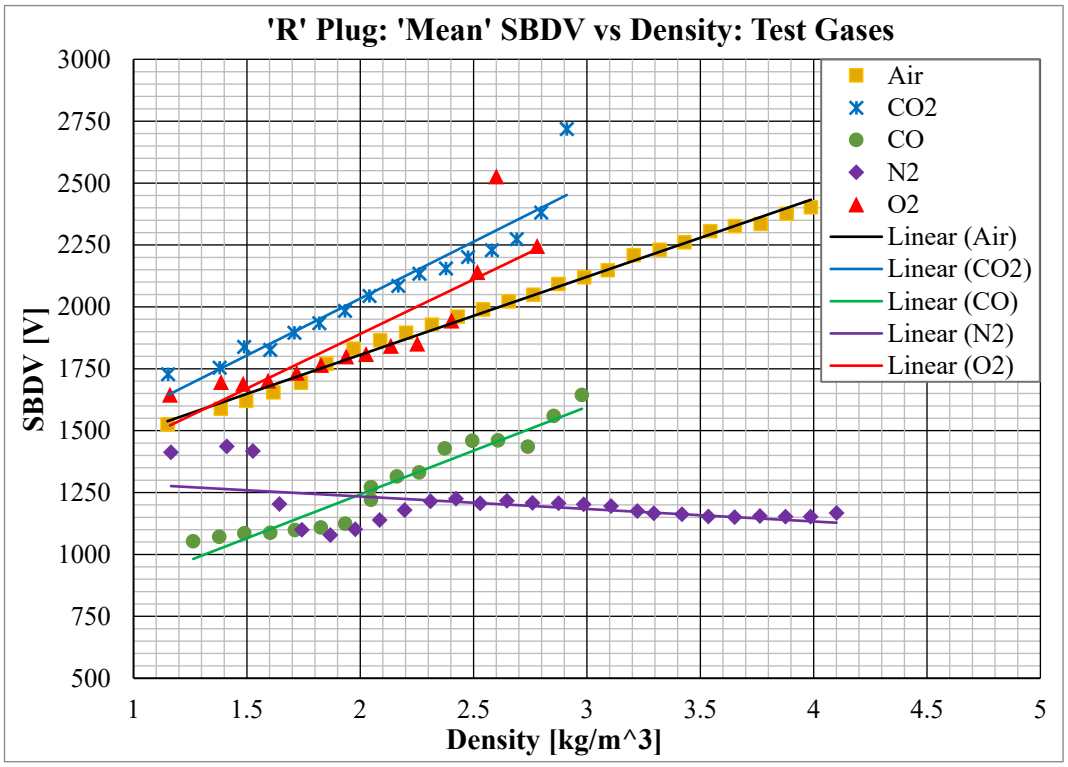

Figure F7-42: 'Mean' SBDV vs Density of Test gases using the 'R' Plug

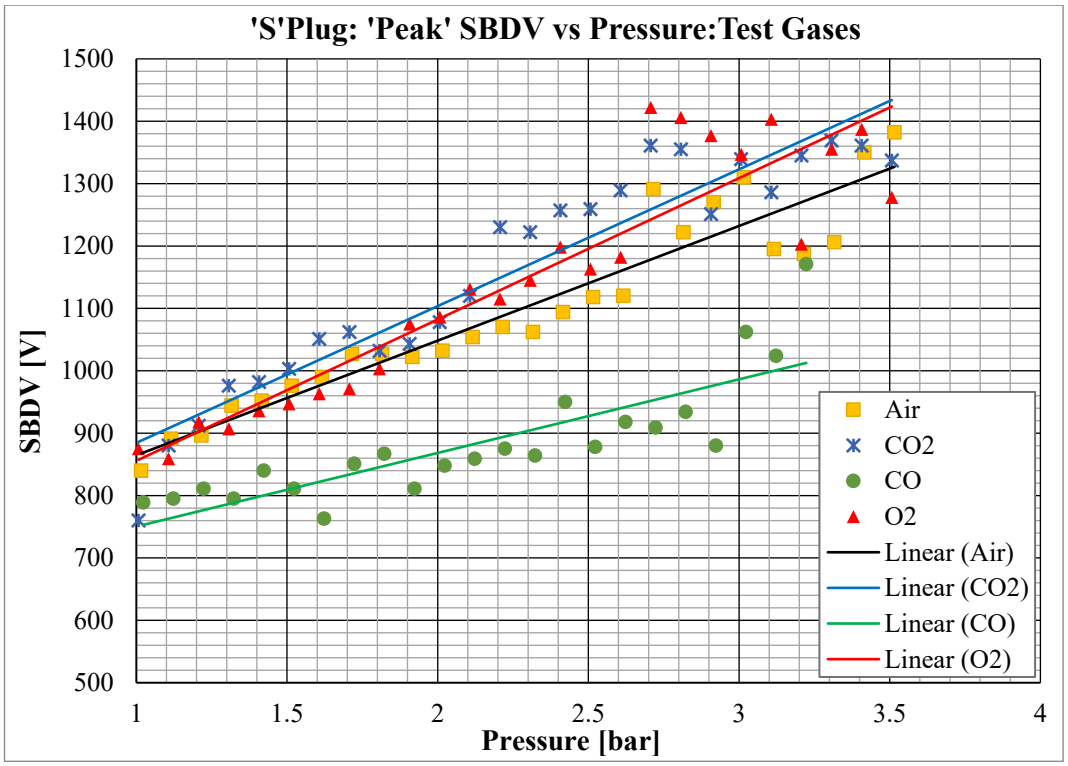

Figure F7-43: 'Peak' SBDV vs Pressure of Test gases using the Shrouded 'S' Plug

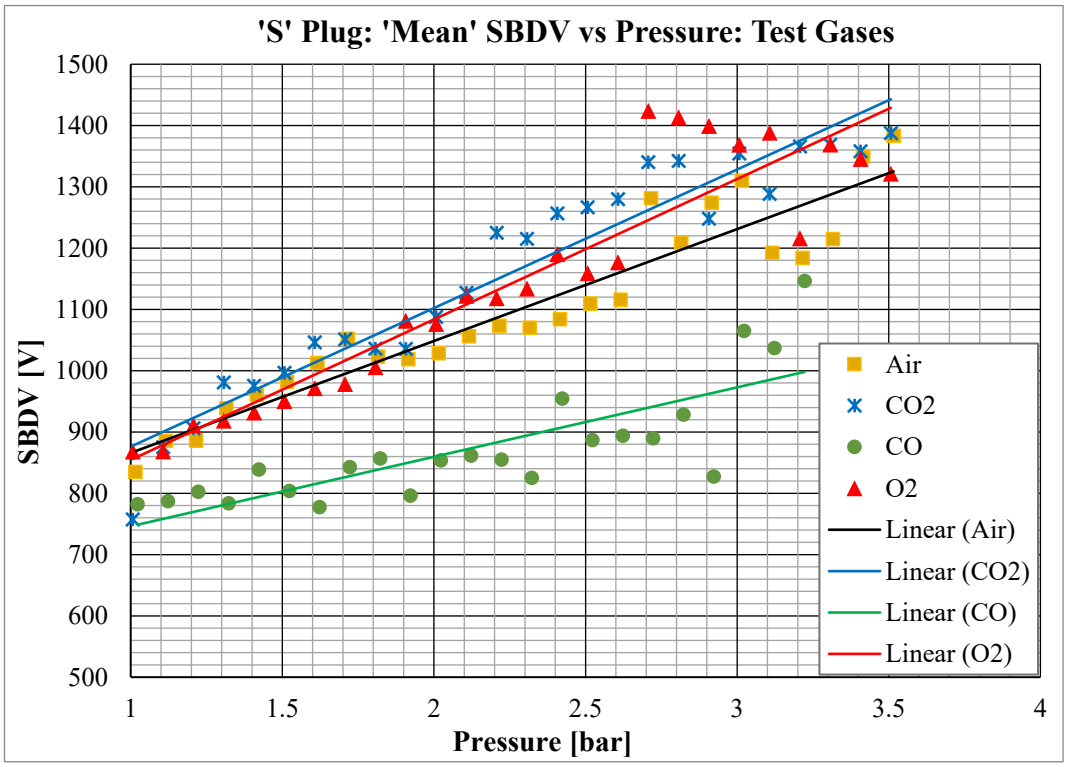

Figure F7-44: 'Mean' SBDV vs Pressure of Test gases using the Shrouded 'S' Plug

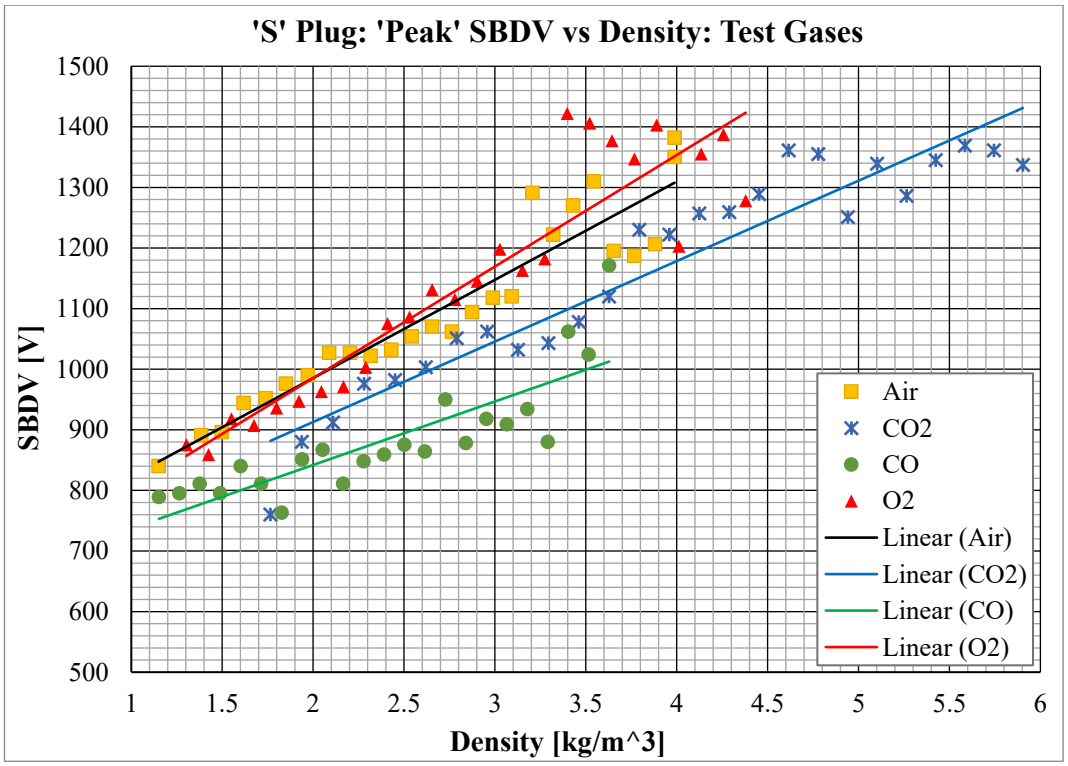

Figure F7-45: 'Peak' SBDV vs Density of Test gases using the Shrouded 'S' Plug

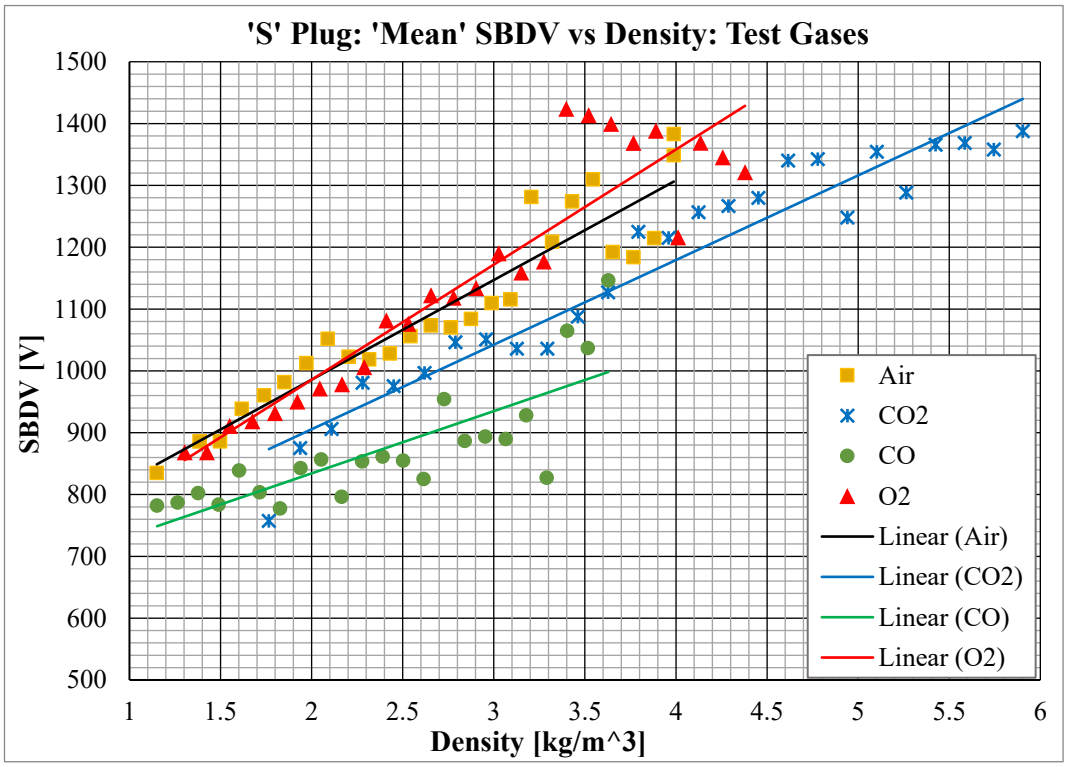

Figure F7-46: 'Mean' SBDV vs Density of Test gases using the Shrouded 'S' Plug

7.5 COMPARISON OF SPARK PLUG TYPES AS A GAS SENSOR

7.5.1 THE ‘J’ TYPE PLUG

The test results for the ‘J’ plug show a clear difference in spark breakdown voltage between the different gases except Air and Oxygen which SBDV vs Pressure results overlap. The relationship extends to a higher pressure in Air than Oxygen. Probably due to the influence of Nitrogen in Air. The spark break-down voltage difference between Carbon Monoxide and Carbon Dioxide however is significant, reaching approximately 1750V.

7.5.2 THE ‘R’ TYPE PLUG

The test results for the ‘R’ plug show a clear difference in spark breakdown voltage at all pressures between all the gases with no overlap between Oxygen and Air. The maximum pressure in which spark break-down can be generated is greater than the ‘J’ plug however, that may be due to the slightly smaller spark gap distance.

7.5.3 THE ‘S’ TYPE PLUG

The test results for the ‘S’ type plug show a clear difference in spark breakdown voltage at all pressures between all the gases tested. Although the voltage differences are smaller than the ‘J’ or ‘R’ plug the highest pressure in which spark break-down can be generated is significantly higher.

7.5.4 COMPARISON

All plug types could be used as gas sensors. The S type plug would produce spark break-down events at significantly higher pressures than the other two plugs. However, the ‘J’ and ‘R’ plugs are functional spark plugs for ignition whereas the ‘S’ plug ability for that function is not known.

Table T7-1: Mathematical Relationships: 'Peak' SBDVp for Pressure of Air, O_2, CO_2, CO and N_2 using 'J', 'R' and 'S' type spark plugs

Peak SBDVp		Linear		Polynomial		Exponential	
		Equation	mrs [%]	Equation	mrs [%]	Equation	mrs [%]
Air	J Plug	352.86x + 1264.6	94.31	$-45.266x^2 + 548.83x + 1071.4$	94.77	$1372.9e^{0.177x}$	93.30
	R Plug	360.44x + 1184.4	99.26	$-33.17x^2 + 512.38x + 1028$	99.63	$1311e^{0.1827x}$	98.14
	S Plug	183.81x + 680.72	90.30	$3.2601x^2 + 169.03x + 695.$	90.31	$742.83e^{0.1683x}$	91.66
CO_2	J Plug	538.25x + 1416.6	96.64	$149.31x^2 - 8.5739x + 1884$	98.10	$1587.9e^{0.223x}$	97.26
	R Plug	478.59x + 1178.3	96.32	$130.22x^2 + 1.2013x + 1586.7$	97.74	$1336.3e^{0.2316x}$	97.55
	S Plug	219.21x + 665.25	90.23	$-73.19x^2 + 549.59x + 333.59$	94.74	$734.18e^{0.1974x}$	87.75
CO	J Plug	140.89x + 484.56	90.14	$58.344x^2 - 95.983x + 707.49$	93.82	$531.38e^{0.1804x}$	91.64
	R Plug	371.22x + 581.8	92.50	$169.4x^2 - 256.07x + 1128.6$	95.97	$736.96e^{0.2887x}$	94.00
	S Plug	118x + 632.3	69.24	$78.667x^2 - 216.02x + 952.25$	80.01	$668.28e^{0.1287x}$	72.60
N_2	J Plug	24.845x + 1153.6	56.44	$21.302x^2 - 72.731x + 1254.1$	74.88	$1155.3e^{0.0203x}$	56.38
	R Plug	-59.601x + 1338.3	22.83	$69.999x^2 - 387.18x + 1681.5$	37.90	$1328.3e^{-0.045x}$	20.90
O_2	J Plug	189.02x + 1561.2	42.15	$-95.114x^2 + 517.75x + 1293.6$	43.80	$1583.1e^{0.1007x}$	42.56
	R Plug	488.95x + 1037	75.37	$485.11x^2 - 1186.7x + 2400.1$	86.90	$1215e^{0.2493x}$	79.96
	S Plug	226.54x + 629.17	86.02	$-42.802x^2 + 419.75x + 435.21$	87.40	$712.52e^{0.2026x}$	87.88

Table T7-2: Mathematical Relationships: 'Mean' SBDVp for Pressure of Air, O_2, CO_2, CO and N_2 using 'J', 'R' and 'S' type spark plugs

Mean SBDVp		Linear		Polynomial		Exponential	
		Equation	mrs [%]	Equation	mrs [%]	Equation	mrs [%]
Air	J Plug	$351.41x + 1265.4$	94.37	$-50.914x^2 + 571.84x + 1048.1$	94.97	$1372.6e^{0.1766x}$	93.42
	R Plug	$356.31x + 1187.1$	99.24	$-36.278x^2 + 522.49x + 1016$	99.70	$1310.8e^{0.1813x}$	98.00
	S Plug	$182.58x + 683.3$	89.78	$2.3539x^2 + 171.91x + 694.07$	89.78	$744.16e^{0.1674x}$	90.84
CO_2	J Plug	$502.62x + 1468.7$	96.01	$154.79x^2 - 64.276x + 1953.2$	97.79	$1621.1e^{0.209x}$	96.70
	R Plug	$502.98x + 1142.9$	90.57	$220.03x^2 - 303.66x + 1832.9$	94.02	$1321.8e^{0.2396x}$	94.07
	S Plug	$226.08x + 650.05$	92.34	$-63.794x^2 + 514.05x + 360.96$	95.63	$724.62e^{0.2031x}$	89.59
CO	J Plug	$158.3x + 446.3$	86.92	$99.275x^2 - 274.53x + 897$	92.66	$513.46e^{0.1963x}$	88.91
	R Plug	$400.38x + 539.68$	93.92	$140.09x^2 - 118.37x + 991.86$	95.35	$713.75e^{0.3103x}$	94.10
	S Plug	$113.36x + 632.8$	63.40	$77.559x^2 - 215.95x + 948.25$	73.79	$667.47e^{0.1242x}$	65.94
N_2	J Plug	$2.1367x + 1205.7$	2.09	$26.438x^2 - 94.737x + 1288.5$	64.83	$1205.6e^{0.0018x}$	2.16
	R Plug	$56.267x + 1331.2$	23.14	$60.108x^2 - 337.56x + 1625.9$	35.77	$1322.8e^{-0.043x}$	21.43
O_2	J Plug	$158.3x + 446.3$	86.92	$99.275x^2 - 274.53x + 897$	92.66	$513.46e^{0.1963x}$	88.91
	R Plug	$400.38x + 539.68$	93.29	$77.559x^2 - 215.95x + 948.25$	73.79	$713.75e^{0.3103x}$	91.40
	S Plug	$113.36x + 632.8$	63.40	$140.09x^2 - 118.37x + 991.86$	95.35	$667.47e^{0.1242x}$	65.94

Table T7-3: Mathematical Relationships: 'Peak' SBDVd for Density of Air, O_2, CO_2, CO and N_2 using 'J', 'R' and 'S' type spark plugs

Peak SBDVd		Linear		Polynomial		Exponential	
		Equation	mrs [%]	Equation	mrs [%]	Equation	mrs [%]
Air	J Plug	316.69x + 1248.8	94.18	$-37.326x^2 + 500.54x + 1041.7$	94.67	$1362e^{0.1589x}$	93.17
	R Plug	318.82x + 1173	99.38	$-21.203x^2 + 429.62x + 1042.6$	99.63	$1303.1e^{0.1617x}$	98.40
	S Plug	162.18x + 660.94	89.92	$6.3792x^2 + 128.31x + 701.3$	90.00	$728.77e^{0.1489x}$	91.73
CO_2	J Plug	319.21x + 1392	96.72	$52.273x^2 - 11.706x + 1882.6$	98.16	$1571.8e^{0.1322x}$	97.35
	R Plug	437.27x + 1151.3	96.04	$117.55x^2 - 47.149x + 1618.9$	97.68	$1318.6e^{0.2117x}$	97.38
	S Plug	132.75x + 647.4	90.66	$-25.3x^2 + 327.22x + 312.68$	94.70	$722.26e^{0.1196x}$	88.28
CO	J Plug	129.99x + 477.76	90.02	$46.603x^2 - 80.335x + 698.67$	93.52	$526.89e^{0.1664x}$	91.40
	R Plug	318.82x + 1173	99.38	$-21.203x^2 + 429.62x + 1042.6$	99.63	$1303.1e^{0.1617x}$	98.40
	S Plug	162.18x + 660.94	89.92	$6.3792x^2 + 128.31x + 701.3$	90.00	$728.77e^{0.1489x}$	91.73
N_2	J Plug	22.878x + 1152.8	56.41	$17.971x^2 - 67.901x + 1256.2$	74.63	$1154.5e^{0.0187x}$	56.34
	R Plug	-53.415x + 1342.2	23.03	$55.705x^2 - 351.89x + 1702$	38.29	$1332.2e^{-0.04x}$	21.09
O_2	J Plug	148.27x + 1560.5	40.75	$-61.7x^2 + 418.49x + 1281.5$	42.36	$1582.1e^{0.0791x}$	41.28
	R Plug	433.36x + 1029.9	76.14	$323.48x^2 - 849.81x + 2230.7$	85.07	$1210.8e^{0.2209x}$	80.73
	S Plug	184.1x + 617.12	86.04	$-28.129x^2 + 344.02x + 413.81$	87.40	$704.9e^{0.1647x}$	87.90

Table T7-4: Mathematical Relationships: 'Mean' SBDVd for Density of Air, O_2, CO_2, CO and N_2 using 'J', 'R' and 'S' type spark plugs

Mean SBDVd		Linear		Polynomial		Exponential	
		Equation	mrs [%]	Equation	mrs [%]	Equation	mrs [%]
Air	J Plug	315.41x + 1249.6	94.25	$-41.827x^2 + 521.42x + 1017.6$	94.87	$1361.8e^{0.1585x}$	93.30
	R Plug	315.21x + 1175.7	99.39	$-23.714x^2 + 439.13x + 1029.9$	99.71	$1302.9e^{0.1605x}$	98.29
	S Plug	161.15x + 663.5	89.47	$5.2184x^2 + 133.44x + 696.52$	89.52	$730e^{0.1482x}$	91.00
CO_2	J Plug	298.1x + 1445.7	96.10	$54.323x^2 - 45.793x + 1955.5$	97.86	$1605.6e^{0.124x}$	96.80
	R Plug	459.11x + 1115.3	90.14	$191.49x^2 - 330.05x + 1877.1$	93.84	$1304.1e^{0.2189x}$	93.76
	S Plug	161.15x + 663.5	89.47	$5.2184x^2 + 133.44x + 696.52$	89.52	$730e^{0.1482x}$	91.00
CO	J Plug	127.14x + 489.05	87.07	$65.163x^2 - 166.96x + 797.94$	94.01	$537.7e^{0.1602x}$	89.42
	R Plug	353.67x + 535.07	93.36	$94.862x^2 - 48.429x + 936.8$	94.97	$711.56e^{0.2739x}$	94.01
	S Plug	100.69x + 632.8	63.40	$61.192x^2 - 191.82x + 948.25$	73.79	$667.47e^{0.1103x}$	65.94
N_2	J Plug	20.044x + 1170.8	62.89	$19.435x^2 - 78.133x + 1282.7$	93.86	$1172.1e^{0.0163x}$	63.05
	R Plug	-50.425x + 1334.9	23.33	$47.93x^2 - 307.24x + 1644.4$	36.19	$1326.5e^{-0.038x}$	21.62
O_2	J Plug	145.49x + 1568.4	38.19	$-58.613x^2 + 402.2x + 1303.3$	39.60	$1588.7e^{0.0776x}$	38.80
	R Plug	440.43x + 1009.7	72.68	$355.53x^2 - 969.87x + 2329.5$	82.65	$1198.7e^{0.224x}$	77.54
	S Plug	186.23x + 613.17	86.95	$-25.02x^2 + 328.47x + 432.32$	88.01	$703.24e^{0.1661x}$	88.89

7.6 COMPARISON OF TESTING RESULTS WITH PUBLISHED INFORMATION

The published results quoted in this thesis are based on the Law relationship provided by Paschen (Paschen, 1889) described in chapter three, which states that spark break-down voltage (V_s), is a function of the product of pressure x spark gap. For any gas, this relationship was found to be to depend upon the electrode configuration, material and surface condition. Hence, the relationship between the product of pressure and spark gap, in any gas is a function of the electrodes. As noted in chapter three and six, spark plug electrodes are different from those used by previous researchers. However, it is necessary to demonstrate how the results of the testing carried out for this work relate to publish results and if these demonstrate consistent differences.

The published expressions provided by three researchers relating spark break-down voltage and the pressure of Air, is provided below. These are repeated from chapter three for the reader's convenience. The expressions include values for 'A' and 'B' constants which relate to empirically derived characteristics of the electrodes used.

$$V(Air)_s = Apd + B\sqrt{pd} \qquad \text{(Eq. 7-1)}$$

The constants derived by the researchers can be noted as being slightly different. It will be seen from comparison with SBDV results, the differences in theses constants used may have been the alterative use of Peak or Mean spark break-down voltage values.

(Ritz. H., 1932) $V_s(Air) = 24.55pd + 6.66\sqrt{pd}$ (kV) (Eq. 7-2)

(Holzer. W., 1932) $V_s(Air) = 23.85pd + 7.85\sqrt{pd}$ (kV) (Eq. 7-3)

(Bruce. F.M., 1947) $V_s(Air) = 24.22pd + 6.08\sqrt{pd}$ (kV) (Eq. 7-4)

7.6.1 CONVERSION OF TEST RESULTS

The tests results obtained in Air at different pressures, using different types of spark plugs were previously presented using pressure (bar) and spark gaps (mm). These were converted for comparison with published information which is presented using the Torr (mmHg) pressure unit (1bar = 750.062 torr) and spark gap in centimetre (cm) length unit (1mm = 0.1cm).

The values of pressure obtained from testing were then converted as noted above and multiplied by the spark gap length for each spark plug type 'J' = 0.06cm, 'R' = 0.055cm and 'S' = 0.03cm. These values were combined to provide Pressure (P) x Gap Length (d) and plotted separately against corresponding values for 'Peak' and 'Mean' spark Break-down voltage. The converted Peak and Mean spark break-down voltage vs pressure, described above are presented below for each Spark plug type in Figures F7-47 to 50. Curve fitting was applied to each plot individually to obtain a polynomial expression. Regression analysis (R^2) values are included for each curve which all show a high level of data confidence. This form of expression matches that of the published information and thus allows a direct comparison between the factors 'A' and 'B' which result from the testing carried out for the present work. The 'A' and 'B' values obtained from Figures F7-47 to 52 are then summarised in Tables T7-5 and 6 which include the 'A' and 'B' values taken from published work previously covered in chapter three for comparison.

The comparative Peak and Mean, SBDV vs P*d, performance of the three spark plug types are presented in Figure F7-53 and 54. These are then also presented in Figure F7-55 and 56 to visually compare with 'A' and 'B' values in tables T7-5 and 6 obtained from published works. It should be noted the 'C' value obtained from the test results relates to the offset from zero pressure/volts and therefore does not relate to the shape of the SBDV vs Pd curve. This term is not included in published information and therefore the comparison between curves are based at zero.

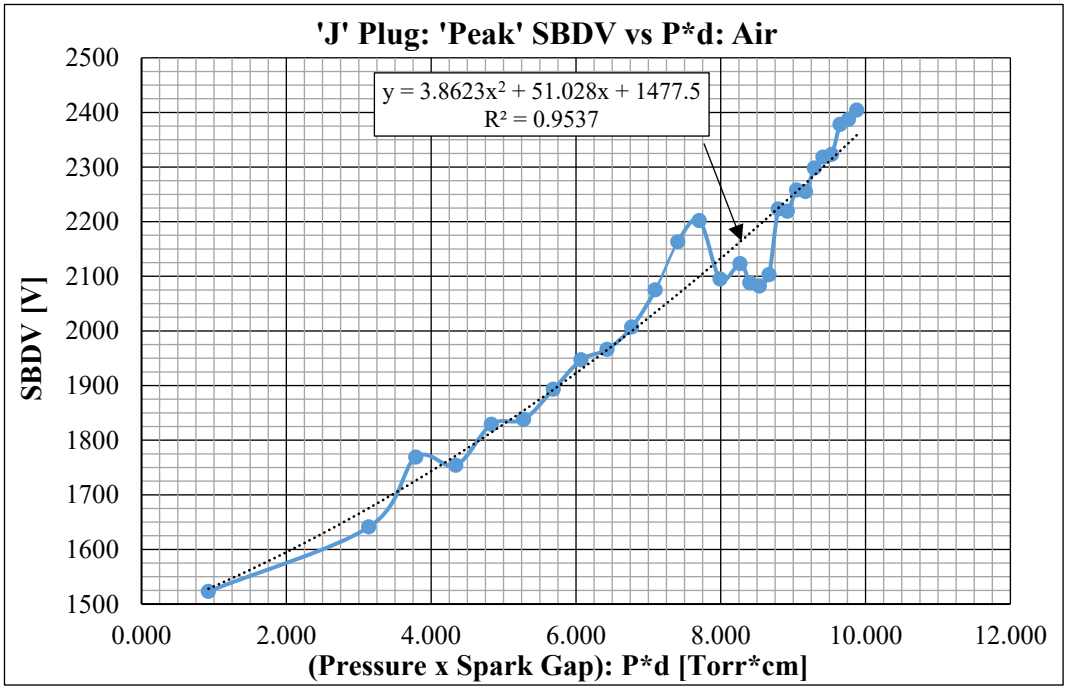

Figure F7-47: 'J' Plug: 'Peak' SBDV vs P*d: Air

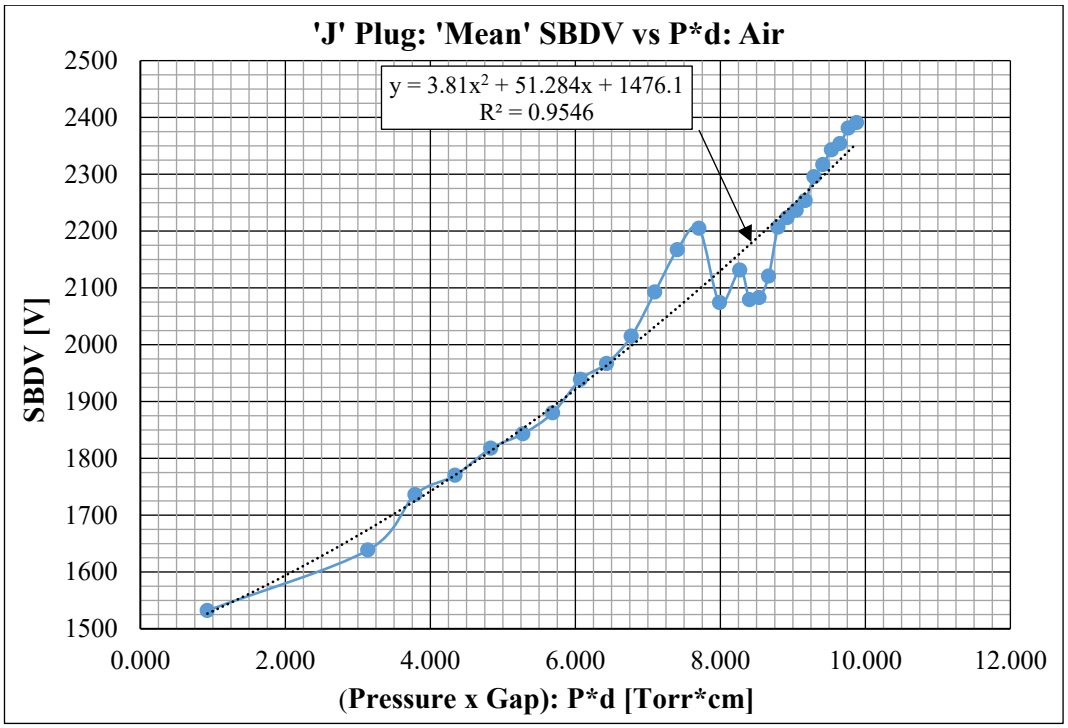

Figure F7-48: 'J' Plug: 'Mean' SBDV vs P*d: Air

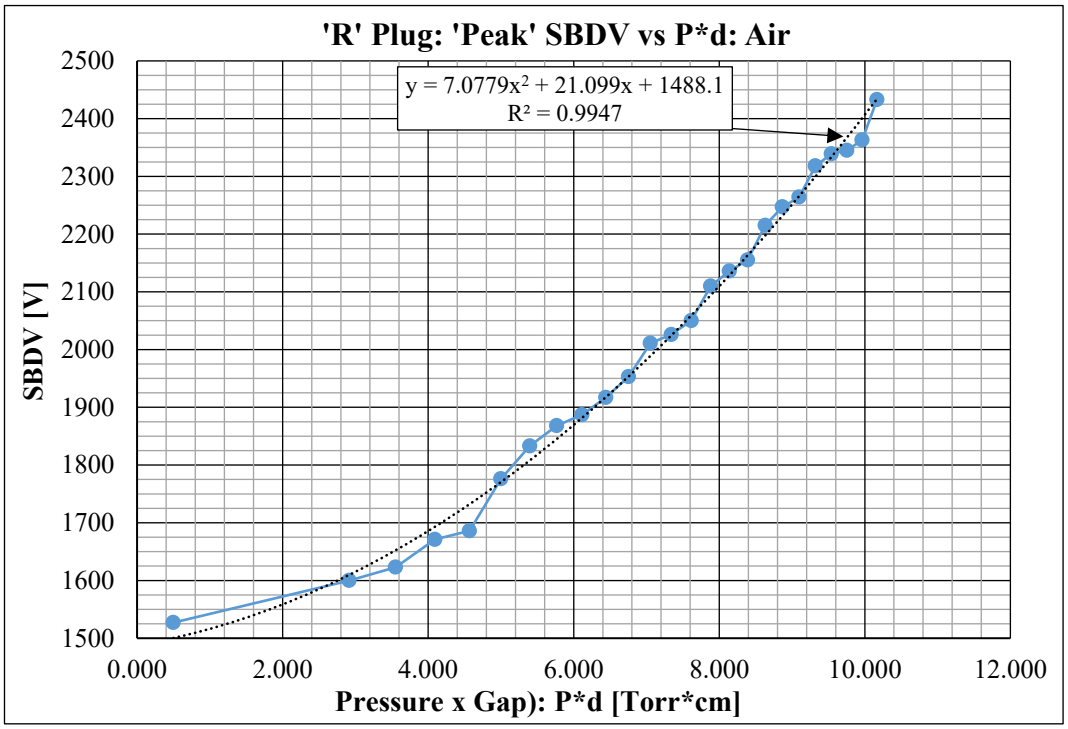

Figure F7-49: 'R' Plug: 'Peak' SBDV vs P*d: Air

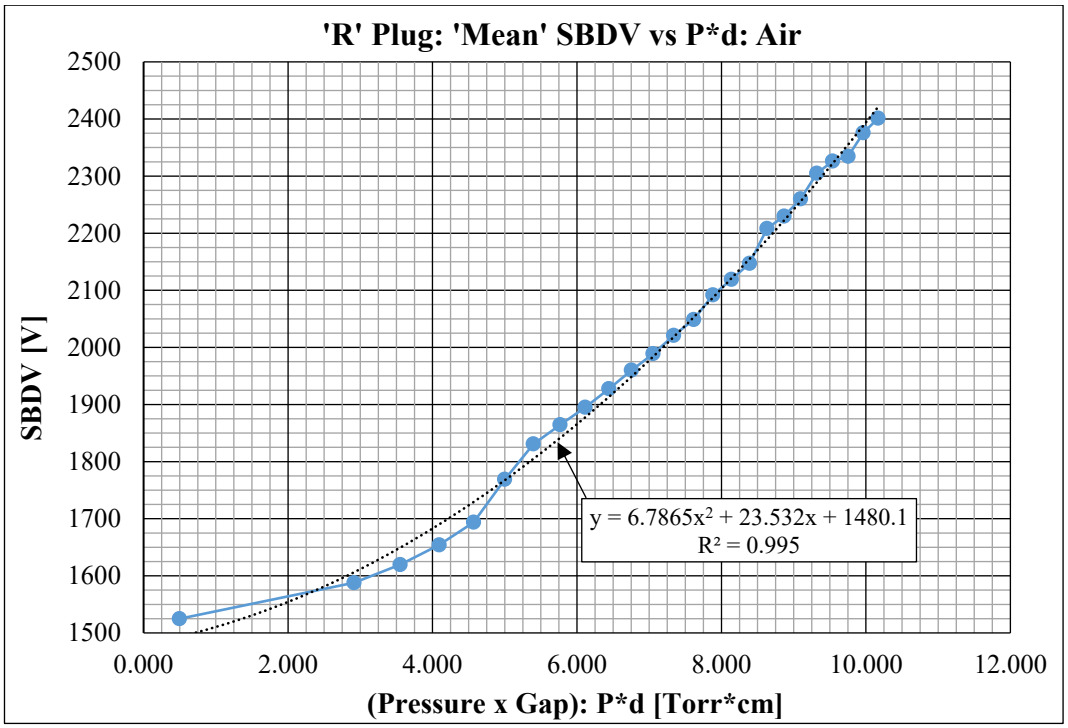

Figure F7-50: 'R' Plug: 'Mean' SBDV vs P*d: Air

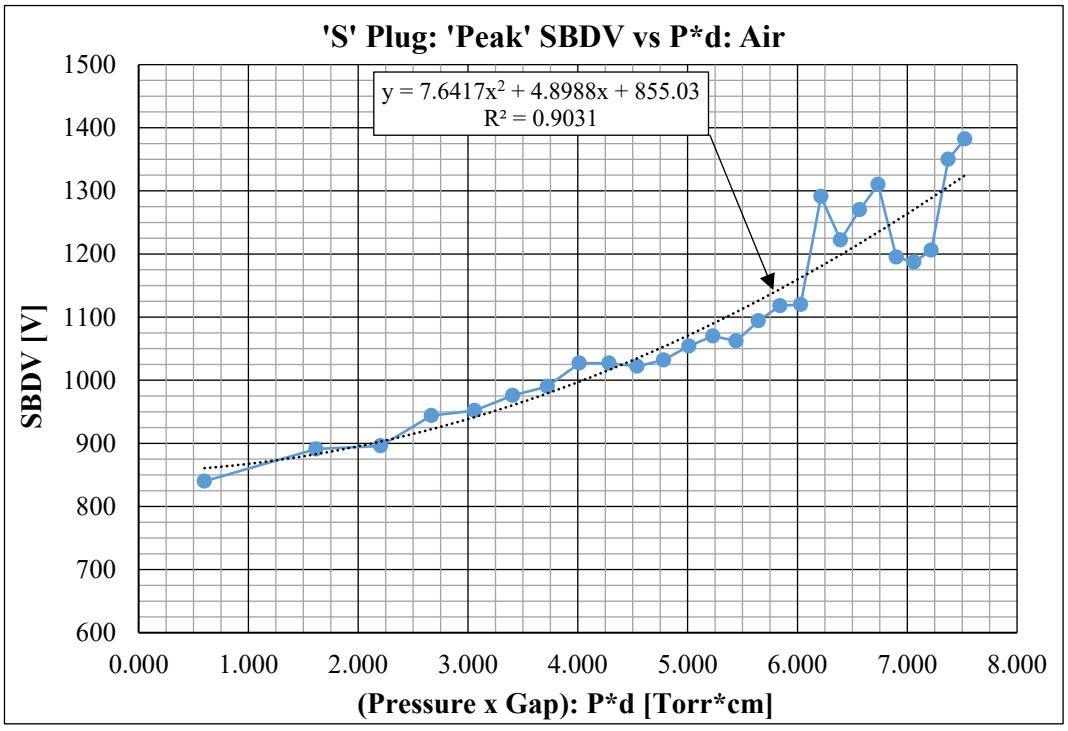

Figure F7-51: 'S' Plug: 'Peak' SBDV vs P*d: Air

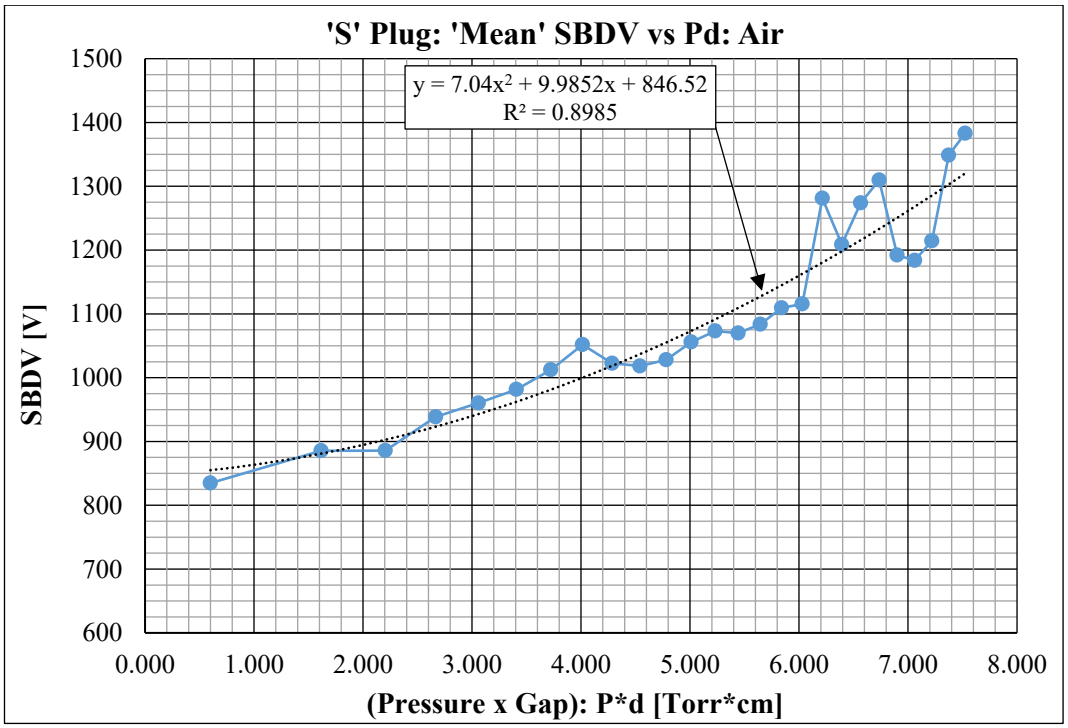

Figure F7-52: 'S' Plug: 'Mean' SBDV vs P*d: Air

Table T7-5: Table of 'A' and 'B' factors: 'Peak' SBDV from testing and published work

Peak	A	B	C (measured)	C (used)
J Plug	3.8623	51.028	1477.5	0
R Plug	7.0779	21.099	1488.1	0
SP Plug	7.6417	4.8988	855.03	0
Ritz	24.55	6.66	-	-
Holzer	23.85	7.85	-	-
Bruce	24.22	6.08	-	-
Schroder	24.36	6.72	-	-

Table T7-6: Table of 'A' and 'B' factors: 'Mean' SBDV from testing and published work

Mean	A	B	C (measured)	C (used)
J Plug	3.81	51.284	1476.1	0
R Plug	6.7865	23.532	1480.1	0
SP Plug	7.04	9.9852	846.52	0
Ritz	24.55	6.66	-	-
Holzer	23.85	7.85	-	-
Bruce	24.22	6.08	-	-
Schroder	24.36	6.72	-	-

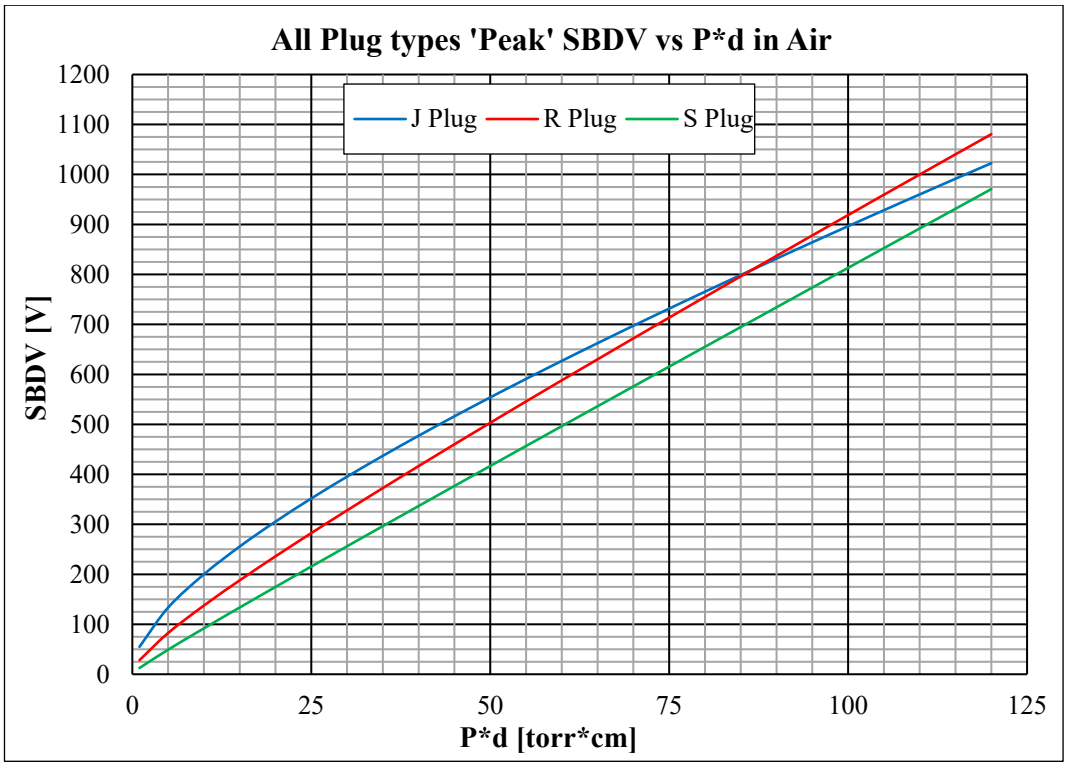

Figure F7-53: Comparison of 'Peak' SBDV vs P*d: Spark Plug Types in Air

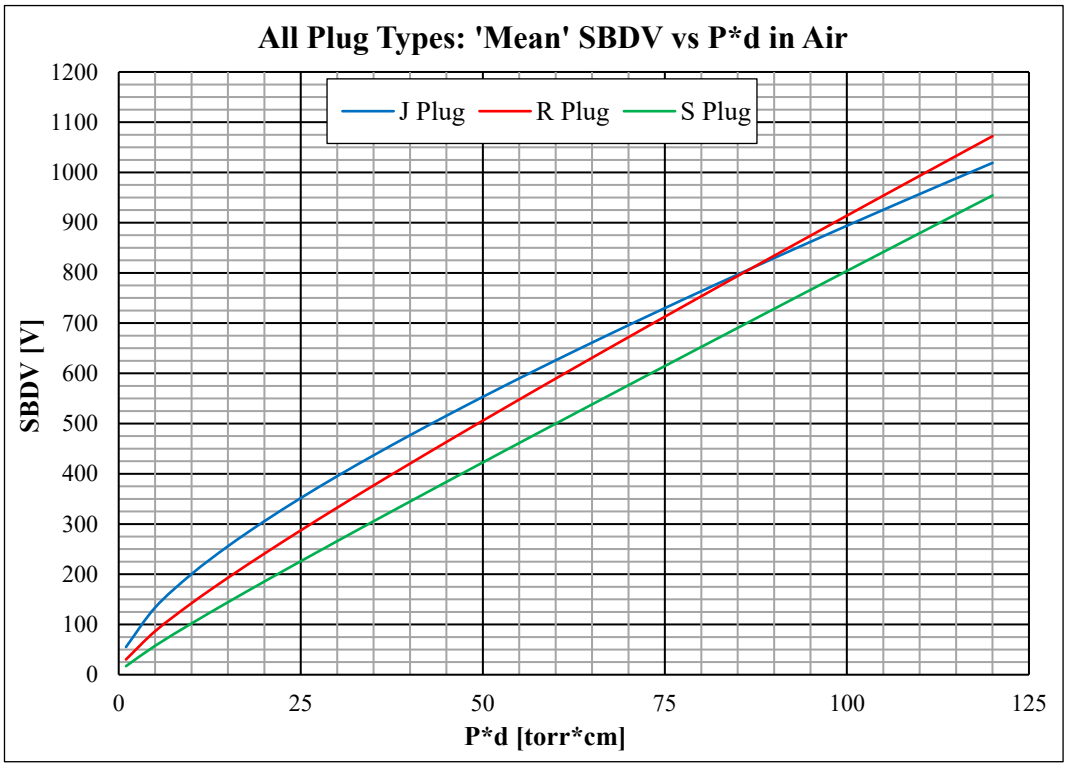

Figure F7-54: Comparison of 'Mean' SBDV vs P*d: Spark Plug Types in Air

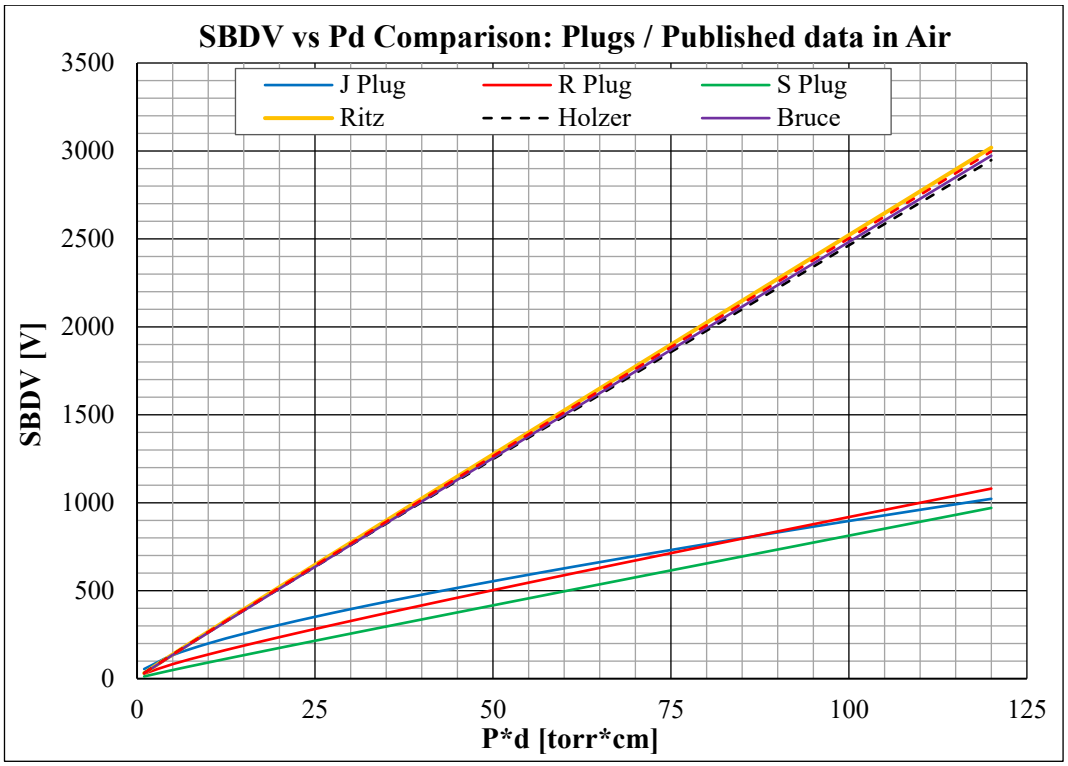

Figure F7-55: Comparison of 'Peak' SBDV vs P*d: Test Results and Published work

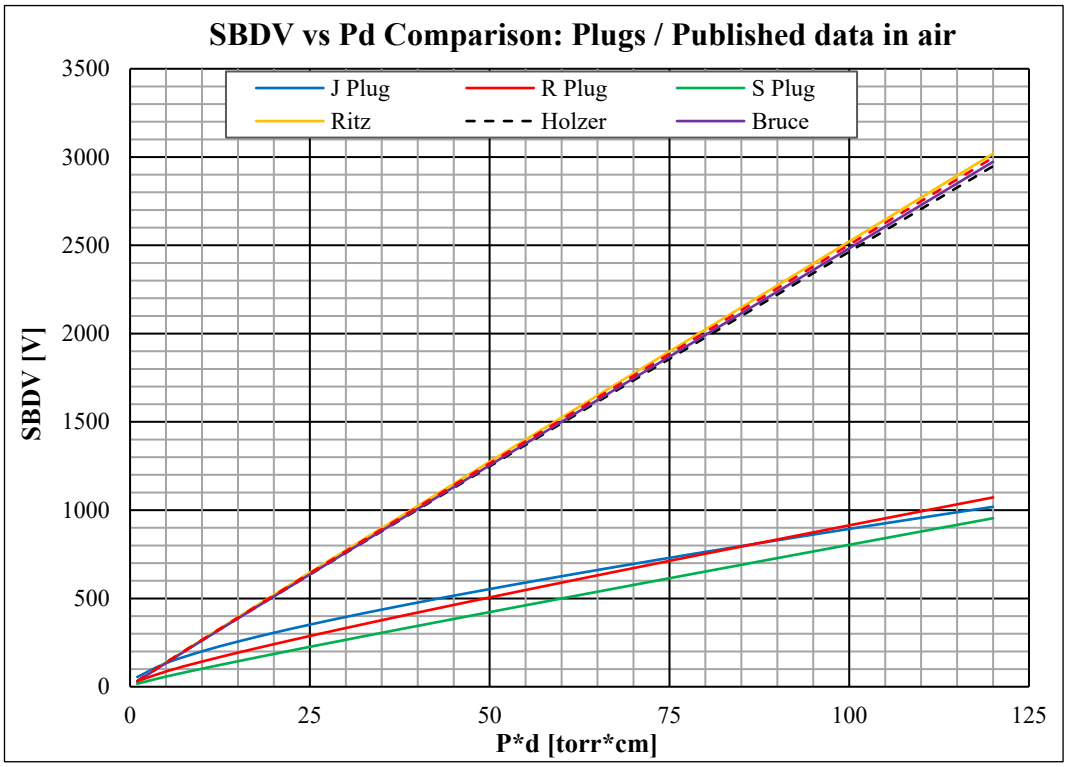

Figure F7-56: Comparison of 'Mean' SBDV vs P*d: Test Results and Published work

7.6.2 SUMMARY OF RESULTS

This shows five key points:

1) The voltage required by the spark plugs for any spark gap length (using a spark length between 0.3mm to 0.6mm), is significantly lower than from published work. This may be due to a combination of non-uniform electrode shape and electrode material.
2) The effect of using ‘Peak’ or ‘Mean’ spark break-down voltage is not significant.
3) The relationship between spark break-down voltage and Pressure x spark gap length is effectively linear when measured using any of the spark plugs tested with the SBDV system.
4) The difference between the published values of empirically derived ‘A’ and ‘B’ constants, possibly results from the alternative use of the peak or mean spark break-down voltages.
5) Over the pressures and spark gap lengths tested, the variation between P*d for the spark plugs used is greater than the variation which results from using the relationships given by published work. However, the variation of P*d is consistent over most of the range tested and at its largest value (P*d = 120) the difference is only around four times that resulting from the variation resulting from the use of the relationships provided in published work. This variation is considered very small considering the relative testing procedures.

7.6.3 COMPARISON BETWEEN TEST RESULTS AND SILSBEE FORMULA

Silsbee (Silsbee, 1925), proposed a simple expression which relates spark break-down voltage required by a Spark Plug to the relative density of the in-cylinder dielectric gas. He stated, the expression fitted the observed data "fairly well" and was "convenient to use", noting that the density of gas increases the spark voltage approximately linearly according to the equation (Eq. 7.8).

The formula presented by Silsbee specifically concerns the spark break-down voltage characteristics of Spark Plugs and represent the use of 'non-uniform' mass-produced electrodes. Consequently, the Silsbee formula is significantly more representative to the present work than other expressions given in published work which Silsbee considered "rather elaborate formula for sphere gaps".

$$E_\delta = E_1 (1 + K^*(\delta - 1)) \qquad \text{(Eq. 7.8)}$$

Where:

δ = density of air relative to standard temperature and pressure

E_1 = sparking voltage at relative density =1

E_s = sparking voltage at relative density = δ

K = a constant representing the spark plug electrodes.

Silsbee recommended a value for K be taken from 0.5 to 0.7 which depends on the shape of the spark plug electrodes where the larger value was appropriate for 'blunter' electrodes. The Silsbee formula represents a straightforward method to obtain in-cylinder gas density from proportional values of spark breakdown voltage. This was investigated by comparing the results of relative density using the Silsbee formula with SBDV values obtained from the testing carried out for the present work. The results of this investigation are presented in Figure 7-57 to 62 which use 'Peak' and 'Mean' SBDV values obtained for 'J', 'R' and 'S' type plugs in Air. In each graph, a base line value for *'K'* of 0.6 was used which is midway between 0.5 and 0.7. The measured SBDV values for Air Density are plotted together with the linear relationship obtained for each spark plug type. An alternative 'Silsbee' plot is then overlaid which was produced using a manual interpolation to obtain a 'best fit' to the measured SBDV data. This provided the modified 'K' factor listed in the key for each graph.

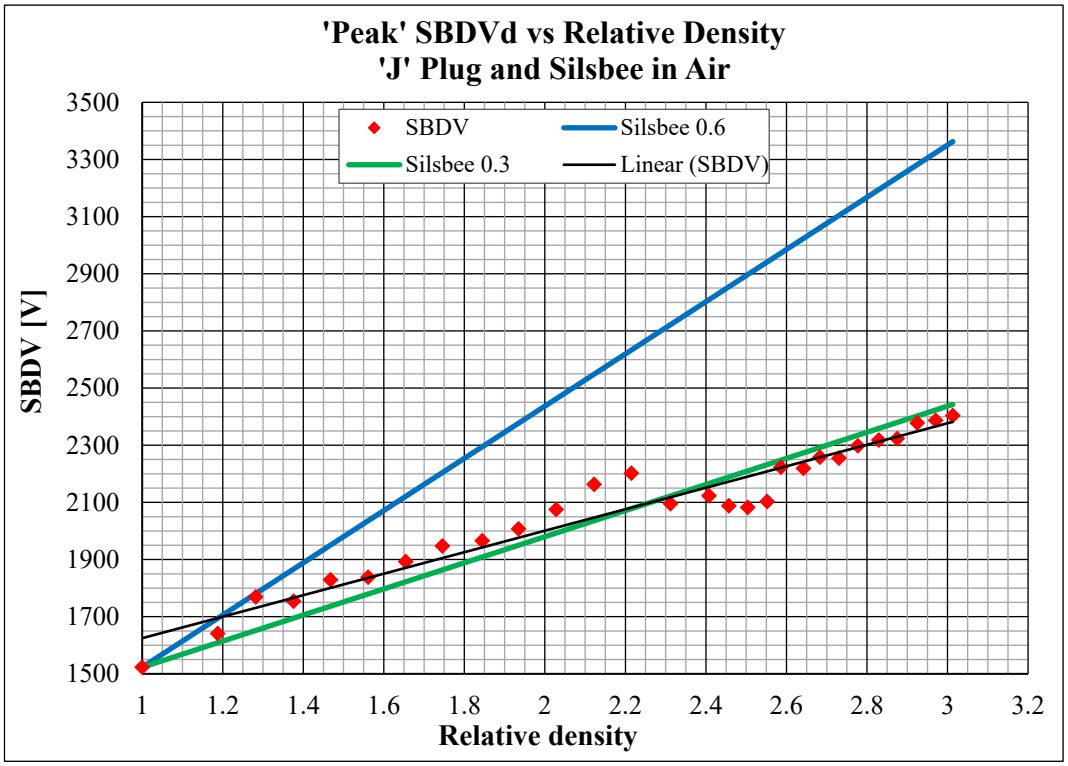

Figure F7-57: 'Peak' SBDVd vs Relative Density: 'J' Plug and Silsbee in Air

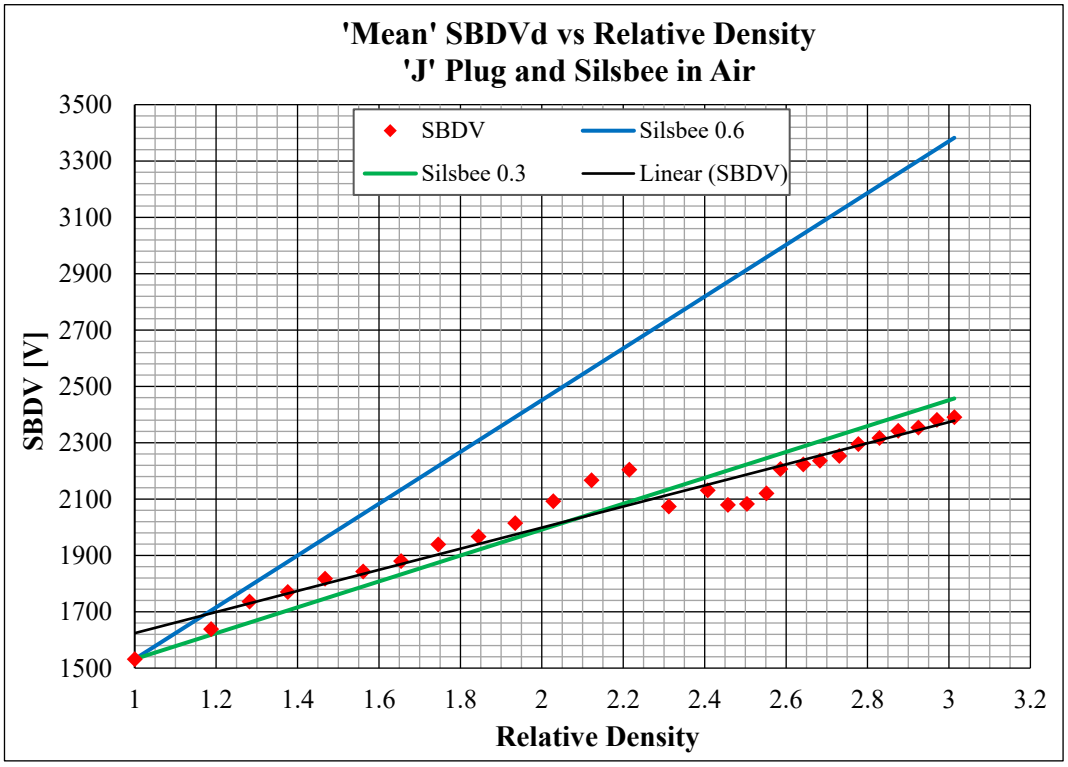

Figure F7-58: 'Mean' SBDVd vs Relative Density: 'J' Plug and Silsbee in Air

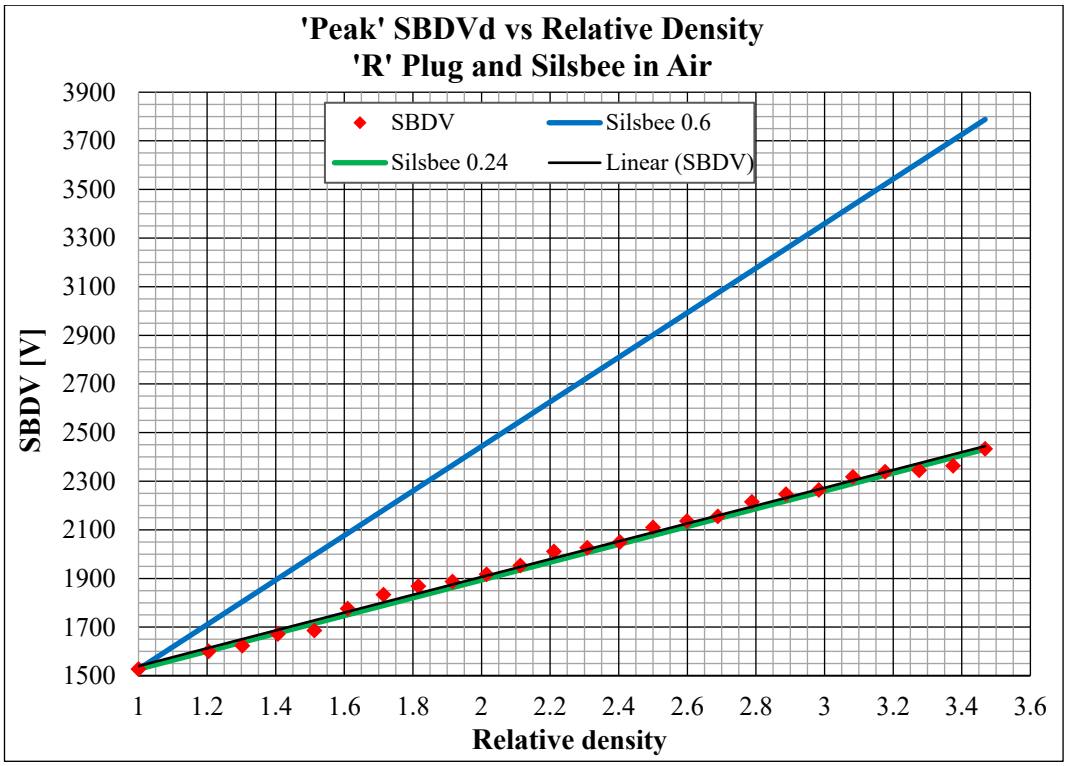

Figure F7-59: 'Peak' SBDVd vs Relative Density: 'R' Plug and Silsbee in Air

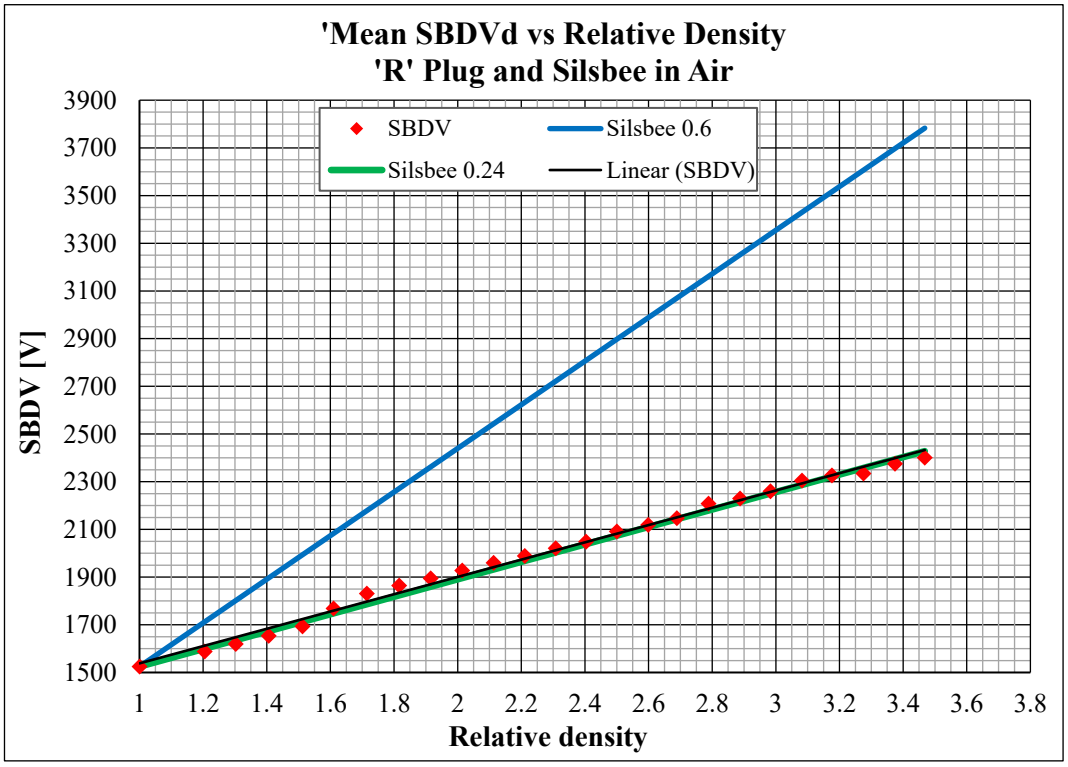

Figure F7-60: 'Mean' SBDVd vs Relative Density: 'R' Plug and Silsbee in Air

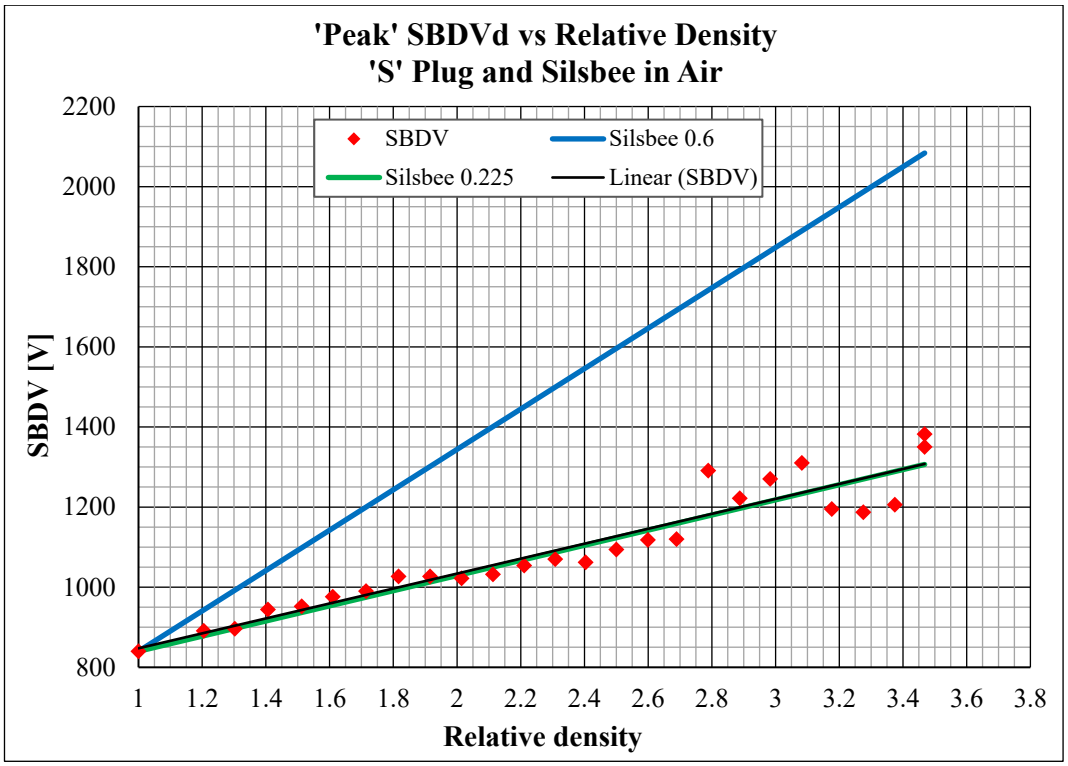

Figure F7-61: 'Peak' SBDVd vs Relative Density: 'S' Plug and Silsbee in Air

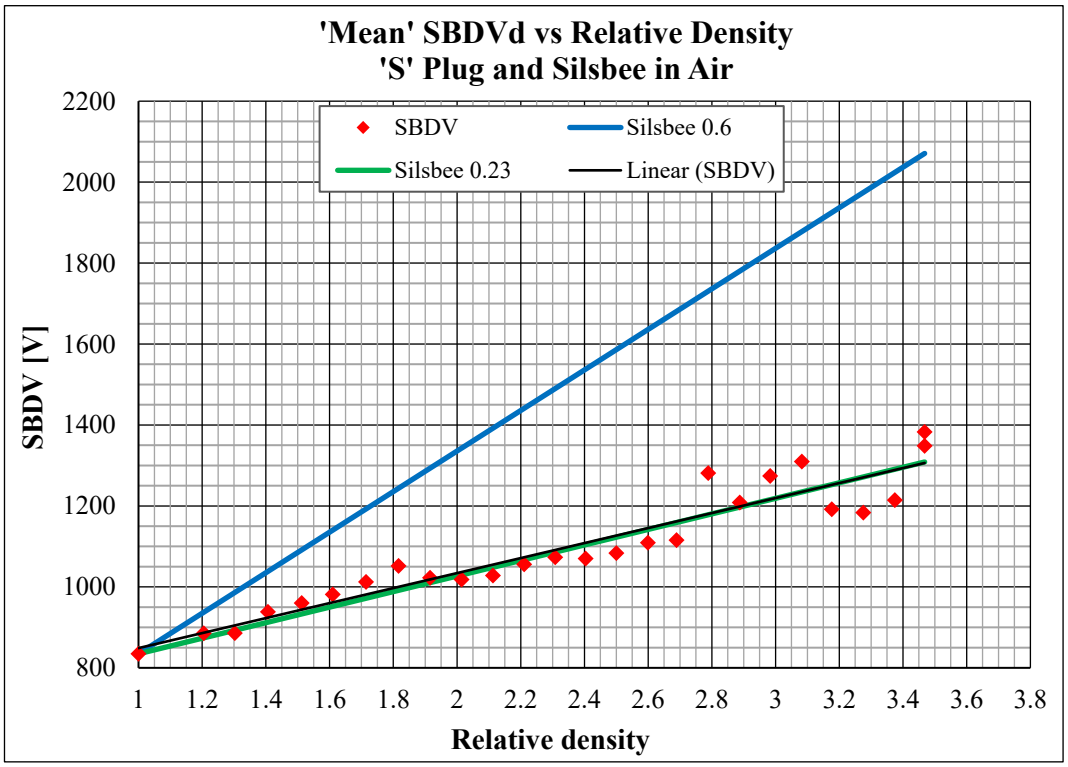

Figure F7-62: 'Mean' SBDVd vs Relative Density: 'S' Plug and Silsbee in Air

7.6.4 SUMMARY OF COMPARISON OF RESULTS WITH 'SILSBEE' FORMULA

The test results of the present work in air for three types of spark plugs with equivalent results given by the Silsbee formula (Eq. 7.8) are shown graphically in Figures F7-57 to F7-62 above. These show remarkably close alignment when the 'K' factor is modified and the influence of the 'K' factor is clearly apparent. The 'K' factor correction for each plug type is summarised below in Table T7-7.

These confirm the formula provided by Silsbee, with 'K' factor correction depending on spark plug type and the use of 'Peak' or 'mean' SBDV provides a very close approximation to the linear relationship with air density determined from testing for the present work.

Table T7-7: Silsbee 'K' factor for 'J', 'R' and 'S' Spark Plugs in Air

SILSBEE' Formula 'K' factor (Air)			
Spark Plug Type	SBDV		Accuracy to Testing Linear Relationship
	Peak	Mean	
J	0.3	0.3	GOOD
R	0.24	0.24	EXCELLENT
S	0.225	0.23	EXCELLENT

7.6.5 THE EFFECT OF HUMIDITY

The test results for the present work were obtained in an engine test cell which was supplied with Air from the exterior atmosphere which was not deliberately modified or conditioned. No specific tests were carried out for the present work to explore the potential effect of on SBDV. Published work shows humidity does affect SBDV but the measured variation depends on the electrode configuration.

Feser (Feser. K., 1972), observed that if breakdown occurs without 'pre-breakdown' the effect of humidity on breakdown is slight (0.25% / gr/m). However, impulse-like pre-breakdown glow corona precedes the breakdown at the positive electrode, is greatly influenced by humidity. Impulse-less glow corona being described as a form of discharge which can be observed in AC and DC voltages particularly at sharp edges and on thin wires confirmed breakdown voltage in a nonhomogeneous field (as is the case with all spark plugs) is influenced by the absolute humidity. However, the observation was conditionally obtained from impulse-less glow corona. Feser, predicted the reduction of breakdown

voltage as humidity increases could lie in the absorption of photons the breakdown characteristics or rod gaps are influenced by humidity, the effect depending on the SBDV form, polarity and over-breakdown voltage. For the new SBDV system this would be consistent to correlate breakdown voltage data the measure values are corrected to a standard humidity of 11gm. / m^3, corresponding to a relative humidity of 64% at 20°C.

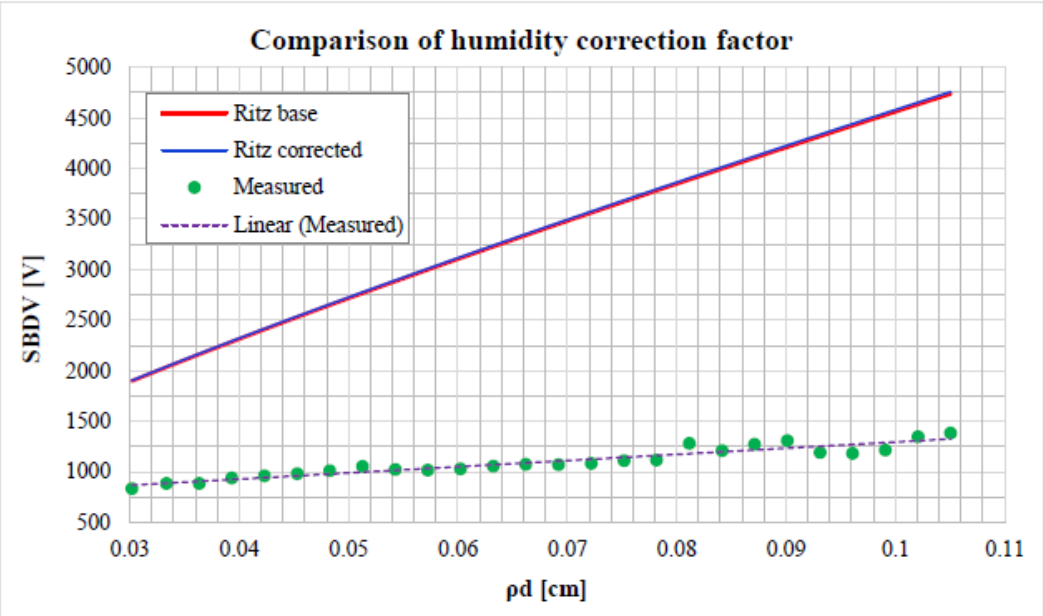

Figure F7-63: Comparison between Published and Measured Humidity Correction

7.7 GAS SPECIES IDENTIFICATION

The previous content in this chapter has shown that individual gases can be related to spark break-down voltages at different pressures. The use of those relationships would potentially allow individual gas species to be identified to satisfy the objectives of the present work. However, the proposed engine control strategy requires fast and precise gas speciation identification which objective justified consideration of all potential sources of information from the generated spark break-down events.

In chapter four the characteristic profile of individual spark break-down events shown was described as part of the work concerning bench testing of the SBDV system. That information is shown below in Figure F7-64, entitled 'SBDV Consecutive events' for the reader's convenience. This shows the key features of the individual spark break-down event shape or the Spark Breakdown Event Profile (SBDVEP).

Considering four different phases of signal are overlaid separately.

a) The maximum voltage attained during the 'single spark discharge cycle' phase, must represent the overall dielectric strength of the gas between the electrode gap. This break-down voltage is defined by the voltage at the sharply pointed strike point.
b) Following the strike point, the voltage reduces sharply back to a level where an arc forms. Unlike an ignition event, the SBDV system has cut off the supply voltage leaving only the residual ionization and heat to produce an arc. The duration of the arc is therefore very short. The interesting features of this phase being: 1) As the pressure increases the arc phase voltage remains comparatively stable leaving the voltage difference between the arc phase and the strike point to increase almost independently. 2) The shape defining the arc varies for each event, which is not surprising as any heat related activity will be to some extent chaotic in nature. However, there exist common frequencies in this phase.
c) The breakdown build-up phase must represent the increasing ionization on the power electrode and define the progress of the ionization cascade by collision with the gas molecules in the electrode gap. The shape of this phase must consist of the frequencies of those collisions and the energy required for these to occur. Thus, if the shape of this phase begins rapidly it could be concluded the build-up of ionization which initiates the break-down process across the electrode gap is also rapid. Differences in this behaviour could be an indicator of the electrode

profile/surface and or material but then for any gas be consistent for that electrode (depending on wear etc). Overall, the shape of this phase must contain significant information about the gas between the electrode gap.

d) The shape of the 'single spark discharge' phase must indicate the speed and therefore the rate of energy release for break-down of the gas to occur and a spark to form. This phase does not contain multiple frequencies as would be expected. However, the start of this phase appears to be triggered by a burst of ultra-high frequencies which could be used as an indicator of the breakdown phase initiation.

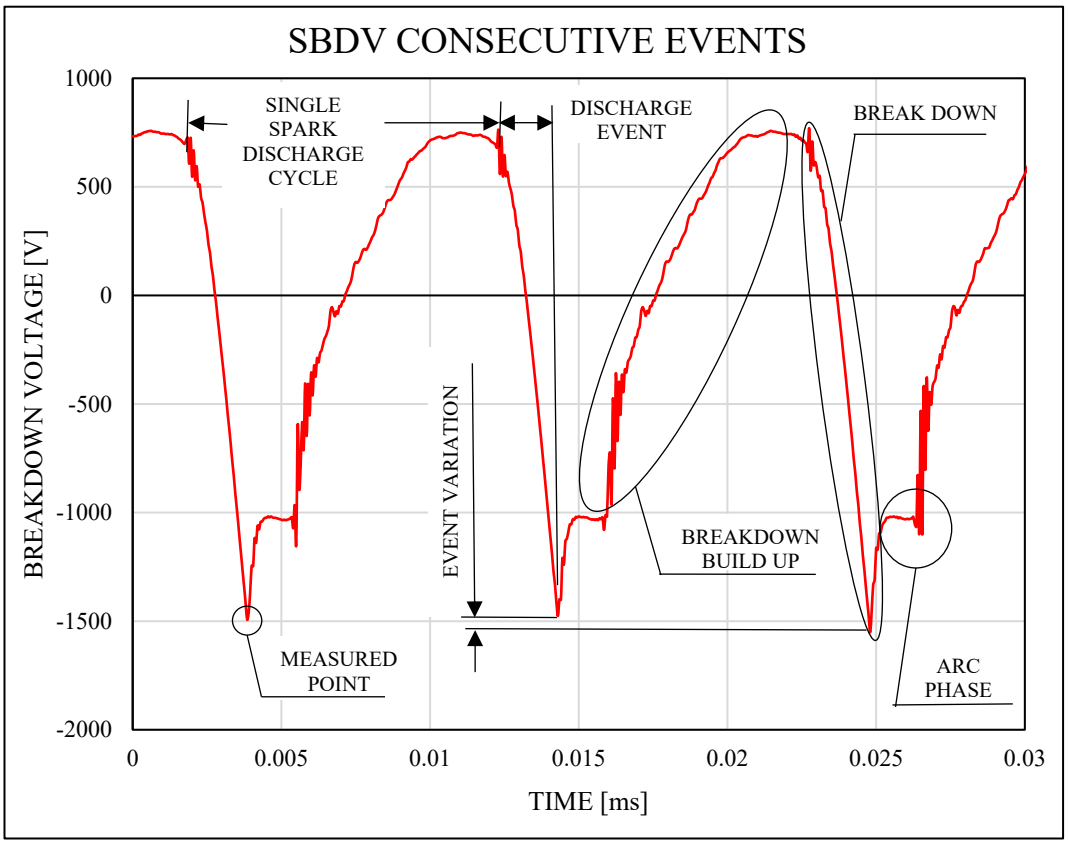

Figure F7-64: The Phases of each Spark Breakdown Event (SBDVEP)

If it is considered the SBDVEP consists of a history of each break-down event. As would be expected for the same gas and conditions, the key features of the events are repeated. (Note although only two events are shown for clarity, the repeating profile can be confirmed by inspection of any sample file). Previously, the present work has focused on the value of and differences between, the breakdown voltage which is represented by the sharp strike-point annotated above as the 'measured event'. However, it can be seen by

inspection, that there is a considerable amount of comparative information in the shapes which constitute characteristic features of the repeated events. Potentially, every part of the event indicates a part of the mechanism whereby the voltage potential between the electrodes gathers, then starts to cause ionization by collision until the gas between the gap 'breaks-down' to allow a spark to pass. Thus, the profile of each event is considered to represent the molecular level obstruction or dielectric resistance at close to 100,000 times per second which is worthy of greater investigation as a potential method to identify and differentiate between gas species. This can be visualised by referring to Figure F7-65. This shows an overlay of two SBDVEP in air at four different pressures starting at ambient to one bar above ambient.

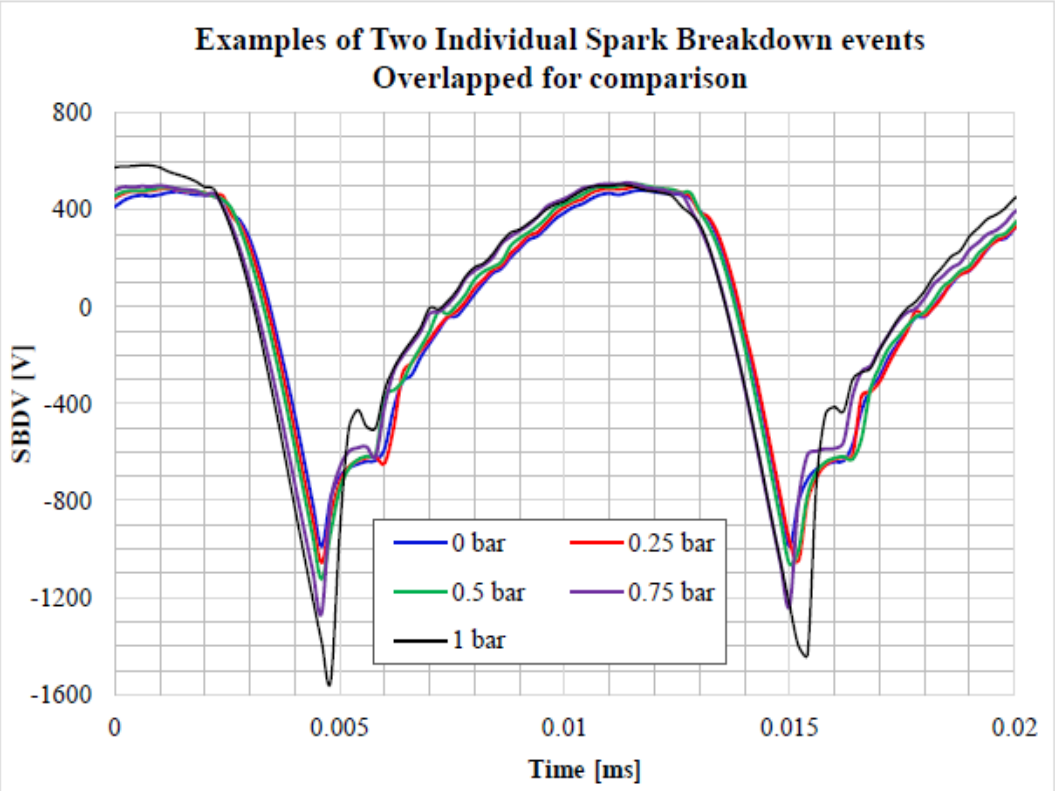

Figure F7-65: Overlay of Two Spark Breakdown events at four different pressures in Air

It is apparent from the previous descriptions of the individual phases of break-down there was potentially a significant amount of information to be obtained which could be used to identify different gas species from a very limited number of samples.

For comparison with the sample previously considered for Air, similar information is presented below in Figures F7-66 & 67, which show characteristic SBDVEP for 'J', 'R' and the shrouded plug extracted from samples of the test gases at the same pressure.

The three examples of SBDVEP signals demonstrate the influence of the spark plug electrodes and their effect on the break-down process in different gases. Of interest is the pre-break-down behaviour which can be observed in Nitrogen with the 'J' and 'R' plug examples. Overall, the influence of the spark plug type and the gas species can be clearly seen from these three examples.

A deeper investigation of the effect of the spark plug electrodes and the related effect on the individual phases of the break-down events was not included in the present work. However, it was considered the overall content of the frequencies constituting a SBDV sample could potentially identify different gases. The process used to extract and obtain this information is presented in the following section.

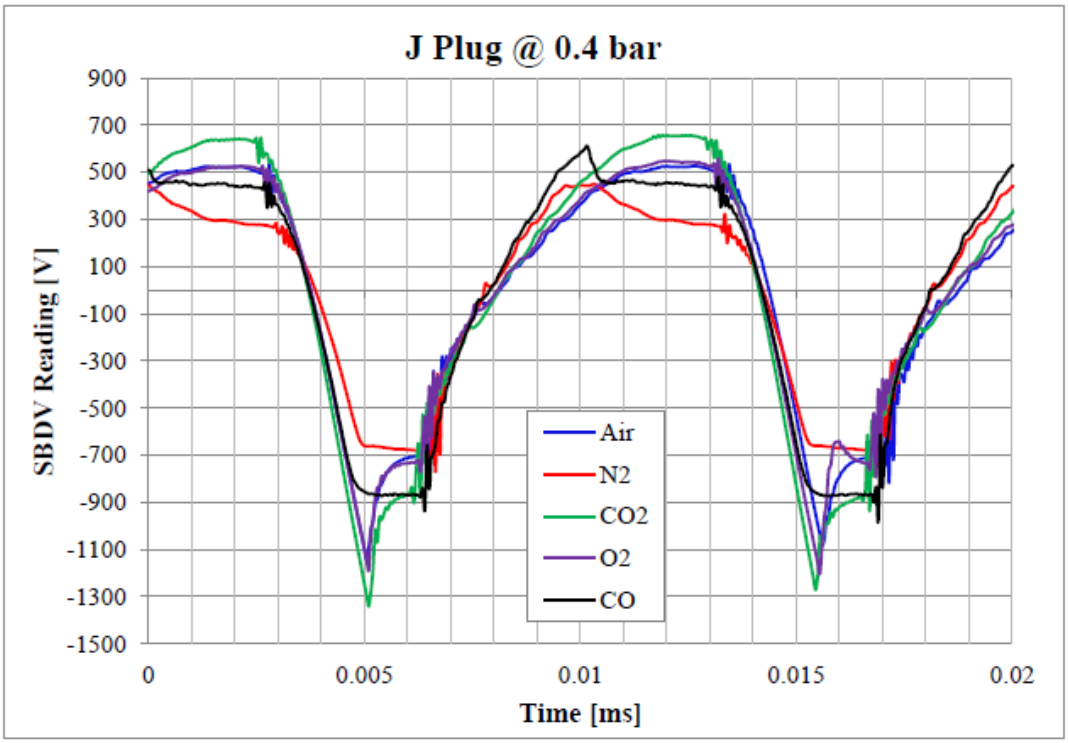

Figure F7-66: Comparison of SBDV events @ 0.4 bar in various gases: 'J' type Plug

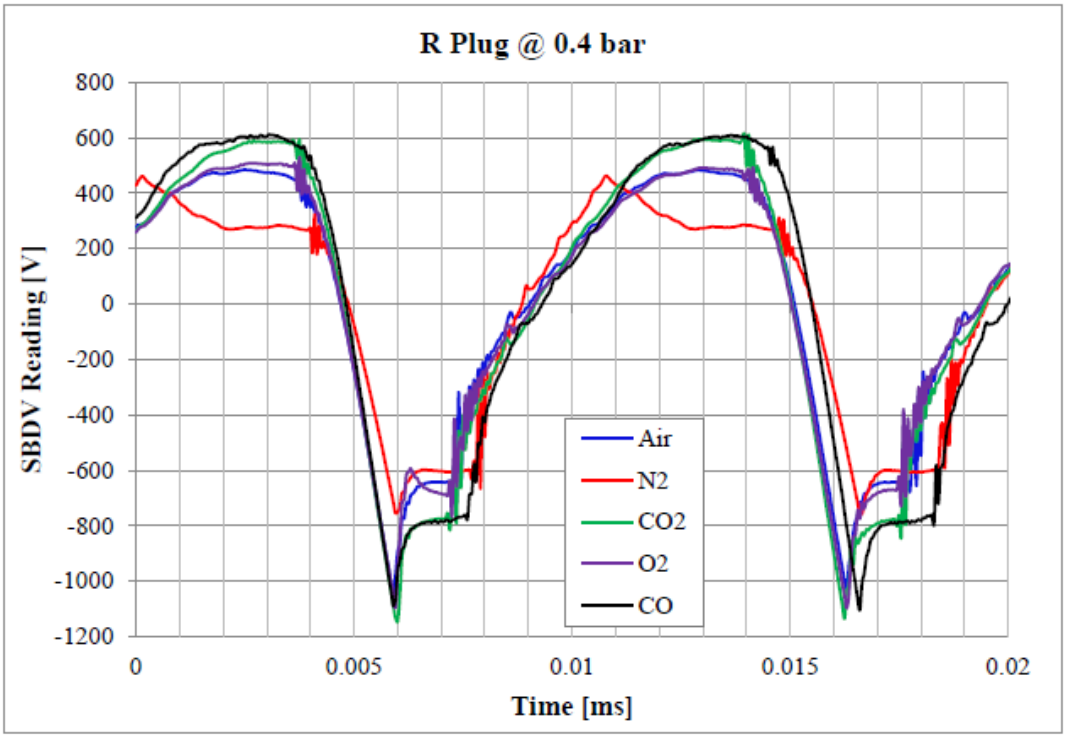

Figure F7-67: Comparison of SBDV events @ 0.4 bar in various gases: 'R' type Plug

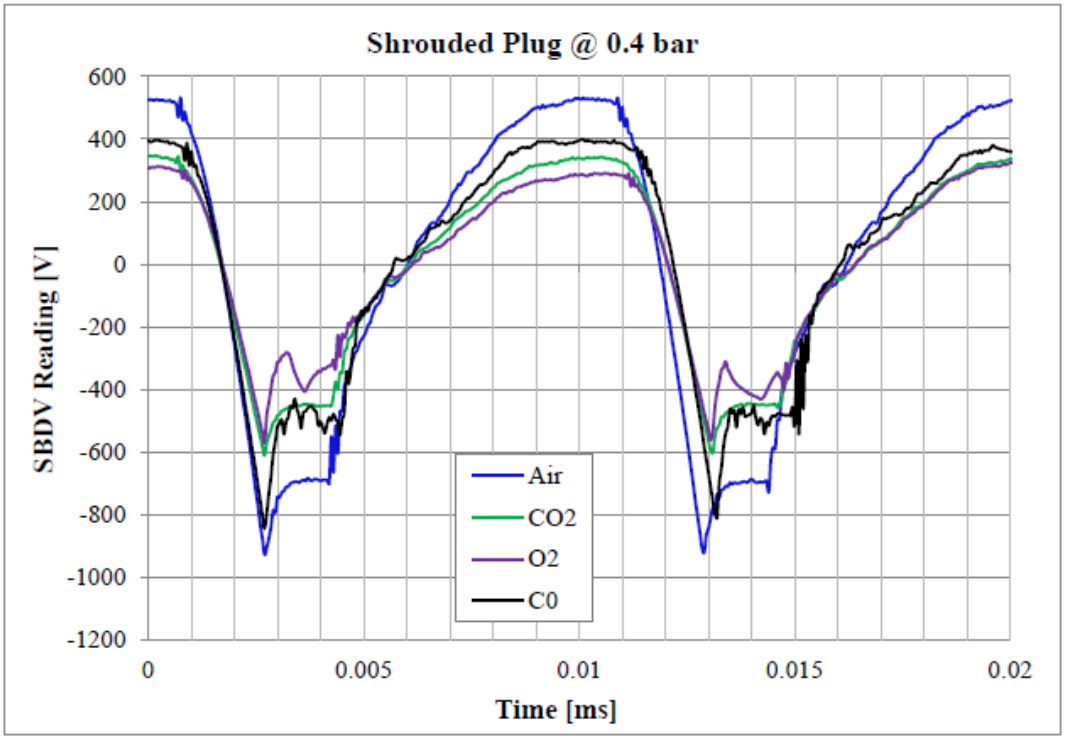

Figure F7-68: Comparison of SBDV events @ 0.4 bar in various gases: S type Plug

7.8 FFT ANALYSIS

Examples of individual SBDV signals generated in different gases show the shape of the signals differs for each gas species. The shape of each signal consists of a characteristic group of individual frequencies which are repeated during each event. This observation has not been found in the literature review for the present work. This is particularly interesting in the section following the breakdown itself which includes the short arc phase and the building process that proceeds the start of the subsequent breakdown. This observation is considered by the author to represent the formation of the ions on the surface of the central electrode and the effort required to create an ionised path along which breakdown can occur. The characteristic frequencies in different gases could be at least partly explained as the vibrational response of different molecules. These vibration frequencies vary depending upon the inter-molecular bonds and degrees of freedom they allow.

Waveforms which consist of multiple frequencies are conventionally analysed using the Fast Fourier Transform technique (FFT). This method separates out the individual frequencies from the overall combined signal and was applied using the 'PWELCH' function in 'Matlab', to the SBDV signals recorded for different gases at using the 'R' type spark plug, at 0.4bar shown in Figures F7-65.

The FFT for each gas, was obtained from one millisecond of SBDV signal which represented approximately ten individual breakdown events. These signals were extracted from a ten milli-second sampling period. The results of the FFT analyses for Air, CO, CO_2 and O_2 are presented in Figures F7-69, 70, 71 and 72. The FFT images represent the 'energy' levels (in the vertical axis) against the individual frequencies at which they occur (in the horizontal axis). The differences in the FFT image for each gas can be clearly seen. This is important because existing electronics are able to efficiently recognise different 'energy' levels at different frequencies. This can be achieved using hardware components thus avoiding complex software needed for FFT processing. This is proposed as the potential method to develop the very fast gas speciation recognition system required to meet the objectives of the present work.

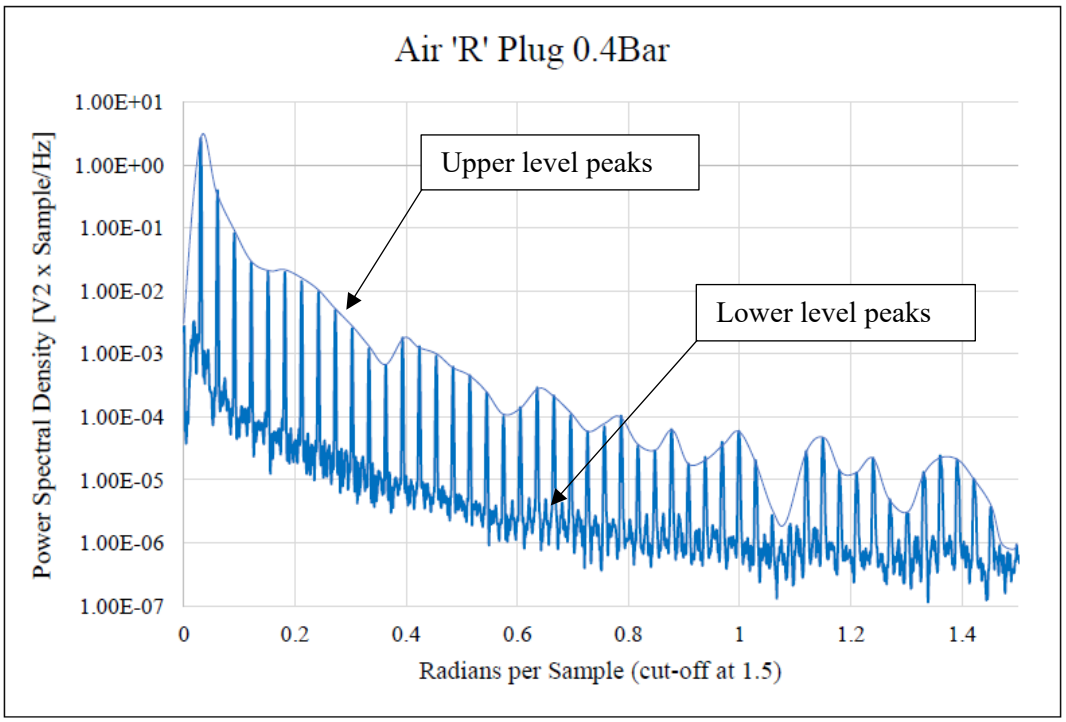

Figure F7-69: Spectrum of all SBDV frequencies averaged from ten continuous separate one millisecond samples - in Air at 0.4 Bar using 'R10' Plug

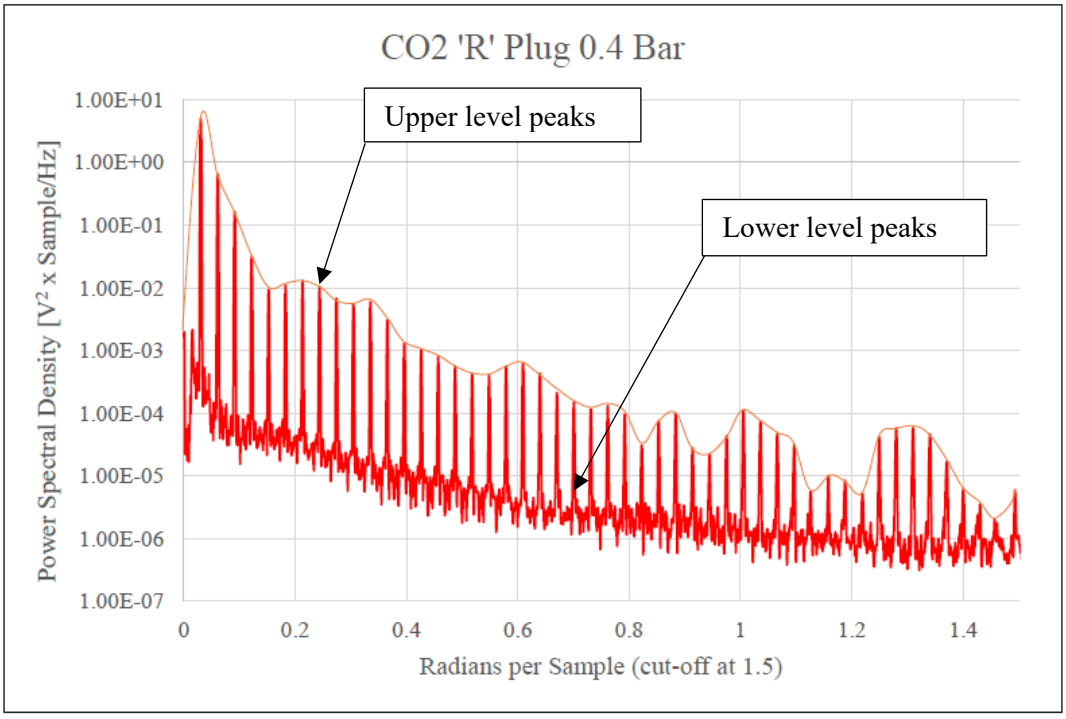

Figure F7-70: Spectrum of all SBDV frequencies averaged from ten continuous separate one millisecond samples - in CO_2 at 0.4 Bar using 'R10' Plug

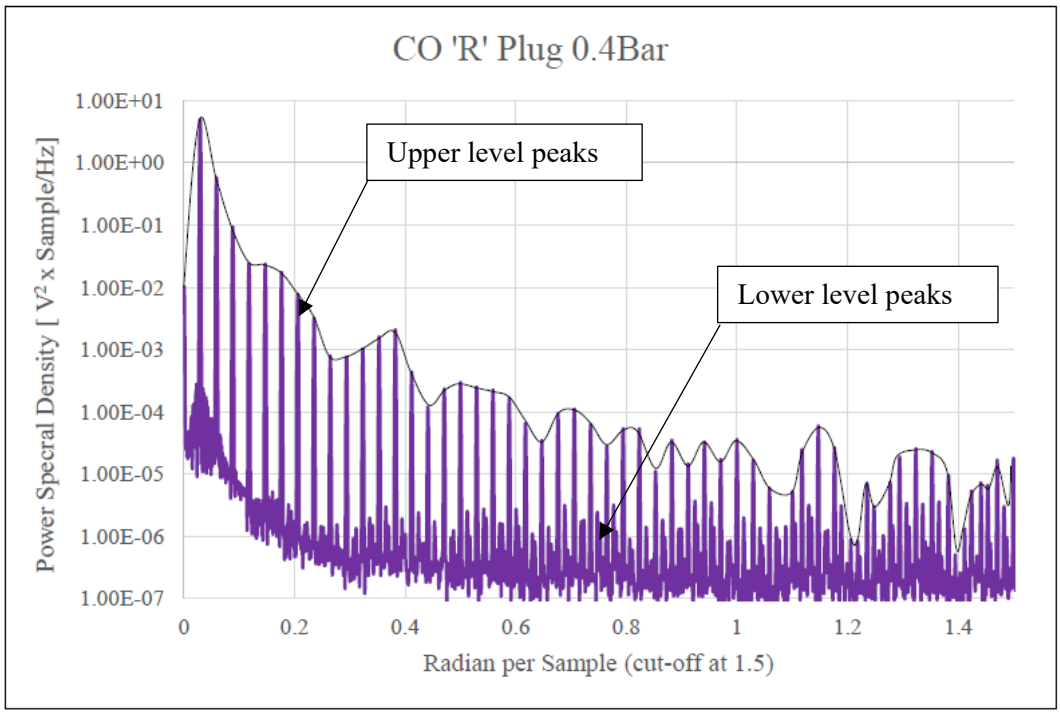

Figure F7-71: Spectrum of all SBDV frequencies averaged from ten separate continuous one millisecond samples - in CO at 0.4 Bar using 'R10' Plug

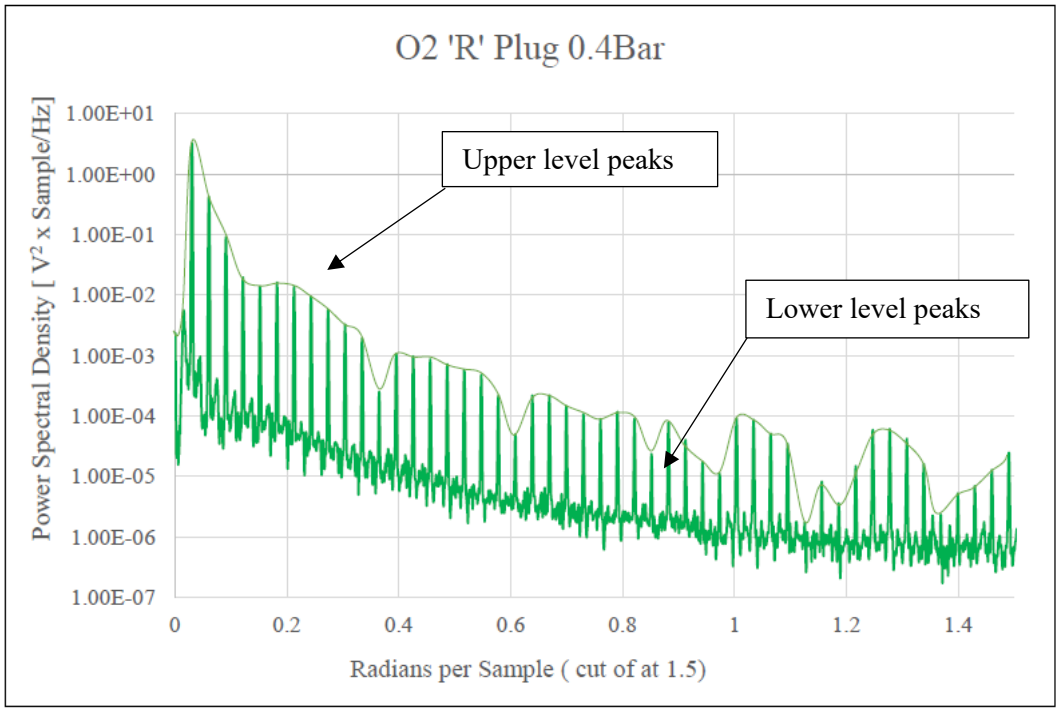

Figure F7-72: Spectrum of all SBDV frequencies averaged from ten separate continuous one millisecond samples - in O_2 at 0.4 Bar using 'R10' Plug

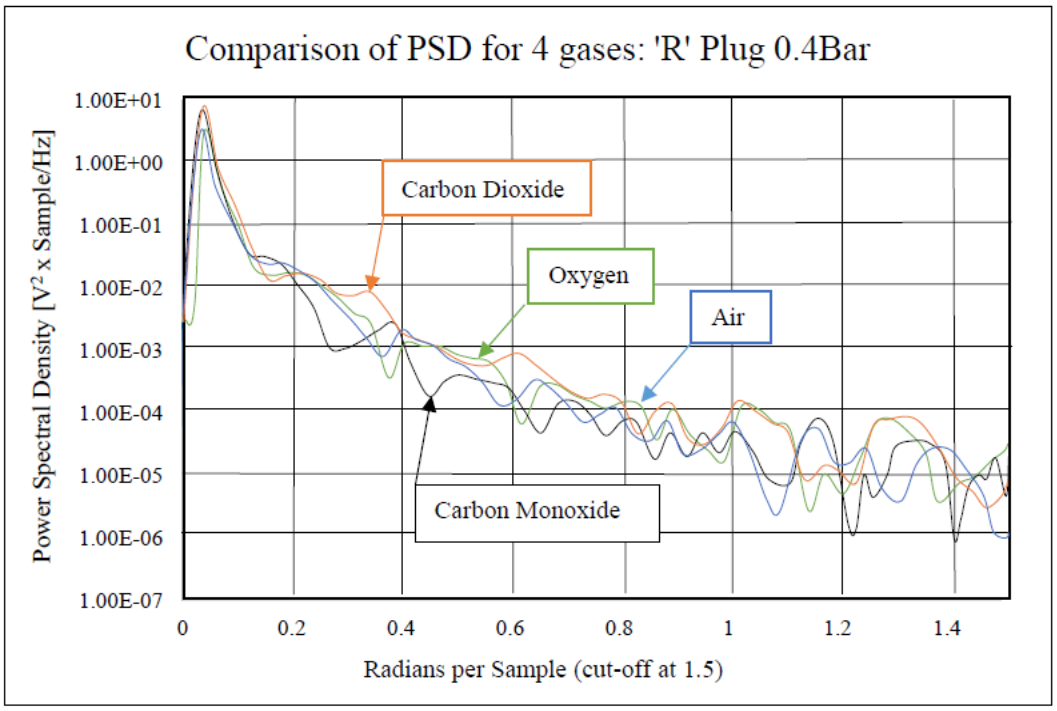

Figure F7-73: Comparison of Spectrum of upper level SBDV frequencies averaged from ten separate continuous one millisecond samples – all test gases @ 0.4 Bar: 'R10' Plug

The comparison of spectrum samples shown in Figure F7-73 is considered significant. This plots the upper level spectrum traces of all the frequencies in ten separate, one millisecond samples of signals in ten milliseconds. This appears to show different individual characteristic signatures for the different gases tested. The variations are believed to represent the natural frequencies of the different gas molecules. This was not investigated further in the present work. However, this would provide a method to identify individual gases within the cylinder and therefore meet one on the key objectives of the thesis.

An additional analysis was carried out by which integrated the area under each FFT signal curve. The curves are the average of ten samples of one millisecond samples. These are intended to represent an average value of the SBDV signals. These values are plotted at each pressure test step from atmospheric to approximately 3.5 Bar. The maximum pressure attainable depended on the dielectric strength of each gas and limited by the maximum voltage generated by the new SBDV circuit.

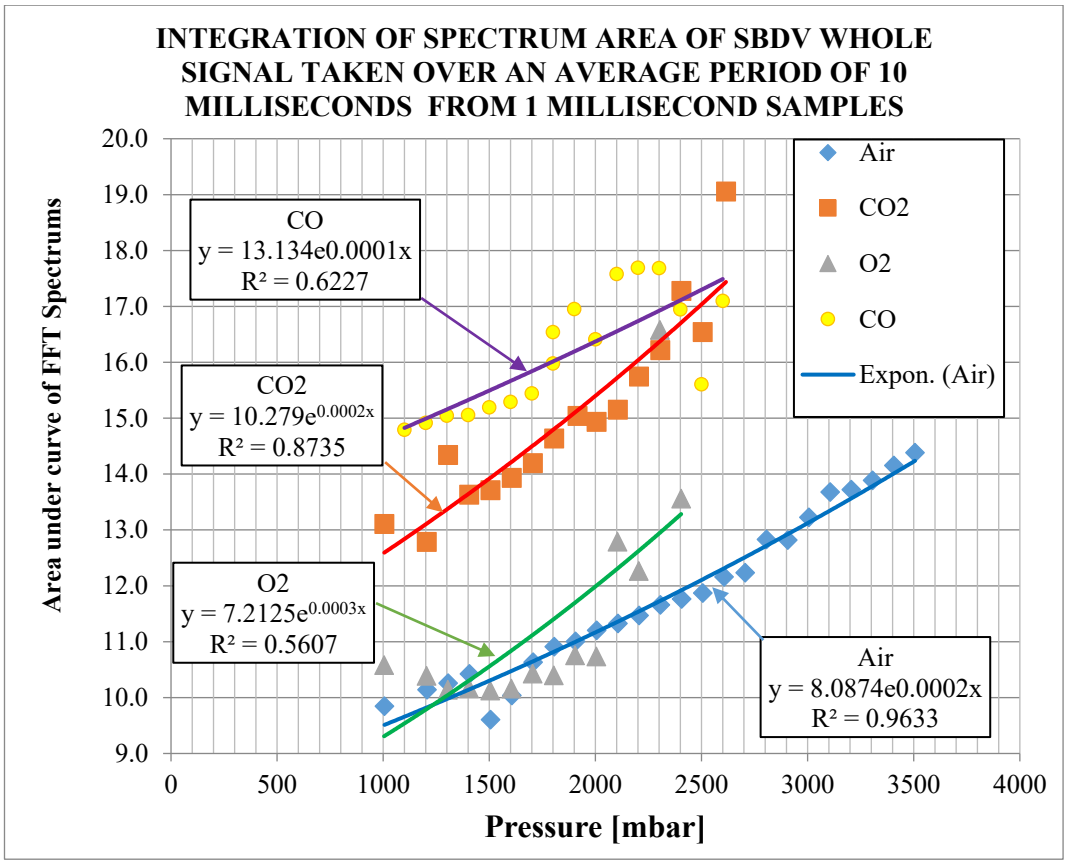

Figure F7-74: Integrated spectrum area of SBDV whole signal over average 1 millisecond

7.9 CHAPTER SUMMARY

Static testing has shown that SBDV could be used to identify the gases which are most significant to combustion. Test results were presented which show accurate Linear relationships between spark break-down voltage for each gas type. The results demonstrated these characteristics from ambient to approximately 2 bar pressure.

Comparison with a simplified formula provided in published work carried out by NACA (Silsbee, 1925) confirmed the formula could be applied using a corrected 'K' factor to determine relative gas density from spark break-down voltage.

The separate identification of gases using SBDV to promote resonance of the various molecules as shown in Figure F7-73 has similarities with other proven methods of gas identification.

The relationships shown in Figure F7-74 show the FFT spectrum results relative to pressure. The test results for CO_2 and Air show a reliable trend, whereas those for O_2 and CO less so.

Overall, the author considers the testing reported in this chapter to have demonstrated the spark plug, despite having non-unified electrode profiles with very short gap lengths in comparison with classic SBDV measuring equipment, could be used as a gas sensor. The results of the static testing indicate a new very fast and accurate method of gas identification is possible.

CHAPTER EIGHT

SBDV TESTING OF VARIOUS EXHAUST GASES

8.0 INTRODUCTION

The previous chapter reported on testing carried out to determine the SBDV characteristics in air and various individual gas mixtures. The results, obtained in static conditions, showed that O_2, CO_2, CO, N_2, can be differentiated from Air using SBDV signals. These gases were termed 'significant to combustion' as they represent the most dominant gases in that process. In an operating engine, these gases undergo transformations due to combustion and collectively termed 'exhaust gases'. Exhaust gases consist of gas species which are indicative of the Air/Fuel ratio burned. Some of these gases, when not completely burned, retain some residual combustibility. Exhaust gases which are not scavenged from the cylinder occupy some of the volume which would ideally be fresh charge. Consequently, the relative proportions of air and exhaust gases present in the cylinder must be determined accurately to determine the amount of combustible charge present and hence the amount of fuel to be added.

This chapter reports on testing carried out to determine if SBDV signals obtained from the spark plug sensor, representing different 'air and exhaust gas mixtures' inside the cylinder, could be identified and mathematical expressions derived to distinguish differences between them. Such expressions could then be used to determine variations of the major constituent gases and or the proportions of air and burned exhaust gases in the various trapped mixed charges which occur cyclically in an engine.

8.1 TESTING ARRANGEMENTS

The objective of the testing reported in this Chapter was to obtain SBDV signals for various exhaust gases. The testing method used to obtain SBDV values for Air and pure gases could not be used to obtain SBDV values in various exhaust gases. This was because exhaust gases were not available in compressed form for supply into the Constant Volume Sparking Chamber which could then be manually adjusted to enable calibrations to be obtained in regular pressure increments. Therefore, a different method to create the required pressure differences had to be used. Two different series of test procedures were used which are described below. The Constant Pressure Sparking Chamber shown in Figure F4-14 was not used for either test.

8.3 QUASI-STATIC SBDV TESTS OF EXHAUST GASES

The first series of tests to obtain spark break-down voltages for different exhaust gases at different pressures were carried out using the 'Rotax Senior Max' test engine as shown in Figure F4-28. The intention being to achieve a slowly increasing (quasi-static), pressure change in the cylinder by slowly rotating the crankshaft manually to move the piston upwards. The AC electric motor could not be used as it would rotate the test engine crankshaft too quickly.

Due to limited working space, the torque required to manually rotate the crankshaft of the 'Rotax Senior Max' test engine had to be reduced. This was achieved by adding a 13mm thick spacer piece between the top of the cylinder and the cylinder head. This addition significantly increased the clearance volume which decreased the compression ratio, reduced the maximum cylinder pressure. This modification to the test engine also enabled the crankshaft angle over which SBDV signals could be reliability obtained from subsequent motored testing to be increased over a greater proportion of each engine revolution.

Compressing the gases at slow speed, in the test engine cylinder could not be achieved using the steel piston ring fitted to the standard piston. The piston ring provides minimal gas leakage at higher engine speeds but this leak rate is too great when the piston is moved slowly. To provide an adequate gas seal for tests up to approximately 3.0 bar the piston of the test engine was modified as shown in Figure F8-1.

The piston ring groove was enlarged by machining to enable fitting of a 3mm section 'O' ring. The material chosen for this 'O' ring was 'Viton' rubber. This material was chosen as it is tough and pliable, however, to avoid scuffing of 'O' ring surface the face was wiped with a smear of light oil. The dimensions of the 'O' ring groove in the piston were machined to provide 0.1mm of seal compression against the cylinder wall. If the bore of the cylinder did not have ports into which the 'O' ring could protrude and be damaged this compression would have been increased. During the tests, this clearance (and compression) was marginal and only just provided sufficient sealing however, the pressure variation could not be well controlled and this resulted in a limited sampling points especially in the transition pressure range.

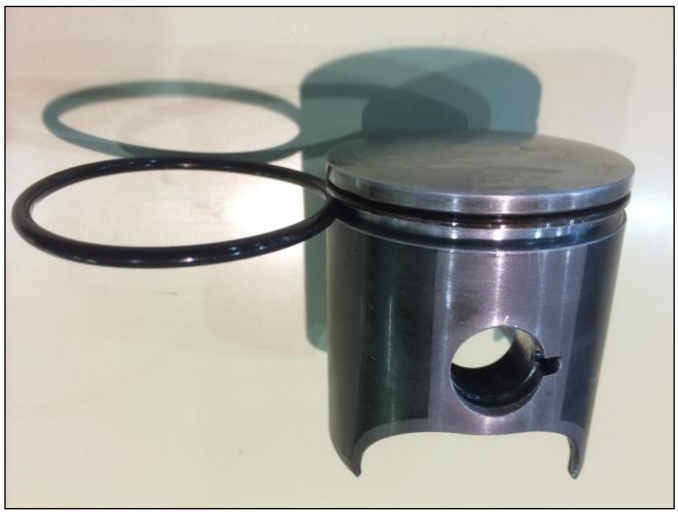

Figure F8-1: ‘O’ ring Piston seal used for Quasi-Static Exhaust Gas Testing

For previous calibration tests (reported in Chapter Seven), carried out using the Constant Volume Sparking Chamber, the gas pressure was measured using a 100mm Diameter pressure gauge. Although not suitable for static pressure measurements the ‘Optrand’ 0-7 bar pressure sensor which was fitted to the test engine cylinder head as shown in Figure F4-15 was used to measure the cylinder pressure when the test engine crankshaft was rotated manually.

Exhaust gases were supplied to the test engine from the 40cc ‘Blata B1’ Auxiliary engine described in section 4.13 and shown in Figure F4-29 and 30, through piping shown in Figure F4-32, via the inlet system described in section 4.14 and shown in Figure F4-33.

The exhaust gases supplied to the test engine would be diluted if any fresh air was included into the charge tested and invalidate the SBDV signal. To prevent air entering the supply to the test the butterfly valve controlling the air entering the intake system was closed which ensured only exhaust gases were delivered and hence, the purity of these gases was maximized. The supply of exhaust gases to the test engine for the ‘Quasi-Static tests followed the procedure detailed in section 8.3.1 below.

The spark plug used for the three ‘hand cranked’ Exhaust gas tests reported below was the ‘R’10 item. This plug had produced the most consistent SBDV signals of all the conventional spark plugs. This spark plug, shown in Figure F6-11, had been used in a running engine and consequently the electrodes of this plug were well-conditioned.

8.3.1 EXHAUST GAS SUPPLY PROCEDURE FOR QUASI-STATIC TESTS

The test engine cylinder was charged with exhaust gas in the following manner:

1) The new SBDV system was started.
2) The Butterfly Air Inlet Valve was closed (see above) and Exhaust Gas inlet valve to the inlet system opened.
3) The Auxiliary engine was started and operated for 30 seconds to reach stability. This gas filled the Test Engine cylinder with the exhaust gas produced by the Auxiliary engine.
4) The Auxiliary engine was stopped while the crankshaft of the Test engine was manually rotated to a position where the exhaust port was closed. This trapped a sample of exhaust gases in the Test engine cylinder.
5) The Picoscope system was turned on to record the SBDV and 'Optrand' pressure signals. The settings used are described in section 8.3.1 below.
6) The Crankshaft of the Test engine was manually turned slowly to compress the gases trapped in the cylinder.
7) The PICOSCOPE files from the three tests were stored. The in-cylinder pressure was recorded synchronously recorded for comparison with the SBDV signal.

Three separate tests were carried out trapping the exhaust gases from the slave engine as described above. For each test the carburation settings of the auxiliary engine carburetion were adjusted to produce 'Lean', 'Stoichiometric' and 'Rich' exhaust gases. These values were not validated scientifically by measurement but were intended to enable 'qualitative' assessments of the new SBDV system's overall capability. The relative fuel settings represented:

A) 'Lean' conditions a fuel adjustment with which the Auxiliary engine would just run and was difficult to start.

B) 'Stoichiometric' conditions a fuel adjustment where by experience the Auxiliary engine ran most strongly.

C) 'Rich' conditions, a fuel adjustment which was at the limit of stability and close to Four-Stroking. It is recognised these assessments were not quantitative but for qualitative purpose only. However, they do represent 'lean', 'Rich' settings and a mid-range value which experience of two-stroke cycle type engine behaviour represents a setting close to 'Stoichiometric'. A table of the tests is included below in Table T8-1.

8.3.2 PICOSCOPE RECORDING AND SIGNAL PROCESSING

A section of a 'Picoscope' recording taken from an exhaust gas test during which the test engine was slowly rotated manually, is shown in Figure F8-2. The SBDV signal, shown in a Grey colour, is negatively earthed which inverts the signal such that SBDV values increase downwards which is indicated by the Red traced line. The cylinder pressure signal is shown in a Green colour, as recorded by the 'Optrand' sensor, rises upwards as pressure increases. The SBDV trace constitutes individual spark breakdown voltage events. These are shown in Figures F8-3 and F8-4 which show 'Picoscope' recordings obtained in the Low and High Pressure sections as the crankshaft was manually rotated.

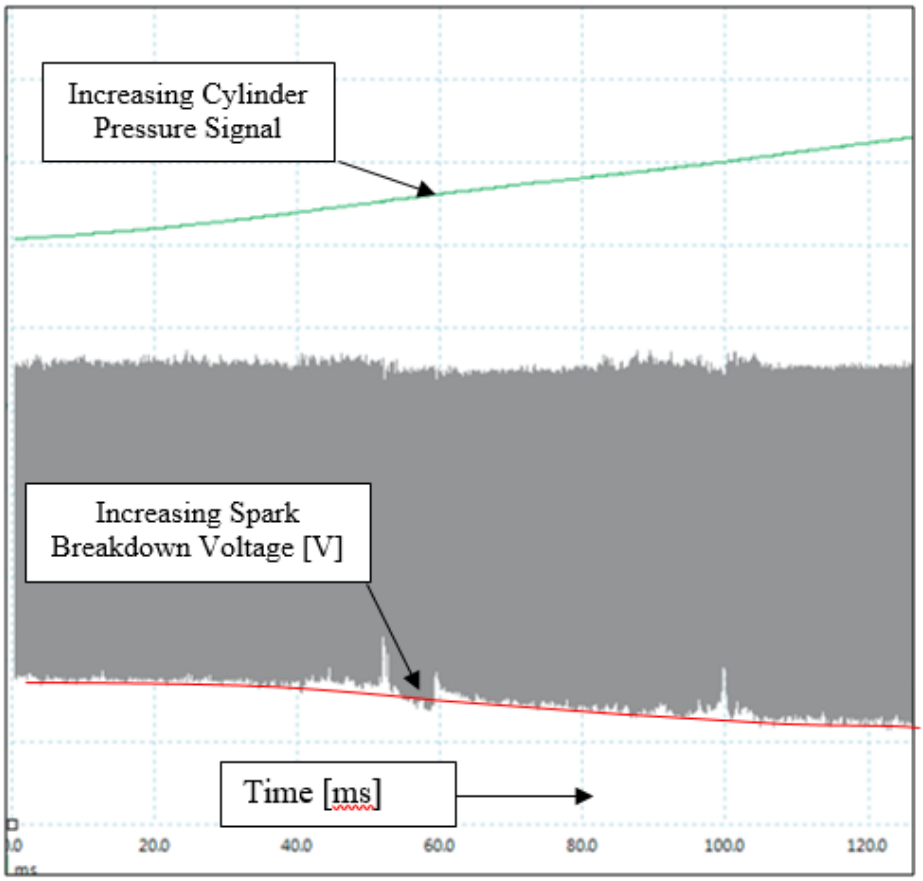

Figure F8-2: Picoscope recording of SBDV and Exhaust Gas Pressure signals

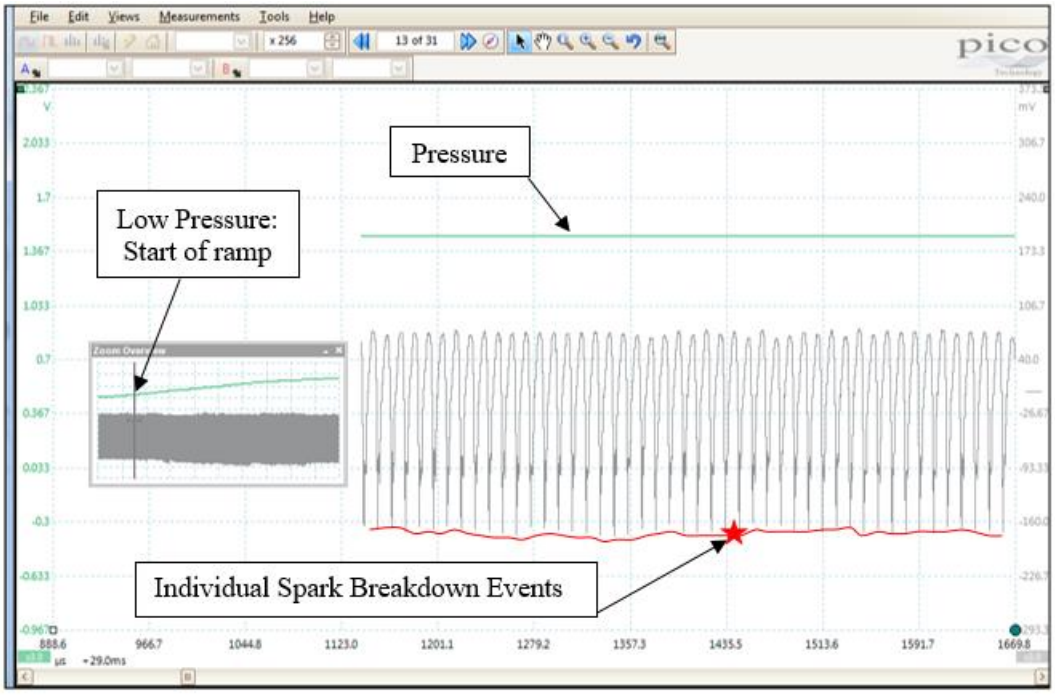

Figure F8-3: Hand cranked Test at Low Pressure (Test: 007-22-08-201)

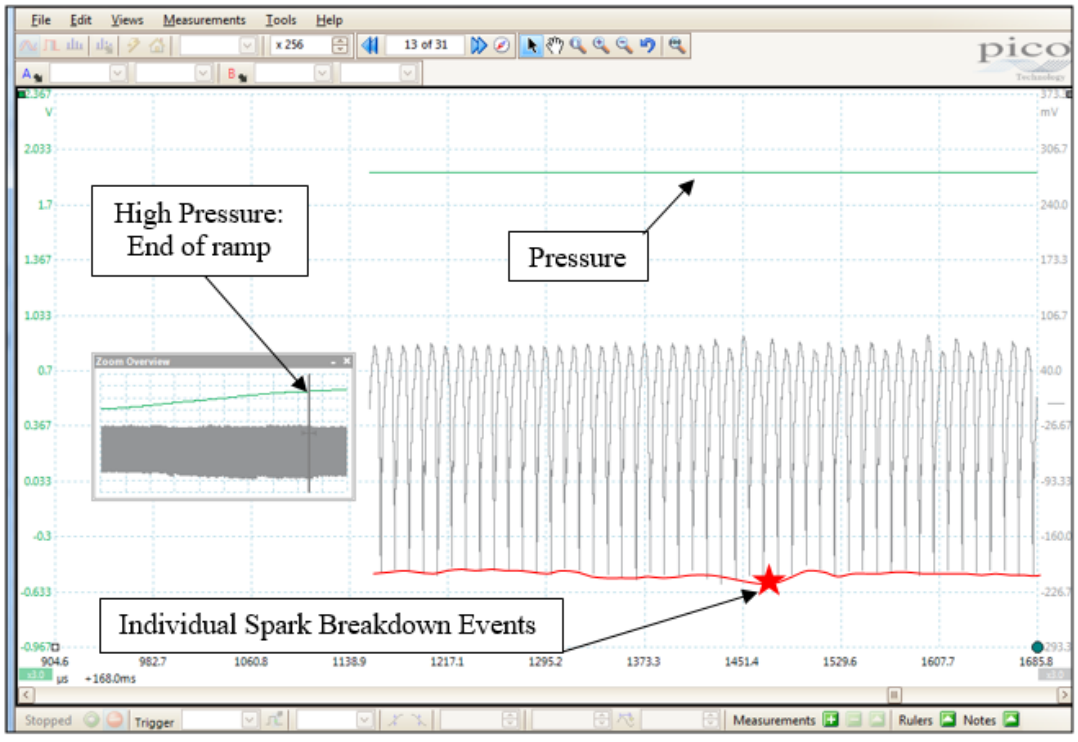

Figure F8-4: Hand cranked Test at High Pressure (Test: 007-22-08-2015)

From each Picoscope 'window' the value of SBDV and coincident pressure (from the OPTRAND pressure sensor) was equated for manually selected signals of 10 millisecond periods. The manually selected periods corresponded to visually flat and consistent SBDV

traces. This approach resulted in different numbers of samples being selected for each exhaust gas test but accurately represent the data. This limited the selection of sample positions to low and high-pressure sections. The restricted continuity of the data over the complete range of hand cranked pressures and limited the samples across the pressure range for each test. For each 10 milli-second sample, the average SBDV was determined using the method described in Chapter Four.

8.3.3 RESULTS OF QUASI-STATIC EXHAUST GAS TESTING

The simultaneously recorded values of SBDV and Pressure for each of the three 'hand cranked' exhaust gas tests are shown plotted below in Figures F8-5, 6 and 7.

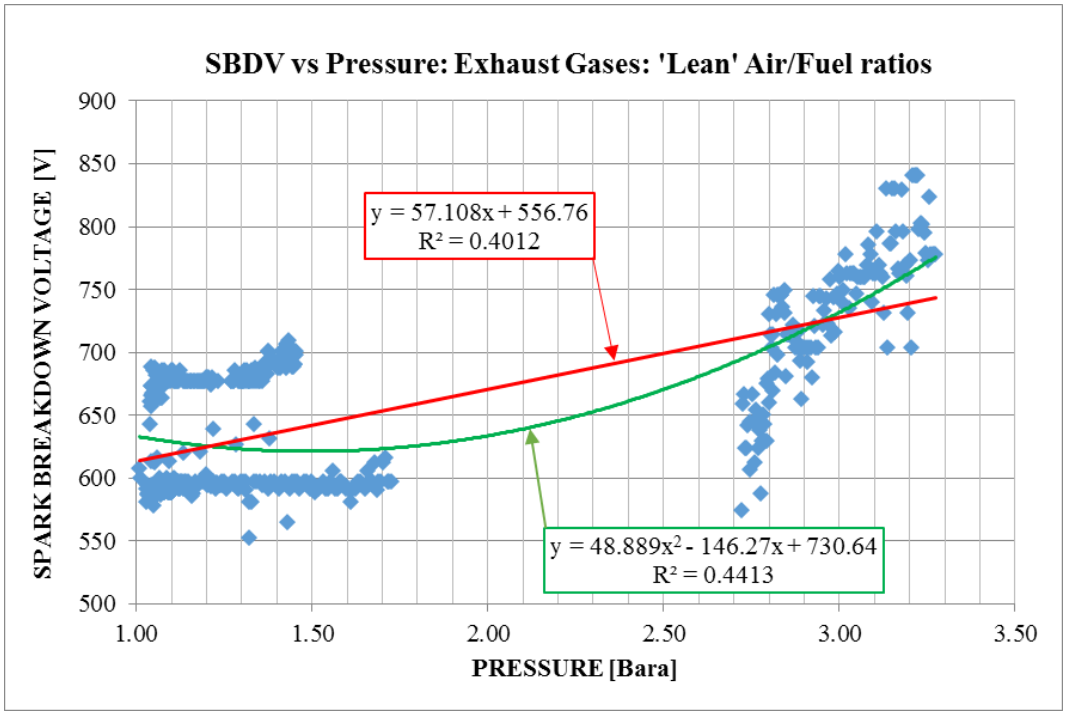

Figure F8-5: SBDV vs Pressure: Exhaust Gases: 'Lean' Air/Fuel ratio

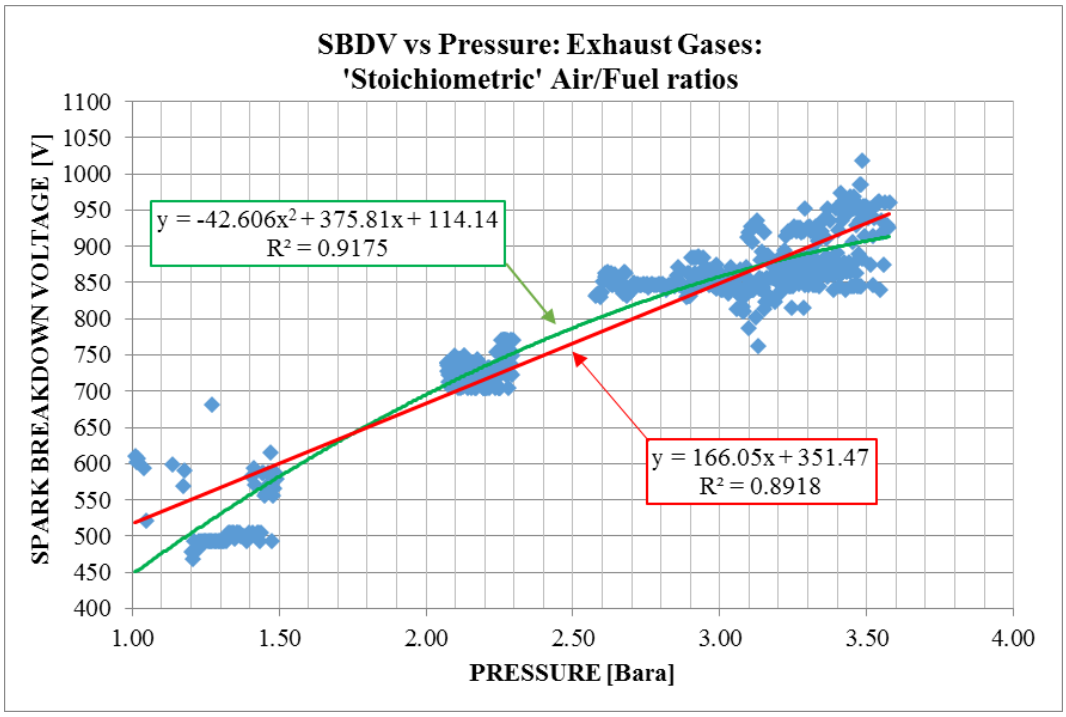

Figure F8-6: SBDV vs Pressure: Exhaust Gases: 'Stoichiometric' Air/Fuel ratio

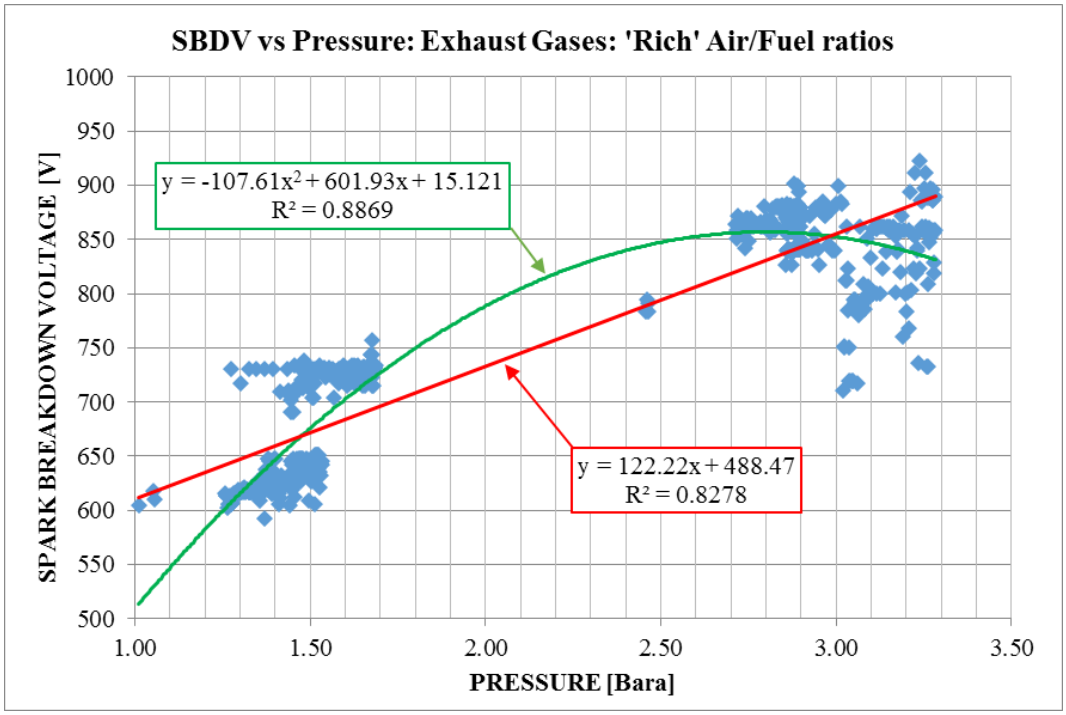

Figure F8-7: SBDV vs Pressure: Exhaust Gases: 'Rich' Air/Fuel ratio

8.3.4 SBDV PASHEN'S LAW RELATIONSHIPS FOR EXHAUST GASES

Further analysis was carried out to consider the test results obtained from the hand cranked exhaust gas tests to relate these to Paschen's Law which expresses spark breakdown voltage as a function of pressure and spark gap.

$$V_s = f(Pd) \qquad \text{(Eq. 8-1)}$$

Where: V_s = Spark Breakdown Voltage, P = Pressure (Torr) and d = gap (cm)

From the data tabulated above the following curves were plotted. The curves represent the mathematical relationships between Spark Breakdown Voltage and Pressure/Gap. The Mathematical expressions shown in Figure F8-8, were derived from the three 'hand cranked' exhaust tests to provide Pashen's Law relationships for exhaust gases resulting from combustion in 'Stoichiometric', 'Lean' and 'Rich' Air /Fuel ratio conditions.

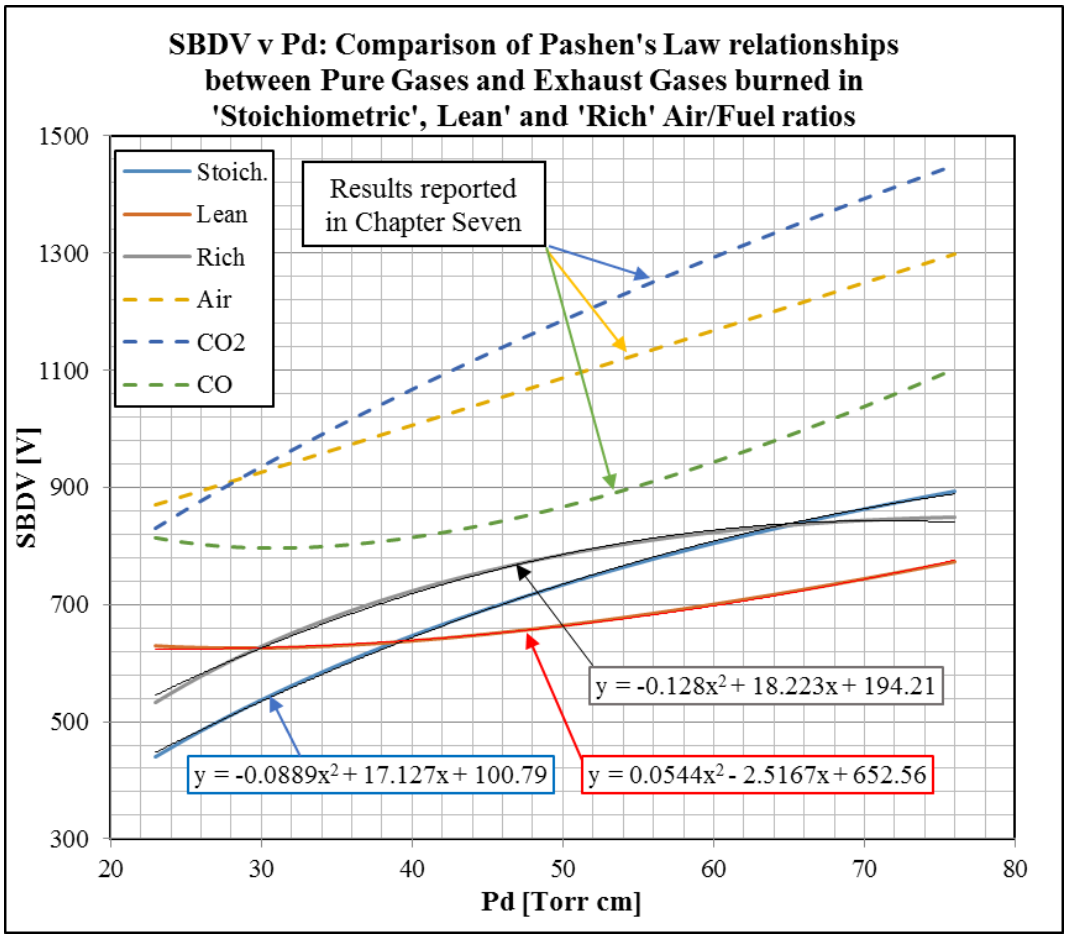

Figure F8-8: Comparison SBDVp vs Pd for different gases and Exhaust Gases

8.3.5 SUMMARY OF RESULTS FROM QUASI-STATIC TESTS

The absence of simultaneous plots of SBDV and Pressure across all pressures restricts the accurate mathematic expressions which could be derived from the data. The most accurate, according to applied regression analysis, being that for exhaust gases resulting from combustion in 'Stoichiometric' conditions. The derived expressions for exhaust gases resulting from combustion in 'Rich' conditions are less accurate. That for exhaust gases resulting from combustion in 'Lean' conditions cannot be applied with confidence. However, in the absence of more accurate values the derived mathematical expressions were used as calibration values for subsequent tests to derive comparative cyclic cylinder exhaust contents described in Chapter Nine.

The plotted relationships for SBDV in exhaust gases burned in all Air/Fuel conditions and at all pressures is significantly lower than those for pure gases. This indicates the breakdown event occurs more readily in burned mixtures of pure gases. The most likely reason for this being the residual ionization which would be present in burned gases. It appears that although the level of ionization would not be used for ionization control feedback there is still sufficient effect to influence breakdown. This effect may be increased due to the AC shuttling effect discussed previously (in chapter four), where the ions between the spark plug electrodes are retained as the voltage direction changes.

All the combusted gases will contain significantly reduced Oxygen (O_2) levels although about 0.5% remains, irrespective of the Air/Fuel ratio (Hamamoto, 1971). Oxygen is a strongly electronegative gas the presence of which increases the rate of ion re-combination. The absence of this gas in the exhaust gas mixtures will lead to the retention of ions for longer and therefore render breakdown at lower voltages.

The plotted values for exhaust gases burned in Stoichiometric conditions appears to show the influence of the largest amount of CO_2 which would be present in the three exhaust gases. The SBDV values which were obtained in the larger range of pressures provided the most inclined linear relationship. The trend of the relationship for Stoichiometric exhaust gas is similar for CO_2 shown as a Pashen's Law relationship in Figure F8-8.

8.4 MOTORED SBDV EXHAUST GAS TESTS

The second series of tests to obtain spark break-down voltages for different exhaust gases at different pressures was also carried out using the 'Rotax Senior Max' test engine as shown in Figure F4-28. The purposely manufactured motored test apparatus described in Chapter Four was utilised for these tests. To minimise unnecessary variable effects, the test engine was motored using the 7hp AC electric motor and held stable at 2500rpm for all tests.

The objective of this series being to determine if SBDV signals could be obtained for a wide range of Air and Exhaust gas mixtures delivered into the motored test engine and the differing amounts of residual exhaust gas in the cylinder determined.

A 40cc 'Origami B1' engine as shown in Figures F4-29 & 30, was used as an auxiliary engine to provide various amounts of burned exhaust gas into the test engine intake system. The Auxiliary engine was retro-fitted with a 'Tillotson' carburettor, shown in Figure F4-31, which features two external fuel jets, one for 'Low' speed and one for 'High' speed running but which in practice these influences overlap. The jets were adjusted as tabulated to provide 'Lean', 'Stoichiometric' and 'Rich' Air/Fuel ratios to the burned gases provided to the test engine. The exhaust gas from the 'auxiliary' engine was connected into the intake system immediately downstream of the butterfly throttle valve described above. The Air/Fuel ratio burnt in the auxiliary engine and therefore supplied to the intake system of the test engine could be varied.

The supply of different mixtures of Air and Exhaust gases to the test engine was achieved using the separate flow controls for each as described in section 4.16. The Butterfly Air inlet valve, was adjusted manually to five different angular (opening) positions, from fully open to fully closed. The associated exhaust gas isolation valve as shown in Figure F4-35 was adjusted for each test. The effect of these adjustments is described in detail below in section 8.6.1 and the associated test schedule is given in Table T8-1.

When motored with the standard compression ratio, the gas pressure in the cylinder would reach approximately 10 Bar. However, the static pressure calibrations had shown the SBDV system to provide a stable signal only up to a maximum of 3 Bar which varied depending upon the gas tested. This nominal operational limit was sufficient to provide information during the first 10 Degrees of closed cycle compression shown in Figure F9-15. However, for the present work, it was preferred to maximise the range of operation over which the relationship between pressure and SBDV could be achieved. This could be achieved in a

non-firing engine by increasing the clearance volume and hence reduce the maximum motored cylinder pressure. Then the SBDV signal would be extended over a wider crankshaft rotation angle and be more consistent and extended over a greater period. Therefore, a 13.0mm spacer between the top of the cylinder and cylinder head was installed. This option was only possible because the engine was motored and not fired. During these tests, the maximum cylinder pressure obtained was approximately 7 Bar. The 0 - 7 Bar 'Optrand' pressure sensor was used for all the tests described in this chapter.

The SBDV circuit was connected to the engine together with the PICOSCOPE and other instrumentation. The SBDV circuit was powered by a stand-alone power supply to avoid variations during testing. The electrical supply was set at 15.0 Volts. The electrical power drawn by the SBDV circuit varied, as drawn, between 1.9 and 2.2 Amps.

Previous investigations had shown the SBDV signal obtained from a spark plug is affected by gas turbulence. The improved signal stability of the shrouded plug compared with conventional types had been demonstrated. Therefore, to minimise these effects on the spark breakdown signal the shrouded plug was used.

8.6.1 LIST OF MOTORED TESTS

Using the test arrangement described above, a series of 20 individual tests as shown in Table T8-1 were carried out. The Air/Fuel ratio was not measured for any of these tests but was 'assessed' by comparison of the relative air and exhaust valve opening. The tabulated carburettor settings were considered to represent 'Lean', Stoichiometric' and 'Rich' mixtures of Air and Exhaust gases of various concentrations. The testing carried out was to evaluate the responsiveness of SBDV to a wide range of Air/Fuel ratio and residual exhaust gas cylinder contents. Irrespective of the accuracy of the settings and the inability to assign actual chemistry values the 20 tests were considered to represent a very wide range of operating engine cylinder contents. The results from five tests were selected and are presented in Figure F8-12. These tests were selected to represent the range of results. Due to the testing methodology, the gases represented the greatest proportion of exhaust gas burned with 'Richest' Air/Fuel ratio to smallest proportion of exhaust gas burned with 'Leanest' Air- Fuel ratio.

In summary, the relative fuel settings thus considered to be represented were:

A) The ‘Lean’ value being a combination of the ‘Lean’ mixture of the burnt exhaust gas and the largest Air valve opening. This would represent the cylinder contents with very little residual exhaust gas. Fuel adjustment with which the Auxiliary engine would just run and was difficult to start.
B) The ‘Rich’ value being a combination of ‘Rich’ mixture of burned exhaust gas with the Inlet Air Valve closed (allowing on exhaust gas into the motored engine). This would represent the cylinder contents full of residual exhaust gas running with ‘Rich’ Air/Fuel ratio settings. Fuel adjustment which was at the limit of stability and close to Four Stroking.
C) The ‘Stoichiometric’ being a combination of some residual burnt exhaust gas resulting from combustion with the most powerful engine settings but a large proportion of fresh charge. Fuel adjustment where by experience the Auxiliary engine ran most strongly.

Table T8-1: Tests of Exhaust Gases: Range between 100% – 0% exhaust gas burned using 'Rich' to 'Lean' Air/Fuel ratios

TEST NUMBER	AIR INLET VALVE POSITION	EXHAUST INLET VALVE POSITION	AUXILIARY ENGINE CARBURETTOR SETTINGS		ASSIGNED COMBINATION FACTOR (RICH: RED)	SELECTED FOR FFT COMPARISON (Figure F8-10)
			LOW SPEED	HIGH SPEED		
001	1 (OPEN)	FULL OPEN	3/4 TURN OPEN	3 1/4 TURNS OPEN	5	
002	2	FULL OPEN	3/4 TURN OPEN	3 1/4 TURNS OPEN	6	
003	3	FULL OPEN	3/4 TURN OPEN	3 1/4 TURNS OPEN	7	
004	4	FULL OPEN	3/4 TURN OPEN	3 1/4 TURNS OPEN	8	
005	5 (CLOSED)	FULL OPEN	3/4 TURN OPEN	3 1/4 TURNS OPEN	10	√
006	1 (OPEN)	1/2 OPEN	3/4 TURN OPEN	3 1/4 TURNS OPEN	3	
007	2	1/2 OPEN	3/4 TURN OPEN	3 1/4 TURNS OPEN	4	√
008	3	1/2 OPEN	3/4 TURN OPEN	3 1/4 TURNS OPEN	5	
009	4	1/2 OPEN	3/4 TURN OPEN	3 1/4 TURNS OPEN	6	√
010	5 (CLOSED)	1/2 OPEN	3/4 TURN OPEN	3 1/4 TURNS OPEN	7	
016	1 (OPEN)	FULL OPEN	1/2 TURN OPEN	1 TURN OPEN	2	√
017	2	FULL OPEN	1/2 TURN OPEN	1 TURN OPEN	3	
018	3	FULL OPEN	1/2 TURN OPEN	1 TURN OPEN	4	
019	4	FULL OPEN	1/2 TURN OPEN	1 TURN OPEN	5	
020	5 (CLOSED)	FULL OPEN	1/2 TURN OPEN	1 TURN OPEN	6	
021	1 (OPEN)	1/2 OPEN	1/2 TURN OPEN	1 TURN OPEN	1	√
022	2	1/2 OPEN	1/2 TURN OPEN	1 TURN OPEN	2	
023	3	1/2 OPEN	1/2 TURN OPEN	1 TURN OPEN	3	
024	4	1/2 OPEN	1/2 TURN OPEN	1 TURN OPEN	4	
025	5 (CLOSED)	1/2 OPEN	1/2 TURN OPEN	1 TURN OPEN	5	

8.5 SPARK BREAKDOWN IN EXHAUST GASES

In Chapters Six and Seven the effect of pure gases on spark breakdown characteristics across the electrodes was investigated. This was displayed in signature SBDV Distribution Curves which constitute approximately 20,000 individual repetitions of spark breakdown recorded on a 0.2 second period. These curves have been shown to respond to changes in individual electrode configurations and condition, gas species and pressure. Two SBDV Distribution Curves are shown in Figure F8-9 which were both recorded using the 'R10' spark plug at ambient pressure and temperature therefore display results related to gas species only. The exhaust gas sampled was burned in a Stoichiometric Air/Fuel ratio. These results show that sparking events in exhaust gases are likely to be inherently more consistent than in Air. The significantly lower comparable breakdown voltage recorded confirms the results shown in Figure F8-9. This is thought to be due to the significant reduction of Oxygen and increased presence of residual ions in combusted gases. SBDV curves for Air at increasing pressure were presented in Chapter Five. Similar curves have not been found during the literature review for the current work.

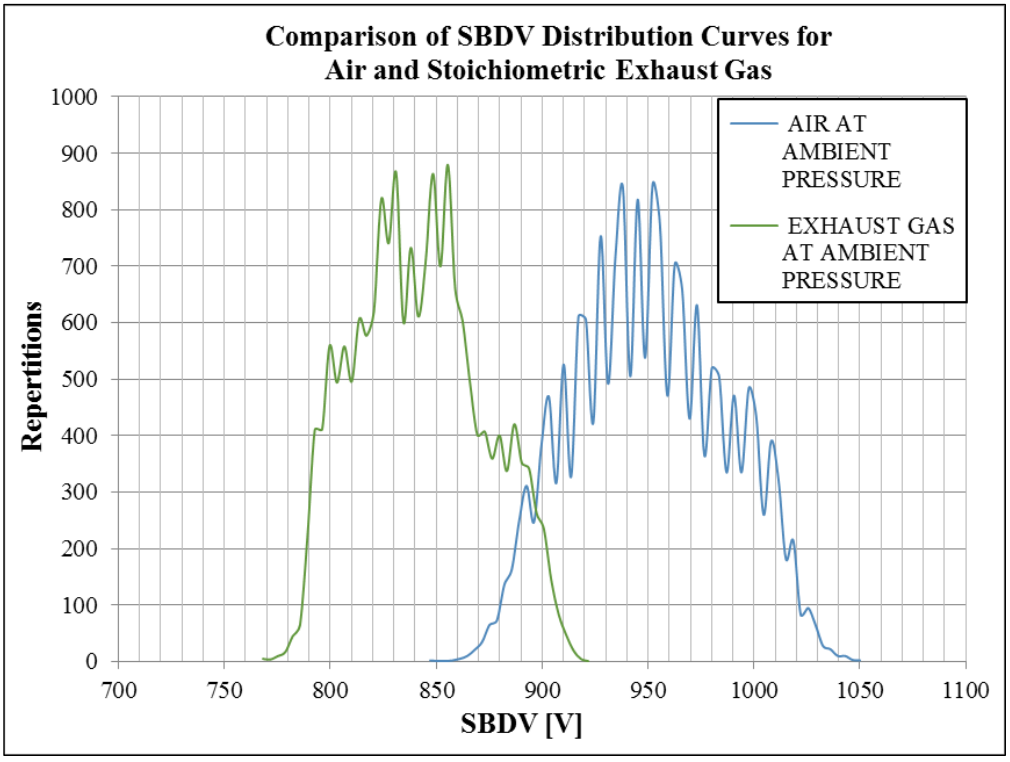

Figure F8-9: SBDV Distribution Curves for Air and Exhaust Gas

8.6 SBDV SIGNATURE IDENTIFICATION OF EXHAUST GASES

The individual spark breakdown events generated in air and other test gases were shown in Chapter Seven and mathematical relationships were proposed. Although the results showed varying levels of confidence, it was noted these relationships are different for each gas and change almost linearly in response gas to pressure. It was proposed the voltage profiles of these events could be used to represent a signature for each gas. This proposal assumed the same spark plug is used as differences in the profiles of each gas obtained at the same pressure were found for different spark plugs. If a similar analysis method could be used to identify differences in exhaust gases this could be used as a key aspect to cycle by cycle control. This was investigated using two different approaches and the results from the three 'hand cranked' and the 20 motored tests reported previously in this chapter.

8.6.1 COMPARISON OF INDIVIDUAL SPARK BREAK-DOWN EVENTS

Examples of four individual spark breakdown events using the 'R10' spark plug, recorded in Exhaust gases, at ambient pressure and temperature, burned in 'Lean', 'Stoichiometric' and 'Rich' Air/Fuel ratios are shown in Figure F8-10. These events were extracted from the 'Picoscope' recordings of the hand cranked tests reported in section 8.4. These events display variations similar with those in pure gases which were subjected to FFT analysis in Chapter Seven. This similar behaviour is not perhaps a surprise as the individual gases present in the exhaust gas mixtures change as previously introduced in Chapter Two. Variations of O_2, CO_2 and CO would be expected to be displayed in the signals of individual SBDV events. However, the largest variation is apparent in the recorded SBDV profile for 'Lean' Exhaust gas. This shows a very similar characteristic as that recorded for pure Nitrogen (N_2) in Figure F7-21. Noting that both of these SBDV events were obtained using the same spark plug. It is considered this could be a response to the presence of NOx as this is produced in Lean combustion conditions.

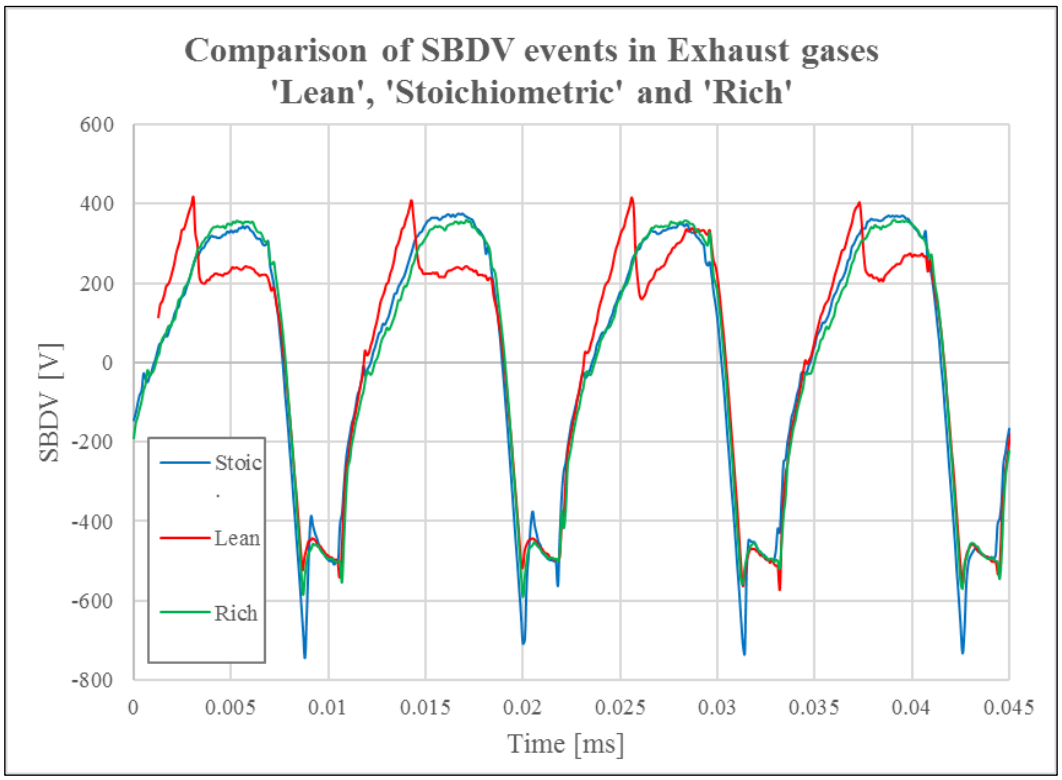

Figure F8-10: Comparison of SBDV events in Exhaust Gases

8.6.2 MOTORED FFT ANALYSIS

For practical application in an operating engine, differences in trapped exhaust gas mixtures require identification in dynamically changing conditions. Five of the tests described in section 8.6.1 and listed in Table T8-1, were assigned between a notional range between 1-10. Within this range '1' being very lean 'LEAN' and 10 being 'RICH'. The signals from three additional tests which were considered notionally representative of mid - range conditions between 'Lean' and 'Rich' (1 - 10) were also selected. Thus, the SBDV signals from tests 005, 007, 009, 016 and 021 selected to represent a wide range of residual exhaust gas mixtures.

From each test selected, a sample period of 10 ms of SBDV signal was randomly selected for FFT analysis using a 'Matlab' code. This code would apply the 'PWELCH' function to create Power Spectral Density curves. These curves represent the combination of individual frequencies which constitute the signature characteristic of individual exhaust gases and concentration mixtures with air. A time-period of 10ms represents approximately 10

Degrees of crankshaft rotation and this time period would have to be reduced with increasing engine speed.

To limit the numerical amplitude of a FFT graphical output a maximum SBDV signal sample time of one millisecond was considered sufficient to produce a representative sample. This signal is unaffected by pressure change and could be extracted for SBDV signals from any sample period and any pressure variation. As a period of 10 ms was used, the 'Matlab' code separated the 10 ms signal into ten separate periods of 1 millisecond. Therefore, the power spectral densities calculated represented a 1ms sample of SBDV signal which is an average of 10 individual periods of 1ms samples. The results from the five separate tests of exhaust gases is shown in Figure F8-11.

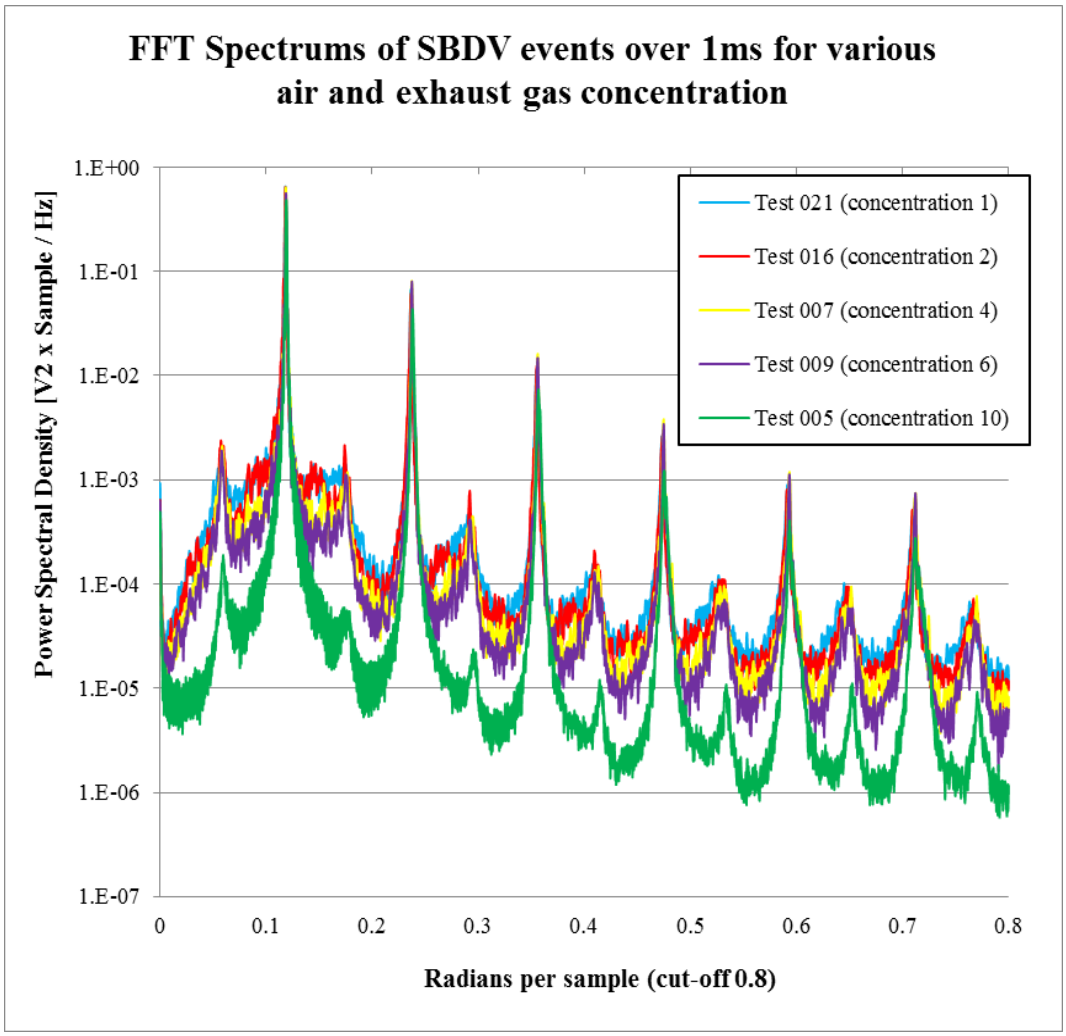

Figure F8-11: An overlay of Power Spectral Density Spectrums
(Showing the effect of exhaust gas proportions and Air/Fuel ratios)

Visual inspection of the individual, overlaid Power Spectral Density PSD curves in Figure F8-11 were considered to show a direct relationship to Exhaust gas concentration. The logarithm base of the vertical graph axis indicated the actual difference between the overlaid signals would be more pronounced than shown. To investigate this relationship in more detail, a further analysis was carried out which calculated the area under the individual PSD curves. The results of the five calculations are presented in Figure F8-12. As described previously in section 8.6.1, the results from the five calculations represent a very wide range of exhaust gas to air proportions burned using very wide Air/Fuel ratios. The relationship between these shown in Figure F8-12 shows a closely linear relationship. This is not an unreasonable result when considering that spark breakdown voltage varies proportionally to gas density. Therefore, it is assumed the density of the exhaust gas varies in proportion to the density of the gases remaining after combustion. Gas density varies with gas temperature and this may be thought to be responsible for the uniformity of plotted results. However, the testing method and apparatus used, which incorporated a gas path with a large heat sink, was intended to deliver exhaust gases at uniform temperature.

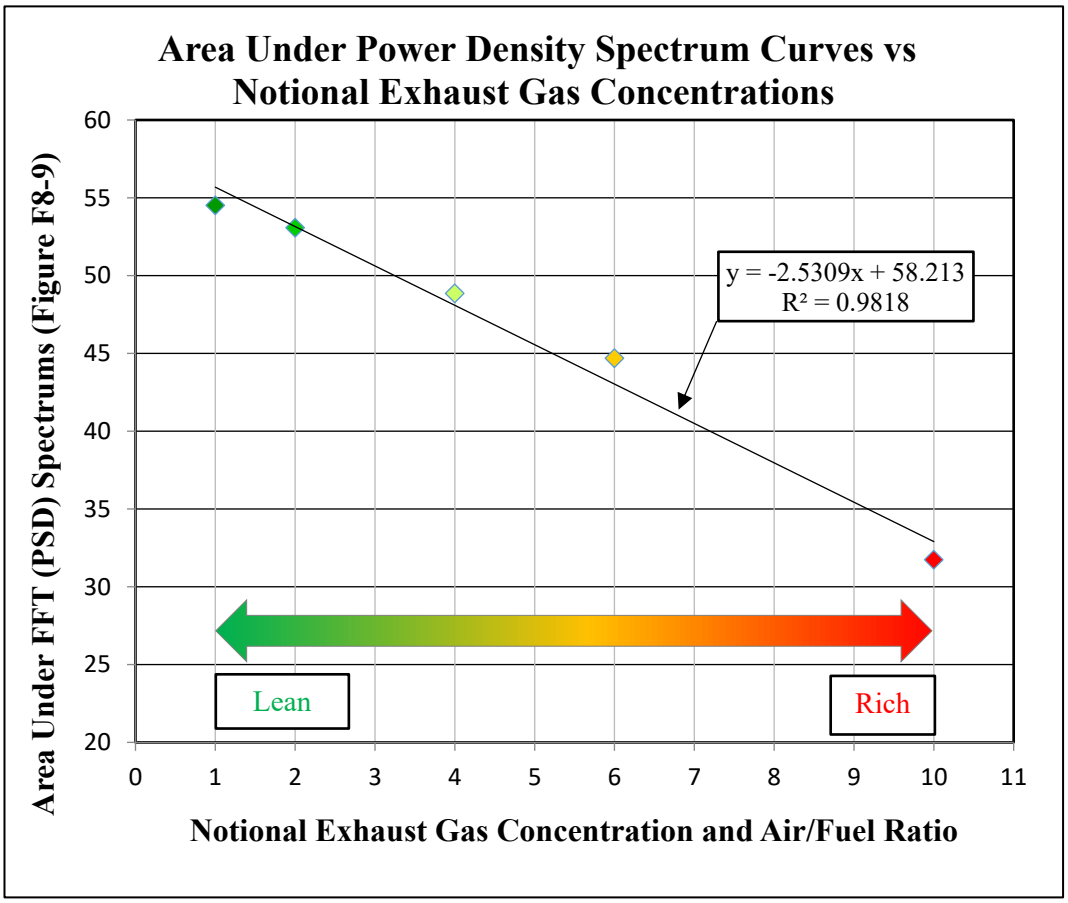

Figure F8-12: Area Under FFT spectrums vs Notional Air/Fuel Ratio
(Ref. Table T8-1 & Figure F8-11)

8.7 CHAPTER SUMMARY

This Chapter reported on two series of tests which were carried out to investigate SBDV behaviour in a wide range of Exhaust Gases burned in Air/Fuel ratios and mixtures of different concentrations of those gases with Air. The tests were carried out in both Quasi-Static and Motored conditions. Both series of tests were carried out using the Rotax Senior Max test engine which ensured the test surroundings were duplicated for both series of tests.

The results of the quasi-static 'hand cranked' tests enabled mathematical expressions between SBDV and pressure for exhaust gases burned respectively in 'Lean', 'Stoichiometric' and 'Rich' conditions. The accuracy of the mathematical expression for 'Stoichiometric' conditions can be more confidently assumed correct than those for' Rich' and 'Lean' conditions due to the gaps in data plots for those gases.

The second series of tests used a motored engine supplied with a range of different Exhaust gases burned in Air/Fuel ratios and mixtures of different concentrations of those gases with Air. It was found that the signature profiles of the SBDV events varied with Air/Fuel ratio similarly to those for the different pure gases reported in Chapter Seven. Additionally, the Spark Distribution Curves introduced in the present work were found to vary in Air and Exhaust gas. The signature SBDV profile for exhaust gas burned in a 'Lean' mixture displayed characteristics similarly to those in pure Nitrogen (N_2). It was considered this may be an indication of a significant presence of NOx which is formed in such combustion conditions (Watson, et al., 1976).

The gas mixtures from five different tests, were evaluated using FFT analysis to investigate the frequencies constituted in SBDV events for each gas. The gases which were evaluated were selected from a manual grading of burned Air/Fuel ratio and mixture combination in Air listed in Table T8-2. This represents the range between very 'Lean' hence diluted with large proportions of Air, through to very 'Rich' with no dilution in Air. The results of these evaluations were plotted in Figure F8-12 and found to display a very closely linear relationship.

CHAPTER NINE

CYCLE BY CYCLE SBDV

9.0 INTRODUCTION

This chapter describes the testing carried out to investigate the capability of the SBDV system to differentiate between different gases in cyclic and dynamically changing conditions. This testing used and built on, the potential of SBDV to differentiate different gases including exhaust gases burned in a wide range of Air/Fuel ratios demonstrated previously in chapters seven and eight.

SBDV signals were obtained from continuous consecutive cycles using the new SBDV system from within a motored engine, not a fired engine using the apparatus described in chapter four.

Motored engine testing has been used by many researchers to simplify the extraction of specific effects such as gas flow (Semenow, 1963) and to evaluate two-stroke engine scavenging efficiency (Ku & Trimble, 1956). The use of a motored engine cycle to investigate the period of compression prior to ignition initiation avoids the complications arising from an operating engine and when evaluation of combustion is not required. As combustion was avoided the effect of temperature variations in the engine was not considered as even in an operating engine heat transfer and heat release varies cycle by cycle and variations of gross heat release rate, by about a factor of 2 it can be largely ignored (Woschni, 1967), (Brunt & Emtage, 1998). Further, whether actual heat transfer rates match calculated values is unclear (Gatowski, et al., 1984). It was therefore considered valid for the cyclic pressure changes in a motored engine during initial compression to be experimentally representative of those which would occur in a fired engine.

An additional benefit of using a non-firing engine was that the compression ratio of the engine could be reduced. Subsequently, for all the cycle by cycle SBDV tests a 13.0mm thick spacer between the top of the cylinder and cylinder head was used. This enabled the range of crankshaft rotational positions for which SBDV signals could be obtained to be extended as described in section 9.3.2.

Initially, an example is presented in Figure F9-1, which shows cyclic SBDV signal behaviour through nine consecutive motored cycles. A more detailed view is shown in

Figure F9-2 in which it can be seen how the signals vary for each cycle especially during the scavenge phase when gas exchange occurs in the cylinder.

In section 9.2, SBDV signals recorded for nine consecutive complete cycles of motored operation are shown. For each cycle, the equivalent pressure calculated by the conversion of SBDV signals, which would occur for Air and three different exhaust gases are shown. The SBDV signal was converted to pressure for Air and Exhaust gases using the calibration values determined by 'Quasi-Static testing reported in Chapter Eight. Finally, the SBDV signals from the same nine cycles but limited to the crankshaft rotation period around immediately following the closed compression cycle are presented with comments.

9.1 CONTINUOUS CONSECUTIVE CYCLIC SBDV SIGNALS

An example of nine cycles of SBDV signal (Grey) and simultaneously recorded cylinder pressure signal (Green) for a typical motored engine test is presented in Figure F9-1. This is included for general discussion of the capability of the new SBDV as a method to identify aspects of engine characteristics which currently cannot be investigated practically outside of an engine test cell. The SBDV signal and how this relates to pressure has been explained in previous Chapters. The Red horizontal line represents the approximate reliable upper voltage limit for the new SBDV system which in turn limits the range of crankshaft rotation period which can be investigated. This includes the period which concerns the objectives of this thesis but does not include the period of turbulent combustion.

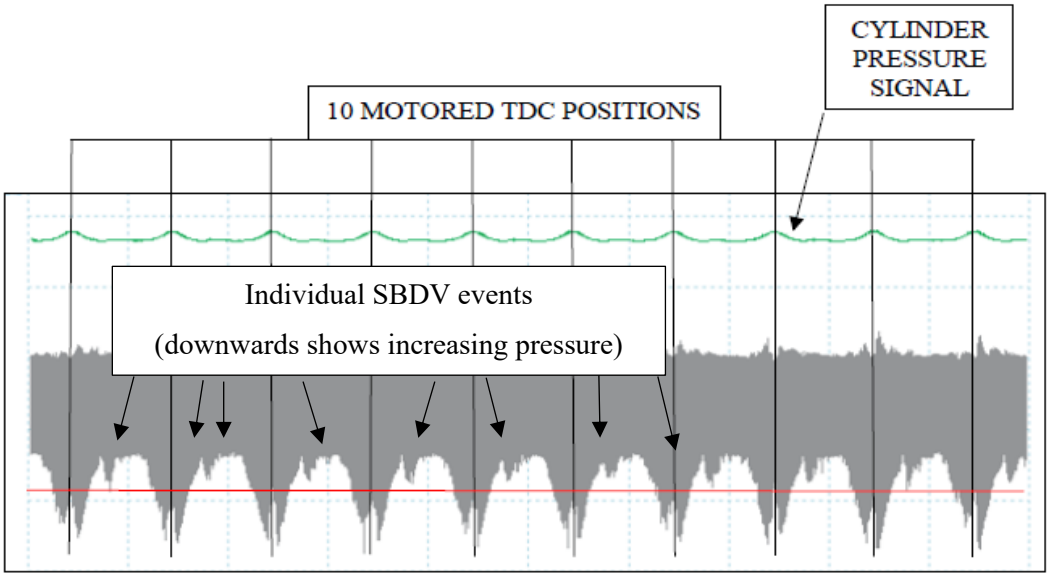

Figure F9-1: SBDV and Pressure signals of Nine Consecutive Motored Engine Cycles

Figure F9-2 shows the SBDV signal in greater detail for four of the ten cycles. Notations indicate the separate phases of engine operation and the approximate positions of Exhaust and Transfer port opening and closing for one cycle. Three of the cycles are notated to highlight the gas exchange period of each cycle. The SBDV shows different profiles over this period for each separate cycle. Reference to Figure F9-1 confirms this behaviour which was clearly apparent in every test carried out.

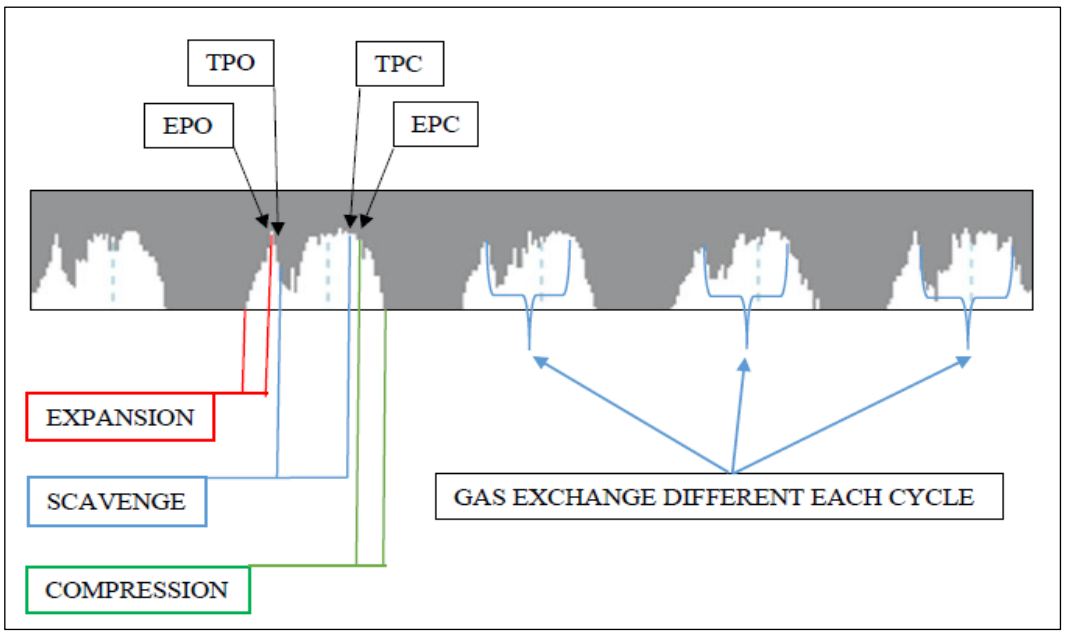

Figure F9-2: Cyclic SBDV signals.

(Note: Cyclic variations occur in each scavenge period during which gases exchange)

To confirm the SBDV signal in this region shows a response to gas exchange, a test was devised in which the exhaust port of the test engine was closed, using a butterfly valve, as shown in Figure F4-28 while the test engine was motored. The closure of this valve prevented any flow of gas through the engine such that no gases could be exchanged in the cylinder. The SBDV signal of one ‘CLOSED’ engine test is shown in Figure F9-3. Note, the pressure signal (Green) is at a larger amplification than shown in Figure F9-1. The comparative absence of SBDV variation in the period when gas exchange would occur in an ‘OPEN’ engine is apparent. The absence of flow into and thus through the engine is confirmed by reference to the output of the two mass airflow sensors in the test engine inlet system (ref Figure F9-3). The signal for these can be seen to diminish over eight gas exchange periods. Careful inspection of the signal shows the simultaneous diminishing of any gas exchange activity with the inlet mass flow rate. Four individual tests were carried

out for Air and three exhaust gases. These tests are not included in full detail within the present work however, some points are included for comparison.

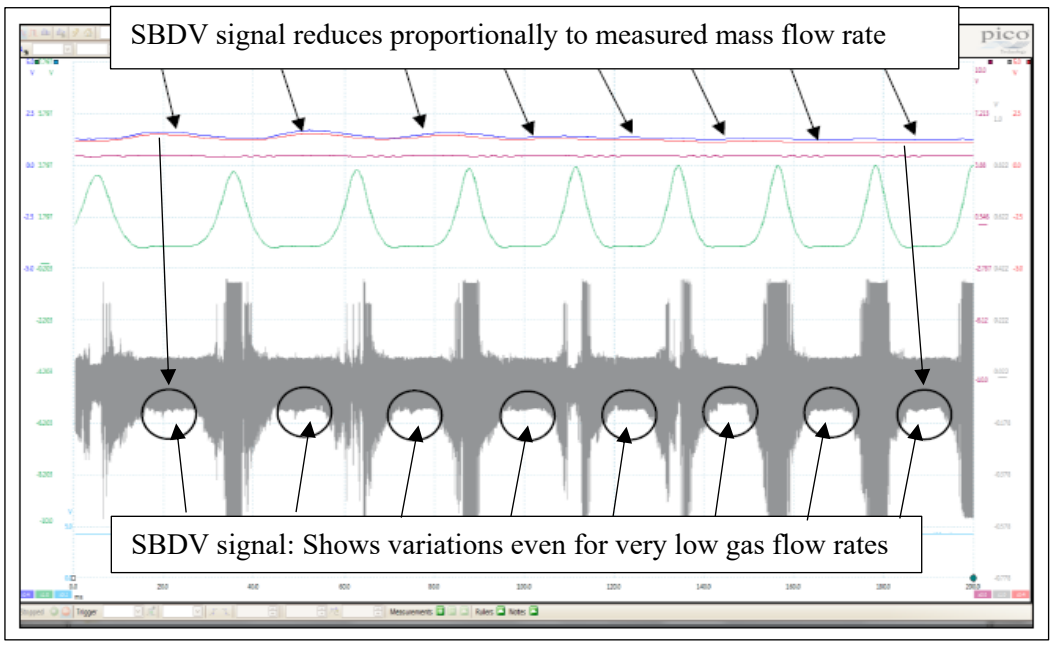

Figure F9-3: Cyclic SBDV signal with closed exhaust port.
(Note: No gas exchange during scavenging periods)

In summary, there is a considerable amount of information that could be interpreted from the SBDV signals. This especially includes the behaviour during the gas exchange period which clearly identifies varying cyclic behaviour. This could be cyclically determined for the first time, from the SBDV signals however, this is not included in the present work.

9.2 CYCLIC COMPARISON OF IN-CYLINDER GASES

Examples of nine motored engine cycles are presented below in Figures F9-4 to 12. These show continuous cycles of cylinder pressure, obtained from the OPTRAND pressure sensor and SBDV signals simultaneously recorded for test 002-16-06-2015.

The spark breakdown signal for each waveform sample was converted into an equivalent pressure using 'Matlab' following the process described previously in Chapter Four. The 'Direct' expressions derived from testing relating Pressure and equivalent SBDV for Air and three Exhaust gases previously described in Chapters Seven and Eight were utilised. However, these required to be transposed to provide an equivalent pressure from SBDV. The Direct and Transposed relationships used are provided in Table T9-1.

Table T9-1: Mathematical Relationships for Air and Exhaust Gases
(Burned in 'Lean', Stoichiometric' and 'Rich' Air/Fuel ratios)

Test	Gas	Direct Equation	Transposed Equation
	Air	SBDV = 161.16P + 663.69	P = 0.00786574(SBDV) - 3.12920383
009	'Lean' Exhaust Gas	SBDV = 59.571P + 554.02	P = 0.00879858(SBDV) - 4.06261432
007	'Stoichiometric' Exhaust Gas	SBDV = 166.05P + 351.47	P = 0.00537059(SBDV) – 1.59867601
011	'Rich' Exhaust Gas	SBDV = 122.22P + 488.47	P = 0.00677349(SBDV) – 2.93394473

The plots of Cycles 1 to 9, in Figures F9-4 to 12 below show the equivalent cylinder pressures for 'Air', 'Lean Exhaust', 'Stoichiometric Exhaust' and 'Rich Exhaust' gas converted from SBDV using the values obtained from the spark plug using the mathematical expressions shown in Table T9-1. Note, SBDV converted to pressure is designated with a 'p' suffix, hence SBDVp. The traces are plotted against cylinder pressure measured (Green trace) by the 0-7 Bar, 'Optrand' pressure sensor as recorded for each cycle. The equivalent pressure for each of the various gases are shown using different coloured traces as listed in the 'key' for each cycle. The equivalent pressures shown for each gas, assumes the same gas is transported throughout the engine during each of the nine cycles. This will not occur in an operating engine due to the gas exchange process. However, if the gas species were identified as presented and discussed in previous chapters the same process could be applied to generate variations in continuous one millisecond intervals although this was not included within the present work.

The cyclic plots presented thus include both the motored compression and expansion phases which are included to demonstrate the overall capabilities of the new SBDV system. The present work is only concerned with the initial stage of closed cycle compression which is discussed in section 9-3. However, as previously noted, a considerable amount of information is available from the SBDV signal through the expansion phase.

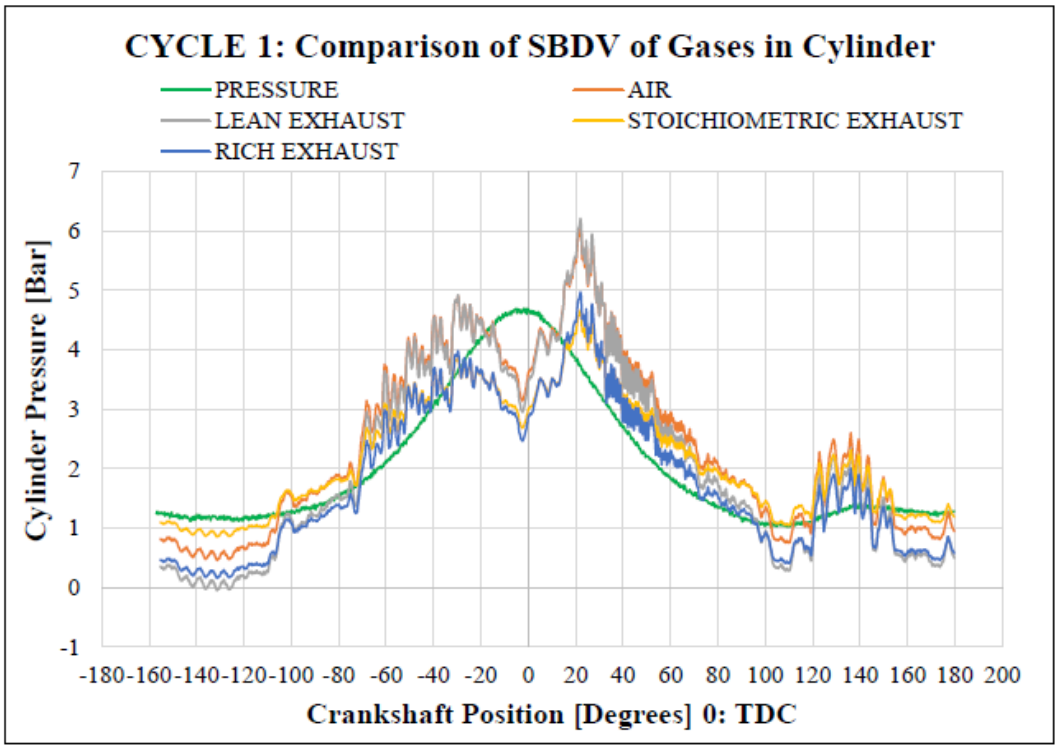

Figure F9-4: SBDVp vs Pressure: Test 002-16-06-2015 Cycle No. 1

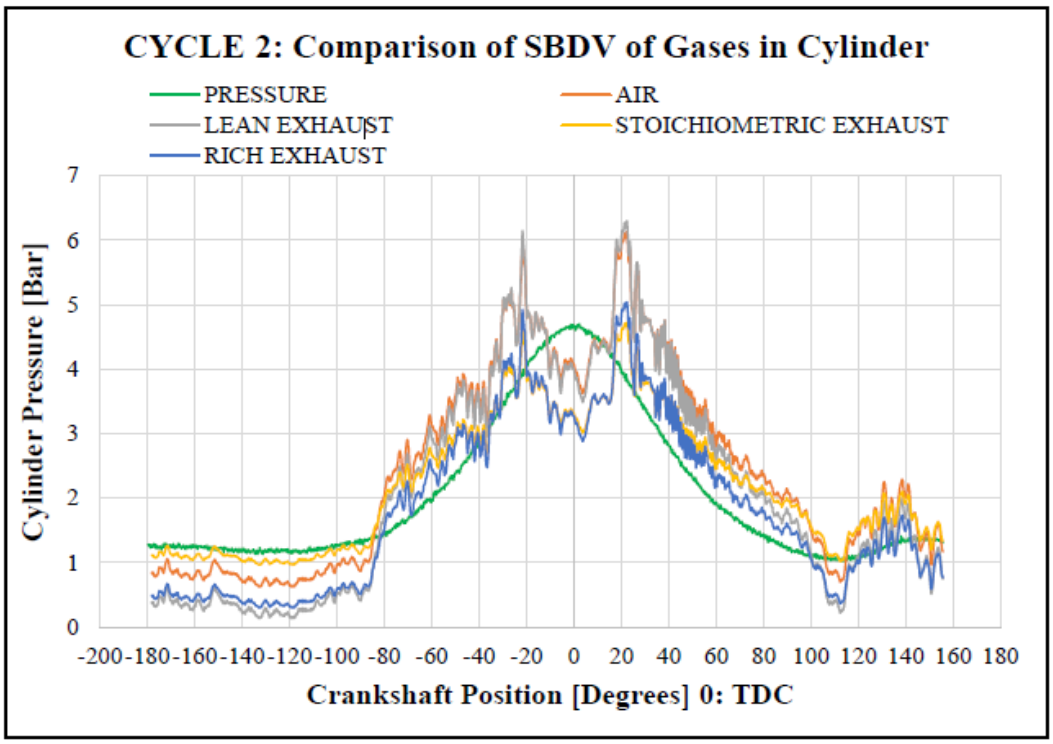

Figure F9-5: SBDVp vs Pressure: Test 002-16-06-2015 Cycle No. 2

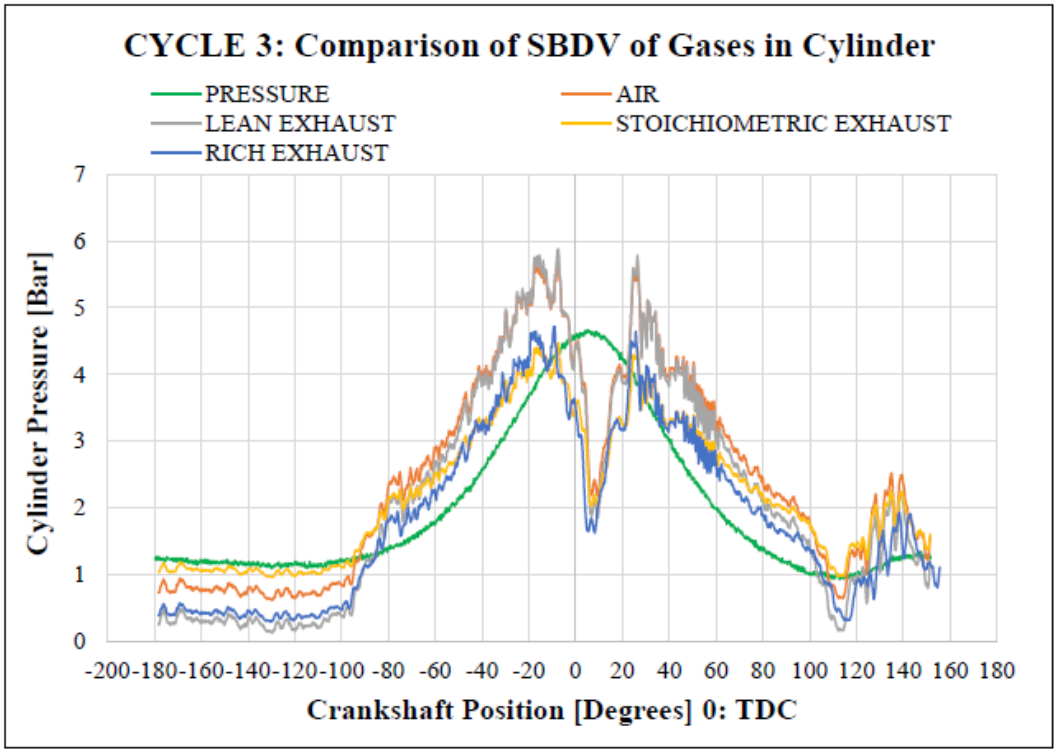

Figure F9-6: SBDVp vs Pressure: Test 002-16-06-2015 Cycle No. 3

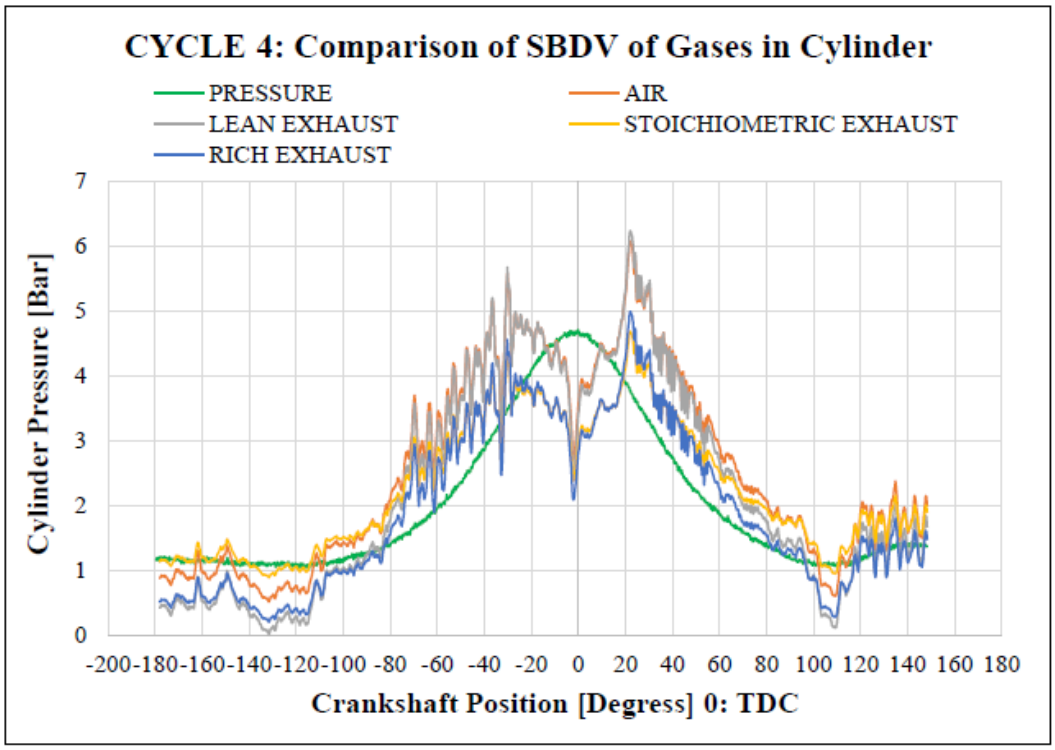

Figure F9-7: SBDVp vs Pressure: Test 002-16-06-2015 Cycle No. 4

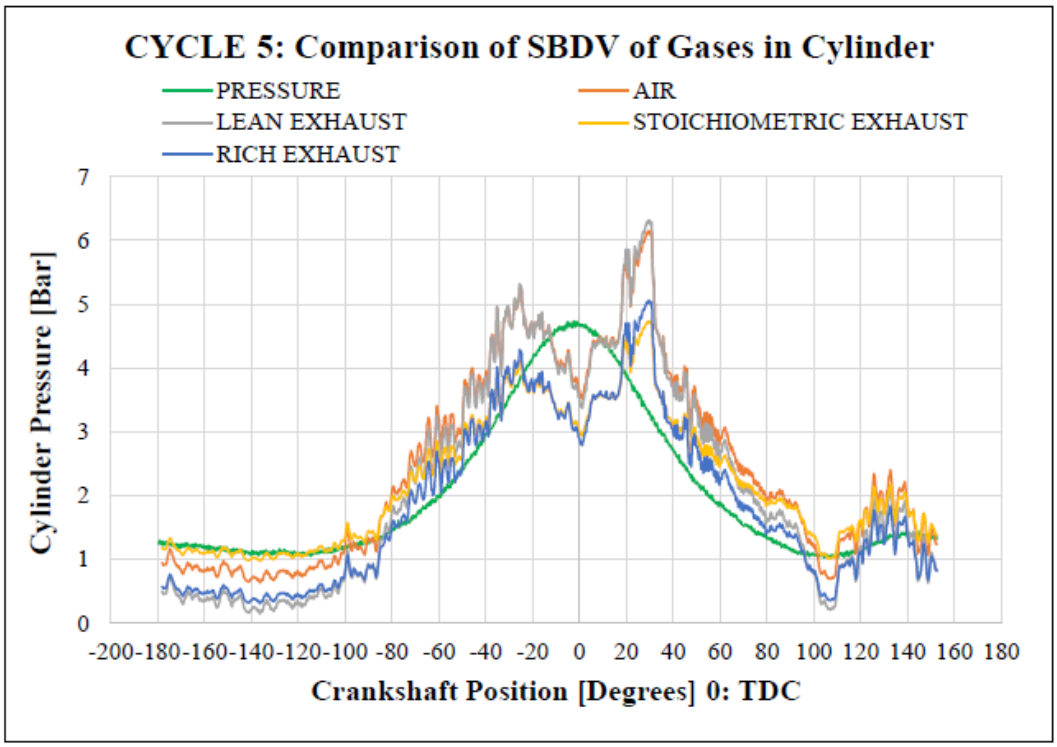

Figure F9-8: SBDVp vs Pressure: Test 002-16-06-2015 Cycle No. 5

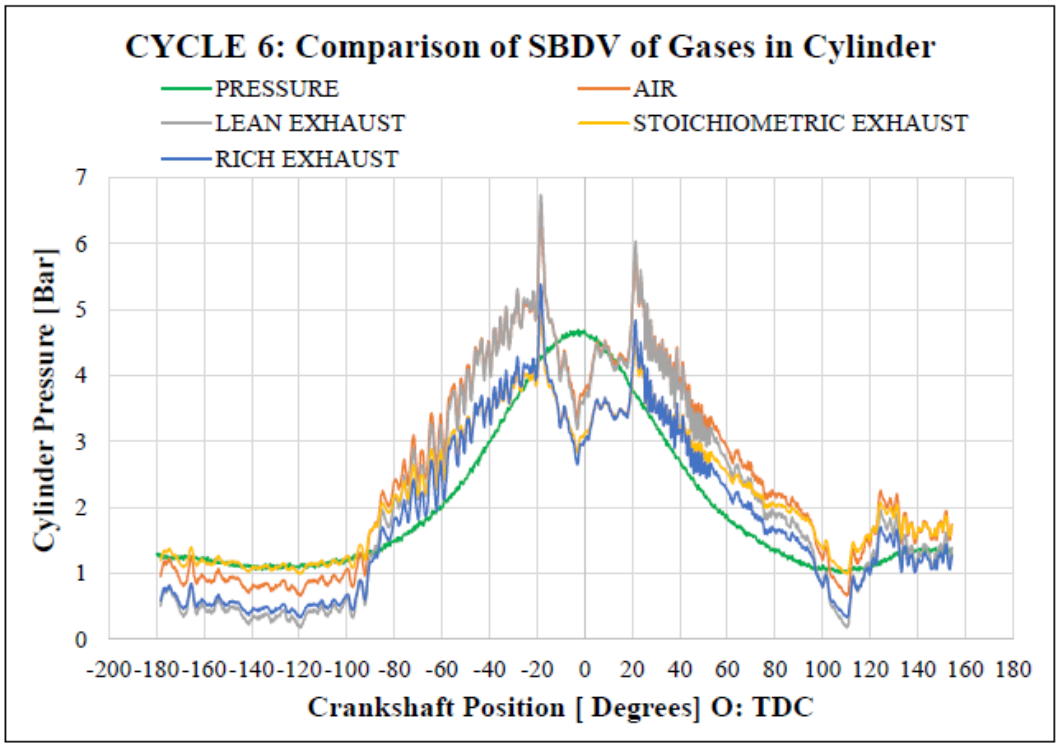

Figure F9-9: SBDVp vs Pressure: Test 002-16-06-2015 Cycle No. 6

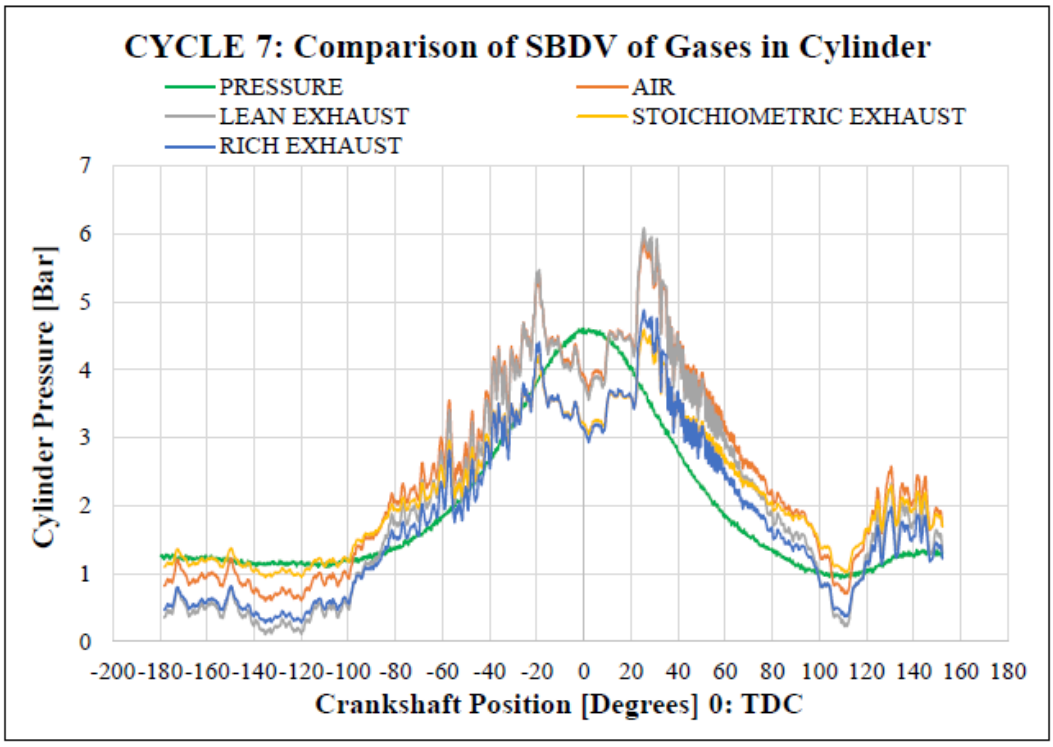

Figure F9-10: SBDVp vs Pressure: Test 002-16-06-2015 Cycle No. 7

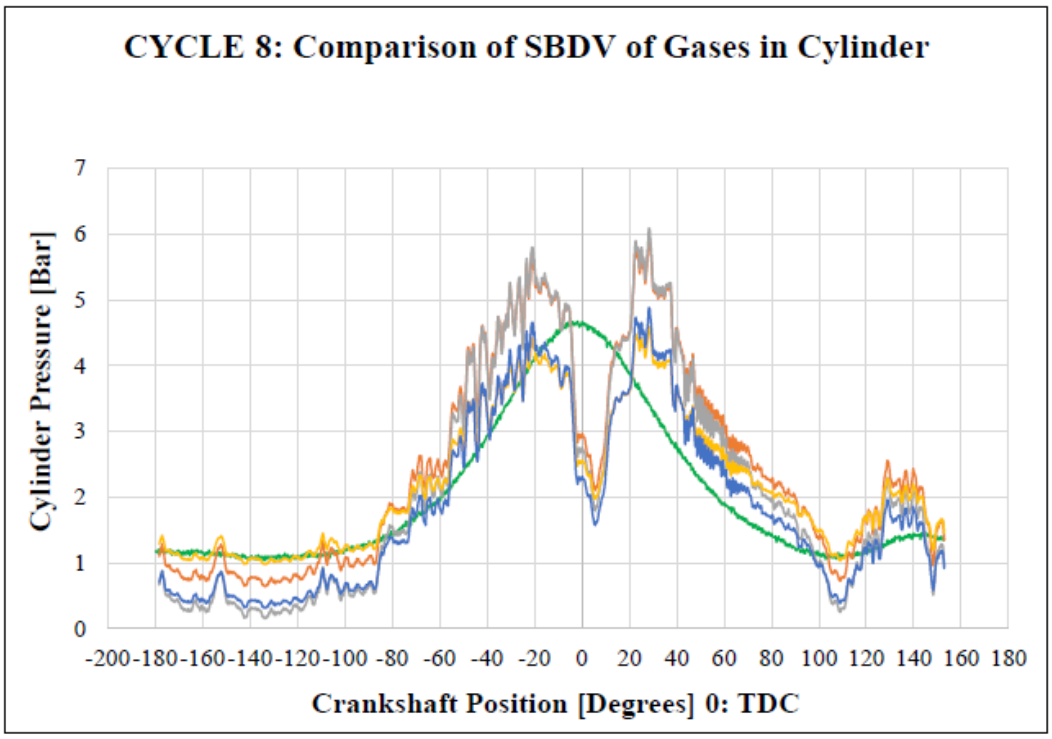

Figure F9-11: SBDVp vs Pressure: Test 002-16-06-2015 Cycle No. 8

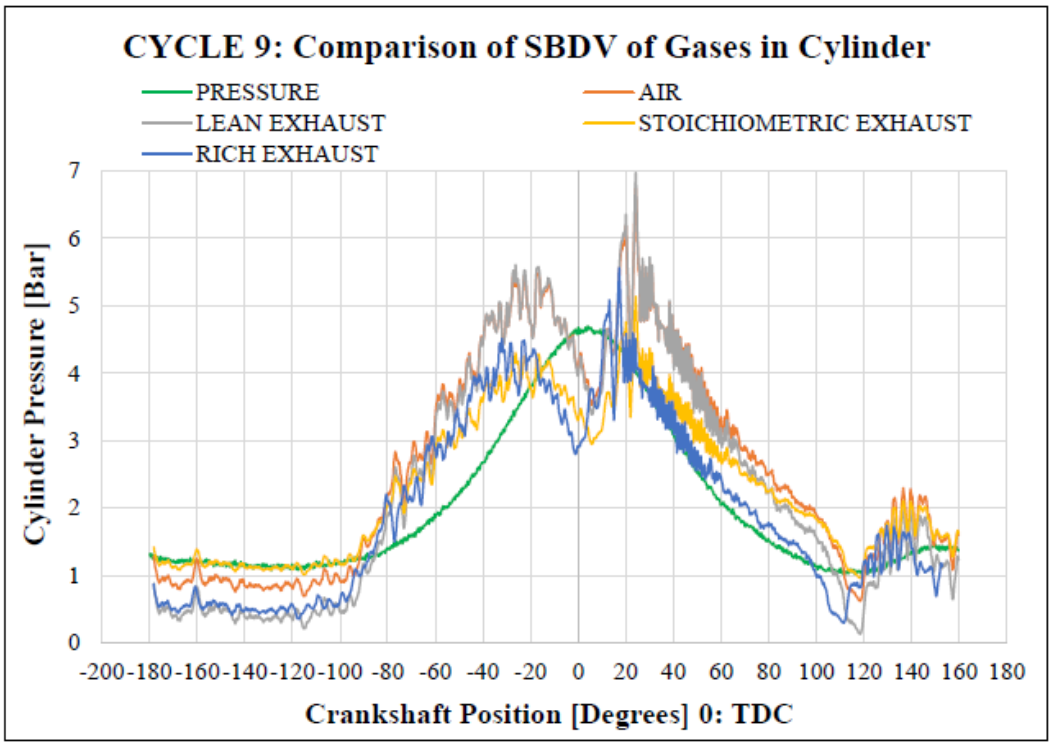

Figure F9-12: SBDVp vs Pressure: Test 002-16-06-2015 Cycle No. 9

The SBDV signals in Figure F9-4 to 12, for Air and the three Exhaust gases can be seen to vary significantly in comparison to the recorded cylinder pressure. Changes of slope in SBDV signal following exhaust port closure can be clearly identified. Although this position is obviously fixed by engine geometry the SBDV signals can be seen to change position from cycle to cycle.

This activity is due to the actual phasing of the pressure wave in the exhaust port. In the motored test engine, in which combustion is not occurring, and into which a fixed exhaust gas is supplied, the gas entering the engine each cycle will be very similar, to the existing gases trapped in the engine and resident in the exhaust pipe. Therefore, there will be expected for the changes of SBDV signals for the relative expressions air and three exhaust gases the four gases to response largely only due to pressure variations. These signals will also vary in response to the gas compressibility (factor Z) which are different for each gas and temperature change therefore, responding to changes in the 'Specific Heat' of the changing gases. The slope of the SBDV signal during the closed cycle would also be expected to vary cyclically and respond to the gas temperature and heat transfer with surrounding cylinder and piston wall surfaces as previously indicated in Figure F4-18.

The SBDV signals for all four gases in the cyclic plots presented above can be seen to become increasingly variable as compression pressure increases above around 2 Bar. The compression pressure and hence the crankshaft angle at which the SBDV signal displays increasingly variable behaviour is expected to increase if the generated spark voltage is raised. In an operating engine, the crankshaft angle and closed compression period is expected to be larger than in a motored engine as gas density is reduced due to the presence of combustion gases. These gases will be at higher temperatures than those in the non-firing, motored test engine used for these tests and it is therefore expected for the SBDV signal to be interrupted at a predetermined crankshaft position. This position would enable the required SBDV signal to be obtained reliably in all engine operating conditions as proposed in section 9.3.

The configuration of the 'Rotax Senior Max' test engine (MSA, 2011), incorporates a variable timing exhaust port. This feature is enabled by a retractable steel blade which has the effect of providing dual stage timing across the operational speed of the engine. This blade does not seal tightly against the piston or the sides of the exhaust port so gas leakage is inevitable. In an operating engine, this is not of significant consequence as the mass flow rate of gas out of the exhaust port is significantly larger than the potential leakage past the steel blade. However, in a motored engine this leakage confused the interpretation of cylinder pressure when closed compression begins due to the partial closure of the exhaust port of the exhaust valve. The closing timing points provided by the fixed steel blade and the following positive closing point provided by the roof of the exhaust port is shown in Figure F9-13. The exhaust valve can also be seen in the photograph looking down from the top of the cylinder bore in Figure F9-14. This shows the valve does not seal the exhaust port completely around the edges of the bore/port wall.

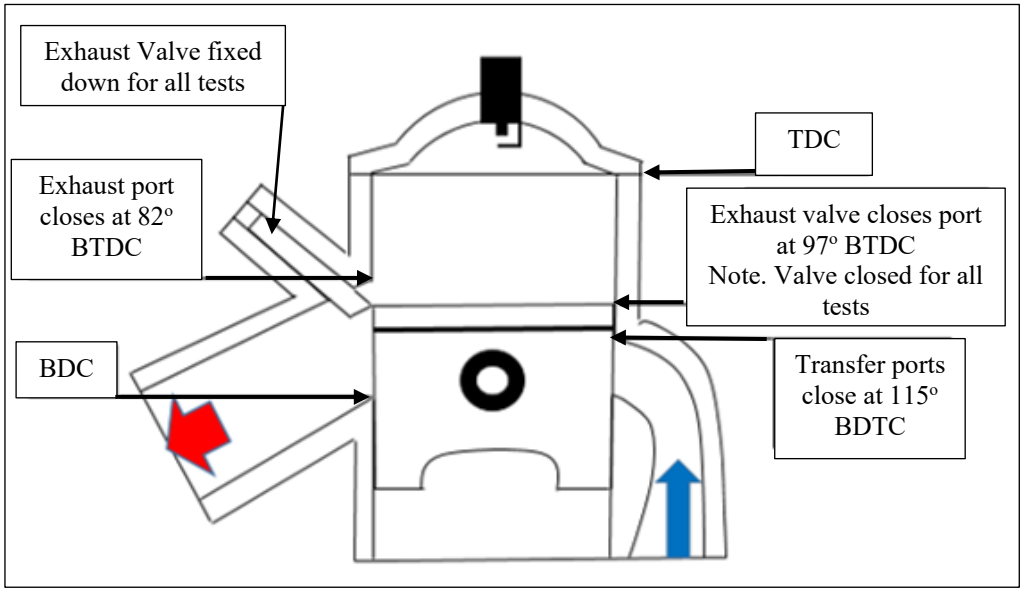

Figure F9-13: Diagram showing piston in cylinder and Port Timings

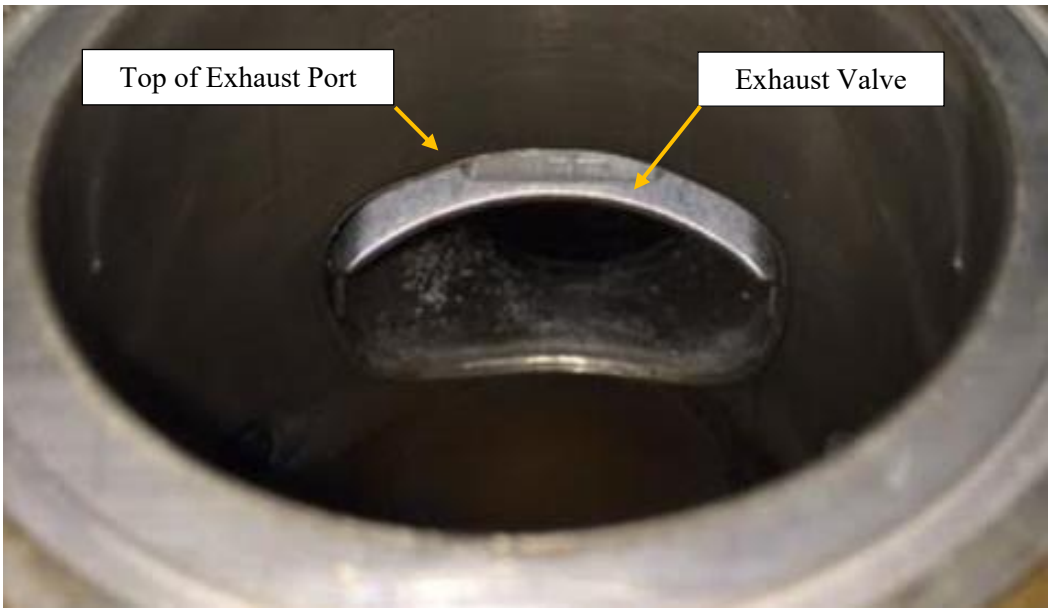

Figure F9-14: Photograph showing the exhaust valve in the exhaust port

9.3 SBDV DURING THE INITIAL STAGE OF COMPRESSION

The objectives of the present work require a practical method to determine the gas species present and in-cylinder pressure of an engine during the initial stages of compression. Consequently, this section focuses on the SBDV behaviour around and during that region

of crankshaft movement. The information presented was extracted from the complete cycle histories (1 to 9), shown in Figures F9-4 to 12.

Although the pressure in the cylinder can vary significantly due to combustion, the in-cylinder pressure variations during the initial stage of compression do not vary in proportion to combustion pressure and are small in comparison to that achieved during combustion (Heywood & Sher, 1999).

The cylinder pressure during initial stage of compression results from wave dynamics in the exhaust system and the crankcase/transfer ports. The wave pressures overlap but are not synchronised with the pressure resulting from the previous combustion. Therefore, there is no straightforward relationship between a preceding combustion event and cylinder pressure during the subsequent following early stage of compression. However, the gases exchanged while the exhaust and transfer ports are open vary with these overlapping pressures. Consequently, the in-cylinder pressure variations during the early stage of each compression contain considerable amounts of information as they respond to delivery ratio, trapping efficiency and pressure wave reflection effects (Blair, 1996). This is important as these pressure changes therefore relate directly to the mixture of gases trapped in the cylinder. These gases will vary each cycle and when compressed provide the charge for each combustion event. As the gases trapped in the cylinder contain different proportions of fresh and burned charge, gas pressure alone will not define the gases present. Additionally, the temperature of the trapped charge and thus it's density, will vary in proportion to the relative amounts of burned charge, which is hot, to fresh charge, which is cool. Similarly, the relative proportions of fresh and burned charge will vary the proportions of gas species present.

9.3.1 SBDV SAMPLING RATE

The exhaust port of a two-stroke cycle type engine typically closes between 90 to 80 Degrees BTDC. To allow sufficient time for calculation of fuel quantity, injection period and ignition initiation timing the period available for SBDV closed cycle sampling was proposed to be 10 Degrees of crankshaft rotation. To enable accurate sampling during this short period, it was considered SBDV events (hence individual samples) should be obtained as a minimum at every degree, hence giving a minimum of ten samples. This requirement was a fundamental aspect of setting the parameters of the SBDV system presented in this work. In review:

The SBDV system has a nominal frequency of 94 kHz which equates (as been seen previously) to provide a potential gas sample 94,000 times per second.

For realistic application in a high speed two-stroke cycle type engine a maximum working engine speed of 15,000 rpm should be considered. If the SBDV frequency is fixed the number of samples which can be obtained over a fixed crankshaft rotation period will decrease as engine rotational speed increases.

Thus: comparing the new SBDV system sampling speed of 94 kHz with the proposed engine speed of 15,000 rpm.

15,000 rpm represents 15000/60 = 250 crankshaft revolutions per second or

250*360 = 90,000 Degrees (of crankshaft revolution) per second.

If the SBDV sampling speed = 94,000 per second

A SBDV event will occur 90000/94000 = 0.957 of each degree of crankshaft revolution.

Therefore, during a 10 Degree period of rotation 10 / 0.957 = 10.449 SBDV sample (10) events would occur. This sample rate matches the procedure reported in Chapters Seven and Eight which was showed the sampling capability of the new SBDV system to identify the gas species or Air-Fuel ratio and gas concentration (Figure F8-12).

The number of SBDV sample events which occur at the engine speed of 2,500 rpm, at which the motored testing for the present was carried out is larger where:

Over a 10 Degree period of crankshaft revolution:

The number of SBDV sample points = 10.449 x 15000/2500 = 62.694

or one sample every 0.156 Degree or crankshaft rotation.

9.3.2 THE EFFECT OF THE SPACER TO REDUCE COMPRESSION RATIO

To maximise the range of crankshaft movement over which SBDV could be obtained for these motored tests the

The pressure in the cylinder of a motored engine changes primarily due to piston displacement which is a fixed geometric relationship. The absolute pressure in the cylinder

varies depending upon the ratio of swept volume to final trapped volume. This relationship is termed ‘the compression ratio’. If the trapped volume is increased relative to the swept volume, the peak pressure and the rate of change of pressure as the piston rises will also be reduced. This relationship was exploited in the motored cyclic tests to maximise the crankshaft movement over which a SBDV signal could be obtained before becoming unsteady. This was achieved by inserting a 13.0 mm thick spacer between the top of the cylinder and the cylinder head.

The effect of reducing the compression ratio using the spacer on in-cylinder pressure is shown in Figure F9-15. This shows the differences between measured and calculated cylinder pressure history around the first ten degrees of closed compression. Thus, Figure F9-15 shows the range of cylinder pressures in which the SBDV system would be required to operate in the Test engine with and without the reduced compression spacer fitted. As annotated:

- The ‘Green’ trace is the measured pressure signal with the spacer fitted. Note the ‘Green’ trace is unfiltered.
- The ‘Red’ trace is the measured but pressure change in the unmodified test engine without the spacer fitted. Note, the red trace has been filtered for clarity.
- The ‘Blue’ trace shows a calculated idealised pressure plot for a test engine with the spacer fitted. Note, the calculation assumes the change of in-cylinder pressure is due to piston displacement only and all displacement occurs in a closed cylinder.
- The ‘Yellow’ trace shows a calculated idealised pressure plot for an unmodified test engine without the spacer fitted. Note, the calculation assumes the change due to piston displacement only and all displacement occurs in a closed cylinder.

Adding the spacer and reducing the compression ratio thus reduced the in-cylinder pressure (over the crankshaft rotation period of interest) by between approximately 0.1 to 0.25 Bar. Although this represented a small difference of pressure during the first 10 Degrees after EPC, the overall range of crankshaft movement over which SBDV events could stably occur over every cycle was greater.

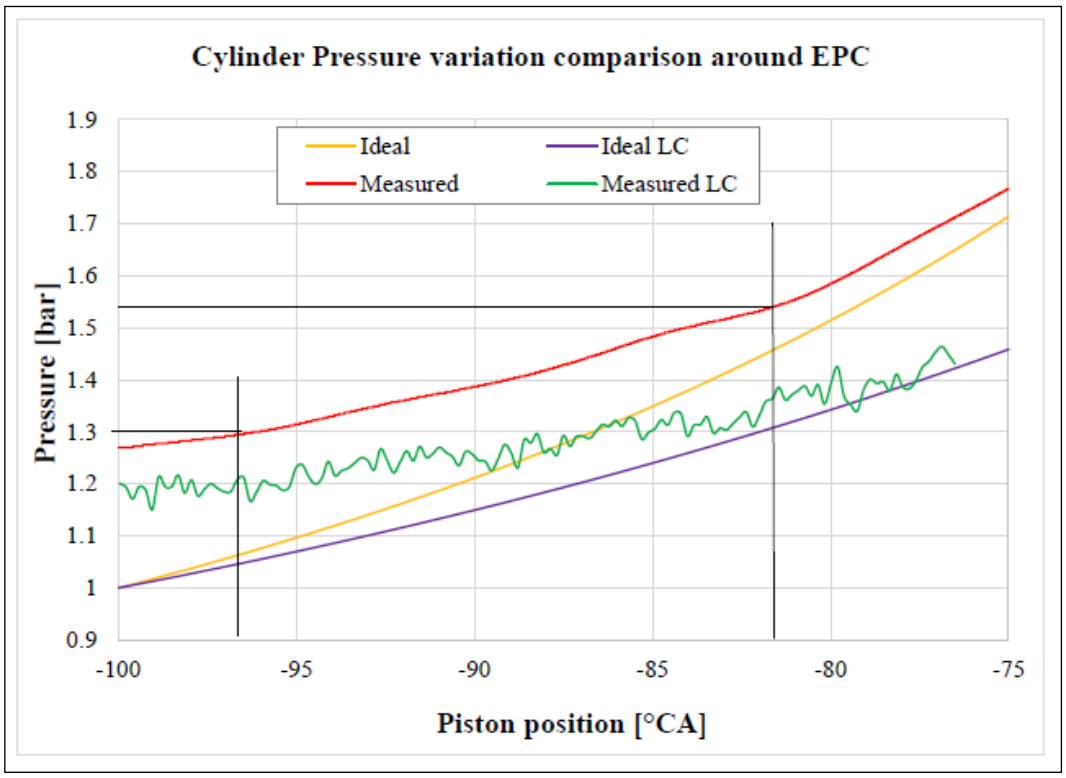

Figure F9-15: Pressure variation in the first ten degrees of closed compression

9.4 CYCLIC COMPARISON OF IN-CYLINDER GASES DURING EARLY STAGE CLOSED COMPRESSION

The SBDV signal during the period following the 10 Degree period of crankshaft rotation after EPC requires interpretation to determine the gases trapped in the cylinder and available for subsequent combustion. Therefore, the response and accuracy of which this signal can respond to changes of gases present during this period is very important.

The plots presented in Figures F9-16 to 24 show localised versions of the whole cycle plots presented previously in Figures F9-4 to 12. The dual exhaust port closing positions at 82 and 97 Degrees BTDC as shown in Figure F9-13, are shown for reference in each cycle.

The plots such show cycle by cycle comparisons between measured pressure and SBDV converted to pressure for each of the four different gases determined using the transposed formulas given in Table T9-1.

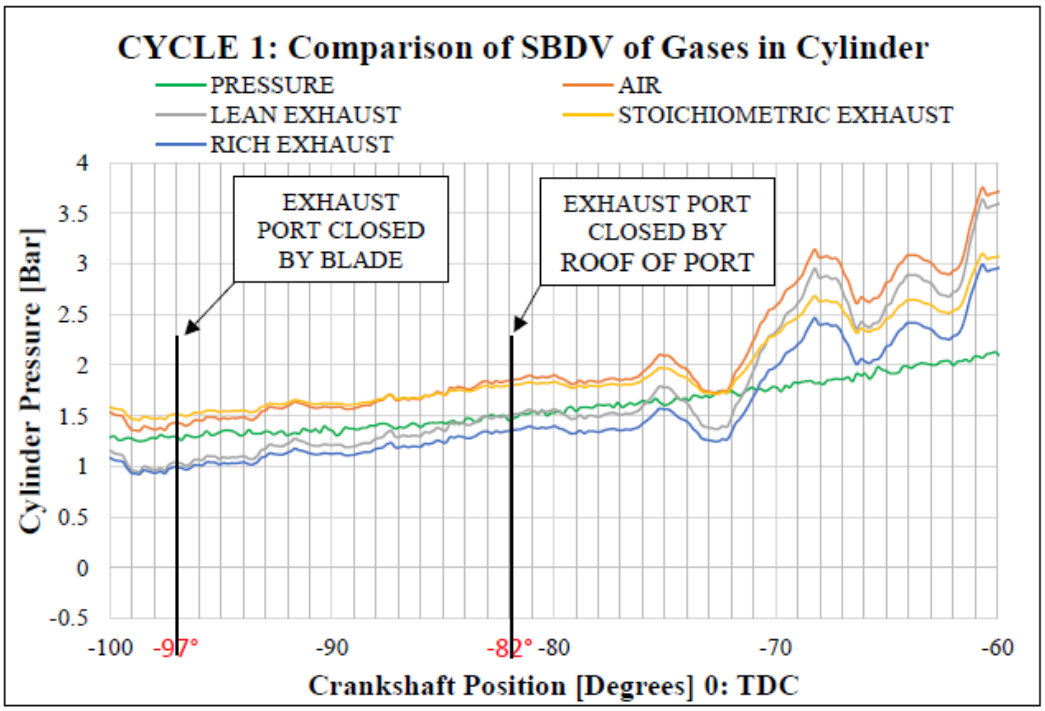

Figure F9-16: Cylinder Pressure and SBDVp for Air and Exhaust Gases: Cycle 1 (during initial stage of compression)

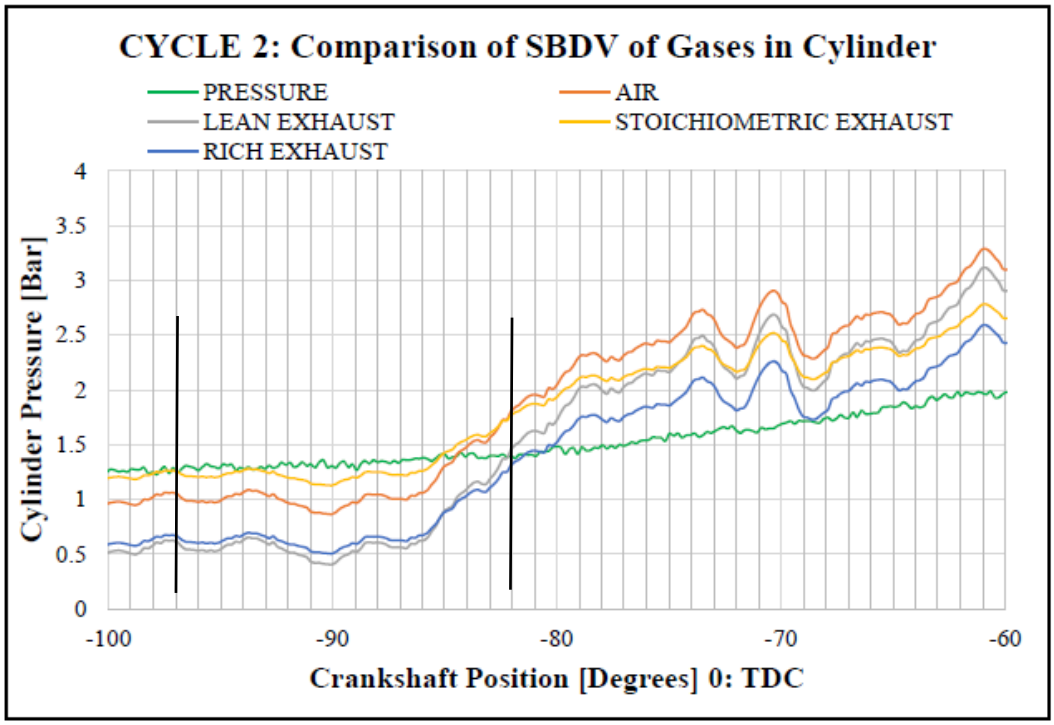

Figure F9-17: Cylinder Pressure and SBDVp for Air and Exhaust Gases: Cycle 2 (during initial stage of compression)

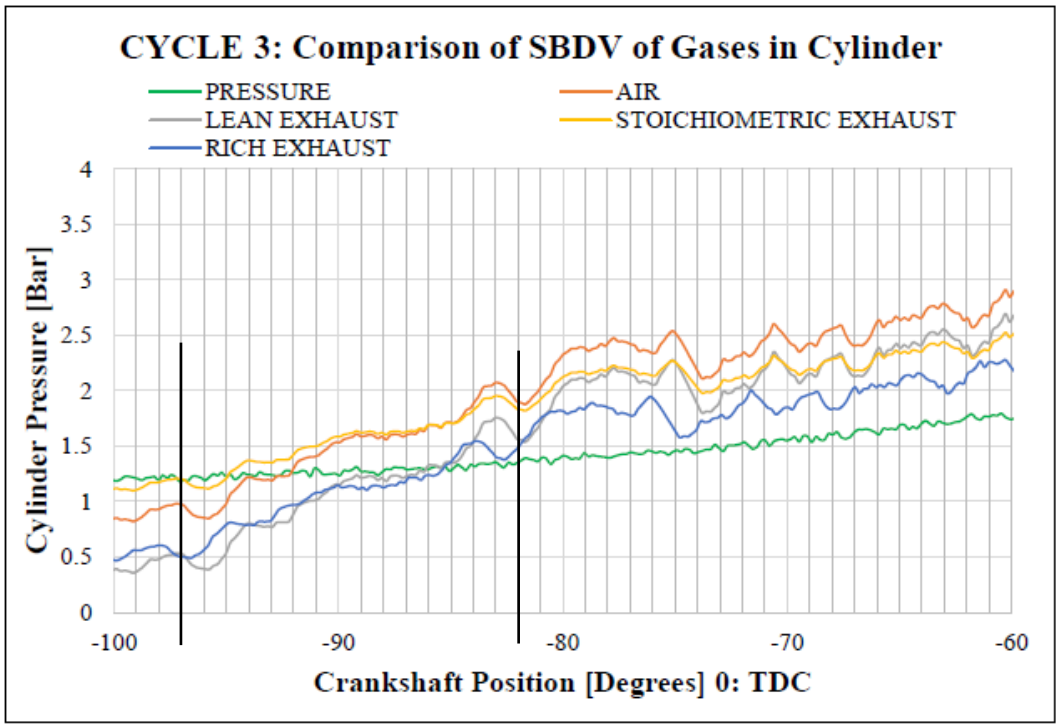

Figure F9-18: Cylinder Pressure and SBDVp for Air and Exhaust Gases: Cycle 3 (during initial stage of compression)

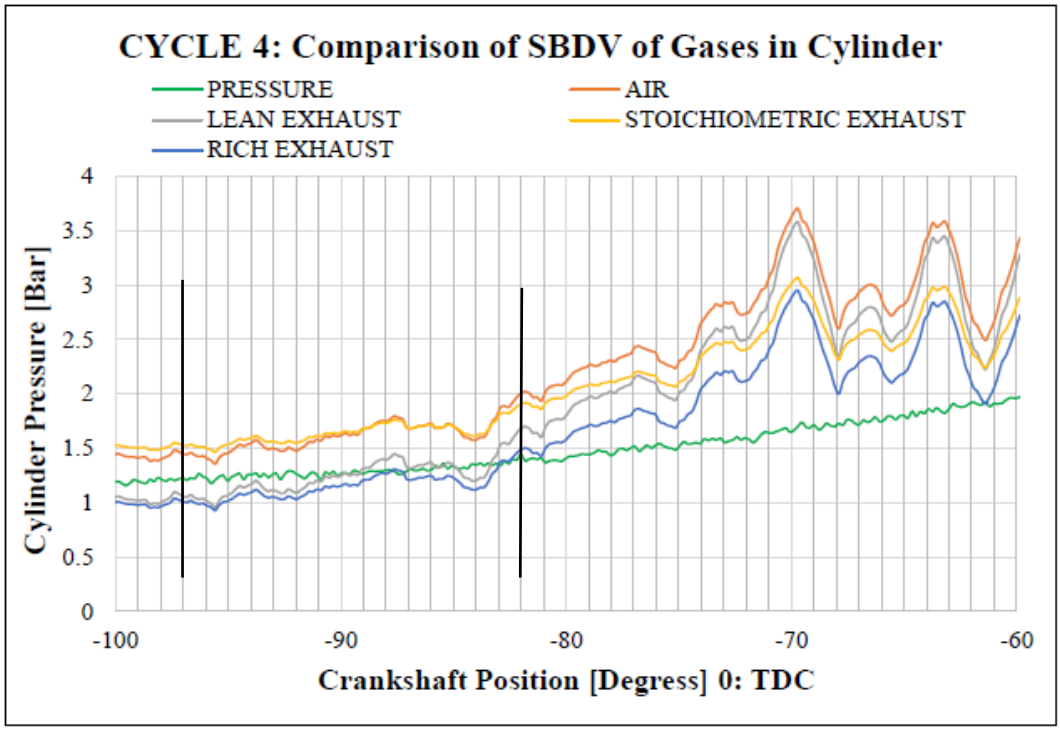

Figure F9-19: Cylinder Pressure and SBDVp for Air and Exhaust Gases: Cycle 4 (during initial stage of compression)

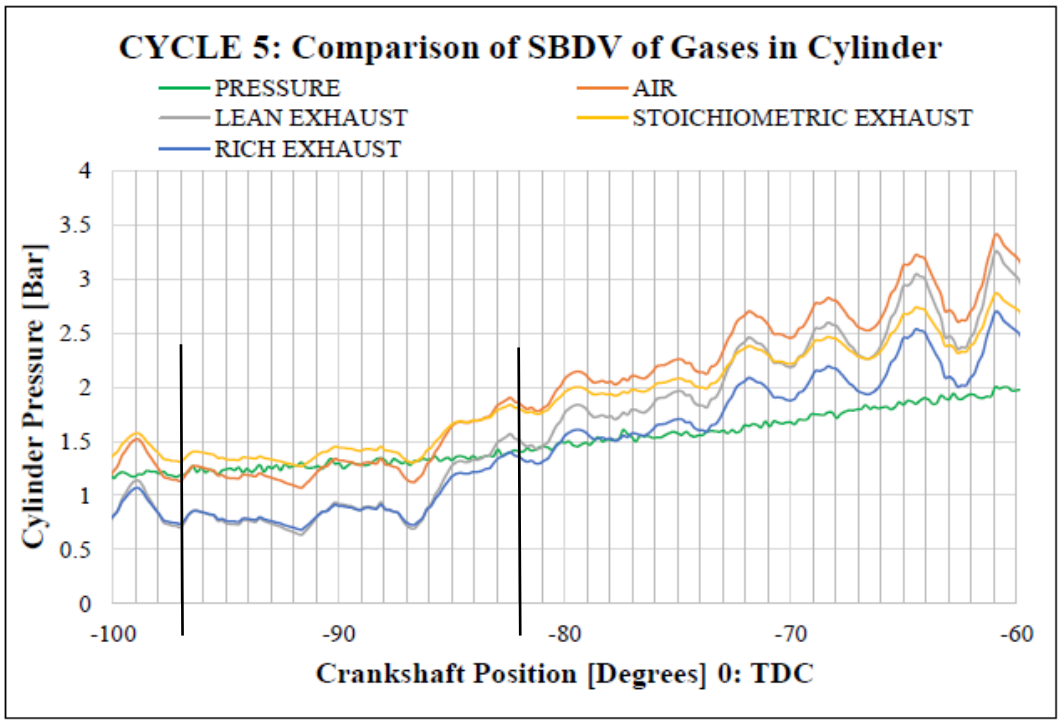

Figure F9-20: Cylinder Pressure and SBDVp for Air and Exhaust Gases: Cycle 5 (during initial stage of compression)

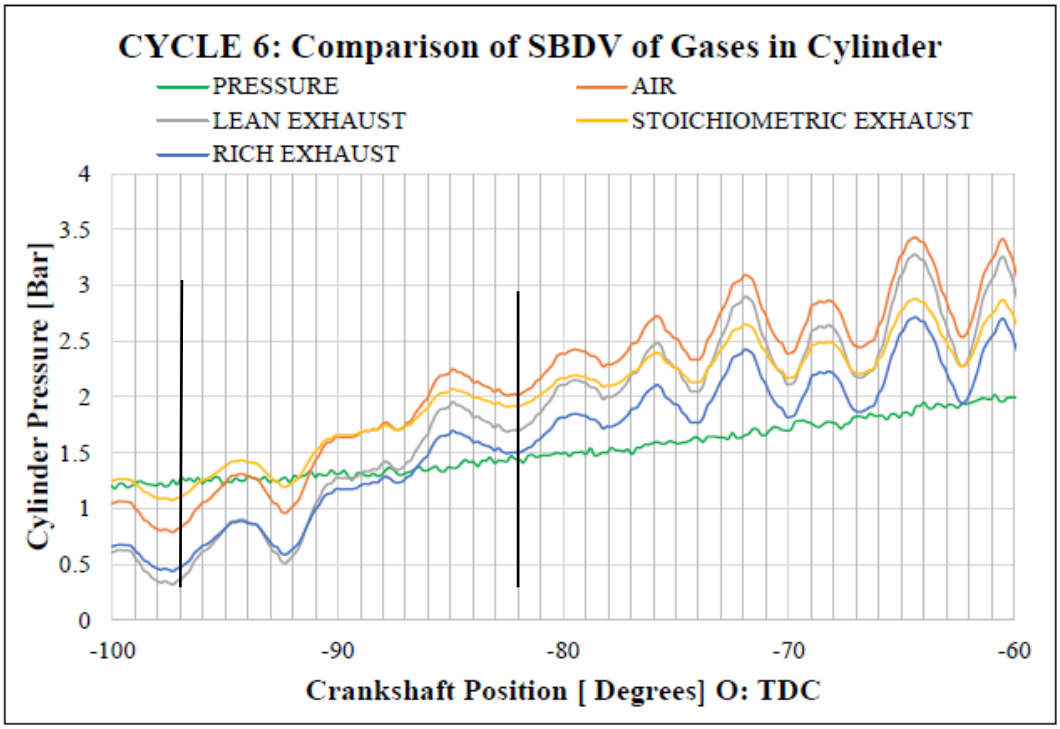

Figure F9-21: Cylinder Pressure and SBDVp for Air and Exhaust Gases: Cycle 6 (during initial stage of compression)

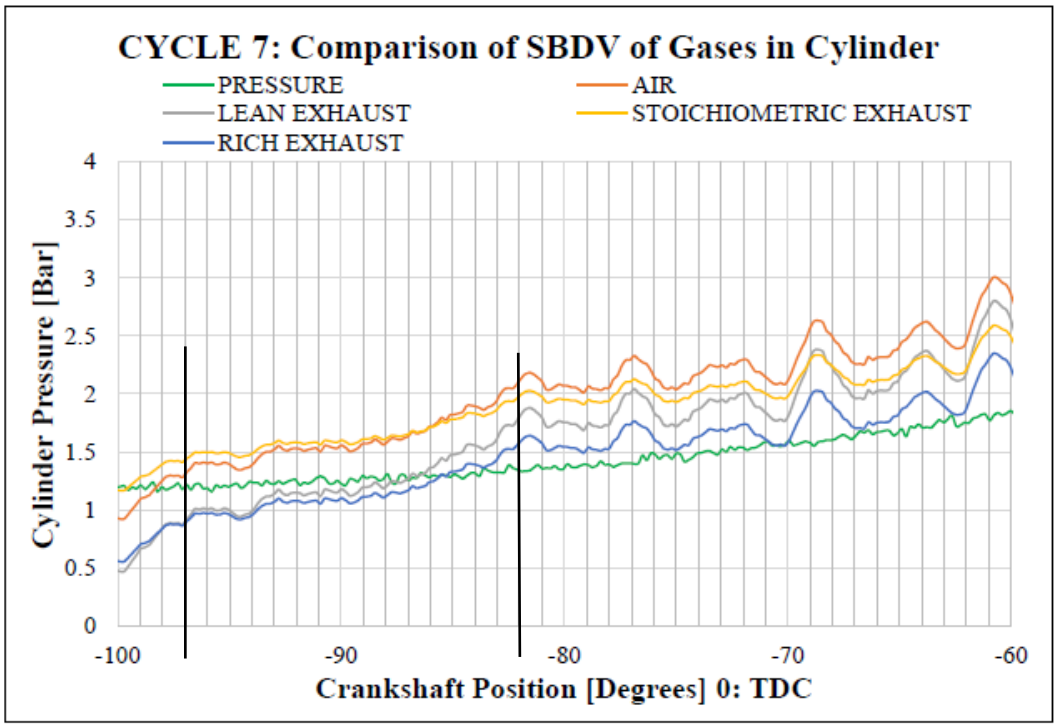

Figure F9-22: Cylinder Pressure and SBDVp for Air and Exhaust Gases: Cycle 7 (during initial stage of compression)

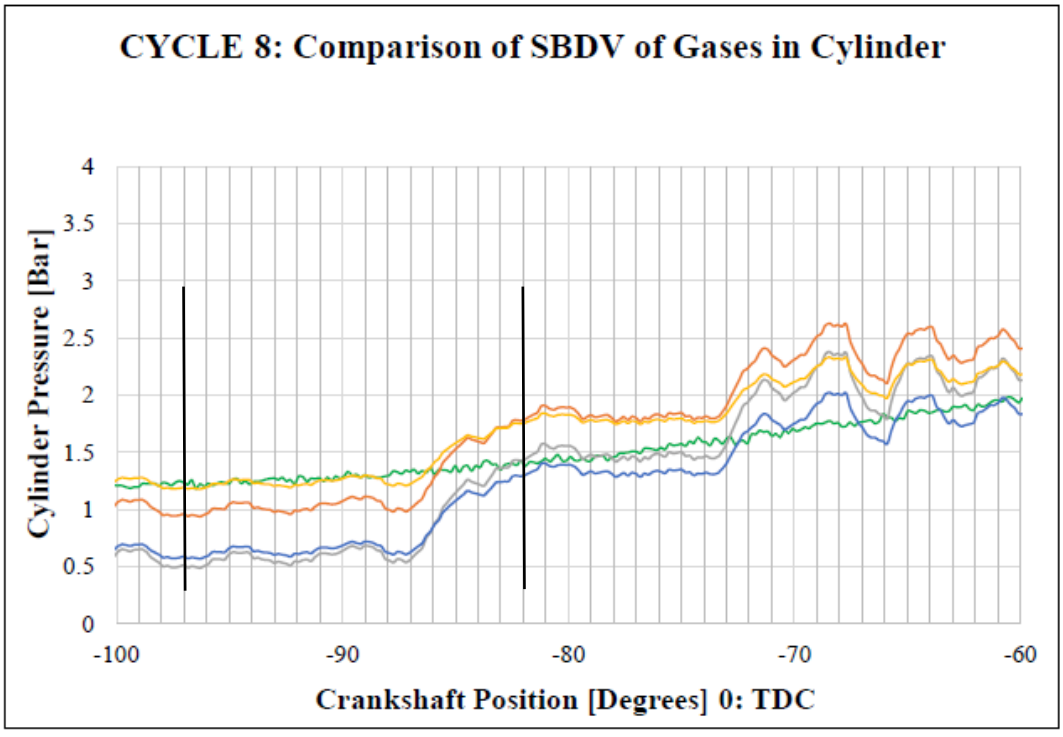

Figure F9-23: Cylinder Pressure and SBDVp for Air and Exhaust Gases: Cycle 8 (during initial stage of compression)

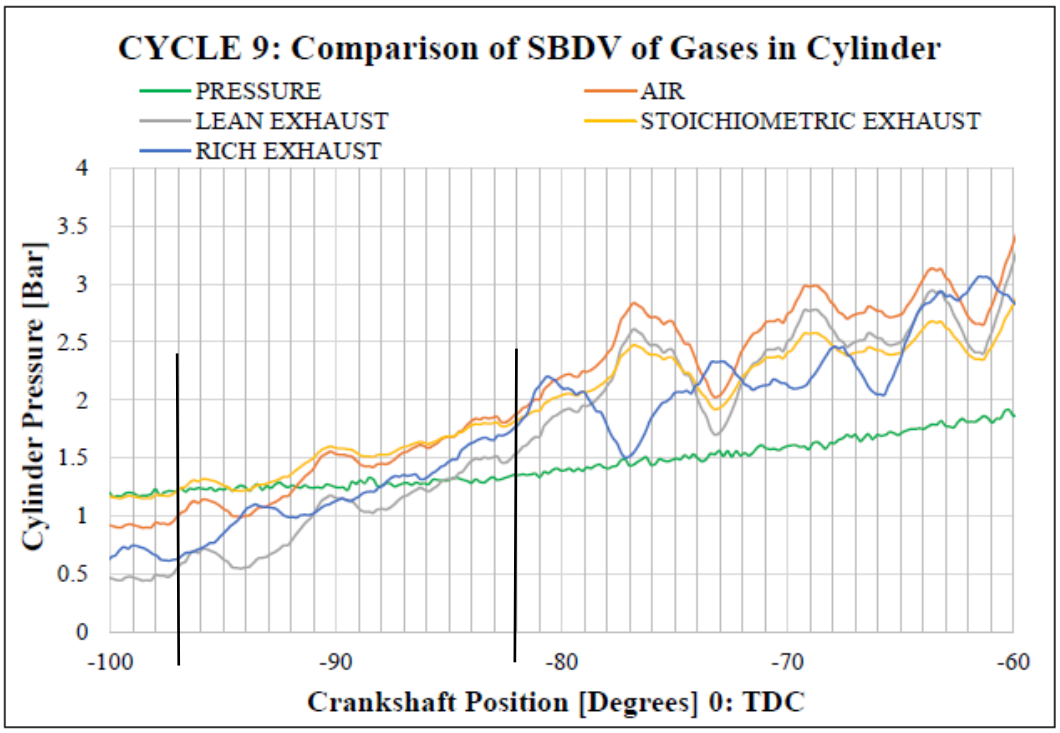

Figure F9-24: Cylinder Pressure and SBDVp for Air and Exhaust Gases: Cycle 9 (during initial stage of compression)

9.4.1 OBSERVATIONS ON FIGURES F9-16 TO 24

a) The SBDVp traces can be seen to replicate the pressure trace. This demonstrates the SBDV system described in the present work could, within imposed functional range / crankshaft angle limits, be used as a low-cost replacement for an in-cylinder pressure sensor.

b) A discontinuous step in the slope of SBDVp traces can be seen to occur corresponding well to exhaust port closure positions. Cyclic variations to this behaviour are clearly evident. These follow, but are more distinct from the pressure trace. These cyclic variations are thought to display the differences in the pressure value and arrival time of the pressure wave returned backwards the engine down the exhaust port. Note, this effect will be considerably greater in a firing engine. Cycle two (Figure F9-17) and Cycle four (Figure F9-19) display this behaviour most clearly.

c) The difference in the pressure value, at specific reference points, between each of the gases represents the relative gas density as per Silsbee's formula Eq. 7.8.

d) The plotted traces for the four different gases in all nine cycles are clearly distinct from one another.

e) Visually, the SBDVp trace for Stoichiometric exhaust gas follows that for Air more closely and consistently than those of Lean or Rich exhaust gases.
f) The traces for Lean and Rich exhaust gases are consistently close together and distinct from the traces for both Air and Stoichiometric exhaust gas.
g) Oscillations in the SBDVp traces are present but can be seen to vary each cycle. This behaviour is considered attributable to gas turbulence around the spark plug electrodes. It can be seen, if SBDVp oscillations occur when the exhaust port is open they continue after the port is closed. Alternatively, if the SBDVp signal is relatively smooth while the exhaust port is open, the start of oscillations is delayed by some 5 -10 Degrees. Note, these signals are obtained at a location approximately 30mm away from the point of port closure. Assuming a pressure wave transmission speed of 250m/s there would be a delay of 0.00012 seconds or 0.12 milliseconds which is approximately 1/10 of the time between successive SBDV events occurring at 94kHz. Thus, the SBDVp signals can be considered to reflect the pressure changes at the port although not obtained at that location.
h) It is concluded that if pressure was measured, the equivalent pressure for various exhaust gases could be determined by comparison.
i) It is concluded that if pressure was measured and gas speciation was determined as discussed in chapter eight, the SBDVp could be determined during the early stage of closed compression as required by the objectives stated in chapter one.
j) It is concluded that if the reverse of the mathematical transposition was used, the in-cylinder pressure could be determined for different gas species present.

9.5 CHAPTER SUMMARY

The contents of this chapter demonstrate that high frequency SBDV applied across spark plug electrodes from successive cycles in a motored engine, can be converted to equivalent pressure which varies dependant on the burned air fuel ratio of in-cylinder exhaust gas. The signals are comparable with those obtained by a proprietary pressure sensor but show significantly greater variation.

The conversion of SBDV to equivalent pressure was achieved by applying the mathematical relationships derived in Chapter 8.0. The converted SBDV signals for the various exhaust gases are distinct and can be individually identified from that of Air. Critically, the signals change around the start of closed cycle compression with cyclic variations which could be attributable to small variations of resonance in the exhaust pipe. The effect of increased compression at the point when the exhaust port is closed can be

seen to progress and influence the initial gas compression in the closed cycle period. This behaviour during the initial period of compression is particularly critical to this thesis and its stated objectives. Further work is required to interpret the information provided by this new analysis tool. However, such activity is outside of the scope of the present work.

CHAPTER TEN

SBDV ENABLED CYCLE BY CYCLE COMBUSTION CONTROL

10.0 INTRODUCTION

The present work has shown a capability to use SBDV to differentiate between different pure gases and different exhaust gases when the pressure of such gases is below approximately 3bar at ambient temperature. This Chapter concerns how the new method to determine the nature of the gases trapped in the cylinder prior to combustion could be used, to enable Cycle by Cycle Combustion Control (CBCC) as proposed and justified in Chapter One.

The Literature review, in Chapter Two, showed that CBCC has been a key objective of automotive engine researchers but has not yet be achieved practically in an operating engine. Methods provided by existing research which could be adapted using SBDV sensing in order to enable CBCC are presented and discussed.

Cycle by Cycle Control represents a control system which would maximise cyclic combustion efficiency. Such a system would have two primary objectives which are summarised below and considered separately in sections 10.2 and 10.3.

1) To provide an amount of fuel to precisely match the mass of air available to burn in a predetermined Air/Fuel ratio. The fuel quantity would be adjusted by the system, for each combustion cycle, to suit variations of overall trapped mass and percentage of residual burned exhaust gases present and available for combustion for each cycle.
2) To initiate an ignition event at a predetermined timing to maximise the heat released and subsequent cylinder pressure to maximise the torque applied to the engine crankshaft. The timing of the ignition event would be adjusted by the system, for each combustion cycle, to compensate for predicted flame speed and acceleration resulting from cyclic variations of cylinder contents and applicable conditions.

This thesis is concerned only on causes of combustion variability resulting from changes of combustible mass of trapped charge which can be identified using the new SBDV system. The following assumptions are made:

a) Overall optimum combustion control can only be achieved if each and every combustion event receives an accurate quantity of fuel to match the mass of trapped combustible gas.

b) In order to control an upcoming combustion event, the major factors which determine the outcome of that event have to be known and acted on in advance of the event.

c) The ability of an engine to deliver fresh charge into the cylinder and then to prevent its escape through the exhaust port and the ability to expel burned gases from previous events varies with engine speed and load.

d) In the case of the two-stroke cycle type engine, (as explained in chapter 2), this ability also varies due to the pressure and flow variations in the exhaust system.

e) The flows inside an engine are unsteady and vary with time. These factors combine and interact differently from cycle to cycle to cause cyclic variations of the mass of combustible charge.

f) The gases available for each combustion event are those gases trapped in the cylinder after valve closure as the piston compresses the gases for the forthcoming combustion event.

g) If the contents were measured at or following the point of exhaust port closure the information will accurately represent the gas charge available for combustion.

h) Following the point when the exhaust port is closed by the piston as it ascends towards each combustion event the system becomes thermodynamically ‘closed’.

i) As the system is ‘closed’ with the exception of fuel added or small amounts of leakage past the piston the change in mass of charge trapped in the cylinder is negligible.

j) For any type of internal combustion engine, the major factor which determines the result of each combustion event is: The mass of combustible gas trapped in the cylinder.

k) For a directly injected, spark ignition engine. If this mass is known sufficiently early in each cycle the values which require control functions to be provided could be determined.

l) The mass of fuel required to provide a given air/fuel ratio must be cyclically estimated.

m) The flame speed which will vary in relation to the mixture of fresh charge, burnt exhaust gases, unburned previous fresh charge and the predetermined Air/Fuel ratio delivered.

n) The fuel quantity injected into the combustion volume and ignition timing can be changed electronically for each cycle.

10.2 THE BENEFITS AND LIMITATIONS OF SBDV ENABLED CBCC

The S.I. internal combustion engine is not a simple device. Complex inter-reactions exist between the mechanical components and the combustion events which convert and transmit created energy. These interactions become even more complex when the engine is required to quickly change speed or load and therefore respond by burning different amounts of fuel. Consequently, combustion efficiency is not consistent for every cycle of operation. This is especially true for two-stroke type engines due to the variability of cylinder charging and trapping efficiencies resulting from their mechanical simplicity. The various contributing factors were presented in Figure F2-6, some of which are a direct result of inherent engine design constraints or issues which require separate improvements. Hence, not all the contributing reasons for cyclic combustion variability would be addressed or controlled by improving the cyclic accuracy of air / fuel ratio or the timing of spark ignition initiation.

However, if cycle by cycle combustion control (CBCC), were improved the result would undoubtedly be improved engine efficiency, reduced fuel consumption and emissions. The significant contributing reasons for these improvements are listed and discussed separately below.

a) A reduction of cyclic combustion variation.

A reduction of cyclic variations would be the primary target of CBCC. The two-stroke cycle type engine suffers the most of all engine types it has been shown that cyclic variation of the trapped mass fraction of residual burned exhaust gases is a major contributing factor to cyclic combustion variations (Abraham & Prakash, 1992), (Hamamoto, 1971). This has shown measured variations of total energy release between 0-1500 kJ within 40 cycles of normal operation. As the delivery ratio reduces the average mass of residual burned exhaust gases increase. This delays flame development which in turn results in partially burned combustion cycles which rapidly further migrate to misfiring. This inhibits combustion of

subsequent cycles. Similarly, a combustion event which results in high pressure optimally timed can lead to many subsequent relatively poor combustion events due to lack of cylinder scavenging. Under low load and low engine speed operation a good combustion to good combustion period of 30 cycles has been noted (Carretti, 2015). The primary cause of this is poor engine scavenging, deliberate skip firing intervention may provide the improvements at low speed.

b) A defined Air/Fuel ratio and homogeneously mixed cylinder charge.

If CBCC were achieved a pre-determined Air/Fuel ratio would be the principle result and improvement. The homogeneous mixing may be improved by achieving a more consistent combustion and reducing the cycle by cycle variations of differential pressures which control the mass flow rate of cylinder charging.

c) A maximum fresh charge and thus Oxygen content.

CBCC would ensure that whatever the mass of oxygen was present it was matched by a pre-determined mass of fuel. Thus, if the available amount of fresh charge and hence Oxygen changed from one cycle to another, the individual combustion events would not waste the opportunity to maximise the average heat energy available.

d) A minimised amount of residual burned exhaust gas to avoid fresh charge dilution but sufficient to assist the creation of dendrite pathways during turbulent spread of the flame front.

Two-stroke cycle engines are notoriously poor at scavenging residual exhaust gases from the cylinder. CBCC would not change that basic characteristic which is fundamental and inherent to the design of the engine. This would also apply to CBCC applications to HCCI and highly variable four-stroke cycle type engine designs. However, the potential ability to determine cyclic variations in the amount of residual exhaust gases would enable the development of sub-controlled devices to influence that behaviour. Knowing the amount of residual burned and thus largely inert gas would potentially enable a cyclic flame speed correction factor to be applied to the ignition initiation point. This would require consideration of how the amount of residual exhaust gas effects flame speed. CBCC would increase the average amount of power produced by an engine.

e) *An ignition initiation point which considers the speed of the combustion flame such that its maximum acceleration will occur at TDC.*

CBCC requires the cyclic determination of the crankshaft position at which ignition is initiated. Conventionally, this event is timed to achieve maximum effect from the increase of cylinder pressure relative to leverage imposed on the crankshaft, which point is termed Maximum Brake Torque (MBT). This point is also conventionally considered to correspond with the burning of 50% of the fuel in the combustible charge and the maximum rate of burning and flame speed. The derivative of flame speed is flame acceleration. Whereas MBT timing is considered as approximately 15 Degrees ATDC, variable and relatively insensitive. However, MBT is optimised if the point of maximum flame acceleration is fixed at TDC. The improved control of cyclic Air/Fuel ratio and knowledge of the amount of burned gases present is expected enable the determination of the ignition initiation timing relative to TDC using this relationship.

f) *Warm spark plug electrodes with clean existing surface conditioning.*

If CBCC were achieved variation of heat input into the spark plug electrodes would be reduced. The temperature of spark plug electrodes is affected by the voltage required to produce an ignition spark breakdown. The voltage delivered across the electrodes is, within the limits of the ignition system, (as noted to be fundamental to the topic of this thesis) self-determining. Additionally, the greatest spark plug temperature is caused by reflected heat back from the expanding flame front. Greater control of each combustion is therefore considered to potentially reduce the thermal variables involved which would prevent excessive spark plug electrode (and associated ceramic) temperatures. Surface conditioning and electrode cleanliness is considered likely to be improved as a result of the large number of spark breakdown events which would occur during the initial stage of each compression. This is considered likely to scour the electrode surface ahead of each subsequent ignition event.

g) *Minimal flow disturbance around the spark kernel until it has formed a self-sustaining flame.*

This will be unaffected if CBCC is achieved. However, the development of new spark plug electrode designs and concepts introduced in the present work, such as Spark Distribution Curves, may lead to improved performance in this area.

h) A slightly richer than stoichiometric Air/Fuel ratio pocket of charge around the initial flame kernel.

To achieve a consistent pocket of gas which is best suited to promote combustion, first the actual gases present in the closed cylinder have to be understood. As the conditions around the cylinder generally and around the spark plug, especially, vary each cycle. The incorporation of the method presented in this work could enable that to be provided.

i) Maximised gas turbulence to spread a stable and concentrically developed self-sustaining flame.

This effect could be improved by CBCC if a more consistent cylinder charging mass flow rate were achieved.

j) The surrounding cylinder, cylinder head and piston temperature to be hot enough not to over quench the temperature of the expanding combustion but cool enough to prevent auto-ignition or knock.

The temperature of the engine parts surrounding the gases trapped in the cylinder is directly affected by the heat input from combustion. Improved combustion control which would result if CBCC were achieved, would inevitably improve the cyclic variations of heat and therefore render improved thermal transfer and control of those parts. Additionally, although not investigated as part of the present work, the new SBDV system would enable instantaneous temperature calculation and cyclic feedback of gas temperature variations. Previous work has shown that SBDV could be used to sense the onset of knock.

k) A descending piston speed which is just slower than the expanding charge rate.

This is likely to be improved if CBCC were achieved as cyclic control would be expected to better match the piston speed variations which occur as result of combustion variations and operational demands.

l) Improved engine torque, operational characteristics and drivetrain reliability.

Consistent cyclic combustion would ensure the contribution of each individual combustion event was maximised. Currently that does not and cannot occur especially in transient conditions where the cyclic variability of fresh charge cannot be accurately matched by the system which controls the cyclic supply of fuel. If the contribution of each combustion were maximised the average torque output would be increased. Additionally, reduced variation of combustion pressure and its peak value relative to crankshaft position would reduce perceived engine vibration. The response of the engine to changing acceleration demands and overall operational behaviour would be improved. An example of this potential improvement in a two-stroke engine occurs at low engine speed and load. Here combustion events occur infrequently (up to around 30 cycles between combustions). The low friction of the engine allows this behaviour to occur. However, the operator senses significant speed reductions and 'blips' the throttle as an instinctive reaction. This behaviour alone, which the author has not found reference to in any related report, contributes significantly to unnecessary fuel efficiencies and emissions levels.

10.3 CHAPTER SUMMARY

The intent of this Chapter was to discuss the potential for the new SBDV system to be used to enable the development of cycle by cycle combustion control (CBCC).

Aspects of existing research quoted in this work could be used in conjunction with SBDV gas sensing to address the key issues which require overcoming to enable CBCC. The present work has shown SBDV gas sensing can provide functional signals which can be interpreted to indicate in-cylinder gases and conditions. This technology can be developed and used as a stand-alone methodology or used in conjunction with existing diagnosis and estimation methods. The application of this would increase the efficiency of directly injected two-stoke cycle and other engine types to reduce worldwide vehicle emissions.

The potentials and limitations of what factors may be influenced, and those which would probably, not be were clarified. The potential effects of SBDV cycle-by-cycle combustion control are shown in Figure F10-2. This diagram is a modified version of the diagram in Figure F2-6, which showed the principle reasons for cyclic combustion variations. The factors which would be improved or negated are highlighted in 'yellow'. The factors which could be beneficently influenced of improved are highlighted in 'blue'. The factors which would not be influenced are left uncoloured. The overall effect on cyclic combustion

variations can be seen to be significant. The factors which are not influenced are due to in-cylinder flows which are subject to improvements by engine design.

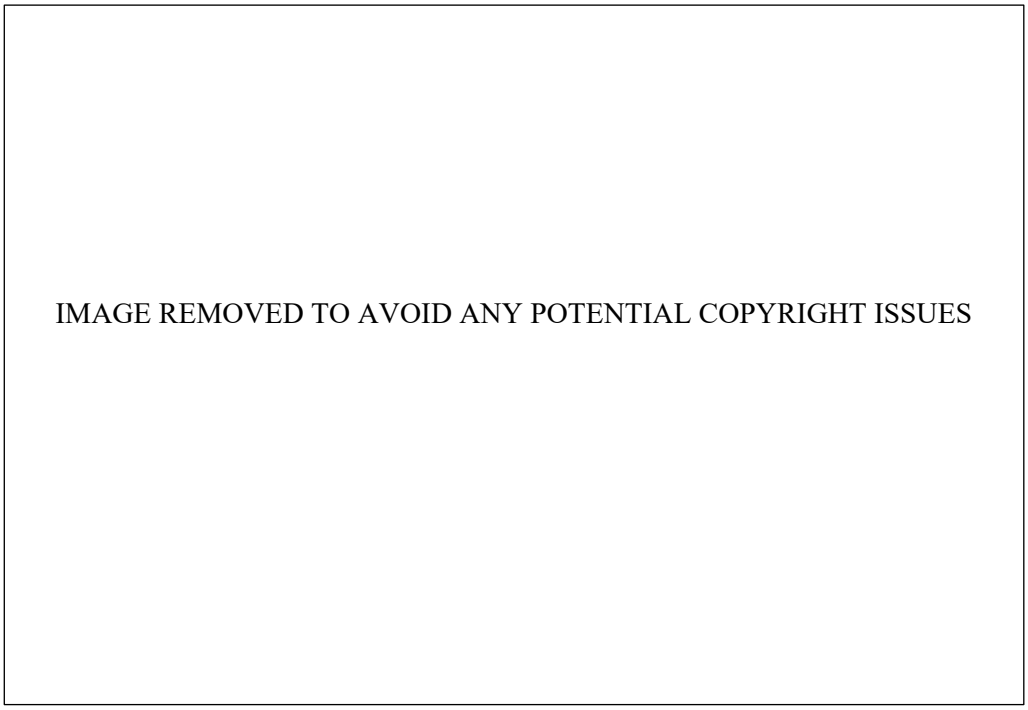

Figure F10-1: Revised CCV contributions diagram showing effects of SBDV improvements

CHAPTER ELEVEN

CONCLUSIONS, LIMITATIONS AND DIRECTIONS FOR FURTHER WORK

11.0 INTRODUCTION

This chapter provides conclusions from the investigations and findings obtained against the stated objectives of the project. Limitations of the present work are explained. Further work is suggested from considerations, conclusions and limitations of the present work.

11.1 CONCLUSIONS

The research was successful, the stated objectives were met and a powerful new in-cylinder, gas analysis tool for combustion control is presented. The use of Spark Breakdown Voltage in the manner proposed in this thesis is novel technology. The results of the research presented have successfully demonstrated a new, non-intrusive, cost effective method to improve combustion control by optimization of each individual cycle is achievable. The present work is principally focused on small two-stroke cycle type engines for which this technology is considered most useful. However, the technology can be used in all types of engines, especially those which exhibit large cyclic combustion variations resulting from changes in-cylinder gas contamination levels.

The testing apparatus which was purposely designed and manufactured testing apparatus for the study of SBDV in a two-stroke cycle spark ignited engines functioned reliably and as intended. The combined use of a motored test engine and an auxiliary engine to supply different exhaust gases functioned in a simple and reliable manner. The Static Sparking chamber and Motored apparatus were both modified and adapted to enable a wide range of tests. The use of a two-stroke cycle test engine enabled simple maintenance and instrumentation access. Further potential improvements have been identified to improve the test apparatus and SBDV system to assist the speed and accuracy of further research.

The present work demonstrates that a spark plug can function as a gas diagnostic sensor working as a part of the new High Frequency SBDV system. A new method to calibrate the characteristics of individual spark plugs was found. From testing results a prototype spark plug was manufactured with the design objective of improving the stability of the SBDV signal, especially in turbulent gas conditions. This was successfully demonstrated.

The new SBDV system can differentiate between different gas species most significant to combustion in the cylinder. The system was used to obtain appropriate signals over a range of pressures associated with the scavenging period and initial stages of closed cycle compression within a 1ms sample duration. The new SBDV system was also shown able to differentiate between a very wide range of Air and Exhaust gas mass fraction mixtures appropriate to a working engine. A method was derived by which this capability included the ability to differentiate the Air/Fuel ratio of the burned exhaust gases.

The new SBDV system was shown able to produce reliable cycle by cycle signals from within a motored test engine. The crankshaft period over which the SBDV signal was obtained being limited by the upper value of generated voltage and the breakdown voltage characteristic of the gas species. The dynamic limits of the SBDV voltage signal were noted to be slightly greater than those achieved in static calibration testing. The present research work contributes the following to the knowledge in the field of internal combustion engines:

The development of an electronic system for using spark breakdown events to determine gas density:

The objective was successfully met. The author specified the requirements of the new system which was designed and manufactured by G.E.M.S Ltd. A total of three variants of SBDV circuit were manufactured and tested. The development of the electronic circuit centred on increasing the power of transformer and reliability of components subjected to high voltage. The circuit behaved reliably and produced repeatable results.

Manufacture test apparatus to determine Spark Breakdown Voltage values for various gases and pressures:

The objective was successfully met. A test apparatus was designed and manufactured for this work. The equipment was reliable and functioned as intended. The Constant Volume Sparking Chamber was used to obtain static pressure calibrations. The maximum gas pressure for which SBDV signals could be obtained from this equipment was raised by the addition of an extension tube and a filter which reduced the gas movement in the test chamber. The gas temperature in the chamber was not significantly affected by heat from the SBDV sparking events.

Investigate the characteristics and experimental variability of typical spark plugs when subjected to spark breakdown events when using the spark plug as a sensor:

The objective was successfully met. The effect of spark electrode gap, material and configuration was evaluated. The effect of turbulent flow on the SBDV signal was assessed. A spark plug was modified which successfully reduced the SBDV signal variability resulting from turbulence. This spark plug was subsequently used to obtain SBDV signals from dynamically changing pressure of air and exhaust gases from within the test engine cylinder when motored at 2500 rpm.

Derive reliable gas density values from spark breakdown voltage events obtained from static conditions and form cycle by cycle events:

The objective was successfully met. SBDV signals contain information which has not been measured in a practical manner by researchers previously. Mathematical relationships for Air, CO, CO_2, N_2, O_2 and exhaust gas were obtained. The accuracy of the SBDV expression obtained from the spark plug in Air at pressures from ambient to 2.5 bar was compared with published data relating to Paschen's Law showed a R^2 value of 0.99. This was considered an excellent result in consideration of the comparative electrode, sampling speed and conditions used.

The SBDV signal from cyclic events shows the entry of fresh charge into the cylinder and points when transfer and exhaust ports open and close. Cyclic variations of pressure are easily identified from multiple engine revolutions.

Signal recognition software was developed to extract and process cyclic SBDV signals values for large and complex samples of data using 'Matlab'.

Investigate the relationships between Spark Breakdown Voltage and the density and speciation of gases present within the combustible charge trapped in the cylinder of an engine:

The objective was successfully met. Mathematical relationships were extracted directly from results for various gases in static and dynamically varying conditions. These were compared with results from FFT spectrums obtained from the spark breakdown events for various gases. The results show that gas speciation could be achieved cyclically from calibrated information.

11.3 LIMITATIONS

The scope of the present work was deliberately wide and was concerned with covering the maximum breath of SBDV technology possibilities. This limited the depth of detail which

could be applied to all of the individual areas investigated. In particular this effected the investigation of exhaust gas mixtures especially the relationships indicated by the FFT investigation.

11.4 DIRECTIONS FOR FURTHER WORK

The present work was intended to investigate wide areas of potential SBDV technology. Several opportunities for more detailed investigations are thus created.

The research reported in the present work used two items of mechanical apparatus which were used for static and dynamic testing. Both these items of mechanical apparatus functioned as intended but could be improved for further work.

The static sparking chamber could be increased in volume and the gas inlet and pressure regulation system improved. The objective of these modifications would be to avoid any gas movement around the spark plug electrodes during testing which did not occur for reasons other than the application of SBDV. The filter used in this testing should be discarded if possible, or modified, as its material was thought to react to pure oxygen and result in contamination. This was believed to be the cause of SBDV variations which reduced the confidence of the assumed mathematical relationship between SBDV and pressure in oxygen and possibly other gases. The time allowed between SBDV calibration tests should be increased to ensure the gases are consistent for each test. This action may reduce the variations and increase the accuracy of SBDV values relative to pressure in all gas calibration tests. The static sparking chamber could also be more sophisticated and perhaps modified to include a variable volume and or method to deliberately vary gas temperature. The constant volume sparking chamber used was constructed with a central copper bar which was intended to be heated by a clamped on electrical heater but those tests were not completed. The ability to vary gas density would allow specific tests to obtain SBDV measurements for varying gas density in addition to varying gas pressure.

The dynamic test apparatus used could also be improved in several ways. The use of an exhaust valve in the test engine cylinder introduced an unnecessary complication to the interpretation of the SBDV and pressure variation during the early stage of compression. This could be avoided in further work by using a cylinder from a ‘Rotax Junior Max’ engine which does not feature such a valve. Knowledge of the precise location of the exhaust port closing position would assist understanding of the pressure and SBDV signal round the point of exhaust port closure. The addition of a sensor triggered by the edge of the piston

at this point would be a preferable alternative to an additional crankshaft position sensor or the interpretation of position.

The incorporation of a valve in the exhaust port of the test engine enabled the gas exchange process in the test engine to be prevented. The valve used for the present work was either fully open or closed and it was operated by hand. Further work could include greater variation and flow control through this valve. In these circumstances, the valve type could be changed to provide a linear flow variation with valve position which is not provided by the butterfly valve used for the present work. The automotive hot film flowmeters should be accurately individually and comparatively calibrated and the addition of a traditional orifice flowmeter arrangement considered.

The auxiliary engine used to supply burned exhaust gases could be improved by adding engine speed and throttle position sensors. Additionally, the engine could be changed to a four-stroke cycle type with direct injection. The objective would be to provide better control of the burned exhaust gases fed to the test engine for SBDV evaluation. The present work used the length and configuration of the auxiliary gas supply to remove heat from the exhaust gas produced by the auxiliary engine. This attempted to ensure the temperature of such gases was stabilised, close to ambient, before entering the test engine so to limit the effects of temperature variations and not confuse the SBDV signal interpretation. Further work should provide more precise control and monitoring of the exhaust gases fed into the test engine to ensure more precise temperature control and or variation. This could be improved using a gas to water-cooled exchanger.

It would be useful for further work to incorporate additional instrumentation. The accuracy of both static and dynamic testing would be improved if a pressure sensor optimised for the pressures tested were used rather than to one used for the present work which had a wider that necessary, 0 -70 Bar range. An additional pressure sensor should be added into the exhaust port to assist interpretation and understanding of the pressure and SBDV changes around the point when the exhaust port closes. A similar item should be added into the transfer port passage for the same reason. Additional fast response ‘K’ type thermocouples should be placed wherever possible to obtain relevant gas and cylinder wall temperatures. The above suggestions have excluded more sophisticated and very expensive in-cylinder measurement techniques on the assumption these would be unavailable.

The PICOSCOPE 4824 functioned perfectly to provide eight channels of high speed sampling however, one or more such items could be used to record additional information simultaneously.

The testing carried out to evaluate SBDV in exhaust gases provided a wide range qualitative assessment. The apparatus used for the present work incorporated direct fuel injectors to provide solenoid activated sample valves but these were not used. Further work could obtain information using a similar arrangement and link this to a mass spectrometry gas sampling system to obtain quantitive values for each gas. Software for both manual and electronic switching of such valves should be enabled to extract gas samples as close as possible to where SBDV sampling is being made. Commercial sample valve systems are also available.

The SBDV circuit used for testing functioned acceptably but provided a reliably consistent signal in a limited pressure range. The maximum output (breakdown) voltage of the SBDV system was proven sufficiently high to prove the capabilities and relationships intended. The upper pressure limit where a consistent SBDV signal could be obtained depended upon the gas being sampled. When the spark breakdown voltage approaches its generated limit the SBDV signal became unstable which limited its accuracy and consistency.

Further work should seek to further develop the electronic circuit to extend the upper pressure limit in which reliable SBDV signals can be obtained. This would be achieved by increasing the generated spark voltage which was also directly linked to the rate of sparking.

The maximum pure gas pressure that could be calibrated statically was limited for CO_2 and CO to approximately 1.8 bar. However, values obtained from within the motored test engine successfully matched values over twice this limit. In an operating engine, the gases in the cylinder would be expected to be hotter and of lower density. In these conditions, the upper pressure limit would be expected to be extended and the SBDV signal to be more stable at lower pressures. Such improvements should also extend the range of pressures and SBDV which could be obtained from within an operating engine.

During initial testing the maximum gas pressures reached only approximately 1 bar before the SBDV signal became unstable or ceased. This was believed to be to disturbance of the spark travel produced by gas turbulence. Instability of SBDV signals was addressed and reduced by modifying the spark plug to incorporate a shroud around the central electrode. The incorporation of the shroud was found to enhance the behaviour of the spark plug as a

gas sensor especially in dynamically changing pressure conditions. The shrouded design reduces the spark breakdown voltage signal variations by limiting the spark gap distance variations the spark can make. The electrode gap distance of the prototype was nominally 0.3mm. For practical reasons, the earth electrode of the prototype shrouded plug was manufactured from carbon steel. Additionally, the spark plug which was adapted using a spark plug which was not the same type as the others tested and it was used prior to the testing in a running engine. It is known the electrode material and surface condition influences the spark breakdown voltage required and the reliability of the spark events. The prototype component produced and tested also provided a sharply defined non-uniform electrode configuration. These features caused the spark to be considerably more stable than plugs with a conventionally shaped earth electrode. Simple 'blowing' tests described in the thesis demonstrated the reason for this.

Further work could be carried out with a spark plug manufacturer to optimise a productionised shrouded spark plug design. This would require further investigation work on materials and construction. It is suggested the surrounding earth electrode be faced in some manner with materials which have a low ionizing potential and high erosion resistance. This would reduce the spark breakdown voltage required for any spark gap distance and increase the gas density range that could be 'sensed' for any spark breakdown voltage. However, it is possible the requirements of the spark plug as a SBDV sensor cannot be successfully optimised with those of required by an ignition initiator. In which case other solutions would need to be explored.

The Spark Breakdown Voltage relationship with pressure in Air was found to be different from published values and relationships. These differences were considered to result from the arrangement and material of the spark plug electrodes which are considerably different from those used in previous calibration testing. The 'breakdown' mechanism or the effect of the high frequency sampling was not fully investigated by the present work and is an opportunity for considerable further work.

The calibration of high frequency spark breakdown voltage across various types of spark plugs to differentiate between gases significant to combustion and exhaust gases containing different amounts of oxygen, CO_2 and CO has been started in this thesis. This is an area that further work could expand greatly. The present work did not investigate the presence of Oxides of Nitrogen (NOx) although SBDV signals for Nitrogen showed marked differences with other gases. The level of production of these gases is significantly less in a two-stroke cycle type engine than a four-stroke or diesel type due to reduced combustion

temperature. However, these gases are very important contributors to pollution and SBDV is likely to offer functional in-cylinder sensing.

The range and accuracy of exhaust gas measurements was limited by the testing method used in the present work. Further work should seek to obtain accurate information and a deeper understanding of the relationships between SBDV and all exhaust gas mixtures. This would require a different calibration testing method which delivers compressed exhaust gases to the static sparking chamber or compressed them in situ. However, the relationships indicated by the FFT investigation presented in the present work could be developed and used as a method. to determine the residual exhaust gases trapped in the cylinder of an engine.

The testing carried out for the present work did not extend into a running (firing) engine. The behaviour of the new SBDV system was not investigated in those conditions. Further work should investigate SBDV behaviour and associated signals in gases containing different quantities and proportions of exhaust gases in an operating engine. Differences from those measurements taken in the present work would occur if ionization of the residual exhaust gases had not decayed significantly.

The opportunities created by the SBDV method require further work to provide information to a functional combustion control system. As described in Chapter Ten, the required information obtained from SBDV signals would enable fuel quantities and ignition initiation timing to be determined for each cycle. This potential system requires further work and research to determine optimal solutions which are likely to require algorithms and or neural network solutions. Testing of the SBDV system has shown the speed, sensitivity and potential to determine the mass of exhaust gas in the cylinder of an engine. It has been shown that a detection period of 1 ms is sufficient to collect the signal for reference to pre-calibrated information. Further work would allow time to develop the SBDV system to obtain samples at pre-defined crankshaft angles of specific interest.

The research reported in the present work successfully demonstrates the application of high frequency spark breakdown voltage to the spark plug can be used as an in-cylinder gas sensing system which is sufficiently fast to provide virtual ‘real-time’ data.

End of Thesis

REFERENCES

Aas, H. P., 2010. *Designing a Cylinder Head with Direct Injection for a High Performance Two Stroke Engine. MSc Dissertation.* Oxford, England: Oxford Brookes University.

Abraham, M. & Prakash, S., 1992. *A Theory of Cyclic Variations in Small Two-Stroke Cycle Spark Ignited Engines - An Analytical Validation of Experimentally Observed Behaviour. SAE Paper No: 920426,* Warrendale. PA: Society of Automotive Engineers.

Adbel-Rehim, A. A., 2013. Impact of Spark Plug Number of Ground Electrodes on Engine Stability. *Ain Shams Engineering Journal. Vol. 4,* pp. 307 - 316.

Ahmedi, A. et al., 2003. *Prediction Tool for the Ion Current in SI Combustion. SAE Paper No: 2003-01-3136,* Warrendale. PA: Society of Automotive Engineers.

Akkerman, V. Y., 2007. *Turbulent Burning, Flame Acceleration. Explosion Triggering. PhD Thesis,* Umea: Umea University.

Aleiferis, P. et al., 2000. *Cyclic Variations of Initial Flame Growth in a Honda VTEC Lean Burn Engine. SAE Paper No: 2000-01-1207,* Warrendale. PA: Society of Automotive Engineers.

Aleksandrov, N. L. & Bazelyan, E. M., 1999. Ionization Processes in Spark Discharge Plasmas. *Plasma Scources Sci. Technol,* Volume 8, pp. 285 - 294.

Alger, T., Hall, M. & Matthews, R. D., 2000. *Effects of Swirl and Tumble on In-Cylinder Fuel Distribution in a Central Injected DISI Engine. SAE Paper No: 2000-01-0533,* Warrendale. PA: Society of Automotive Engineers.

Alger, T., Mangold, B., Mehta, D. & Roberts, C., 2006. *The Effect of Spark Plug Design on Initial Flame Kernel Development and Spark Plug Performance. SAE Paper No: 2006-01-0224,* Warrendale. PA: Society of Automotive Engineers.

Amsden, A. A. et al., 1992. *Comparisons of Computed and Measured Three Dimensional Flow Fields in a Motored Two-Stroke Engine. SAE Paper No: 920418,* Warrendale. PA: Society of Automotive Engineers.

Anderson, J. et al., 2003. *Comparison of an E10 Direct Injection Two-Stroke Cycle Engine and an E85 Four-Stroke Cycle Engine. SAE Paper No: 2003-32-0077,* Warrendale. PA: Society of Automotive Engineers.

Andersson, I., 2004. *A Comparison of Combustion Temperature Models for Ionization Current Modelling in an SI Engine. SAE Paper No: 2004-01-1465,* Warrendale. PA: Society of Automotive Engineers.

Annand, C. A., 1985. *Cylinder Pressure Measurement and its use in Engine Research. SAE Paper No. 852067,* Warrendale, PA: Society of Automotive Engineers.

Annand, C. A., 1995. Classical Combustion Diagnostics for Engine Research. In: *SAE. Fuels and Lubricants.* Warrendale. PA: Society of Automotive Engineers, pp. 168 Vol 94.

Archer, M. & Bell, G., 2001. *Advanced Electronic Fuel Injection Systems - An Emissions Solution for both 2 and 4 Stroke Small Vehicle Engines SAE Paper No. 2001-01-0010),* Warrendale. PA: Society of Automotive Engineers.

Arcoumanis, C. & Bae, C. S., 1992. *Correlation between Spark-Ignition Characteristics and Flame Development in a Constant-Volume Combustion Chamber. SAE Paper No. 920413,* Warrendale. PA: Society of Automotive Engineers.

Arnone, L., Janeck, M., Marcacci, M. & Kirchberger, R., 2001. *Development of a Direct Injection Two-Stroke Engine for Scooters. SAE Paper No: 2001-01-1782,* Warrendale. PA: Society of Automotive Engineers.

Asanuma, T. & Yanagihara, S., 1962. *Gas Sampling Valve for Measuring Scavenging Efficiency in High-Speed Two-Stroke Engines. SAE Transactions, 70 pp 420-433,* Warrendale. PA: Society of Automotive Engineers.

Astanei, D., Pellerin, S., Hnatiuc, B. & Eugen, H., 2011. The Study of Electrical Parameters and the Exhaust Gas Analysis for a Double Plug. *Annals of the University of Craiova. Geeorghe, Asachi, Iasi, Romania.,* Electrical Engineering Series (35), pp. 47 - 52.

Aust, V., Zimmermann, G., Manz, P.-W. & Hentschel, W., 1999. *Crank-Angle Resolved Temperature in SI Engines Measured by Emission-Absorption Spectroscopy. SAE Paper No: 1999-01-3542,* Warrendale. PA: Society of Automotive Engineers.

Backer, S. a., 1990. *Correlation of Flame Propagation and In-Cylinder Pressure in a Spark-Ignited Engine. SAE Paper No. 902126,* Warrendale. PA: Society of Automotive Engineers.

Ballal, D. R. & Liefebvre, A. H., 1975. The Influence of Spark Discharge Characteristics on Minimum Ignition Energy in Flowing Gases. *Combust and Flame,* Feb-June, Volume 24, pp. 99-108.

Ball, J. K., Bowe, M. J., Stone, C. R. & McFadden, P. D., 2000. *Torque Estimation and Misfire Detection using Block Angular Acceleration. SAE Paper No: 2000-01-0560,* Warrendale. PA: Society of Automotive Engineers.

Batoni, G., 1978. *An Investigation into the Future of Two-Stroke Motorcycle Engine. SAE Paper No: 780710,* Warrendale. PA: Society of Automotive Engineers.

Bauer, W., Tam, C., Heywood, J. B. & Zeigler, C., 1997. *Fast Gas Temperature Measurement by Velocity of Sound for IC Engine Applications. SAE Paper No: 972826,* Warrendale. PA: Society of Automitive Engineers.

Bazelyan, E. M., 1988. Ionization Processes in Spark Discharge Plasmas. *Plasma sources Science and Technology,* Volume 8, pp. 285 - 294.

Bazika, V. & Rodig, J., 1963. *A Method of Determining the Scavenging Efficiency of Oil Cylinders. The Engineers Digest No. 24.,* s.l.: s.n.

Beck, K. W. et al., 2008. *Ion Current Measurement in Small Two-Stroke Engines. SAE Paper No: 2008-32-0037,* Warrendale. PA: Society of Automotive Engineers.

Bella, G. & Chiatti, G., 1989. *Optimisation of the Performance of Two-Stroke Spark-Ignition Engines using a Capacitor in the Exhaust Manifold. SAE Paper No: 891807,* Warrendale. PA: Society of Automotive Engineers.

Bendix, K. H., 1993. *Optimizing of the Non-Steady Operational Behaviour of High Performance Two-Stroke Engines. SAE Paper No: 931509,* Warrendale. PA: Society of Automotive Engineers.

Benson, R. S., 1977. A New Gas Dynamic Model for the Gas Exchange Process in Loop and Cross Scavenged Engines. *International Journal of Mechanical Engineering Science,* Volume 19, pp. 693-711.

Benson, R. S. & Brandham, P. T., 1969. A Method for Obtaining a Quantative Assessment of the Influence of Charge Efficiency in Two-Stroke Engine Performance. *Internationl Journal for Mechanical Science,* Volume 11, pp. 303 - 312.

Berlusconi, G. & Colombo, P., 2001. *Dell'orto Electronic Carburetor. SAE Paper No: 2001-01-1862,* Warrendale. PA: Society of Automotive Engineers.

Bertola, A., Dolt, R. & Howling, J., 2015. *The use of Spark Plug Pressure Transducer for Engine Indication Measurements. Possibilities and Limits. SAE Paper No: 2015-26-0041,* Warrendale. PA: Society of Automotive Engineers.

Betz, G. & Ellermann, J., 1981. *Knock Related Piston Damage in Gasoline Engines. Knock Measurement Technique. Aspect of Piston Failure Prevention.* Wolfsburg, International Symposium on Knocking in Combustion Engines. Nov 26-27..

Biswas, J. C. & Mitra, V., 1979. High Frequency Breakdown and Paschen's Law. *Applied Physics. Vol. 19,* pp. 377 - 381.

Bizard, N. C. & Keck, J. C., 1974. *Experimental and Theoretical Investigation of Turbulent Burning Model for Internal Combustion Engines. SAE Paper No: 740191,* Warrenedale. PA: Socientry of Automotive Engineers.

Bjerkborn, S., 2011. *Development and validation of a Turbulent Flame Propagation Model. MSc Thesis.* s.l.:Lund University.

Blair, G. P., 1988. *The Correlation of Theory and Experiment for Scavenging Flow in Two-Stroke Cycle Engines. SAE Paper No: 881265,* Warrendale. PA: Society of Automotive Engineers.

Blair, G. P., 1993. *Correlation of an Alternative Method for the Prediction of Engine Performance Characteristics with Measured Data. SAE Paper No: 930501,* Warrendale. PA: Society of Automotive Engineers.

Blair, G. P., 1996. *Design and Simulation of Two Stroke Engines. SAE R-161.* 1st ed. Warrendale. PA: Society of Automobile Engineers.

Blair, G. P. & Ashe, M. C., 1976. *The Unsteady Gas Exchange Charcteristics of a Two-Cycle Engine. SAE Paper No: 760644,* Warrendale. PA: Society of Automotive Engineers.

Blair, G. P., Hinds, E. T. & Fleck, R., 1979. *Predicting the Performance Characteristics of Two-Cycle Engines fitted with Reed Induction Valves. SAE Paper No: 790842,* Warrendale. PA: Society of Automotive Engineers.

Bolt, J. A. H. D. L., 1967. *The Effects of Mixture Motion upon the Lean Limit and Combustion of Spark-Ignited Mixtures. SAE Paper No: 670467,* Warrendale. PA: Society of Automotive Engineers.

Boylett, F. D. A. & Looms, J. S. T., 1963. Effect of Discharge Products upon Corona Discharge and Spark Breakdown Voltage. *Proceedings of IEEE,* 110(12).

Bradley, D. et al., 1994. *CARS Temperature Measurements and the Cyclic Dispersion of Knock in Spark Ignition Engines.* s.l., The Combustion Institue, pp. 125 - 133.

Bregnsbo, M. A. C. a., 1979. Experimental Study on the Onset of Positive Corona in Atmospheric Air. *Journal of Applied Pyhsics. Vol. 50,* pp. 6797 - 6805.

Brehob, D. D., 1989. *An Exhaust Ionization Sensor for Detection of Late Combustion with EGR. SAE Paper No: 892084,* Warrendale. PA: Society of Automotive Engineers.

Brereton, G. H. & Rani, M. A. A., 1998. *Some Effects of Spark Plug Electrode Geometry and Orientation on Small Engines. SAE Paper No: 982057,* Warrendale. PA: Society of Automotive Engineers.

Brown, S. C., 1951. *High Frequency Discharge Breakdown. Technical report No. 195,* Cambridge, MA. USA: Massachusetts Institue of Technology.

Bruce, F. M., 1947. Calibration of Uniform-Field Spark-Gaps for High Voltage Measurement at Power Frequencies (Based on E.R.A. Report Ref. L/T152 April, 1947)). *Journal of the Institue of Electrical Engineers,* 94(II), p. 138.

Brunt, M. F. J. R. H. & Emtage, A. L., 1998. *The Calculation of Heat Release Energy from Engine Cylinder Pressure Data. SAE Paper No: 981052,* Warrendale. PA: Society of Automotive Engineers.

Burgett, R. R., Leptich, J. M. & Sangwan, V. S., 1972. *Measuring the Effects of Spark Plug and Ignition System Design on Engine Performance. SAE Paper No: 720007,* Warrendale. PA: Society of Automotive Engineers.

Byttner, S. & Rognvaldsson, T., 2001. *Estimation of Combustion Variability using In-Cylinder Ionization Measurements. SAE Paper No: 2001-01-3485,* Warrendale. PA: Society of Automotive Engineers.

Caicedo, M. A. R. et al., 2012. *A Parameter Varying Observer for the Enclosed Mass in a Spark-Ignited Engine.* Rueil-Malmaison, France, IFAC, The International Federation of Automatic Control, pp. 318 - 325.

Caicedo, M. A. R., Witrant, E., Sename, O. & Hegelin, P., 2012. *A High Gain Observer for Enclosed Mass Estimation in a Spark Ignited Engine..* Montreal, QC, Canada, IEEE.

Carlucci, A. P., Ficarella, A., Laforgia, D. & Longo, M., 2015. *An Easy and Inexpensive way to Estimate the Trapping Efficiency of a Two-Stroke engine.* New York, Elsevier Ltd., pp. 17-22.

Carretti, A., 2015. *In-Cylinder Pressure Measurements using Spark Breakdown Voltage. MSc Dissertation.,* Oxford: Oxford Brookes University.

Cartwright, A. F. R., 1994. *A Detailed Investigation of Exhaust System Design in High Performance Two-Stroke Engines. SAE Paper No: 942515,* Warrendale. PA: Society of Automotive Engineers.

Casarella, M. V. et al., 1997. *Spray Combustion and Emissions in a Direct Injection Two-Stroke Engine with Wall-Stabilisation and an Air-Assisted Spray. SAE Paper No: 970360,* Warrendale. PA: Society of Automotive Engineers.

Ceviz, M. A., Oner, I. V., Kaya, F. & Karacali, T., 2011. Analysis of the Thermal Efficiency and Cyclic Variations in a SI Engine Under Lean Combustion Conditions. ISSN 1300-3615. *Journal of Thermal Science and Technology,* Volume 31, pp. 121 - 127.

Chae, J. O. & al, e., 1999. *The Measurement of Combustion Gas Density Fluctuation in a Cylinder of Internal Combustion Engine by Spark-Plug for Detection of Transient Misfire. 3rd KSME-JSME Thermal Engineering Conference. Vol. 2. pp 355-358..* s.l., s.n.

Chen, C. & Wallace, F. J., 1987. *A Generalised Isobaric and Isochoric Thermodynamic Scavenging Model. SAE Paper No: 871657,* Warrendale. PA: Society of Automotive Engineers.

Chen, C. & Wallace, F. J., 1987. *A Phenomenological Unsteady Jet Model for Uniflow Scavenging. SAE Paper No: 871658,* Warrendale. PA: Society of Automotive Engineers.

Choi, I., Chun, K. M., Park, C. & Hann, J. W., 2000. *End-Gas Temperature Measurements in a DOHC Spark-Ignition Engine using CARS. SAE Paper No: 2000-01-0237.,* Warrendale. PA: Society of Automotive Engineers.

Chubb, L. W. & Fortesque, C., 1913. The Calibration of the Sphere Gap Voltmeter. *Journal of A.I.E.E.,* 32(2), pp. 627 - 638.

Chu, T. D., 1992. *High Frequency Breakdown Voltage. Report No. SSCL- 539. Contract No - DE-AC35-89ER40486,* Dallas: Universities Research Association. Inc. USA.

Clark, C. J. & Ryan, H. J., 1914. Sphere Gap Discharge Voltages at High Frequencies. *Proceedings of A.I.E.E..*

Clarke, W. A., Clark, W. E., M, A. & West, R., 2002. *Reinventing the Internal Combustion (IC) Engine Head and Exhaust Gaskets. SAE Paper No: 2002-01-0332,* Warrendale. PA: Society of Automotive Engineers.

Clark, R. J. D., 1926. *Transactions of the Faraday Society No. 22 page 338,* London: The Faraday Society.

Cobine, J. D., 1958. *Gaseous Conductors. Theory and Engineering Apllications..* New York: Dover Publications Inc..

Collings, N., 1988. *A New Technique for Measuring HC Concentration in Real Time in a Running Engine. SAE Paper No: 880517,* Warrendale. PA: Society of Automotive Engineers.

Cowart, J., 2002. *A Comparison of Transient Air-Fuel Measurement Techniques. SAE Paper No: 2002-01-2753,* Warrendale. PA.: Society of Automotive Engineers.

Craver, R. J., Poliak, R. S. & Miller, R. D., 1970. *Spark Plug Design Factors and their Effect on Engine Performance. SAE Paper No: 700081,* Warrendale. PA: Society of Automotive Engineers.

Crawford, J. G. & Wallace, J. S., 1996. *Validation Tests for a Fast Response Flame Ionisation Detector for In-Cylinder Sampling Near the Spark Plug. SAE Paper No: 961201,* Wareendale. PA: Society of Automotive Engineers.

Cudina, M., 2004. Model Testing the Two Phase Scavenging System in a Two-Stroke Eengine. *Proceedings of the Institue of Mechanical Engineers,* Volume 218 part D: J Automobile Engineering, pp. 1307 - 1316.

Curry, S., 1963. *A Three Dimensional Study of Flame Propagation in a Spark Ignition Engine. SAE 71 p. 628,* Warrendale. PA: Society of Automotive Engineers.

Czekala, M., Johnson, B., Morgani, C. & McRoy, G., 1998. *Matching Ignition System Multi-Spark Calibration to the Burn-Rate of an Engine to Extend Ignitability Limits. SAE Paper No: 981046,* Warrendale. PA: Society of Automotive Engineers.

Dadd, M. W., 1983. Acoustic Thermometry in Gases Using Pulse Tecnology. *High Temperature Technology,* Issue 6.

Daniels, C. F., 1998. *The Comparison of Mass Fraction Burned Obtained from the Cylinder Pressure Signal and Spark Plug Ion Signal. SAE Paper No. 980140,* Warrendale. PA: Society of Automotive Engineers.

Daniels, C. F. & Scilzo, B. M., 1996. *The Effects of Electrode Design on Mixture Ignitabilty. SAE Paper No: 960606,* Warrendale. PA: Society of Automotive Engineers.

Daniels, C. F., Zhu, G. G. & Winkelman, J., 2003. *Inaudible Knock and Partial Burn Detection using In-Cylinder Ionization Signal. SAE Paper No: 2003-01-3149,* Warreandale. PA: Society of Automotive Engineers.

Davaine, J., 1993. *Measurement and Analysis of Intra-Cyclic RPM changes. SAE Paper No: 930397,* Warrendale. PA: Society of Automotive Engineers.

Davenport, D., Duke, R., Bingham, J. T. & Kemmerer, D., 2003. *Low-Pressure In-Cylider Fuel Injection. SAE Paper No: 2003-32-0082,* Warrendale. PA: Society of Automotive Engineers.

De-Soete, G. C., 1983. Propagation behaviour of Spark Ignited Flames in Early Stages. *IMechE- Combustion in Engineering,* Vol. 1 C59/83, pp. 93 -100.

De-Swart, J. A. M. et al., 2006. Detailed Analysis of the Mass Burning Rate of Stretched Flames including Perferential Diffusion Effects. *Combust and Flame 145,* pp. 245 - 258.

Douglas, R. & Blair, G. P., 1982. *Fuel Injection of a Two-Stroke Cycle Spark Ignition Engine. SAE Paper No: 820952,* Warrendale. PA: Society of Automotive Engineers.

Downs, D. & Wheeler, R. W., 1951. Recent Developments in Knock Research. *Procedings of Automotive Division of the Institution of Mechanical Engineers,* 5(1), pp. 88-89.

Eriksson, l., 1998. *Requirement for a Systematic Method for Identifying Heat Release Model Parameters. SAE Paper No: 980626,* Warrendale. PA: Society of Automotive Engineers.

Essig, G., 1981. *Piston Loading at Knock Combustion (Detonation).* Wolfburg, International Symposium on Knocking in Combustion Engines. Nov. 26-27.

Fansler, T. D. & French, D. T., 1988. *Cycle-Resolved Laser-Velocimetry Measurements in a Re-Entrant-Bowl-in-Piston Engine. SAE Paper No: 880377,* Warrendale. PA: Society of Automotive Engineers.

Faraday, M., 1844. *Experimental Researches in Electricity.* London: Richard and John Edward Taylor.

Feser, K., 1972. Influence of Humidity on the Breakdown Voltage of D.C and A.C. Voltages in Air. *Translated from ASE 63,* Volume 6, pp. 278 - 282.

Ficker, T., 2009. Electrical Breakdown in Gases via a New Mechanism of Avalanche and Streamer Multiplications. *The Japan Society of Plasma Science and Nuclear Fusion Research,* Volume 8, pp. 744 - 749.

Fleck, R., Blair, G. P. & Houston, A. R., 1987. *An Improved Model for Predicting Reed Valve Behaviour in Two-Stroke Cycle Engines. SAE Paper No: 871654,* Warrendale. PA: Society of Automotive Engineers.

Forster, J., Gunther, A., Ketterer, M. & Wald, K., 1999. *Ion Current Sensing for Spark Ignition Engines. SAE Paper No: 1999-01-0204,* Warrendale. PA: Society of Automotive Engineers.

Foster, H. H., Schuricht, F. R. & Tauschek, M., 1949. *Experimental Study of Loop-Scavenged Compression Ignition Cylinder for Gas use. Report RM No. E8L30,* Washington. USA: NACA.

Foudray, H. Z. & Ghandhi, J. B., 2003. *Scavenging Measurements in a Direct-Injection Two-Stroke Engine. SAE Paper No: 2003-32-0081,* Warrendale. PA: Society of Autmotive Engineers.

Franke, A., Einwall, P., Larsson, A. & Reinmann, R., 2003. *Analysis of the Ionization Equilibrium in the Post Flame Zone. SAE Paper No: 2003-01-0715,* Warrendale. PA: Society of Automotive Engineers.

Franke, A. & Reinmann, R., 2000. *Calorimetric Characterization of Commercial Ignition Systems. SAE Paper No: 2000-01-0548,* Warrendale. PA: Society of Automotive Engineers.

Fritton, J. & Nates, R., 1996. *Knock Erosion in Spark-Ignition Engines. SAE Paper No: 962102,* Warrendale. PA: Society of Automotive Engineers.

Fujikawa, T. & Ohtsu, M., 1991. *Development of an Automatic Exhaust Valve Control Device for 2 Stroke Engines. SAE Paper No: 911226,* Warrendale. PA: Society of Automomotive Engineers.

Galindo, J., Climent, H., Pla, B. & Jimenez, V. D., 2010. Correlations for Wiebe Function Parameters for Combustion Simulation in Two-Stroke Small Engines. *Applied Thermal Engineering,* Volume 31 (6-7), p. 1190.

Galloni, E., 2010. Analyses about parameters that affect Cyclic Variation in a Spark Ignition Engne.. *Applied Thermal Engineering, 29 (5-6),* p. 1131.

Gatowski, J. A., Balles, E. N., Chan, K. M. & Nelson, F. E., 1984. *Heat Release Analysis of Engine Pressure Data: SAE Paper No: 841359,* Warrendale. PA: Society of Automotive Engineers.

Gatowski, J. A. & Heywood, J. B., 1985. *Effects of Valve-Shrouding and Squish on Combustion in a Spark-Ignition Engine, SAE Paper No: 85209,* Warrendale PA: Society of Automotive Engineers.

Geiser, F., Wytrykus, F. & Spicher, U., 1998. *Combustion Control with the Optical Fibre Fitted Production Spark Plug. SAE Paper No: 980139,* Warrendale. PA: Society of Automotive Engineers.

Ghandi, J. B. & Bracco, F. V., 1995. *Fuel Distribution Effects on the Combustion of a Direct-Injection Stratified-Charge Engine. SAE Paper No; 950460,* Warrendal. PA: Society of Automotive Engineers.

Ghandi, J. B., Felton, P. G., Gajdeczko, B. F. & Bracco, F. V., 1994. *Investigation of the Fuel Distribution in a Two-Stroke Engine with Air-Assited Injector. SAE Paper No: 940394,* Warrendale. PA: Society of Automotive Engineers.

Gillespie, L., Lawes, M., Sheppard, C. G. W. & Woolley, R., 2000. *Aspects of Laminar and Turbulent Burning Velocity Relevant to SI Engines. SAE Paper No: 2000-01-0192,* Warrendale. PA: Society of Automotive Engineers.

Glavmo, M., Spadafora, P. & Bosch, R., 1999. *Closed Loop Start of Combustion Control Utilizing Ionization Sensing in a Diesel Engine. SAE Paper No: 1999-01-0549,* Warrendale. PA: Society of Automotive Engineers.

Gorczakowski, A. & Jarossinski, J., 2000. *The Pnenomena of Flame Propagation in a Cylindrical Combustion Chamber with a Swirling Mixture. SAE Paper No: 2000-01-0195,* Warrendale. PA: Society of Automotive Engineers.

Gozy, G., 1974. *'L' Injection Electronique Direct Sur le Motobecane 500cc, VTJ,* s.l.: s.n.

Grandin, B. & Denbratt, I., 2002. *The Effect of Knock on Heat Transfwr in SI Engines. SAE Paper No: 2002-01-0238,* Warrendale. PA: Society of Automotive Engineers.

Grasso, J. B., Pennisi, S., Paparo, M. & Patti, D., 2013. *Estimation of In-Cylinder Pressure using Spark Discharge Current Measurements,* s.l.: 2013 European Conference on Circuit Theory and Design.

Griffin, S. E., Crane, M., Leone, D. M. & Schneider, S. W., 1998. *A Study of Engine Sensitivty to Spark Plug Rim-Fire. SAE Paper No: 981453,* Warrendale. PA: Society of Automotive Engineers.

Grupp, D. J. & Martin, J. K., 2002. *Ignition System Characteristics and Effects on Combustion for Two-Stroke Engines. SAE Paper. No: 2002-01-0644,* Warrendale. PA: Society of Automotive Engineers.

Guindehi. S, 1970. Effect of air humidity on the breakdown voltage in air in various types of voltage and forms of electrodes.. *Bull. SEV 61,* pp. 97 - 104.

Halldin, C., 1992. *Velocity and Turbulence Measurements Close to a Spark Plug. SAE Paper No: 920154,* Warrendale. PA: Society of Automotive Engineers.

Hallgren, B. E. & Heywood, J. B., 2003. *Effects of Substantial Spark Retard on SI Engine Combustion and Hydrocarbon Emissions. SAE Paper No: 2003-01-3237,* Warrendale. PA: Society of Automotive Engineers.

Hamamoto, O. a., 1971. *Cylinder Gas Composition of Small 2-Stroke Cycle Gasoline Engine. SAE Paper No. 710143,* Warrendale. PA: Society of Automotive Engineers.

Hanashi, K., Ishino, Y., Osamura, H. & Hashizume, K., 2001. *Development of New Concept Iridium Plug. SAE Paper No: 2001-01-1201, (DOI org/ 10.4271/ 2001-01-1201),* Warrendale. PA: Society of Automotive Engineers.

Han, Y., 1997. *Spark Plug Based Diagnostics for Fuel - Air Ratio Determination. MSc Thesis.* Toronto: University of Toronto.

Han, Z., Fan, L. & Reitz, R. D., 1997. *Multidimensional Modelling of Spray Atomization and Air-Fuel Mixing in Direct-Injection Spark-Ignition Engine. SAE Paper No: 979884,* Warrendale. PA: Society of Automotive Engineers.

Harari, R. & Sher, E., 1993. *The Effect of Ambient Pressure on the Performance Map of a Two-Stroke SI Engine. SAE Paper No. 930503,* Warrendale. PA: Society of Automotive Engineers.

Hardalupas, Y. et al., 2004. Chemiluminescence Sensor for Local Equivalence Ratio of Reacting Mixtures of Fuel and Air (FLAMESEEK). *Applied Thermal Engineering 24,* pp. 1619 - 1632.

Hardcastle, J., 2013. *Automotive Council Tecnology Work Groups. Consensus Roadmaps and Workstream Feedback. Presentation at Low Carbon Vehicle Event.* s.l., s.n.

Harigaya, Y., Toda, F., Ohyagi, S. & Tsuji, H., 1989. *Surface Temperature and Wall Heat Flux in a Spark-Ignition Engine under Knocking and Non-Knocking Conditions. SAE Paper No: 891795,* Warrendale. PA: Society of Automotive Engineers.

Hart, M., Zeigler, M. & Loefeld, O., 1998. *Adaptive Estimation of Cylinder Air Mass using the Combustion Pressure. SAE Paper No: 980791,* Warrendale. PA: Society of Automotive Engineers.

Hashimoto, E., Tottori, T. & Terata, S., 1982. *Scavenging Performance Measurements of High Speed Two-Stroke Engines. SAE Paper No: 850182,* Warrendale. PA: Society of Automotive Engineers.

Hata, N., Fujita, T. & Matsuo, N., 1981. *Modification of Two-Stroke Engine Intake System for Improvement of Fuel Consumption and Performance through the Yamaha Energy Induction System (YIES). SAE Paper No. 810923,* Warrendale. PA: Society of Automotive Engineers.

Hata, N. & Lio, T., 1981. *Improvement of Two-Stroke Engine Performance with the Yamaha Power Valve System. SAE Paper No: 810922,* Warrendale. PA: Society of Automotive Engineers.

Haworth, D. C., Huebler, M. S., EL Tahry, S. H. & Matthes, W. R., 1993. *Multidimensional Calculations for a Two Stroke Cycle Engine. A Detailed Scavenging Model Validation. SAE Paper No: 932712,* Warrendale. PA: Society of Automotive Engineers.

Hayashi, F., 1914. Spark Breakdown Voltages of Pure and Gas Mixtures to 75 Atmosheres. *Ann. De Physik,* 45(4), p. 431.

Herweg, R., Begleris, P. H., Zettlitz, A. & Ziegler, G. F. W., 1988. *Flow Field Effects on Flame Kernel Formation in a Spark Ignition Engine. SAE Paper No: 881639,* Warrendale. PA: Society of Automotive Engineers.

Heywood, J. B., 1988. *Internal Combustion Engine Fundamentals.* New York: McGraw-Hill.

Heywood, J. B., 1994. *Combustion and its Modelling in Spark-Ignition Engines.* s.l., COMODIA, pp. 1 - 15.

Heywood, J. B. & Sher, E., 1999. *The Two-Stroke Cycle Engine - Its Development, Operation and Design (ISBN: 1-56032-831-2).* First ed. Warrendale. PA: Society of Automotive Engineers.

Higashino, I., Hitomi, M. & Yoshizawa, J., 1966. *A Method to Measure an Exhaust Gas Temperature with Ultrasound. Memoirs of the Faculty of Engineering. Vol. 8,* Osaka: Osaka City University.

Hill, B. W. & Blair, G. P., 1983. *Further Tests on Reducing Fuel Consumption with a Carburetted Two-Stroke Cycle Engine. SAE Paper No: 831303,* Warrendale. PA: Society of Automotive Engineers.

Hill, P. G. & Kapil, A., 1989. *The Relationship Between Cyclic Variations in Spark-Ignition Engines and Small Structure of Turbulence.* Amsterdam, Elsevier Ltd., pp. 237-247.

Hires, S. D., Tabaczynski, R. J. & Novak, J. M., 1978. *The Pediction of Ignition Delay and Combustion Intervals for a Homogeneous Charge Spark Ignition Engine. SAE Paper No: 780232,* Warrrendale. PA: Society of Automotive Engineers.

Hirz, M., Korman, M., Eichlseder, H. & Kirchberger, R., 2004. *Potential of the 50cc Two Wheeler Motor Vehicle Class in Respect of Future Exhaust Emission Targets. SAE Paper No: 2004-32-0050,* Warrendale. PA: Society of Automotive Engineers.

Holzer, W., 1932. Zeits. f Phhysik 77, 676. *ibid. 26,* p. 43.

Holzleitner, H., 1991. *Snowmobile 340ccm Formula 1 - Kart 100ccm Racing Engines: Two Extremes in terms of High-Performance Two-Stroke Engine Layouts. SAE Ppaer No. 911312,* Warrendale. PA: Society of Automotive Engineers.

Honda et al, 2004. *A Study of Mixture Formation and Combustion for Spray Guided DISI. SAE Paper No. 2004-01-0046,* Warrendale. PA: Society of Automotive Engineers.

Honda Racing Corporation, 1993. *PGM - F1 For NSR500.* Japan: HRC.

Hood, S., 1990. *The V-Grooved Electrode Spark Plug. SAE Paper No: 901535,* Warrendale. PA: Society of Automotive Engineers.

Hopkinson, B., 1914. The Charging of Two-Stroke Cycle Internal Combustion Engines. *Transactions of NW Coast Instn. Engrs. Shipbuilders,* Volume 30, p. 433.

Hori, T., Shibata, M., Okabe, S. & Hashizume, K., 2003. *Super Ignition Spark Plug with Fine Centre and Ground Electrodes. SAE Paper No: 2003-01-0404 (Doi.org/10.4271/2003-01-0404,* Warrendale PA: Society of Automotive Engineers.

Huber, E. W., 1971. *Measuring the Trapping Efficiency of Internal Combustion Engines through Continuous Exhaust Gas Analysis. SAE Paper No: 710144,* Warrendale. PA: Society of Automotive Engineers.

Hull, W. et al., 2003. *Optimisation of a Direct-Injected 2-Stroke Cycle Snowmobile SAE Paper No: 2003-32-0074,* Warrendale. PA: Society of Automotive Engineers.

Hung, D. L. S. et al., 2008. *Gasoline Fuel Injector Spray Measurement and Characterization - A New SAE J2715 Recommended Practice. SAE Paper No: 2008-01-1068 (Doi.org/10.4271/2008-01-1068),* Warrendale. PA: Society of Automotive Engineers.

Hunicz, J., Piernikarski, D. & Niewczas, A., 2004. *Transient In-cylinder AFR Management Based on Optical Emissions Signals. SAE Paper No: 2004-01-0516,* Warrendale. PA: Society of Automotive Engineers.

Hutton, J. G., 1947. Determination of Corona Starting Voltages for Non uniform fields in Air. *Transactions of the AIEE,* Volume 66, pp. 1674-1680.

Hu, Z., 1996. *Non-Linear Instabilities of Combustion Processes and Cycle-to-Cycle Variations in Spark Ignition Engines. SAE Paper No: 961197,* Warrendale. PA: Society of Automotive Engineers.

Ikeda, Y., Nishiyama, A. & Baritaud, T., 2008. *Flame Speed Measurement of a Racing Engine by IR Method and Chemiluminescence Method,* Lisbon, Portugal: s.n.

Ishiguro, H., Kanao, K., Okabe, S. & Hashizume, K., 2005. *Super Carbon Fouling Resistive Small Size Spark Plug. SAE Paper No: 2005-01-1158,* Warrendale. PA: Society of Automotive Engineers.

Isigami, S., Tanaka, Y. & Tamari, M., 1963. *The Trapping Efficiency Measurement of Two-Stroke Cycle Diesel Engine by Tracer Gas Method. Bulletin of JSME, 6. pages 541-31,* Tokyo: JSME.

Ivansson, N., 2003. *Estimation of the Residual Gas Fraction in an HCCI-engine using Cylinder Pressure. Thesis Reg. nr. LiTH-ISY-EX-3441,* Linkoping: Linkoping University.

James, K., Chen, R. & Turner, J., 2010. *Ionization and Ionization Rate in a Two-Stroke HCCI Engine Fueled with E85 For Control Feedback. SAE Paper No: 2011-01-1247,* Warrendale. PA: Society of Automotive Engineers.

Jante, A., 1968. *Scavenging and other problems of Two-Stroke Cycle Spark-Ignition Engines. SAE Paper No: 680468,* Warrendale. PA: Society of Automotive Engineers.

Jaulmes, M. E., 1977. Le Moteur a Deux-Temps a Injection Electronique. *Ingenieurs de L'Automobile,* pp. 11-77.

Javan, S., Hosseini, S. V. & Alaviyoun, S. S., 2012. An Experimental Investigation of Spark Plug Temperature in Bi-Fuel Engine and its effect on Eectrode Erosion. *International Journal of Automotive Engineering,* 2(1), pp. 21 - 29.

Jennings, G., 1973. *Two-Stroke Tuners Handbook (41-ISBN 0-912656-41-7).* 1st ed. Tucson. Arizona: H.P. Books.

Johansson, B., 1996. *Cycle to Cycle Variations in SI Engines- The Effects of Fluid Flow and Gas Composition in the Vicinity of the Spark Plug on Early Combustion. SAE Paper No: 962084,* Warrendale. PA: Society of Automotive Engineering.

Karagiorgis, S. et al., 2006. *Residual Gas Fraction Measurement and Estimation on a Homogeneous Charge Compression Ignition Engine Ultizing the Negative Valve Overlap Strategy. SAE Paper No: 2006-01-3276,* Warrendale. PA: Society of Automotive Engineers.

Karmakar, S., 2012. An Experimental Study of Air Breakdown Voltage and its effects on Solid Insulation. *Journal of Electrical Systems,* 8(2), pp. 209-217.

Kato, T., Akiyama, K. N. T. & Shimizu, R., 2007. *Development of Combustion Behaviour Analysis Techniques in the Ultra High Engine Speed Range. SAE Paper No: 2007-01-0643,* Warrendale. PA: Society of Automotive Engineers.

Kawamura, Y. et al., 1988. *MBT Control through Individual Cylinder Pressure. SAE Paper No. 881779,* Warrendale. PA: Society of Automotive Engineers.

Keck, J. C., 1982. *Turbulent Flame Structure and Speed in Spark-Ignition Engines.* Haifa, Israel, The Combustion Institue, Elsevier, pp. 1451-1466.

Keck, J. C., Heywood, J. B. & Noske, G., 1987. *Early Flame Development and Burning Rates in Spark Ignition Engines and their Cyclic Variabilty. SAE Paper No. 870164,* Warrendale. PA: Scociety of Automotive Engineering.

Khou, L. Y. C. & Yang, Z., 1984. *Minimisation of Inverse Inlet Flow and Consequent Reduction in Specific Fuel Consumption in Gasoline Engines. SAE Paper No: 841093,* Warrendale. PA: Society of Automotive Engineers.

Kim, J. & Anderson, R. W., 1995. *Spark Anemometry of Bulk Gas Velocity at the Plug Gap of a Firing Engine. SAE transactions, 104(3) (1995) 2256-2266,* Warrendale. PA: Society of Automotive Engineers.

Kinoshita, H. & Motoyama, Y., 1999. *The Relationship between Port Shape and Engine Performance for Two-Stroke Engines. SAE Paper No: 1999-01-3333/JSAE 9938088,* Warrendale. PA: Society of Automotive Engineers.

Kirchberger, R., Eichiseder, H., Winkler, F. & Hirz, M., 2007. *Potential of High Technology 50cc³ Two Stroke and Four Stroke Engines. SAE Pparer No: 2007-32-0013 / JSAE 20076513,* Warrendale. PA: Society of Automotive Engineers.

Knaus, D., Gouldin, F., Hinze, P. & Miles, P., 1999. *Measurement of Instantaneous Flamelet Surface Normals and the Burning Rate in a SI Engine. SAE Paper No: 1999-01-3543,* Warrendale. PA: Society of Automotive Engineers.

Koehler, F. & Bargende, M., 2004. *A Model for a Fast Prediction of the Residual Gas Fraction in IC Engines. SAE Paper No: 2004-01-3053,* Warrendale. PA: Society of Automotive Engineers.

Koliatene, F., Sili, E. & Cambronne, J.-P., 2011. Temperature Dependance of Electrical Breakdown Mechanisms on the left of the Paschen Minimum. *IEEE Transactions. Plasma Science,* 11, 39(11), pp. 3173-3179.

Komotori, K. & Watanabe, E., 1969. *A Study of the Delivery Ratio Characteristics of Crankcase Scavenged Two-Stroke Cycle engines. Parts 1 & 2. SAE Paper No. 690136,* Warrendale. PA: Society of Automotive Engineers.

Kubota, S., 2010. *Evaluation of the Calculation Accuracy of Local Air-Fuel Ratio using VECTIS/WAVE. Ricardo User Conference,* s.l.: Honda R&D Co. Ltd..

Kuffel, E., Zaengl, W. S. & Kuffel, J., 2000. *High Voltage Engineering Fundamentals. ISBN 0 75 06 3634 3.* 2nd ed. Oxford: Butterworth-Heinemann.

Ku, P. M. & Trimble, T. F., 1956. Scavenging Characteristics of a Two-Stroke Cycle Engine as determined by Skip-Cycle Operation. *Journal of Research of National Bureau of Standards,* Research Paper 2721 Vol. 57(6), pp. 325 - 331.

Kusano, K. & Kurosaka, H., 1991. *Development of Programmed - Fuel Injection for Two-Stroke Cycle Racer Engine. SAE Paper No: 911224,* Warrendale. PA: Society of Automotive Engineers.

Ladammatos, N., 1992. Cyclically Resolved Measurements of Hydrocarbons in Cylinders of Internal Combustion Engines by Means of a Fast Flame Ionization Detector. *Journal of the Institue of Energy,* Volume 65 (463), pp. 94 - 101.

Laimbock, F. J., 1991. *The Potential of Small Loop Scavenged Spark Ignition Single Cylinder Two-Stroke Engines. SAE Paper No. 910675,* Warrendale. PA: Society of Automotive Engineers.

Lancaster, D. R., 1976. *Effects of Engine Variables on Turbulence in a Spark-Ignition Engine. SAE Paper No: 760159,* Warrendale. PA: Society of Automotive Engineers.

Lancaster, D. R., Krieger, R. B., Sorenson, S. C. & Hull, W. L., 1976. *Effects of Turbulence on Spark-Ignition Engine Combustion. SAE Paper No: 760160,* Warrendale. PA: Society of Automotive Engineers.

Lee, K. H., Ohira, T., Nakajima, T. & Masumoto, R., 1990. Measurement of Gas Flow Velocity in the Combustion Chamber of a Two-Stroke S.I engine by Laser Doopler Velocimeter. *JSME International,* Feb, 1(1), pp. 163-170.

Lee, M. J., Hall, M., Ezekoye, O. A. & Matthews, R. D., 2005. *Voltage and Energy Deposition Characteistics of Spark Ignition Systems. SAE Paper No: 2005-01-0231,* Warrendale. PA: Society of Automotive Engineers.

Lee, Y. G. & Boehler, J. T., 2005. *Flame Kernel Development and its Effects on Engine performance with Various Spark Plug Electrode Configurations,* Warrendale. PA: Society of Automotive Engineers.

Lee, Y. G., Grimes, D. A., Boehler, J. T. & Flavin, C., 2000. *A Study of the Effects of Spark Plug Electrode Design on 4-Cycle Spark-Ugnition Engine Performance. SAE Paper No: 2000-01-1210,* Warrendale. PA: Society of Automotive Engineers.

Leroy, T., Chauvin, J. & Petit, N., 2008. *Controlling Air and Burned Gas Masses of Turbocharged VVT SI Engines.* Cancun. Mexico, IEEE.

Litak, G. et al., 2008. Combustion Processes in a Spark Ignition Engine: Analysis of Cyclic Maximum Pressure and Peak Pressure Angle. *Mechanica,* Feb, 44(1), pp. 1-11.

Litak, G., Kaminski, T., Rusinek, R. & Wendeker, M., 2008. Patterns in the Combustion Process in a Spark Ignition Engine. *Science Direct. Chaos, Solutions and Fractals 35,* pp. 578-585.

Livengood, J., Taylor, C. & Wu, P., 1958. *Mesurement of Gas Temperatures in an Engine by the Velocity of Sound Method. SAE Transactions. Vol. 66.,* Warrendale. PA: Society of Automotive Engineers.

Loeb, L. B. & Silsbee, F. B., 1920. *Effect of Temperature and Pressure on Sparking Voltage. NACA Report No. 54,* Washington: NACA.

Lorenz, N., T, B. & Wilson, B., 2005. *Design of a Direct Injection Retrofit Kit for Small Two-Stroke Engines. SAE Paper No. 2005-32-0095 (JSAE: 20056601),* Warrendale. PA: Society of Automotive Engineers.

Lucas, J. R., 2001. *High Voltage Engineering.* s.l.:University of Moratuwa.

Lu, J.-H. & Lee, Y.-B., 1996. *Analysis and Measurements of Cyclic Variations and Emissions of Single Cylinder Two Stroke Engines at Low Loads. SAE Paper No: 960746,* Warrendale. PA: Society of Automotive Engineers.

Lu, J.-H. & Wang, C.-M., 1995. *Studies on the Cyclic Variations of Single Cylinder Two Stroke Engines- Cycle Analysis SAE Paper No: 950225,* Warrendale. PA: Society of Automotive Engineers.

Maekawa, 1957. *Text of course. JSME G36. Vol. 23,* s.l.: s.n.

Malaczynski, G., Roth, G. & Johnson, D., 2013. *Ion-Sense-Based Real-Time Combustion Sensing for Closed Loop Engine Control. SAE Paper No: 2013-01-0354,* Warrendale. PA: Society of Automotive Engineers.

Maly, R., Klein, R., Peters, N. & Konig, G., 1990. *Theoretical and Experimental Investigation of Knock Induced Surface Destruction. SAE Paper No; 900025,* Warrendale. PA: Society of Automotive Engineers.

Maly, R., Meinel, H. & Wagner, E., 1983. Novel Method for Determining General Flow Parameters from Conventional Spark Discharge. *Proceedings of IMechE,* Volume C67/83, pp. 27-32.

Maly, R. & Vogel, M., 1979. *Initiation and Propoagation of the Flame Front in Lean CH - Air Mixtures by Three Modes of Ignition Spark.* s.l., Elsevier, pp. 821 - 831.

Maly, R. & Ziegler, G., 1982. *Thermal Combustion Modelling - Theorectical and Experimental Investigation of the Knocking Process. SAE Paper No: 820759,* Warrendale. PA: Society of Automotive Engineers.

Manivannan, P., Poola, R. B., Ramesh, A. & Dhinagar, S. J., 1995. *Ignition Enhancement in a Two-Stroke Spark Ignition Engine. SAE Paper No: 951780,* Warrendale. PA: Society of Automotive Engineers.

Mantel, T., 1992. *Three Dimensional Study of Flame Kernel Formation Around a Spark Plug. SAE Paper No: 920587,* Warrendale. PA: Society of Automotive Engineers.

Martin, J. K., Plee, S. L. & Remboski, D. J., 1988. *Burn Modes and Prior-Cycle Effects on Cyclic Variations in Lean-Burn Spark Ignition Engine Combustion. SAE Paper No: 880201,* Warrendale. PA: Society of Automotive Engineers.

Martychenko, A. A., Park, J. K. & Ko, J. S., 1999. *A Study on the Possibility of Estimation of In-Cylinder Pressure by means of Measurement of Spark Gap Breakdown Voltage. SAE Paper No: 1999-01-1115,* Warrendale. PA: Society of Automotive Engineers.

Matekunas, F. A., 1983. *Modes and Measures of Cyclic Combustion Variability. SAE Paper No. 830337,* Warrendale. PA: Society of Automotive Engineers.

Mc Allister, I. W., Crichton, G. C. & Bregnsbo, E., 1989. An Experimental Method to Determine the Electrostatic Field Enhancement Factor of a Practical Conductor. *IEEE Transactions Electrical Insulation,* Volume 24, pp. 325-333.

MECA, 2014. *Emission Control of Two and Three Wheeled Vehicles,* Washington: Manufacturers of Emission Controls Association.

Meek, J. M. & Craggs, J. D., 1953. *Electrical Breakdown of Gases (1st Ed).* London: Clarendon Press.

Mendra, K. Z., 2004. Thermodynamic Properties of Working Fluid of Inetrnal Combustion Engine. *Jornal of KONES Internal Combustion Engines,* 11(3-4), pp. 53-60.

Merker, G. P. & Gerstle, M., 1997. *Evaluation on Two Stroke Engines Scavenging Models. SAE Paper No: 970358,* Warrendale. PA: Society of Automotive Engineers.

Meyer, R. C., Kubesh, J. T., Shahed, S. M. & Davis, J. K., 1993. *Simultaneous Application of Optical Spark Probe and Head Gasket Ionization Probe to a Production engine. SAE Paper No: 930464,* Warrendale. PA: Society of Automotive Engineers.

Miadek, M. & Onder, C., 2000. *A Model for the Estimation of Induced Air Mass and Residual Gas Fraction using Cylinder Pressure Measurements. SAE Paper No: 2000-01-0958,* Warrendale. PA: Society of Automotive Engineers.

Miller, C. D., 1941. *A Study by High-Speed Photography of Combustion and Knock in a Spark-Ignition Engine. NACA Report No. 727,* Washington: NACA.

Mitianiec, W., 2003. *Formation of Fuel Mixture in a SI Two Stroke Engine with Direct Pneumatic Injection. SAE Paper No: 2003-01-3164,* Warrendale. PA: Society of Automotive Engineers.

Mitianiec, W., 2012. *Factors Determining Ignition and Efficient Combustion in Modern Engines Operating on Gaseous Fuels,* s.l.: INTECH.

Mogi, K., Ohno, E. & Nakamura, N., 1992. *Spark Plug Fouling and Counter Measures. SAE Paper. No: 922093,* Warrendale. PA: Society of Automotive Engineers.

MSA, 2011. *Homologation details for the Rotax Senior Max FR125 engine. No.01/ENG/11.* London: United Kingdom Motor Sports Association.

Muebe, C. E., 1965. *AC Breakdown in Gases. M.I.T. Tecnhnical report No. 380,* Massachusett. USA: Massachusetts Institute of Technology.

Nagao, F. & Shimamoto, Y., 1967. *The Effect of Crankcase Volume and Inlet System on the Delivery Ratio of Two-Stoke Cycle Engines. SAE Paper No. 670030,* Warrendale. PA: Society of Automotive Engineers.

Naidu, M. S. & Kamaraju, V., 1996. *High Voltage Engineering.* 2nd ed. New York. USA: McGraw-Hill.

Naitoh, H. & Nomura, K., 1971. *Some New Development Aspects of Two-Stroke Cycle Motorcycle Engines. SAE Paper No. 710084,* Warrendale. PA: Society of Automotive Engineers.

Naito, H. & Taguchi, M., 1966. *Some Development Aspects of Two-Stroke Cycle Motorcycle Engines. SAE Paper No: 880394,* Warrendale. PA: Society of Automotive Engineers.

Namazian, M. et al., 1980. *Schlieren Visualisation of the Flow and Density Fields in the Cylinder of a Spark-Ignition Engine. SAE Paper No: 800044,* Warrendale. PA: Society of Automotive Engineers.

Nam, J. W., Rahaman, H. & Nam, S. H., 2011. Behaviour of a Spark Gap Pulser at High Repetition Rate. *Journal of the Korean Physical Society, (Conference code EAPPC/BEAMS, 2010),* 59(6), pp. 3536 - 3541.

NASA, n.d. *Paschen Breakdown in the Martian Atmosphere,* s.l.: s.n.

Nicholson, D. E. & Witze, P. O., 1993. *Flame Measurement in a Production Engine using Ionization Probes Embedded in Printed Circuit Board Heat Gasket. SAE Paper No: 930390,* Warrendale. PA: Society of Automotive Engineers.

Nilsson, J., 2008. *AC jonstromsinterface: AC Ion Current Interface. Degree Project,* Karlstad: Karlstads Universitet.

Nishioka, S., Hanashi, K. & Okabe, S., 2008. *Super Ignition Spark Plug with Wear Resistive Electrode. SAE Paper No: 2008-01-0092,* Warrendale. PA: Society of Automotive Engineers.

Nishio, K., Osima, T. & Sher, E., 1994. *Cyclic Variabilty in Spark Ignition Engines. SAE Paper No: 940987,* Warrendale. PA: Society of Automotive Engineers.

Nishiyama, A., Kawahara, N. & Tomita, E., 2003. *In-Situ Fuel Concentration Measurement near Spark Plug by 3.39um Infrared Absorption Method (Application to Spark Ignition Engine) SAE Paper No: 2003-01-1109,* Warrendale. PA: Society of Automotive Engineers.

Nomura, K., Hirano, S., Gotoh, T. & Motoyama, Y., 1983. *Improvement of Fuel Consumption with Variable Exhaust Port Timing in a Two-Stroke Gasoline Engine. SAE. Paper No: 850183,* Warrendale. PA: Society of Automotive Engineers.

Nuti, M., 1986. *Direct Fuel Injection: An Opportunity for Two-Stroke SI Engines in Road Vehicle Use. SAE Paper No: 860170,* Warrendale. PA: Society of Automotive Engineers.

Nuti, M. & Martorano, L., 1985. *Short Circuit Ratio Evaluation in the Scavenging of Two-Stroke S.I. Engines. SAE Paper No: 850177,* Warrendale. PA: Society of Automotive Engineers.

Nuti, M., Pardini, R. & Caponi, D., 1997. *FAST Injection System: PIAGGIO Solution for ULEV 2T SI Engines: SAE Paper No: 970362,* Warrendale. PA: Society of Automiotive Engineers.

Ohigashi, S. & Hamamoto, Y., 1971. *Cylinder Gas Composition of Small 2-Stroke Cycle Gasoline Engine. SAE Paper No: 710143,* Warrendale. PA: Society of Automotive Engineers.

Ohigashi, S., Hamamoto, Y. & Tanabe, S., 1969. *A New Digital Method for Measuring Gas Flow Velocity by Electric Discharge. SAE Paper No: 690180,* Warrendale. PA: Society of Automotive Engineers.

Ohita, T., 1989. *Initiations of Engine Knock: Traditional and Modern. Flame Structure..* Alma-Ata, Nagoya Intsitue of Technology.

Oler, C. B., 1954. The use of Sphere Gaps at Radio Frequencies. *Proceedings of A.I.E.E. ,* 73(4), pp. 329 - 332.

Olsson., J. O., Tunestal, P. & Johansson, B., 2001. *Closed Loop Control of an HCCI Engine. SAE Paper No: 2001-01-1031,* Warrendale. PA: Society of Automotive Engineers.

Onishi, S., Souk, H.-J., Pan, D.-J. & Kato, S., 1984. *Multi-Layer Stratified Scavenging (MULS) - A New Scavenging Method for Two-Stroke Engine. SAE Paper No: 840420,* Warredale. PA: Society of Automotive Engineers.

Oppenheim, A. K., 1988. *Quest for Controlled Combustion Engines. SAE Paper No. 880572 (DOi.org//10.4271/88572),* Warrendale. PA: Society of Automotive Engineers.

Oppenheim, A. K., Stewart, H. E. & Hom, K., 1990. *Pulsed Jet Combustion Generator for Premixed Charged Engines.* USA, Patent No. 4,926,818.

Osakabe, T., 1991. *Electronically-Controlled Motorcycle Carburettors. SAE Paper No: 911223,* Warrendale. PA: Society of Automotive Engineers.

Osamura, H., 2000. *Development of Long Life and High Ignitabilty Iridium Spark Plug. Paper Reference No. F2000A144.* Seoul, FISITA.

Ostiguy, J. E., 1993. Longitudinal Profile and Effective Length of a Conventional Dipole Magnet. *Journal of the IEEE,* pp. 2901-2903.

Oswald, R., Ebner, A. & Kirchberger, R., 2010. *High efficient 125-250 cm3 LDPI Two-Stroke Engines, a Cheap and Robust Alternative to Four-Stroke Solutions? SAE Paper No: 2010-32-0019,* Warrendale. PA: Society of Automotive Engineers.

Oxley, M., 2009. *Stealing Speed. ISBN-13: 978-1844256891.* 1st ed. s.l.:Haynes, J H & Co. Ltd.

Ozdor, M., Dulger, M. & Sher, E., 1994. *Cyclic Variability in Spark Ignition Engines; A Literature Survey. SAE Paper 940987,* Warrendale. PA: Society of Automotive Engineers.

Ozdor, M., Dulger, M. & Sher, E., 1996. *An Experimental Study of the Cyclic Variabilty in Spark Ignition Engines. SAE Paper No: 960611,* Warrendale. PA: Society of Automotive Engineers.

Park, J. K. et al., 2000. *The Temperature Interpretation in Gasoline Engine using Breakdown Voltage Characteristics. SAE Paper No: 2000-05-0119,* Warrendale. PA: Society of Automotive Engineers.

Park, J. K. et al., 1999. *The Misfire Detection and Intensity Interpretation using Spark Breakdown Voltage. SAE Paper No:1999-01-2934,* Warrendale. PA: Society of Automotive Engineering.

Paschen, F., 1889. On the Potential Difference required for Spark Initiation in Air, Hydrogen and Carbon Dioxide at Differential Pressures. Ueber die zum Funkenubergang in Luft, Wasserstoff un Kohlensaure bei Verschiedenen Drucken Erfordliche Potentialdifferenz. *Annals der Physik und Chemie,* 273(5), pp. 69-96.

Pashley, N. & Stone, R., 2000. *Ignition System Measurement Technique and Correlations for Breakdown and Arc Voltages and Currents. SAE Paper No: 2000-01-0245,* Warrendale. PA: Society of Automotive Engineers.

Patterson, C. C. & Campbell, N. R., 1918. *The Sparking Potential of Sparking Plugs. Report No. 214,* Oxford: British National Physics Laboratory.

Patterson, C. C. & Campbell, N. R., 1919. Some Characteristics of the Spark Discharge and its Effect in Igniting Explosive Mixtures. *Physics Society Procedures,* Volume 31, p. 168.

Patterson, D. J., 1966. *Cylinder Pressure Variations, A Fundamental Combustion Problem. SAE Paper No: 66129,* Warrendale. PA: Society of Automotive Engineers.

Pedersen, A., 1967. Calculation of Spark Breakdown or Corona Starting Voltages in Nonuniform Fields. *Transactions on Power Apparatus and Systems,* PAS-86(2), pp. 200 - 206.

Pedersen, A., 1989. On the Electrical Breakdown of Gaseous Dielectrics. *IEEE Transactions on Electrical Insulation,* 24(5), pp. 721 - 738.

Peek, F. W., 1914. The Sphere Gap as a means of Measuring High-Voltage. *Proccedings of A.I.E.E,* XXXIII(1), pp. 923 - 949.

Pen-Tung-Sah. A., 1927. Studies of Sparking in Air. *Proc. of A.I.E.E. Volume XLVI,* pp. pp 604-615.

Peschke, E., 1969. Effect of Humidity on the Breakdown and Flash-Over at High DC Voltages in Air. *ETZ-A 90,* Volume 1, pp. 7-13.

Peters, N., 1997. *Four Lectures on Turbulent Combustion., ERCOFTAC Summer school,* Aachen: Institut fur Technische Mechanik RWTH Aachen.

Piah, M. A. M., Ping, P. A. & Buntat, Z., 2008. *Development of Mathematical Equation for Determining Breakdown Voltage of Electrode Gap.* Johor Baharu. Malaysia, IEEE, pp. 1509 - 1513.

Pichard, J., 1977. *Two-Cycle Stratified Charge Engine.* s.l., s.n.

Pim, J. A., 1948. The Electrical Strength of Air at Ultra-High Frequencies. *IEEE Journal,* Volume Radio, pp. 117 - 129.

Pinca-Bretotean, C. R. S. & Stoica, D., 2012. Mathematical Model for Cylinder Pressure in a Spark Ignition Engine. *Annals of Faculty Enhineering Hunedoara - International Journal of Engineering,* Tome X(3), pp. 285 -290.

Pischinger, S., 1989. *Effects of Spark Plug Design Parameters on Ignition and Flame Development on an SI-Engine. PhD Thesis,* Massachusetts. USA: Massachusetts Institue of Technology.

Pischinger, S. & Heywood, J. B., 1988. *A Study of Flame Development and Engine Performance with Breakdown Ignition Systems in a Visualization Engine. SAE Paper No: 880518,* Warrendale. PA: Society of Automotive Engineers.

Pischinger, S. & Heywood, J. B., 1990. *A Model for Flame Kernel Development in a Spark-Ignition Engine.* s.l., s.n., pp. 1033 - 1040.

Pischinger, S. & Heywood, J. B., 1990. *How Heat Losses to Spark Plug Electrodes affect Flame Kernel Development in an SI Engine. SAE Paper No: 900021,* Warrendale. PA: Society of Automotive Engineers.

Pontoppidan, M., Gaviai, G., Bella, G. & de Maio, A., 2004. *Optimization by CFD simulation of Spray formation Parameters to adapt Direct Injection High Pressure Fuel Injectors to High-Speed SI engines. SAE Paper No: 2004-01-0539,* Warrendale. PA: Society of Automotive Engineers.

Powell, T., 1978. *High-Output Small Displacement Two-Stroke Engines. SAE Paper No: 780737,* Warrendale. PA: Society of Automotive Engineers.

Pundir, B. P., Zvonow, V. A. & Gupta, C. P., 1981. *Effect of Charge Non-Homogeneity on Cycle-by-Cycle Variations in Combustion in SI Engines. SAE Paper No: 819774,* Warrendale. PA: Society of Automotive Engineers.

Quader, A. A., 1976. *What Limits Lean Operation in Spark Ignition Engines- Flame Initiation or Propagation. SAE Paper No. 760760,* Warrendale. PA: Society of Automotive Engineers.

Rager, J. et al., 2006. *Design and Materials for Long Life Spark Plugs. SAE Paper No: 2006-01-0617,* Warrendale. PA: Society of Automotive Engineers.

Rassweiler, G. M. & Withrow, L., 1980 (originally published 1938). *Motion Pictures of Engine Flames Correlated with Pressure Cards. SAE Paper No: 800131,* Warrendale. PA: Society of Automobile Engineers.

Reukema, L. E., 1928. The Relationship between Frequency and Spark-Over Voltage in a Sphere-Gap Voltmeter. *Transactions of A.I.E.E,* 47(1), pp. 38 - 48.

Ritz, H., 1932. Breakdown Field Strength of Isolators. Uberschlagfeldstarke von Isolatoren. *Archiv fur Elekrotechnik,* 1 Jan, 26(1), p. 219.

Rivas, M. et al., 2011. *Validation and Application of a New 0D Flame/Wall Interaction Sub Model for SI. Engines. SAE Paper No: 2011-01-1893,* Warrendale. PA: Society of Automotive Engineers.

Rivin, B., Dulger, M. & Sher, E., 1999. *Extending Lean Misfire Limit of Methane-Air Mixtures by Means of an Enhanced Spark Discharge. SAE Paper No: 1999-01-0573,* Warrendale. PA: Society of Automotive Engineers.

Robinet, C. & Higelin, P., 1998. *Crossed Study of Residual Gas Rate - Firing Device for Better Understanding of SI Engines Cycle-to-Cycle Variations. SAE Paper No: 981434,* Warrendale. PA: Society of Automotive Engineers.

Rogowski, A. R. & Bouchard, C. L., 1938. *Scavenging a Piston Ported Two-Stroke Cylinder. NACA Report: TN-712,* Washington: National Advisory Committee for Aeronautics.

Rogowski, W. & Rengier, H., 1926. Ebene Funkenstrecke mit richtiger Randausbilung. *Archive of Elektrotechnik (ibid.),* 16(1), pp. 73-75.

Rohwein, G. J., 1997. An Efficient, Over-Enhanced Ignition System.. *IEEE Transactions on Plasma Science,* 25(2), pp. 306 - 310.

Rosskamp, H., Kimmek, A., Pretzasch, P. & Mugele, M., 2001. *Scavenge Loss Mechanisms and their Driving Forces in Loop-Scavenged High Performance Two-Stroke Engines. Presented at SETI 2001 (PISA). SAE Paper No: 2001-01-1826,* Warrendale. PA: Society of Automotive Engineers.

Russ, S. G., Peet, G. & Stockhausen, W. F., 1997. *Measurements of the Effect on Flame Development and Cycle to Cycle Variations using a Ionization Probe Head Gasket. SAE Paper No: 970507,* Warrrendale. PA: Society of Automotive Engineers.

Saitzkoff, A., Reinmann, R. & Mauss, F. G. M., 1997. *In-Cylinder Pressure Measurement using the Spark Plug as an Ionization Sensor. SAE Paper No: 970857,* Warrendale. PA: Society of Automoble Engineers.

Sanborn, D. S., Blair, G. P. & Kenny, R. C., 1980. *Experimental Asessment of Scavenging Efficiency of Two-Stroke Cycle Engines. SAE Paper No: 800975,* Warrendale. PA: Society of Automotive Engineers.

Sanborn, D. S. & Roeder, W. M., 1985. *Single Cycle Simulation Simplifies Scavenging Study. SAE Paper No: 850175,* Warrendale. PA: Society of Autmotive Engineers.

Sankar, P. B., 2011. *Measurement of Air Breakdown Voltage and Electrical Field using Standard Sphere Gap Method. Master of Technology Thesis.,* Rourkela, India: Department of Electrical Engineering, National Institue of Technology.

Sato, T. & Nakayama, M., 1987. *Gasoline Direct Injection for a Loop Scavenged Two-Stroke Cycle Engine. SAE Paper No: 871690,* Warrendale. PA: Society of Automotive Engineers.

Saxena, M., Mathur, H. B. & Radzimirski, S., 1989. *Reduction of Fresh Charge Losses by Selective Exhaust Gas Recirculation (SEGR) in Two-Stroke Engines. SAE Paper No: 891806,* Warrendale. PA: Society of Automotive Engineers.

Scheitzer, P. H., De Luca, F. & Frank, J., 1942. *The Tracer Gas Method of Determining the Charging Effficiency of Two-Stroke Cycle Diesel Engines. NACA TN-838,* Washington: NACA.

Schemmann, G. S., 2003. *Travelling Spark Ignition. SAE Paper No: 2003-01-0633,* Warrendale. PA: Society of Automotive Engineers.

Schmidt, S., Winkler, F., Schoegl, O. & Pontoppidan, M., 2004. *Development of a Combustion Process for a High-Performance 2-Stroke Engine with High-Pressure Direct Injection. SAE Paper No: 2004-01-2942,* Warrendale. PA: Society of Automotive Engineers.

Schnauffer, K., 1934. Engine Cylinder Flame Propagation Studies by New Methods.. *SAE Journal,* pp. 1-17.

Schoder, G. A., 1961. Zeitsch fur Angew. *Annal der Physik,* p. 296.

Schumann, W. O., 1923. Elektrische Durchbruchfeldstarke von Gasen. ISBN 978-3-662-25891-0. *Archiv fur Elekrotechnik 12,* p. 593.

Sellnau, M. C., Matekunas, F. A., Battiston, P. A. C. C.-F. & Lancaster, D. R., 2000. *Cylinder Pressure Based Engine Control using Pressure Ratio Management and Low-Cost Non-Intrusive Cylinder Pressure Sensors. SAE Paper No: 2000-01-0932,* Warrendale. PA: Society of Automotive Engineers.

Semenow, E. S., 1963. *Studies of Turbulent Gas Flow in Piston Engines. NASA Technical Translation F-97,* Houston: NASA.

Serway, R. A. & Jewett Jnr, J. W., 2014. *Physics for Scientists and Engineers (with Modern Pyhsics) ISBN: T3:978-1-133-95405-7.* 9th ed. Boston: Brookes / Cole.

Shah, J. & Harshadeep, N., 2001. *Urban Pollution from Two Stroke Engine Vehicles in Asia: Technical and Policy Options, 2001. Presented at the Regional Workshop on Reduction of Emissions from 2-3 Wheelers. Sep 5-7, Hanoi, Vietnam.,* New York: The World Bank.

Shelkin, K. I., 1947. *On Combustion in a Turbulent Flow. NACA RN-1110.,* Washington: NACA.

Sher, E., Hacohen, Y., Refael, S. & Harari, R. 1990. *Minimising Short-Circuiting Losses in 2-S Engines by Throttling the exhaust pipe. SAE Paper No: 901665,* Warrendale. PA: Society of Automotive Engineers.

Sher, E., Benyaish, J., Pokryvailo, A. & Spector, Y. 1992. *A Corona Spark Plug System for Spark-Ignition Engines. SAE Paper No: 920810,* Warrendale. PA.: Society of Automotive Engineers.

Sher, E., 1984. *The Effect of Atmospheric Conditions on the Peformance of an Air-Bourne Two-Stroke Spark-Ignited Engine. SAE Paper No: 844962,* Warrendale. PA: Society of Automotive Engineers.

Sher, E., 1985. *A New Practical Model for the Scavenging Process in a Two-Stroke Cycle Engine. SAE Paper No: 850085,* Warrendale. PA: Scociety of Automotive Engineers.

Sher, E., 1986. Spark Ignition in Combustible Gas Mixtures. *Combust and Flame 66,* pp. 17 - 25.

Sher, E., 1990. Scavenging the Two-Stroke Engine. *Progress in Energy and Combustion Science,* Volume 16, pp. 95-124.

Shimanokami, Y., Matsubara, Y., Suzuki, T. & Wataru, M., 2004. *Development of High Ignitabilty with Small Size Spark Plug. SAE Paper No: 2004-01-0987,* Warrendale. PA: Society of Automotive Engineers.

Shimasaki, Y. et al., 1993. *Spark-Plug Voltage Analysis for Monitoring Combustion in an Internal Combustion Engine. SAE Paper No; 930461,* Warrendale. PA: Society of Automotive Engineers.

Shimizu, Y., 1991. *2-Cycle Engine Exhaust Control Device. SAE Paper No: 911228,* Warrendale. PA: Society of Automotive Engineers.

Shoobert, G. W., 1962. Iridium Electrodes Increase Spark Plug Life: Resistanace to Attack by Lead Compounds. *Platium Metals Review,* 6(3), pp. 92 - 94.

Sigmond, R. S. et al., 2004. The Aiming of the Bolt: How Flashover Finds the Weak Spot. *IEEE Transactions on Plasma Science,* 32(5), pp. 1812 - 1818.

Silsbee, F. B., 1920. *Heat Energy of Various Ignition Sparks. NACA Report No. 56,* Washington: NACA.

Silsbee, F. B., 1920. *Spark Plug Defects and Tests. NACA Report No. 51. Parts I,II,III,* Washington: NACA.

Silsbee, F. B., 1925. *The Sparking Voltage of Spark Plugs. NACA Report TR-202,* Washington: United States Government - Bureau of Standards.

Silsbee, F. B. & Honaman, R. K., 1920. *Properties and Preparation of Ceramic Insulators for Spark Plugs. NACA Report No. 53. Parts I,II,III,IV,* Washington: NACA.

Silsbee, F. B. & Randolp, D. W., 1925. *Flame Speed and Spark Intensity. Report No. 187,* Washington: NACA.

Smith, L. A., Fickenscher, T. & Osbourne, R. P., 1999. *Engine Breathing - Steady Speed Volumetric Efficiency and its Validity Under Transient Engine Operation: SAE Ppaer No: 1999-01-0212,* Warrendale. PA: Society of Automotive Engineers.

Smokers, R., Vermeulen, R., van Meighem, R. & Gense, R., 2006. *Review and Analysis of the Reduction Potential and Costs of Technological and other Measures to reduce CO2-Emissions from Passenger Cars.,* Delft: TNO Science and Industry.

Soda, H. & Sato, T., 1999. *Detonation Counter for Production Racing Motorcycle. SAE Paper No: 1999-01-3324,* Warrendale. PA: Society of Automotive Engineers.

Soderbeg, F. J. B. & Lindoff, B., 1998. *Wavelet Analysis of In-Cylinder LDV Measurements and Correlation against Heat Release. SAE Paper No: 980483,* Warrendale. PA: Society of Automotive Engineers.

Sogawa, M. & Kato, M., 2001. *Development of the High-Pressure Direct Injection (HPDI) System for Two-Stroke Outboard Motor. SAE Paper No: 2001-01-1786,* Warrendale. PA: Society of Automotive Engineers.

Sohst, H., 1962. Zeitsch fur Angew. *Physik,* Volume 14, p. 620.

Song, J., Seo, Y. & Sunwoo, M., 2000. *Effects of Ignition Energy and System on Combustion Characteristics in a Constant Volume Combustion Chamber. F2000A003.* Seoul, FISITA World Automotive Congress.

Spicher, U. & Backer, H., 1990. *Correlation of Flame Propagation and In-Cylinder Pressure in a Spark-Ignited Engine. SAE Paper No. 902126,* Wareendale. PA: Society of Automotive Engineers.

Spicher, U. & Velji, A., 1984. *Measurements of Spatial Flame Propagation and Flow Velocities in a Spark Ignited Engine..* s.l., s.n., p. 19.

Stevens, R. & Ewart, P., 2003. *Single Shot Measurement of Temperature and Pressure using Laser-Induced Thermal Gratings with Long Probe Pulse. ,* Oxford: Charendon Laboratory.

Stiebels, B. & Sakak, A. S., 1996. *Development of a New Measurement Technique for the Investigation of End Gas Auto-ignition and Engine Knowledge. SAE Paper No: 960827,* Warrendale. PA: Society of Automotive Engineers.

Stone, C. R., Brown, A. C. & Beckwith, P., 1996. *Cycle by Cycle Variations in Spark Ignition Engine Combustion-Part II: Modelling of Flame Kernel Displacements as a Cause of Cycle by Cycle Variations. SAE Paper No: 960613,* Warrendale. PA: Society of Automotive Engineers.

Stone, R., 2012. *Introduction to Internal Combustion engines. SAE R-391, 2012-09-30, ISBN 978-0-7680-2084-7.* 4th ed. Hong Kong: SAE International and Macmilllan Press.

Streit, E. E. & Borman, G. L., 1971. *Mathematical Simulation of a Large Turbo-Charged Two-Stroke Diesel Engine. SAE Paper No: 710176,* Warrendale. PA: Society of Automotive Engineers.

Stueck, P., Egbers, C. & Geyer, W., 2003. *Visualisation of the Flow Inside the Transfer Channels of Small Two-Stroke Cylinders. SAE Paper No. 2003-32-0008,* Warrrendale. PA: Society of Automotive Engineers.

Stumbo, M. T., 2013. *Paschen Breakdown in a CO2 Atmosphere,* San Luis. California: California Polytechnic State University for The American Institue of Aeronatics and Astronautics.

Subramniam, M. N. et al., 2010. *A Multi-Cylinder Airflow and Residual Gas Estimation Tool Applied to a Vechilcle Demonstrator, SAE Paper No: 2010-01-0169,* Warrendale. PA: Society of Automotive Engineers.

Sweeney, M. E. G., Kenny, R. G., Swann, G. B. G. & Blair, G. P., 1985. *Single Cycle Gas Testing Method for Two-Stroke Engine Scavenging. SAE Paper No: 850178,* Warrendale. PA: Society of Automotive Engineers.

Sweeney, M. E. G., Swann, G. B. G., Kenny, R. G. & Blair, G. P., 1985. *Computational Fluid Dynamics Applied to Two-Stoke Engine Scavenging. SAE Paper No: 851519,* Warrendale. PA: Society of Automotive Engineers.

Swett, C. C., 1948. *Investigation of Spark Gaps subject to Altitude and Air Velocity Conditions. NACE RM No. E8117,* Washingon. USA: NACA.

Swett, C. C., 1949. *Spark Ignition of Flowing Gases I - Energies to Ignite Propane-Air Mixtures in Pressure Range of 2 to 4 inches Mercury Absolute. NACA Report RM-E9E17,* Washington. USA: NACA..

Swett, C. C., 1951. *Spark Ignition of Flowing Gases II- Effect of Electrode Parameters on Energy Required to Ignite a Propane-Air Mixture. NACA Report RM-E51J12,* Washinton. USA: NACA.

Swett, C. C., 1954. *Spark Ignition of Flowing Gases IV-Theory of Ignition in Non-Turbulent and Turbulent Flow using Long-Duration Discharges. NACA Report RM E54F29a,* Washingto. USA: NACA.

Swett, C. C., 1955. *Spark Ignition of Flowing Gases V-Application of Fuel-Air Ratio and Initial-Temperature data to Ignition Theory. NACA RM E55I16,* Washington. USA: NACA.

Swett, C. C. & Donlon, R. H., 1953. *Spark Ignition of Flowing Gases- III Effect of Turbulence Promotor on Energy Required to Ignite a Propane- Air Mixture. NACA Report No. RM E52J28 -,* Washington. USA: NACA..

Tabaczynski, R. J. & Ferguson, C., 1977. *A Turbulent Entrainment Model for Spark-Ignition Engine Combustion. SAE Paper No: 770647,* Warrendale. PA: Society of Automotive Engineers.

Tanoue, K. et al., 2010. *Extension of Lean and Diluted Combustion Stability Limits by Using Repetitive Pulse Discharges. SAE Paper No: 2010-01-0173,* Warrendale. PA: Society of Automotive Engineers.

Taylor, C. F. & Rogowski, A. R., 1956. *Scavenging the Two-Stroke Engine. SAE Trans, 62, 486,* Warrendale. PA: Society of Automotive Engineers.

Taylor, S. C., 1991. *Burning Velocity and the Influence of Flame Stretch. PhD Thesis,* Leeds: University of Leeds.

Teets, R. E. & Sell, J. A., 1988. *Calorimetry of Ignition Sparks. SAE Paper No: 880204,* Warrendale. PA: Society of Automotive Engineers.

The Scott Owners Club, 2016. *Scottownersclub.org.* [Online] [Accessed 30th May 2016].

Theil, J., 2014. *Private Communication.* s.l.:s.n.

Thomson, J. J., 1908. *Conduction of Electricity Through Gases.* Cambridge: Cambridge Uiversity Press.

Thomson, W., 1860. Collected Papers on Electrostatics and Magnetism. p. 247.

Tobis, B. J. et al., 1994. *Scavenging of a Firing Two-Stroke Spark-Ignition Engine. SAE Paper No: 940393,* Warrendale. PA: Society of Automotive Engineers.

Tomita, E. & Kwahara, N., 2004. Real Time HC Concentration Measurement in Exhaust Gas from a Spark-Ignition Engine by using 3.392um Absorbtion Method.. *Journal of KONES,* 11(3-4), pp. 280 -287.

Torrens, H. S., 1991. *Joseph Day 1855 - 1946 and the Development of the Two Stroke Internal Combustion Engine. (ISBN 0-9518602-0-8).* 1st ed. Bath: Bath Industrial Heritage Trust.

Townsend, J. S. E., 1915. *Electricity in Gases.* 1st ed. Oxford: Wexford College Press.

Tsuchiya, K. & Hirano, S., 1975. *Characteristics of 2-Stroke Motorcycle Exhaust HC Emission and Effect of Air/Fuel Ratio and Ignition Timing SAE Paper No: 750908,* Warrendale. PA: Society of Automotive Engineers.

Tsuchiya, K., Hirano, S., Okamura, M. & Gotoh, T., 1980. *Emission Control of Two-Stroke Motorcycle Engines by Butterfly Exhaust Valve. SAE Paper No: 800973,* Warrendale. PA: Society of Automotive Engineers.

Tsuchiya, K., Nagai, Y. & Gotoh, T., 1983. *A Study of Irregular Combustion in 2-Stroke Cycle Gasoline Engines. SAE Paper No. 830091,* Warrendale. PA: Society of Automotive Engineers.

Ugale, R., 2014. *Digital DC CDI for Small Engines: Low Cost Solution and Challenges with 8 bit Microcontroller. SAE Paper No. 2014-01-2860,* Warrendale. PA: Society of Automotive Engineers.

Valavala, M. & Kanchanapalli, B., 2013. Measurement of Air Breakdown Voltage using Stadard Sphere Gap Method. *Journal of Electrical Engineering,* Jan.pp. 1-6.

Vieilledent, E., 1978. *Low Pressure Electronic Fuel Injection System for Two-Stroke Engines. SAE Paper No: 780767,* Warrendale. PA: Society of Automotive Engineers.

W.H.O., 2000. *World Health Organisation Fact Sheet No. 187,* s.l.: WHO.

Wadhwa, C. L., 2007. *High Voltage Engineering (ISBN-10: 1906574723).* 1st ed. New Delhi: New Age Publishers Ltd.

Wagner, R. M., Drallmeier, J. A. & Daw, C. S., 1998. *Prior Cycle Effects in Lean Spark Ignition Combustion - Fuel/Air Charge Considerations. SAE Paper No: 981047,* Warrendale. PA: Society of Automotive Engineers.

Walker, L. R., Lin, H. T., Levina, I. & Lykowski, J., 2005. *SEM and EPMA Analysis of Spark Plug Electrode Erosion..* Honolulu, Hawaii, Oak Ridge National Laboratory..

Wallace, F. J. & Cave, P. R., 1971. *Experimental and Analytical Scavenging Studies of Two-Stroke Opposed Piston Diesel Engine. SAE Paper No: 710175,* Warrendale. PA: Society of Automotive Engineers.

Wallace, F. J. & Nasif, M. H., 1954. Airflow in a Naturally Aspirated 2 Stroke Engine. *Proceedings of the Institution of Mechanical Engineers,* 168(18).

Walter, B., 1899. On the Formation of Electrical Sparks: Ueber die Entstehungsweise des Electrischen Funkens. *Weid. Ann. d. Phys. 66 & 68, lxvi / lxviii,* 302(12), pp. pp. 636-648.

Warburg, E., 1896. The Effect of Light on the initiation of electrical sparks. Ueber die wWirkung des Lichts auf die Funkenentladung. *Annalen der Physik und Chemie,* 295(9), p. 223.

Watanabe, I. & Kuroda, H., 1981. *Effect of Atmospheric Temperature on the Power Output of a Two-Stroke Cycle Crankcase Compression Gasoline Engine. SAE Paper No: 810295,* Warrendale. PA: Society of Automotive Engineers.

Watson, H. C., Goldsworthy, L. C. & Milkins, E. E., 1976. *Cycle by Cycle Variations of HC, CO and NOX. SAE Paper No: 760753,* Warrendale. PA: Society of Automotive Engineers.

Weclas, M., Melling, A. & Durst, F., 1997. Characteristics of Scavenging Flow in Transfer Ports of a Motored Two-Stroke Engine.. *Proceedings of the Institution of Mechanical Engineers,* Volume 211. Part D.

Weidemann, J. E. & Ebert, H., 1888. The Influence of Ultra-Violet Light on Spark Discharge. Ueber Electrische Entadungen in Gasen und Flammen. *Annalen der Physik. Weid. Ann. 33 (xxxiii),* 271(10), p. 241.

Weinhart, H., 1939. *Knocking in the Otto-Cycle Engine. NACA Report No. T.M. No. 911,* Washington: NACA.

Wijeyakulasuriya, S. D. & Nalim, M. R., 2007. *Simulation of Scavenging in a Small Two-Stroke Gasoline Engine Typical in South Asia. SAE Paper No. 2007-01-3554,* Warrendale. PA: Society of Automotive Engineers.

Wilstermann, H. et al., 2000. *Ignition System Integrated AC Ion Current Sensing for Robust and Reliable Online Engine Control. SAE Paper No: 2000-01-0553,* Warrendale. PA: Society of Automotive Engineers.

Winkelnkemper, H. & Baucke, W., 1969. Effect of Humidity on the Breakdown of Air in High AC Voltage. *ETZ-A 90,* pp. 667 - 670.

Winkler, F., Oswald, R., Schogl, O. & Kirchberger, R., 2008. *Application of Low Pressure Direct Injection and Semi-Direct Injection to a Small Capacity Two-Stroke Engine. SAE Paper No: 2008-32-0059,* Warrendale. PA: Society of Automotive Engineers.

Winterbourne, D. E. & Pearson, R. J., 1999. *Design Techniques for Engine Manifolds - Wave Action Methods for IC Engines (ISBN 1 86058 179 X).* 1st ed. Bury St. Edmunds: Professional Engineering Publishing.

Withrow, L. & Rassweiler, G. M., 1936. Slow Motion Shows Knocking and Non-Knocking Explosions. SAE Paper No: 360126. *SAE Journal,* 39(2), pp. 297-303, 312.

Witze, P. O., 1980. *A Critical Comparison of Hot-Wire Anemometry and Laser Doppler Velocimetry for I.C. Engine Applications. SAE Paper No: 800132,* Warrendale. PA: Society of Automotive Engineers.

Witze, P. O., 1989. *Cycle-Resolved Multipoint Ionization Probe Measurements in a Spark Ignition Engine. SAE Paper No: 892099,* Warrendale. PA: Society of Automotive Engineers.

Witze, P. O., Hall, M. J. & Bennett, M. J., 1990. *Cycle Resolved Measurements of Flame Kernel Growth and Motion Correlated with Combustion Duration. SAE Paper No: 900023,* Warrendale. PA: Society of Automotive Engineers.

Witze, P. O. & Mendes-Lopez, J. M. C., 1986. *Direct Measurements of the Turbulent Burning Velocity in a Homogeneous-Charge Engine. SAE Paper No: 861531,* Warrendale. PA: Society of Automotive Engineers.

Woschni, G., 1967. *A Universally Applicable Equation for the Intantaneous Heat Transfer Coefficient in the Internal Combustion Engine. SAE Paper No: 670931,* Warrendale. PA: Society of Automotive Engineers.

Wyczalek, F. A., 1991. *Two-Stroke Engine Technology in the 1990's. SAE Paper No: 910663,* Warrendale. PA: Society of Automotive Engineers.

Yamada, T., Matsubara, Y. & Kondo, N., 1999. *Characteristics of Multi-Spark Ignition System. SAE Paper No: 1999-01-0205,* Warrendale. PA: Society of Automotive Engineers.

Yamaga, J. & Shibata, S., 1969. *Measurement of Combustion Gas Temperature of Internal Combustion Engine by the use of Ultrasonic Wave. Bulletin of JSAE 535.55:662.613:621.2.029,* Warrendale. PA: Japanese Society of Automotive Engineers.

Yamagishi, G., Sato, T. & Iwasa, H., 1972. *A Study of Two-Stroke Cycle Fuel Injection for Exhaust Gas Purification. SAE Paper No: 720195,* Warrendale. PA: Society of Automotive Engineers.

Yamamoto, H. & Misumi, M., 1987. *Analysis of Cyclic Combustion Variation in a Lean Operating S.I. Engine. SAE Paper No: 870547,* Warrendale. PA: Society of Automotive Engineers.

Yorita, H., Okabe, S., Ishiguro, H. & Shibata, M., 2007. *Ignition Simulation and Visulatization for Spark Plug Electrode Design. SAE Paper No: 2007-01-0940,* Warrendale. PA: Society of Automotive Engineers.

Yoshiyama, S., Horita, E., Tabuchi, N. & Matsumoto, K., 2003. *Combustion Diagnostics of a Spark Ignition Engine by Using a Gasket Ion Sensor - Relation between Waveforms of Ion Current and Flame Propagation Process. SAE Paper No: 2003-01-1801,* Warrendale. PA: Society of Automotive Engineers.

Yoshiyama, S., Tomita, E. & Hamamoto, Y., 2000. *Fundamental Study on Combustion Diagnostics using Spark Plug as Ion Probe. SAE Paper No: 2000-01-2828,* Warrendale. PA: Society of Automotive Engineers.

Young, M. B., 1981. *Cyclic Dispersion in the Homogeneous-Charge Spark Ignition Engine- A Literature Survey. SAE Paper No: 810020,* Warrendal. PA: Society of Automotive Engineers.

Yucel, N., Karaasian, S., Hepkaya, E. & Dinler, N., 2013. High Speed Gas Sampling System for Engine Cylinder Emission Analysis. *Journal of Clean Energy Technologies,* April, 1(2), pp. 144 - 147.

Yui, S. & Ohnishi, S., 1969. *A New Concept of Stratified Charge Engine, Yui and Ohnishi Combustion Process (YOCP). SAE Paper No. 690468,* Warrendale. PA: Society of Automotive Engineers.

Zareei, J. & Kakaee, A. H., 2013. Study and the Effects of Ignition Timing on Gasoline Engine Performance and Emissions. *European Transport Research Review,* June, Volume 5, pp. 109 - 116.

Zdenek, J. S. & Anthenien, R., 2004. *Ion Based High-Temperature Pressure Sensor AIAA-2004-0470 / ADA453070,* Washington: American Institue of Aeronautics and Astronautics.

Zhou, L., Yao, C. & Yang, Z., 1984. *Minimization of Inverse Inlet Flow and Consequent Reduction in Specific Fuel Consumption in Gasoline Engines. SAE Paper No: 841093,* Warrendale. PA: Society of Automotive Engineers.

Zublin, B., 1997. *A Technical Report : MSD-6A Multiple Spark Discharge System. Rev 02,* San Diego: Zublin Engineering.